USGS
science for a changing world

The Pu‘u ‘Ō‘ō-Kūpaianaha Eruption of Kīlauea Volcano, Hawai‘i: The First 20 Years

Professional Paper 1676

U.S. Department of the Interior
U.S. Geological Survey

COVER

Lava flows from Pu'u ʻŌʻō wrap around Puʻu Halulu (foreground) during eruptive episode 46. View southwestward; photograph taken by J. D. Griggs at 0956 H.s.t., June 2, 1986.

The Pu‘u ‘Ō‘ō-Kūpaianaha Eruption of Kīlauea Volcano, Hawai‘i: The First 20 Years

Edited by Christina Heliker, Donald A. Swanson, and Taeko Jane Takahashi

The ongoing Pu‘u ‘Ō‘ō-Kūpaianaha eruption, which began in January 1983, is the longest and largest rift-zone eruption of Kīlauea Volcano in more than 600 years.

Professional Paper 1676

U.S. Department of the Interior
U.S. Geological Survey

U.S. Department of the Interior
Gale A. Norton, Secretary

U.S. Geological Survey
Charles G. Groat, Director

U.S. Geological Survey, Reston, Virginia: 2003

For additional copies please contact:
U.S. Geological Survey Information Services
Box 25286, Denver Federal Center
Denver, CO 80225

This report and any updates to it are available at http://geopubs.wr.usgs.gov/prof-paper/pp1676/
Additional USGS publications can be found at http://geology.usgs.gov/products.html

For more information about the USGS and its products:
Telephone: 1-888-ASK-USGS (1–888–275–8747)
World Wide Web: http://www.usgs.gov/

Text edited by George A. Havach and Peter H. Stauffer
Layout and graphic design by Jenda A. Johnson
Manuscript approved for publication, March 19, 2003

Library of Congress Cataloging-in-Publication Data

The Pu'u O'o-Kupaianaha eruption of Kilauea Volcano, Hawai'i : the first 20 years /
edited by Christina Heliker, Donald A. Swanson, and Taeko Jane Takahashi.
p. cm. -- (Professional paper ; 1676)
Includes bibliographical references.
1. Kilauea Volcano (Hawaii)--Eruptions. 2. Earth movements--Hawaii--Kilauea Volcano. 3. Volcanism--Hawaii. I. Heliker, C. C. II. Swanson, Donald A. (Donald Alan), 1938- III. Takahashi, Taeko Jane, 1941- IV. U.S. Geological Survey professional paper ; 1676.

QE523.K5P89 2003
551.21'09969'1--dc21

2003053114

Preface

The Pu‘u ‘Ō‘ō-Kūpaianaha eruption started on January 3, 1983. The ensuing 20-year period of nearly continuous eruption is the longest at Kīlauea Volcano since the famous lava-lake activity of the 19th century. No rift-zone eruption in more than 600 years even comes close to matching the duration and volume of activity of these past two decades.

Fortunately, such a landmark event came during a period of remarkable technological advancements in volcano monitoring. When the eruption began, the Global Positioning System (GPS) and the Geographic Information System (GIS) were but glimmers on the horizon, broadband seismology was in its infancy, and the correlation spectrometer (COSPEC), used to measure SO_2 flux, was still very young. Now, all of these techniques are employed on a daily basis to track the ongoing eruption and construct models about its behavior.

The 12 chapters in this volume, written by present or past Hawaiian Volcano Observatory staff members and close collaborators, celebrate the growth of understanding that has resulted from research during the past 20 years of Kīlauea’s eruption. The chapters range widely in emphasis, subject matter, and scope, but all present new concepts or important modifications of previous ideas—in some cases, ideas long held and cherished.

This volume complements Professional Paper 1463, which includes a discussion of the first 1½ years of the eruption, and the first chapter includes a bibliography that augments the material presented in both professional papers.

Readers will note that many Hawaiian words are spelled differently in the two Professional Papers. Improved technology now allows the full complement of diacritical marks to be used, both to satisfy the new standards of the Board on Geographic Names and to honor the Hawaiian language after more than a century of neglect. Our principal sources are *The Hawaiian Dictionary* (by M.K. Pukui and S.H. Elbert, ©1986) and *Place Names of Hawaii* (by M.K. Pukui, S.H. Elbert, and E.H. Mookini, 2nd edition, ©1974), published by the University of Hawai‘i Press. We depart from both the Board of Geographic Names and the *Place Names* dictionary in using the spelling “Halemaumau” for the largest pit crater in Kīlauea’s caldera, because local Hawaiian groups use two pronunciations. This spelling, without diacritical marks, permits both pronounciations.

Many persons have contributed to this work. We would like to acknowledge those whose contributions have not been noted elsewhere but without whose assistance and support this volume would have taken much longer to complete:

Jenda Johnson worked through the ins and outs of text, tables, and figures to seamlessly lay out each paper with a discerning eye.

Ed Bonsey, Lee Ann Chattey, Susan Dieterich, and especially Deb Sheppard, HVO library volunteers, researched all the references in these papers to produce accurate citations, including the many variations on the spelling of “Pu‘u ‘Ō‘ō.”

The librarians at the U.S. Geological Survey library at Menlo Park, Calif., provided reference and citation support. Without their assistance, we could not have properly edited the References Cited sections. Finally, Peter Stauffer, George Havach, and Susan Mayfield of the Western Publications Group in Menlo Park put up with our contretemps and numerous queries and guided the volume to completion.

The ongoing Kīlauea eruption has long since evolved from a scientific curiosity into a part of daily life in Hawai‘i. Though terribly destructive during its first eight years, it has also provided economic opportunities, visceral excitement, and artistic inspiration for the local community. In this light, we thought it appropriate to introduce the volume with a new poem, a tale about how Pu‘u ‘Ō‘ō acquired its name.

The editors

Contents

Contributors to This Professional Paper

Hawaiian Volcano Observatory

Brantley, Steven R.
Cervelli, Peter F.
Elias, Tamar
Heliker, Christina
Johnson, Jenda A.
Kauahikaua, Jim
Miklius, Asta
Nakata, Jennifer S.
Okubo, Paul G.
Sherrod, David R.
Sutton, A. Jeff
Takahashi, Taeko Jane

U.S. Geological Survey
P.O. Box 51
Hawaii Volcanoes National Park, HI 96718

Cascades Volcano Observatory

Lisowski, Michael
Thornber, Carl R.

U.S. Geological Survey
1300 SE Cardinal Court, Suite 100
Vancouver, WA 98683

Menlo Park

Dieterich, James H.
Mangan, Margaret

U.S. Geological Survey
345 Middlefield Road
Menlo Park, CA 94025

Reston

Helz, Rosalind Tuthill

U.S. Geological Survey
12201 Sunrise Valley Drive
Reston, VA 20192

Others

Barker, Stephen R.
Geoscience Department
University of Cambridge
Cambridge, U.K.

Cashman, Katharine V.
Department of Geology
University of Oregon
Eugene, OR 97403

Cayol, Valérie
Université B. Pascal
Clermont Ferrand, France

Gansecki, Cheryl A.
Volcano Video Productions
P.O. Box 909
Volcano, HI 96785

Hon, Ken
Department of Geology
University of Hawaii
Hilo, HI 96720

Mattox, Tari N.
Department of Geology
Grand Valley State University
Allendale, MI 49401

FACING PAGE

Low fountains erupt from Pu‘u ‘Ō‘ō, an hour after the start of eruptive episode 47.
View southwestward; photograph taken by G.E. Ulrich at 0522 H.s.t., on June 26, 1986.

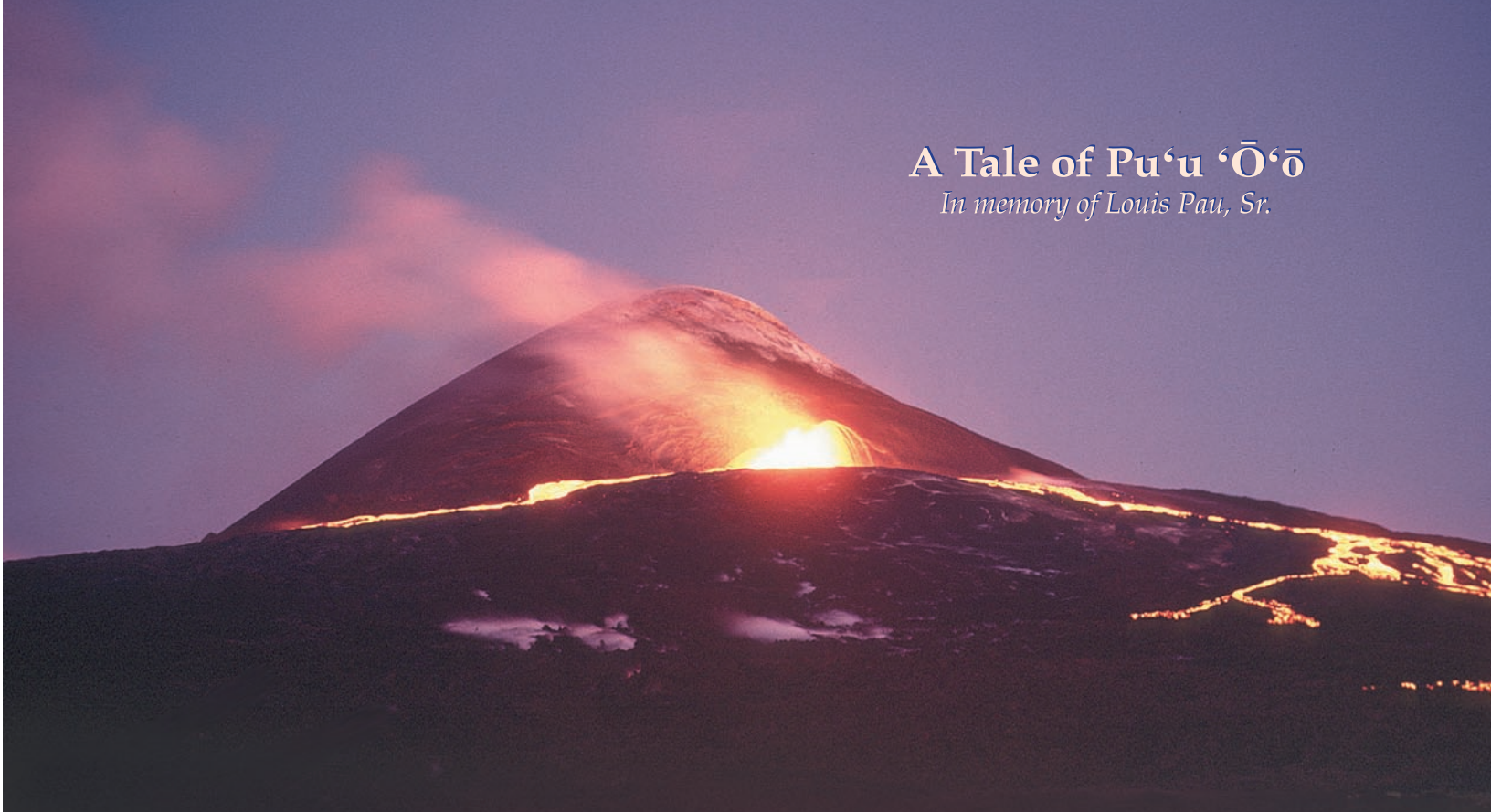

A Tale of Pu‘u ‘Ō‘ō

In memory of Louis Pau, Sr.

It started right on cue, fuming and spattering from vents uprift and down before merging into one, shooting molten rock high into the night. The puka formed neatly on “o” on the map’s “Flow of 1965,” so we called it “Pu‘u O.” It teased us, intrigued us, enduring beyond reason; it assumed a Hawaiian meaning. Pele the goddess pierced and thrusted, spilling lava into Royal Gardens subdivision.

To take on the mana of naming the new cone, we deferred to the elders of Kalapana to make it their own. Their stories grew long—as long as the night. “Oh-oh, it’s getting late—we’d better stop talking and give it a name,” Louis Pau said. Thus it went from ‘Ō to ‘Ō‘ō, the stick for piercing to the one for digging. Transcending nomenclature, Pele, creator and destroyer, dug silently and unseen. . . .

A new mystery, Kūpaianaha, was revealed. Its flows blanketed the land and (under cover) slid down to the sea. Who could have known so much lava would flow so far, so long? “She’s winding down,” the scientist said. But Pele, indifferent to theory, ate up the land. Inland she turned at Hākuma, covering the history of Kalapana, and poured her heart out into the bay. The ocean boiled, and birds feasted on steamed seafood washed upon a dark new shore.

A black cat crossed a molten sea, burned its paws and earned the name “Raku.” The Star of the Sea Church—moved at dawn, the storied landmarks—gone. Queen’s Bath, Kaimū, Kamoamoa and the heiau Waha‘ula (whose red mouth Pele filled), Louis’ homestead and Louis, too, are pau. “You can talk to the stones,” he said, “but watch out if they start talking back to you.” They do, Louis: we call it “geology.” Pele, glowing, moved on.

Taeko Jane Takahashi
September 2002

The First Two Decades of the Pu‘u ‘Ō‘ō-Kūpaianaha Eruption: Chronology and Selected Bibliography

By Christina Heliker *and* Tari N. Mattox

Abstract

The Pu‘u ‘Ō‘ō-Kūpaianaha eruption on the east rift zone of Kīlauea Volcano, Island of Hawai‘i, began on January 3, 1983. The early years of the eruption are vividly remembered for lava fountains as high as 470 m that erupted episodically from the Pu‘u ‘Ō‘ō vent. For the last 16 year, however, the activity has been dominated by near-continuous effusion, low eruption rates, and emplacement of tube-fed pāhoehoe flows. The change in eruptive style began when the activity shifted to the Kūpaianaha vent in mid-1986, and has continued since the eruption returned to flank vents on Pu‘u ‘Ō‘ō in 1992. To date, the total volume of lava erupted, 2.1 km^3, accounts for about half the volume erupted by Kīlauea in the past 160 years. This chapter includes a selected bibliography winnowed from the more than 1,000 reports and abstracts published about this eruption.

Introduction

The Pu‘u ‘Ō‘ō-Kūpaianaha eruption of Kīlauea Volcano, Island of Hawai‘i (fig. 1), ranks as the most voluminous outpouring of lava on the volcano’s east rift zone in the past 6 centuries. By the beginning of 2002, more than 2 km^3 of lava had been erupted, covering an area of 105 km^2 on the volcano’s south flank and adding 210 ha of new land to the island.

Since the eruption began, lava flows have repeatedly invaded communities on Kīlauea’s south coast, destroying 186 houses and a visitor center in Hawai‘i Volcanoes National Park (fig. 1*A*). The composite flow field spans 14.5 km at the coastline, forming a lava plain 10 to 35 m thick.

The eruption has progressed through three main epochs: 3½ years of episodic fountaining, mainly from the Pu‘u ‘Ō‘ō central vent, producing a cinder-and-spatter cone and ‘a‘ā flows; 5½ years of continuous effusion from the Kūpaianaha vent, creating a lava shield and tube-fed pāhoehoe flows; and more than 11 years (as of January 2003) of nearly continuous effusion from flank vents on Pu‘u ‘Ō‘ō, again creating a lava shield and tube-fed pāhoehoe flows.

This chapter provides a brief overview of the Pu‘u ‘Ō‘ō-Kūpaianaha eruption, followed by general observations on eruptive phenomena that have spanned most of the eruption, with emphasis on topics not covered elsewhere in this volume. The final section of this chapter is a selected bibliography culled from the more than 1,000 publications pertaining directly to the eruption.

Eruption Chronology

Setting the Stage

Before the Pu‘u ‘Ō‘ō-Kūpaianaha eruption, Kīlauea’s longest rift zone eruption in the past 2 centuries was at Mauna Ulu (fig. 1*A*), which erupted on the upper east rift zone in 1969–74 (Swanson and others, 1979; Tilling and others, 1987). The site of the current eruption, on the middle east rift zone, was host to several eruptions from 1963 to 1969, all of them short-lived. After the M7.2 earthquake in 1975 on Kīlauea’s south flank, magmatic activity in the middle east rift zone was dominated by intrusions. A total of 10 intrusions and a single brief eruption occurred in this section of the rift zone between 1977 and 1980 (Dzurisin and others, 1984; Klein and others, 1987). Leveling and geoelectric measurements in 1979–80 identified an intrusive body within 100 m of the eventual site of Pu‘u ‘Ō‘ō (Jackson, 1988). Three intrusions into the upper east rift zone from September through December 1982 (Jackson, 1988; Koyanagi and others, 1988; Okamura and others, 1988) may have primed the magmatic system for the January 1983 intrusion.

January 1983–April 1983 (Episodes 1–3): Fissures Erupt and Pu‘u Halulu Forms

The eruption began on January 3, 1983, after a 24-hour-long seismic swarm propagated down Kīlauea’s east rift zone at the leading edge of a basaltic dike. The initial outbreak was from a fissure in Nāpau Crater, within Hawai‘i Volcanoes National Park (fig. 1*A*). Over the next 4 days, fissures extended nearly 8 km northeastward along a remote section of the east rift zone (Wolfe and others, 1988).

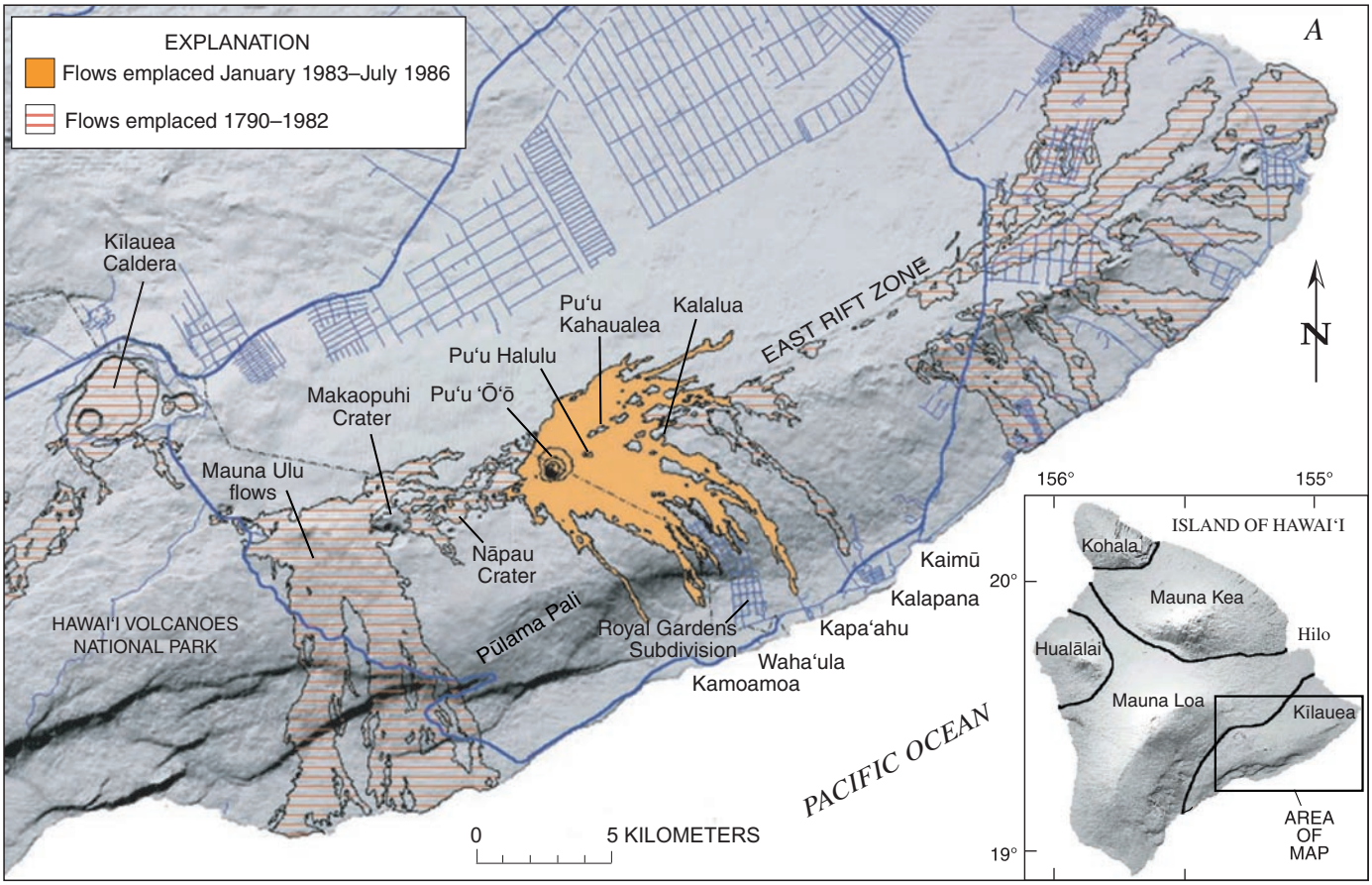

Figure 1. Summit and east rift zone of Kīlauea Volcano, Island of Hawai'i, showing development of Pu'u 'Ō'ō-Kūpaianaha flow field. *A*, Flows emplaced during 2 centuries before 1983 and flows erupted from January 3, 1983, through July 18, 1986. *B* (facing page), Flows emplaced as of February 1, 1997. *C*, Flows emplaced as of March 2002. Composite flow field has covered much of the same ground many times. In particular, episode 55 flows have buried most of episodes 50–53 flow field and parts of episodes 1–48 flow fields.

Effusion then became localized along a 1-km-long segment of the fissure system south of Pu'u Kahauale'a. This segment included the "1123 vent," later renamed Pu'u Halulu, which was the main locus of eruptive activity during episodes 2 and 3 (table 1). Fountains from Pu'u Halulu built a small (60 m high) cinder-and-spatter cone, the only substantial vent structure formed during this eruption, aside from Pu'u 'Ō'ō and Kūpaianaha. The vent later named "Pu'u 'Ō'ō" first erupted during episode 2.

June 1983–June 1986 (Episodes 4–47): Episodic High Fountaining at Pu'u 'Ō'ō

Pu'u 'Ō'ō made its solo debut in June 1983 (episode 4) and was the primary vent for the next 3 years. The eruption assumed an increasingly regular schedule, with brief (mostly less than 24 hour long) episodes, separated by repose periods averaging 24 days in length. These eruptive episodes were characterized by high effusion rates and spectacular lava fountains that reached a height of 470 m (fig. 2). Effusion rates (averaged over the length of an episode) increased through episode 39, reaching a maximum of 1.4×10^6 m^3/h (George Ulrich, unpub. data, 1986). Fountain heights gradually increased through episode 23 and were at a maximum during episodes 24 through 30 (table 1). Fallout from the fountains built a cinder-and-spatter cone 255 m high and 1.4 km in diameter at its base.

Tiltmeters recorded cycles of gradual inflation of Kīlauea's summit between eruptive episodes and rapid deflation, averaging 13 μrad, during fountaining episodes. The deflation was accompanied by high-amplitude tremor both at the summit and on the east rift zone. As the summit reinflated during repose periods, the rift zone was slowly repressurized, causing extension and uplift across the rift zone near the vent (Hoffmann and others, 1990). During the same interval, the magma column gradually rose within the Pu'u 'Ō'ō conduit, becoming visible within days to weeks after an eruptive episode.

The style of the eruption at Pu'u 'Ō'ō progressively changed through its first year from low fountains and pāhoehoe rivers to high fountains and 'a'ā fans. Episodes 4 through 19

(June 1983–May 1984) were characterized by channeled pāhoehoe flows that spilled from a lava pond at the base of the fountains (Wolfe and others, 1988). These fluid rivers carried most of the lava away from the cone before making the transition to ʻaʻā 1 to 2 km from the vent.

Beginning in episode 20 (June 1984), fountain-fed ʻaʻā flows became the norm, mainly because of a substantial increase in fountain heights. During the early Puʻu ʻŌʻō episodes, fountain heights rarely exceeded 250 m, but during episodes 20 through 39, fountains consistently reached heights greater than 300 m and, during about half of these episodes, greater than 400 m. Flows were fed directly by fallback from the fountains, resulting in lava with a higher viscosity and yield strength, owing to the loss of heat and volatile components (Sparks and Pinkerton, 1978). When sustained fountain heights decreased during episodes 42 through 47 in 1986, channeled pāhoehoe flows were observed once again.

From January 1983 through mid-1986, lava flows covered an area of 42 km^2 (for detailed maps, see Wolfe and others, 1988; Heliker and others, 2001). Flows soon threatened the sparsely populated Royal Gardens subdivision, located on a steep slope 6 km from the vent (fig. 1*A*). ʻAʻā flows reached the subdivision in as little as 13 hours during several eruptive episodes and destroyed 16 houses in 1983 and 1984 (Wolfe and others, 1988).

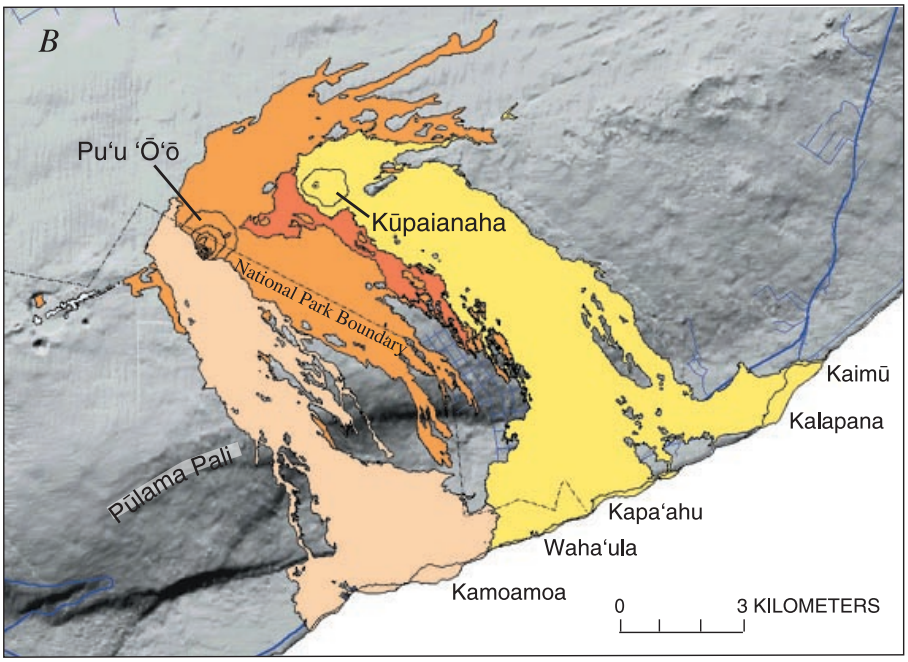

Episode	Area originally covered by lava (km^2)	Area exposed in January 2002 (km^2)
1–48b	42.0	17.7
48	41.0	34.7
49	3.9	3.9
50	1.0	0.2
51–52	12.3	0.8
53	19.4	10.7
54	0.2	0 .2
55	37.0	37.0
Total		105.2

EXPLANATION

February 1997–March 2002
Episode 55: Puʻu ʻŌʻō flank vents, mainly tube-fed pāhoehoe

January 1997
Episode 54: fissure vents, pāhoehoe

February 1992–January 1997
Episodes 50–53: Puʻu ʻŌʻō flank vents, mainly tube-fed pāhoehoe

November 1991
Episode 49: fissure vents, pāhoehoe

July 1986–February 1992
Episode 48: Kūpaianaha vent, mainly tube-fed pāhoehoe

January 1983–July 1986
Episodes 1–48b: Mainly Puʻu ʻŌʻō central vent, mainly ʻaʻā

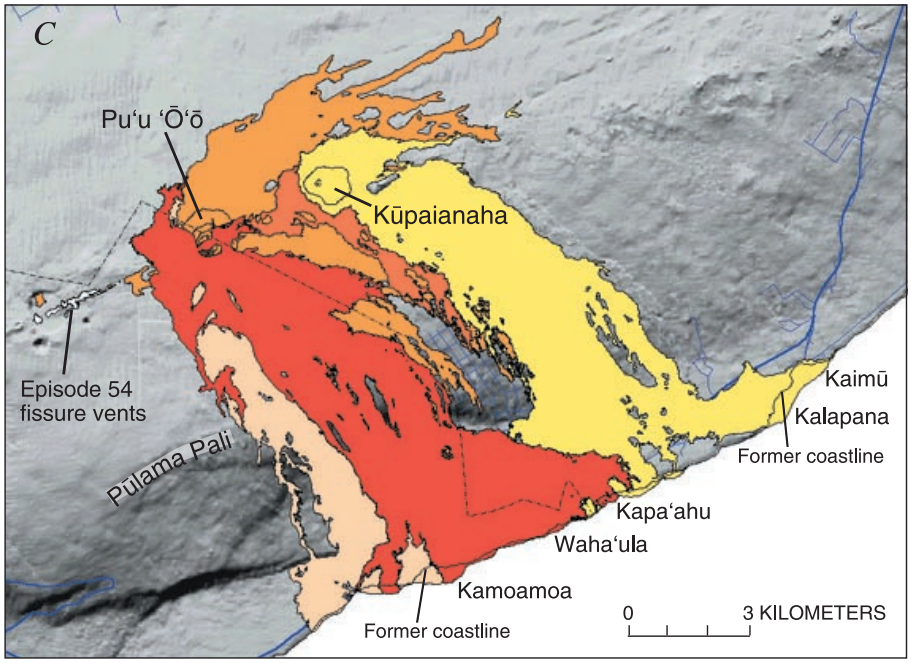

Table 1. Eruption statistics, 1983–2001.

[Raw lava volumes for episodes 1 through 40 were determined from flow areas and measured flow thicknesses. Lack of aerial photographs and accurate flow areas forced us to estimate lava volumes for episodes 41 through 47 from amount of deflation recorded by Uwēkahuna tiltmeter at Kīlauea's summit. During the first few months of episode 48, volumes were determined from area and estimated thickness of flows. Once tube-fed lava flows began entering the ocean, we had no accurate way of estimating volumes except to note constant rate of deflation recorded by Uwēkahuna tiltmeter. Beginning in 1988, volumes were estimated from geoelectrical measurements of lava flux, using very low frequency (VLF) profiles over lava tube (see Kauahikaua and others, 1996; Sutton and others, this volume). DRE, dense-rock equivalent (3 g/cm^3). Maximum fountain heights for episodes 2 through 47 were measured either directly by theodolite or indirectly from digitized time-lapse movie-camera film. Data for episodes 1 through 20 from Wolfe and others, 1988; for episodes 21 through 47 from George Ulrich unpub. data, 1986.]

Episode	Episode start		Episode end		Repose period before episode (days)	Episode length (days)	Area covered by lava (km^2)	Raw volume (10^6 m^3)	DRE volume (10^6 m^3)	Maximum fountain height (m)
	Date	Time (H.s.t.)	Date	Time (H.s.t.)						
1	01/03/83	0031	01/23/83	0000	0.0	4.1	4.8	14	9.8	--
2	02/25/83	0900	03/04/83	1451	33.0	7.3	2.7	14	9.8	117
3	03/28/83	0100	04/09/83	0257	23.5	12.1	7.9	38	26.6	278
4	06/13/83	1025	06/17/83	1413	65.3	4.2	2.2	11	7.7	57
5	06/29/83	1251	07/03/83	0715	11.9	3.8	3.4	13	9.1	61
6	07/22/83	1530	07/25/83	1630	19.3	3.0	2.0	9	6.3	129
7	08/15/83	0741	08/17/83	1600	20.6	2.3	3.7	14	9.8	86
8	09/06/83	0511	09/07/83	0526	19.5	1.0	2.0	8	5.6	160
9	09/15/83	1541	09/17/83	1920	8.4	2.2	2.1	8	5.6	200
10	10/05/83	0106	10/07/83	1650	17.2	2.7	2.7	14	9.8	237
11	11/05/83	2350	11/07/83	1845	29.3	1.8	4.3	12	8.4	58
12	11/30/83	0447	12/01/83	1545	22.4	1.5	3.0	8	5.6	65
13	01/20/84	1724	01/22/84	1123	50.1	1.8	2.6	10	7.0	116
14	01/30/84	1745	01/31/84	1318	8.3	.8	2.1	6	4.2	195
15	02/14/84	1940	02/15/84	1501	14.3	.8	2.2	8	5.6	350
16	03/03/84	1450	03/04/84	2231	17.0	1.3	3.2	12	8.4	389
17	03/30/84	0448	03/31/84	0324	25.3	1.0	3.0	10	7.0	177
18	04/18/84	1800	04/21/84	0533	18.6	2.5	6.6	24	16.8	217
19	05/16/84	0500	05/18/84	0050	25.0	1.8	1.4	2	1.4	128
20	06/07/84	2104	06/08/84	0625	20.8	.4	1.6	4	2.8	331
21	06/30/84	1028	06/30/84	1827	22.2	.3	1.9	5.7	4.0	318
22	07/08/84	1930	07/09/84	1017	8.0	.6	2.7	7.7	5.4	--
23	07/28/84	1200	07/29/84	0540	19.1	.8	3.3	9.5	6.7	322
24	08/19/84	2152	08/20/84	1725	21.7	.8	3.7	11.6	8.1	407
25	09/19/84	1604	09/20/84	0532	29.9	.6	3.3	11.1	7.8	467
26	11/02/84	1140	11/02/84	1636	43.3	.2	1.6	6.6	4.6	394
27	11/20/84	0005	11/20/84	1006	17.3	.4	2.3	8.4	5.9	--
28	12/03/84	1905	12/04/84	0941	13.4	.6	3.6	12.4	8.7	421

Table 1. Continued.

Episode	Episode start		Episode end		Repose period before episode (days)	Episode length (days)	Area covered by lava (km^2)	Raw volume (10^6 m^3	DRE volume (10^6 m^3)	Maximum fountain height (m)
	Date	Time (H.s.t)	Date	Time (H.s.t)						
29	01/03/85	1315	01/04/85	0504	29.1	.7	3.8	13 .0	9.1	464
30	02/04/85	0546	02/05/85	0246	31.0	.9	4.1	14.1	9.9	445
31	03/13/85	0600	03/14/85	0455	36.1	1.0	4.8	19.4	13.6	309
32	04/21/85	1516	04/22/85	0906	38.4	.8	4.8	16.3	11.4	391
33	06/12/85	2306	06/13/85	0453	51.6	.3	2.2	7.9	5.5	--
34	07/06/85	1903	07/07/85	0850	23.6	.6	2.3	10.6	7.4	410
35	07/26/85	0252	07/26/85	0952	18.8	.3	2.9	12	8.4	--
35a fissure	07/27/85	0414	08/12/85	0430	0.7	16.0	0.8	4.5	3.2	8
36	09/02/85	1400	09/02/85	2335	21.1	.4	2.7	11.5	8.1	441
37	09/24/85	1808	09/25/85	0619	21.8	.5	4.4	14.7	10.3	352
38	10/21/85	0300	10/21/85	1124	25.9	.4	3.9	14.8	10.4	--
39	11/13/85	1534	11/14/85	0124	23.2	.4	4.2	13.7	9.6	436
40	01/01/86	1309	01/02/86	0238	48.5	.6	4.0	11.6	8.1	264
41	01/27/86	2035	01/28/86	0757	25.8	.5	5.0	13.7	9.6	--
42	02/22/86	1515	02/23/86	0420	25.3	.5	3.5	12.1	8.5	--
43	03/22/86	0450	03/22/86	1556	27.1	.5	4.8	10.3	7.2	269
44	04/13/86	2054	04/14/86	0756	22.2	.5	5.2	11.5	8.1	308
45	05/07/86	2241	05/08/86	1106	23.6	.5	5.5	9.4	6.6	257
46	06/02/86	0229	06/02/86	1320	24.6	.5	4.6	9.8	6.9	223
47	06/26/86	0419	06/26/86	1635	23.6	.5	3.8	8.8	6.2	224
48a-b fissure	07/18/86	1205	07/19/86	0930	21.8	.9	4.5	7.2	5.0	30
Subtotal							42	*559*	*391*	--
48	07/20/86	0830	02/07/92	--	1.0	2, 028.0	41	--	500	5
49	11/08/91	0445	11/26/91	--	0	17.8	3.9	--	11	3
50	02/17/92	~1930	03/03/92	0130	10.0	14.3	1	--	4.5	<4
51	03/07/92	1245	09/27/92	~0600	4.5	197.7	--	--	--	10
52	10/03/92	~0330	02/20/93	1450	5.9	140.5	--	--	--	8
51-52	--	--	--	--	--	--	*12.3*	--	*78*	--
53	02/20/93	1450	01/29/97	1852	0	1,439.2	19.4	--	535	15
54	01/30/97	0240	01/31/97	0033	.3	.9	.2	--	.3	30
55	02/24/97	0700	ongoing	--	24.3	ongoing	37	--	667	15
Grand total									*2,190*	--

Eruptions from fissures or discrete vents on or near the base of the Pu‘u ‘Ō‘ō cone accompanied nine of episodes 4 through 47. Most of these vents opened just before, or concurrently with, the start of high fountaining from the main Pu‘u ‘Ō‘ō vent, and most died within a few hours once fountaining relieved some of the pressure on the magmatic system. Episode 35 was a conspicuous exception: a fissure on the uprift flank of the cone erupted early in the episode, propagated 2.5 km uprift after the high fountaining ended, and then erupted for the next 16 days.

July 1986–February 1992: Continuous Effusion from Kūpaianaha

On July 18, 1986, the conduit beneath Pu‘u ‘Ō‘ō ruptured, and lava was erupted through new fissures at the base of the cone. Fissures A and B of episode 48 were active for only 22 hours, but fissure C, which opened 3 km downrift of Pu‘u ‘Ō‘ō on July 20, evolved into a single vent, later named “Kūpaianaha” (fig. 1*B*). This event marked the end of the beginning of 5½ years of nearly continuous, quiet effusion (the main phase of episode 48). A tadpole-shaped lava pond, 140 by 300 m in diameter, formed over the new vent, and its frequent overflows built a broad, low shield 1 km in diameter and about 56 m high (fig. 3).

After weeks of continuous eruption, the main channel leaving the pond gradually evolved into a lava tube as crust at the sides of the channel extended across the lava stream, forming a roof. By the end of 1986, this tube became a persistent outlet to the pond; thereafter, the pond rarely overflowed, and shield growth declined.

A broad field of tube-fed pāhoehoe spread slowly toward the coast, 12 km to the southeast, taking 3 months to cover the same distance that ‘a‘ā flows from Pu‘u ‘Ō‘ō traveled in less than a day. Inflated pāhoehoe sheet flows dominated the composite flow field on the low-angle slope near the coast (Hon and others, 1994; Kauahikaua and others, 1998 and this volume). Over the next 5 years, the Kūpaianaha flow field covered an area of 41 km^2 (fig. 1*B*).

Late in November 1986, flows reached the ocean for the first time during this eruption, cutting a swath through the community of Kapa‘ahu (fig. 1*B*) and closing the coastal highway. A few weeks later, the lava took a more easterly course and overran 14 homes on the northwest edge of Kalapana in a single day. This flow abruptly stagnated when the tube became blocked near Kūpaianaha.

From mid-1987 through 1989, most of the lava that erupted from Kūpaianaha flowed through lava tubes to the

Figure 2. Spectacular lava fountain, 450 m high, erupts from the Pu‘u ‘Ō‘ō vent during eruptive episode 25. View southwestward from Pu‘u Halulu; photograph taken September 19, 1984.

Figure 3. Overflows from Kūpaianaha lava pond quickly built a lava shield. View southwestward; photograph taken November 24, 1986.

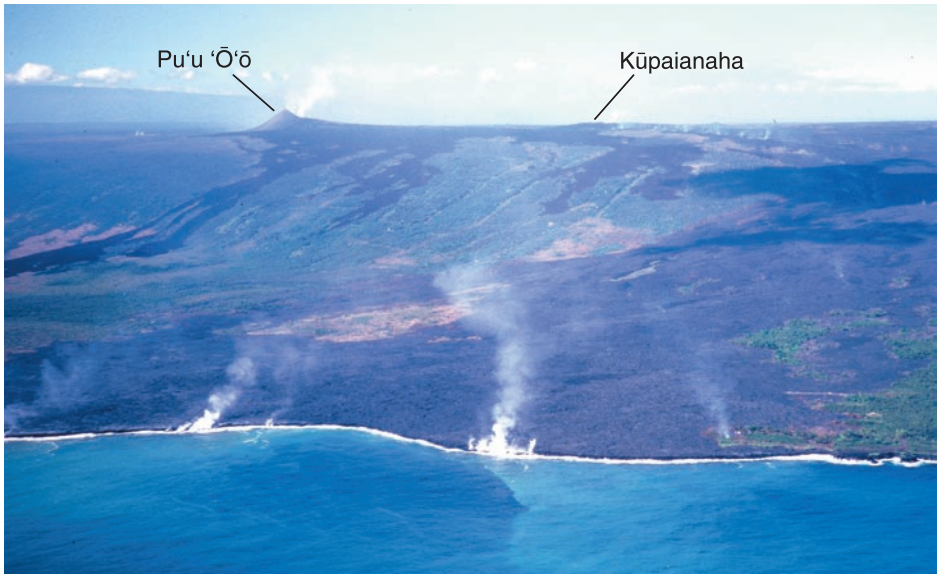

Figure 4. Steam plumes mark sites where lava flows from Kūpaianaha enter ocean on Kīlauea's south coast. Line of fume to right of Kūpaianaha reveals trace of tube feeding lava to coast. Streets of Royal Gardens subdivision, which lie on steep slope below vents, are partly covered by ‘a‘ā flows from Pu‘u ‘Ō‘ō. Photograph taken December 28, 1987.

sea, a distance of 12 km (fig. 4). The long-lived lava-tube system extending from the vent to the ocean began to break down in spring 1989, and lava flows encroached on new territory, overrunning the Waha‘ula Visitor Center in Hawai‘i Volcanoes National Park.

In March 1990, the eruption entered its most destructive period to date when the flows turned toward Kalapana, a village on the flat coastal plain 12 km southeast of Kūpaianaha (fig. 1*B*). Over the next several months, a succession of pāhoehoe sheet flows inundated the community (Mattox and others, 1993; Heliker and Decker, in press). Lava reached the sea at Kaimū and filled the shallow bay, extending the shoreline 300 m seaward. In May 1990, a Federal Disaster Declaration was issued for Kalapana and all other areas previously affected by the eruption.

In late 1990, a new tube diverted lava away from Kalapana and back into the national park, where flows once again entered the ocean. During Kūpaianaha's tenure, from 1986 to 1992, lava entered the ocean approximately 68 percent of the time (fig. 5), creating about 130 ha of new land.

Although Pu‘u ‘Ō‘ō did not produce any lava flows during the 5½ years that Kūpaianaha erupted, Pu‘u ‘Ō‘ō remained actively linked to the conduit that fed magma from Kīlauea's summit to Kūpaianaha. Beginning in June 1987, repeated collapses over the Pu‘u ‘Ō‘ō vent formed a crater approximately 300 m in diameter. A lava pond began to appear intermittently at the bottom of the crater in 1987; by mid-1990, the pond was present most of the time.

Except for a week-long pause in the eruption in 1988 (table 2), lava effusion from Kūpaianaha was continuous

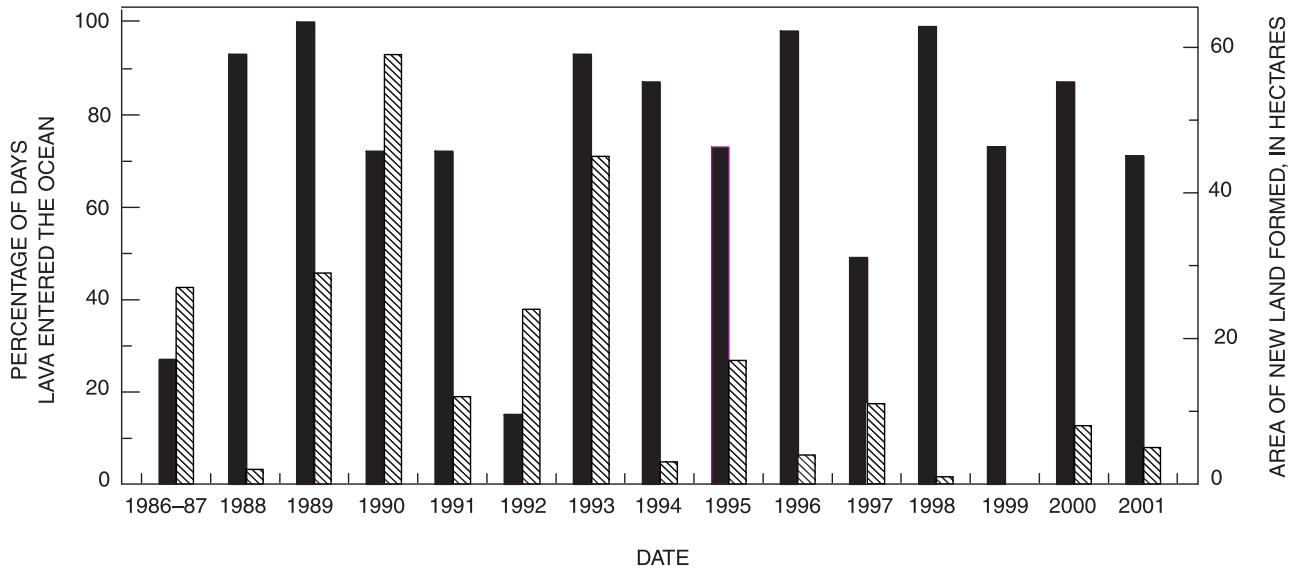

Figure 5. Percentage of days per year when lava entered ocean (black bars) since flows from Kūpaianaha first reached coast in November 1986, and area of new land created (shaded bars). Greatest area of new land formed during 1990 and 1993, when flows filled two largest embayments on coastline, at Kaimū and Kamoamoa, respectively.

Table 2. Eruptive pauses, intrusions, surges, and large earthquakes, 1983–2001.

[Start and end times for episodes in italics. Tilt plots for the 1990 pauses were reexamined, and start and stop times for pauses were picked in a manner consistent with current practice: in general, pause starts at bottom of brief interval of steep deflation at summit and ends at top of intervening summit inflation. Last three pauses originally reported for 1990 (Heliker and Wright, 1991; Mattox and others, 1993) were omitted, because, although instrumental signature resembled those of earlier pauses, we had insufficient evidence that eruption actually stopped. Start and stop times for intrusions and magmatic surges are based solely on beginning and end of period of elevated seismicity at summit. Seismicity tends to tail off gradually, and so end time is much more uncertain than start time. Deformation and eruptive changes associated with these events continue much longer than seismicity. All earthquakes of M>5.5 since 1983 are listed, along with two smaller earthquakes near vent that may have affected eruptive activity.]

Event start		Event end		Pause length	Comments
Date	Time (H.s.t.)	Date	Time (H.s.t.)	(days)	
09/09/83	0630	--	--	--	M=5.7 earthquake, Kīlauea's south flank, 6 km SSE. of Nāpau Crater.
11/16/83	0613	--	--	--	M=6.7 earthquake, Kaʻōiki, 19 km west of Kīlauea's summit.
04/24/88	a.m.	05/01/88	a.m.	7.00	Pause 48.0.
06/25/89	1727				M=6.2 earthquake, Kalapana, 1.5 km WNW. of Hākuma Point.
02/06/90	0800	02/09/90	1330	3.23	Pause 48.1.
03/19/90	0400	03/21/90	1600	2.50	Pause 48.2.
04/04/90	0200	04/06/90	1700	2.63	Pause 48.3.
05/06/90	0000	05/09/90	1000	3.42	Pause 48.4.
05/28/90	1500	05/30/90	1400	1.96	Pause 48.5.
06/17/90	0400	06/19/90	2200	2.75	Pause 48.6.
07/31/90	0400	08/02/90	0000	1.83	Pause 48.7.
08/09/90	1200	08/11/90	0000	1.50	Pause 48.8.
08/13/90	2200	08/14/90	2200	1.00	Pause 48.9.
12/04/90	1628	12/04/90	~1900	--	Intrusion—upper east rift zone. Brief (<24 h) surge in Puʻu ʻŌʻō.
03/26/91	0532	03/26/91	~0830	--	Intrusion—upper east rift zone. No change in effusion rate at Kūpaianaha, but see below.
03/26/91	0700	--	---	--	Explosion in Puʻu ʻŌʻō's crater, possibly triggered by rockfall into crusted pond.
08/21/91	1100	08/21/91	~1300	--	Intrusion (?)—summit, SE. of Kīlauea caldera. No deformation data.
11/08/91	*0445*	*11/26/91*	---	--	*Episode 49—fissure eruption lasts 18 days.*
02/07/92	--	--	---	--	*Kūpaianaha vent shuts down—end of episode 48.*
02/07/92	--	*02/17/92*	*~1930*	*10.00*	*Eruption hiatus.*
02/17/92	*~1930*	--	---	--	*New fissure erupts—episode 50 begins.*
03/03/92	0045	03/03/92	~0930	--	Intrusion—upper east rift zone. Triggered eruption pause.
03/03/92	0130	03/07/92	1245	4.47	Pause 50.1.
03/07/92	*1245*	---	---	--	*Episode 50 fissure extends—episode 51 begins.*
03/07/92	2100	03/07/92	2400	.13	Pause 51.2.
03/12/92	1519	03/14/92	1130	1.84	Pause 51.3.
03/15/92	1800	03/17/92	0600	1.50	Pause 51.4.
03/18/92	0300	03/18/92	0600	.13	Pause 51.5.
03/26/92	1400	03/29/92	0930	2.81	Pause 51.6.
03/31/92	0000	03/31/92	1230	.52	Pause 51.7.
04/19/92	2000	04/23/92	1100	3.63	Pause 51.8.
04/28/92	1130	05/04/92	0539	5.76	Pause 51.9.
05/22/92	1400	05/27/92	0320	4.56	Pause 51.10.
05/28/92	2020	06/02/92	~0530	4.38	Pause 51.11.
06/05/92	~1700	06/06/92	0400	.46	Pause 51.12.
06/07/92	~0630	06/10/92	1325	3.29	Pause 51.13.
06/16/92	~0500	06/20/92	2314	4.76	Pause 51.14.
07/22/92	p.m	07/27/92	1030	~4.5	Pause 51.15.
08/11/92	~2000	08/15/92	~1300	3.70	Pause 51.16.
08/29/92	~0800	09/02/92	1400	4.25	Pause 51.17.
09/09/92	0900	09/12/92	1700	3.33	Pause 51.18.

Table 2. Continued.

Event start		Event end		Pause length (days)	Comments
Date	Time (H.s.t.)	Date	Time (H.s.t.)		
09/27/92	~0600	10/03/92	~0330	5.90	Pause 51.19.
10/02/92	1951	--	--	--	M=4.2 earthquake, Kīlauea's south flank, 4 km SSE. of Pu‘u ‘Ō‘ō; tremor at Pu‘u ‘Ō‘ō increased.
10/03/92	*~0330*	--	--	--	*New fissure erupts—episode 52 begins.*
09/27/92	*1530*	--	--	--	*Episode 51 vent restarts.*
10/16/92	*p.m.*	--	--	--	*Last observed activity at 52 vent.*
01/03/93	1600	01/04/93	1528	.98	Pause 52.20.
02/07/93	2325	02/08/93	~0400	--	Intrusion—upper east rift zone. Triggered eruption pause; Pu‘u ‘Ō‘ō's crater floor collapsed <24 h later.
		--	--		
02/08/93	0400	02/16/93	1200	8.33	Pause 52.21.
02/20/93	*1450*	--	--	--	*New vent erupts—episode 53 begins.*
06/08/93	0257	--	--	--	M=4.8 earthquake, Kīlauea's south flank, 8 km WSW. of Nāpau Crater. May have triggered drop in Pu‘u ‘Ō‘ō's pond level.
03/02/94	2230	03/03/94	0600	.31	Pause 53.1.
03/12/94	1330	03/14/94	1400	2.02	Pause 53.2.
04/14/94	1600	04/16/94	0400	1.50	Pause 53.3.
10/05/94	0130	10/07/94	1100	2.40	Pause 53.4.
10/24/94	2100	10/26/94	1200	1.63	Pause 53.5.
11/29/94	1500	12/01/94	0900	1.75	Pause 53.6.
03/16/95	1000	03/17/95	0400	.75	Pause 53.7.
04/11/95	0000	04/11/95	2000	.83	Pause 53.8.
08/22/95	2000	08/25/95	0800	2.50	Pause 53.9.
11/10/95	1500	11/11/95	1800	1.13	Pause 53.10.
12/14/95	1500	12/16/95	2400	2.38	Pause 53.11.
02/01/96	0809	02/01/96	~1210	--	Magmatic event—Kīlauea's summit. Surge in effusion rate.
02/01/96	1130	02/02/96	p.m.	--	Surge in effusion rate—tailed off gradually.
02/04/96	2000	02/14/96	0000	9.17	Pause 53.12.
03/24/96	1036	03/24/96	1151	--	Magmatic event—Kīlauea's summit. Small surge in effusion rate.
05/29/96	2000	06/04/96	1030	5.60	Pause 53.13.
08/21/96	0800	08/22/96	0800	1.00	Pause 53.14.
11/18/96	0900	11/19/96	0900	1.00	Pause 53.15.
01/29/97	1841	01/30/97	0240	--	Intrusion—Nāpau Crater.
--	1930	--	--	--	Onset of summit deflation; probable end of episode 53.
--	~2100	--	--	--	Probable time of collapse of Pu‘u ‘Ō‘ō's crater floor and west wall of cone.
01/30/97	*0240*	*01/31/97*	*0033*	*24.20*	*Episode 54—fissure eruption lasts 22 h.*
01/31/97	*0033*	*02/24/97*	*~0700*	--	*Eruption hiatus.*
02/24/97	*~0700*	--	---	--	*Lava returns to Pu‘u ‘Ō‘ō's crater—start of episode 55.*
05/03/97	0000	05/03/97	0530	.23	Pause 55.1.
05/10/97	0700	05/10/97	1230	.23	Pause 55.2.
05/11/97	2000	05/12/97	0600	.42	Pause 55.3.
05/12/97	2139	05/13/97	0030	.13	Pause 55.4.
05/14/97	0200	05/14/97	0700	.21	Pause 55.5.
05/23/97	0630	05/23/97	2134	.63	Pause 55.6.
05/27/97	0430	05/27/97	0654	.10	Pause 55.7.
06/06/97	2330	06/07/97	1005	.44	Pause 55.8.
06/16/97	1600	06/16/97	2027	.19	Pause 55.9.
06/17/97	1010	06/18/97	~0530	0.81	Pause 55.10.

Table 2. Continued.

Event start		Event end		Pause length (days)	Comments
Date	Time (H.s.t.)	Date	Time (H.s.t.)		
01/14/98	1815	01/15/98	0600		Magmatic event—Kīlauea's summit. Surge in effusion rate. Triggered pause.
01/15/98	1030	01/16/98	1100	1.02	Pause 55.11.
01/26/98	1130	01/27/98	0600	0.77	Pause 55.12.
02/21/98	0000	02/21/98	2400	1.00	Pause 55.13.
03/02/98	0400	03/02/98	1600	0.50	Pause 55.14.
03/09/98	1400	03/10/98	0800	0.75	Pause 55.15.
04/04/98	0400	04/05/98	0041	0.85	Pause 55.16.
05/19/98	0350	05/20/98	2230	1.77	Pause 55.17.
06/19/98	~1400	06/20/98	~0100	0.46	Pause 55.18.
07/16/98	2100	07/19/98	0200	2.21	Pause 55.19.
08/12/98	~1500	08/14/98	~0930	1.75	Pause 55.20.
11/07/98	~0600	11/08/98	~1000	1.17	Pause 55.21.
02/06/99	0400–0800	02/07/99	~0300	.90	Pause 55.22.
04/16/99	1456	--	--	--	M=5.6 earthquake, 6 km NNW. of Pahala.
05/04/99	~1300	05/05/99	~2200	1.38	Pause 55.23.
06/14/99	0010	06/17/99	2300	3.96	Pause 55.24.
08/21/99	~2000	08/22/99	~2000	1.00	Pause 55.25.
09/12/99	0131	09/12/99	~0600	--	Intrusion—upper east rift zone. Triggered pause. Pu‘u ‘Ō‘ō crater floor partially collapsed; new collapse pit formed in west gap.
09/12/99	0131	09/23/99	1100	11.40	Pause 55.26.
10/03/99	~2200	10/05/99	0900	1.46	Pause 55.27.
11/07/99	1400	11/08/99	1015	.85	Pause 55.28.
11/11/99	~1530	11/14/99	1030	2.79	Pause 55.29.
02/23/00	1342	02/23/00	~1600	--	Intrusion—upper east rift zone. Effusion may have slowed or paused briefly (<7 h).
08/23/00	~2300	08/26/00	~1900	2.83	Pause 55.30.
09/24/00	1300	09/25/00	2200	--	Magmatic event—Kīlauea's summit (Dog Day Surge). Surge in effusion rate for ~8 h.
09/25/00	0005	--	--	--	First breakouts on upper flow field.
12/15/00	1715	12/17/00	~0200	1.40	Pause 55.31.
05/20/01	1630	05/21/01	0200	--	Magmatic event—Kīlauea's summit. Surge—two periods of increased effusion rate.
05/20/01	1918	05/21/01	~0400	--	First surge in effusion rate.
05/23/01	~0800	05/23/01	~1800	--	Second surge in effusion rate, associated with summit deflation.

until 1990. From February through August 1990, nine pauses, lasting from less than 1 to 3 days, interrupted the steady effusion of lava.

The 1990 pauses accelerated the demise of the Kūpaianaha lava pond, which had been gradually diminishing in size since late 1987. During the first pause, the pond drained to a depth of 35 to 40 m. When the eruption resumed, the pond partly refilled, but a broad, inner ledge reduced its diameter to 50 m. After subsequent pauses, the shrinking pond was active for a few days when the eruption restarted, and then crusted over. Shortly after the sixth pause in June 1990, the lava pond crusted over for good.

The lava output from Kūpaianaha began to decrease in mid-1990 and steadily declined through 1991 (Kauahikaua and others, 1996). This change also was probably triggered by the frequent pauses, which induced cooling and constriction in the conduit between Pu‘u ‘Ō‘ō and Kūpaianaha (Mangan and others, 1995; Kauahikaua and others, 1996). Concurrently, the level and activity of the Pu‘u ‘Ō‘ō lava pond rose.

In response to pressurization of the magmatic system uprift of Kūpaianaha, fissures opened on the northeast flank of Pu‘u ‘Ō‘ō in November 1991 and quickly propagated 2 km downrift to the base of the Kūpaianaha shield. The downrift end of the fissure system erupted for 3 weeks (episode 49), creating a channeled flow that extended 6.5 km along the western margin of the Kūpaianaha flow field (Mangan and others, 1995). Kūpaianaha continued to erupt during this event, but its output waned. By February 7, 1992, the Kūpaianaha vent was dead.

1992–96: The Return to Pu‘u ‘Ō‘ō

Ten days after Kūpaianaha died, the eruption returned to Pu‘u ‘Ō‘ō. Lava erupted in low fountains along a radial fissure on the west flank of the massive cone (episode 50). New flank vents opened nearby in March 1992 (episode 51), October 1992 (episode 52), and February 1993 (episode 53; Heliker and others, 1998a, b). As at Kūpaianaha, the style of the eruption was nearly continuous, quiet effusion. Flows from the flank vents quickly built a lava shield that banked up against the south and west slopes of Pu‘u ‘Ō‘ō. Spatter cones formed over the initial fissure vents (fig. 6), and during the first 4 months of episode 51, a tube from one of these cones fed a perched lava pond.

By July 1992, new lava tubes formed that bypassed the perched pond. Within a few months, the active vents were completely crusted over, feeding directly into tubes. Tube-fed pāhoehoe flows gradually advanced toward the coastal plain. In November 1992, flows crossed Chain of Craters Road in Hawai‘i Volcanoes National Park and entered the ocean at Kamoamoa, an archeological site and campground 11 km from the vents (figs. 1*B*, 7). From the end of 1992 through January 1997, tubes fed lava to the ocean almost continuously, forming approximately 93 ha of new land. Surface breakouts from the lava-tube system broadened the new flow field, which was mostly contained within the national park.

During the first year of flank-vent activity at Pu‘u ‘Ō‘ō, the eruption was erratic, with frequent pauses, multiple vents, and two intrusions on the upper east rift zone (table 2; fig. 8). Once episode 53 began in late February 1993 (fig. 9), no more pauses occurred for a year. Pauses resumed in March 1994, with a series of 15 pauses that continued through November 1996.

By 1993, the shield produced by the flank vents was pockmarked with collapse pits, which formed as lava tubes eroded vertically as much as 29 m through the thick deposits of tephra on the downwind side of the Pu‘u ‘Ō‘ō cone (Heliker and others, 1998b). The level of the magma column in the vents feeding the tubes dropped in tandem with the downcutting tubes. As the magma column in the vents dropped, so did the level of the pond in the Pu‘u ‘Ō‘ō crater (fig. 10), demonstrating the hydraulic connection between the flank vents and the crater's pond. The downcutting tubes and the drop in elevation of the magma column beneath the flank vents opened voids that undermined the west side of the Pu‘u ‘Ō‘ō cone.

In addition to the collapse pits on the shield, pits formed on the side of the Pu‘u ‘Ō‘ō cone upslope of the flank vents. The largest of these features, known as the "Great Pit," had engulfed most of the west flank by the end of 1996 (see Heliker and others, this volume).

Figure 6. The cone of Pu‘u ‘Ō‘ō. Spatter cones on skyline to left mark site of episode 51 vents. Lines across lower part of cone are foot trails. View northward; photograph taken December 15, 1992.

Figure 7. Lava flow beginning to fill bay at Kamoamoa on November 12, 1992. Narrow flow has not yet covered picnic ground visible on near side of flow. Dark flows in distance are from Kūpaianaha.

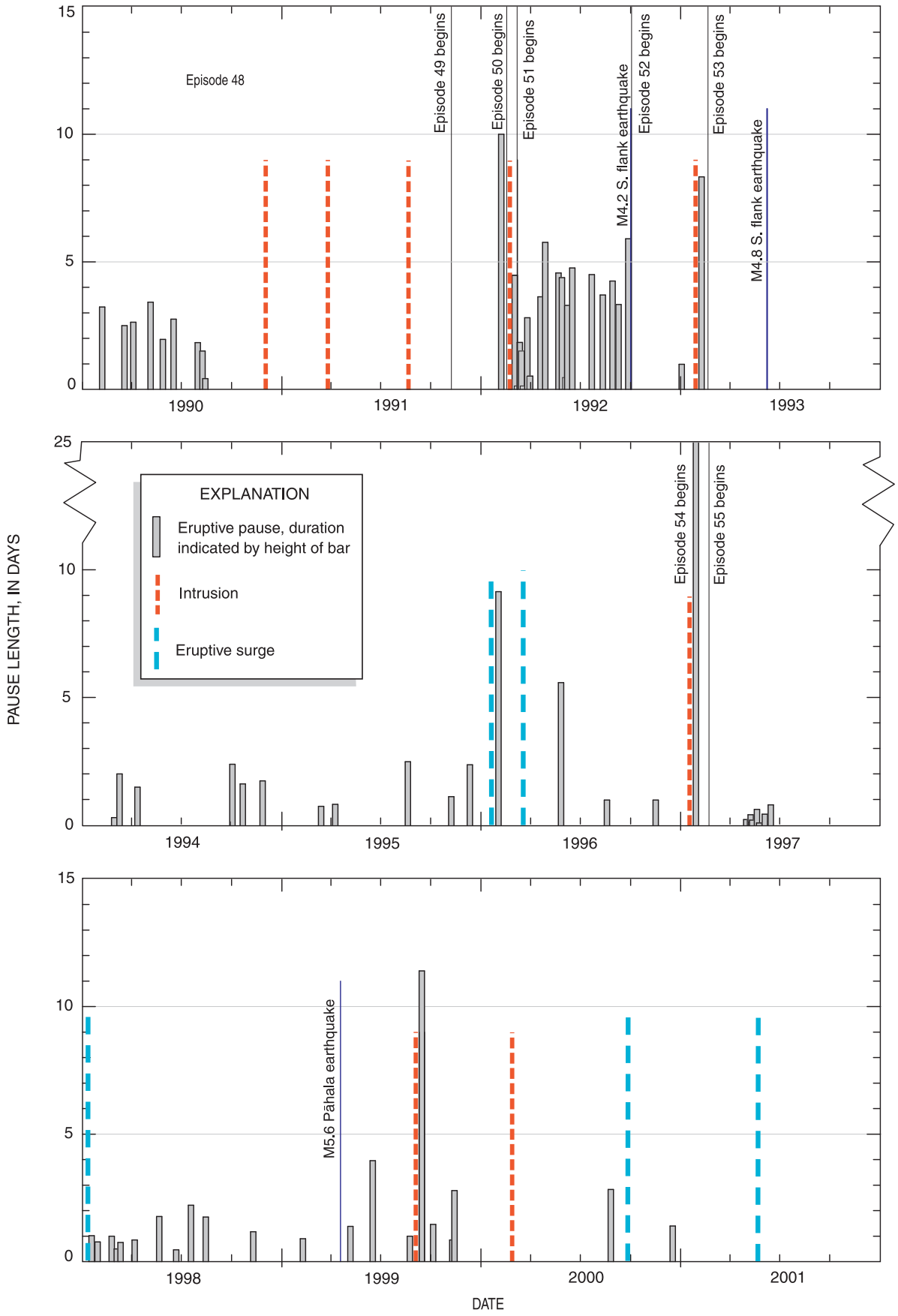

Figure 8. Timeline showing pauses, intrusions, and eruptive surges during Pu‘u ‘Ō‘ō-Kūpaianaha eruption, from 1990 through 2001.

January 1997: Cone Collapse and Fissure Eruption

On the night of January 29, 1997, the conduit leading from the summit reservoir to Pu‘u ‘Ō‘ō was depressurized as magma was diverted to an intrusion uprift of Pu‘u ‘Ō‘ō (Owen and others, 2000; Thornber, 2001; Thornber and others, in press). In rapid sequence, the Pu‘u ‘Ō‘ō conduit drained, the crater floor dropped about 150 m, and the west flank of the cone collapsed, producing a plume of red rock dust that blanketed an area of more than 4 km^2. When the dust settled, Pu‘u ‘Ō‘ō had a nearly vertical walled crater 210 m deep, and the Great Pit had been replaced by a 115-m-wide gap in the west flank of the cone. The height of the cone was reduced by 34 m.

A few hours later, fissures began to erupt in, and downrift of, Nāpau Crater, 4 km uprift of Pu‘u ‘Ō‘ō (figs. 1*C*, 11). The fissure eruption (episode 54) lasted less than a day and was notable for producing lava with the first major differences in whole-rock chemistry in the eruption since 1985—a result of the dike incorporating older magma stored within the rift zone (Thornber, 2001; Thornber and others, in press). Episode 54 was also the first fissure eruption to occur since continuous Global Positioning System (GPS) monitoring of the east rift zone began, resulting in a detailed geodetic record of dike emplacement (Owen and others, 2000; Segall and others, 2001).

February 1997 to Present: Eruption of Pu‘u ‘Ō‘ō Flank Vents Resumes

Episode 54 was followed by the longest eruptive hiatus in more than 10 years. Twenty-four days passed before episode 55 began on February 24, 1997, when lava rose through the rubble on the floor of the crater to form a new pond. Lava first erupted outside the crater on March 28, after the pond had risen to within 50 m of the crater rim. Over the next 3 months, several new vents opened on the west and southwest flanks of the cone (see Heliker and others, this volume). As during episodes 50 through 53, the new flank vents initially formed spatter cones (fig. 12) and fed short surface flows onto the shield. Within weeks, however, each vent crusted over and fed lava directly into tubes rather than to surface flows. Before all the vents sealed over, the episodes 50–55 shield grew rapidly. By the end of 1997, the shield was about 80 m high and 0.8 by 1.8 km wide.

In April 1997, the active lava pond in the Pu‘u ‘Ō‘ō crater was replaced by a single vent on the west side of the crater. Flows from this vent intermittently ponded at the crater’s east end. In June 1997, the lava rose until it overtopped the gap in the west wall of Pu‘u ‘Ō‘ō formed by the January 1997 collapse. Lava spilled from the crater for the first time in 11 years (fig. 13). Subsequent crater overflows in 1997 also overtopped the east crater rim and extended as far as 1.5 km downrift. The spillovers were brief events, ending when the lava pond

Figure 9. Episode 53 vent on southwest flank of the Pu‘u ‘Ō‘ō cone. Photograph taken February 21, 1993, 1 day after vent began erupting.

Figure 10. Throughout early 1990s, lava pond in the Pu‘u ‘Ō‘ō crater was typically circular and occupied east end of the crater. Depth to crater floor is 37 m, and pond is about 80 m in diameter. Photograph by M.T. Mangan, taken from north rim of crater on April 16, 1992.

Figure 11. Fuming fissures and fresh black pāhoehoe mark episode 54 fissures, which stopped erupting a few hours before photograph was taken on January 31, 1997. Pu‘u ‘Ō‘ō, in background, is tinted red from rock dust deposited during collapse of crater floor and west side of cone.

drained through conduits in the crater floor. Crater overflows continued intermittently through January 1998 and plated the west gap and east flank of the cone with fresh pahoehoe.

From February 1998 through 2001, eruptive activity within the crater dropped to its lowest level since early 1990, relieved only by a 2-month interval of spattering and extrusion of small flows after a pause in September 1999. In early 2002, crater activity again became conspicuous, with multiple vents contributing lava flows that resurfaced the crater floor and raised its level to within 10 m of the east rim (fig. 14).

Tube-fed flows from the episode 55 flank vents reached the ocean in July 1997 near the east boundary of Hawai‘i Volcanoes National Park. Episode 55 flows have subsequently buried much of the episodes 50–53 flow field (fig. 1*C*). In early 2000, flows crossed the east boundary of the park and encroached on private property. During the next 2 years, lava overran five abandoned houses in Royal Gardens subdivision, bringing the total number of structures destroyed by this eruption to 189 by the end of May 2002.

Flank-vent activity continued to undermine the Pu‘u ‘Ō‘ō cone during episode 55. In December 1997, a new collapse pit, Puka Nui, formed on the southwest flank of the cone. During the next year, Puka Nui expanded rapidly by coalescing with pits on the adjacent shield. Several spatter cones formed within Puka Nui in September–October 1999 and again in April–May 2002; lava flows floored the shield part of the pit on both occasions. By mid-2002, Puka Nui was 180 by 200 m in diameter, and headward erosion of the upper edge of the pit had carved a notch in the rim of the cone.

A total of 31 pauses had interrupted episode 55 as of May 2002 (fig. 8), two-thirds of which occurred during the first 2 years of the episode. The latest pause was in December 2000.

Long-Term Observations

Effusion and Magma-Supply Rates

The estimated long-term effusion rate averaged over the first 19 years of the Pu‘u ‘Ō‘ō-Kūpaianaha eruption is about 0.12 km^3/yr (dense-rock equivalent; using methods given in table 1. Sutton and others (this volume) average VLF-and SO_2-emission-derived efusion rates to obtain 0.13 km^3/yr.) Tiltmeters at Kīlauea’s summit have recorded long-term deflation during the eruption (see Cervelli and Miklius, this volume), indicating that nearly all the magma entering the shallow summit reservoir passes through it to the eruption site. According to several workers who have used geodetic data to model long-term deformation of Kīlauea’s south flank, however, the effusion rate does not approximate the full magma-supply rate (Delaney and others, 1993; Owen and others, 1995; Cayol and others, 2000). Their models invoke an extensional source within the deep rift zone that requires diversion of a significant proportion of the magma supply to fill the space opened by this source. Depending on the details of the source geometry, this component of the magma supply rate has been variously estimated at 0.025 km^3/yr (Delaney and others, 1993) and 0.06 km^3/yr (Owen and others, 1995). Added to the effusion rate, these estimates give a magma-supply rate of 0.15 to 0.18 km^3/yr over the course of this eruption.

Alternative models (both old and new) for south-flank deformation do not include a deep rift-zone source (for

Figure 12. Episode 55 flank vent, viewed from the west slope of Pu‘u ‘Ō‘ō. Lava from spatter cone is feeding lava pond to left. Photograph taken April 24, 1997.

example, Douglas and Cervelli, 2002). If these models are correct, then the effusion rate during sustained eruptions does approximate the magma-supply rate, as proposed by Swanson (1972) and Dvorak and Dzurisin (1993). The current effusion rate of about 0.12 km^3/yr is essentially the same as their estimated average magma-supply rates of 0.11 and 0.09 km^3/yr, respectively.

Our estimate of the total volume of lava erupted in 1983–2001 omits the 7 intrusions in the upper east rift zone and 1 intrusion in the middle east rift zone that have occurred since late 1990 (table 2; fig. 15). The volumes of the upper-east-rift-zone intrusions were small: for example, the volume of the September 1999 intrusion was approximately $3.3x10^6$ m^3 (Cervelli and others, 2002), or about a 1-week magma supply to the eruption. The middle-east-rift-zone intrusion of January 1997, which preceded the episode 54 fissure eruption, was much larger, with a modeled volume of $23x10^6$ m^3 (Owen and others, 2000). (The January 1997 event is considered an intrusion because the volume of lava erupted—about $0.3x10^6$ m^3—was small relative to the volume of magma intruded.) On the basis of these figures, the total volume of all eight intrusions would not significantly increase the estimated magma-supply rate.

By updating estimates of the total volume of lava erupted by Kīlauea since 1840 (Dvorak and Dzurisin, 1993), we calculate that about half this total volume is from the Pu‘u ‘Ō‘ō-Kūpaianaha eruption. The ongoing eruption has produced nearly twice the volume erupted during Kīlauea’s sustained summit activity from 1840 to 1932.

Volcanic Air Pollution

Once the eruption shifted to Kūpaianaha in mid-1986, the continuous emission of SO_2 from the vent resulted in persistent volcanic smog, called vog, downwind of Kīlauea. SO_2 in the eruption plume reacts with O_2, dust particles, and atmospheric moisture to form H_2SO_4 droplets and solid sulfate particles that result in vog and acid rain (Sutton and others, 1997). The west side of the island, 125 km from the eruption site, is most persistently impacted, because prevailing trade winds cause the vog to accumulate along the Kona coast. The health effects of vog on island residents are still under study, but vog is known to aggravate preexisting respiratory problems.

Another persistent and conspicuous type of gas release during this eruption is created where tube-fed lava enters the ocean. The resulting large steam plume contains a mixture of HCl, concentrated seawater, and particulates created when seawater boils and vaporizes (Gerlach and others, 1989; Sutton and others, 1997). The acidity of this plume decreases rapidly with distance from its source and so is a much more localized hazard than vog.

The Slow Process of Building New Land

Since November 1986, lava flows have entered the ocean more than 70 percent of the time (fig. 5), by far the longest such interval in Hawai‘i in the past 500 years. The longest lived ocean entry was active for 15½ months (May 1988–Aug. 1989); 30 others lasted longer than 2 months (see Kauahikaua and others, this volume).

New land formed as lava deltas build seaward over steep, prograding submarine slopes of hyaloclastite debris and pillow lava (Kelly and others, 1989; Hon and others, 1993; Kauahikaua and others, this volume). These slopes are inherently unstable and prone to slumping, which removes support for the active, leading edge of the lava delta, or “bench.” The catastrophic collapse of a bench can submerge several hectares

Figure 13. Lava from crater of Pu‘u ‘Ō‘ō flows through west gap in cone. View eastward; photograph by J.P. Kauahikaua, taken October 20, 1997.

Figure 14. Crater of Pu‘u ‘Ō‘ō. Fume rises from several vents on crater floor, which is covered with pāhoehoe erupted in 2002. View westward; photograph taken April 11, 2002.

of land in a matter of minutes or hours. Large collapses commonly precipitate violent littoral explosions when the severed lava tubes are exposed to the surf (Mattox and Mangan, 1997). Not all bench collapses are dramatic, however; small, piecemeal collapse has been the dominant process at many benches.

More than 210 ha of new land has been created during this eruption—a net value that does not include new land claimed by calving of active benches or by wave erosion of inactive ones. Owing to these processes, in some years a net decrease was noted in the total area of new land, even though flows entered the ocean the entire year. Both the steep offshore slope and the exposure of the coastline to storm surf have contributed to the slow rate at which new land has formed.

The continuous interaction of lava and seawater at the ocean entry points created black sand that was entrained in the southwest-bound longshore current. Kīlauea's wave-battered coastline has few places sheltered enough to capture and retain sand, and so most of the black sand beaches that formed during this eruption were small and ephemeral. The largest beach (approximately 400 m long by 40 m wide) began to form at Kamoamoa (fig. 1*B*) in January 1988. For the next 2 years, it was fed by ocean entries 2 to 4 km to the northeast. This beach subsequently was buried by lava flows from Pu‘u ‘Ō‘ō flank vents in November 1992 (fig. 7).

Eruptive Pauses, Intrusions, and Surges

When the eruption paused for a week in 1988, the event seemed completely anomalous, occurring midway through 42 months of continuous effusion from Kūpaianaha. In 1990, however, the first of 4 series of pauses began (fig. 8). From February through August 1990, 9 pauses, each lasting approximately 1–3½ days, punctuated the steady effusion of lava. The Kūpaianaha pauses were preceded by sharp, but small, deflation of the summit reservoir and increasing summit tremor (Okubo and others, 1990). After each pause began, the summit inflated rapidly, summit tremor decreased, and microearthquakes beneath the summit increased. The supply from the summit probably resumed at the peak of inflation. The eruption started 4 to 8 hours later.

The 1990 pauses ended in mid-August, and no more pauses occurred as the output of lava from Kūpaianaha declined over the next 17½ months. During this interval, however, three magmatic intrusions took place in the upper east rift zone, followed by a fourth shortly after Kūpaianaha stopped erupting and all activity returned to Pu‘u ‘Ō‘ō (Okubo and others, 1991). These were the first intrusions anywhere on the volcano since the eruption began in 1983.

Since the era of Pu‘u ‘Ō‘ō flank-vent eruptions began, long intervals of frequent pauses have been the norm. During episodes 50 through 52 (Feb. 1992–Feb.1993), 21 pauses occurred, lasting a total of 65 days. About 50 percent of these pauses were immediately preceded by slight summit deflation, but many comparable intervals of deflation were not followed by pauses (see discussion in Heliker and others, 1998b). The most consistent change at the summit was inflation during most pauses. The episodes 50–52 pauses occurred at irregular intervals, separated by periods as short as 8 hours or as long as 90 days, and each pause lasted an average of 3 days.

The last pause in this series was triggered by the fifth upper-east-rift-zone intrusion in February 1993 (Heliker and others, 1998b). Episode 53 began shortly thereafter, and throughout the next year no pauses occurred. In March 1994,

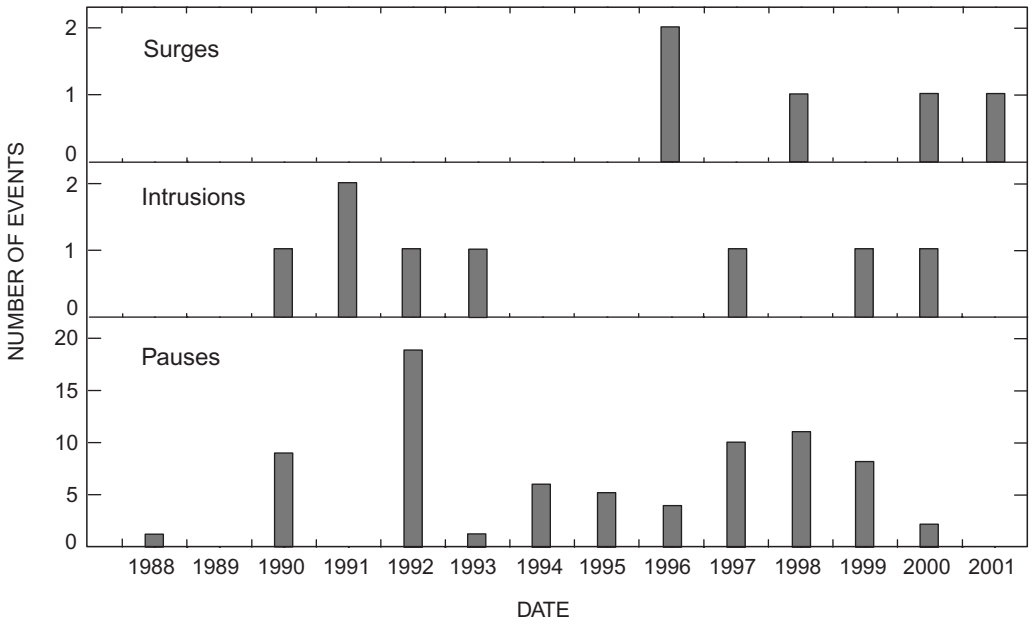

Figure 15. Frequency of eruptive pauses, intrusions, and eruptive surges during Pu‘u ‘Ō‘ō-Kūpaianaha eruption, from 1988 through 2001.

a new series of pauses began (Thornber and others, 1995), with 15 pauses occurring over the next 2¾ years of episode 53. Overall, these pauses had an instrumental signature similar to those during the previous series. The episode 53 pauses, however, were briefer, on average, and less frequent (figs. 8, 15).

The eruption was especially erratic after the long hiatus that followed the cone collapse in early 1997 (see Heliker and others, this volume). The first 2 years of episode 55 were marked by 21 pauses; another 10 pauses punctuated the eruption in 1999–2000. No pauses occurred from January 2001 through 2002.

During the first half-year of episode 55, the tremor amplitude recorded at the closest seismic station (sta. STC, 2.1 km WSE of the Pu‘u ‘Ō‘ō crater), fell to background levels during each pause. This decrease in tremor contrasted markedly with many of the episode 53 pauses, which were accompanied by little detectable change in the station STC tremor. As episode 55 progressed, however, defining a “typical” pause became increasingly difficult. Most episode 55 pauses occurred without any increase in summit tremor; many had no seismic signature either at the summit or on the rift. Yet the last pause in 2000 was preceded by 41 hours of high tremor at the summit that dropped off a few hours after the pause began.

The criteria for picking the start and stop times of pauses have evolved over time. Through episode 53, we generally picked the start of the pause by visual evidence of flagging activity at a vent. This evidence was difficult to obtain when vents had crusted over and flows were encased in lava tubes all the way to the ocean. Our first indication of a pause commonly came only when the steam plume at the ocean entry point died, sometimes more than a day after the eruption stopped. With the advent of a much more sensitive tiltmeter, installed at Kīlauea’s summit during episode 55, the summit tilt signal became the most consistent indicator of the beginning of a pause. Many pauses were preceded by a brief interval of steep deflation at the summit. This interval seemed to mark the point at which the magma supply to the eruption site was interrupted; most pauses ended after an interval of summit inflation.

The precursory tilt changes at the summit indicate that most eruptive pauses were initiated by a shutoff of magma supply from the summit. The episodes 50–55 pauses varied widely in their instrumental signature, however, and some were probably triggered locally by transient blockages in the connections between the main Pu‘u ‘Ō‘ō conduit and the flank vents. A new generation of borehole tiltmeters, extending from the summit down the east rift zone to the Pu‘u ‘Ō‘ō cone, may yield the answers to the origin of the pauses once the next series begins.

Two more upper-east-rift-zone intrusions occurred in episode 55: the first in September 1999 (Cervelli and others, 2002), and the second in February 2000. During the past 5½ years, we have also witnessed a different type of magmatic event that begins at the summit and results in a substantial surge in effusion rate at the eruption site. The first of these “surge” events occurred on February 1, 1996 (Lisowski and others, 1996; Okubo and others, 1996; Thornber and others, 1996), and four others occurred before the end of 2001 (table 2; figs. 8, 15). The surges varied in duration, amplitude, and instrumental signature but generally were characterized by increasing seismicity and rapid inflation at the summit, followed by rapid summit deflation and a surge in effusion rate at the eruption site (for a discussion of four of these events, see Cervelli and Miklius, this volume).

The surge in effusion rate caused by these events is striking. Long-dormant vents in the crater become active, and flows break out of the tube on the upper flow field, where breakouts are uncommon. These breakouts generally originate from preexisting skylights in the lava tube, and low fountains are typical at the breakout points during the first few hours of a surge, when effusion rates may be 10 times higher than normal.

The Show Goes On

The chronology of the first 2 decades of the Pu‘u ‘Ō‘ō-Kūpaianaha eruption lacks a final chapter. Our ability to predict the onset of a Kīlauea eruption far exceeds our ability to predict its end. In the early years of this eruption, we speculated that a large earthquake might disrupt the rift-zone plumbing and bring the activity to a close. Although the eruption has not yet been tested by an M≥7 earthquake, the activity has proven remarkably impervious to lesser tectonic and magmatic events.

In its first decade, the eruption weathered the M6.6 Ka‘ōiki earthquake of 1983 and the M6.1 Kalapana earthquake of 1989. In March–April 1984, Mauna Loa erupted for 3 weeks, while at Pu‘u ‘Ō‘ō, episode 17 occurred on schedule, and the two volcanoes erupted simultaneously (Wolfe and others, 1988). In 1997, Pu‘u ‘Ō‘ō revived after substantial edifice collapse and a prolonged hiatus in activity. Thus far, the Pu‘u ‘Ō‘ō-Kūpaianaha eruption has withstood all of these events and shows no sign of faltering; the eruption continues unabated.

Selected Bibliography for the Pu‘u ‘Ō‘ō-Kūpaianaha Eruption

Our initial search of the Hawai‘i Bibliographic Database (Wright and Takahashi, 1998) yielded more than 1,000 references pertaining to the eruption published between 1983 and early 2002. We first culled the list for all references in the geosciences. Additional selection criteria included (1) abstracts containing material not published elsewhere; (2) the most recent, inclusive publication by the same author(s) on an identical topic; (3) articles published in journals with widespread distribution, favored over publications with limited distribution; (4) M.S. and Ph.D. theses not published elsewhere that contained a unique dataset; and (5) USGS Open-File Reports with unique datasets not published in mainstream publications.

Including every report written about every aspect of this eruption is impossible. Readers interested in a complete listing for a particular topic should consult the Hawai‘i Bibliographic Database. Updated instructions on how to access this remarkable research tool are posted on the Hawaiian Volcano Observatory Web site, at URL http://wwwhvo.wr.usgs.gov/products/database.html. To find every reference about this eruption, we recommend searching for the keyword “kl.erz.1983” and for any of the following words within the abstract or title: Kīlauea *and* East Rift, Pu‘u ‘Ō‘ō, and Kūpaianaha.

Acknowledgments

We thank all the staff geologists who served at the Hawaiian Volcano Observatory during the past 20 years for their countless contributions to monitoring and understanding the eruption: Edward Wolfe, Tina Neal, George Ulrich, Ken Hon, Margaret Mangan, Carl Thornber, David Sherrod, and Richard Hoblitt. We also thank the geology group’s constant collaborator, Jim Kauahikaua. Don Swanson and Tamar Elias provided thoughtful reviews of this manuscript. Compilation of the selected bibliography would have been much more difficult without the Hawai‘i Bibliographic Database, which owes its existence to the tireless and ongoing work of Thomas Wright and Jane Takahashi.

References Cited

Cayol, Valérie, Dieterich, J.H., Okamura, A.T., and Miklius, Asta, 2000, High magma storage rates before the 1983 eruption of Kilauea, Hawaii: Science, v. 288, no. 5475, p. 2343–2346.

Cervelli, P.F., Segall, Paul, Amelung, Falk, Garbeil, Harold, Meertens, C.M., Owen, S.E., Miklius, Asta, and Lisowski, Michael, 2002, The 12 September 1999 Upper East Rift Zone dike intrusion at Kilauea Volcano, Hawaii: Journal of Geophysical Research, v. 107, no. B7, p. ECV 3–1 – ECV 3–13.

Delaney, P.T., Miklius, Asta, Árnadóttir, Thóra, Okamura, A.T., and Sako, M.K., 1993, Motion of Kilauea Volcano during sustained eruption from the Puu Oo and Kupaianaha vents, 1983–1991: Journal of Geophysical Research, v. 98, no. B10, p. 17801–17820.

Douglas, Anne, and Cervelli, Paul, 2002, Continuous GPS monitoring of deformation at Kilauea Volcano during the latter half of the Pu‘u ‘O‘o eruption [abs.]: Eos (American Geophysical Union Transactions), v. 83, no. 47, supp., p. F1440.

Dvorak, J.J., and Dzurisin, Daniel, 1993, Variations in magma supply rate at Kilauea Volcano, Hawaii: Journal of Geophysical Research, v. 98, no. B12, p. 22255–22268.

Dzurisin, Daniel, Koyanagi, R.Y., and English, T.T., 1984, Magma supply and storage at Kilauea Volcano, Hawaii, 1956–1983: Journal of Volcanology and Geothermal Research, v. 21, no. 3–4, p. 177–206.

Gerlach, T.M., Krumhansl, J.L., Fournier, R.O., and Kjargaard, J.I., 1989, Acid rain from the heating and evaporation of seawater by molten lava; a new volcanic hazard [abs.]: Eos (American Geophysical Union Transactions), v. 70, no. 43, supp., p. 1421.

Heliker, C.C., and Decker, R.W., in press, The Hawai‘i Island eruptions of Kīlauea, 1983 to 2001, and Mauna Loa, 1984; living with lava*, in* Guffanti, M.C., Miller, C.D., and Ewert, J.W., eds., Responding to volcanic eruptions and unrest—1980–2000; two decades of scientific experience in applied volcanology: U.S. Geological Survey Circular 1250.

Heliker, C.C., Mangan, M.T., Mattox, T.N., and Kauahikaua, J.P., 1998a, The Pu‘u ‘Ō‘ō-Kūpaianaha eruption of Kīlauea, November 1991–February 1994; field data and flow maps: U.S. Geological Survey Open-File Report 98–103, 10 p., 2 sheets, scale 1:50,000.

Heliker, C.C., Mangan, M.T., Mattox, T.N., Kauahikaua, J.P., and Helz, R.T., 1998b, The character of long-term eruptions; inferences from episodes 50–53 of the Pu‘u ‘Ō‘ō-Kūpaianaha eruption of Kīlauea Volcano: Bulletin of Volcanology, v. 59, no. 6, p. 381–393.

Heliker, C.C., Ulrich, G.E., Margriter, S.C., and Hoffmann, J.P., 2001, Maps showing the development of the Pu‘u ‘Ō‘ō-Kūpaianaha flow field, June 1984–February 1987, Kīlauea Volcano, Hawaii: U.S. Geological Survey Miscellaneous Investigations Series Map I–2685, 4 sheets, scale 1:50,000.

Heliker, C.C., and Wright, T.L., 1991, The Pu‘u ‘O‘o-Kupaianaha eruption of Kilauea: Eos (American Geophysical Union Transactions), v. 72, p. 521, 526, 530.

Hoffmann, J.P., Ulrich, G.E., and Garcia, M.O., 1990, Horizontal ground deformation patterns and magma storage during the Puu Oo eruption of Kilauea volcano, Hawaii; episodes 22–42: Bulletin of Volcanology, v. 52, no. 6, p. 522–531.

Hon, K.A., Kauahikaua, J.P., Denlinger, R.P., and Mackay, Kevin, 1994, Emplacement and inflation of pahoehoe sheet flows; observations and measurements of active lava flows on Kilauea Volcano, Hawaii: Geological Society of America Bulletin, v. 106, no. 3, p. 351–370.

Hon, K.A., Mattox, T.N., Kauahikaua, J.P., and Kjargaard, J.I., 1993, The construction of pahoehoe lava deltas on Kilauea volcano, Hawaii [abs.]: Eos (American Geophysical Union Transactions), v. 74, no. 43, supp., p. 616.

Jackson, D.B., 1988, Geoelectric observations (including the September 1982 summit eruption), chap. 8 *of* Wolfe, E.W., ed., The Puu Oo eruption of Kilauea Volcano, Hawaii; episodes 1 through 20, January 3, 1983, through June 8, 1984: U.S. Geological Survey Professional Paper 1463, p. 237–251.

Kauahikaua, J.P., Cashman, K.V., Mattox, T.N., Heliker, C.C., Hon, K.A., Mangan, M.T., and Thornber, C.R., 1998, Observations on basaltic lava streams in tubes from Kilauea Volcano, island of Hawai‘i: Journal of Geophysical Research, v. 103, no. B11, p. 27303–27323.

Kauahikaua, J.P., Mangan, M.T., Heliker, C.C., and Mattox, T.N., 1996, A quantitative look at the demise of a basaltic vent; the death of Kupaianaha, Kilauea Volcano, Hawai‘i: Bulletin of Volcanology, v. 57, no. 8, p. 641–648.

Kelly, K.M., Hon, K.A., and Tribble, G.W., 1989, Bathymetric and submarine studies of an active lava delta near Kupapau Point,

Kilauea volcano, Hawaii [abs.]: Eos (American Geophysical Union Transactions), v. 70, no. 43, p. 1202.

Klein, F.W., Koyanagi, R.Y., Nakata, J.S., and Tanigawa, W.R., 1987, The seismicity of Kilauea's magma system, chap. 43 *of* Decker, R.W., Wright, T.L., and Stauffer, P.H., eds., Volcanism in Hawaii: U.S. Geological Survey Professional Paper 1350, v. 2, p. 1019–1185.

Koyanagi, R.Y., Tanigawa, W.R., and Nakata, J.S., 1988, Seismicity associated with the eruption, chap. 7 *of* Wolfe, E.W., ed., The Puu Oo eruption of Kilauea Volcano, Hawaii; episodes 1 through 20, January 3, 1983, through June 8, 1984: U.S. Geological Survey Professional Paper 1463, p. 183–235.

Lisowski, Michael, Owen, S.E., and Segall, Paul, 1996, The Kilauea Volcano, Hawaii, continuous GPS network; recent results [abs.]: Eos (American Geophysical Union Transactions), v. 77, no. 46, supp., p. F808.

Mangan, M.T., Heliker, C.C., Mattox, T.N., Kauahikaua, J.P., and Helz, R.T., 1995, Episode 49 of the Pu'u 'O'o-Kupaianaha eruption of Kilauea volcano—breakdown of a steady-state eruptive era: Bulletin of Volcanology, v. 57, no. 2, p. 127–135.

Mattox, T.N., Heliker, C.C., Kauahikaua, J.P., and Hon, K.A., 1993, Development of the 1990 Kalapana flow field, Kilauea Volcano, Hawaii: Bulletin of Volcanology, v. 55, no. 6, p. 407–413.

Mattox, T.N., and Mangan, M.T., 1997, Littoral hydrovolcanic explosions; a case study of lava-seawater interaction at Kilauea Volcano: Journal of Volcanology and Geothermal Research, v. 75, no. 1–2, p. 1–17.

Okamura, A.T., Dvorak, J.J., Koyanagi, R.Y., and Tanigawa, W.R., 1988, Surface deformation during dike propagation, chap. 6 *of* Wolfe, E.W., ed., The Puu Oo eruption of Kilauea Volcano, Hawaii; episodes 1 through 20, January 3, 1983, through June 8, 1984: U.S. Geological Survey Professional Paper 1463, p. 165–182.

Okubo, P.G., Nakata, J.S., Chouet, B.A., and Dawson, P.B., 1996, The February 1, 1996, Kilauea summit earthquake swarm [abs.]: Eos (American Geophysical Union Transactions), v. 77, no. 46, supp., p. F798.

Okubo, P.G., Okamura, A.T., and Miklius, Asta, 1991, Intrusive earthquake swarms and the continuing Kilauea eruption [abs.]: Eos (American Geophysical Union Transactions), v. 72, no. 44, supp., p. 566.

Okubo, P.G., Tomori, A.H., Nakata, J.S., Largo, A.J., and Fukunaga, P.N., 1990, Spatial and temporal patterns of seismicity related to the on-going eruption of Kilauea Volcano, Hawaii [abs.]: Eos (American Geophysical Union Transactions), v. 71, no. 43, p. 1711.

Owen, S.E., Segall, Paul, Freymueller, J.T., Miklius, Asta, Denlinger, R.P., Árnadóttir, Thóra, Sako, M.K., and Bürgmann, R.B., 1995, Rapid deformation of the south flank of Kilauea volcano, Hawaii: Science, v. 267, no. 5202, p. 1328–1332.

Owen, S.E., Segall, Paul, Lisowski, Michael, Miklius, Asta, Murray, Michael, Bevis, M.G., and Foster, James, 2000, January 30, 1997 eruptive event on Kilauea Volcano, Hawaii, as monitored by continuous GPS: Geophysical Research Letters, v. 27, no. 17, p. 2757–2760.

Segall, Paul, Cervelli, P.F., Owen, S.E., Lisowski, Michael, and Miklius, Asta, 2001, Constraints on dike propagation from continuous GPS measurements: Journal of Geophysical Research, v. 106, no. B9, p. 19301–19317.

Sparks, R.S.J., and Pinkerton, Harry, 1978, Effect of degassing on rheology of basaltic lava: Nature, v. 276, no. 5686, p. 385–386.

Sutton, A.J., Elias, Tamar, Hendley, J.W., II, and Stauffer, P.H., 1997, Volcanic air pollution—a hazard in Hawaii: U.S. Geological Survey Fact Sheet 169–97, 2 p.

Swanson, D.A., 1972, Magma supply rate at Kilauea Volcano, 1952–1971: Science, v. 175, no. 4018, p. 169–170.

Swanson, D.A., Duffield, W.A., Jackson, D.B., Peterson, D.W., 1979, Chronological narrative of the 1969–71 Mauna Ulu eruption of Kilauea Volcano, Hawaii: U.S. Geological Survey Professional Paper 1056, 55 p.

Thornber, C.R., 2001, Olivine-liquid relations of lava erupted by Kīlauea Volcano from 1994 to 1998; implications for shallow magmatic processes associated with the ongoing east-rift-zone eruption: Canadian Mineralogist, v. 39, no. 2, p. 239–266.

Thornber, C.R., Heliker, C.C., Reynolds, J.R., Kauahikaua, J.P., Okubo, P.G., Lisowski, Michael, Sutton, A.J., and Clague, D.A., 1996, The eruptive surge of February 1, 1996; a highlight of Kilauea's ongoing east rift zone eruption [abs.]: Eos (American Geophysical Union Transactions), v. 77, no. 46, supp., p. F798.

Thornber, C.R., Heliker, C.C., Sherrod, D.R., Kauahikaua, J.P., Miklius, Asta, Okubo, P.G., Trusdell, F.A., Budahn, J.R., Ridley, W.I., and Meeker, G.P., in press, Kilauea east rift zone magmatism: an episode 54 perspective: Journal of Petrology.

Thornber, C.R., Mattox, T.N., Sutton, A.J., Elias, Tamar, Okubo, P.G., Tomori, A.H., and Denlinger, R.P., 1995, The eruptive pulse of Kilauea Volcano as revealed by continuous temperature monitoring of an active lava tube [abs.]: (American Geophysical Union Transactions), v. 76, no. 46, supp., p. F681.

Tilling, R.I., Christiansen, R.L., Duffield, W.A., Endo, E.T., Holcomb, R.T., Koyanagi, R.Y., Peterson, D.W., and Unger, J.D., 1987, The 1972–1974 Mauna Ulu eruption, Kilauea Volcano; an example of quasi-steady-state magma transfer, chap. 16 *of* Decker, R.W., Wright, T.L., and Stauffer, P.H., eds., Volcanism in Hawaii: U.S. Geological Survey Professional Paper 1350, v. 1, p. 405–469.

Wolfe, E.W., Neal, C.A., Banks, N.G., and Duggan, T.J., 1988, Geologic observations and chronology of eruptive events, chap. 1 *of* Wolfe, E.W., ed., The Puu Oo eruption of Kilauea Volcano, Hawaii; episodes 1 through 20, January 3, 1983, through June 8, 1984: U.S. Geological Survey Professional Paper 1463, p. 1–97.

Wright, T.L. and Takahashi, T.J., 1998, Hawaii bibliographic database: Bulletin of Volcanology, v. 59, no. 4, p. 276–280.

Selected Bibliography

LETTER CODES FOR KEY WORDS

D Deformation	**Gp** Geophysics	**M** Maps	**S** Seismology
E Eruption chronology	**H** Hazards	**P** Petrology/mineralogy	**V** Physical volcanology
G Gas and water geochemistry	**I** Instrumentation	**R** Remote sensing	

V Anderson, S.W., Stofan, E.R., Smrekar, S.E., Guest, J.E., and Wood, B.J, 1999, Pulsed inflation of pahoehoe lava flows; implications for flood basalt emplacement: Earth and Planetary Science Letters, v. 168, no. 1–2, p. 7–18.

V Anderson, S.W., Stofan, E.R., Smrekar, S.E., Guest, J.E., and Wood, B.J, 2000, Reply to Self et al discussion of "Pulsed inflation of pahoehoe lava flows; implications for flood basalt emplacement": Earth and Planetary Science Letters, v. 179, no. 2, p. 425–428.

G Andres, R.J., Kyle, P.R., Stokes, J.B., and Rose, W.I., 1989, SO_2 from episode 48A eruption, Hawaii; sulfur dioxide emissions from the episode 48A east rift zone eruption of Kilauea volcano, Hawaii: Bulletin of Volcanology, v. 52, no. 2, p. 113–117.

V, R Baloga, S.M., Glaze, L.S., Crisp, J.A., and Stockman, S.A., 1998, New statistics for estimating the bulk rheology of active lava flows; Puu Oo examples: Journal of Geophysical Research, v. 103, no. B3, p. 5133–5142.

Gp Bartel, L.C., Hardee, H.C., and Jacobson, R.D., 1983, An electrical resistivity measurement in molten basalt during the 1983 Kilauea eruption: Bulletin Volcanologique, v. 46, no. 3, p. 271–276.

P Burkhard, D.J.M, 1997, Redox state and crystallizations of recent basalt lava from the East Rift, Kilauea, Hawaii [abs.]: Eos (American Geophysical Union Transactions), v. 78, no. 46, supp., p. F648.

P Burkhard, D.J.M., 2000, Kinetics of crystallization; example of micro-crystallization in basalt lava [abs.]: Eos (American Geophysical Union Transactions), v. 81, no. 46, p. F1291.

S Caplan-Auerbach, Jacqueline, and Duennebier, F.K., 2001, Seismic and acoustic signals detected at Loʻihi Seamount by the Hawaiʻi Undersea Geo-Observatory: G^3 (Geochemistry, Geophysics, Geosystems), v. 2, paper 2000GC000113.

S Caplan-Auerbach, Jacqueline, Fox, C.G., and Duennebier, F.K., 2001, Hydroacoustic detection of submarine landslides on Kilauea volcano: Geophysical Research Letters, v. 28, no. 9, p. 1811–1813.

P, V Cashman, K.V., and Kauahikaua, J.P., 1997, Reevaluation of vesicle distributions in basaltic lava flows: Geology, v. 25, no. 5, p. 419–422.

P, V Cashman, K.V., and Mangan, M.T., 1994, Physical aspects of magmatic degassing, II. Constraints on vesiculation processes from textural studies of eruptive products, chap. 11b *of* Carroll, M.R., and Holloway, J.R., eds., Volatiles in magmas: Reviews in Mineralogy, v. 30, p. 447–478.

P, V Cashman, K.V., Mangan, M.T., and Newman, Sally, 1994, Surface degassing and modifications to vesicle size distributions in active basalt flows: Journal of Volcanology and Geothermal Research, v. 61, no. 1–4, p. 45–68.

P, V Cashman, K.V., Thornber, C.R., and Kauahikaua, J.P., 1999, Cooling and crystallization of lava in open channels, and the transition of pāhoehoe lava to ʻaʻā: Bulletin of Volcanology, v. 61, no. 5, p. 306–323.

D, S Cayol, Valérie, Dieterich, J.H., Okamura, A.T., and Miklius, Asta, 2000, High magma storage rates before the 1983 eruption of Kilauea, Hawaii: Science, v. 288, no. 5475, p. 2343–2346.

D Cervelli, P.F., Segall, Paul, Amelung, Falk, Garbeil, Harold, Meertens, C.M., Owen, S.E., Miklius, Asta, and Lisowski, Michael, 2002, The 12 September 1999 Upper East Rift Zone dike intrusion at Kilauea Volcano, Hawaii: Journal of Geophysical Research, v. 107, no. B7, p. ECV 3–1 – ECV 3–13.

G Chartier, T.A., Rose, W.I., and Stokes, J.B., 1988, Detailed record of SO_2 emissions from Puʻu ʻOʻo between episodes 33 and 34 of the 1983–86 ERZ eruption, Kilauea, Hawaii: Bulletin of Volcanology, v. 50, no. 4, p. 215–228.

S, D Chouet, B.A., and Dawson, P.B., 1997, Observations of very-long-period impulsive signals accompanying summit inflation at Kilauea Volcano, Hawaii, in February 1997 [abs.]: Eos (American Geophysical Union Transactions), v. 78, no. 46, supp., F429–430.

S, D Chouet, B.A., Dawson, P.B., Ohminato, Takao, and Okubo, P.G., 1997, Broadband measurements of magmatic injection beneath Kilauea Volcano, Hawaii [abs.]: Seismological Research Letters, v. 68, no. 2, p. 317.

S, G Chouet, B.A., and Shaw, H.R., 1991, Fractal properties of tremor and gas piston events observed at Kilauea Volcano, Hawaii: Journal of Geophysical Research, v. 96, no. B6, p. 10177–10189.

V Coltelli, Mauro, Heliker, C.C., Okamura, A.T., and Ulrich, G.E., 1991, Lava lakes in the effusive phase of Kilauea's current eruption [abs.]: Eos (American Geophysical Union Transactions), v. 72, no. 44, supp., p. 565.

R, V Crisp, J.A., and Baloga, S.M., 1991, Thermal processes in lava flows: Lunar and Planetary Science Conference Abstracts of Papers, v. 22, p. 257–258.

V Crisp, J.A., Sakimoto, S.E.H., and Baloga, S.M., 1995, Lava tube pressure & gravity driving forces; constraints on tube lengths, flow rates & surface breakout locations [abs.]: Eos (American Geophysical Union Transactions), v. 76, no. 46, supp., p. F667.

G Crowe, B.M., Finnegan, D.L., Zoller, W.H., and Boynton, W.V., 1987, Trace element geochemistry of volcanic gases and particles from 1983–1984 eruptive episodes of

Kilauea volcano: Journal of Geophysical Research, v. 92, no. B13, p. 13708–13714.

D Delaney, P.T., and Denlinger, R.P., 1999, Stabilization of volcanic flanks by dike intrusion; an example from Kilauea: Bulletin of Volcanology, v. 61, no. 6, p. 356–362.

D Delaney, P.T., Miklius, Asta, Árnadóttir, Thóra, Okamura, A.T., and Sako, M.K., 1993, Motion of Kilauea Volcano during sustained eruption from the Puu Oo and Kupaianaha vents, 1983–1991: Journal of Geophysical Research, v. 98, no. B10, p. 17801–17820.

D Denlinger, R.P., 1997, A dynamical balance between magma supply and eruption rate at Kilauea volcano, Hawaii: Journal of Geophysical Research, v. 102, no. B8, p. 18091–18100.

S Dietel, C.M., Chouet, B.A., Aki, Keiiti, Ferrazzini, Valérie, Roberts, P.M., and Koyanagi, R.Y., 1989, Data summary for dense GEOS array observations of seismic activity associated with magma transport at Kilauea Volcano, Hawaii: U.S. Geological Survey Open–File Report 89–113, 171 p.

D, S Dieterich, J.H., Cayol, Valérie, and Okubo, P.G., 2000, The use of earthquake rate changes as a stress meter at Kilauea volcano: Nature, v. 408, no. 6811, p. 457–460.

D, S Dvorak, J.J., 1994, An earthquake cycle along the south flank of Kilauea Volcano, Hawaii: Journal of Geophysical Research, v. 99, no. B5, p. 9533–9541.

V, D Dvorak, J.J., and Dzurisin, Daniel, 1993, Variations in magma supply rate at Kilauea Volcano, Hawaii: Journal of Geophysical Research, v. 98, no. B12, p. 22255–22268.

D, S Dvorak, J.J., and Okamura, A.T., 1985, Variations in tilt rate and harmonic tremor amplitude during the January–August 1983 east rift eruptions of Kilauea Volcano, Hawaii: Journal of Volcanology and Geothermal Research, v. 25, no. 3–4, p. 249–258.

D, S Dvorak, J.J., Okamura, A.T., English, T.T., Koyanagi, R.Y., Nakata, J.S., Sako, M.K., Tanigawa, W.R., and Yamashita, K.M., 1986, Mechanical response of the south flank of Kilauea volcano, Hawaii, to intrusive events along the rift systems: Tectonophysics, v. 124, no. 3–4, p. 193–209.

G Elias, Tamar, and Sutton, A.J., 2002, Volcanic air pollution in our backyard; gas advisory system helps alert people of Hawai‘i [abs.]: Geological Society of America Abstracts with Programs, v. 34, no. 5, p. A–11.

G Elias, Tamar, and Sutton, A.J., 2002, Sulfur dioxide emission rates from Kilauea Volcano, Hawaii, an update; 1998–2001: U.S. Geological Survey Open-File Report 02–460, 10 p., figs. 23 p.

G Elias, Tamar, Sutton, A.J., Stokes, J.B., and Casadevall, T.J., 1998, Sulfur dioxide emission rates of Kilauea Volcano, Hawaii, 1979–1997: U.S. Geological Survey Open-File Report 98–462, 40 p.

S, G Ferrazzini, Valérie, Aki, Keiiti, and Chouet, B.A., 1991, Characteristics of seismic waves composing Hawaiian volcanic tremor and gas-piston events observed by a near-source array: Journal of Geophysical Research, v. 96, no. B4, p. 6199–6209.

V Fink, J.H., and Zimbelman, J.R., 1986, Rheology of the 1983 Royal Gardens basalt flows, Kilauea Volcano, Hawaii: Bulletin of Volcanology, v. 48, no. 2–3, p. 87–96.

G Finnegan, D.L., Miller, T.L., and Zoller, W.H., 1990, Iridium and other trace-metal enrichments from Hawaiian volcanoes, *in* Sharpton, V.L., and Ward, P.D., eds., Global catastrophes in Earth history: Geological Society of America Special Paper 247, p. 111–116.

R Flynn, L.P., and Mouginis-Mark, P.J., 1992, Cooling rate of an active Hawaiian lava flow from nighttime spectroradiometer measurements: Geophysical Research Letters, v. 19, no. 17, p. 1783–1786.

R Flynn, L.P., and Mouginis-Mark, P.J., 1994, Temperature of an active lava channel from spectral measurements, Kilauea Volcano, Hawaii: Bulletin of Volcanology, v. 56, no. 4, p. 297–301.

R Flynn, L.P., Mouginis-Mark, P.J., Gradie, J.C., and Lucey, P.G., 1993, Radiative temperature measurements at Kupaianaha lava lake, Kilauea Volcano, Hawaii: Journal of Geophysical Research, v. 98, no. B4, p. 6461–6476.

R Flynn, L.P., Mouginis-Mark, P.J., and Horton, K.A., 1994, Distribution of thermal areas on an active lava flow field; Landsat observations of Kilauea, Hawaii, July 1991: Bulletin of Volcanology, v. 56, no. 4, p. 284–296.

P, V Folley, M.J., 1999, Crystallinity, rheology, and surface morphology of basaltic lavas, Kilauea Volcano, Hawai‘i: Eugene, University of Oregon, M.S. thesis, 205 p.

P, V Friedman, R.C., Taylor, G.J., Keszthelyi, L.P., and Thornber, C.R., 1996, Petrographic textures as indicators of Kilauea lava flow emplacement history [abs.]: Eos (American Geophysical Union Transactions), v. 77, no. 46, supp., p. F807.

V Gaonac’h, Helene, Lovejoy, Shaun, and Stix, John, 1992, Scale invariance of basaltic lava flows and their fractal dimensions: Geophysical Research Letters, v. 19, no. 8, p. 785–788.

P Garcia, M.O., Ho, R.A., Rhodes, J.M., and Wolfe, E.W., 1989, Petrologic constraints on rift-zone processes: Bulletin of Volcanology, v. 52, no. 2, p. 81–96.

P Garcia, M.O., Ito, Emi, Eiler, J.M., and Pietruszka, A.J., 1998, Crustal contamination of Kilauea Volcano magmas revealed by oxygen isotope analyses of glass and olivine from Puu Oo eruption lavas: Journal of Petrology, v. 39, no. 5, p. 803–817.

P Garcia, M.O., Pietruszka, A.J., Rhodes, J.M., and Swanson, K.A., 2000, Magmatic processes during the prolonged Pu‘u ‘O‘o eruption of Kilauea Volcano, Hawaii: Journal of Petrology, v. 41, no. 7, p. 967–990.

P Garcia, M.O., Rhodes, J.M., Trusdell, F.A., and Pietruszka, A.J., 1996, Petrology of lavas from the Puu Oo eruption of Kilauea Volcano; III. The Kupaianaha episode (1986–1992): Bulletin of Volcanology, v. 58, no. 5, p. 359–379.

P Garcia, M.O., and Wolfe, E.W., 1988, Petrology of the erupted lava, chap. 3 *of* Wolfe, E.W., ed., The Puu Oo eruption of Kilauea Volcano, Hawaii; episodes 1 through 20, January 3, 1983, through June 8, 1984: U.S. Geological Survey Professional Paper 1463, p. 127–143.

P Garcia, M.O., Wolfe, E.W., Ulrich, G.E., and Ho, R.A., 1992, Petrology of lavas from episodes 2–47 of the Puu Oo eruption of Kilauea Volcano, Hawaii; evaluation of magmatic processes: Bulletin of Volcanology, v. 55, no. 1, p. 1–16.

G Gerlach, T.M., 1986, Exsolution of H_2O, CO_2, and S during eruptive episodes at Kilauea volcano, Hawaii: Journal of Geophysical Research, v. 91, no. B12, p. 12177–12185.

G Gerlach, T.M., 1993, Oxygen buffering of Kilauea volcanic gases and the oxygen fugacity of Kilauea basalt: Geochimica et Cosmochimica Acta, v. 57, no. 4, p. 795–814.

G Gerlach, T.M., 1993, Thermodynamic evaluation and restoration of volcanic gas analyses; an example based on modern collection and analytical methods: Geochemical Journal, v. 27, no. 4–5, p. 305–322.

G Gerlach, T.M., and Graeber, E.J., 1985, Volatile budget of Kilauea volcano: Nature, v. 313, no. 6000, p. 273–277.

G, H Gerlach, T.M., Krumhansl, J.L., Fournier, R.O., and Kjargaard, J.I., 1989, Acid rain from the heating and evaporation of seawater by molten lava; a new volcanic hazard [abs.]: Eos (American Geophysical Union Transactions), v. 70, no. 43, supp., p. 1421.

G Gerlach, T.M., McGee, K.A., Sutton, A.J., and Elias, Tamar, 1998, Rates of volcanic CO_2 degassing from airborne determinations of SO_2 emission rates and plume CO_2/SO_2; test study at Pu′u ′O′o cone, Kilauea volcano, Hawaii: Geophysical Research Letters, v. 25, no. 14, p. 2675–2678.

G Gerlach, T.M., and Taylor, B.E., 1990, Carbon isotope constraints on degassing of carbon dioxide from Kilauea Volcano: Geochimica et Cosmochimica Acta, v. 54, no. 7, p. 2051–2058.

G Gill, J.B., Williams, R.W., and Bruland, K.W., 1985, Eruption of basalt and andesite lava degasses $^{(222)}$Rn and $^{(210)}$Po: Geophysical Research Letters, v. 12, no. 1, p. 17–20.

S Gillard, Dominique, Rubin, A.M., and Okubo, P.G., 1996, Highly concentrated seismicity caused by deformation of Kilauea's deep magma system: Nature, v. 384, no. 6607, p. 343–346.

S Gillard, Dominique, Wyss, Max, and Okubo, P.G., 1996, Type of faulting and orientation of stress and strain as a function of space and time in Kilauea's south flank, Hawaii: Journal of Geophysical Research, v. 101, no. B7, p. 16025–16042.

S Goldstein, Peter, and Chouet, B.A., 1994, Array measurements and modeling of sources of shallow volcanic tremor at Kilauea Volcano, Hawaii: Journal of Geophysical Research, v. 99, no. B2, p. 2637–2652.

R Gradie, J.C., Mouginis-Mark, P.J., Hayashi, J.N., and Flynn, L.P., 1988, Surface temperature and variability of an active lava lake; lessons to be applied to Io [abs.]: Lunar and Planetary Science Conference Abstracts of Papers, v. 19, no. 1, p. 407–408.

G Greenland, L.P., 1984, Gas composition of the January 1983 eruption of Kilauea Volcano, Hawaii: Geochimica et Cosmochimica Acta, v. 48, no. 1, p. 193–195.

G Greenland, L.P., 1986, Gas analyses from the Pu′u O′o eruption in 1985, Kilauea volcano, Hawaii: Bulletin of Volcanology, v. 48, no. 6, p. 341–348.

G Greenland, L.P., 1988, Gases from the 1983–84 east-rift eruption, chap. 4 *of* Wolfe, E.W., ed., The Puu Oo eruption of Kilauea Volcano, Hawaii; episodes 1 through 20, January 3, 1983, through June 8, 1984: U.S. Geological Survey Professional Paper 1463, p. 145–153.

G Greenland, L.P., and Aruscavage, P.J., 1986, Volcanic emission of Se, Te, and As from Kilauea volcano, Hawaii: Journal of Volcanology and Geothermal Research, v. 27, no. 1–2, p. 195–201.

G, D Greenland, L.P., Okamura, A.T., and Stokes, J.B., 1988, Constraints on the mechanics of the eruption, chap. 5 *of* Wolfe, E.W., ed., The Puu Oo eruption of Kilauea Volcano, Hawaii; episodes 1 through 20, January 3, 1983, through June 8, 1984: U.S. Geological Survey Professional Paper 1463, p. 155–164.

D Hall Wallace, M.K., and Delaney, P.T., 1995, Deformation of Kilauea volcano during 1982 and 1983; a transition period: Journal of Geophysical Research, v. 100, no. B5, p. 8201–8219.

P Halleran, A.D., and Russell, J.K., 1990, Trace elements formulated as Pearce element ratios II; recognition of open system behaviour, chap. 12 *of* Russell, J.K., and Stanley, C.R., eds., Theory and application of Pearce element ratios to geochemical data analysis: Geological Association of Canada Short Course Notes, v. 8, p. 243–269.

R, V Hanley, D.J., and Zimbelman, J.R., 1998, Topographic control of lava flow morphology; putting a number to it [abs.]: Lunar and Planetary Science Conference Abstracts of Papers, v. 29, abstract 1749, n.p.

V Hardee, H.C., 1983, Heat transfer measurements in the 1983 Kilauea lava flow: Science, v. 222, no. 4619, p. 47–48.

R Harris, A.J.L., Flynn, L.P., Keszthelyi, L.P., Mouginis-Mark, P.J., Rowland, S.K., and Resing, J.A., 1998, Calculation of lava effusion rates from Landsat TM data: Bulletin of Volcanology, v. 60, no. 1, p. 52–71.

R Harris, A.J.L., Flynn, L.P., Rothery, D.A., Oppenheimer, Clive, and Sherman, S.B., 1999, Mass flux measurements at active lava lakes; implications for magma recycling: Journal of Geophysical Research, v. 104, no. B4, p. 7117–7136.

R, E Harris, A.J.L., Keszthelyi, L.P., Flynn, L.P., Mouginis-Mark, P.J., Thornber, C.R., Kauahikaua, J.P., Sherrod, D.R., and Trusdell, F.A., 1997, Chronology of the episode 54 eruption at Kilauea Volcano, Hawaii, from GOES-9 satellite data: Geophysical Research Letters, v. 24, no. 24, p. 3281–3284.

V Harris, A.J.L., and Rowland, S.K., 2001, FLOWGO; a kinematic thermo-rheological model for lava flowing in a channel: Bulletin of Volcanology, v. 63, no. 1, p. 20–44.

R Harris, A.J.L., and Thornber, C.R., 1999, Complex effusive events at Kīlauea as documented by the GOES satellite and remote video cameras: Bulletin of Volcanology, v. 61, no. 6, p. 382–395.

V Head, J.W., III, and Wilson, Lionel, 1987, Lava fountain heights at Pu′u ′O′o, Kilauea, Hawaii; indicators of amount and variations of exsolved magma volatiles: Journal of Geophysical Research, v. 92, no. B13, p. 13715–13719.

V Head, J.W., III, and Wilson, Lionel, 1987, Magma migration and Hawaiian-style eruptions in shield volcano rift zones;

the Puʻu ʻOʻo eruptive episodes, Kilauea East Rift, Hawaii [abs.]: Lunar and Planetary Science Conference Abstracts of Papers, v. 18, no. 2, p. 411–412.

V Head, J.W., III, and Wilson, Lionel, 1988, Lateral migration and eruption of magma in volcanic edifice rift zones; the Puʻu ʻOʻo eruptions of the east rift zone of Kilauea Volcano, Hawaii [abs.]: Lunar and Planetary Science Conference Abstracts of Papers, v. 19, no. 2, p. 471–472.

H Heliker, C.C., and Decker, R.W., in press, The Hawai‘i Island eruptions of Kīlauea, 1983 to 2001, and Mauna Loa, 1984; living with lava*, in* Guffanti, M.C., Miller, C.D., and Ewert, J.W., eds., Responding to volcanic eruptions and unrest—1980–2000; two decades of scientific experience in applied volcanology: U.S. Geological Survey Circular 1250.

E, V Heliker, C.C., Hoffmann, J.P., Rowland, S.K., Greenland, L.P., Reason, M.D., and Wright, T.L., 1985, Fissure activity near Puʻu Oʻo, Kilauea Volcano, HI [abs.]: Eos (American Geophysical Union Transactions), v. 66, no. 46, p. 851.

M Heliker, C.C., Mangan, M.T., Mattox, T.N., and Kauahikaua, J.P., 1998, The Puʻu ʻŌʻō-Kūpaianaha eruption of Kīlauea, November 1991–February 1994; field data and flow maps: U.S. Geological Survey Open-File Report 98–103, 10 p., 2 sheets, scale 1:50,000.

V, E Heliker, C.C., Mangan, M.T., Mattox, T.N., Kauahikaua, J.P., and Helz, R.T., 1998, The character of long-term eruptions; inferences from episodes 50–53 of the Puʻu ʻŌʻō-Kūpaianaha eruption of Kīlauea Volcano: Bulletin of Volcanology, v. 59, no. 6, p. 381–393.

M Heliker, C.C., Ulrich, G.E., Margriter, S.C., and Hoffmann, J.P., 2001, Maps showing the development of the Puʻu ʻŌʻō-Kūpaianaha flow field, June 1984–February 1987, Kīlauea Volcano, Hawaii: U.S. Geological Survey Miscellaneous Investigations Series Map I–2685, 4 sheets, scale 1:50,000.

E Heliker, C.C., and Wright, T.L., 1991, The Puʻu ʻOʻo-Kupaianaha eruption of Kilauea: Eos (American Geophysical Union Transactions), v. 72, no. 47, p. 521, 526, 530.

P Helz, R.T., Banks, N.G., Heliker, C.C., Neal, C.A., and Wolfe, E.W., 1995, Comparative geothermometry of recent Hawaiian eruptions: Journal of Geophysical Research, v. 100, no. B9, p. 17637–17657.

P Helz, R.T., and Hearn, B.C., Jr., 1998, Compositions of glasses from the Puʻu Oʻo-Kupaianaha eruption of Kilauea Volcano, Hawaii, January 1983 through December 1994: U.S. Geological Survey Open-File Report 98–511, 75 p.

G Hildebrand, A.R., Boynton, W.V., and Zoller, W.H., 1984, Rhenium enriched Kilauea volcano aerosols; evidence for a volcanogenic component in the K/T boundary clay layer [abs.]: Bulletin of the American Astronomical Society, v. 16, no. 3 (pt. 1), p. 679.

G Hilton, D.R., McMurtry, G.M., and Kreulen, Rob, 1996, Helium-carbon relations of Kilauea volcano, Hawaii (USA); implications for magmatic degassing processes and the nature of the Hawaiian hotspot [abs.]: Eos (American Geophysical Union Transactions), v. 77, no. 46, supp., p. F807.

G Hinkley, T.K., 1991, Distribution of metals between particulate and gaseous forms in a volcanic plume: Bulletin of Volcanology, v. 53, no. 5, p. 395–400.

G Hinkley, T.K., Le Cloarec, M.-F., and Lambert, Gerard, 1994, Fractionation of families of major, minor, and trace metals across the melt-vapor interface in volcanic exhalations: Geochimica et Cosmochimica Acta, v. 58, no. 15, p. 3255–3263.

G Hinkley, T.K, Wilson, S.A., Lamothe, P.J., Landis, G.P., Finnegan, D.L., Gerlach, T.M., and Thornber, C.R., 1997, Metal emissions from Kilauea—proportions, source strength, and contribution to current estimates of volcanic injection to the atmosphere [abs.]: Eos (American Geophysical Union Transactions), v. 78, no. 46, supp., p. F803.

D Hoffmann, J.P., Ulrich, G.E., and Garcia, M.O., 1990, Horizontal ground deformation patterns and magma storage during the Puu Oo eruption of Kilauea volcano, Hawaii; episodes 22–42: Bulletin of Volcanology, v. 52, no. 6, p. 522–531.

S Ho-Liu, Phyllis, Johnson, C.E., Mantagner, J.-P., Kanamori, Hiroo, and Clayton, R.W., 1988, Three-dimensional attenuation structure of Kilauea east rift zone, Hawaii [abs.]: Seismological Research Letters, v. 59, no. 1, p. 30.

V Hon, K.A., Heliker, C.C., and Kjargaard, J.I., 1988, Limu o Pele; a new kind of hydroclastic tephra from Kilauea Volcano, Hawaii [abs.]: Geological Society of America Abstracts with Programs, v. 20, no. 7, p. A112–A113.

V Hon, K.A., Kauahikaua, J.P., Denlinger, R.P., and Mackay, Kevin, 1994, Emplacement and inflation of pahoehoe sheet flows; observations and measurements of active lava flows on Kilauea Volcano, Hawaii: Geological Society of America Bulletin, v. 106, no. 3, p. 351–370.

V Hon, K.A., Kauahikaua, J.P., and Mackay, Kevin, 1993, Inflation and cooling data from pahoehoe sheet flows on Kilauea volcano: U.S. Geological Survey Open-File Report 93–342–A, 27 p.

V Hon, K.A., Mattox, T.N., Kauahikaua, J.P., and Kjargaard, J.I., 1993, The construction of pahoehoe lava deltas on Kilauea volcano, Hawaii [abs.]: Eos (American Geophysical Union Transactions), v. 74, no. 43, supp., p. 616.

R Horton, K.A., 1995, Airborne and satellite infrared imaging spectroscopy of active volcanism at Kilauea volcano, Hawaii: Honolulu, University of Hawaii, Ph.D. dissertation, 343 p.

S, V Ida, Yoshiaki, 1996, Cyclic fluid effusion accompanied by pressure change; implication for volcanic eruptions and tremor: Geophysical Research Letters, v. 23, no. 12, p. 1457–1460.

Gp Jackson, D.B., 1988, Geoelectric observations (including the September 1982 summit eruption), chap. 8 *of* Wolfe, E.W., ed., The Puu Oo eruption of Kilauea Volcano, Hawaii; episodes 1 through 20, January 3, 1983, through June 8, 1984: U.S. Geological Survey Professional Paper 1463, p. 237–251.

D Johnson, D.J., 1992, Dynamics of magma storage in the summit reservoir of Kilauea Volcano, Hawaii: Journal of Geophysical Research, v. 97, no. B2, p. 1807–1820.

V Jones, A.C., 1993, The cooling rates of pahoehoe flows; the importance of lava porosity [abs.]: Lunar and Planetary Science Conference Abstracts of Papers, v. 24, p. 731–732.

R, V Jones, A.C., 1994, Remote sensing and thermal modelling of active lava flows, Kilauea Volcano, Hawai'i: Lancaster, U.K., Lancaster University, Ph.D. dissertation, 288 p.

V, Gp Kauahikaua, J.P., Cashman, K.V., Mattox, T.N., Heliker, C.C., Hon, K.A., Mangan, M.T., and Thornber, C.R., 1998, Observations on basaltic lava streams in tubes from Kilauea Volcano, island of Hawai'i: Journal of Geophysical Research, v. 103, no. B11, p. 27303–27323.

V, Gp Kauahikaua, J.P., Mangan, M.T., Heliker, C.C., and Mattox, T.N., 1996, A quantitative look at the demise of a basaltic vent; the death of Kupaianaha, Kilauea Volcano, Hawai'i: Bulletin of Volcanology, v. 57, no. 8, p. 641–648.

D, S Kedar, Sharon, Chouet, B.A., and Dawson, P.B., 1997, Broadband analysis of the February 1996 inflation episode of Kilauea caldera, Hawaii [abs.]: Eos (American Geophysical Union Transactions), v. 78, no. 46, p. F442.

V Kelly, K.M., Hon, K.A., and Tribble, G.W., 1989, Bathymetric and submarine studies of an active lava delta near Kupapau Point, Kilauea volcano, Hawaii [abs.]: Eos (American Geophysical Union Transactions), v. 70, no. 43, p. 1202.

V Kent, R.M., and Pinkerton, Harry, 1994, Modelling the flow and heat transfer of magma in dikes using computational fluid dynamics [abs.]: Lunar and Planetary Science Conference Abstracts of Papers, v. 25, no. 2, p. 693–694.

V Kerr, R.C., 2001, Thermal erosion by laminar lava flows: Journal of Geophysical Research, v. 106, no. B11, p. 26453–26465.

V Keszthelyi, L.P., 1994, Calculated effect of vesicles on the thermal properties of cooling basaltic lava flows: Journal of Volcanology and Geothermal Research, v. 63, no. 3–4, p. 257–266.

V Keszthelyi, L.P., 1995, A preliminary thermal budget for lava tubes on the Earth and planets: Journal of Geophysical Research, v. 100, no. B10, p. 20411–20420.

V Keszthelyi, L.P., 1995, Measurements of the cooling at the base of pahoehoe flows: Geophysical Research Letters, v. 22, no. 16, p. 2195–2198.

V Keszthelyi, L.P., and Denlinger, R.P., 1996, The initial cooling of pahoehoe flow lobes: Bulletin of Volcanology, v. 58, no. 1, p. 5–18.

P Kilinc, A.I., and Lammert, Penny, 1992, Oxidation state of the episode 5 basalt flow, Kilauea, HI [abs.]: Geological Society of America Abstracts with Programs, v. 24, no. 7, p. 262.

S Koyanagi, R.Y., and Nakata, J.S., 1990, Seismicity related to eruption at Kilauea Volcano, Hawaii, 1983–1989 [abs.]: Eos (American Geophysical Union Transactions), v. 71, no. 28, p. 955.

S Koyanagi, R.Y., Tanigawa, W.R., and Nakata, J.S., 1988, Seismicity associated with the eruption, chap. 7 *of* Wolfe, E.W., ed., The Puu Oo eruption of Kilauea Volcano, Hawaii; episodes 1 through 20, January 3, 1983, through June 8, 1984: U.S. Geological Survey Professional Paper 1463, p. 183–235.

D Lisowski, Michael, Miklius, Asta, Sako, M.K., Owen, S.E., and Cervelli, P.F., 1999, Temporal changes in deformation of Kilauea Volcano, Hawaii [abs.]: Eos (American Geophysical Union Transactions), v. 80, no. 46, supp., p. F958.

D Lisowski, Michael, Owen, S.E., and Segall, Paul, 1996, The Kilauea Volcano, Hawaii, continuous GPS network; recent results [abs.]: Eos (American Geophysical Union Transactions), v. 77, no. 46, supp., p. F808.

P Lowther, J.S., and Brunstad, K.A., 1998, Microtextures and microanalysis of olivine in the 1992 Kalapana, Hawaii, lava flow [abs.]: Geological Society of America Abstracts with Programs, v. 30, no. 7, p. 376.

P, V Mangan, M.T., and Cashman, K.V., 1996, The structure of basaltic scoria and reticulite and inferences for vesiculation, foam formation, and fragmentation in lava fountains: Journal of Volcanology and Geothermal Research, v. 73, no. 1, p. 1–18.

P, V Mangan, M.T., Cashman, K.V., and Newman, Sally, 1993, Vesiculation of basaltic magma during eruption: Geology, v. 21, no. 2, p. 157–160.

E, V Mangan, M.T., Heliker, C.C., Mattox, T.N., Kauahikaua, J.P., and Helz, R.T., 1995, Episode 49 of the Pu'u 'O'o-Kupaianaha eruption of Kilauea volcano—breakdown of a steady-state eruptive era: Bulletin of Volcanology, v. 57, no. 2, p. 127–135.

P Mangan, M.T., Heliker, C.C., Mattox, T.N., Kauahikaua, J.P., Helz, R.T., and Hearn, B.C., Jr., 1995, The Pu'u 'O'o-Kupaianaha eruption of Kilauea Volcano; June 1990 through August 1994 lava sample archive: U.S. Geological Survey Open-File Report 95–496, n.p.

E Mattox, T.N., Heliker, C.C., Hoffmann, J.P., Hon, K.A., Mangan, M.T., Neal, C.A., Ulrich, G.E., and Wolfe, E.W., 1994, Timelapse film logs from the Pu'u 'O'o-Kupaianaha eruption of Kilauea Volcano; January 1983 through September 1994: U.S. Geological Survey Open-File Report 94–713, 237 p.

V Mattox, T.N., Heliker, C.C., Kauahikaua, J.P., and Hon, K.A., 1993, Development of the 1990 Kalapana flow field, Kilauea Volcano, Hawaii: Bulletin of Volcanology, v. 55, no. 6, p. 407–413.

V Mattox, T.N., and Mangan, M.T., 1997, Littoral hydrovolcanic explosions; a case study of lava-seawater interaction at Kilauea Volcano: Journal of Volcanology and Geothermal Research, v. 75, no. 1–2, p. 1–17.

R McGee, K.A., and Gerlach, T.M., 1998, Airborne volcanic plume measurements using a FTIR spectrometer, Kilauea volcano, Hawaii: Geophysical Research Letters, v. 25, no. 5, p. 615–618.

G McMurtry, G.M., and Goff, Fraser, 1992, Anomalous deuterium and tritium in magmatic water from Kilauea and Mount St. Helens; implications for deep Earth processes [abs.]: Eos (American Geophysical Union Transactions), v. 73, no. 14, p. 348.

P Meeker, G.P., and Hinkley, T.K., 1993, The structure and composition of microspheres from the Kilauea volcano, Hawaii: American Mineralogist, v. 78, no. 7–8, p. 873–876.

P Meeker, G.P., and Thornber, C.R., 2000, A three dimensional view of basalt crystallization in "lava straws" from Kilauea [abs.], *in* Williams, D.B., and Shimizu, Ryuichi, eds., Microbeam analysis 2000; International Union of Microbeam Analysis Societies Conference, 2d, Proceedings: London, Institute of Physics Publishing, Symposium 9, ser. no. 165, p. 297–298.

P Meeker, G.P., Thornber, C.R., and Hinkley, T.K., 2000, Natural "fly ash" from Kilauea volcano, Hawaii [abs.], *in* Williams, D.B., and Shimizu, Ryuichi, eds., Microbeam analysis 2000; International Union of Microbeam Analysis Societies Conference, 2d, Proceedings: London, Institute of Physics Publishing, Symposium 9, ser. no. 165, p. 309–310.

G Miller, T.L., Zoller, W.H., Crowe, B.M., and Finnegan, D.L., 1990, Variations in trace metal and halogen ratios in magmatic gases through an eruptive cycle of the Puʻu Oʻo vent, Kilauea, Hawaii; July–August 1985: Journal of Geophysical Research, v. 95, no. B8, p. 12607–12615.

R Mouginis-Mark, P.J., Rowland, S.K., Garbeil, Harold, and Flament, Pierre, 1991, AVHRR observations of the Kupaianaha eruption, Hawaii [abs.]: Eos (American Geophysical Union Transactions), v. 72, no. 44, supp., p. 562.

S, E Nakata, J.S., and others, 1986–2001, Hawaiian Volcano Observatory summaries, part I, seismic data (annually), 1986–2001: U.S. Geological Survey Open-File Reports 92–301, 92–333, 94–169, 91–564, 91–578, 94–432, 98–147, 99–415, 00–326, 00–353, 00–354, 00–408, 00–406, 00–433, 01–332, 02–157.

P Neal, C.A., Duggan, T.J., Wolfe, E.W., and Brandt, E.L., 1988, Lava samples, temperatures, and compositions, chap. 2 *of* Wolfe, E.W., ed., The Puu Oo eruption of Kilauea Volcano, Hawaii; episodes 1 through 20, January 3, 1983, through June 8, 1984: U.S. Geological Survey Professional Paper 1463, p. 99–126.

S Ohminato, Takao, Chouet, B.A., Dawson, P.B., and Kedar, Sharon, 1998, Waveform inversion of very long period impulsive signals associated with magmatic injection beneath Kilauea Volcano, Hawaii: Journal of Geophysical Research, v. 103, no. B10, p. 23839–23862.

D Okamura, A.T., Dvorak, J.J., Koyanagi, R.Y., and Tanigawa, W.R., 1988, Surface deformation during dike propagation, chap. 6 *of* Wolfe, E.W., ed., The Puu Oo eruption of Kilauea Volcano, Hawaii; episodes 1 through 20, January 3, 1983, through June 8, 1984: U.S. Geological Survey Professional Paper 1463, p. 165–182.

D Okamura, A.T., Miklius, Asta, and Sako, M.K., 1991, Relation between the Kilauea east-rift-zone eruption and surface deformation of the summit and southwest rift zone, island of Hawaii [abs.]: Eos (American Geophysical Union Transactions), v. 72, no. 44, supp., p. 566–557.

S Okubo, P.G., 1994, Seismicity associated with the continuing eruption at Kilauea Volcano, Hawaii [abs.]: Seismological Research Letters, v. 65, no. 1, p. 55.

S Okubo, P.G., 1997, An evolving seismological view of Kilauea's east rift zone [abs.]: Eos (American Geophysical Union Transactions), v. 78, no. 46, supp., p. F634.

S Okubo, P.G., Nakata, J.S., Chouet, B.A., and Dawson, P.B., 1996, The February 1, 1996, Kilauea summit earthquake swarm [abs.]: Eos (American Geophysical Union Transactions), v. 77, no. 46, supp., p. F798.

S Okubo, P.G., Okamura, A.T., and Miklius, Asta, 1991, Intrusive earthquake swarms and the continuing Kilauea eruption [abs.]: Eos (American Geophysical Union Transactions), v. 72, no. 44, supp., p. 566.

S Okubo, P.G., Seidl, Dieter, and Hellweg, Margaret, 1994, The broadband wavefield at the Puu Oo vent of Kilauea Volcano, Hawaii [abs.]: Eos (American Geophysical Union Transactions), v. 75, no. 44, supp., p. 714.

S Okubo, P.G., Tomori, A.H., Nakata, J.S., Largo, A.J., and Fukunaga, P.N., 1990, Spatial and temporal patterns of seismicity related to the on-going eruption of Kilauea Volcano, Hawaii [abs.]: Eos (American Geophysical Union Transactions), v. 71, no. 43, p. 1711.

G Olmez, Ilhan, Finnegan, D.L., and Zoller, W.H., 1986, Iridium emissions from Kilauea volcano: Journal of Geophysical Research, v. 91, no. B1, p. 653–663.

D Owen, S.E., Segall, Paul, Lisowski, Michael, Miklius, Asta, Denlinger, R.P., and Sako, M.K., 2000, Rapid deformation of Kilauea Volcano; global positioning system measurements between 1990 and 1996: Journal of Geophysical Research, v. 105, no. B8, p. 18983–18998.

D Owen, S.E., Segall, Paul, Lisowski, Michael, Miklius, Asta, Murray, Michael, Bevis, M.G., and Foster, James, 2000, January 30, 1997 eruptive event on Kilauea Volcano, Hawaii, as monitored by continuous GPS: Geophysical Research Letters, v. 27, no. 17, p. 2757–2760.

P Oze, C.J.-P., and Winter, J.D., 1997, A petrographical study of blue glassy pahoehoe from Kilauea Volcano, Hawaiʻi [abs.]: Geological Society of America Abstracts with Programs, v. 29, no. 6, p. A–137.

G, P Paces, J.B., and Rose, W.I., 1984, Hourly volatile and chemical evolution during phase 16 of the 1983–84 Kilauea east rift zone eruption [abs.]: Eos (American Geophysical Union Transactions), v. 65, no. 45, p. 1130–1131.

V Parfitt, E.A., and Wilson, Lionel, 1994, The 1983–86 Puʻu ʻOʻo eruption of Kilauea volcano, Hawaii; a study of dike geometry and eruption mechanisms for a long-lived eruption: Journal of Volcanology and Geothermal Research, v. 59, no. 3, p. 179–205.

V Parfitt, E.A., and Wilson, Lionel, 1995, Explosive volcanic eruptions; IX. The transition between Hawaiian-style lava fountaining and Strombolian explosive activity: Geophysical Journal International, v. 121, no. 1, p. 226–232.

V, G Parfitt, E.A., Wilson, Lionel, and Neal, C.A., 1995, Factors influencing the height of Hawaiian lava fountains; implications for the use of fountain height as an indicator of magma gas content: Bulletin of Volcanology, v. 57, no. 6, p. 440–450.

R Peitersen, M.N., and Crown, D.A., 1999, Downflow width behavior of Martian and terrestrial lava flows: Journal of Geophysical Research, v. 104, no. E4, p. 8473–8488.

R Peitersen, M.N., and Crown, D.A., 2000, Correlations between topography and intraflow width behavior in Martian and terrestrial lava flows: Journal of Geophysical Research, v. 105, no. E2, p. 4123–4134.

R Perry, D.L., Gunderson, K.W., Herd, D.G., Kauahikaua, J.P., Lange, J.J., McCord, T.B., and Ross, J.P., Jr., 1995, Predicted and measured thermal infrared signatures of Kilauea lava tubes [abs.]: Eos (American Geophysical Union Transactions), v. 76, no. 17, p. S300.

V Pinkerton, Harry, and Herd, R.A., 1996, Field measurements of the rheological properties of basaltic lavas on Kilauea, Hawaii [abs.], *in* Whitehead, P.W., ed., Long lava flows: Chapman Conference on Long Lava Flows, Townsville, Australia, 1996, Abstracts, p. 52–53.

V Pinkerton, Harry, James, Mike, and Jones, Alun, 2002, Surface temperature measurements of active lava flows on Kilauea volcano, Hawai'i: Journal of Volcanology and Geothermal Research, v. 113, no. 1–2, p. 159–176.

V Pinkerton, Harry, and Wilson, Lionel, 1994, Factors controlling the lengths of channel-fed lava flows: Bulletin of Volcanology, v. 56, no. 2, p. 108–120.

P, V Polacci, Margherita, Cashman, K.V., and Kauahikaua, J.P., 1999, Textural characterization of the pāhoehoe-'a'ā transition in Hawaiian basalt: Bulletin of Volcanology, v. 60, no. 8, p. 595–609.

P Putirka, K.D., 1997, Magma transport at Hawaii; inferences based on igneous thermobarometry: Geology, v. 25, no. 1, p. 69–72.

G Quick, J.E., Hinkley, T.K., Reimer, G.M., and Hedge, C.E., 1991, Tritium concentrations in the active Pu'u O'o Crater, Kilauea volcano, Hawaii; implications for cold fusion in the Earth's interior: Physics of the Earth and Planetary Interiors, v. 69, no. 1–2, p. 132–137.

R Realmuto, V.J., Hon, K.A., Kahle, A.B., Abbott, E.A., and Pieri, D.C., 1992, Multispectral thermal infrared mapping of the 1 October 1988 Kupaianaha flow field, Kilauea volcano, Hawaii: Bulletin of Volcanology, v. 55, no. 1, p. 33–44.

R, G Realmuto, V.J., Sutton, A.J., and Elias, Tamar, 1997, Multispectral thermal infrared mapping of sulfur dioxide plumes; a case study from the East Rift Zone of Kilauea Volcano, Hawaii: Journal of Geophysical Research, v. 102, no. B7, p. 15057–15072.

R, G Realmuto, V.J., and Worden, H.M., 2000, Impact of atmospheric water vapor on the thermal infrared remote sensing of volcanic sulfur dioxide emissions; a case study from the Pu'u 'O'o vent of Kilauea Volcano, Hawaii: Journal of Geophysical Research, v. 105, no. B9, p. 21497–21508.

P Reinitz, I.M., and Turekian, K.K., 1991, The behavior of the uranium decay chain nuclides and thorium during the flank eruptions of Kilauea (Hawaii) between 1983 and 1985: Geochimica et Cosmochimica Acta, v. 55, no. 12, p. 3735–3740.

G Resing, J.A., and Sansone, F.J., 1999, The chemistry of lava-seawater interactions; the generation of acidity: Geochimica et Cosmochimica Acta, v. 63, no. 15, p. 2183–2198.

G Resing, J.A., and Sansone, F.J., 2002, The chemistry of lava-seawater interactions II; the elemental signature: Geochimica et Cosmochimica Acta, v. 66, no. 11, p. 1925–1941.

P Roeder, P.L., Thornber, C.R., Poustovetov, A.A., and Grant, A.C., in press, Morphology and composition of spinel Pu'u 'O'o lava (1996–1998), Kilauea volcano, Hawai'i: Journal of Volcanology and Geothermal Research.

R, Gp Roggenthen, W.M., 1994, A ground-penetrating radar survey of the active Kamoamoa delta, Kilauea Volcano, Hawaii [abs.]: Geological Society of America Abstracts with Programs, v. 26, no. 7, p. A–118.

P, G Rose, W.I., Paces, J.B., and Chartier, T.A., 1985, Complex magma mixing and degassing patterns revealed by tephra sampling during Kilauea east rift zone eruptions, 1984–85 [abs.]: Eos (American Geophysical Union Transactions), v. 66, no. 46, p. 1133.

R Rosen, P.A., Hensley, Scott, Zebker, H.A., Webb, F.H., and Fielding, E.J., 1996, Surface deformation and coherence measurements of Kilauea Volcano, Hawaii, from SIR-C radar interferometry: Journal of Geophysical Research, v. 101, no. E10, p. 23109–23125.

R Rowland, S.K., MacKay, M.E., and Garbeil, Harold, 1999, Topographic analyses of Kīlauea Volcano, Hawai'i, from interferometric airborne radar: Bulletin of Volcanology, v. 61, no. 1, p. 1–14.

S Rubin, A.M., Gillard, Dominique, and Got, J.-L., 1998, A reinterpretation of seismicity associated with the January 1983 dike intrusion at Kilauea Volcano, Hawaii: Journal of Geophysical Reseach, v. 103, no. B5, p. 10003–10015.

S Saccorotti, Gilberto, Chouet, B.A., and Dawson, P.B., 2001, Wavefield properties of a shallow long-period event and tremor at Kilauea Volcano, Hawaii: Journal of Volcanology and Geothermal Research, v. 109, no. 1–3, p. 163–189.

V Sakimoto, S.E.H., and Zuber, M.T., 1998, Flow and convective cooling in lava tubes, *in* Cashman, K.V., Pinkerton, Harry, and Stephenson, Jon, eds., Long lava flows: Journal of Geophysical Research, v. 103, no. B11, p. 27465–27487.

G Sansone, F.J., Benitez-Nelson, C.R., DeCarlo, E.H., Liangzhong, Zhuang, Heath, J.A., and Huebert, B.J., 2000, Chemical composition of the steam plume resulting from the ocean lava entry at Kilauea Volcano, Hawaii [abs.]: Eos (American Geophysical Union Transactions), v. 81, no. 46, supp., p. F1275.

G, V Sansone, F.J., and Resing, J.A., 1995, Hydrography and geochemistry of sea surface hydrothermal plumes resulting from Hawaiian coastal volcanism: Journal of Geophysical Research, v. 100, no. C7, p. 13555–13569.

G, V Sansone, F.J., Resing, J.A., Tribble, G.W., Sedwick, P.N., Kelly, K.M., and Hon, K.A., 1991, Lava-seawater interactions at shallow-water submarine lava flows: Geophysical Research Letters, v. 18, no. 9, p. 1731–1734.

G, V Sedwick, P.N., McMurtry, G.M., and Tribble, G.W., 1991, Chemical alteration of seawater by lava from Kilauea Volcano, Hawaii: Marine Geology, v. 96, no. 1–2, p. 151–158.

D Segall, Paul, Cervelli, P.F., Owen, S.E., Lisowski, Michael, and Miklius, Asta, 2001, Constraints on dike propagation from continuous GPS measurements: Journal of Geophysical Research, v. 106, no. B9, p. 19301–19317.

S Seidl, Dieter, Hellweg, Margaret, Okubo, P.G., Rademacher, Horst, and Gresta, Stefano, 1996, A preliminary survey of the broadband seismic wavefield at Puu Oo, the active vent of Kilauea Volcano, Hawaii: Annali di Geofisica, v. 39, no. 2, p. 283–297.

V Self, Stephen, Keszthelyi, L.P., and Thordarson, Thorvaldur, 2000, Discussion of "Pulsed inflation of pahoehoe lava flows; implications for flood basalt emplacement", by S.W. Anderson, E.R. Stofan, E.R. Smrekar, J.E. Guest and B. Wood [Earth Planet. Sci. Lett. 168 (1999) 7–18]: Earth and Planetary Science Letters, v. 179, no. 2, p. 421–423.

P, V Sharma, Kirti, Self, Stephen, Thornber, C.R., and Keszthelyi, L.P., 1999, Textural variations through inflated pahoehoe flow lobes from Kilauea, Hawaii [abs.]: Eos (American Geophysical Union Transactions), v. 80, no. 46, supp., p. F1090.

R, V Smith, J.R., 1993, Extent and depositional processes of hyaloclastite and lava delta debris offshore Kilauea Volcano, Hawaii [abs.]: Eos (American Geophysical Union Transactions), v. 74, no. 43, supp., p. 617.

G Sutton, A.J., and Elias, Tamar, 1993, Annotated bibliography; volcanic gas emissions and their effect on ambient air character: U.S. Geological Survey Open-File Report 93–551–E, 26 p.

G Sutton, A.J., Elias, Tamar, Gerlach, T.M., and Stokes, J.B., 2001, Implications for eruptive processes as indicated by sulfur dioxide emissions from Kīlauea Volcano, Hawai'i, 1979–1997: Journal of Volcanology and Geothermal Research, v. 108, no. 1–4, p. 283–302.

G, H Sutton, A.J., Elias, Tamar, Hendley, J.W., II, and Stauffer, P.H., 1997, Volcanic air pollution—a hazard in Hawaii: U.S. Geological Survey Fact Sheet 169–97, 2 p.

G, H Sutton, A.J., Elias, Tamar, and Navarrete, R.M., 1994, Volcanic gas emissions and their impact on ambient air character at Kilauea Volcano, Hawaii: U.S. Geological Survey Open-File Report 94–569, 34 p.

G, S Thomas, D.M., and Koyanagi, R.Y., 1986, The association between ground gas radon concentrations and seismic and volcanic activity at Kilauea volcano [abs.]: Eos (American Geophysical Union Transactions), v. 67, no. 44, p. 905.

I Thornber, C.R., 1997, HVO/RVTS–1; a prototype remote video telemetry system for monitoring the Kilauea east rift zone eruption, 1997: U.S. Geological Survey Open-File Report 97–537, 19 p.

P Thornber, C.R., 2001, Olivine-liquid relations of lava erupted by Kīlauea Volcano from 1994 to 1998; implications for shallow magmatic processes associated with the ongoing east-rift-zone eruption: Canadian Mineralogist, v. 39, no. 2, p. 239–266.

E Thornber, C.R., Heliker, C.C., Reynolds, J.R., Kauahikaua, J.P., Okubo, P.G., Lisowski, Michael, Sutton, A.J., and Clague, D.A., 1996, The eruptive surge of February 1, 1996; a highlight of Kilauea's ongoing east rift zone eruption [abs.]: Eos (American Geophysical Union Transactions), v. 77, no. 46, supp., p. F798.

P Thornber, C.R., Sherrod, D.R., Siems, D.F., Heliker, C.C., Meeker, G.P., Oscarson, R.L., and Kauahikaua, J.P., 2002, Whole-rock and glass major-element geochemistry of Kilauea Volcano, Hawaii, near-vent eruptive products; September 1994 through September 2001: U.S. Geological Survey Open-File Report 02–17, 41 p.

P Thornber, C.R., Heliker, C.C., Sherrod, D.R., Kauahikaua, J.P., Miklius, Asta, Okubo, P.G., Trusdell, F.A., Budahn, J.R., Ridley, W.I., and Meeker, G.P., in press, Kilauea east rift zone magmatism: an episode 54 perspective: Journal of Petrology.

V Tribble, G.W., 1991, Underwater observations of active lava flows from Kilauea volcano, Hawaii: Geology, v. 19, no. 6, p. 633–636.

D Troise, Claudia, de Natale, Giuseppe, Pingue, Folco, and Dvorak, J.J., 1999, Variable opening of dike-fed eruptive fissures determined from geodetic data; the 1971 and 1983 rift-zone eruptions of Kilauea Volcano, Hawaii: Journal of Geodynamics, v. 27, no. 1, p. 75–88.

E Ulrich, G.E., Wolfe, E.W., Heliker, C.C., and Neal, C.A., 1987, Puʻu ʻOʻo IV; evolution of a plumbing system [abs.], *in* Decker, R.W., Halbig, J.B., Hazlett, R.W., Okamura, R.T., and Wright, T.L., eds., Hawaii Symposium on How Volcanoes Work, Hilo, Hawaii, 1987, Abstract volume: Honolulu, University of Hawaii, Hawaii Institute of Geophysics, p. 259.

G Vergniolle, Sylvie, and Jaupart, Claude, 1990, Dynamics of degassing at Kilauea volcano, Hawaii: Journal of Geophysical Research, v. 95, no. B3, p. 2793–2809.

V, G Wallace, P.J., and Anderson, A.T., Jr., 1998, Effects of eruption and lava drainback on the H_2O contents of basaltic magmas at Kilauea Volcano: Bulletin of Volcanology, v. 59, no. 5, p. 327–344.

P White, A.F., and Hochella, M.F., 1992, Surface chemistry associated with the cooling and subaerial weathering of recent basalt flows: Geochimica et Cosmochimica Acta, v. 56, no. 10, p. 3711–3721.

V Wilson, Lionel, and Head, J.W., III, 1988, Nature of local magma storage zones and geometry of conduit systems below basaltic eruption sites; Puʻu ʻOʻo, Kilauea east rift, Hawaii, example: Journal of Geophysical Research, v. 93, no. B12, p. 14785–14792.

V Wilson, Lionel, Parfitt, E.A., and Head, J.W., III, 1995, Explosive volcanic eruptions—VIII. The role of magma recycling in controlling the behavior of Hawaiian-style lava fountains: Geophysical Journal International, v. 121, no. 1, p. 215–225.

E Wolfe, E.W., Garcia, M.O., Jackson, D.B., Koyanagi, R.Y., Neal, C.A., and Okamura, A.T., 1987, The Puu Oo eruption of Kilauea Volcano, episodes 1–20, January 3, 1983, to June 8, 1984, chap. 17 *of* Decker, R.W., Wright, T.L., and Stauffer, P.H., eds., Volcanism in Hawaii: U.S. Geological Survey Professional Paper 1350, v. 1, p. 471–508.

E, M Wolfe, E.W., Neal, C.A., Banks, N.G., and Duggan, T.J., 1988, Geologic observations and chronology of eruptive events, chap. 1 *of* Wolfe, E.W., ed., The Puu Oo eruption of Kilauea Volcano, Hawaii; episodes 1 through 20, January 3, 1983 through June 8, 1984:U.S.Geological Survey Professional Paper 1463, p. 1-97.

The Rise and Fall of Pu‘u ‘Ō‘ō Cone, 1983–2002

By Christina Heliker, Jim Kauahikaua, David R. Sherrod, Michael Lisowski, *and* Peter F. Cervelli

Abstract

The Pu‘u ‘Ō‘ō-Kūpaianaha eruption of Kīlauea Volcano, Hawai‘i, began on January 3, 1983. From June 1983 through June 1986, 44 episodes of high fountaining at the Pu‘u ‘Ō‘ō vent constructed a complex basaltic cone, 255 m high and 1.4 km wide at its base, composed of lava flows, agglutinated spatter, and cinder, with an asymmetric shape determined largely by the prevailing trade winds. The steeper slope (36°) on the west side of the cone was controlled by unconsolidated cinder and agglutinated spatter, and the gentler slope (8°) on the east side by lava flows. These two sectors of the cone were separated by transitional zones of rootless spatter flows. At its maximum size, the volume of the cone was ~136x10^6 m^3 (dense-rock equivalent, 67x10^6 m^3) and composed about 20 percent of the total volume of eruptive deposits produced during the 3 years of its growth.

In July 1986, the eruption shifted 3 km downrift to a new vent, Kūpaianaha, which became the locus of activity for the next 5½ years. Episodic collapse from mid-1987 through 1988 resulted in a central crater, 180 m deep and 200 m wide, at Pu‘u ‘Ō‘ō. The elevation of the crater floor stabilized at about the same elevation as the Kūpaianaha lava pond, and a lava pond appeared intermittently in the new crater of Pu‘u ‘Ō‘ō.

In February 1992, Kūpaianaha stopped erupting, and the activity returned to Pu‘u ‘Ō‘ō, where a series of flank vents on the west and southwest sides of the cone have been erupting ever since. The west wall of the cone was gradually undermined by shallow subsurface magma movement associated with flank vents, and collapse pits began to form high on the west flank of the cone in 1993. In January 1997, the magmatic system beneath Pu‘u ‘Ō‘ō was depressurized by an intrusion and a brief fissure eruption 4 km uprift. The crater floor dropped 150 m, and the west wall of the cone collapsed, removing 13x10^6 m^3 of material and enlarging the elliptical crater to 240 by 400 m. The cumulative volume of crater and west-wall collapse since 1987 is 28x10^6 m^3. In addition to catastrophic collapse, the cone is undergoing long-term subsidence. Repeated surveys of bench marks on the cone recorded 63 to 83 cm/yr of subsidence near the crater from 1998 to 2002.

Recent geodetic data from borehole tiltmeters on and near the cone indicate the presence of a deformation source less than 400 m below the preeruption surface. Gravity measurements suggest that the cone is underlain by an elongate zone, parallel to the rift zone, with a density contrast of 0.5 g/cm^3 relative to the surrounding rock. We have modeled the gravity data as a low-density zone, approximately 500 m wide, 1,500 m long, and 300 m thick, occupying a volume 70 to 370 m below the preeruption surface; this low-density zone probably represents brecciated rock laced with magma-filled fractures.

Introduction

The ongoing Pu‘u ‘Ō‘ō-Kūpaianaha eruption (fig. 1), which began in January 1983, is the longest lived eruption on Kīlauea’s rift zones in more than 500 years. Monitoring this eruption has provided ample opportunity to witness catastrophic changes in the landscape on a time scale from days to months. The most striking landform created during this prolonged eruption is Pu‘u ‘Ō‘ō, a basaltic cone composed of cinder, agglutinated spatter, and lava flows. Constructed during 3 years of episodic high lava fountaining, the cone grew to a height of 255 m above the pre-1983 surface. By 1986, Pu‘u ‘Ō‘ō was the most prominent vent structure on either rift zone of Kīlauea, more than 140 m higher than any other cone on the volcano.

Studies of complex basaltic cones (those not composed predominantly of cinder) are rare, and, with the exception of an overview by Head and Wilson (1989), the contribution of rootless agglutinated-spatter flows to basaltic vent structures is little noted in the literature. Since the late 1990s, however, basaltic and andesitic rootless spatter flows have been the focus of studies at Izu-Oshima Volcano (Sumner, 1998) and Asama Volcano (Maya Yasui and Takehiro Koyaguchi, written commun., 2002) in Japan and at Vulcan cone, part of the basaltic Albuquerque Volcanoes, in New Mexico (Smith and others, 1999). These recent studies highlight the need for better documentation of such features, particularly where the eruption is witnessed.

Both the duration and scale of the collapse of Pu‘u ‘Ō‘ō are unique in the recorded history of Kīlauea. The ongoing collapse of the crater and west flank of the cone has resulted from two processes: (1) short-term events that abruptly divert magma from the eruption site, depressurize the magmatic system, and trigger catastrophic collapse; and (2) long-term downcutting by the lava tubes leading from the flank vents that has progressively undermined the west flank of the cone.

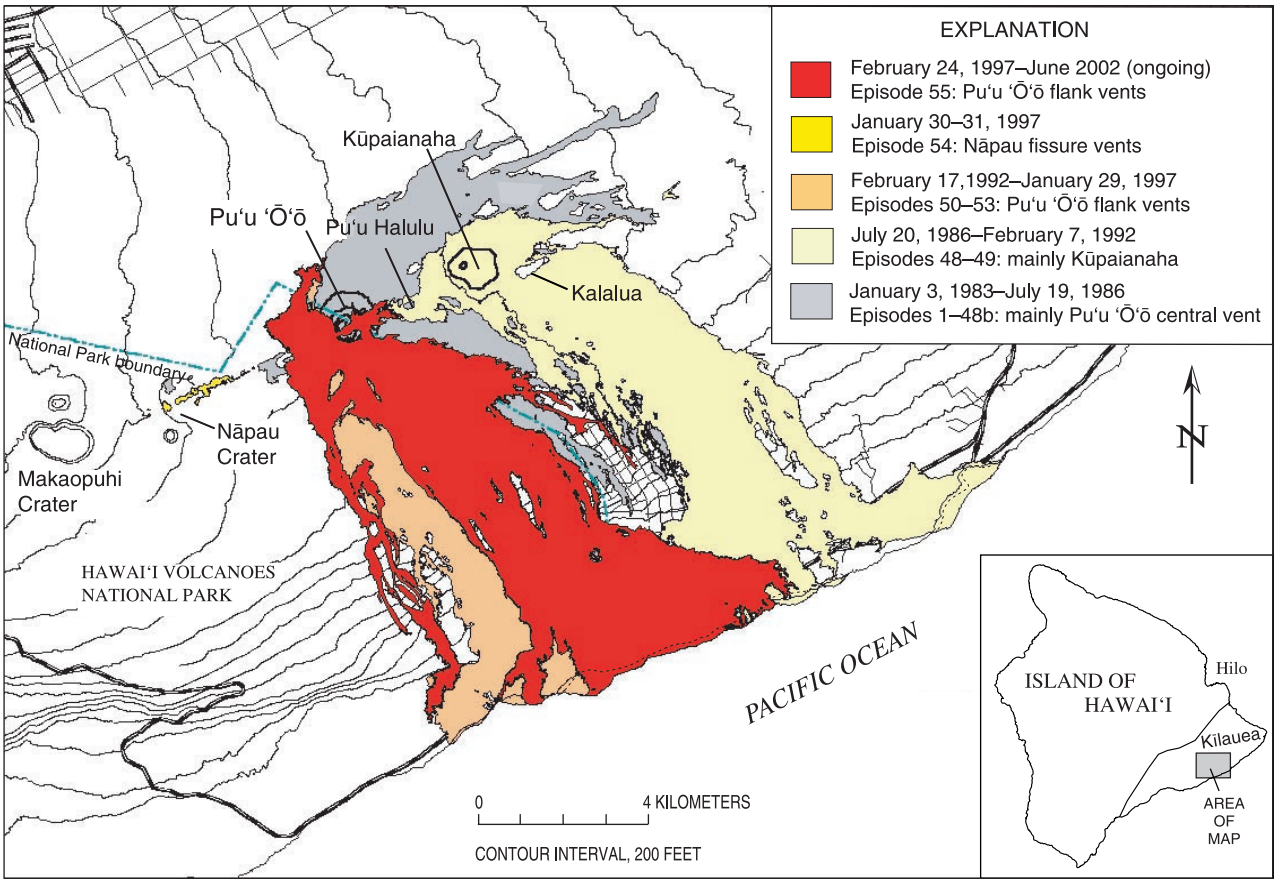

Figure 1. Kīlauea Volcano, Island of Hawai‘i, showing location of Pu‘u ‘Ō‘ō-Kūpaianaha eruption site on east rift zone and lava flows emplaced during eruptive episodes.

Recently obtained gravity and geodetic data, interpreted in the light of the ongoing collapse and the growing number of flank vents, give us a better understanding of the shallow magmatic system beneath Pu‘u ‘Ō‘ō.

The scope of this chapter is limited to those events that bear directly on the growth and later collapse of the Pu‘u ‘Ō‘ō cone. For a full chronology of the eruption, see Heliker and Mattox (this volume).

The Rise of Pu‘u ‘Ō‘ō, June 1983–July 1986

How the Cone Got Its Shape

Within 6 months of its onset in January 1983, the eruption had localized at the Pu‘u ‘Ō‘ō vent (fig. 1). By mid-1984, the activity had settled into a pattern of brief (<24 hour) eruptive episodes, separated by repose periods averaging 25 days in length (George Ulrich and others, The Pu‘u ‘Ō‘ō-Kūpaianaha eruption of Kīlauea Volcano, Hawaii: episodes 21 through 48, U.S. Geological Survey Open-File Report, in preparation). Over the next 3 years, 44 episodes of high fountaining built a cinder-and-spatter cone, 255 m high and 1.4 km in diameter at its base (fig. 2).

Within its first few months, the cone developed an asymmetric shape, because the prevailing northeasterly trade winds deflected most of the tephra to the southwest side of the vent. This asymmetry became more pronounced in mid-1984, when maximum fountain heights increased from less than 250 to 300–470 m, with a corresponding increase in the volume of tephra deposits. The summit gained as much as 27 m in height during each high fountaining episode and, by July 1986, stood 86 m higher than the vent (fig. 3). The southwest side of the cone rose like a backstop behind the fountains.

The rapid increase in cone height slowed markedly after October 1985 (table 1; fig. 4), because fountain heights were substantially lower and southwesterly winds prevailed during half of the remaining high-fountaining episodes. The vent continued to increase in elevation, however, which may have contributed to the end of high fountaining at Pu‘u ‘Ō‘ō in mid-1986.

By December 1983, the Pu‘u ‘Ō‘ō vent had consolidated into a single circular opening approximately 20 m in diameter. The conduit below the vent was a vertical pipe of constant diameter, visible to approximately 50-m depth. During its first year, the vent was situated in a shallow crater. Lava overflowed from the crater into spillways, which had been established on the east side of the cone during its first 6 months (Wolfe and others, 1988). Generally, the lava exited through one or two spillways that persisted through several eruptive

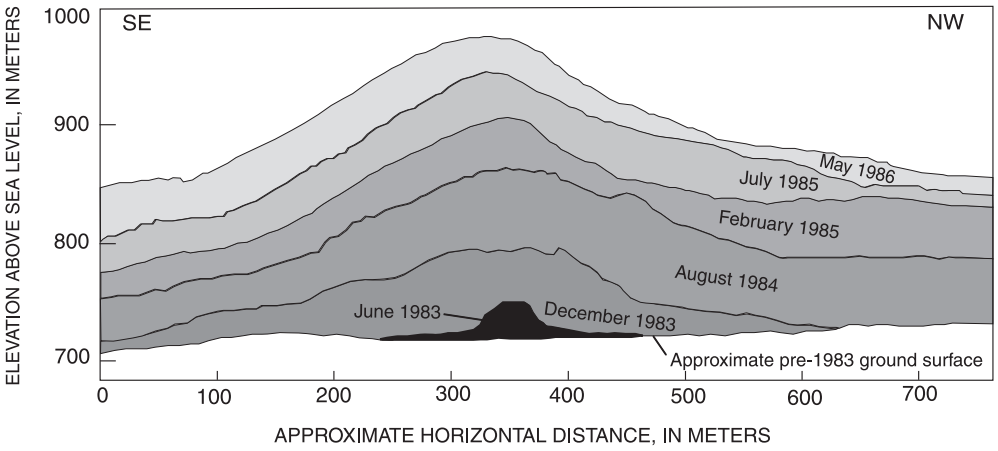

Figure 2. Profiles showing growth of Pu‘u ‘Ō‘ō cone, June 1983 through May 1986, traced from photographs taken from Pu‘u Halulu. Vertical scale constrained by cone-height measurements taken by theodolite at end of each eruptive episode; horizontal scale from topographic surveys. Profiles for June and December 1983 from Wolfe and others (1988).

episodes. After low-level effusion during episode 19 (May 1984), the crater was filled to the level of the spillways (Wolfe and others, 1988), creating an amphitheater opening eastward. The increasing breadth of the fountains flattened the area around the vent, and, by episode 34 (July 1985), a broad ramp sloped from the vent toward the spillways (fig. 5).

By mid-1985, the cone's morphology was firmly established, with lava spillways to the east of the vent and a steep, cinder-covered flank to the west. These two sectors of the cone were separated by transitional zones of rootless spatter flows, partly buried by cinder, on the north and south flanks (fig. 5). The slope of the west (summit) side of the cone, which was controlled by unconsolidated cinder and agglutinated spatter, was 36°, whereas the slope of the east (spillway) side was only 8°.

The Components of the Cone

Lava Flows

The style of the eruption at Pu‘u ‘Ō‘ō changed progressively throughout its first year from low fountains that fed pāhoehoe flows to high fountains that fed ‘a‘ā flows. Episodes 4 through 19 (June 1983–May 1984) were characterized by channeled pāhoehoe flows that spilled from a lava pond at the base of the fountains (Wolfe and others, 1988). These fluid rivers carried most of the lava away from the cone before the flows underwent the transition to ‘a‘ā 1 to 2 km from the vent (Wolfe and others, 1988).

Beginning with episode 20 (June 1984), fountain-fed ‘a‘ā flows became the norm, mainly because fountain heights increased substantially. Maximum fountain heights fluctuated widely in the early Pu‘u ‘Ō‘ō episodes but were rarely more than 250 m. From episodes 20 through 41, however, maximum fountain heights were consistently more than 300 m, and during about half of these episodes, more than 400 m. The flows were fed directly by fallback from the fountains, resulting in lava with a higher viscosity and yield strength, owing to the loss of heat and volatile components during fountaining (Sparks and Pinkerton, 1978). When sustained fountain heights decreased during episodes 42 through 47 in 1986, channeled pāhoehoe flows were observed once again. A similar correlation between fountain height and flow type was documented during the 1961 Askja eruption in Iceland (Sparks and Pinkerton, 1978).

The predominance of ‘a‘ā flows near the vent caused a substantial buildup of the adjacent terrain on the north, east, and south sides of the cone, blurring the distinction between the cone and the surrounding lava-flow field. Lava rivers flowing down the spillways coalesced at the foot of the cone to form broad, thick fans of ‘a‘ā that piled up near the cone for several hours at the beginning of each episode.

Agglutinated Spatter and Rootless Flows

Spatter falling from the fountains fed all of the lava flows erupted during high-fountaining episodes. Although such spatter-fed flows are generally defined as clastogenic rather than coherent (Wolff and Sumner, 2000), this distinction is not useful in the field for Hawaiian eruptions, where complete coalescence of clasts takes place at the base of the fountain. A distinction can be made, however, between channeled flows

Figure 3. Pu‘u ‘Ō‘ō during episode 46, June 2, 1986. Summit is 86 m higher than vent, owing to prevailing trade winds. View southward.

Table 1. The Pu‘u ‘Ō‘ō cone and central-vent heights, measured by theodolite from Pu‘u Halulu at the end of each eruptive episode.

[Horizontal distance to cone determined periodically by electronic distance meter. Data for episodes 4 through 20 from Wolfe and others (1988).]

Date	Episode	Cone height (meters above pre-1983 surface)	Cone height (meters above sea level)	Vent height (meters above pre-1983 surface)	Vent height (meters above sea level)
06/17/83	4	25	744	--	--
12/01/83	12	80	799	--	--
03/04/84	16	100	819	--	--
04/21/84	18	118	837	--	--
05/18/84	19	120	839	--	--
06/08/84	20	130	849	--	--
06/31/84	21	142	861	--	--
07/09/84	22	145	864	--	--
08/21/84	24	150	869	--	--
09/20/84	25	162.5	881.5	--	--
10/28/84	--	157	876	--	--
11/05/84	26	164	883	--	--
11/20/84	27	184	903	--	--
11/28/84	--	167	886	--	--
12/04/84	28	187	906	--	--
12/30/84	--	174	893	135	854
01/04/85	29	201	920	129	848
01/17/85	--	193	912	--	--
02/05/85	30	194	913	133	852
03/15/85	31	206	925	131	850
04/22/85	32	214	933	132	851
04/29/85	--	209	928	--	--
06/13/85	33	212	931	136	855
07/07/85	34	228	947	--	--
08/09/85	35	232	951	--	--
09/03/85	36	242	961	140	859
09/25/85	37	243	962	140	859
10/21/85	38	251	970	141	860
11/29/85	39	250	969	144	863
01/02/86	40	250	969	147	866
01/28/86	41	250	969	148	867
02/23/86	42	250	969	--	--
03/22/86	43	255	974	--	--
04/14/86	44	255	974	154	873
05/08/86	45	255	974	--	--
06/02/86	46	255	974	--	--
06/27/86	47	255	974	169	888
07/19/86	48	255	974	--	--
10/06/88	48	253.5	972.5	--	--
01/17/91	48	236.5	955.5	--	--
09/17/91	48	235.5	954.5	--	--
01/13/92	48	235.5	954.5	--	--
02/02/92	48	234.5	953.5	--	--
03/25/93	53	234	953	--	--
03/04/94	53	234	953	--	--
08/11/95	53	233	952	--	--
06/27/96	53	233	952	--	--
01/09/97	53	232.5	951.5	--	--
01/31/97	54	198	917	--	--
01/18/01	55	189	908	--	--

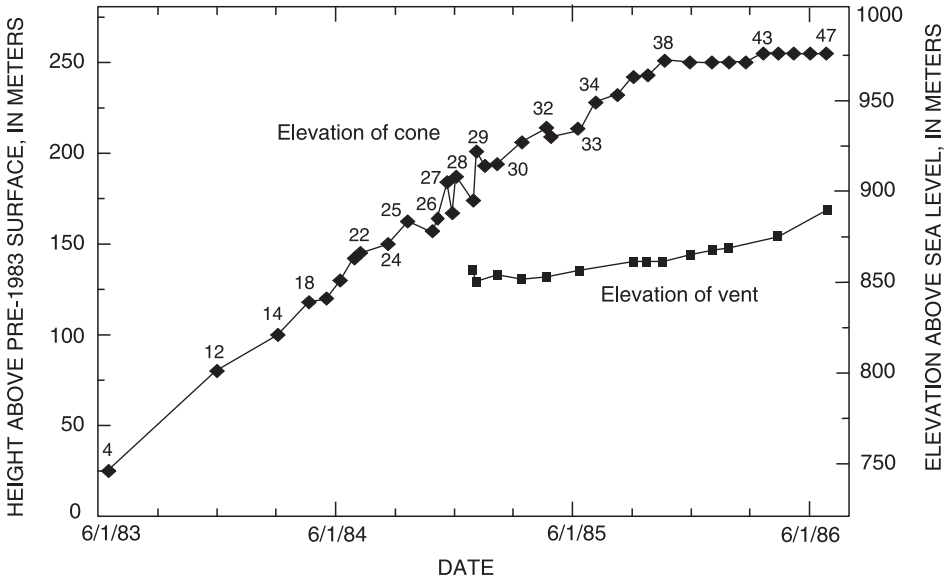

Figure 4. Growth of the Pu‘u ‘Ō‘ō cone during episodes 4 through 47, as determined by theodolite measurements from Pu‘u Halulu. Decreases in cone elevation are due to slumping of agglutinated spatter at summit soon after the end of an eruptive episode. Data from episodes 4 through 20 from Wolfe and others (1988).

fed by continuous fallout from the fountains and rootless flows fed by a discontinuous supply of spatter. Rootless flows are commonly referred to as clastogenic flows at other volcanoes, but we avoid this term to prevent confusion.

By episode 10 (October 1983), most channeled lava flows were funneled through spillways on the east side of the cone. Intense but intermittent spatter fallout on the steep north and south slopes of the cone, however, created thick, broad, rootless flows that extended as far as 3 km from the vent (Wolfe and others, 1988). Rootless flows on the west and southwest sides of the cone were short and stubby because the growing summit blocked deposition on this flank.

Some rootless flows resulted from steady accumulation of spatter near the edge of the fountain; others started after an abrupt change in fountain trajectory quickly slopped a huge load of spatter onto the rim. When fountains were highest, waves of fluid spatter intermittently spilled down the slopes. The largest rootless flows began several hours into a high-fountaining episode, after a substantial volume of agglutinated spatter had accumulated on the upper slopes of the cone.

Many remobilized spatter flows were more than 5 m thick on the upper slopes of the cone. The initial spatter deposits apparently had sufficient yield strength to impede immediate mobilization, probably because of cooling during intermittent deposition. The spatter accumulated and compacted until gravitational stress overcame the yield strength of the massive deposit.

Close to the vent, the larger rootless spatter flows consisted of thick sheets of agglutinate that became deeply fissured as the deposit began to slide (fig. 6)**.** Midway down the cone, where the slope was steepest, the sheets broke apart into a chaotic jumble of truck-size blocks. With continued movement, the blocks split into progressively smaller pieces that slid or rolled downhill; rootless flows that reached the base of the cone fanned out into lobes that resembled a typical ‘a‘ā flow but lacked flow channels (fig. 7).

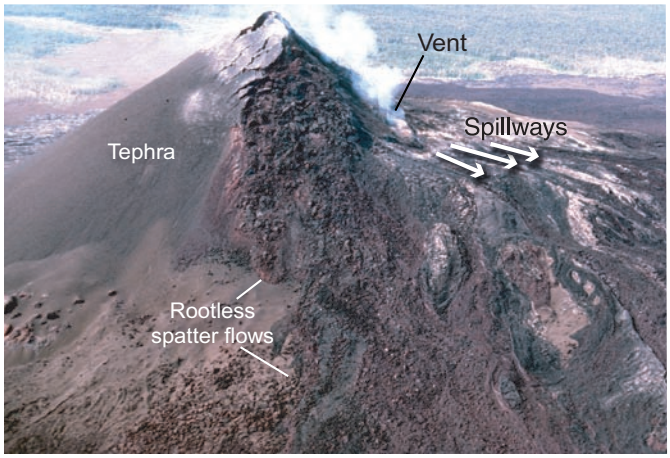

Figure 5. Pu‘u ‘Ō‘ō cone after episode 38. View northward; photograph taken by J.D. Griggs on November 12, 1985.

Figure 6. Agglutinated spatter forms deeply fissured carapace on upper slopes of Pu‘u ‘Ō‘ō cone after episode 29. View northwestward; photograph taken by G.E. Ulrich, on February 1, 1985.

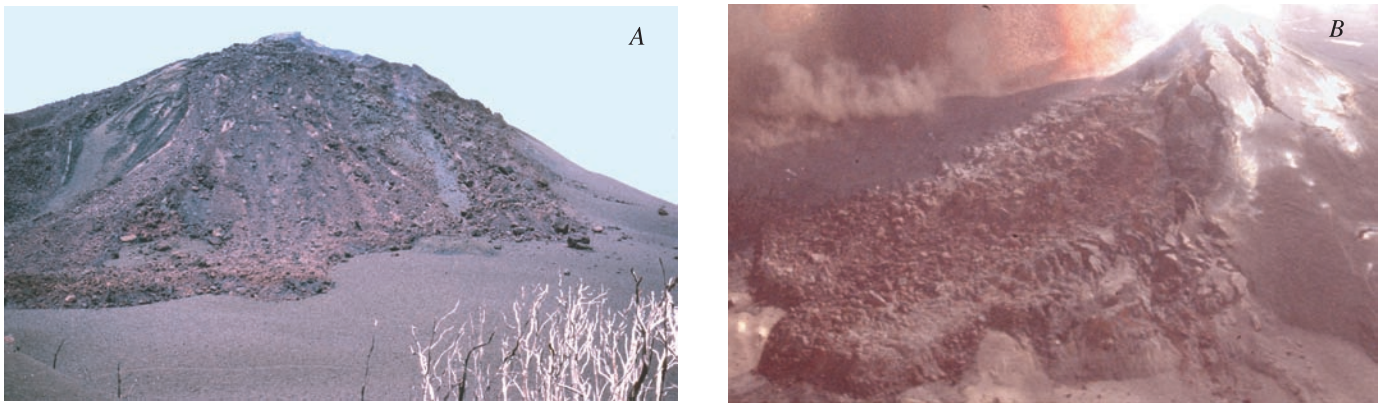

Figure 7. The Pu‘u ‘Ō‘ō cone. *A*, Rootless spatter flows on west side of cone emplaced during episode 33. Relief from top to bottom of flow is about 175 m. Photograph taken June 13, 1985. *B*, Rootless spatter flow on northwest side of cone emplaced during episode 29 (January 1985). Lobe at lower left is 11 m thick. Photograph taken by J.D. Griggs on February 4 1985.

Some rootless flows mobilized entire sectors of the rim or upper slopes of the cone, leaving conspicuous scarps in their wake. Such flows sometimes were reported as cone collapses. This terminology obscures their actual origin, however, because the flows formed during or immediately after high fountaining and mobilized deposits of still-hot agglutinate.

Several rootless flows are still exposed on the cone, although all have been beheaded by widening of the crater. The best-preserved rootless flow formed during episode 45 (May 1986) on the northwest slope of the cone. Transverse fissures, 5 m deep, cut the head of the 30-m-wide flow. Just below the deeply fissured area is an undulating, concave surface where the agglutinate slid as a single mass. At a steep break in slope, the flow broke into large blocks and ploughed aside ridges of cinder and agglutinate blocks as it advanced. Near the flow terminus, 400 m from the rim of the cone, the blocks were reduced to a size typical of ‘a‘ā. Striations are ubiquitous, both on loose blocks and on the slip surfaces that floor the deep fissures at the head of the flow (fig. 8).

Tephra

After episode 33 (June 1985), the cone’s summit, by then 75 m higher than the vent, became a barrier that prevented the thick accumulation of spatter needed to generate large rootless flows. Thereafter, except for small summit-capping rootless flows, the south and west sides of the cone were covered by a smooth blanket of unconsolidated tephra that extended 2 km southwestward of the cone. The tephra consisted predominantly of cinder lapilli but also included bombs of spatter and reticulite, as well as fine Pele’s tears and hair.

During a typical eruptive episode with northeasterly trade winds, 1 to 1.5 m of unconsolidated tephra accumulated at the southwest base of the cone and 4 to 5 m on the upper flanks. A collapse pit that later formed in this area exposed 14 m of unconsolidated tephra, a minimum final thickness of the tephra layers overlying earlier rootless spatter flows in that area.

Theodolite measurements of the cone’s height after each eruptive episode were used to estimate the accumulation rate

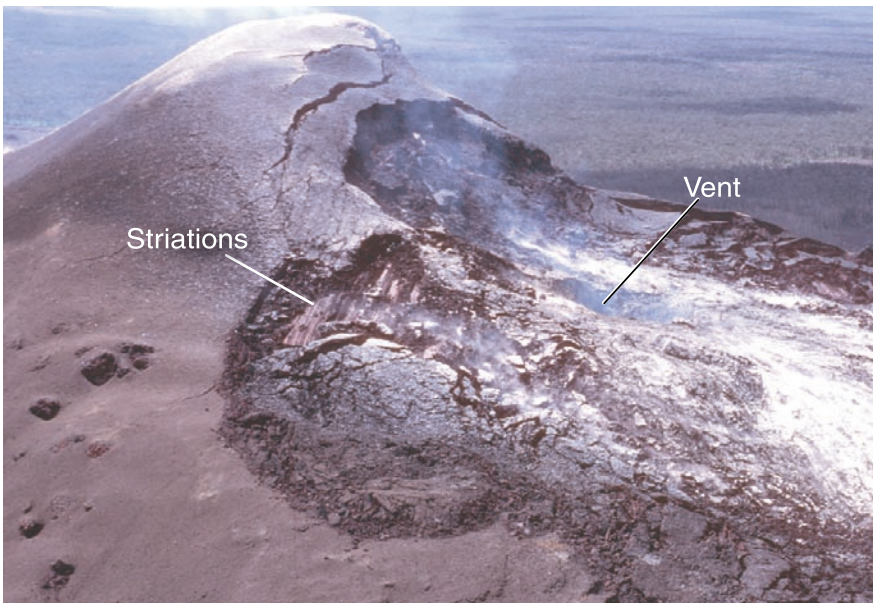

Figure 8. Striated surface on south shoulder of cone, formed by sliding mass of agglutinated spatter during or shortly after episode 30. View northwestward; photograph taken by J.D. Griggs on March 4, 1985.

Figure 9. (facing page) The Pu‘u ‘Ō‘ō crater walls on August 30, 1990. View southwestward; photograph taken by J.D. Griggs.

of fallout deposits. During three episodes, the summit grew more than 20 m in height, and the average instantaneous accumulation rate was 2 to 3 cm per minute—less than the actual rate, both because of compaction and mass flow of tephra from the summit during high fountaining.

After trade-wind-dominated episodes, clean-edged cracks, as much as 10 m wide, formed in the tephra on the summit and shoulders of the cone, parallel to the rim (figs. 5, 7*B*, 8). Observed from the air shortly after fountaining ended, the interiors of these cracks were incandescent. Investigation of similar cracks preserved on the cone reveals that they cut agglutinated deposits, capped by a thin veneer of loose cinder, and are not slumps in unconsolidated tephra. Cinder deposited on the summit and shoulders of the cone was directly exposed to the heat of the lava fountains and may have reheated enough to weld. The deposits subsequently cracked and slid, sometimes leaving striated surfaces above the vent or on the shoulders of the cone (fig. 8).

Cone Stratigraphy

When a large crater formed over the Pu‘u ‘Ō‘ō vent, strata of agglutinated spatter, lava flows, and unconsolidated tephra were exposed. The crater wall beneath the cone’s summit (since removed by collapse) displayed layers of dense gray agglutinated spatter, 1 to 3 m thick, and less dense red to brown agglutinate and unconsolidated tephra, 2 to 8 m thick (fig. 9). The gray agglutinate probably owes its color to a higher degree of compaction that prevented subsequent oxidation.

The red layers thickened beneath the summit and probably represented most of the fallout, whereas the gray layers had a more uniform thickness and were draped over successive summits. Prominent layers beneath the summit could be traced around the south crater wall, where they thinned and pinched out near the east rim. Beneath the east rim, the layers are thinner and include lava flows, as well as agglutinated spatter. Spillway positions are marked by discontinuities in the strata.

A white precipitate that coats the planar faces of the gray agglutinate makes them conspicuous and easy to trace, but the red to brown layers blend together and are impossible to identify individually from a distance. For many years, the crater walls could be viewed only from the rim, and the few available hand specimens were deposited by infrequent explosions that littered the northwest slope of the cone with lithic blocks excavated from the interior of the cone.

Part of the crater-wall stratigraphy became accessible when the west wall of the cone collapsed in 1997 to form the “West Gap” (figs. 10, 11*D*). When examined closely, some of the red units in the north wall of the West Gap prove to be sequences grading upward from 2 to 3-m thick, dark-red, moderately dense agglutinate (0.95–1.90 g/cm^3)

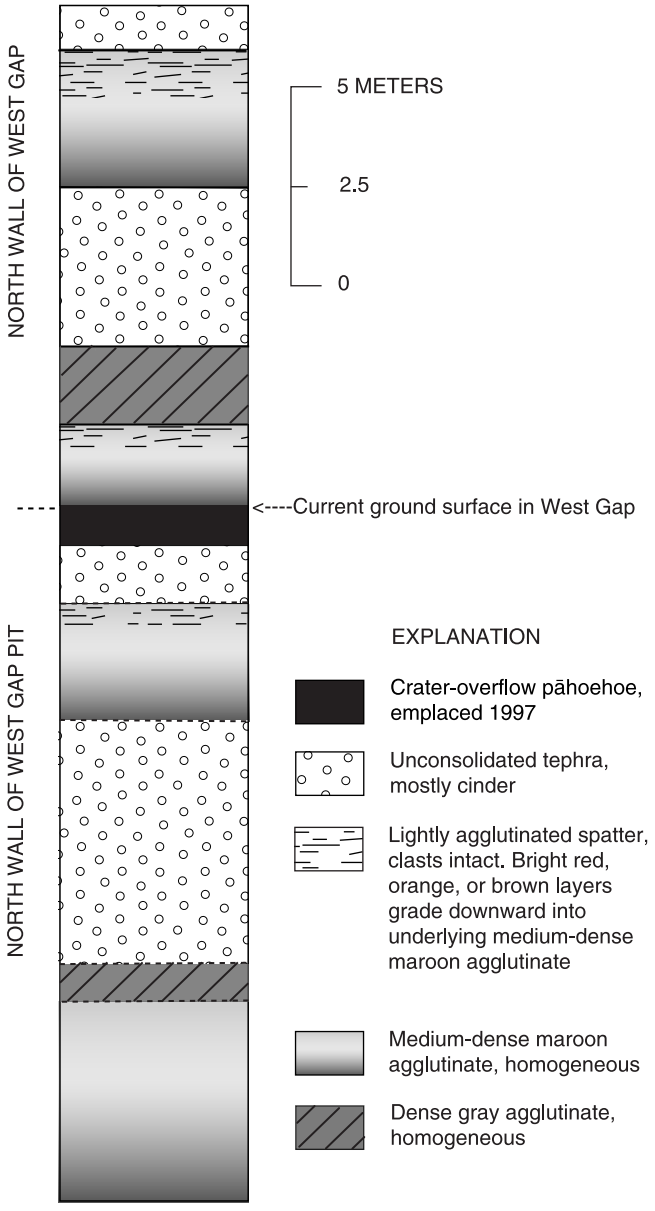

Figure 10. Stratigraphic section of north wall of West Gap in the Pu‘u ‘Ō‘ō cone. Collapse of January 1997 exposed 12.4 m of wall; enlargement of collapse pit at base of wall in September 2000 exposed an additional 17.5 m. Wall of pit is mapped from rim, and so thickness of layers is approximate. Dip of strata, 32°.

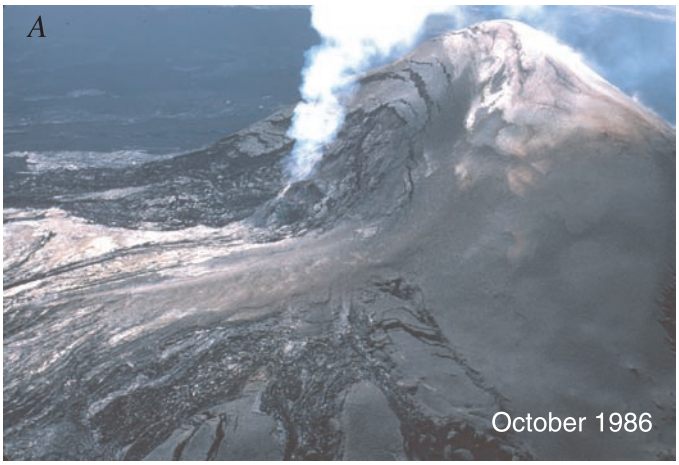

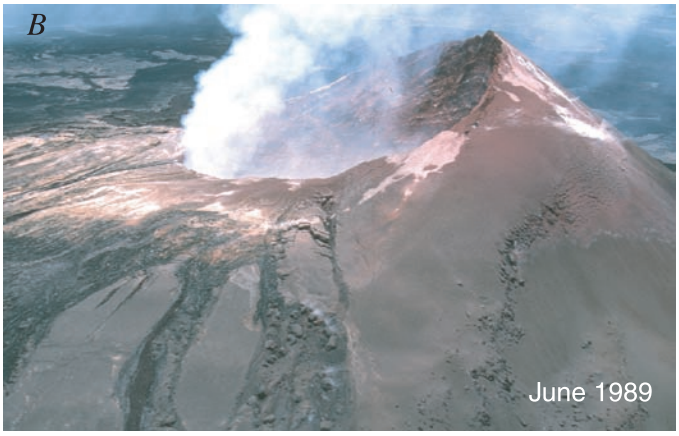

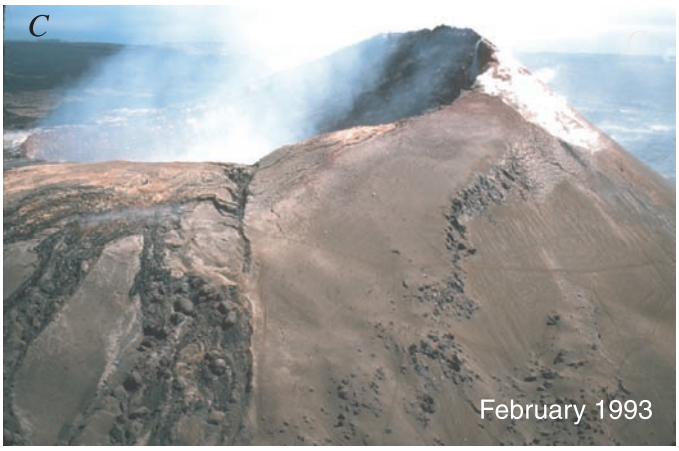

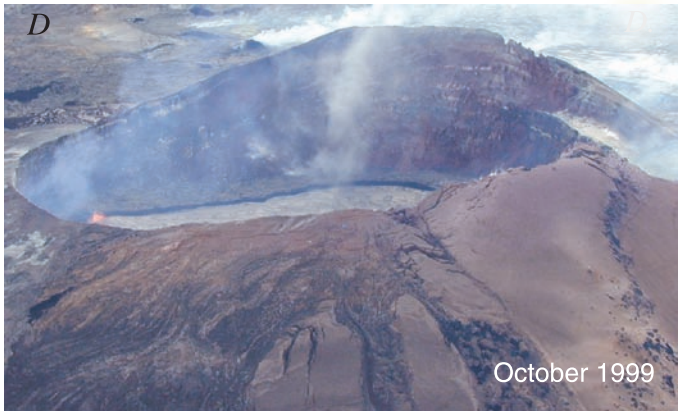

to thin, porous layers oxidized bright orange or red (fig. 10). Similar sequences are visible in rootless spatter flows on the flanks of the cone. The most voluminous component of the agglutinate sequences consists of homogeneous maroon layers with densities of about 1.5 g/cm^3. Clast outlines are rarely visible in outcrop in these layers. The porous layers capping the sequences consist of barely deformed spatter bombs sintered at the contact points with adjacent clasts. The gray agglutinate layer accessible in the wall is homogeneous in color and density (2.3 g/cm^3), except for a thin, dark-red, vesicular top.

The north wall of the West Gap (including the section exposed by an adjacent collapse pit) also includes three layers of unconsolidated tephra, 1.5 to 6 m thick, sandwiched between thick layers of agglutinated spatter (fig. 10). Each of the high fountaining episodes in 1985–86 had about the same duration and eruption rate, and so the widely varying degree of welding at this site apparently resulted from differences in fountain trajectory—which varied by as much as 15° from vertical during some eruptive episodes—and wind direction. These factors determined the size and temperature of the fallout clasts and the rate and continuity of their accumulation.

Some of the thickest gray layers are exposed beneath the southeast rim of the present-day crater, where rootless spatter flows originated during nearly every episode of high fountaining. The densest agglutinate (2.9 g/cm^3) preserved on the surface of the cone forms the basal layer of a rootless flow on the northwest flank. The basal layer was compressed and degassed as thick layers of overlying agglutinate slid across it, leaving behind grooves and striations. The denser gray agglutinate layers in the crater walls, traceable for some distance, may represent basal agglutinate units that were slip surfaces for rootless flows (for example, striated surface, fig. 8).

Volume and Bulk Density of the Cone and Its Components

The maximum volume of the Puʻu ʻŌʻō cone, approximately 136x10^{6}m^3, was estimated by digitizing the contours of the late 1986 (precollapse) cone, then using Geographic Information System (GIS) software to calculate the difference between these and the preeruption digital elevation model (DEM). A bulk density of 1.5 g/cm^3 for the cone, derived from the estimated proportion and density of its various components (table 2), was used to reduce the raw volume to a dense-rock-equivalent (DRE) volume of 67x10^{6}m^3.

Figure 11. Puʻu ʻŌʻō, showing evolution of crater. View southward. *A*, Vent is 20 m wide and topped by small spatter cone in October 1986, after shift in eruption site to Kūpaianaha. *B*, Crater is about 210 m in diameter in June 1989, after 2 years of collapse over central vent. *C*, By February 1993, crater is 240 by 320 m. *D*, Crater and West Gap (to right) in October 1999, after collapse in January 1997 removed west wall of cone. Photographs in figures 11*A* and 11*B* by J.D. Griggs.

Table 2. Estimated density of the Pu‘u ‘Ō‘ō cone and its components.

[Dense-rock equivalent density, 3 g/cm^3. Bulk density of tephra estimated by packing tephra into known volume and weighing it; bulk density of lava based on average of bulk densities for Pu‘u ‘Ō‘ō ‘a‘ā, as determined by D.J. Johnson (Wolfe and others, 1987); bulk density of agglutinated spatter based on average of density measurements on 10 samples, weighted according to estimated proportion of different types of agglutinate.]

Component	Raw volume (10^6 m^3)	Estimated percent	Bulk density (g/cm^3)	Dense-rock-equivalent volume (10^6 m^3)
Unconsolidated tephra	20	15	0.32	2.2
Lava	41	30	2.0	27
Agglutinated spatter	75	55	1.5	38
Totals	136	100		67

Our estimated raw volume is similar to that of Rowland and others (1999), who calculated a volume of 122x10^6 m^3 by subtracting the preeruption DEM volume from an airborne interferometric-radar TOPSAR DEM volume measured in 1993. Though relatively precise, the TOPSAR data have a vertical accuracy no better than ±5 m, owing to the difficulty in matching the vertical datum of pre-1983 topographic maps. Another source of uncertainty is an aspect-ratio distortion—for at least the upper part of the Pu‘u ‘Ō‘ō cone—as judged by our machine contouring of the TOPSAR DEM data provided by S.K. Rowland. A more subjective difference between our method and Rowland’s arises over the difficulty in delineating the cone’s outer boundary, which is abrupt only on the south and west flanks. Thus, the analytical uncertainty for each method is probably about 10 percent.

The estimated DRE volume of the cone is about 20 percent of the total volume of eruptive deposits produced during the 3-year period of cone growth (episodes 4–47). Lava flows predominate in the deposits beyond the base of the cone, along with a very small amount of tephra. Tephra was measured in downwind transects during episodes 25 through 34, the period of highest fountain heights and greatest fallout. During these 10 episodes, tephra volumes (DRE) ranged from 0.8 to 4.1 percent (avg of 1.9 percent) of the total volume of eruptive deposits.

End of Cone Building, July 1986

In July 1986, the conduit beneath Pu‘u ‘Ō‘ō ruptured, and fissures erupted for a day, first on the uprift, then on the downrift, side of the cone. Then, 2 days later, a new fissure opened 3 km downrift of Pu‘u ‘Ō‘ō. This fissure evolved into the Kūpaianaha shield, which became the focus of the eruption for the next 5½ years. During that time, no lava flows issued from Pu‘u ‘Ō‘ō, although ample evidence indicated that it was still linked to the magmatic conduit leading from Kīlauea’s summit reservoir to Kūpaianaha. For a year after the eruption shifted to Kūpaianaha, the Pu‘u ‘Ō‘ō vent remained incandescent, a chimney venting gases from magma on its way to Kūpaianaha. During this period, 500–1,000 t of SO_2 per day were released from Pu‘u ‘Ō‘ō (Elias and others, 1998).

The Fall of Pu‘u ‘Ō‘ō, June 1987 to Present

Central Crater Formation, 1987–92

On June 25, 1987, nearly a year after the eruption shifted to Kūpaianaha, the Pu‘u ‘Ō‘ō vent abruptly collapsed, forming a vertical-walled crater about 100 m deep and 30 to 40 m in diameter. Piecemeal collapse continued to the end of the year, when the new crater was 150 m deep. Lava appeared briefly on the floor of the new crater 3 days after the initial collapse and again at the end of 1987. For the rest of Kūpaianaha’s tenure, active lava was observed intermittently at the bottom of the Pu‘u ‘Ō‘ō crater. The cylindrical crater deepened episodically until December 1988, when it stabilized at a depth of approximately 180 m, which remained more or less constant through mid-1990. The diameter of the crater, about 200 m at the end of 1988, continued to increase gradually (fig. 11).

At the end of 1988, the volume of the Pu‘u ‘Ō‘ō crater was approximately 5.6x10^6 m^3 (table 3). The elevation of active lava on the crater floor was nearly the same as that of the Kūpaianaha lava pond; the feeding conduits at both vents were thus in hydrostatic equilibrium (figs. 12*A*,12*B*). We surmise that the crater formed as material subsided into voids created when the conduit beneath the cone drained and the eruption shifted to Kūpaianaha, 226 m lower in elevation than the Pu‘u ‘Ō‘ō vent.

Eruption Returns to Pu‘u ‘Ō‘ō, February 1992

In mid-1990, the lava pond in the Pu‘u ‘Ō‘ō crater rose to 80 m below the rim as the conduit linking Pu‘u ‘Ō‘ō and Kūpaianaha began to constrict (Mangan and others, 1995; Kauahikaua and others, 1996). Thereafter, a lava pond was nearly always present at the bottom of the crater (fig. 9). As output from Kūpaianaha steadily declined through 1991, activity within the Pu‘u ‘Ō‘ō crater intensified, and the lava pond continued to rise. In November 1991, a fissure eruption

Table 3. (facing page) The Pu‘u ‘Ō‘ō crater’s depths, dimensions, and volume of major crater-collapse events.

[Crater depths, from low point on east rim, estimated by various methods, ranging from estimates made by airborne observers to direct measurements made by lowering cable from the rim (for description, see Heliker and others, 1998a). Measurements in 1992–2002 are generally accurate to within ±5 m except during January–February 1997, with crater at its deepest and floor visible only from the air. Crater dimensions scaled from aerial photographs (asterisks) where available; crater was nearly circular through mid-1989, and so only one dimension is recorded.]

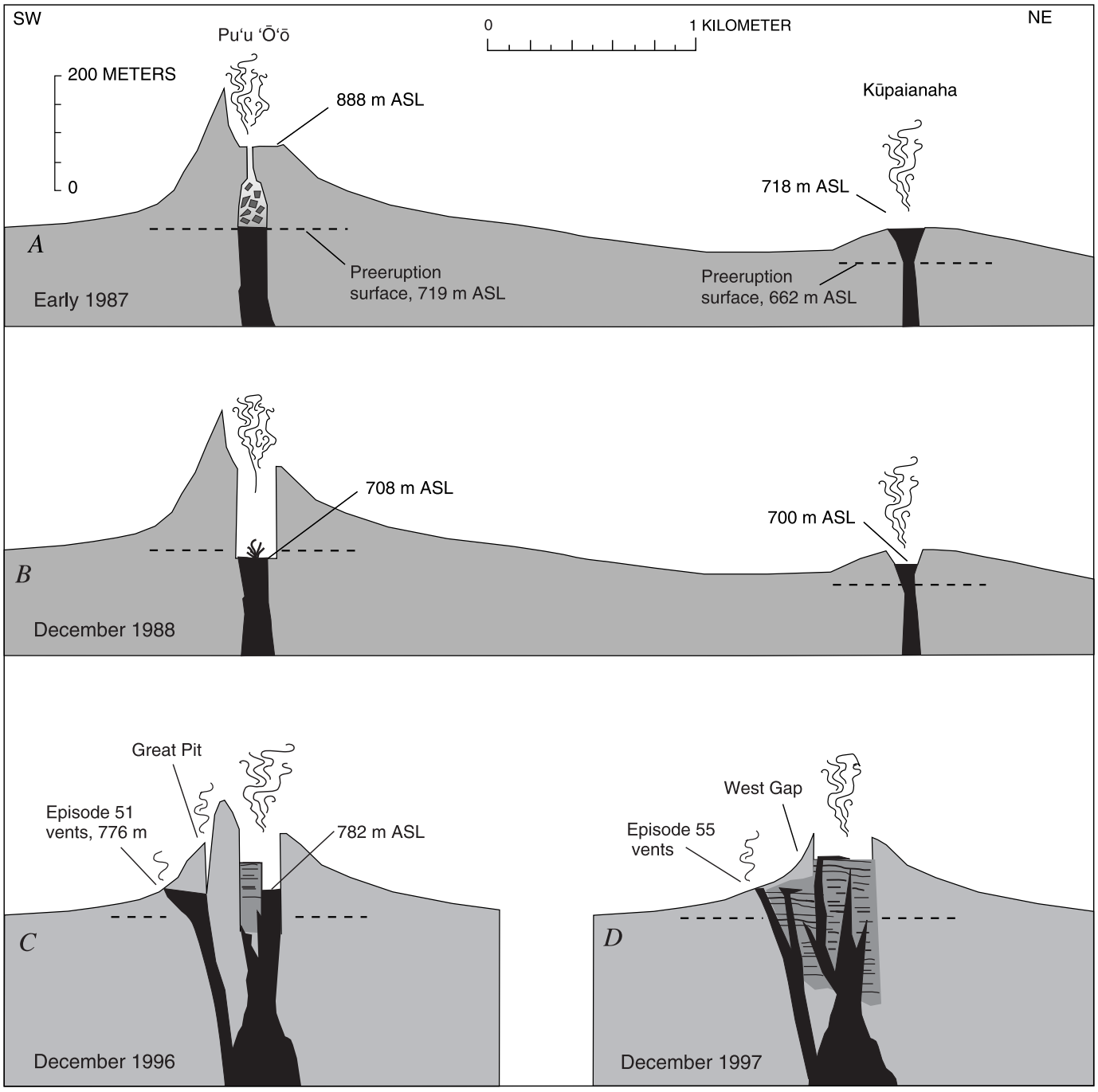

Figure 12. Schematic cross sections showing relative elevations of the Pu‘u ‘Ō‘ō crater floor, flank vents, and Kūpaianaha lava pond. Dashed line, preeruption surface. ASL, above sea level. Vertical exaggeration, 3x. *A*, In July 1986, conduit beneath Pu‘u ‘Ō‘ō fails, and eruption shifts to Kūpaianaha. Pu‘u ‘Ō‘ō is still linked to magma conduit leading from Kīlauea’s summit reservoir to Kūpaianaha. *B*, Collapse of Pu‘u ‘Ō‘ō vent begins in June 1987. Crater stabilizes in December 1988 at 180-m depth below rim. Elevation of lava in crater is nearly the same as that of Kūpaianaha lava pond. *C*, Eruption returns to Pu‘u ‘Ō‘ō in 1992, where radial fissures open on west flank of cone. Great Pit forms upslope of episode 51 vents in 1993 and expands through 1996. *D*, Crater floor and west wall of cone collapse, January 1997. Eruption resumes from episode 55 flank vents on west and south sides of cone.

Date	Crater floor (meters below rim)	Crater floor (meters above sea level)	Crater dimensions (m)	Volume of crater collapse ($10^6 m^3$)	Comments
06/25/87	100	788	30–40	--	
07/24/87	100	788	80*	--	
09/30/87	100	788	120	--	
12/03/87	150	738	150	--	
02/04/88	150	738	150*	--	
08/24/88	--	--	190*	--	
12/31/88	180	690	200	5.6	Cumulative volume of collapse, June 1987–December 1988.
04/30/89	180	690	--	--	
05/18/89	--	--	210*	--	
07/31/89	180	690		--	
08/24/89	180	690	240x210*	--	
12/31/89	180	690	--	--	
08/31/90	80	790	--	--	
12/31/90	80	790	--	--	
06/30/91	80	790	--	--	
08/31/91	40	830	--	--	
10/19/91	36	834	280x240*	--	
11/11/91	120	750	--	3.1	Crater floor collapse, episode 49.
12/23/91	57	809	--	--	
01/24/92	35	831	--	--	
03/27/92	40	826	--	--	
04/16/92	37	829	--	--	
04/24/92	36	830	--	--	
02/08/93	85	781	--	3.1	Crater floor collapse, upper east rift zone intrusion.
02/18/93	--	--	320x240*	--	
02/26/93	60	806	--	--	
10/24/94	--	--	330x240*	--	
09/05/95	60	806	--	--	
02/02/96	57	809	--	--	
06/02/96	--	--	350x240*	--	
12/01/96	60	806	--	--	
01/31/97	210	656	--	13	Crater and west wall collapse, episode 54.
02/24/97	170	696	--	--	
03/21/97	84	782	--	--	
04/01/97	57	809	--	--	
04/18/97	46	820	--	--	
04/29/97	30	836	--	--	
06/16/97	0	866	--	--	Level of pond, not floor. First of 20 crater overflows, averaging about 4 hours, during next 7 months.
07/31/97	45	821	--	--	
10/01/97	45	821	--	--	
01/01/98	30	836	--	--	
01/14/98	0	866	--	--	Level of pond, not floor. Last crater overflow.
02/07/98	30	836	400x240*	--	
03/01/98	30	836	--	--	
06/01/98	35	831	--	--	
10/22/98	40	826	--	--	
04/01/99	55	811	--	--	
09/12/99	120	746	--	<1	Partial crater floor collapse, upper east rift zone intrusion. Estimated depth to collapsed area at center crater.
09/23/99	55	811	--	--	
10/03/99	40	826	400x250*	--	
02/10/00	36	830	--	--	
01/18/01	34	832	--	--	
03/29/02	24	842	--	--	
04/25/02	12	854	--	--	
Total estimated collapse volume				25.8	

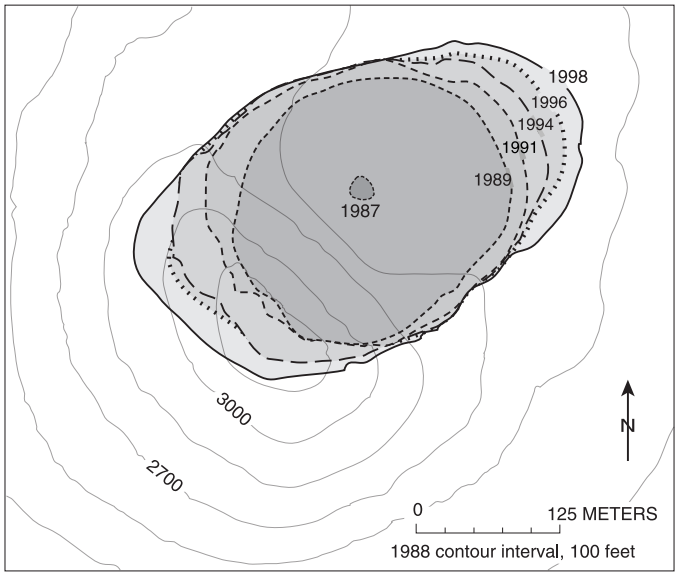

Figure 13. Evolution of the Pu‘u ‘Ō‘ō crater. Crater rims (bold outlines) traced from orthorectified aerial photographs taken from 1987 to 1998. Topographic base (prepared by Ken Hon) shows shape of cone in 1988.

(episode 49) broke out between Pu‘u ‘Ō‘ō and Kūpaianaha (Mangan and others, 1995), and the level of the Pu‘u ‘Ō‘ō lava pond dropped by 30 m. On the fourth day of the eruption, the crater floor collapsed, removing a volume of 3.1×10^6 m^3 (table 3). When the fissure eruption ended after 3 weeks, the lava pond quickly refilled and began resurfacing the talus on the crater floor with fresh pāhoehoe.

In February 1992, the Kūpaianaha vent died. Eleven days later, a radial fissure, 150 m long, opened on the uprift (west) flank of Pu‘u ‘Ō‘ō (episode 50); (Heliker and others, 1998b). Three weeks later, the fissure extended 35 m up the slope of the cone before the flank eruption localized at two main vents (episode 51 vents) at the east end of the fissure. A second fissure, 250 m to the south, was briefly active in late 1992 (episode 52). Three months later, an isolated vent (episode 53 vent) erupted near the end of the episode 52 fissure and was active for the next year.

Central Crater Slowly Widens, 1992–96

From 1992 through 1996, a lava pond was present in the Pu‘u ‘Ō‘ō crater. When full, the pond overflowed and built up the crater floor, which was generally 35 to 60 m below the east rim. The high level of the magma column buttressed the crater walls, and crater expansion was limited to (1) mass wasting of the steep wall beneath the summit and (2) undercutting of the northeast wall by the lava pond, which occupied the northeast end of the crater from January 1991 through April 1995. By these processes, the crater slowly elongated along the trend of the rift zone (fig. 13). The only large collapse of the crater between 1992 and 1996 was triggered by an upper-east-rift-zone intrusion in February 1993, when the lava pond drained and the crater floor collapsed. The volume of this collapse—3.1×10^6 m^3—was about the same as that of November 1991 (table 3).

Flank Vents Undermine Cone, 1992–96

Support for the west wall of the cone was gradually undermined by shallow subsurface magma movement associated with the flank vents. By mid-1992, the episode 51 vents were feeding directly into lava tubes, which rapidly eroded downward through the unconsolidated tephra at the base of the cone. The level of the magma column in the vents dropped in tandem with the downcutting tubes. From 1992 to 1994, the magma column feeding the active flank vents dropped 29 m (Heliker and others, 1998b), and the spatter cones that once marked the vents were consumed by collapse pits. The level of the lava pond within the central crater dropped in concert with the flank vents.

In March 1993, the “Great Pit” formed on the west flank of the cone upslope of the episode 51 flank vents (figs. 14*A*, 14*B*). Lava was intermittently visible at the bottom of the new pit, which probably formed over the east tip of the radial dike that fed the episode 51 vents. The Great Pit enlarged and coalesced with the pits over the episode 51 vents until, by the end of 1996, only a knife-edged ridge separated the composite west-flank pit from the central crater (fig. 14*C*).

Crater Expansion Resumes, Brings Down West Wall of Cone, January 1997

In January 1997, the conduit leading from the summit reservoir to Pu‘u ‘Ō‘ō depressurized as magma was diverted to an intrusion and subsequent fissure eruption (episode 54) in and near Nāpau Crater (fig. 1; Thornber and others, 1997; Owen and others, 2000). In rapid sequence, the Pu‘u ‘Ō‘ō conduit drained, the crater floor collapsed, and part of the cone’s west wall collapsed to leave a gap, 115 m wide (figs. 14*D*, 15). The crater floor dropped approximately 150 m and formed a vertical-walled crater, 210 m deep, with its floor about 65 m below the pre-1983 surface (fig. 16). The January 1997 collapse removed approximately 13×10^6 m^3 of material (table 3) and reduced the height of the cone by 34 m.

The fissure eruption in the Nāpau Crater area lasted only 1 day (Jan. 30–31) and was followed by the longest eruptive hiatus in more than 10 years. Twenty-four days passed before lava rose through the rubble on the floor of the crater, and another 31 days before flank vents resumed erupting.

Cone Burial, 1992–98

Even as the cone was diminished by ongoing collapse, its west and south flanks were being buried beneath the lava shield built by flank vents (fig. 15). The shield grew in several

discrete spurts during periods of eruptive instability (such as the first 6 months of episode 55, in 1997) characterized by shifting vent locations and frequent eruptive pauses. Both of these conditions inhibited lava-tube formation and caused short flows to stack up within 1 km of the vents. About 90 m of the southwest side of the cone disappeared beneath the rising tide of pāhoehoe, while the height of the cone dropped 68 m, owing to collapse.

In June 1997, lava flows poured from the main Pu‘u ‘Ō‘ō crater for the first time since high fountaining ended in 1986. Drain holes in the crater floor periodically clogged, and the lava pond in the crater overflowed the West Gap. Then, 2 months later, lava also overtopped the east rim of the crater, sending flows 1.5 km downrift. These brief spillovers, which continued intermittently through early 1998, plated more of the original cone surface with fresh pāhoehoe (fig. 17).

Southwest Flank Collapse, 1998–Present

A new collapse pit, Puka Nui, formed in December 1997 on the southwest flank of the cone, centered between the rim of the cone and the shield (figs. 18*A,* 18*B*). The pit was initially funnel shaped—50 m in diameter in the loose cinder at the surface, narrowing to 15 to 20 m in width where it intersected layers of agglutinate, with a small, incandescent hole at the bottom. The surface layer of cinder was approximately 20 m deep on this flank, which was along the main trajectory of windborne tephra during the high-fountaining era. As Puka Nui grew, the slope of the cone above the pit slumped into it. Puka Nui quickly assumed the shape of a broad, shallow basin, unlike the Great Pit (fig. 14*B*), where the cinder was not so deep.

Through 1998, Puka Nui expanded rapidly, by coalescing first with a new pit that formed adjacent to it on the slope of the cone, then with pits on the adjacent shield. Collapse slowed in 1999 and 2000, but expansion resumed in 2001 along the eastern margin of the pit. Several spatter cones formed inside Puka Nui during September–October 1999, and fresh lava flows resurfaced the shield part of the pit (fig. 18*C*). As of June 2002, Puka Nui is 180 by 200 m across, and headward erosion of the pit has carved a notch in the rim of the Pu‘u ‘Ō‘ō cone. A zone of circumferential cracks that extends as far as 50 m beyond the pit’s south rim (fig. 19) augurs future collapse.

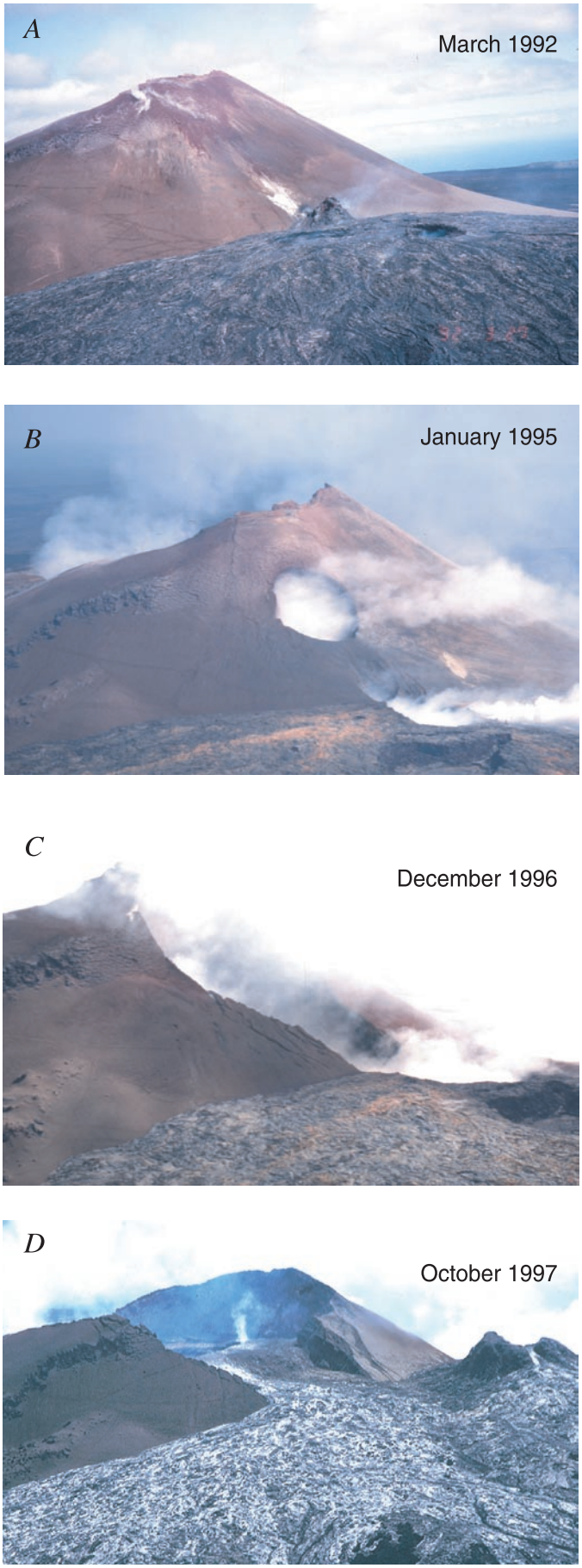

Figure 14. West flank of Pu‘u ‘Ō‘ō. *A*, Spatter cones mark episode 51 vents on west flank of cone in March 1992. *B*, “Great Pit” in January 1995. The pit began to form in early 1993 as flank-vent activity undermined slope. *C*, In December 1996, pits on cone merge with those over episode 51 vents. *D*, By October 1997, the West Gap, formed by January 1997 collapse, is coated by overflows from crater.

Beneath the Cone: the Pu‘u ‘Ō‘ō Plumbing

Previous Work

Previous models of the Pu‘u ‘Ō‘ō magmatic system were predicated on data from the initial 1983 dike emplacement at the beginning of the eruption and from the high-fountaining episodes of 1983–86. In January 1983, a dike linked to the summit reservoir was emplaced in the east rift zone. On the basis of geodetic data, estimates of the dike's dimensions ranged from ~2 to 3.5 m wide, 11.4 to 15 km long, and 2.4 to 4.4 km high (Dvorak and others, 1986; Okamura and others, 1988; Hall Wallace and Delaney, 1995). Seismicity associated with dike emplacement was centered about 2.5 km beneath Makaopuhi (fig. 1), deepening to 3.5 km below Kalalua (Klein and others, 1987). The dike ascended to intersect the surface along a 7.5-km stretch of the rift zone from Nāpau Crater to Kalalua (Wolfe and others, 1987).

After the eruption became localized at Pu‘u ‘Ō‘ō, Wolfe and others (1987, 1988) postulated that the vent was connected to the original dike by a vertical, cylindrical pipe, 38 to 66 m in diameter in its upper 1,000 m. This model, based on the volume of gas-enriched melt erupted during the highest fountains early in an episode, assumed that gas accumulates in the upper 1,000 m of the pipe. Greenland and others (1988) calculated a similar diameter (50 ±30 m) for a cylindrical pipe about 2,200 m high, on the basis of both SO_2 emissions and summit inflation during repose periods. They also calculated a volume range of 7–11x10^6 m^3 for the pipe.

Hoffmann and others (1990) used near-vent deformation measurements during high-fountaining episodes to model the shallow magma reservoir beneath Pu‘u ‘Ō‘ō as a tabular body, 2.5 km high, 1.6 km long, and 2.5 to 3 m wide, with a volume of 10 x10^6 to 12x10^6 m^3. They inferred the top of this modeled dike to be 400 m below the surface and postulated that the dike was linked to the surface by a cylindrical conduit, 20 m in diameter.

Wilson and Head (1988) argued that the shallow plumbing of Pu‘u ‘Ō‘ō, at more than a few hundred meters depth, must be planar and less than a few meters wide. They proposed, on the basis of fluid dynamics of the high-fountaining episodes, that a shallow tabular body, about 3.5 m wide, 1 km high, and 100 m long, with a volume of 7.5x10^5 m^3, was linked to the surface by a cylindrical conduit, 10 m in diameter and no more than a few hundred meters high.

In 1988, while Kūpaianaha was the active vent, Goldstein and Chouet (1994) deployed a dense array of seismometers near Pu‘u ‘Ō‘ō to model the source of volcanic tremor recorded near the cone. They determined that the tremor sources were beneath, or in close proximity to, Pu‘u ‘Ō‘ō, within an area about 400 m in diameter. They concluded that these sources, which could be resonating fluid-filled cracks or point sources, such as exploding gas bubbles in magma, were located mainly within a few hundred meters of the surface.

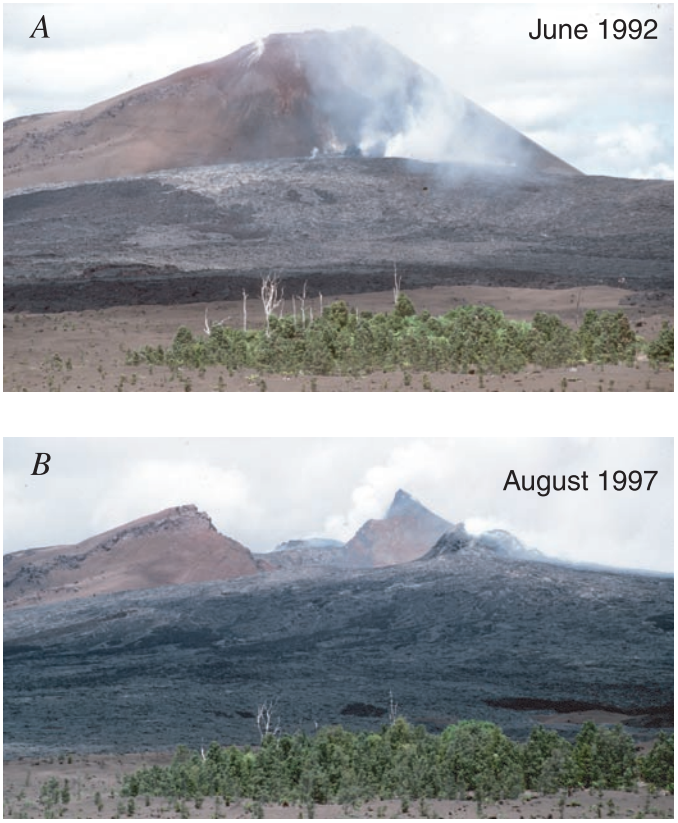

Figure 15. Pu‘u ‘Ō‘ō cone in June 1992 (*A*) and August 1997 (*B*), after collapse of west wall of cone and growth of episodes 50–55 shield. Spatter cones on shield mark episode 51 (1992) and episode 55 (1997) flank vents. Photograph in figure 15*A* taken by T.N. Mattox.

New Geophysical Evidence

Geodetic Data

In February 1999, a borehole tiltmeter (sta. POO; fig. 20*A*) was installed 1.9 km northwest of the Pu‘u ‘Ō‘ō crater. During steady eruption, this tiltmeter rarely records any changes greater than the diurnal variation in the signal. The tiltmeter has responded, however, to several short-term magmatic events, including upper-east-rift-zone intrusions and pauses in the eruption. During such events, the station POO tiltmeter generally tracked the borehole tiltmeter at Kīlauea's summit, recording inflation of the rift zone during pauses, and deflation as the eruption resumed. During the largest events recorded by station POO (the Sept. 11, 1999, and Feb. 23, 2000, intrusions), the tilt vectors pointed to a source 1.5 to 2.3 km uprift from the center of the crater (fig. 20*A*), presumably the dike leading from the summit to Pu‘u ‘Ō‘ō.

In January 2000, another borehole tiltmeter (sta. POC; fig. 20*A*) was installed on the northwest flank of the Pu‘u ‘Ō‘ō cone at about the elevation of the crater floor. This tiltmeter has proved highly responsive to short-term magmatic events, including the February 2000 upper-east-rift-zone intrusion and

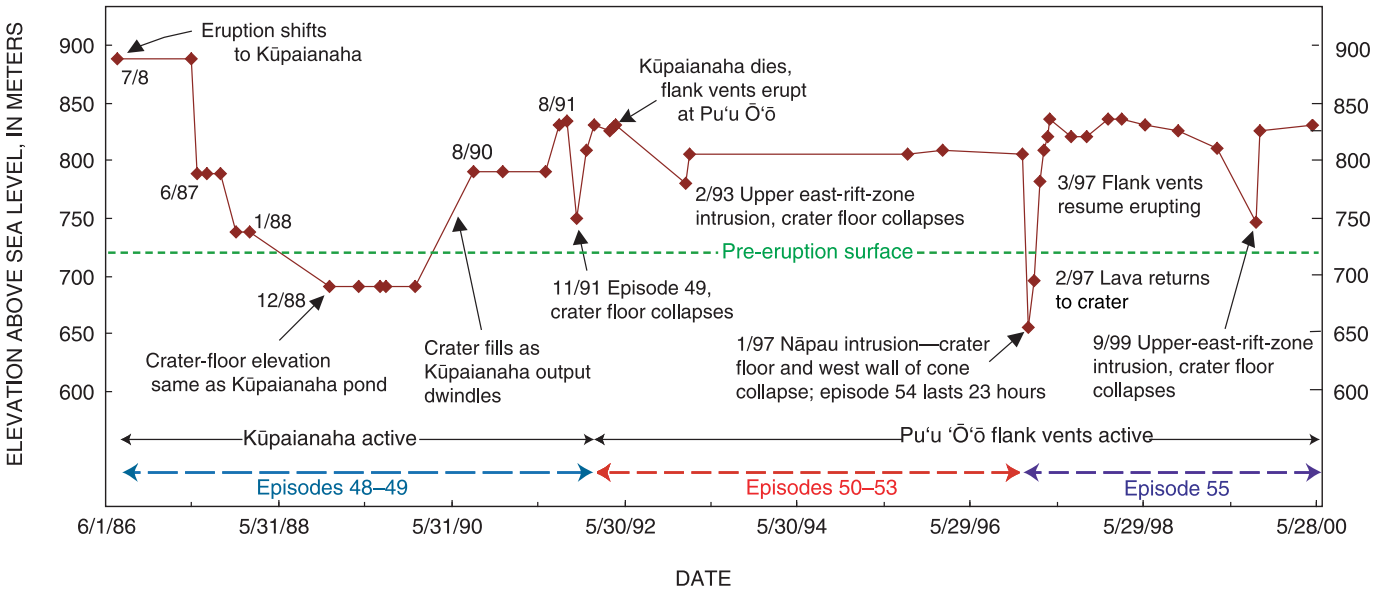

Figure 16. Timeline of Pu'u 'Ō'ō crater formation, showing crater-floor elevations from June 1986 to June 2000. Elevation of crater floor did not change significantly from June 2000 through end of 2001.

several pauses and surges in effusion rate. During such events, the azimuth of tilt ranges from 132° to 149°, pointing just west of the center of the crater. Most of the magmatic events recorded at station POC are not detected by the more distant station POO tiltmeter, which indicates that the deformation source at Pu'u 'Ō'ō is both local and shallow—probably less than 400 m below the preeruption surface.

In April 2002, a third tiltmeter (sta. POS; fig. 20*A*) was installed on the northeast flank of Pu'u 'Ō'ō, just in time to record a large magmatic event that produced a surge in effusion rate at Pu'u 'Ō'ō. The results of modeling the data from the two tiltmeters on the cone suggest a radially symmetric deformation source, approximately 250 m below the preeruption surface.

The station POC tiltmeter has recorded not only rapid tilt changes in response to short-lived magmatic events, but also long-term, quasi-steady tilting down toward the eastern side of the crater. The long-term tilt signal is corroborated by a continuously recording, single-frequency (L1) Global Positioning System (GPS) receiver installed on the northwest flank of Pu'u 'Ō'ō in 1999 (sta. L1; fig. 20*A*). The L1 station data for 2000–01 show approximately 9 cm/yr of steady subsidence relative to another GPS receiver located near the station POO tiltmeter.

A set of bench marks along the east rift zone at the Pu'u 'Ō'ō cone was surveyed in January 1998 and April 2002, using kinematic GPS and total-station methods. Vertical precision is better than 5 cm for the GPS survey and better than 1 cm for the total station data. For illustrative purposes, the along-rift locations are projected onto a line and referenced by their distance from pin 4 at the northeast end of the line (fig. 20*A*). Cumulative subsidence over the 4.3-year interval increases toward the cone and ranges from 63 to 83 cm in the crater area (north spillway to sta. L1, fig. 20*B*), corresponding to an average subsidence rate of 16 to 21 cm/yr. Maximum observed subsidence of 193 cm was found in the West Gap, an area of highly broken ground that has had a complex subsidence pattern since cone collapse in January 1997.

The long-term subsidence recorded by the two surveys and by the continuously recording instruments on the cone probably results from a combination of causes, including the cone settling under its own weight, gravitational failure of the cone's flanks, and long-term subsidence of the rift zone.

Gravity Data

Between January 1998 and February 2000, more than 100 gravity measurements—including 4 on the crater floor—were made at 84 stations within a 2-km radius of the Pu'u 'Ō'ō crater (fig. 21*A*). The elevation of each site was determined by using a combination of differential GPS measurements and total-station surveying; vertical precision ranged from 1 to 5 cm. The gravity measurements have a typical error of 25 to 30 μGal and were reduced to a standard free-air anomaly.

The densities of the cone and the surrounding lava flows erupted since 1983 are probably lower than those of most Hawaiian rocks. Detailed knowledge of the topography and density of these deposits was needed to further reduce the data to reveal subsurface structures. In 1999, much of Pu'u 'Ō'ō was surveyed with the total-station instrument. The results of the survey were used in conjunction with aerial photographs to produce a topographic map (fig. 17). The topography of areas outside this map was estimated from site elevations by using the 1993 radar DEM data of Rowland and others (1999) as a guide.

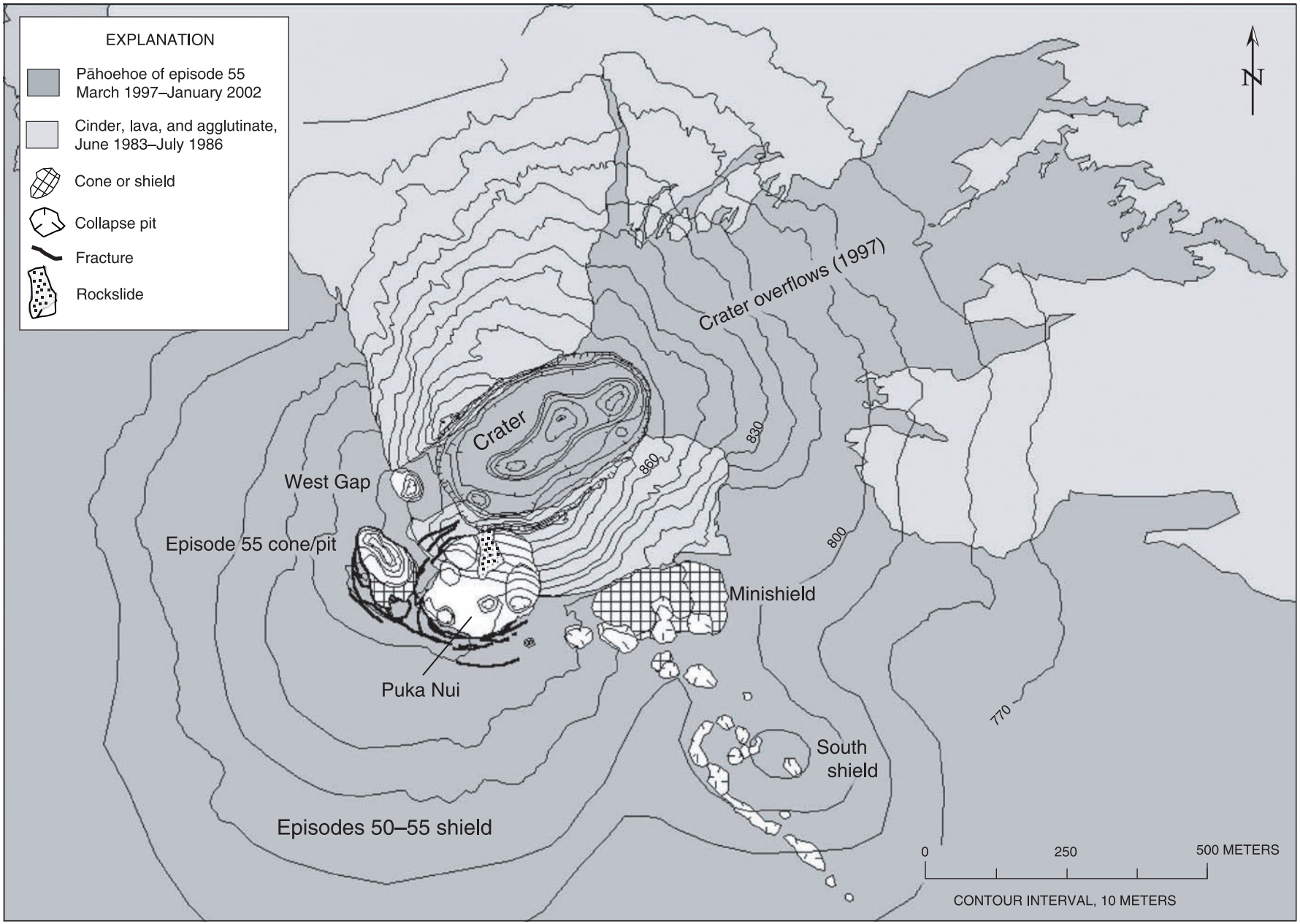

Figure 17. Map of the Pu‘u ‘Ō‘ō cone. Contours from topographic survey in 1999, using total-station data in conjunction with aerial photographs. Contours inside crater and collapse pits as of July 2001.

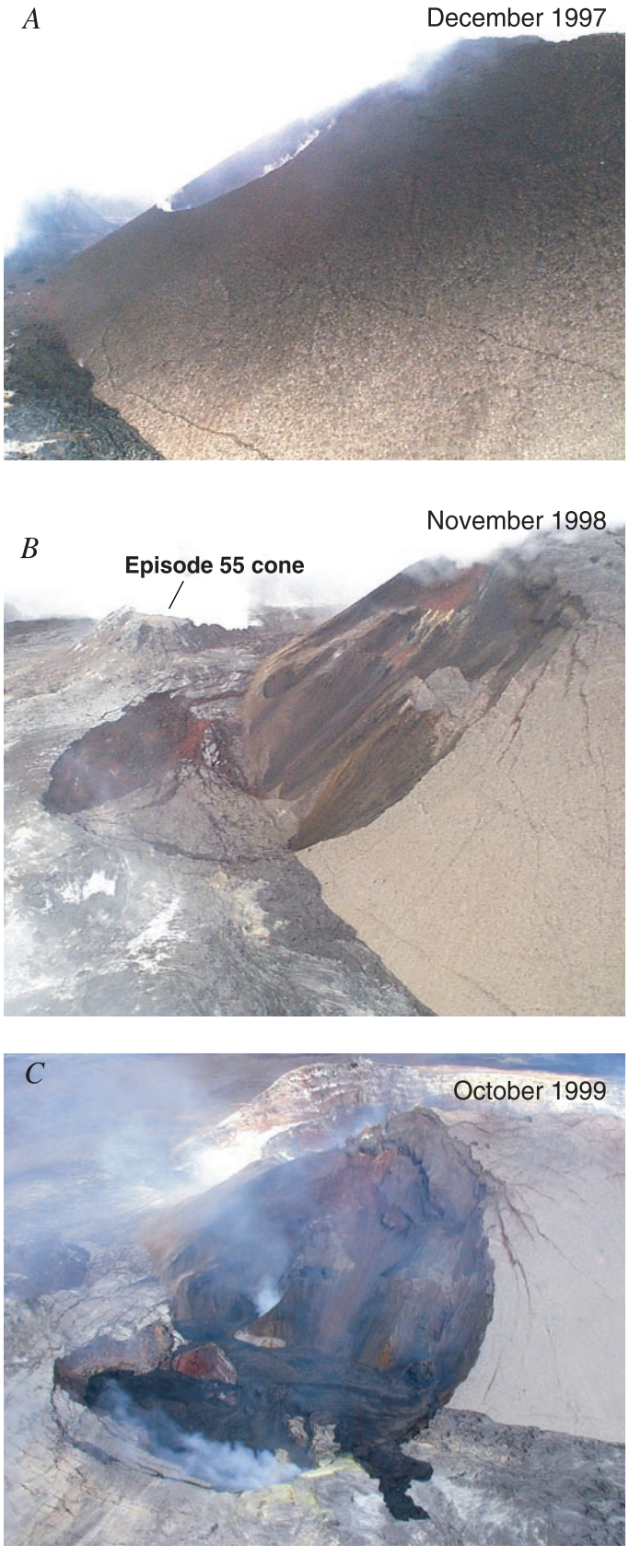

Figure 18. Southwest flank of Pu‘u ‘Ō‘ō. *A*, In December 1997, Puka Nui forms high on flank of cone. *B*, In November 1998, composite pit expands and merges with pits undermining adjacent shield. *C*, In September–October 1999, four spatter cones form inside pit, which partly fills with pāhoehoe. Small tongue of black pāhoehoe spills out of pit on lower right.

An average density of 1.50 g/cm^3 was estimated for the Pu‘u ‘Ō‘ō cone by computing the proportional density contribution from the tephra, lava flow, and agglutinate units (table 2). A density of 2.0 g/cm^3 was assumed for the shield lava flows that mantle the west and south flanks. We used these densities and the above-derived topography to compute the cone's gravitational response with the USGS computer program GRAVPOLY (Godson, 1983). The residual values computed from the formula

residual = free-air anomaly - (1.50 g/cm^3 [cone] + 2.0 g/cm^3 [shield])

are mapped in figure 21*A*. The isogal contours define two features: a chevron pattern pointing east-northeastward downrift and a narrow, oblong trough of low residuals centered over the crater south of the chevron ridge axis. The chevron pattern is an expression of the general rift-zone gravity high (see Kauahikaua and others, 2000, fig. 2). We interpret the trough to be a low-density zone, approximately 500 m wide and 1,500 m long (fig. 21*B*).

One model we can use to explain the trough is a body with a density contrast of -0.5 g/cm^3 in a volume 300 m thick, between 350 m and 650 m above sea level (70–370 m below the preeruption surface). The modeled depth range is not unique but is consistent with the shallow deformation source indicated by the tiltmeter data. The low-density zone lies within pre-Pu‘u ‘Ō‘ō lava flows—assumed to have a density of approximately 2.0 g/cm^3—giving an estimated model density of 1.5 g/cm^3.

Discussion

The Shallow Plumbing System

Roche and others (2001), in recent experimental work on crater-collapse mechanisms, modeled collapse over an underpressurized magma reservoir. In experiments using roof-aspect ratios (roof thickness/roof width) >1, they found that the initial subsidence is subsurface and noncoherent; that is, "chaotic stoping accompanies intense brecciation of the reservoir roof." Subsurface collapse over a cylindrical reservoir left a cavity capped by a stable roof. With continued subsidence, the cavity migrated upward until the surface abruptly collapsed. In their experimental model, the end result was a crater underlain by a cylinder of brecciated material occupying about twice the volume of the same material before collapse. By analogy, we can expect that, in the aftermath of the January 1997 collapse, an elongate volume of brecciated rock underlies the crater and the west wall of the cone.

The low-density trough inferred from the gravity map probably represents brecciated rock, created by repeated cone collapse, riddled with magma-filled fractures. The brecciated

rock beneath the cone originally had a density of 1.5 to 2.0 g/cm^3. If it now takes up twice its original volume, its density would be halved. In the depth range 70–370 m below the base of the cone, magma averages about 70 percent bubbles and has a density of ~0.8 g/cm^3 (Mangan and others, 1993).

The volume of material lost during the January 1997 collapse, 13x10^6 m^3, gives us a minimum for the current size of the shallow magma system at Pu‘u ‘Ō‘ō. Data from tiltmeters near and on the cone indicate that the deformation source is less than 400 m below the preeruption ground surface, with a deeper source 1.5 to 2.3 km uprift of the crater (fig. 20*A*). These observations weigh against the notion of a vertical conduit, about 50 m in diameter, extending ≥1,000 m below the crater, as postulated in earlier studies (for example, Wolfe and others, 1988). Such a conduit would probably produce a much greater tilt signal than we observe. Although the geometry of the deformation source beneath the cone remains unclear in detail, models based on tiltmeter data suggest that the source is more likely radially symmetrical than tabular.

Changing Vent Distributions

The January 1997 collapse caused significant changes in the subsurface plumbing that were reflected in the distribution of flank vents. From 1992 through 1996 (episodes 50–53), the flank vents evolved from eruptive fissures aligned along the trace of the rift zone or subparallel to it (Heliker and others, 1998b). When episode 55 began, after the January 1997 collapse, the first flank vent to erupt was at the base of the newly formed West Gap, close to the pre-collapse vents. Thereafter, eruptive activity quickly migrated southward around the cone, with lava effusion shifting back and forth among four to six vents that were not aligned along fissures (fig. 22).

As these early episode 55 vents were erupting, we debated whether they were true vents fed from below the preeruption ground surface, or rootless vents fed by a deep tube leading from vents at the base of the West Gap. No links between any of the episode 55 vents were detected by very low frequency

Figure 19. Southwest flank of Pu‘u ‘Ō‘ō and collapse features. Dashed line encloses composite collapse pit, Puka Nui; another collapse pit engulfs episode 55 cone. Concentric cracks on shield extend well beyond present pits. Photograph taken by R.P. Hoblitt on February 7, 2002.

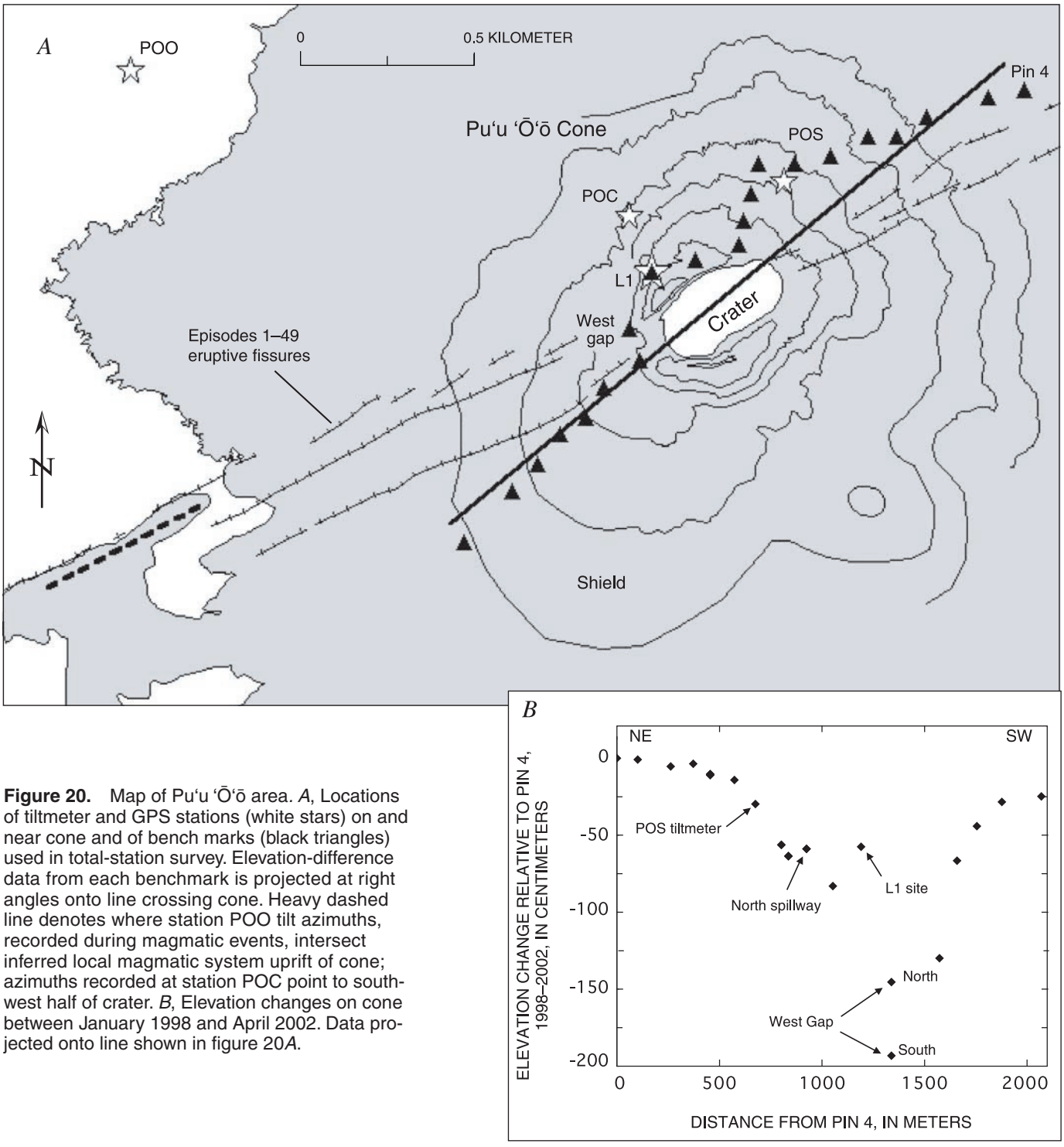

Figure 20. Map of Pu‘u ‘Ō‘ō area. *A*, Locations of tiltmeter and GPS stations (white stars) on and near cone and of bench marks (black triangles) used in total-station survey. Elevation-difference data from each benchmark is projected at right angles onto line crossing cone. Heavy dashed line denotes where station POO tilt azimuths, recorded during magmatic events, intersect inferred local magmatic system uprift of cone; azimuths recorded at station POC point to southwest half of crater. *B*, Elevation changes on cone between January 1998 and April 2002. Data projected onto line shown in figure 20*A*.

(VLF) measurements, a geoelectrical technique that can detect lava tubes a few tens of meters below the surface (Kauahikaua and others, 1996). Yet within a year, a string of collapse pits in the episodes 50–55 shield linked the West Gap with the uppermost detectable part of the lava tube feeding surface flows (figs. 19, 22). Incandescence and, rarely, moving lava have been glimpsed at the bottom of these collapse pits, but none has had the appearance of a normal skylight over a tube containing a fast-moving stream of lava.

In September–October 1999, in response to heightened pressure in the magmatic system after an 11-day pause in the eruption, five spatter cones formed within collapse pits on the southwest flank of the cone (fig. 22). Two of the spatter cones in Puka Nui arose from the collapsed wall of the Pu‘u ‘Ō‘ō cone, rather than from the shield, and so were clearly not connected to any existing lava tube.

These observations lead us to conclude that the episode 55 vents are fed by one or more dikes rather than by a shallow

lava tube. The distribution of these vents indicates that dike emplacement beneath the cone, at least at shallow levels, is no longer controlled by the tensional regime parallel to the rift zone. The arcuate trend of episode 55 vents suggests that their position is controlled by deep, concentric fracturing on the west side of the cone resulting from the catastrophic collapse of January 1997.

The distribution of vents inside the crater also was permanently disrupted by the January 1997 collapse. The lava pond that was almost continuously active from 1990 through 1996 was replaced by a succession of vents on the crater floor, apparently because the central conduit that had long fed the crater was blocked by rubble and replaced by multiple feeders.

Future Outlook for Pu‘u ‘Ō‘ō

As of mid-2002, the Pu‘u ‘Ō‘ō cone continues to collapse. Flank-vent activity on the southwest side of the cone is ongoing, and the composite collapse pit, Puka Nui, is enlarging. Another event that depressurizes the magmatic system beneath Pu‘u ‘Ō‘ō, as did the January 1997 intrusion, is almost certain to trigger collapse of the southwest wall of the cone.

To date, the cone has lost 27 percent of its original height because of collapse. On the south and west flanks, the lower third of the cone has disappeared beneath the lava shield created by multiple flank vents. If the eruption continues in the

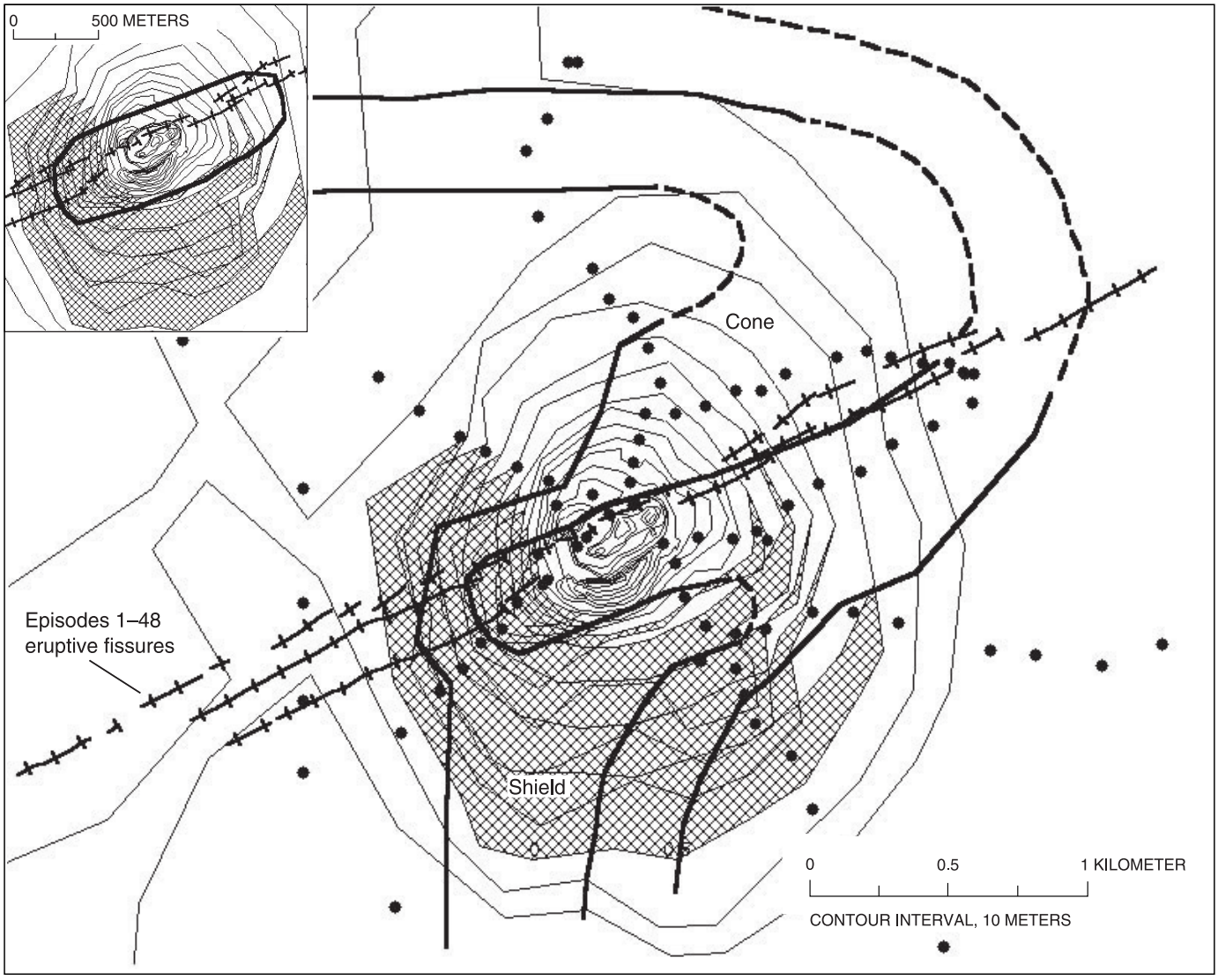

Figure 21. Gravity data on the Pu‘u ‘Ō‘ō cone and adjacent shield. Generalized 10-m elevation contours (thin lines) subdivided to assign different densities for modeling purposes. Shield is distinguished from cone by stippling. GRAVPOLY software-computed gravitational attraction model is made up of 10-m-thick slabs with vertical edges. Thick lines are 1-mGal contours of free-air anomaly minus gravitational attraction of cone (1.5 g/cm^3) and shield (2.0 g/cm^3), dashed where inferred. *Inset*, Oblong outline centered on Pu‘u ‘Ō‘ō is boundary of modeled low-density area suggested by pattern of gravity contours.

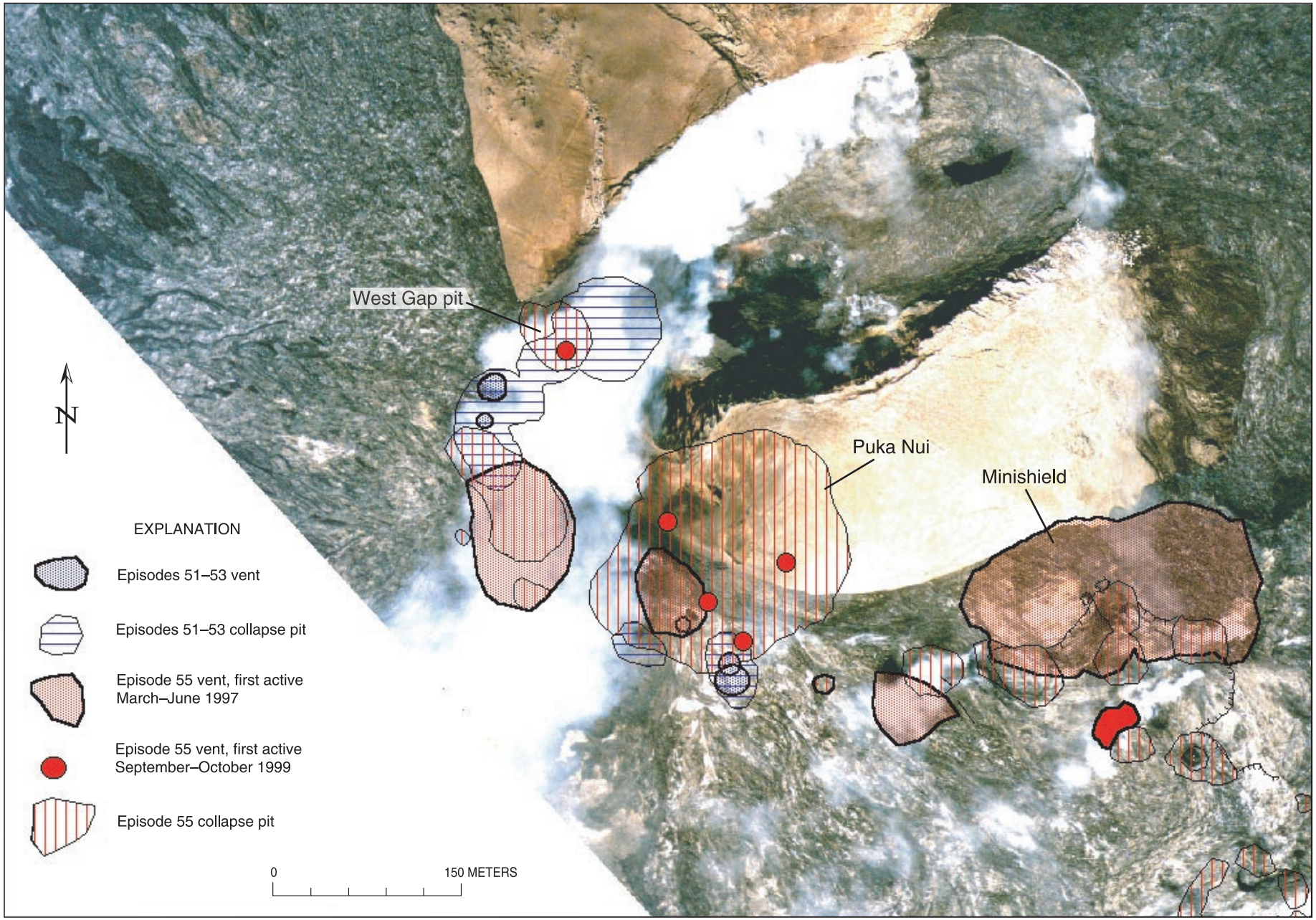

Figure 22. Episodes 51–55 vents and collapse pits on west and south flanks of Pu‘u ‘Ō‘ō superimposed on orthorectified aerial photograph taken February 1998.

same mode, Pu‘u ‘Ō‘ō will eventually evolve into a low shield with a compound crater formed by coalescence of the central-vent crater and the collapse pits on the southwest slope of the cone. The cone’s foundation of tephra, lava, and agglutinated spatter will be obscured by an overplating of pāhoehoe from crater overflows and flank vents.

Acknowledgments

We gratefully acknowledge the expertise and opinions shared by our colleagues, past and present, at the Hawaiian Volcano Observatory (HVO) and the able assistance supplied by countless volunteers and student workers. Former staff geologists George Ulrich, Ken Hon, Margaret Mangan, Tari Mattox, and Carl Thornber all contributed to collecting the data and making the interpretations presented here. Discussions in the field with Don Swanson and Maya Yasui were helpful in clarifying our thoughts about rootless spatter flows. We thank Robert Tilling and Richard Hoblitt for their careful reviews of the manuscript. During the 2 decades of this eruption, HVO has relied heavily on the exceptional skills of two helicopter pilots, David Okita and Bill Lacey III, whom we thank for all their contributions to our work.

References Cited

Dvorak, J.J., Okamura, A.T., English, T.T., Koyanagi, R.Y., Nakata, J.S., Sako, M.K., Tanigawa, W.R., and Yamashita, K.M., 1986, Mechanical response of the south flank of Kilauea volcano, Hawaii, to intrusive events along the rift systems: Tectonophysics, v. 124, no. 3–4, p. 193–209.

Elias, Tamar, Sutton, A.J., Stokes, J.B., and Casadevall, T.J., 1998, Sulfur dioxide emission rates of Kilauea Volcano, Hawaii, 1979–1997: U.S. Geological Survey Open-File Report 98–462, 40 p.

Godson, R.H., 1983, GRAVPOLY; a modification of a three-dimensional gravity modelling program: U.S. Geological Survey Open-File Report 83–346, 53 p.

Goldstein, Peter, and Chouet, B.A., 1994, Array measurements and modeling of sources of shallow volcanic tremor at Kilauea Volcano, Hawaii: Journal of Geophysical Research, v. 99, no. B2, p. 2637–2652.

Greenland, L.P., Okamura, A.T., and Stokes, J.B., 1988, Constraints on the mechanics of the eruption, chap. 5 *of* Wolfe, E.W., ed., The Puu Oo eruption of Kilauea Volcano, Hawaii; episodes 1 through 20, January 3, 1983, through June 8, 1984: U.S. Geological Survey Professional Paper 1463, p. 155–164.

Hall Wallace, M.K., and Delaney, P.T., 1995, Deformation of Kilauea volcano during 1982 and 1983; a transition period: Journal of Geophysical Research, v. 100, no. B5, p. 8201–8219.

Head, J.W., III, and Wilson, Lionel, 1989, Basaltic pyroclastic eruptions; influence of gas-release patterns and volume fluxes on fountain structure, and the formation of cinder cones, spatter cones, rootless flows, lava ponds and lava flows: Journal of Volcanology and Geothermal Research, v. 37, no. 3–4, p. 261-271.

Heliker, C.C., Mangan, M.T., Mattox, T.N., and Kauahikaua, J.P., 1998a, The Puʻu ʻŌʻō-Kūpaianaha eruption of Kīlauea, November 1991–February 1994; field data and flow maps: U.S. Geological Survey Open-File Report 98–103, 10 p., 2 sheets, scale 1:50,000.

Heliker, C.C., Mangan, M.T., Mattox, T.N., Kauahikaua, J.P., and Helz, R.T., 1998b, The character of long-term eruptions; inferences from episodes 50–53 of the Pu‘u ‘Ō‘ō-Kūpaianaha eruption of Kīlauea Volcano: Bulletin of Volcanology, v. 59, no. 6, p. 381–393.

Hoffmann, J.P., Ulrich, G.E., and Garcia, M.O., 1990, Horizontal ground deformation patterns and magma storage during the Puu Oo eruption of Kilauea volcano, Hawaii; episodes 22–42: Bulletin of Volcanology, v. 52, no. 6, p. 522–531.

Kauahikaua, J.P., Hildenbrand, T.G., and Webring, M.W., 2000, Deep magmatic structures of Hawaiian volcanoes, imaged by 3D gravity models: Geology, v. 28, no. 10, p. 883–886.

Kauahikaua, J.P., Mangan, M.T., Heliker, C.C., and Mattox, T.N., 1996, A quantitative look at the demise of a basaltic vent; the death of Kupaianaha, Kilauea Volcano, Hawai‘i: Bulletin of Volcanology, v. 57, no. 8, p. 641–648.

Klein, F.W., Koyanagi, R.Y., Nakata, J.S., and Tanigawa, W.R., 1987, The seismicity of Kilauea’s magma system, chap. 43 *of* Decker, R.W., Wright, T.L., and Stauffer, P.H., eds., Volcanism in Hawaii: U.S. Geological Survey Professional Paper 1350, v. 2, p. 1019–1185.

Mangan, M.T., Cashman, K.V., and Newman, Sally, 1993, Vesiculation of basaltic magma during eruption: Geology, v. 21, no. 2, p. 157–160.

Mangan, M.T., Heliker, C.C., Mattox, T.N., Kauahikaua, J.P., and Helz, R.T., 1995, Episode 49 of the Pu‘u ‘O‘o-Kupaianaha eruption of Kilauea volcano—breakdown of a steady-state eruptive era: Bulletin of Volcanology, v. 57, no. 2, p. 127–135.

Okamura, A.T., Dvorak, J.J., Koyanagi, R.Y., and Tanigawa, W.R., 1988, Surface deformation during dike propagation, chap. 6 *of* Wolfe, E.W., ed., The Puu Oo eruption of Kilauea Volcano, Hawaii; episodes 1 through 20, January 3, 1983, through June 8, 1984: U.S. Geological Survey Professional Paper 1463, p. 165–182.

Owen, S.E., Segall, Paul, Lisowski, Michael, Miklius, Asta, Murray, Michael, Bevis, M.G., and Foster, James, 2000, January 30, 1997 eruptive event on Kilauea Volcano, Hawaii, as monitored by continuous GPS: Geophysical Research Letters, v. 27, no. 17, p. 2757–2760.

Roche, Olivier, van Wyk de Vries, Benjamin, and Druitt, T.H., 2001, Sub-surface structures and collapse mechanisms of summit pit craters: Journal of Volcanology and Geothermal Research, v. 105, no. 1, p. 1–18.

Rowland, S.K., MacKay, M.E., and Garbeil, Harold, 1999, Topographic analyses of Kīlauea Volcano, Hawai‘i, from interferometric airborne radar: Bulletin of Volcanology, v. 61, no. 1, p. 1–14.

Smith, G.A., Florence, P.S., Castrounis, M.L., Luongo, Mark, Moore, J.D., Throne, John, and Zelley, Karin, 1999, Basaltic

near-vent facies of Vulcan cone, Albuquerque volcanoes, New Mexico, *in* Pazzaglia, F.J., and Lucas, S.G., Albuquerque geology: New Mexico Geological Society Guidebook, v. 50, p. 211–219.

Sparks, R.S.J., and Pinkerton, Harry, 1978, Effect of degassing on rheology of basaltic lava: Nature, v. 276, no. 5686, p. 385–386.

Sumner, J.M., 1998, Formation of clastogenic lava flows during fissure eruption and scoria cone collapse; the 1986 eruption of Izu-Oshima Volcano, eastern Japan: Bulletin of Volcanology, v. 60, no. 3, p. 195–212.

Thornber, C.R., Sherrod, D.R., Heliker, C.C., Kauahikaua, J.P., Trusdell, F.A., Lisowski, Michael, and Okubo, P.G., 1997, Kilauea's ongoing eruption; Nāpau Crater revisted after 14 years [abs.]: Eos (American Geophysical Union Transactions), v. 78, no. 17, supp., p. S329.

Wilson, Lionel, and Head, J.W., III, 1988, Nature of local magma storage zones and geometry of conduit systems below basaltic eruption sites; Puʻu ʻOʻo, Kilauea east rift, Hawaii, example: Journal of Geophysical Research, v. 93, no. B12, p. 14785–14792.

Wolfe, E.W., Garcia, M.O., Jackson, D.B., Koyanagi, R.Y., Neal, C.A., and Okamura, A.T., 1987, The Puu Oo eruption of Kilauea Volcano, episodes 1–20, January 3, 1983, to June 8, 1984, chap. 17 *of* Decker, R.W., Wright, T.L., and Stauffer, P.H., eds., Volcanism in Hawaii: U.S. Geological Survey Professional Paper 1350, v. 1, p. 471–508.

Wolfe, E.W., Neal, C.A., Banks, N.G., and Duggan, T.J., 1988, Geologic observations and chronology of eruptive events, chap. 1 *of* Wolfe, E.W., ed., The Puu Oo eruption of Kilauea Volcano, Hawaii; episodes 1 through 20, January 3, 1983, through June 8, 1984: U.S. Geological Survey Professional Paper 1463, p. 1–97.

Wolff, J.A., and Sumner, J.M., 2000, Lava fountains and their products, *in* Sigurdsson, Haraldur, Houghton, B.F., McNutt, S.R., Rymer, Hazel, and Stix, John, eds., Encyclopedia of volcanoes: San Diego, Calif., Academic Press, p. 321–329.

Correlation Between Lava-Pond Drainback, Seismicity, and Ground Deformation at Pu‘u ‘Ō‘ō

By Stephen R. Barker, David R. Sherrod, Michael Lisowski, Christina Heliker, *and* Jennifer S. Nakata

Abstract

The crater of Pu‘u ‘Ō‘ō, a vent along Kīlauea Volcano’s east rift zone on the island of Hawai‘i, is occupied periodically by a lava pond. During the 50 days from September 30 to November 19, 1999, pond activity comprised periods of slow filling and rapid drainback. Pond filling typically occurred without measurable changes in seismicity or ground deformation. In contrast, the beginning of each drainback event was closely matched by heightened seismic tremor, as measured by a seismometer 2 km west-southwest of the lava pond. Intensified tremor typically continued after the end of visible drainback, lasting another 45–90 minutes before tremor returned to background level. Ground deformation, monitored by a borehole tiltmeter 1.8 km northwest of the lava pond, also correlated with pond drainback. The onset and cessation of local inflationary tilt more or less coincided with the beginning and completion of pond drainback.

Lava-pond filling is thought to be due to vesiculation within the magma column beneath the vent. The magma column expands, but pressurization within the system is minimized, owing to the free surface at the top of the column. Pond drainback is initiated by an abrupt release of gas at the vent orifice as vesiculation proceeds sufficiently to shred through the magma column. Within seconds, the downpipe flow of ponded lava occludes the conduit and inhibits gas escape. Pressurization increases until the vent clears, a cycle recorded by the tiltmeter as short-lived inflation, lasting only as long as is needed to drain the pond. The common absence of a lava pond for much of the time since 1997 suggests that systemic permeability in the Pu‘u ‘Ō‘ō edifice has increased, likely by stoping of the cone. Cycles of pond filling and drainback may occur when the system is resealed by infiltrating magma.

Setting

Kīlauea, one of the world’s most active volcanoes, has been in a state of near-constant eruption since 1983 (for example, Wolfe and others, 1988; Mangan and others, 1995; Garcia and others, 1996; Heliker and others, 1998). Tholeiitic basaltic melt generated by hotspot processes is supplied to a magma chamber 1 to 4 km beneath the volcano’s summit (Klein and others, 1987; Dawson and others, 1999). From there it travels 20 km through a shallow dike system along the east rift zone to the currently active vent, Pu‘u ‘Ō‘ō (fig. 1). From this vent, lava is more or less at the land’s surface, flowing downslope through lava tubes to the ocean or periodically spilling from the tubes to form pāhoehoe and ‘a‘ā flows.

In this chapter we describe events that occurred between September 30 and November 19, 1999, a period when a lava pond intermittently filled and drained within the crater of Pu‘u ‘Ō‘ō. During this time, a remote-surveillance camera monitored lava-pond activity, and nearby geophysical instruments monitored ground deformation and seismicity; the instruments provided records that correlate closely with lava-pond activity.

Pu‘u ‘Ō‘ō’s crater is elliptical, about 240 by 400 m in diameter (figs. 1, 2); its long axis parallels the east rift zone. From late September 1999 until January 2002, the crater’s main floor remained about 35 m below the lowest crater-rim points. Inset into the floor during much of that time was an irregular elongate trough 285 m long and about 15 to 20 m deeper than the main crater floor. Through early 2000, this trough filled periodically to form a lava pond. Depth from the crater rim to the main crater floor shallowed only slightly as a few thin lava flows partly mantled the crater floor during overflow from the trough. The lava level from the main crater floor to the floor of the central trough subsided gradually after the trough was emptied.

During periods of pond activity, vesicular lava issued from vents at the east end of the trough and spread uprift to the west, flooding the trough to form a pond with a volume of as much as 4.2×10^5 m^3. Typically lava in the pond drained into the vent orifice after partly or completely filling the trough; more rarely it overflowed the trough to add a new coating to the main crater floor. The influx of lava and filling of the pond was commonly a steady, lengthy process, but drainback generally occurred abruptly and rapidly, in events typically lasting 20–50 minutes. During heightened activity, the complete filling-and-draining cycle varied from tens of minutes to several hours; at other times, the lava pond remained empty and essentially inactive for periods of 24 hours or more.

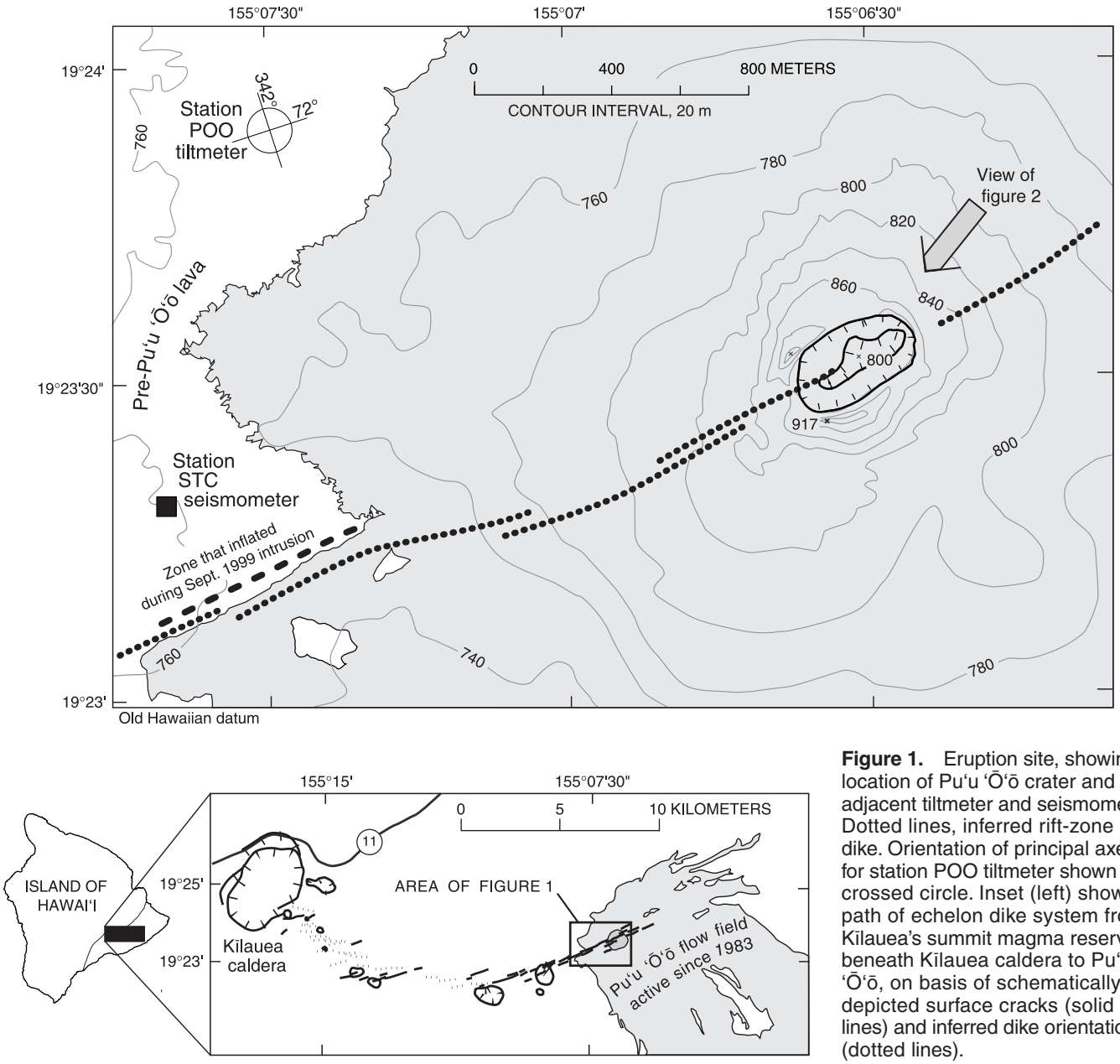

Figure 1. Eruption site, showing location of Pu'u 'Ō'ō crater and adjacent tiltmeter and seismometer. Dotted lines, inferred rift-zone dike. Orientation of principal axes for station POO tiltmeter shown by crossed circle. Inset (left) shows path of echelon dike system from Kīlauea's summit magma reservoir beneath Kīlauea caldera to Pu'u 'Ō'ō, on basis of schematically depicted surface cracks (solid lines) and inferred dike orientations (dotted lines).

Monitoring Equipment and Results for 1-Day Sampling Periods

Remote-Surveillance Camera

Lava-pond activity in Pu'u 'Ō'ō's crater was monitored visually by a remote-surveillance camera that transmitted digital images to the Hawaiian Volcano Observatory (HVO; Thornber, 1997). This camera system is the latest stage in a lengthy history of monitoring that has included time-lapse 8-mm movie cameras and, more recently, video camcorders placed on the vent's rim (fig. 2). In its 1999 configuration, the remote-surveillance camera received images about once every 5–10 s. An image-storing cycle occurred every 5 minutes, when 2 to 20 images were collected during a 1–minute interval. Thus, the approximate error when ascribing times to filling and drainback events that began between image-storing cycles was about 2.5–3.0 minutes.

Although fume, fog, or rain obscured the view of the lava pond in some images, these conditions were surprisingly sparse during the period of interest. Apparently enough heat was generated by active lava that steam was unable to condense or was driven off as updrafts ventilated the crater. Thus, if the pond was active, incandescent lava could commonly be seen in the images. Electronic failure at the camera site or in the image-processing software prevented the logging of images from October 7 to14 (UTC Julian days 280.5–287.9), 7 days of the 50-day period discussed here.

The near-constant depth of the drained central trough during October and November 1999 allows us to describe the depth of the lava pond by reference to its height below the main crater floor (from –1 m when full to –20 m when empty). For ease of representation, overflows onto the main floor were assigned heights between +3 and +5 m, depending on their thickness on the crater floor. The sequence and magnitude of 1 day's pond-filling events are listed in table 1, and the results for three representative days are plotted in figure 3.

Near-Vent Seismometer

Since August 7, 1985, a high-gain, short-period seismometer has operated at a site known as Steam Cracks (sta. STC, fig. 1), 2 km west-southwest of Pu‘u ‘Ō‘ō. The station STC seismic record has been dominated by shallow-source tremor.

For the period September 30–November 19, 1999, an analysis of tremor variations was performed manually on analog printouts from the station STC seismometer by identifying times when distinctly higher amplitude tremor was superimposed upon a varying level of background tremor, forming banded tremor (fig. 4). The well-defined periods of increased tremor, which commonly lasted 0.5–2 hours, correlated closely with pond-drainback events (figs. 3*A*, 3*B*). (Pond filling lacked noticeable tremor.) Typically, high-amplitude tremor began at the onset of pond drainback, persisted throughout the drainback event, and continued for as much as 30–45 minutes after the end of visible drainback. Tremor for different events could begin a few minutes before, coincident with, or a few minutes after the start of drainback (table 1).

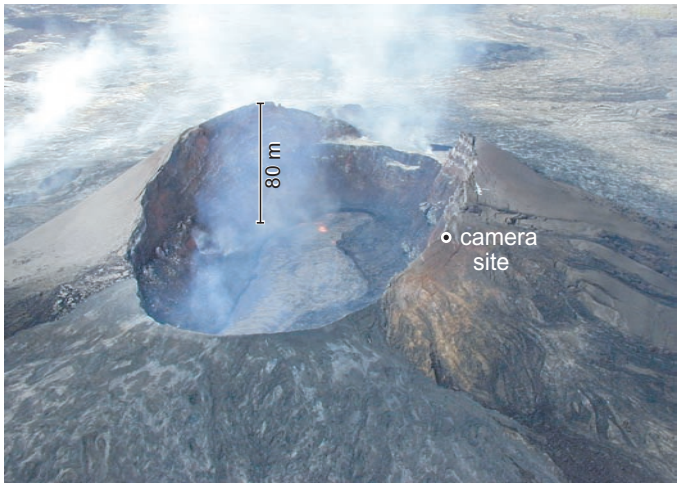

Figure 2. Pu‘u ‘Ō‘ō crater and central trough holding active lava pond on crater floor. View orientation is indicated in figure 1. Crater, 400 m long by 240 m wide, has floor 35 m below low point on west rim and about 80 m below rim's highest point on south (left) side. View southwestward; photograph taken October 12, 1999.

This variability may stem from the relatively large imprecision associated with camera observations, probably the greatest weakness in the data set.

The banded tremor that we used for correlation with the video-camera data required low background tremor for its recognition. When other sources of high-amplitude tremor dominated the seismic record, the high-amplitude signal of banded

Table 1. Start and finish times for pond filling and drainback, high-amplitude seismic tremor, and abrupt inflationary tilt during a 24-hour period in 1999.

[Day is UTC Julian day 294, shown here as local time 1400 H.s.t. October 20 to 1400 H.s.t. October 21. Dashes denote events for which no banded tremor was present or, for tilt, no inflationary event occurred (see fig. 3*A*)]

	Drainback event			Banded tremor			Abrupt inflation		
Event	Start	Finish	Duration	Start	Finish	Duration	Start	Finish	Duration
October 20									
1	1436	1501	0:25	1445	1530	0:45	1430	1500	0:30
2	1551	1616	0:25	--	--	--	1550	1630	0:40
3	1736	1827	0:51	1730	1830	1:00	1730	1830	1:00
4	1951	2031	0:40	2000	2100	1:00	2000	2030	0:30
5	2141	2206	0:25	--	--	--	--	--	--
6	2231	2247	0:16	2230	2330	1:00	2230	2300	0:30
7	2331	2351	0:20	--	--	--	2330	2350	0:20
October 21									
8	0336	0401	0:25	0330	0415	0:45	0330	0400	0:30
9	0436	0456	0:20	0445	0530	0:45	0440	0500	0:20
10	0641	0711	0:30	0645	0745	1:00	0640	0710	0:30
11	1011	1100	0:49	1015	1145	1:30	1010	1100	0:50
12	--	--	--	1300	1400	1:00	1300	1340	0:40

tremor was obscured. For example, at 0930 H.s.t. on November 8, tremor amplitude increased substantially and remained high for 42 hours (fig. 3*C*). This period of high background tremor overwhelmed most or all of the component of tremor originating from drainback events. During this and similar periods, pond drainback and tilt correlated well, but tremor correlation was difficult to determine, owing to the high background signal.

Shallow Borehole Tiltmeter

In February 1999 an Applied Geomechanics 722 tiltmeter was installed 1.8 km northwest of Pu‘u ‘Ō‘ō (sta. POO, fig. 1). The borehole tiltmeter was positioned at 4.2-m depth (14 ft). Its dynamic range, precision, and accuracy were about 250, 0.002, and 0.02 µrad, respectively. Data were gathered every minute and relayed back to HVO at 10-minute intervals. The tiltmeter performed flawlessly, providing a complete record for the period September 30–December 1, 1999.

The horizontal axes of the tiltmeter were oriented north-northwest and east-northeast, the *y*-axis toward azimuth 342° and the *x*-axis toward azimuth 072° (fig. 1). The largest events recorded at station POO since its installation have been dike intrusions on September 11, 1999, and February 23, 2000. During these events, the axis of greatest response recorded inflation south-southwest at azimuth 192°, toward a source along the east rift zone about 2.3 km uprift of Pu‘u ‘Ō‘ō crater (fig. 1). After about 30 minutes during the September 11 event, this axis rotated counterclockwise 30°, pointing south-southeast at azimuth 167°, 1.5 km uprift of the crater. These results probably define a part of the rift-zone dike that supplies magma to Pu‘u ‘Ō‘ō. The dike commonly responds to large changes in pressurization and, possibly, even to the small changes that resulted from the drainback events of October and November 1999.

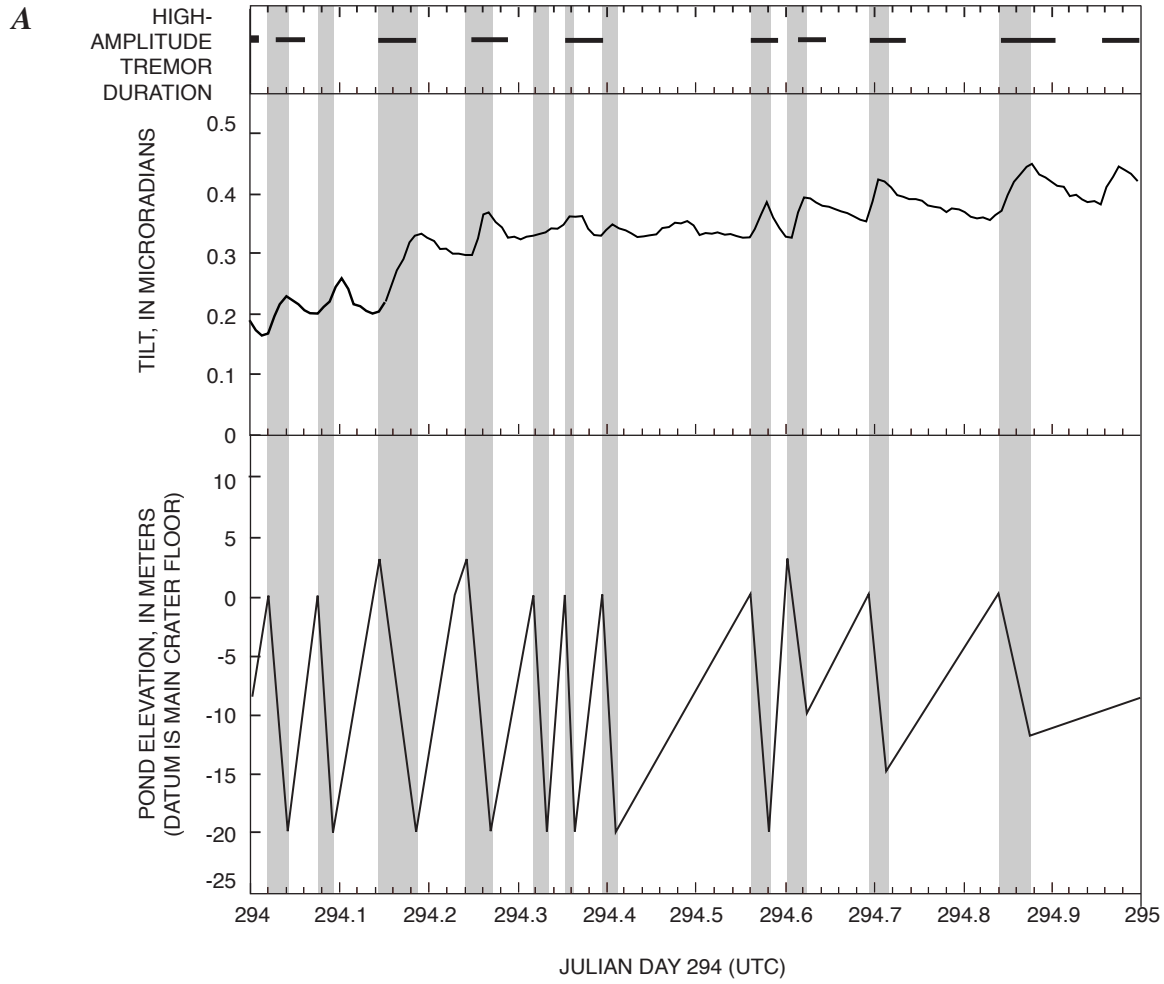

Figure 3. Correlation of pond drainback, tilt, and tremor. Shaded boxes indicate drainback events observed by remote video camera. *A*, Julian day 294, 1999 (1400 H.s.t. Oct. 20 to 1400 H.s.t. Oct. 21, 1999). *B*, Julian day 305, 1999 (1400 H.s.t. Oct. 31 to 1400 H.s.t. Nov. 1, 1999). *C*, Julian day 314, 1999 (1400 H.s.t. Nov. 9 to 1400 H.s.t. Nov. 10, 1999). The seismic trace was characterized by continuous high-amplitude tremor during this 24-hour period, and so correlation is limited to pond drainback and inflationary tilt.

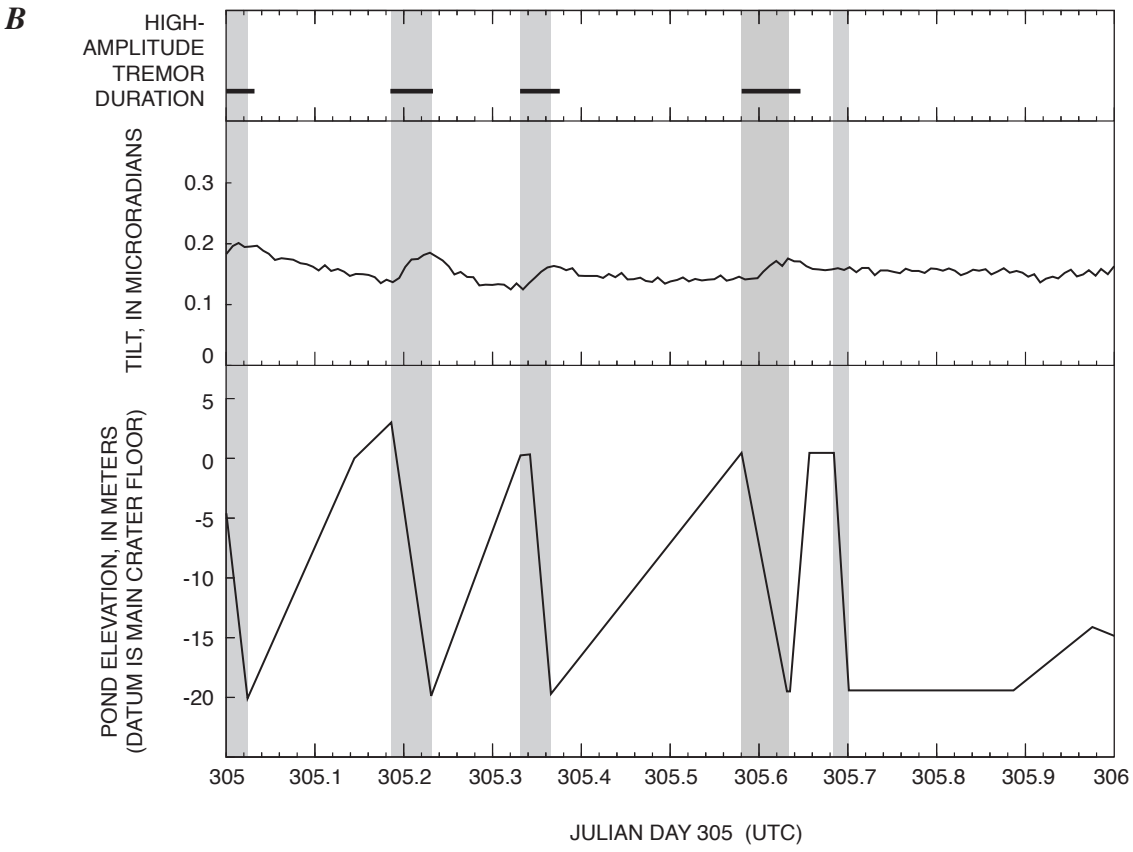

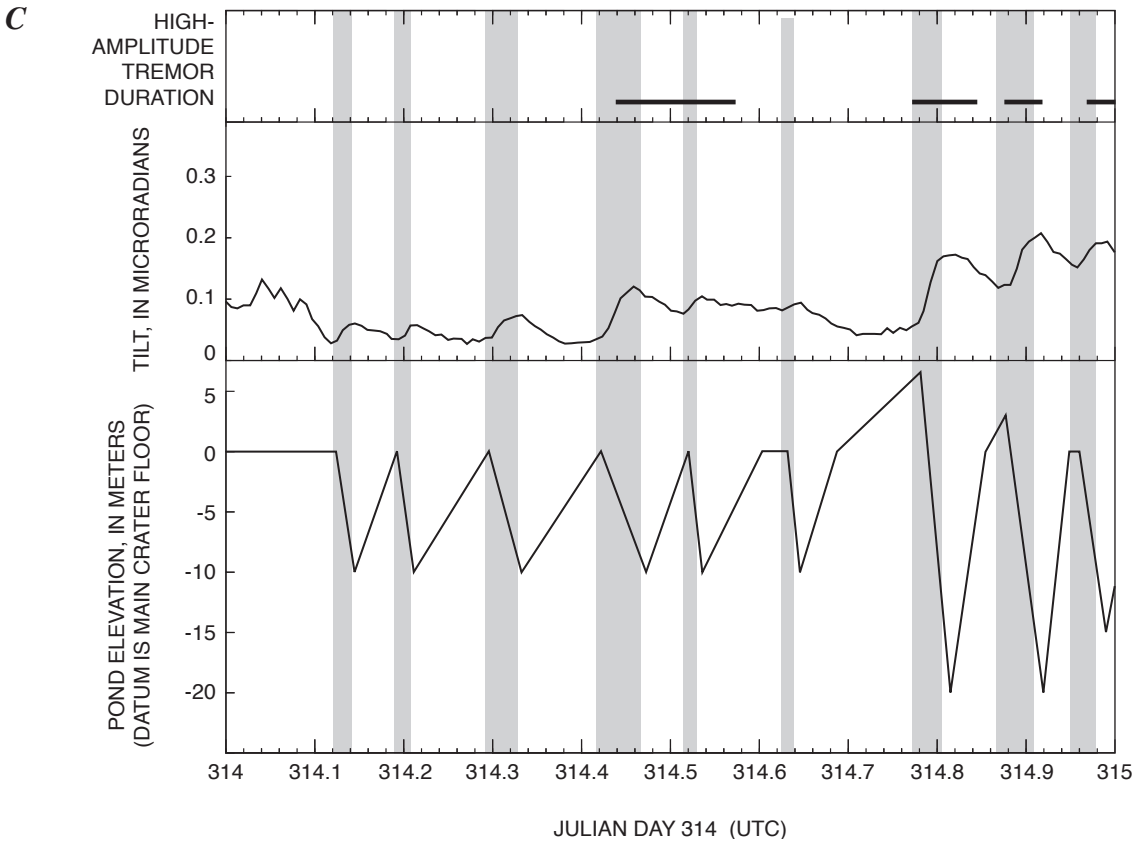

Figure 3. Continued.

During this period, the station POO tiltmeter data for a representative 24-hour period showed abrupt episodes of inflationary tilt (positive slope) that coincided closely with drainback events (table 1). The inflationary event began at the same time as drainback (within the error of timing for the video images) and ended when the lava pond had fully drained or within 10 minutes thereafter. As with the increased tremor, the tilt onset could precede, coincide with, or follow drainback as timed by the camera, probably owing to the imprecision associated with obtaining and analyzing the camera imagery. Deformation at the cone itself likely was similar in style, but no tiltmeter was there to measure it because the on-cone POC tiltmeter was not installed until early in 2000 (see Cervelli and Miklius, this volume).

The high-frequency tilt fluctuation, local to the Puʻu ʻŌʻō area and seen only on the station POO tiltmeter, was superimposed upon a longer-period variation in tilt that resulted from systemwide pressurization and depressurization of Kīlauea's summit and east rift zone. Such systemwide events were recorded simultaneously at several tiltmeters on the volcano.

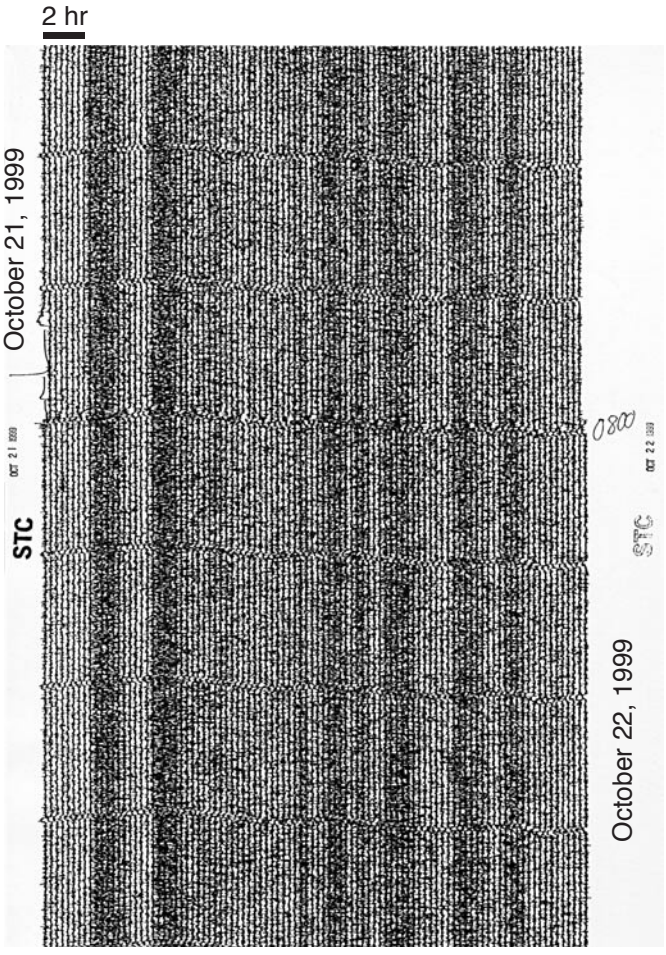

Figure 4. Seismic record at Steam Cracks (sta. STC, fig. 1) from a helicorder, showing part of the 24-hour period from 0800 H.s.t. on October 21 (left) to 0800 H.s.t. on October 22 (right), 1999. Banding is created by interspersed high- and low-amplitude tremor episodes. Abrupt regular steps on each line are 1-minute tickmarks, and each line is a 15-minute cycle of drum.

The high-frequency variation commonly displays a sawtooth pattern reflecting the rapid and localized expression of drainback events. Pond filling resulted in no discernible record in the tiltmeter data.

We interpret the locus of inflation for the drainbacks to be oriented south-southeast (at az approx. 162°) from the station POO tiltmeter, along the tiltmeter's *y*-axis. Thus the locus of inflation is about 1.6 km uprift of the crater. The events were so small that a precise direction was difficult to determine, but we can say with certainty that most changes were broadly in the direction of the tiltmeter's *y*-axis.

Correlations between tilt amplitude and drainback characteristics are obscure. We note a crude positive correlation between tilt amplitude and the duration of each drainback event (fig. 5). Complete draining of the lava pond took from 10 to 80 minutes in most events, and tilt ranged in amplitude from 0.0 to 0.12 μrad. The larger tilt events tended to occur during the longer drainback episodes. Similarly, the data suggest that the larger-amplitude tilt events tended to occur when the largest pond volumes were involved (fig. 5).

50 Days of Record

The temporal correlations that we have described between drainback, tremor, and tilt are characteristic of most days between September 30 and November 15, 1999. About 80 percent of pond-drainback events have correlative episodes of high-amplitude tremor.

When compiled, the daily correlations describe a longer-term (50-day) sequence of pond activity and inactivity (fig. 6). When active, the lava pond filled and drained as frequently as 11 times per day; when inactive, it remained empty for as long as 3 days. When the lava pond was active, as many as nine episodes of banded tremor occurred on any day; when it was inactive, banded tremor was sparse or absent.

Plotting the tilt data for a 50-day period obscures the detailed high-frequency (sawtooth) pattern that correlates with pond-drainback events. Instead, the record is dominated by (1) the long-term, low-frequency inflation and deflation that resulted from systemwide magmatic pressurization and (2) intermediate-frequency events that resulted from diurnal effects, such as earth tides and heating or cooling of the ground—the temperature effects discernible because the borehole was shallow. The presence or absence of high-frequency tilt fluctuations may be shown, however, by indexing the 24-hour average variation from the tilt record. This tilt index (fig. 6) was compiled by measuring the absolute value of the slope for each 10-minute segment of the tilt curve and calculating the mean value for each 24-hour period. A high tilt index generally corresponds to days when the tilt displayed the high-frequency pattern characteristic of pond filling and drainback.

In figure 6, vertical shaded bands are drawn to match the peaks of the tilt index after choosing an arbitrary index value to define the breadth of the peaks. These bands encompass most periods of frequent pond filling and drainback and

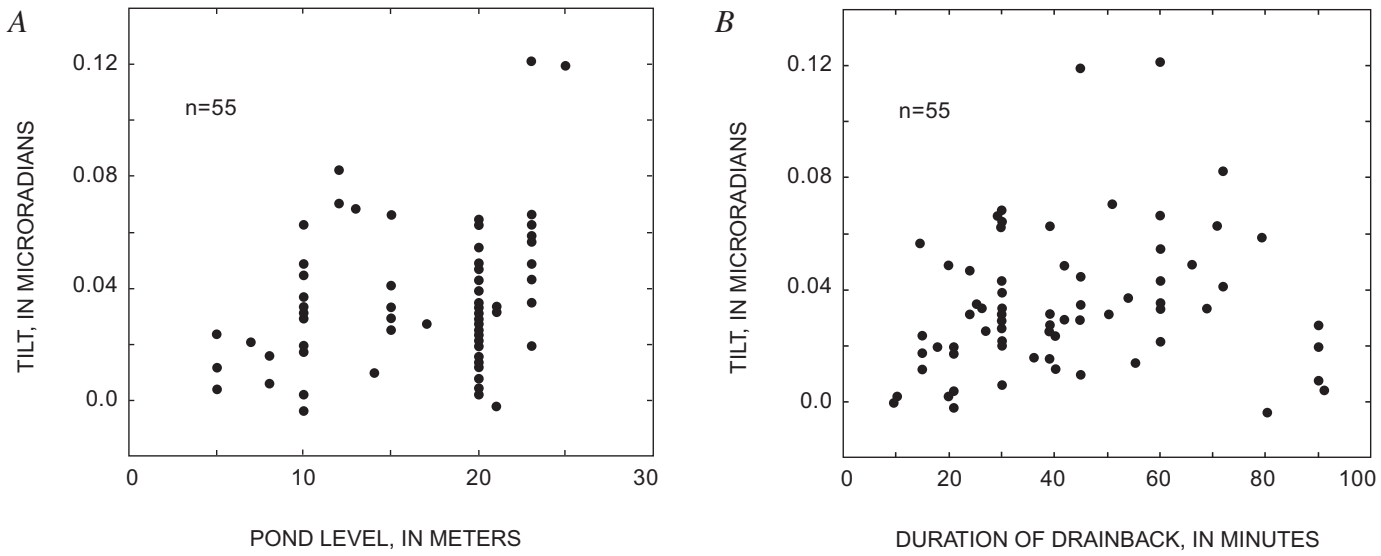

Figure 5. Comparison of tilt magnitude with pond level (*A*) and duration of drainback (*B*).

match fairly closely with days when banded tremor characterized the seismic record.

Another feature of figure 6 suggests a systemwide relation between lava-pond activity and magmatic pressurization during this 50-day period. Beginning on Julian day 279, the low-frequency tilt signal recorded at station POO showed broad inflation or relatively flat tilt during episodes of increased pond activity and banded tremor. In contrast, broad deflation occurred during periods of pond inactivity. Apparently the magmatic system needed suitable pressurization for pond activity to occur.

End of the Pond-Filling and Drainback Episodes

The lava-pond activity at Pu‘u ‘Ō‘ō diminished beginning about November 13, 1999. A final trough-filling event occurred on November 15. Subsequently, new lava flows were barely able to cover the trough's floor during rare extrusive events on November 17 and 18. After November 18, no within-crater extrusion was observed.

Banded tremor persisted in the seismic record until the afternoon of November 11, 1999. At 1530 H.s.t. on that day, a pause in the supply of lava to the flow field interrupted the eruption; however, lava was still present in the pond. The pause ended at 1030 H.s.t. on November 14, 67 hours later, accompanied by onset of high-amplitude tremor at station STC. Tremor amplitude decayed slowly thereafter, but banded tremor was absent from the seismic record.

After November 11, tilt returned to its more customary pattern in which lengthy periods of nearly no inflation or deflation were interspersed with the systemwide, sharp, steep inflations and deflations corresponding to magmatic pauses and restarts. Broad inflationary sequences were once again absent.

Discussion

Vent activity, seismic tremor, and ground deformation have been shown to correlate differently, depending on the location and magmatic scale of events at Kīlauea Volcano. At the volcano's summit, fountain heights during the 1959 Kīlauea Iki eruption correlated closely with tremor amplitude: the higher the fountaining, the higher the tremor (Eaton and others, 1987). The fountaining episodes were matched by broad deflation of the summit area as the magma reservoir discharged lava to the surface. Also well chronicled was the occurrence of deflationary tilt at Kīlauea's summit during eruptions along the east rift zone, such as during the August and October 1968 eruptions (Jackson and others, 1975) or the early years of the current Pu‘u ‘Ō‘ō eruption (Wolfe and others, 1988).

In contrast to those large-scale events are small-scale cycles of pond-filling and -drainback. Previous observers have described short-lived cyclic episodes known as gas-piston events. In the classic Mauna Ulu example described by Swanson and others (1979, p. 6), the magma column rose a few meters to several tens of meters in 15–20 minutes, without spattering. Their description continues:

> The next part of the cycle was violent. Suddenly, vigorous bubbling within the column generated intense spattering, the crust was torn to shreds, and the column withdrew turbulently to its starting level. The time from the onset of bubbling to the completion of withdrawal was generally a minute or two. This type of activity is ascribed to uplift of the column by expanding gases trapped beneath a relatively impermeable crust; eventually gas pressure overcame the strength of the crust, degassing of the column quickly resulted, and the lava withdrew to fill the void evacuated by the lost gas.

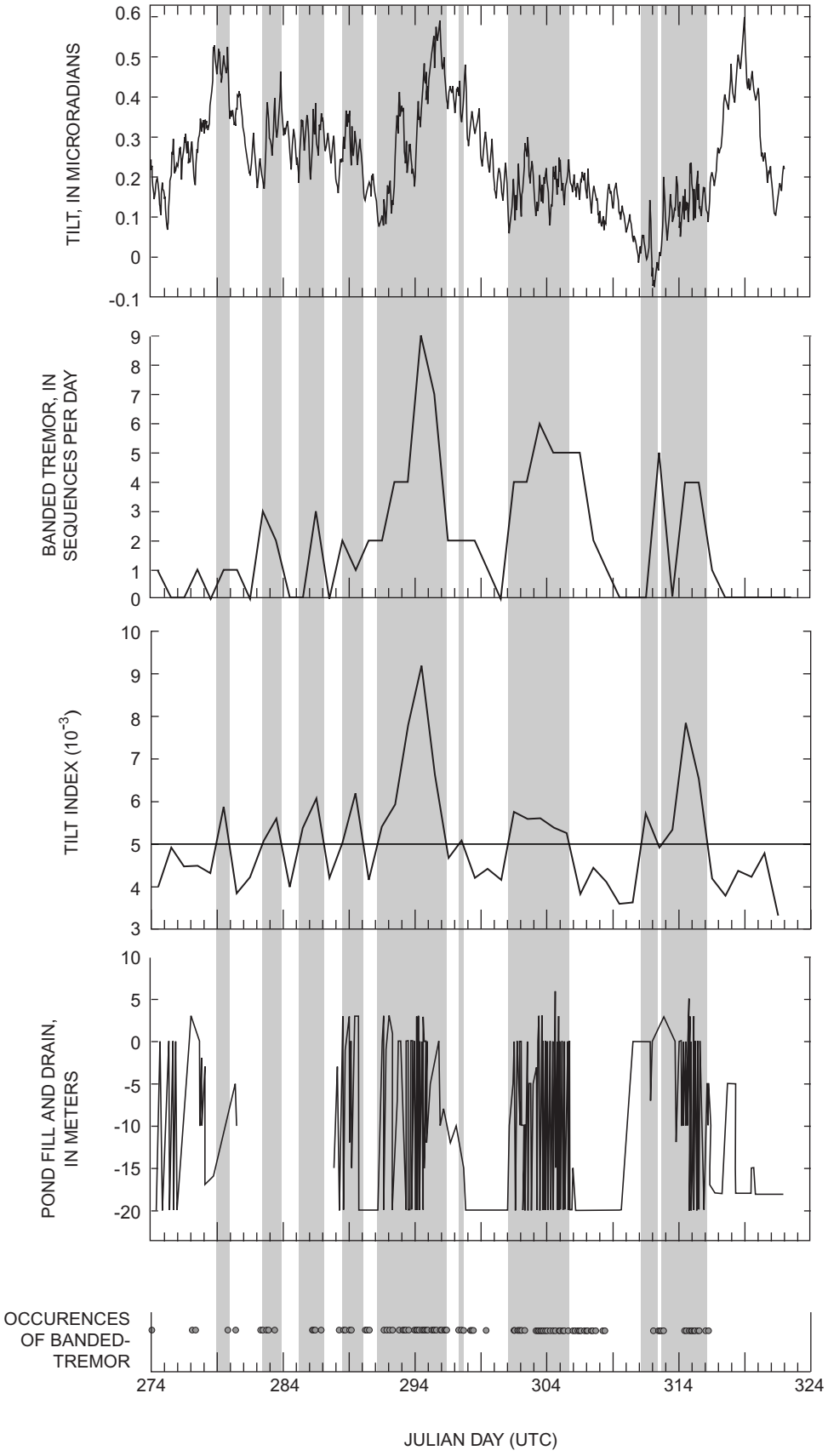

Figure 6. 50-day time series showing tilt, pond-filling and drainback events, banded-tremor occurrences, and indices for banded tremor and tilt (see text). Shaded bands correspond to peaks in tilt index.

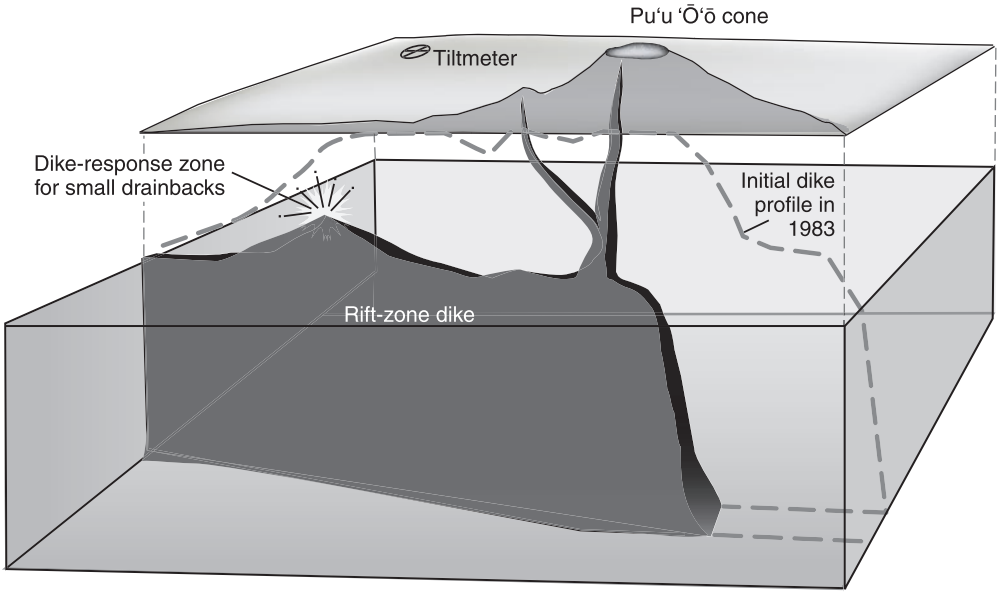

Figure 7. Cross section showing rift-zone dike, conduit into Pu‘u ‘Ō‘ō crater, and site where dike is believed to respond to drainback events from September 30 to November 15, 1999.

Gas-piston events occur sporadically at Pu‘u ‘Ō‘ō. For example, during February 1988, gas pistoning occurred repeatedly at intervals of 10–20 minutes over a period of several hours and produced a characteristic seismic record—a cigar-shaped amplitude envelope with a duration of about 80 s (Ferrazzini and others, 1991). During the February 1988 events, increasing amplitude of the seismic signal corresponded with accelerating rate of degassing as bubble bursts increased in size and number, such that the peak seismic amplitude corresponded to the violent phase of the degassing (Ferrazzini and others, 1991). The tremor sources were thought to lie beneath or close to the crater, within 1 km of the surface (Goldstein and Chouet, 1994).

The pond drainbacks we observed at Pu‘u ‘Ō‘ō in autumn 1999 were a more sustained and less intense version of lava-column rise and drainback than the isolated bursts etched on the seismic record by gas-piston events. Individual drainbacks during these autumn 1999 events ranged mostly from 10 to 80 minutes in duration. Ground deformation, expressed as inflation at or near the vent, was of similar duration. High-amplitude tremor persisted for 45–90 minutes before decaying fairly abruptly to background levels. Cigar-shaped amplitude envelopes were absent in the tremor record.

Interpretation and Conclusions

The most enigmatic part of the Pu‘u ‘Ō‘ō system is the subterranean conduit that feeds lava to the surface. Its connection to the dike system of the east rift zone is poorly understood but believed to lie in the depth range 0.4–2.0 km beneath the cone (fig. 7; Greenland and others, 1988; Wolfe and others, 1988; Hoffman and others, 1990; see Heliker and others, this volume, for more complete explanation). Also speculative are the depth and orientation of conduits that supply lava or gas into Pu‘u ‘Ō‘ō’s crater or that feed lava to the tube system of the adjacent flow field.

At the surface, pond filling and drainback were the events easiest to recognize and correlate among the tremor, tilt, and digital-camera records from September 30 to November 15, 1999. Pond filling was probably driven by vesiculation and expansion of the magma column, in a manner analogous to the vesiculation pump described from the 1959 Kīlauea Iki eruptions (Eaton and others, 1987). Whenever the system was suitably pressurized, the rising lava reached the surface and spilled onto the crater floor. As the pond filled, the top of the column became a slightly denser cap, owing to degassing and cooling. Meanwhile, bubbles presumably coalesced within the maturing magma column and began a more rapid ascent, hollowing out the shallow core of the column. Upon intercepting the pond, this gas-rich core first enhanced surface bubbling and spatter and then, once the gas escaped, initiated drainback. The gas-rich core is an interpretation to explain the mechanism of observed bubbling, spatter, and ensuing rapid drainback.

Lava-pond drainback disrupted the equilibrium of the vesiculating magma column, which became choked with degassed lava flushing down from the pond. Discharge of gas was probably stalled. As a result, the rift-zone dike momentarily swelled, possibly favoring sites where the dike was wider or where existing cracks yielded more readily (fig. 7). Magma entering the system through the dike continued its exit from the conduit that fed the tube system. Flow-field flux may have varied, but our tube-monitoring data were gathered too infrequently to determine the magnitude of changes that resulted from the filling-and-drainback process.

Tremor was heightened during and after drainback. Local inflation and drainback ceased nearly simultaneously, but the tremor began a lengthy response as some cracks drained, some filled, and vesiculation began anew in the upwelling magma column.

Once commonplace at Pu‘u ‘Ō‘ō, a crater-filling lava pond has been largely absent since large-scale disruption of the cone in January 1997. We explain its late September 1999 reappearance by reference to an event on September 12, 1999, when a dike intrusion into the east rift zone led to collapse of the crater floor at Pu‘u ‘Ō‘ō. This event probably created enough instability to close or diminish cracks and minor vents whose conduits might normally have discharged gas or been occupied by small magma columns. Thus lava in the central conduit was able to rise as high as the crater floor. This delicate balance of pressurization ended in November, when the supply of magma from the summit was interrupted. When resupply of magma began, stoping during repressurization probably reopened enough cracks and vents to lower the overall pressurization below some critical level. Thereafter, a vesiculating magma column could swell and shrink only within the subterranean realm, never burdened by the degassed cap of a lava pond.

Acknowledgments

Our work at Pu‘u ‘Ō‘ō has proceeded in collaboration with J.P. Kauahikaua and C.R. Thornber (U.S. Geological Survey), A.J.L. Harris and Dawn Pirie (University of Hawaii), and David Okita (Volcano Helicopters). The manuscript was reviewed by Andy Harris, George Havach, Paul Okubo, Don Swanson, and Jane Takahashi.

References Cited

Dawson, P.B., Chouet, B.A., Okubo, P.B., Villaseñor, Antonio, and Benz, H.M., 1999, Three-dimensional velocity structure of the Kilauea caldera, Hawaii: Geophysical Research Letters, v. 26, no. 18, p. 2805–2808.

Eaton, J.P., Richter, D.H., and Krivoy, H.L., 1987, Cycling of magma between the summit reservoir and Kilauea Iki lava lake during the 1959 eruption of Kilauea Volcano, chap. 48 *of* Decker, R.W., Wright, T.L., and Stauffer, P.H., eds., Volcanism in Hawaii: U.S. Geological Survey Professional Paper 1350, v. 2, p. 1307–1335.

Ferrazzini, Valérie, Aki, Keiiti, and Chouet, B.A., 1991, Characteristics of seismic waves composing Hawaiian volcanic tremor and gas-piston events observed by a near-source array: Journal of Geophysical Research, v. 96, no. B4, p. 6199–6209.

Garcia, M.O., Rhodes, J.M., Trusdell, F.A., and Pietruszka, A.J., 1996, Petrology of lavas from the Puu Oo eruption of Kilauea Volcano; III. The Kupaianaha episode (1986–1992): Bulletin of Volcanology, v. 58, no. 5, p. 359–379.

Goldstein, Peter, and Chouet, B.A., 1994, Array measurements and modeling of sources of shallow volcanic tremor at Kilauea Volcano, Hawaii: Journal of Geophysical Research, v. 99, no. B2, p. 2637–2652.

Greenland, L.P., Okamura, A.T., and Stokes, J.B., 1988, Constraints on the mechanics of the eruption, chap. 5 *of* Wolfe, E.W., ed., The Puu Oo eruption of Kilauea Volcano, Hawaii; episodes 1 through 20, January 3, 1983, through June 8, 1984: U.S. Geological Survey Professional Paper 1463, p. 155–164.

Heliker, C.C., Mangan, M.T., Mattox, T.N., Kauahikaua, J.P., and Helz, R.T., 1998, The character of long-term eruptions; inferences from episodes 50–53 of the Pu‘u ‘Ō‘ō-Kūpaianaha eruption of Kīlauea Volcano: Bulletin of Volcanology, v. 59, no. 6, p. 381–393.

Hoffmann, J.P., Ulrich, G.E., and Garcia, M.O., 1990, Horizontal ground deformation patterns and magma storage during the Puu Oo eruption of Kilauea volcano, Hawaii; episodes 22–42: Bulletin of Volcanology, v. 52, no. 6, p. 522–531.

Jackson, D.B., Swanson, D.A., Koyanagi, R.Y., and Wright, T.L., 1975, The August and October 1968 east rift eruptions of Kilauea Volcano, Hawaii: U.S. Geological Survey Professional Paper 890, 33 p.

Klein, F.W., Koyanagi, R.Y., Nakata, J.S., and Tanigawa, W.R., 1987, The seismicity of Kilauea’s magma system, chap. 43 *of* Decker, R.W., Wright, T.L., and Stauffer, P.H., eds., Volcanism in Hawaii: U.S. Geological Survey Professional Paper 1350, v. 2, p. 1019–1185.

Mangan, M.T., Heliker, C.C., Mattox, T.N., Kauahikaua, J.P., and Helz, R.T., 1995, Episode 49 of the Pu‘u ‘O‘o-Kupaianaha eruption of Kilauea Volcano—breakdown of a steady-state eruptive era: Bulletin of Volcanology, v. 57, no. 2, p. 127–135.

Swanson, D.A., Duffield, W.A., Jackson, D.B., and Peterson, D.W., 1979, Chronological narrative of the 1969–71 Mauna Ulu eruption of Kilauea volcano, Hawaii: U.S. Geological Survey Professional Paper 1056, 55 p., 4 pls. in pocket.

Thornber, C.R., 1997, HVO/RVTS-1; a prototype remote video telemetry system for monitoring the Kilauea east rift zone eruption, 1997: U.S. Geological Survey Open-File Report 97–537, 19 p.

Wolfe, E.W., Neal, C.A., Banks, N.G., and Duggan, T.J., 1988, Geologic observations and chronology of eruptive events, chap. 1 *of* Wolfe, E.W., ed., The Puu Oo eruption of Kilauea Volcano, Hawaii; episodes 1 through 20, January 3, 1983, through June 8, 1984: U.S. Geological Survey Professional Paper 1463, p. 1–97.

Hawaiian Lava-Flow Dynamics During the Pu‘u ‘Ō‘ō-Kūpaianaha Eruption: A Tale of Two Decades

By Jim Kauahikaua, David R. Sherrod, Katharine V. Cashman, Christina Heliker, Ken Hon, Tari N. Mattox, *and* Jenda A. Johnson

Abstract

Two decades of the nearly continuous Pu‘u ‘Ō‘ō-Kūpaianaha eruption have provided many opportunities to study lava-flow dynamics. Many channelized ‘a‘ā flows evolve to form lava tubes that are covered by pāhoehoe lava. Their initial advance rate appears to be a crude function of effusion rate. Pāhoehoe flows have been more common than ‘a‘ā flows during this eruption, dominantly emplaced by inflation on low slopes. Flows with morphologies transitional between ‘a‘ā and pāhoehoe are interpreted as indicators of flow-field conditions. Observation and analysis of both ‘a‘ā and pāhoehoe flows reveal that a substantial increase in microcrystallinity generally results in the liquid solidifying as ‘a‘ā rather than as pāhoehoe. Lava tubes can form in both ‘a‘ā and pāhoehoe flows but are more common in pāhoehoe. A lava stream flowing within a tube has been documented to downcut through its base at a rate of 10 cm per day for a period of several months. Lava features, such as hornitos, rootless shields, and shatter rings, apparently form over tubes carrying an unsteady lava supply. Lava flows entering the ocean develop a unique set of features and behaviors. Many thermal-characterization studies have been done for active lava flows to calibrate satellite-borne sensors. Promising applications include thermal lava-flux monitoring and lava-flow and lava-tube mapping. The ultimate goal of much of this research is improvement of lava-flow hazard assessments and mitigation tools.

Introduction

In the past 2 decades, great advances have been made in our understanding of the physical processes that control basalt-flow emplacement, resulting in improvement of our tools for the mitigation of lava-flow hazards. Earlier studies of the 1969–74 Mauna Ulu eruption of Kīlauea Volcano and the 1984 Mauna Loa eruption provided a strong foundation for these advances. Although this chapter emphasizes the current eruption, we have incorporated data from these and other Hawaiian eruptions in our interpretations. Some of the lessons learned during previous eruptions have been relearned and expanded upon by a new generation of volcanologists.

The past 2 decades have also been unprecedented in modern times for the continuity of eruptive activity. This continuity has made possible both monitoring and experimenting on numerous aspects of lava-flow emplacement, instead of deducing processes from solidified products. Continuous eruptive activity has also allowed repeated experiments and observations on aspects of pāhoehoe-flow emplacement, such as lava flux, flow inflation, changes in bubble content, and the temperature of basaltic lava during transport through lava tubes. These studies, in turn, have provided new quantitative interpretations of the deposits from older eruptions.

The Pu‘u ‘Ō‘ō-Kūpaianaha eruption has produced lava-flow morphologies from ‘a‘ā to pāhoehoe and all the transitional forms between. The relative abundance of morphologic types, however, varied in both time and space. The first 3½ years of eruptive activity were dominated by fountain-fed ‘a‘ā, and the next 16½ years by tube-fed pāhoehoe. All eruptive activity played out on terrain that can be divided into five areas (fig. 1). The first area is the vicinity of the vent, which, for three of the first 3½ years and for the past 11 years, has been Pu‘u ‘Ō‘ō (see Heliker and Mattox, this volume). The second area, the upper flow field, encompasses terrain between the vent area and the top of Pūlama pali (“pali” is a Hawaiian word for escarpment or steep slope). Here, slopes are typically 1º–5º, and stable, long-lived lava tubes dominate the flow activity during periods of steady effusion; less commonly, lava shield and hornito formation dominates during varying or declining effusion. The third area is the face and base of the pali, where slopes are as steep as 20º. On these slopes, surface flows commonly change to ‘a‘ā, only to be resurfaced by pāhoehoe breakouts from established lava tubes. The fourth area is the coastal plain below the pali, with slopes less than 2º. This area is characterized by a prevalence of lava-flow-inflation structures and other features unique to “filled” lava tubes. The fifth area is the coast itself, a narrow (200–300 m) zone of >2º slopes bounded by low seacliffs and steep offshore bathymetry. This area is host to a range of activity related to the physical conditions of ocean entry as emplacement changes from subaerial to submarine.

Together, observations made over space and time have allowed us to address old questions, such as the process of lava-tube formation and the change from pāhoehoe to ‘a‘ā;

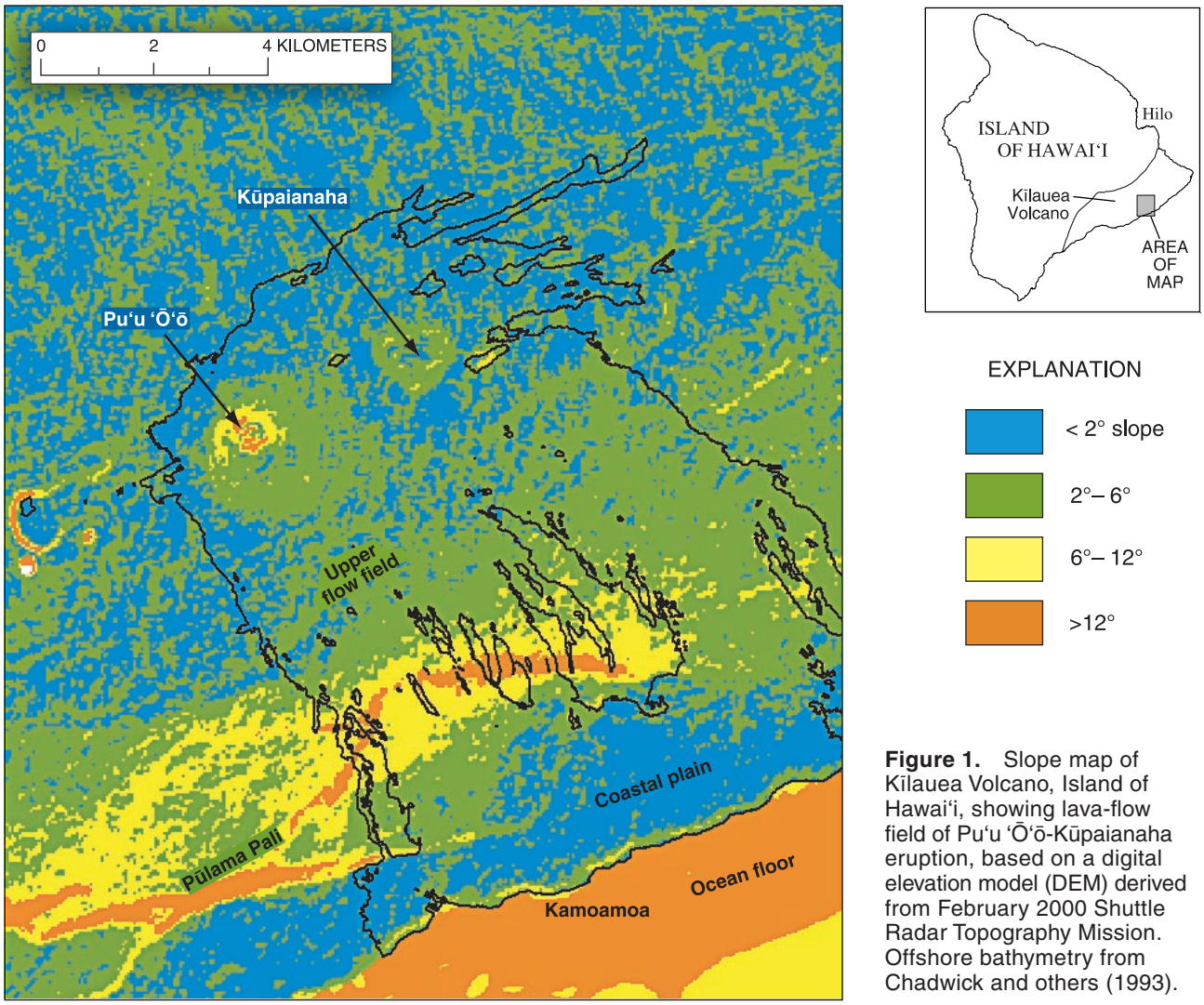

Figure 1. Slope map of Kīlauea Volcano, Island of Hawai'i, showing lava-flow field of Pu'u 'Ō'ō-Kūpaianaha eruption, based on a digital elevation model (DEM) derived from February 2000 Shuttle Radar Topography Mission. Offshore bathymetry from Chadwick and others (1993).

develop new models for lava-flow-emplacement behavior, including flow inflation and the origin of shatter rings; apply new technologies, particularly in the realm of remote sensing; and improve the basis for hazard assessment and mitigation.

Channelized 'A'ā Flows

Channelized 'a'ā flows formed during each of the fountaining episodes (1–47) and thus constituted the primary emplacement style of the first 3½ years of the eruption. Channelized 'a'ā flows also formed during the subsequent 16½ years under the following conditions: (1) unusually high effusion rates (for example, the Feb. 1, 1996, surge event), (2) unsteady fluxes after an eruptive pause (for example, in May 1997), or (3) surface flows that reach the steep slopes of the Pūlama pali. Thus, conditions of 'a'ā-flow generation generally matched those summarized by Macdonald (1953), Peterson and Tilling (1980), and Rowland and Walker (1990), who noted that 'a'ā formation requires high strain rates, as well as increases in apparent viscosity.

Evolution of 'A'ā Channels

A comprehensive summary of the flow behavior during episodes 1 through 20 (Wolfe and others, 1988) provides a description of these fountaining episodes. Detailed observations of channelized 'a'ā flows during the 1984 Mauna Loa eruption—which was concurrent with episode 17—provide additional insight into the general characteristics of 'a'ā flow behavior (Lipman and Banks, 1987).

Lava flows from episodes 1 through 3, the last part of episode 35, and the beginning of episode 48 were fed from fissures that erupted extensive near-vent shelly pāhoehoe, some of which, in turn, fed 'a'ā flows. All the other eruptive episodes earlier than episode 48 involved channelized 'a'ā flows fed from a central vent. During episodes 2 through 19 and 42 through 47 (Wolfe and others, 1988; see Heliker and Mattox, this volume), pāhoehoe flows spilled from a central vent and then were rapidly directed into a narrow open channel, 2 to 5 m deep and 5 to 25 m wide, that typically was rectangular in cross

section. Channel levees were constructed by lateral displacement of ʻaʻā rubble at the flow front and then strengthened over time with repeated coatings by pāhoehoe overflows. During episodes 20 through 41, substantially higher fountains apparently degassed and cooled the lava to the point where the flows started as ʻaʻā (see Heliker and others, this volume).

During episodes 1 through 19, channel formation permitted transport of fluid lava to distances of 2 to 5 km from the Puʻu ʻŌʻō vent. At this distance, the channel surface gradually became increasingly lumpy with incipient clinker. Once established, the position of this transition in surface morphology generally did not change over time. Farther downflow, the stable channel gradually transformed into a zone of dispersed flow at the front (Lipman and Banks, 1987). Fluid velocities in the channel were 10 to 15 m/s within a few tens of meters from the vent but decreased to 1 to 3 m/s 1 km from the vent. Velocities slowed through the transition zone, and the flow fronts advanced at velocities of <0.1 m/s (Lipman and Banks, 1987).

Superb observations of the channelized ʻaʻā flow from the 1984 Mauna Loa eruption included detailed measurements of flow advance and changes in channel flow, lava density, and lava temperature over time and distance from the vent (Lockwood and others, 1985; Lipman and Banks, 1987). These studies, which provided evidence for extensive syneruptive crystallization in response to magma degassing, formed the basis of subsequent examination of the rates of syneruptive and posteruptive crystallization (Crisp and others, 1994) and cooling (Crisp and Baloga, 1994). Together, these studies provide the most complete data set and analysis of a Hawaiian ʻaʻā flow.

Longer lived channelized ʻaʻā flows emplaced during episodes 48 and later progressed to the final stage of the channelization process. With sustained flow, the upper parts of the channel formed stable pāhoehoe crusts that initiated lava-tube development. The insulation provided by the tube roof permitted hot lava from the vent to progress farther downstream and to subsequently bury ʻaʻā levees with pāhoehoe. Given sufficient time, the entire flow would be overrun by pāhoehoe. This process illustrates the importance of thermal efficiency in the transport of pāhoehoe-producing lava flows, as discussed in detail below.

Constraints on Initial Flow-Advance Rates

Two lava-flow parameters of critical importance to hazard assessment are rate of advance and ultimate flow length. Episodic high fountaining from Puʻu ʻŌʻō from 1983 to 1986 allowed us to acquire many data sets of advance rates for ʻaʻā flows (Wolfe and others, 1988; Heliker and others, 2001). Flow length may increase either linearly over time or rapidly at first and then at a slower rate as the flow approaches a final length (fig. 2). Kilburn (1996) described these patterns of flow lengthening in other basaltic-lava flows; he found linear advance to be limited by lava supply, and slowing advance by cooling at the flow front.

To expand our analysis, we have compiled (fig. 2) lava-flow-advance rates for other recent eruptions of Kīlauea (Moore and others, 1980) and Mauna Loa (Finch and Macdonald, 1953; Lipman and Banks, 1987; Barnard, 1990–92). The rapid advance of most recent flows from Mauna Loa's southwest rift zone precluded detailed estimates of flow advance; instead, advance rates had to be estimated from reports of flows crossing known roads or reaching the ocean. Together, these data show a crude correlation between initial rates of lava-flow advance and volumetric effusion rate (Q). We concentrate here on just the first several hours of each advance, not the entire advance history of each flow. Average initial flow-advance rates for $Q \approx 25$ m^3/s are <0.02 m/s, and for $Q \approx 50$–70 m^3/s ~0.08 m/s. In contrast, flows erupted at moderately high effusion rates ($Q \approx 300$ m^3/s) can advance as fast as 0.3 m/s over the first several hours, whereas the extraordinarily high effusion rates ($Q \approx 1{,}000$ m^3/s) of the 1950 Mauna Loa eruption produced flows that advanced 3 to 4 m/s during the first day of emplacement.

The observed correlation between flow-advance rate and volumetric effusion rate for flows that traverse distinct topographic settings suggests that slope is of secondary importance in controlling flow-advance rate. Underlying slope has previously been shown to have no statistically evident control on flow width (Peitersen and Crown, 1999, 2000). Theoretical and empirical expressions for flow length as a function of time (advance rate) show a dependence on the sine of the average ground slope (and, thus, of order <1). Instead, flow advance depends on the square root of the effusion rate (Kilburn and others, 1995). Additionally, the final length of an ʻaʻā flow is best predicted by its effusion rate (Walker, 1973; Pieri, 1986; Pinkerton and Wilson, 1994). These observations point to the importance of accurately determining volumetric effusion rate during the early stages of an ʻaʻā-producing eruption.

Rheology of ʻAʻā Flows

ʻAʻā flows have long been recognized to have non-Newtonian rheologies that control the mechanics of flow emplacement (Robson, 1967; Walker, 1967; Hulme, 1974). ʻAʻā is commonly modeled as a Bingham fluid, which has an apparent yield strength when stress/strain-rate curves measured at high strain rates are extrapolated back to zero shear strain. For a Bingham fluid, flow through a channel is plug-like, and levees form when marginal flow ceases because of yield-strength limitations. The final levee width and channel width have been used to estimate the yield strength (Hulme, 1974). A potential problem with this technique is the observed formation of levees by lateral displacement of solid material at the flow front, rather than by lateral flow limited by lava yield strength.

Data from selected episodes 1–20 ʻaʻā flows, and from the "1 flow" of the 1984 Mauna Loa eruption, provide an opportunity to estimate rheologic changes in flowing lava as a function of emplacement style and transport distance

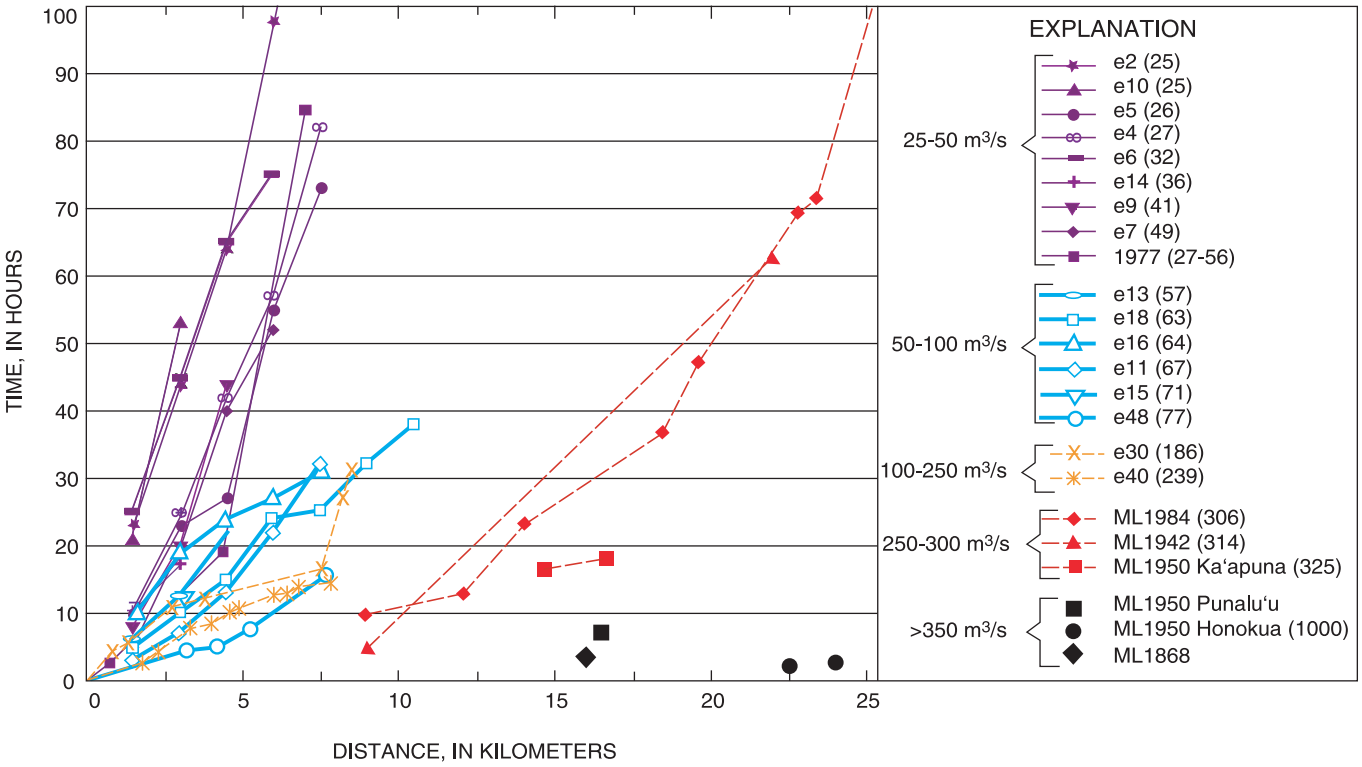

Figure 2. Advance of Hawaiian ‘a‘ā flows grouped by range in effusion rate**.** Rate for each flow given in parentheses; e, Pu‘u ‘Ō‘ō eruptive episode; ML, Mauna Loa.

(Fink and Zimbelman, 1986; Lipman and Banks, 1987; Moore, 1987; Wolfe and others, 1988). Fink and Zimbelman (1986) used measured channel and levee geometries to estimate a 30-fold increase in yield strength and a 10-fold increase in viscosity near the distal end of the 7-km-long, episode 5 ‘a‘ā flow accompanying a 30ºC decrease in temperature along the lowermost 1.7 km. They concluded that the increase in viscosity is explainable by increasing lava crystallinity but that the increase in yield strength most likely reflects both greater crystallinity and more flow-surface brecciation. Fink and Zimbelman (1990) extended their analysis to episodes 2–5 flows, computing yield strengths of 300 to 40,000 Pa and viscosities of 60 to 0.3×10^6 Pa-s, increasing exponentially along the flow lengths. In a similar study of the 1984 Mauna Loa flow, Moore (1987) deduced a 10,000-fold increase in viscosity and 30-fold increase in yield strength along the 25-km length of the flow.

More recently, Baloga and others (1998; 2001) relaxed assumptions of constant flow density and thickness. They used flow width, thickness, along-flow distance, and elevation measured from flow maps for episodes 2 and 18 (Wolfe and others, 1988) as random variables, from which they estimated “statistics” of viscosity variation based on three different rheologic models. They preferred a model that accounts for the flow volume lost to stagnant, stationary components of the flow. The resulting derived viscosity for episode 2 increased by a factor of ~150 along the flow, similar to the viscosity increase calculated by Fink and Zimbelman (1990) for the same flow. Reanalysis of the data for the “1 flow” from Mauna Loa in 1984 (Baloga and others, 2001) shows the importance of incorporating density into viscosity calculations and the spurious findings (Baloga and Pieri, 1986) that can result when flow thicknesses are not corrected for density.

Sakimoto and Gregg (2001) used numerical models to simulate observed channel flow during the 1984 Mauna Loa eruption and episode 51 of the Pu‘u ‘Ō‘ō–Kūpaianaha eruption. Using validating data from numerous polyethylene glycol (wax) analog simulations of channel flow, they found a Newtonian fluid-channel model to be more accurate than either Bingham or Newtonian infinite-sheet models for these flows (for example, Tallarico and Dragoni, 2000).

Pāhoehoe Flows

Pāhoehoe has been the dominant flow type throughout most of the Pu‘u ‘Ō‘ō-Kūpaianaha eruption since mid-1986. During the shorter (1969–74) Mauna Ulu eruption, Swanson and others (1979) and Tilling and others (1987) made excellent observations of pāhoehoe flow and lava-tube formation. These studies, along with others (Greeley, 1971, 1972, 1987; Swanson, 1973; Swanson and Fabbi, 1973; Peterson and Swanson, 1974; Peterson and others, 1994) provided a foundation for future work. Here, we focus on five aspects of pāhoehoe-flow-field development: emplacement mechanisms, the evolution of lava tubes, the origin of different morphologic flow types, and complex interactions of lava and seawater at ocean entries.

Inflation Is the Dominant Emplacement Mechanism of Pāhoehoe on Low Slopes

Close observations of newly emplaced pāhoehoe lava on the coastal plain during episode 48 (Mattox and others, 1993) led to an experimental study of inflating pāhoehoe sheetflows (Hon and others, 1993a, 1994) that complemented earlier deductive fieldwork (Holcomb, 1987; Walker, 1991; Chitwood, 1993, 1994) on flow inflation. The process is straightforward—continual growth of upper and lower crust that surrounds a molten interior continually replenished with fresh lava. The interior is a conduit for molten lava and so acts as a lava tube feeding the advancing flow front. An inflating pāhoehoe flow can thicken from tens of centimeters to meters within a few days as lava influx under hydraulic pressure forces the crust upward and outward. Inflation creates hummocky flows or sheetflows, differing only in scale. In hummocky flows, inflation is localized to form tumuli, from meters to tens of meters wide (Swanson, 1973; Hon and others, 1994). Wholesale inflation of sheetflows occurs over hundreds of meters, commonly leaving broad, flat areas (plateaus) elevated above the surrounding terrain.

The upper crust of inflated flows thickens during flow emplacement and, in solidified inflated flows, is recognizable by its vesicularity, which contrasts with a dense flow interior. Where crustal growth rates are known, the thickness of the upper vesicular crust provides an estimate of the duration of flow emplacement, as demonstrated by a comparison of known and calculated flow durations for specific lobes of the 1990–91 Kalapana flow (Cashman and Kauahikaua, 1997). Additionally, vesicle distribution within the upper crust confirms that the flow interiors are overpressured (Cashman and Kauahikaua, 1997). The source is hydrostatic and is transmitted through the fluid-filled parts of lava tubes or flow interiors. Overpressuring explains several features of lava breakouts from tumuli, including squeezeups through cracks, breakouts that push apart tumuli from within, and the "blue glassy" breakouts that issue from the base of tumuli as dense, vesicle-poor lava which had some of its original gas resorbed in response to the overpressure (Hon and others, 1994).

Extension of the upper crust over the axis of inflation creates a downward-propagating axial crack. Banding caused by alternating brittle- and ductile-failure patterns on the interior crack walls has been interpreted either as pulsed crack formation (Hon and others, 1994), similar to that proposed for columnar-joint formation (DeGraff and Aydin, 1993), or pulsed inflation (Anderson and others, 1999, 2000). The pulsed-inflation interpretation is inconsistent with observations of actively inflating sheetflows (Self and others, 2000).

Once identified in Hawai'i, inflated flows soon were recognized in several different submarine and terrestrial environments. Sea-floor analogs to inflated sheetflows have been documented on submarine extensions of Hawaiian rift zones (Umino and others, 2000; Smith and others, 2002) and in midoceanic environments (Appelgate and Embley, 1992; Gregg and Chadwick, 1996; Chadwick and others, 1999, 2001). Inflated features have recently been recognized in Australian and South African komatiites (Hill and Perring, 1996; Hollamby, 1996; Dann, 2001) and more recent (<200 ka) flows in Queensland, Australia (Atkinson and Atkinson, 1995; Stephenson and others, 1998; Whitehead and Stephenson, 1998).

Identification of Hawaiian-like inflation structures within the Columbia River Basalt Group has led to the suggestion that inflation may be important in the emplacement of large igneous provinces (Self and others, 1996, 1997, 1998, 2000). Tumuli and inflated pāhoehoe flows have been recognized in the older part of the Deccan Volcanic Province, India (Duraiswami and others, 2001), an observation consistent with the low regional slopes of preeruption flood-basalt provinces but raising questions about the limiting conditions of volumetric effusion rate or flow-advance rate in which inflation can occur.

Limited drilling in large igneous provinces in the North Atlantic (Eldholm and others, 1989; Larsen and others, 1994; Duncan and others, 1996) and on the Kerguelen Plateau (Coffin and others, 2000) confirms the presence of inflated basalt flows in both regions, although core samples of 'a'ā and transitional flows are also common. Large basaltic provinces, like those of Hawai'i, probably vary in eruption and emplacement conditions.

Lava Tubes Are Common Within Pāhoehoe Flows and Can Erode Their Bases

As the crust around a pāhoehoe flow thickens, the interior remains molten and continues to flow. Differential movement of solid crust and fluid core constitutes lava-tube flow. Initially, tubes conform to the shape of the flow—wide and not especially tall (low aspect ratio; Cooper and Kauahikaua, 1992). As the crust at the flow margins grows, the flow focuses, and the aspect ratio increases. Lava flowing in a tube may downcut its base in the center, resulting in keyhole-shaped cross sections (Kauahikaua and others, 1998a). Circumstantial evidence indicates that lava either remelts or abrades at the base of a stream (Greeley and others, 1998) and that the surfaces of lava streams within tubes slowly recede from the ground surface without a reduction in stream volume (Peterson and others, 1994). A single field measurement of the rate at which this downcutting can occur—10 cm per day over several months—was obtained during episode 53 (Kauahikaua and others, 1998a). This rate can be modeled by assuming steady forced convective heat transfer by a laminar channel flow at large Péclet numbers (Kerr, 2001).

The process of building a tube from a new vent to the ocean, a distance of 10 to 12 km, has occurred four times during this eruption (episodes 48, 51, and twice during 55), each time taking 2 to 8 months (Heliker and Decker, in press). The complexity of each tube system increased over time as sustained breakouts from the tube formed branches.

Tubes that form on slopes of more than a few degrees generally have headspace (air- and gas-filled space in the

tube above the lava stream), form skylights, and downcut their bases. On flat terrain, such as the coastal plain, tubes generally form as elongate inflated tumuli that remain full and are actually overpressured; downcutting generally does not take place, and skylights generally do not form (Kauahikaua and others, 1998a). Notable exceptions include the Highcastle tube in 1995 and the Lae‘apuki tube in 1996–97, both of which initially formed elongate tumuli. Inflation stopped as soon as downcutting began. Hydrostatic pressure can be transmitted only through the parts of the tube that are full—those that form on flat terrain. Skylights and downcutting are also visible at the coastline in the steeper terrain atop the coastal cliffs.

Flow-field development is controlled by lava-effusion rate. Steady effusion promotes the formation of stable, long-lived tube systems, whereas varying effusion rates result in temporary deflation of tumuli over filled tubes, formation of shatter rings (described below) above wide sections of tubes, or partial collapse of the tube system. Partial collapse commonly results in the formation of a new tube system that widens the flow field.

Lava tubes form readily within pāhoehoe flows. When blockages occur, the lava stream is forced out through the roof onto the ground surface in what is called a breakout. If the blockage is removed, the stream resumes flowing through the tube, cutting off lava supply to the surface breakout. If the blockage persists, the breakout commonly builds another tube that joins the system.

Occasionally a new tube system develops a site of persistent breakouts at the end of a tube segment, at an unusually sharp bend, break in slope, or anywhere else. If breakouts occur on a pali, they form a fan with a surface slope less than that of the original ground slope. If they form on flatter ground, they may transform into rootless shields, as described in detail in the next section.

Several lava falls that were observed in long-lived lava tubes, commonly below skylights, are not necessarily the result of one lava tube flowing into a lower tube, for we observed lava falls forming within a single lava tube (Kauahikaua and others, 1998a). The mechanism seems to be enhanced downcutting and widening of a plunge pool at the base of the falls, rather than headward erosion typical of waterfalls, as had been deduced from observations in ancient tubes (Kempe, 1997). Evidence against headward plucking is provided by the stationary position of lava falls beneath skylights for as long as 20 months, even as the falls’ height increased to approximately 4 m.

The formation of thermally insulated tubes permits lava to be transported great distances without significant cooling. For the Mauna Ulu lava tubes, temperature loss over the entire 12-km-long tube system was less than 15ºC, the estimated precision of the optical pyrometer then in use (Swanson, 1973; Swanson and Fabbi, 1973; Peterson and Swanson, 1974). Advances in obtaining in-place liquid lava temperatures by using glass compositions (Helz and Thornber, 1987; Helz and others, 1995) yield a tool for slightly more precise estimation ($\pm$3ºC) of tube insulation. Helz and others (1993) reported a consistent temperature drop of 9–10ºC over the 12-km distance between the Kūpaianaha lava pond and the coast, decreasing to 7ºC as the tube matured (see Helz and others, this volume). Using the same method, a maximum temperature drop of 6ºC was estimated for lava in both the episode 48 Waha‘ula lava tube and the episode 53 Kamoamoa lava tube (Cashman and others, 1994). Thornber (2001) estimated a maximum temperature drop of 6–15ºC during five sampling runs down episodes 53 and 55 lava tubes between May 1996 and September 1998. These estimates were made on tubes less than 14 km long, in contrast to a similar estimate for a 40-km-long tube system within the A.D. 1445 ‘Ailā‘au lava flows northeast of Kīlauea caldera (Clague and others, 1999). We conclude that lava tubes are remarkable insulators that allow temperature drops of only 6–16ºC ($\pm$3ºC) over 14 km or greater distances ($\leq$1ºC/km).

Lava flowing through tubes continues to degas passively, and large bubbles of gas preferentially rise and escape. Gas escape from surface lava flows and tubes accounts for nearly 1 percent of the overall SO_2 output of the eruption (Cashman and others, 1994). Bubbles continue to nucleate at a rate of about 25 percent of the nucleation rate in the vent conduit. Surface breakouts from the tube, extremely depleted in small vesicles, suggest coalescence of bubbles.

When lava tubes drained during episode 53, especially the Highcastle and Lae‘apuki tubes, we were able to observe and analyze encrustations that formed while the tube was active or while it cooled. Analysis of hollow lava (“soda straw”) stalactites revealed that the outside surfaces are enriched in Fe and depleted in Si, and oxide phases and the vesicle walls are enriched in Ti, as discovered previously by Baird and others (1985). This unique enrichment led to the conclusion that these stalactites and stalagmites formed by remelting of the tube walls (Baird and others, 1985; Thornber and others, 1999).

After the tubes cooled sufficiently for rainwater to enter, various sulfates, primarily hydrous, precipitated when water remobilized sulfur deposited within the tube roof while the tube was active (Finch and Emerson, 1925; Thornber and others, 1999). A visit to the Lae‘apuki lava tube 2 years after it drained found lava falls, soda-straw stalactites, and abundant hydrous sulfate stalactites composed of bloedite and thenardite (Porter, 2000).

Morphologic Subtypes of Lava Flows

Before the current eruption, morphologic types of subaerial basaltic-lava flows were assigned to three main categories: pāhoehoe, ‘a‘ā, and blocky (Jones, 1937, 1943; Wentworth and Macdonald, 1953; Macdonald, 1967). Several morphologic subtypes were also defined: entrail pāhoehoe results from lava dribbled down steep slopes, slabby pāhoehoe has an upper surface festooned with broken slabs of cooled crust, and shelly pāhoehoe has thin crusts around a completely empty interior and occurs mainly near vents. Swanson (1973) described lobelike and sheetlike varieties of shelly pāhoehoe

for the Mauna Ulu eruption. Wentworth and Macdonald (1953) also described entrail, shark-skin, filamented, corded, festooned, elephant-hide, and slabby pāhoehoe.

A distinctive subtype of pāhoehoe that attracted attention during the current eruption was variously described as P-type pāhoehoe (Wilmoth and Walker, 1993), dense-glass pāhoehoe (Hon and others, 1994), or blue-glassy pāhoehoe (Oze, 1997; Self and others, 1998; Sage and Mattox, 2000). The various descriptors each emphasize a distinct characteristic of this subtype: "P-type" indicates pipe-vesicle-bearing, "dense-glass" describes a rind of glass as thick as 1 cm with few vesicles, and "blue-glassy" describes the distinctive gun-metal-blue hue of this type of pāhoehoe, which typically emerges from the base of tumuli. Hon and others (1994) proposed that its unique characteristics resulted from being subjected to 2 to 4 bars of excess pressure within a tumulus, forcing gas back into solution before the lava was extruded and cooled. Cashman and Kauahikaua (1997) documented vesiculation in the crust of an inflating sheetflow as subdued with depth relative to normal vesiculation, an observation supporting the existence of fluid pressures higher than lithostatic within the flow. Alternately, Wilmoth and Walker (1993), Friedman and others (1996), and Self and others (1998) hypothesized that after spending a week or two inside inflating flows, the lava cools, and the bubbles coalesce before a pressure surge from the vent forces them out onto the surface. In frequent observations of blue-glassy flows issuing from 1- to 2-day-old tumuli, we noted that breakouts require a minimum tumulus height and are triggered by a threshold pressure (Hon and others, 1994; Kauahikaua and others, 1998a), rather than a threshold residence time of a week or two. Time-lapse videos of inflating flows confirms the absence of a surge pulse before breakouts (Ka ʻIo Productions, 2000).

The glassy surface of blue-glassy pāhoehoe flows commonly has the shark-skin texture (fig. 3) described by Wentworth and Macdonald (1953), who concluded that the texture results from "the escape of gas from the lava surface, each bubble dragging with it a filament of the enclosing liquid," and attributed the glass surface to "quick chilling . . . as by heavy rain." Observations during this eruption reveal that the dense-glass rind can form without rain and that the rough, shark-skin texture is the result of "olivine phenocrysts that were draped by the highly fluid lava during emplacement" (Hon and others, 1994).

Blue-glassy pāhoehoe is one of three subtypes of pāhoehoe that were used as indicators of robust sheetflow and tumulus inflation during the closely watched lava inundation of Kalapana (Mattox and others, 1993; Heliker and Decker, in press). The other subtypes are a shiny, silvery pāhoehoe, probably equivalent to the S-type pāhoehoe of Wilmoth and Walker (1993) and the "silvery" lobes of Self and others (1998), and a pastier, bulbous, duller, rough-surfaced, gun-metal-gray pāhoehoe. The shiny, silvery pāhoehoe is abundant in an advancing pāhoehoe flow. In contrast, pasty, dull pāhoehoe indicates either a reduced lava supply (Kauahikaua and others, 1996) from a draining tube system or residual lava pushed out of a reoccupied tube. Both surface characteristics (pasty and dull) reflect higher groundmass crystallinities afforded by increased transport time.

Figure 3. Blue-glassy flow surface, showing embedded crystals draped to form "shark-skin" texture.

Hornitos, Rootless Shields, and Shatter Rings Form over Pāhoehoe Lava Tubes

Hornitos (fig. 4) formed at least once during episodes 48 and 53 and three times during episode 55 in 2001–2. Each hornito formed directly over a lava tube or intrusion within 4 km of the vent.

The episode 48 hornitos were observed near Kūpaianaha. One stood 1-m high over a lava tube emerging from the south-southeast side of the shield in August 1986. A cluster of three hornitos formed around the edges of a bulge, believed to be the result of intrusion, on the north side of Kūpaianaha in July 1987. A pair of hornitos developed side by side during episode 53, each no more than 1 m high and 0.5 m in diameter at the base. The episode 55 hornitos were 2 to 12 m high and approximately 2 to 3 m in basal diameter.

Each hornito commonly had spatter and Pele's hair at its base and on the downwind side. Escaping gas could be heard from incandescent holes in the top or sides. The formation of hornitos was commonly preceded or accompanied by a small breakout.

Figure 4. Two hornitos formed in February 2002, about 4 km from Puʻu ʻŌʻō. Hornito above blue case is 15 cm high; distant hornito is 4 m high. Photograph taken February 21, 2002.

The hornitos in 2001–2 began forming when the lava tube under them apparently filled, as inferred from very low frequency (VLF) monitoring measurements. In the upper part of the flow field above Pūlama pali, the lava stream normally occupies only the lower meter or two of the tube beneath a large gas-filled cylindrical cavity (Kauahikaua and others, 1998a), as observed through skylights and by VLF measurements. In several places, we observed hornitos actively forming, spitting lava clots on or immediately adjacent to a VLF tube-monitoring location. Coincident with the hornito activity, the VLF-measured cross-sectional area of lava in the tube showed an abrupt increase that indicated a full tube. When next observed, the VLF-derived cross-sectional area had abruptly decreased, and the hornitos were no longer actively spattering. The local filling of a lava tube could have resulted from a partial obstruction farther downstream that caused lava to back up.

The rootless shields (fig. 5) that form over lava tubes are not fed directly from a deep-seated (>1 km depth) source; instead, the outflowing lava accumulates around the breakout point to create a shieldlike structure. Four rootless shields formed within a period of 2 weeks directly over an active lava tube in September and October 1999, during reoccupation of the tube after an especially long eruptive pause of nearly 12 days. Each breakout site formed a perched pond that overflowed in all directions to eventually form the shields built of predominantly shelly pāhoehoe. The shields can build to 5 to 20 m in height relative to the preshield surface; the largest shield is more than 500 m in diameter and is topped by a flat, ponded-lava surface 175 m across. The four 1999 shields subsequently merged together to form a broad, elongate ridge approximately 2 km long, directly over the lava tube.

Another set of rootless shields that formed in late 2001 to early 2002 at approximately the same distance from Puʻu ʻŌʻō as the 1999 shields were built over continuously active lava tubes, and their growth was not related to a pause. When this episode of shield building started, the shields formed over a tube system that fed two ocean entries. Within about 8 weeks

Figure 5. Rootless lava shield (skyline) at 2,080-ft elevation. Shield is about 500 m wide at its base and nearly 20 m high. View southward; photograph taken January 28, 2002.

after shield building began, both ocean entries stopped, and lava was seen only 1 km beyond the lowest shield. Skylights, never abundant, ceased forming as hornitos and shields were built over the lava tubes.

Shatter rings—broken rubble arranged in approximately concentric circles or ellipses (figs. 6–8)—also form directly over lava tubes on gently sloping ground (Kauahikaua and others, 1998a). Observations during episode 53 and measurements during episode 55 demonstrated that shatter-ring formation is more complex than simple collapse.

As verified by electromagnetic profiles, the shatter rings (two in the upper flow field in episode 53 and four on the coastal plain in episode 55) all formed over active lava tubes. When first noticed, the shatter rings resembled broad, collapsed tumuli. Growth of each shatter ring continued by episodic, nearly constant flexing of the lava-tube roof, as determined by repeat leveling across one of the early episode 55 features and indicated by a persistent grinding sound. The constant flexing breaks the lava-tube roof around the edges of the circular uplifted area. Fractured rock then collects around the rim in circular or ellipsoidal rings, while the remaining tube roof or crust within the center, generally consisting of the original pāhoehoe surface, continues its up-and-down motion. The range of vertical movement in the center can exceed 2 m up or down, with total relief of as much as 4 m relative to the surrounding flow surface (fig. 8). Subsidence into the drained lava tube increases the relief inside some rings (fig. 9). Survey results confirm that only vertical movement takes place, with no net compression or extension.

The two shatter rings formed during episode 53 started building after the eruptive pauses in March and November 1995, respectively, above a lava tube that had made its first ocean entry in November 1992. The first episode 55 shatter ring started to form more than 6 months after the tube was established at that site in July 1997, after the first of two eruptive pauses in January 1998. Coincidentally, this shatter ring was centered on a geophysical profile established during October 1997 that provided pre-shatter-ring baseline data (fig. 9). The most recent shatter ring was first noticed in July 1999 above a lava tube that reached the ocean nearly 12 months earlier. Lava had resumed flowing through the tube in June 1999 after a 4-day pause.

All of these shatter rings formed over unusually wide sections of the active lava tube on slopes less than 5°. Electrical-conductivity signatures indicate that the lava tubes in this low-slope environment are commonly 3 to 5 m, rarely as much as 10 m, wide (Kauahikaua and others, 1998a). In contrast, electrical-conductivity signatures over active shatter rings indicate a lava-tube width of 50 to 100 m. The 1998 shatter ring formed on the coastal plain, where the underlying tube was 80 m wide when first surveyed in October 1997. Similar observations have been made on Hualālai Volcano for a few shatter rings under which the related tube can be explored. In

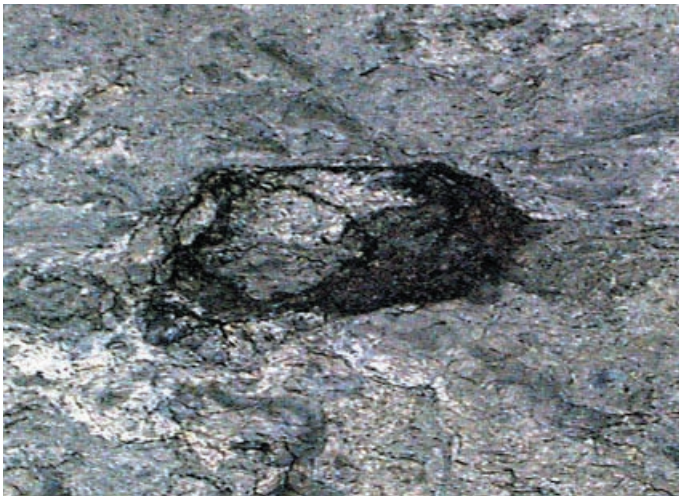

▲**Figure 6.** The 1999 shatter ring on coastal plain when first noticed. Reflective lava inside ring is original ground surface that has not been completely disrupted. Ring is approximately 50 m in diameter. Aerial oblique view northeastward; photograph taken July 22, 1999.

◄**Figure 7.** The 1999 shatter ring on coastal plain. View northward; photograph taken August 10, 1999.

the clearest example, the lava tube is 50 m wide beneath a 60-m-diameter shatter ring. Tubes are less than 7 m in diameter upslope and downslope from all the observed shatter rings.

Shatter rings form during several months of continuous lava-tube activity, when lava issues from breakouts around the outside of the shatter ring. The two episode 53 shatter rings were centered on low rootless shields that formed from breakouts around the ring. The three shatter rings above the 1997–98 Waha‘ula lava tube were actively deforming for about 6 months until the tube was abandoned in early July 1998. The most recent shatter ring (figs. 6, 7) grew for about 3 months until a pause drained the underlying lava tube in September 1999.

The fluctuations in elevation inside the shatter ring directly correlate with variations in the volume of lava moving through the tube. The 1998 shatter ring was resurveyed several times in the first half of the year, when seven pauses in lava supply occurred. During the first several pauses, the interior of the shatter ring subsided; when flow resumed through the tube, the interior of the shatter ring rose significantly. The repeated leveling (fig. 10) captured only the range in elevation changes and one rapid rise after the last pause before the tube was abandoned.

Shatter rings have been recognized and puzzled over worldwide. We have mapped dozens on Hualālai, two in the Koa‘e fault system, and several on the lower end of the main ‘Ailā‘au lava tube (Clague and others, 1999) of Kīlauea. A few shatter rings have been observed on Mauna Loa and Haleakalā. Shatter rings are known outside Hawai‘i as “collapsed tumuli” on the 1614–24 pāhoehoe flows on Mount Etna (Guest and others, 1984), “unusual craters” on the Aden basalts of New Mexico (Summerour, 1989), “craters with raised rims” on the Cave Basalt of Washington (Greeley and Hyde, 1972), and “lava ponds” on the Undara lavas of Queensland, Australia (Atkinson and Atkinson, 1995). They are also reported from Etna (Sonia Calvari, written commun., 1998) and the Hallmundarhraun area of Iceland (Wood, 2001).

Both shatter rings and rootless shields apparently result from unsteady flow of lava through tubes. During the current eruption, shatter rings were initiated by pauses, and rootless shields were built by flows with insufficient lava supply to form tubes. As such, shatter rings and rootless shields provide an estimate of both the longevity and steadiness of tube flow and can be used to assess emplacement conditions of older, solidified lava flows.

Lava Entering the Sea Forms Deltas and Benches, Continues Flowing Underwater, and Alters Nearby Ocean Water

During the 1969–74 Mauna Ulu eruption, lava entering the ocean was described on the basis of depositional environment—subaerial (Peterson, 1976) or submarine (Moore and others, 1973). Lava entered the ocean 5 times between 1969 and 1971, for less than 2 months on each occasion. The pāhoehoe flows built lava deltas, as wide as 400 m and extending nearly 2 km along shore. Small littoral tephra cones grew on the deltas. Lava tubes delivered fluid lava to the ocean floor through the surf zone. Pillow lavas and lava tongues were observed forming and moving on the ocean floor off these entries above 70-m depth, the limit of the diving undertaken.

The current Pu‘u ‘Ō‘ō-Kūpaianaha eruption has produced much longer lived ocean entries than any other eruption of Kīlauea since A.D. 1500 (Don Swanson, oral commun., 2002). Of the nearly 80 ocean entries recorded to date, 30 lasted for

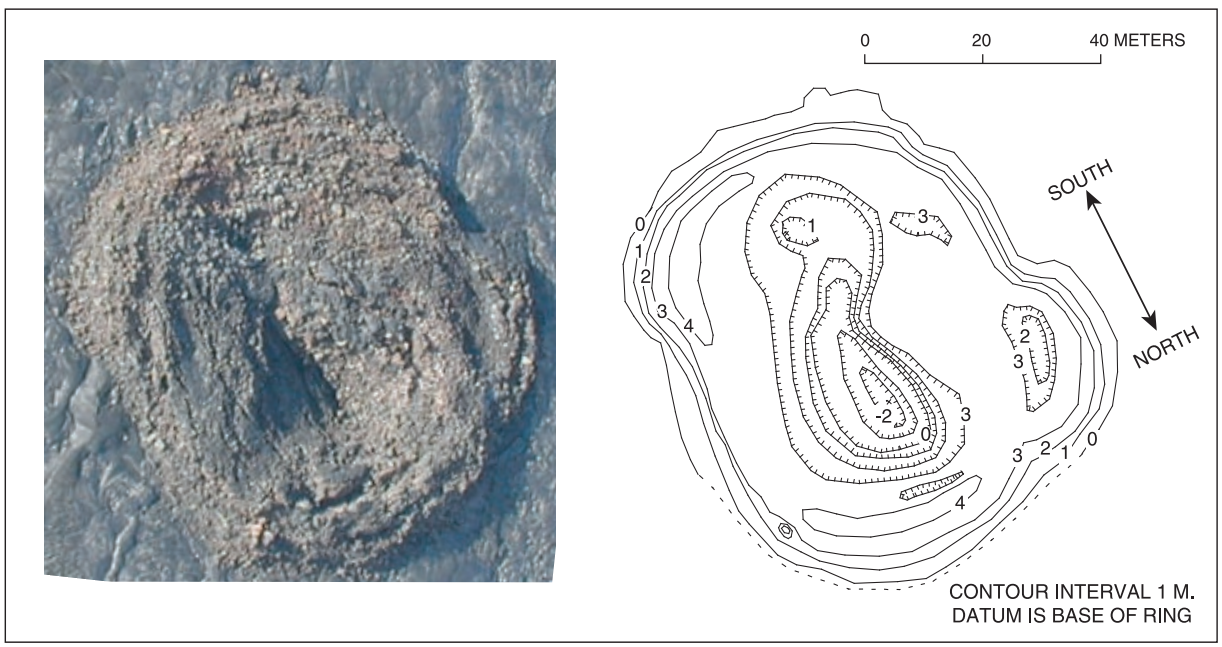

Figure 8. Vertical view and topographic map of 1999 shatter ring. Photograph taken December 23, 1999.

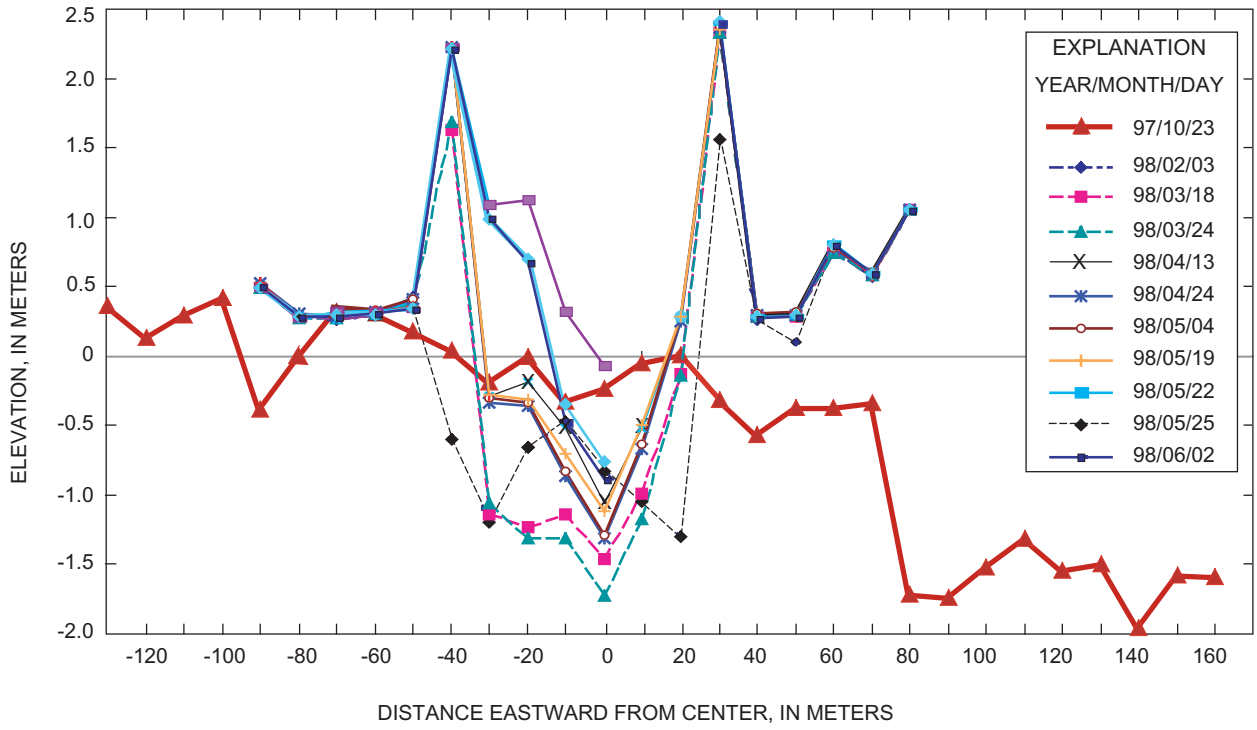

Figure 9. Results of repeat elevation surveys across a shatter ring. First data set, from October 23, 1997 (97/10/23), was measured before initiation of deformation.

more than 2 months, and the longest lasted 15½ months. The first ocean entry occurred in November 1986, and by 1988 the lava deltas were exhibiting a previously unobserved behavior: they were catastrophically collapsing into the ocean (Kelly and others, 1989; Hon and others, 1993b). Collapse resulted from the accumulation of subaerial flows and lava on the delta, which overburdened the hyaloclastite fans on which they were built and caused parts of the delta to calve into the ocean with little warning. The new coastline, which continued building beyond the old one, could be overrun by a new surface flow that would add to the lava delta. This process prompted the following distinction in terminology: A "lava delta" refers to all lava built beyond the preeruption coastline, whereas a "lava bench" refers to a part of the lava delta that has built outward within a previous collapse scar and that could collapse because of its unstable structure. The elevation of a lava bench is therefore abruptly lower than that of a lava delta.

Full or partial bench collapses commonly initiate explosive interactions between lava and ocean water. Mattox and Mangan (1997) describe four different types of explosive events: tephra jets, lithic blasts, bubble bursts, and littoral lava fountains. The explosions result either from open mixing of

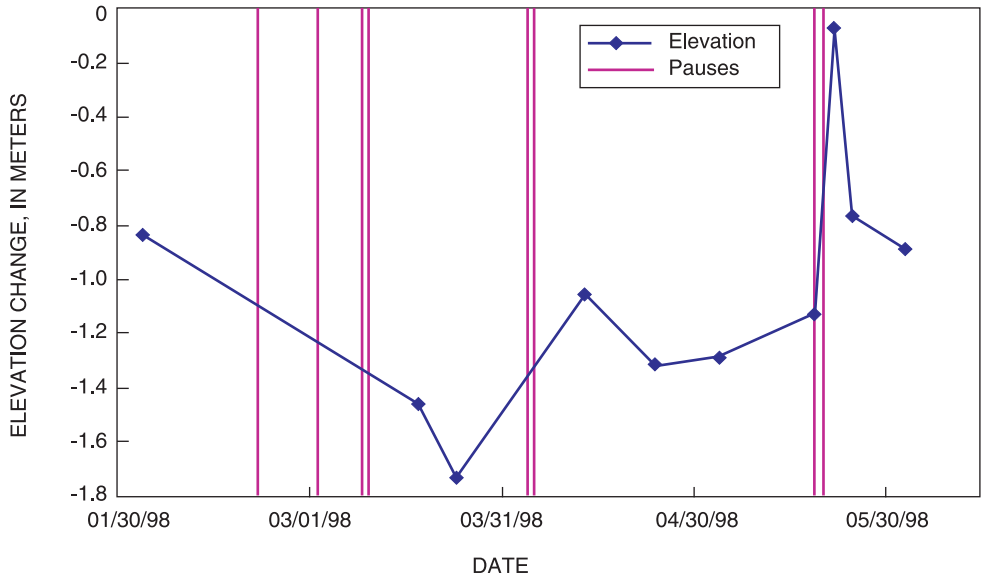

Figure 10. Elevation changes in interior of 1998 shatter ring. Vertical lines denote eruption pauses.

molten lava and seawater induced by wave action or from confined mixing within lava tubes in the bench. The explosions can produce abundant glass lapilli, ash, spatter bombs, Pele's hair, and limu o Pele (Hon and others, 1988). When interactions are persistent, littoral cones can develop.

Lava deltas subside while they are forming (Kauahikaua and others, 1993). Repeated surveying of two lines across the lava delta built off Kamoamoa in 1993 showed that it was subsiding faster at its seaward edge than at the old coastline. The maximum subsidence rate at the new coastline was just less than 1.5 mm per day over the 3 weeks between surveys.

The flexing and subsidence of a lava delta diminish over time after flow activity has ceased, presumably owing to increasing cementation of the submarine hyaloclastite fan. Three survey lines established in 2000 on lava deltas last active in 1996 and 1998 show a vertical change of less than 3 mm in 2 years—the limit of the survey's precision. Notable subsidence characterizes only the outermost survey pin along each line, where the rocks are persistently buffeted by surf. These rocks were visibly downdropped from the position they held when the pin was initially set. On two lines, blocks containing the outermost pins disappeared.

We conclude from these survey data that lava deltas build outward farthest over shallow marine embayments and relatively stable submarine slopes. The slopes then become oversteepened, and later lava flows of the same eruption expand the delta seaward, while supplying the slopes with new hyaloclastic debris. These slopes grow more stable during the decades between major eruptions, and the ground is thus prepared for new seaward growth in the next major eruption.

Elevation profiles of the Kamoamoa lava delta show that the subaerial slope within 250 m inland of the coastline steepens seaward from about 0.4° to 2.3° (Kauahikaua and others, 1993). Examination of the slope map (fig. 1) confirms that this steepening is a common feature of the new coastline. If lava tubes were at an approximately constant depth within the delta, the steepening would result in a marked increase in flow velocity. This fringe of steepened topography immediately behind the new coast is the most common place on the coastal plain for skylights to form, presumably because the lava stream cuts downward, leaving its roof unsupported (Kauahikaua and others, 1998a).

Underwater observers report both pillow lava and highly channelized lava streams flowing down a steep and unconsolidated submarine slope (Tribble, 1991). Partially crusted lava in the 0.75- to 1.5-m-wide channels advances at a velocity of 1 to 3 m/s, similar to the flow velocities through subaerial lava tubes and small channels. Bubbles of water vapor form and collapse constantly on the hot surface and are commonly audible to divers as explosions. A sonobuoy survey on Lō'ihi could detect both these explosions and more constant sounds indicative of mass wasting relating to bench collapse (Caplan-Auerbach and Duennebier, 2001; Caplan-Auerbach and others, 2001).

We conducted two brief, near-shore bathymetric surveys to determine whether our coastal-hazard analysis could be broadened by monitoring changes on the submarine slopes. Previously published maps show bathymetric contours that trend parallel to the coastline and define a slope dipping 21° in the first 1,000 m of water depth (Chase and others, 1981; Chadwick and others, 1993). After an extensive bench collapse in March 1998, we mapped the seafloor at 100- to 1,000-m depth using a small fishing vessel equipped with an ocean-bottom finder (fig. 11). This collapse destroyed not only the bench outboard of the existing seacliff but also a large tract of land behind the seacliff, 10 ha in all. The most conspicuous features of the survey are a set of shallow

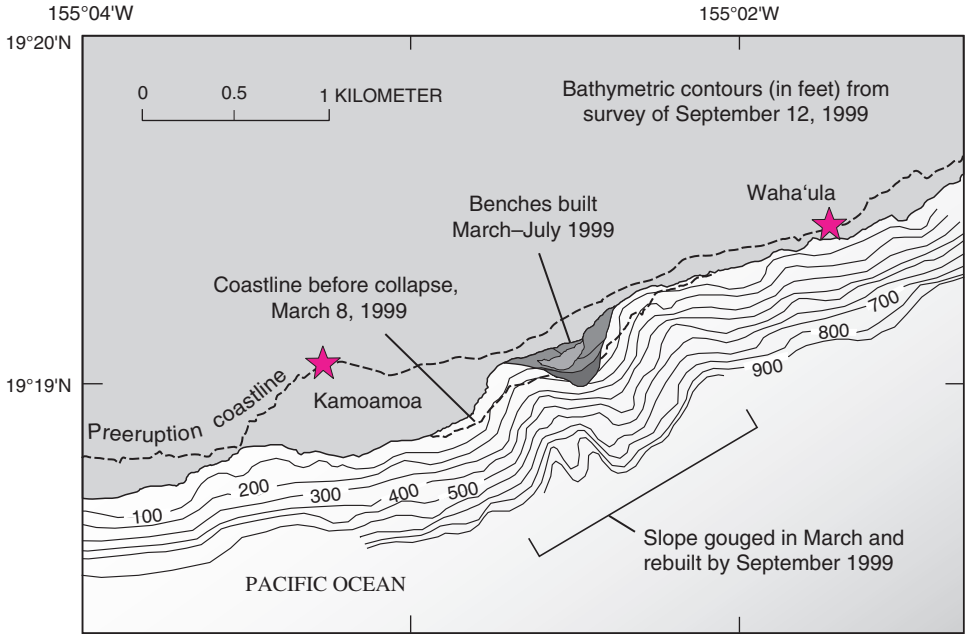

Figure 11. Bathymetry of coastal area near 1999 Kamokuna ocean entry.

canyons in the submarine fan, possibly gouged by collapsing debris. Subsequent regrowth of a lava bench during the 6 months between this collapse and our survey allows an alternative interpretation that the canyons are merely artifacts resulting from bench growth in the intervening sector. We prefer the erosional interpretation because such large canyons are found only along this stretch of our 6-km-long survey, and long-lived lava benches elsewhere along the survey lack conspicuous submarine constructional forms.

The long-lived lava entries have enabled studies of the chemical alteration of the seawater and the composition of the steam plume. Sansone and others (1991), Sansone and Resing (1995), and Resing and Sansone (2002) reported that the seawater near the ocean entry is highly enriched in H_2, Mn, and Si and has high particle concentrations. Temperatures are elevated to at least 69ºC in a surface layer 1 to 2 m thick.

A roil (fig. 12) is frequently observed a few tens of meters offshore from an active ocean entry. These roils are crudely circular areas of calmer water that are generally darker than the light-colored plumes of heated water emanating radially away from the molten-lava-contact point (Realmuto and others, 1992). Commonly, two such light-colored plumes occur with a roil between them (fig. 12). Temperature measurements indicate that the roil is an area where heated water is upwelling over a submarine lava extrusion (Sansone and Resing, 1995). The water temperature and chemistry within a roil are nearly identical to those outside the general ocean-entry area. When a roil is viewed with an infrared video camera, however, small amounts of warm water are seen emerging at the roil's center and spreading out radially (fig. 13). Although the general area of the roil is cooler than the warm plumes to either side, the fine structure confirms that the roils are driven by convection of warm water from the sea floor.

Reversible (?) Transition Between Pāhoehoe and ʻAʻā

The discussion about the transition between pāhoehoe and ʻaʻā became semiquantitative in the reports by Peterson and Tilling (1980) and Kilburn (1981), who described the transition as a relation between viscosity and the rate of internal shear strain. Kilburn (2000) recast the transition in terms of a relation between applied stress and deformation rate, with a primary emphasis on crust formation, and reiterated the long-held belief that the pāhoehoe-ʻaʻā transition is irreversible. The long Puʻu ʻŌʻō-Kūpaianaha eruption presented numerous opportunities to observe this transition.

Observations

For tholeiitic magma, low-effusion-rate eruptions produce pāhoehoe flows, and high effusion-rate eruptions produce ʻaʻā flows, with the threshold at about 5 to 10 m^3/s in Hawaiʻi (Rowland and Walker, 1990). This data set includes ʻaʻā flows from Puʻu ʻŌʻō and episode 48 pāhoehoe from Kūpaianaha. Cashman and others (1999) and Polacci and others (1999) analyzed lava sampled from channels and reported that the lava that solidified to ʻaʻā contains at least 30 to 50 volume percent plagioclase microlites, whereas lava that solidified to pāhoehoe has a much lower microlite crystallinity. These observations suggest that plagioclase microlite abundance might be an index for the transition between these morphologic and behavioral characteristics. Hoover and others (2001) and Saar and others (2001) detailed the establishment and increase of yield strength in a Newtonian fluid with the addition of solid particles, such as crystals. Their results reveal

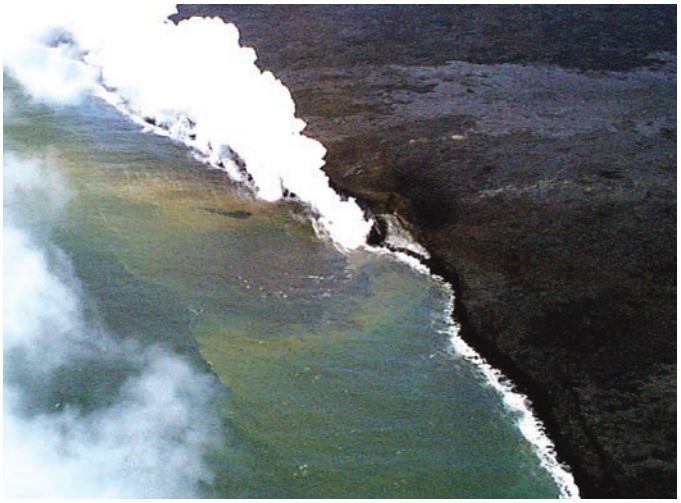

Figure 12. Roil (darker area just outboard of steam plume) between two lighter-colored warm-water plumes. Roil is 23–25°C, and plumes are at least 70°C on either side. Photograph and radiometric temperatures taken May 7, 1998.

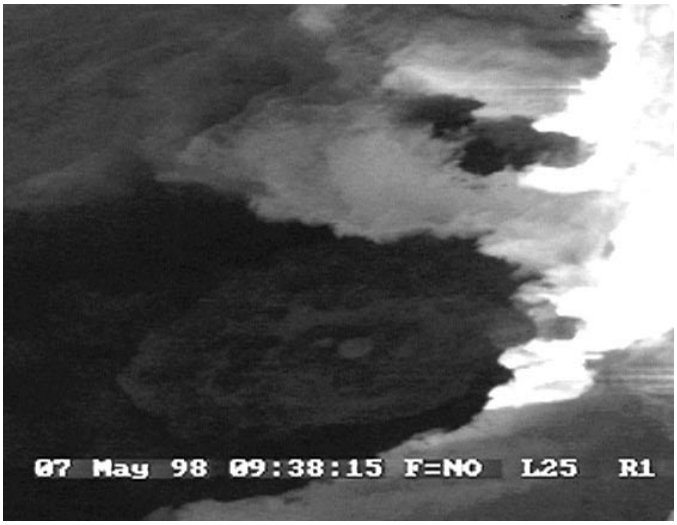

Figure 13. Infrared video image of roil between two warm-water plumes, showing slightly warmer water in center beginning to spread out radially. White area is hot; ocean entry to right. Video taken May 7, 1998.

how microcrystallinity increases the yield strength to the point that a fluid tears under shear stress instead of flowing. The factors that can induce an increase in microlite crystallinity are (1) degassing, either in high lava fountains (see Heliker and others, this volume) or shallow subsurface transport (Lipman and others, 1985); (2) cooling (Cashman, 1993; Crisp and others, 1994); and (3) high internal shear stress, such as that generated gravitationally by flowing over steep slopes.

During the current eruption, lava flows commonly emerged from vents as pāhoehoe over ground that sloped as much as 3º, then changed to ʻaʻā going over Pūlama pali, which slopes as much as 20º, on the way to the coastal plain slope (0º–1º) and the coast. We observed two distinct behaviors of ʻaʻā flows that raise questions about the irreversibility of the pāhoehoe-ʻaʻā transition. In the first case, lava flows initially solidifying as pāhoehoe began to solidify as ʻaʻā as they advanced down steeper slopes, then continued to solidify as a crust transitional to pāhoehoe (see Hon and others, this volume).

In the second case, ʻaʻā fronts stagnated upon reaching the flat terrain and then leaked fluid lava. For example, the initial episode 55 lava flow (July 1997) traveled over the pali as a channelized ʻaʻā flow, moved obliquely down the pali, and turned toward the ocean before stalling. Lava solidifying as pāhoehoe apparently broke out of its core and continued 1 km to the ocean. This flow continued to supply lava to the ocean entry for several months as the ʻaʻā channel fed lava through its front into the tube system of the pāhoehoe flow. The time between the stalling of the ʻaʻā front and the initiation of the pāhoehoe was, at most, hours; in other words, the pāhoehoe was not a later flow reoccupying the previous ʻaʻā channel (Kilburn, 2000). Similar behavior was observed for a 1-km-long tube breakout on November 10, 1998. The initial flow was channelized ʻaʻā that leaked a lava apron which solidified as pāhoehoe. The Mother's Day, 2002, flow advanced rapidly from the flank of Puʻu ʻŌʻō as an ʻaʻā flow for the first 3 km, then stalled and continued as a more fluid lava solidifying as pāhoehoe. Thus, the core of these two ʻaʻā flows was sufficiently fluid to form a pāhoehoe crust. Similar observations were made during the 1991–1993 Mount Etna eruption (Calvari and Pinkerton, 1998).

An Alternative Model

A solidified piece of pāhoehoe cannot convert to a solidified piece of ʻaʻā, and conversely. Thus, any transition must refer to an identified *pāhoehoe liquid* that can solidify as either a pāhoehoe or an ʻaʻā crust. If the liquid begins to host slightly solidified chunks on its surface, we would probably call it an *ʻaʻā liquid* and expect only ʻaʻā crusts to solidify from this liquid. ʻAʻā liquid might be an accurate description of the liquid's surface morphology, but the liquid deeper in the channel could still solidify as either an ʻaʻā or pāhoehoe crust upon leaking to the surface. The transition from low to high microlite crystallinity in the liquid must either precede or accompany the solidification of ʻaʻā crust.

This discussion shows that the designation of a liquid as pāhoehoe or ʻaʻā from its morphologic characteristics can be a poor indicator of its future behavior. We therefore suggest that liquid should be identified as neither pāhoehoe nor ʻaʻā. Those morphologic terms should be used only as the Hawaiians originally used them, for solidified products. The change from one morphology to another along channels can still be defined from solidified products deposited on levees. We can also picture the transition zone as marked by a contour of microlite crystallinity in the liquid. That transition zone might be three dimensional in a channel where the surface liquid solidifies as an ʻaʻā crust, but the deeper liquid is sufficiently insulated to continue down channel and either bleed out the front of the ʻaʻā flow or move farther down channel before coming to the surface and solidifying as a pāhoehoe crust.

Implications for Modeling and Interpretation of Remote-Sensing Data

Thermal Models and Applications

Thermal models of lava flows have applications ranging from remote volcano monitoring to volcanic geothermal energy development. The single study of such development during this eruption sought to measure the convective heat flux available in lava during episode 2 (1.8-8.1 kW/m^2; Hardee, 1983). The application of thermal models to volcano-hazard and lava-flow studies is more numerous.

Cooling of pāhoehoe flows has been studied by using measured internal and surface temperatures, and modeled simply as conduction with no radiation (Hon and others, 1994). The resulting model works well when using crustal thickness for estimating the age of crust on pāhoehoe lobes within a timespan of hours to days. The model extends the conductive crustal-growth model for months to years on the basis of data obtained from the cooling of Makaopuhi lava lake (Wright and Okamura, 1977). Significantly higher temperatures than predicted by conductive cooling alone were measured, however, beneath an advancing pāhoehoe flow (Keszthelyi, 1995); the high temperatures were interpreted as the sudden release of latent heat from crystallization. These data were used to construct a model that included both conductive and radiative cooling (Keszthelyi and Denlinger, 1996). Their intent was to use this model to predict cooling rates not only of Kīlauea lava but also of lava with different rheology in different environments and even on different planets. This model currently works well for only the first 5 minutes of the cooling process.

Much work has been done to characterize lava-flow cooling by using surface temperatures alone to calibrate satellite-based sensors. Cooling models with two thermal components (Crisp and Baloga, 1990) have been used since 1990 for most work on thermal radiation from both lava flows

and lakes. Flynn and Mouginis-Mark (1992) made nighttime measurements on an active episode 50 lava flow. The data were modeled as having a crustal temperature of 768ºC and a hot core of 1,150ºC that composed 3.6 percent of the lava flow area (hot radiating area) upon emplacement. In the next 52 minutes, the crust cooled to 420ºC at rates as high as 15ºC per minute. Flynn and Mouginis-Mark (1994) also made spectroradiometric measurements on an active episode 50 channelized flow. The two-component thermal model was more nearly steady state in this experiment, with a crust at 940ºC, a hot core at 1,120ºC, and a hot radiating area of 60 percent in the channel center and a crust at 586ºC, a hot core at 1,130ºC, and a hot radiating area of 1.2 percent at the channel margin. The thermal-radiance model parameters obtained for Hawai‘i flows and lava lakes are summarized in table 1.

Surface-temperature studies were summarized by Pinkerton and others (2002), who concluded from their extensive ground measurements that a minimum of four thermal components are required to fully characterize Hawaiian lava flows: core (>1,050°C), viscoelastic skin (750–900°C), rigid solid crust (<750°C), and flow margins (<175°C).

Cooling of Hawaiian pāhoehoe flows is thus well understood. The crust and the much hotter core both cool substantially by radiation in the first few minutes after emplacement, then predominantly by conduction to the air. The flow surface cools rapidly while the crust cracks. The flow interior cools by conduction. It is difficult to generalize these results to flows in substantially different environments.

Estimating Lava Volume Rate from Thermal Satellite Data

Harris and others (1998) proposed a method of estimating instantaneous lava-effusion rate from Thematic Mapper measurements of the total thermal flux of active surface flows. This method produced reasonable matches to VLF-based estimates during 1991 (Kauahikaua and others, 1996). Cloud cover limits this method's application. Wright and others (2001) pointed out that use of Harris and others' method with advanced very high resolution radar (AVHRR) data, which are commonly saturated at active-lava-flow temperatures, yields average effusion rates based on flow area rather than instantaneous effusion rates.

Advances in Lava-Flow-Hazard Assessment and Mitigation

A long-lived and much-studied eruption promotes improved monitoring techniques and methods. Increased understanding of the mechanics of eruptions and lava flows can help mitigate future volcanic hazards in Hawai‘i through more precise estimates of both hazard and risk. Low-risk alternatives can then be explored for future land-use planning.

Use of Infrared Imagery in Routine Flow-Field Monitoring

Landsat and other thermal imagery has shown with rare clarity the system of tubes and active flows (Realmuto and others, 1992); however, Landsat images take several weeks to months to acquire, and other specialized imagery may take even longer. Prevalent cloud cover may make it difficult to get a clear view. From July 1999 to July 2002, Landsat 7, which takes an image of the flow field every 16 days, has recorded only three clear views of the entire flow field, 29 views of at least 50 percent of the flow field, and 35 views of mostly clouds. The infrequent acquisition and low yield of cloud-free images make use of this imagery impractical for hazard-mitigation work. Monitoring requires frequent and immediately available imagery.

Beginning with episode 54 in January 1997, the active volcanoes of Hawai‘i have been imaged every 15 minutes, using the AVHRR sensor on the geosynchrous-orbiting environmental satellite (GOES) and processed specifically to detect thermal changes in the current eruption (Harris and others, 1997a, b, 2000; Harris and Thornber, 1999). A Web site, designed and maintained by the Hawai‘i Institute of Geophysics and Planetology, makes these images available to the public at URL http://goes.higp.hawaii.edu/bigisland/latest.shtml. Unless clouds obscure the vent and lava flows, timing of eruption events (lava flows of >10,000 m^2 area) can be documented within the 15-minute sampling rate of the GOES. The tradeoff for frequent images is the crude spatial locations afforded by the 4- by 4-km pixel size of the thermal band.

Handheld infrared video cameras offer a timelier, more spatially precise alternative. Keszthelyi (1993) demonstrated that lava tubes and flows are easily visible with these tools. We have been using uncalibrated forward-looking infrared radiometer (FLIR) video several times a year for the past 10 years. A single pass over the flow field can catalog flows that have been active in the past 4 to 6 weeks, as well as those active currently. In addition, the infrared images can show the location and configuration of lava tubes beneath the surface in areas without significant surface-flow activity.

Use of an uncalibrated infrared video camera is sufficient to map lava flows and tubes (fig. 14). Relative temperatures are all that we need if the studies are aimed only at cataloging the heat sources and not at understanding the process of cooling.

Telemetered Video Images of Pu‘u ‘Ō‘ō

Since 1997, live video images of Pu‘u ‘Ō‘ō's crater have been available at the Hawaiian Volcano Observatory (Thornber, 1997). These images have proved useful for monitoring eruptive activity within the crater, such as the initiation and growth of vents and the filling and draining of the crater. The images are of relatively low resolution but are sufficient to track changes in the crater between observational visits. The real value of continuous imagery is its potential for correlating visible activity with satellite observations and seismic

Table 1. Summary of radiometrically measured or modeled lava temperatures. Episode numbers refer to Pu‘u ‘Ō‘ō-Kūpaianaha eruption.

Crust temperature (°C)	Core temperature (°C)	Hot fraction (per cent)	Average total radiant flux density (kW/m^2)	Comment
--	1,130–1,145	0.5	--	Episode 4 and 18, Mauna Loa 1984, 1 and 1A (Crisp and Baloga, 1990).
768	1,150	3.6	72.2	Emplacement, episode 50 flow (Flynn and Mouginis-Mark, 1992).
410	900	0.5	12.7	52 minutes after emplacement.
940	1,120	60	130	Center of channel, episode-50 (Flynn and Mouginis-Mark, 1994).
586	1,130	1.2	29	Margin of channel.
180–572	900–1,250	<2.1	22	1987–1988 Kūpaianaha lava lake, stage 1, fountaining and overturning crusts (Flynn and others, 1993).
100–340	900–1,250	<0.39	5.3	1987–1988 Kūpaianaha lava lake, stage 2, rifting.
80–345	900–1,250	<0.05	4.9	1987–1988 Kūpaianaha lava lake, stage 3, quiescent.
--	--	--	128–170	7/91 Kūpaianaha lava lake (Harris and others, 1999).
400–505	--	--	--	2/2795–3/10/95 Pu‘u ‘Ō‘ō lava lake (HVO unpub. radiometric data).
220–240	--	--	--	3/11/95 Pu‘u ‘Ō‘ō lava lake (HVO unpub. radiometric data).
--	980–1,110	--	--	1995–2001 various skylights (HVO unpub. radiometric data).

and deformation monitors (Harris and Thornber, 1999). Barker and others (this volume) report on an application of this technique.

Monitoring of Lava-Flow-Field Formation and the Volumetric Rate of Lava Produced

During the past 5 years, lava tubes and flows have been mapped by using hand-held Global Positioning System (GPS) receivers. Both commercial- and military-grade receivers have been used, resulting in an accuracy of 5 to 20 m. Many lava-flow contacts are mapped by walking along with GPS in hand, recording waypoints or trackpoints at intervals of 5 to 20 m. Some of the more difficult parts of a flow field are mapped by GPS in a helicopter, with the pilot flying as close to the contact as possible. At times, partial flow contacts located by GPS are completed freehand by referencing oblique aerial photographs. The GPS data are combined into flow polygons for use with GIS software; the eruption-update maps are GIS products. All the episode 55 flow contacts illustrated by Heliker and Mattox (this volume) and Heliker and others (this volume) were determined in this way.

Lava tubes are mapped on the basis of surface features, such as fume, elongate tumuli, skylights, hornitos, and breakouts, and can be more precisely located by using surface geophysics, such as Geonics EM-16 (VLF) or EM-31 conductivity tools (Zablocki, 1978). Molten lava is electrically conductive and so easily detected by using shallow electromagnetic tools (Kauahikaua and others, 1996). We use these techniques weekly, together with visual observations and active flow mapping, to track active lava tubes and flows. Lava flows commonly originate where a tube ruptures, and so a current map of a lava tube is a basic predictor of where surface flows will originate (Mattox and others, 1993).

In addition to field mapping, numerous digital photographs and some video tapes record flow features from the air and ground. The digital images can be distributed quickly, and the public is then informed, commonly within 24 hours of any new developments, through the HVO website at URL http://hvo.wr.usgs.gov/.

Repeated VLF profiles at fixed spots along a lava tube can be used to estimate its cross-sectional conductance. Lava is the only conductor, and we can independently estimate its conductivity. The estimated conductance allows an easy way to monitor the cross-sectional area of fluid lava in the tube. In combination with velocity measurements made at a nearby skylight with a radar gun, a volumetric flux can be estimated. These measurements can be made nearly anywhere on the lava-tube system, but those nearest a vent on the master tube are better approximations of the total output of the vent. Linearly declining flux estimates accurately predicted the demise of the Kūpaianaha vent in early 1992 (Kauahikaua and others, 1996). Similarly declining flux estimates on just a branch of a lava tube without corresponding decline in either the total flux or the other branches has signaled the end of activity of that branch. These geophysical results have compared favorably with a flux estimated from differences in the volume of the flow field (Rowland and others, 1997), satellite thermal-flux data (Harris and others, 1998), and gas-emission data (Sutton and others, 2001; this volume). Currently, these estimates are made once per week, a frequency that is easily capable of demonstrating long-term behavior but incapable of showing response to short-term events either at Pu‘u ‘Ō‘ō or at Kīlauea’s summit.

Prediction of Lava-Flow Behavior

The ultimate goal of lava-flow-hazard mitigation is prediction of the direction and advance rate of lava flows. That challenge has inspired the development of computer code to simulate lava flows (Ishihara and others, 1989; Young and Wadge, 1990; Miyamoto and Sasaki, 1997, 1998; Harris and Rowland, 2001). Much of the physical parameterization of lava flows in terms of viscosity, yield strength, and density has improved computer simulations. More robust approaches to develop limited forecasting tools include the delineation of lava sheds and preferred pathways for possible lava flows.

Lava Sheds and Preferred-Gravitational-Flow-Path Maps

Rather than simulating lava flows, complete with complex rheology, we may be able to make significant contributions by splitting the prediction question into several parts. A primary question is, where will a lava flow go? Answering that question is a simple terrain analysis problem solvable with standard GIS tools.

A catchment (Guest and Murray, 1979) or lava shed (Kauahikaua and others, 1998b) is an area within which any lava flow will be confined if it is erupted from a vent within that lava shed. Lava sheds are computed as watersheds that drain into the ocean. When an eruption begins and the position and configuration of the vents are known, the vents can be plotted on a lava-shed map. The initial lava flow is predicted to advance within any lava shed that contains a part of the eruptive vent. A lava-shed map can also determine which areas are topographically shielded from lava flows (Guest and Murray, 1979).

A refinement on this idea is to include the major pathways, or paths of steepest descent, predicted for gravitationally driven fluids on the island's surface. These pathways also are easily computed with standard GIS tools. Hanley and Zimbelman (1998) evaluated such computed paths as predictors for lava flows from the first 18 episodes of activity at Pu‘u ‘Ō‘ō and calculated that they account for 60 percent of the flow's location and orientation. A "steepest path" map for part of the Island of Hawai‘i, showing those pathways that drain at least 1 km^2 of surface area for the region including the lower flows erupted from Mauna Loa in 1984, is shown in figure 15. Both the lava sheds and the preferred pathways

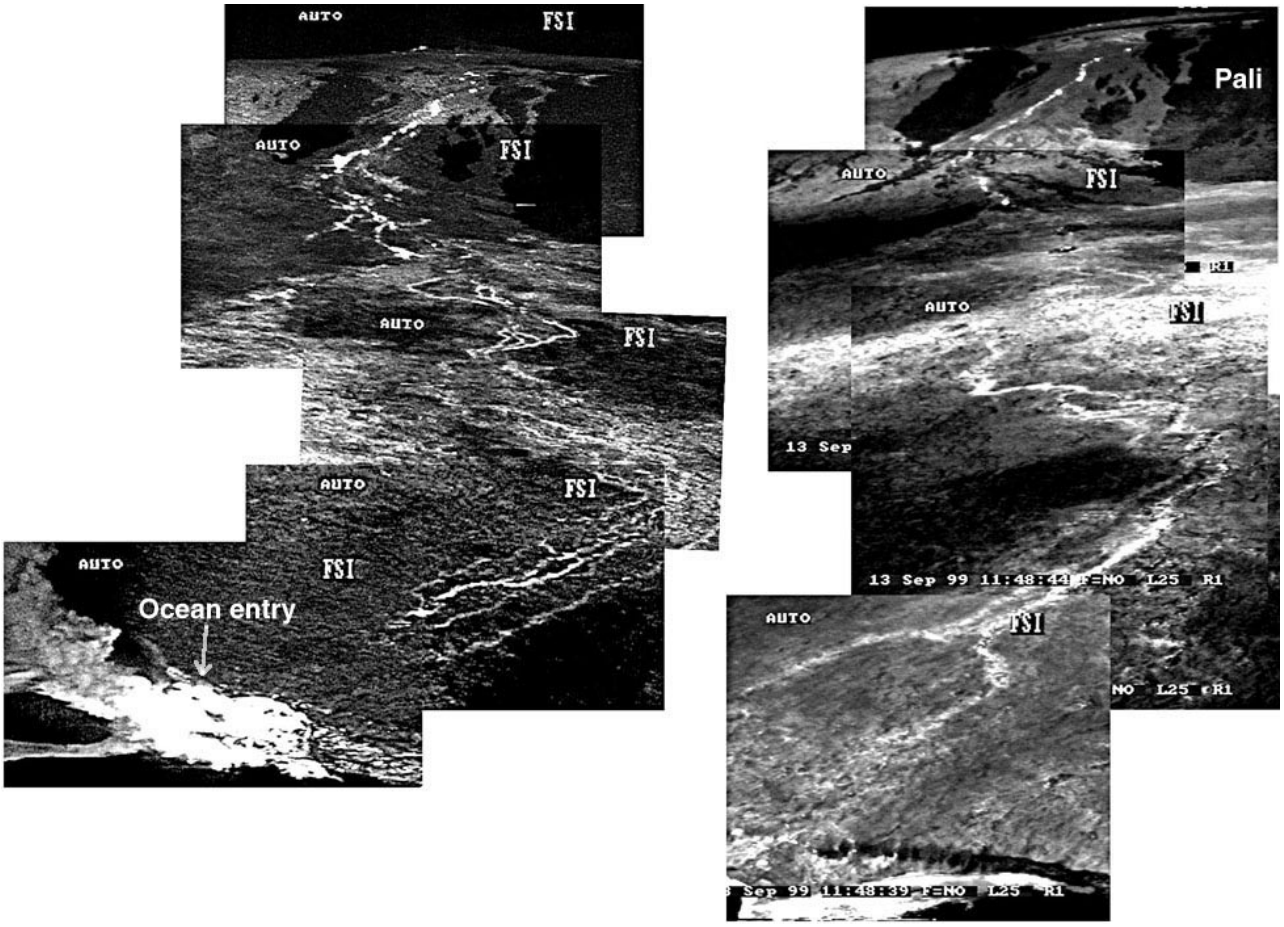

Figure 14. Composite infrared video images of lava-tube system, showing young system with braided streams. In right image, braids have consolidated into a few main braids. Note the redirection of the lower extent of the two braids near coastline. Videos taken December 29, 1998 (left), and September 13, 1999 (right).

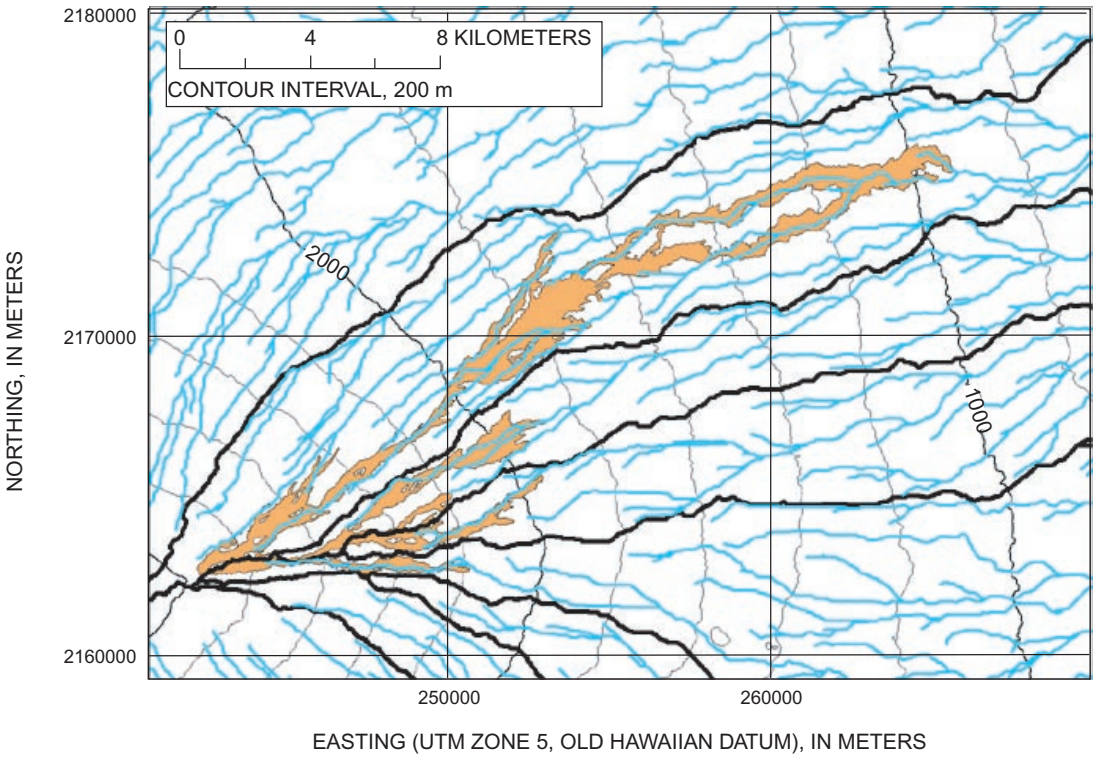

Figure 15. Lower 1984 lava flows from Mauna Loa (orange), Island of Hawai'i. Heavy black lines outline lava sheds; blue lines denote estimated preferred lava pathways.

were estimated from 1978 topography. Note how well both the lava sheds and the preferred pathways would have predicted the ultimate path of the 1984 lava flows. Several such pathways may exist within a single lava shed, and so spatial predictive capability can be further refined.

Estimation of Probabilistic Lava-Flow Hazards

Probabilistic-hazard maps address the question "How often will lava flows inundate a given area?" If we can assume that future inundation will be statistically identical to past inundation, then the question becomes "How often in the past has lava inundated a given area?" Three steps are needed to answer this question. The first step is to obtain a digital geologic map in which each lava flow is mapped and dated. The second step is to determine the distribution of lava-flow-recurrence intervals within subregions. The third step is to choose an appropriate statistical distribution (for example, Poisson or Weibull) to estimate the average recurrence interval from the frequency of lava-flow occurrence. The average recurrence interval can then be used to estimate the probability of future inundation (Kauahikaua and others, 1995a). This methodology was applied to estimating the lava-flow hazard for the east rift zone geothermal subzones (Kauahikaua and others, 1995b) and for a proposed prison site on the northeast rift zone of Mauna Loa (Kauahikaua and others, 1998b). The results give the probability of lava-flow inundation within some nominal period, chosen to be 50 years for those studies.

Two problems arise when estimating inundation probabilities on the basis of past lava-flow frequencies. The first problem is the general condition that younger flows progressively bury older flows, and so an uncorrected frequency-versus-age histogram for any volcano shows exponentially decreasing frequency with age. The second problem is the apparent disparity in eruption frequency between the past 150 years of close observation and previous periods represented only by mappable and datable lava flows. These problems have been overcome; correction methods were compared by Kauahikaua and others (1998b).

An alternative approach is to estimate the probabilities of lava-flow inundation from the combined estimate of the probability of an eruption occurring anywhere on the volcano, the probability of the eruption location, the probability of a lava flow being generated, and the probability of specific lava-flow parameters (such as composition, effusion rate, or temperature; Newhall and Hoblitt, 2002). This approach has been used for Mount Etna (Wadge and others, 1994) where lava flows were simulated by using both a stochastically chosen vent site and a set of parameters from a library of such parameters for lava flows erupted between 1763 and 1989. The resulting map displays the frequency of inundation for areas around the volcano. A total of 380 flows were simulated, representing a 2,400-year period. The zones of greatest hazard were areas inundated by more than 10 flows at an average recurrence interval of less than 240 years. Changes in topography were not

explicitly incorporated into their computer simulations, and so Wadge and others emphasized that the resulting map is not "a map of the likely coverage of lava flows in the next 2,400 years but a map of the potential for inundation by lava flows now"— that is, areas inundated by the most simulated flows are those of highest hazard for the next flow but not necessarily those that will be inundated by the most flows in the next 2,400 years. The next flows will change the topography and alter the paths of all future flows. For comparison, Wadge and others (1994) presented a map of historical frequency of lava-flow inundation for the period 1763–1989, within which the maximum frequency is only six flows. Although this estimate of the lava-flow hazard has been labeled "probabilistic," the result is not easily converted to probability of inundation.

Future Directions in Monitoring

Significant progress in volcano monitoring has been made over the last two decades, but we should not conclude that little is left to do to advance our understanding of lava-flow dynamics. Lava erupting from a vent drives all the flow-field processes, and so we could and should better understand the conduit system within Pu‘u ‘Ō‘ō and exactly how it connects to the lava-tube system. The cause of the numerous collapse structures both inside and outside Pu‘u ‘Ō‘ō crater is unclear. Do they overlie the upper reaches of a deep tube exiting flank vents on the west side of the cone, or are they part of a structure, such as concentric fracturing around the base (see Heliker and others, this volume)?

Further progress could be made by improving our current ability to monitor the lava output from Pu‘u ‘Ō‘ō. Elevation data over the entire flow field (possibly from satellite- or aircraft-borne radar) for time intervals during which no lava entered the ocean could help calibrate or check volume-rate estimates obtained by the currently used techniques of VLF electromagnetic profiles or gas monitoring. New monitoring technologies are being developed to study lava-tube flow by passive seismic listening or active ultrasound probing (Rick Hoblitt, oral commun., 2002). Development and increasing reliability of such tools, in addition to an increase in the frequency of data acquisition by way of telemetered sites, should improve our understanding of the short-term relation between deformation, seismic events, and lava output. We will be better able to correlate short-term flow-field events, such as tube ruptures, breakouts, and shatter-ring and rootless-shield development, with short-term and, possibly, subtle variations in lava supply. Our current monitoring capabilities and weekly data allow resolution of only long-term changes and relations.

More can be learned by combining remote sensing technologies with traditional ground-based observations. Multispectral satellite images are invaluable but are too infrequently obtained to be routinely useful. It would be ideal to be able to acquire the same sort of data on demand rather than waiting for a favorable satellite pass and clear sky, such as by using hand-held multispectral imagers from the ground or a helicopter. Imagers could also be borne on small remote-controlled blimps, balloons, or aircraft. Interferometric radar for measuring topographic changes may be usable from aircraft or from the ground.

We would also like to progress with real-time telemetered information, such as tube-flux monitors based on the VLF electromagnetic technique, microphones for monitoring gas jetting, and stationary video monitors, possibly including infrared sensors. Multiple telemetered sites and continuous data sets could allow synchronous observation of lava vents and tubes, or of several vent sites—data crucial to deciphering vent structure and mechanics.

More quantitative measurements and change detection could be done with oblique digital photographs. We currently take many photographs from the ground and helicopters and can keep track of most changes through familiarity with features by personnel. Subtle changes may be missed, however, until they increase and become more significant. Time-lapse videography has shown great promise in revealing lava flow processes that happen slowly, such as inflation of both pāhoehoe and ‘a‘ā channels (for example, Ka ‘Io Productions, 2000).

Last, but not least, much remains to be understood about lava flow emplacement. Although we have empirical interpretations for the emplacement modes of pāhoehoe and ‘a‘ā, and for the various transitional types of lava morphologies observed in the last two decades, quantifying their emplacement conditions would be a significant advance.

Acknowledgments

We thank the numerous student volunteers who contributed time and effort to acquire many of the data presented here, and Rick Hoblitt, Frank Trusdell, Don Swanson, and Jane Takahashi for their helpful reviews of this manuscript. We also thank helicopter pilot David Okita, who has been part of the research team, as well as a great pilot, for most of the eruption.

References Cited

Anderson, S.W., Stofan, E.R., Smrekar, S.E ., Guest, J.E., and Wood, B.J., 1999, Pulsed inflation of pahoehoe lava flows; implications for flood basalt emplacement: Earth and Planetary Science Letters, v. 168, no. 1–2, p. 7–18.

Anderson, S.W., Stofan, E.R., Smrekar, S.E ., Guest, J.E., and Wood, B.J., 2000, Reply to Self et al discussion of "Pulsed inflation of pahoehoe lava flows; implications for flood basalt emplacement": Earth and Planetary Science Letters, v. 179, no. 2, p. 425–428.

Appelgate, Bruce, and Embley, R.W., 1992, Submarine tumuli and inflated tube-fed lava flows on Axial Volcano, Juan de Fuca Ridge: Bulletin of Volcanology, v. 54, no. 6, p. 447–458.

Atkinson, Anne, and Atkinson, Vernon, 1995, Undara Volcano and its lava tubes: Brisbane, Australia, Vernon and Anne Atkinson, 86 p.

Baird, A.K., Mohrig, D.C., and Welday, E.E., 1985, Vapor deposition in basaltic stalactites, Kilauea, Hawaii: Lithos, v. 18, no. 2, p. 151–160.

Baloga, S.M., Glaze, L.S., Crisp, J.A., and Stockman, S.A., 1998, New statistics for estimating the bulk rheology of active lava flows; Puu Oo examples: Journal of Geophysical Research, v. 103, no. B3, p. 5133–5142.

Baloga, S.M., Glaze, L.S., Peitersen, M.N., and Crisp, J.A., 2001, Influence of volatile loss on thickness and density profiles of active basaltic flow lobes: Journal of Geophysical Research, v. 106, no. B7, p. 13395–13405.

Baloga, S.M., and Pieri, D.C., 1986, Time-dependent profiles of lava flows: Journal of Geophysical Research, v. 91, no. B9, p. 9543–9552.

Barnard, W.M., ed., 1990–92, Mauna Loa—a source book; historical eruptions and exploration: Fredonia, N.Y., Walther M. Barnard, 3 v.

Calvari, Sonia, and Pinkerton, Harry, 1998, Formation of lava tubes and extensive flow field during the 1991–1993 eruption of Mount Etna: Journal of Geophysical Research, v. 103, no. B11, p. 27291–27301.

Caplan-Auerbach, Jacqueline, and Duennebier, F.K., 2001, Seismic and acoustic signals detected at Loʻihi Seamount by the Hawaiʻi Undersea Geo-Observatory: G^3 (Geochemistry, Geophysics, Geosystems), v. 2, paper 2000GC000113.

Caplan-Auerbach, Jacqueline, Fox, C.G., and Duennebier, F.K., 2001, Hydroacoustic detection of submarine landslides on Kilauea volcano: Geophysical Research Letters, v. 28, no. 9, p. 1811–1813.

Cashman, K.V., 1993, Relationship between plagioclase crystallization and cooling rate in basaltic melts: Contributions to Mineralogy and Petrology, v. 113, no. 1, p. 126–142.

Cashman, K.V., and Kauahikaua, J.P., 1997, Reevaluation of vesicle distributions in basaltic lava flows: Geology, v. 25, no. 5, p. 419–422.

Cashman, K.V., Mangan, M.T., and Newman, Sally, 1994, Surface degassing and modifications to vesicle size distributions in active basalt flows: Journal of Volcanology and Geothermal Research, v. 61, no. 1–4, p. 45–68.

Cashman, K.V., Thornber, C.R., and Kauahikaua, J.P., 1999, Cooling and crystallization of lava in open channels, and the transition of pāhoehoe lava to ʻaʻā: Bulletin of Volcanology, v. 61, no. 5, p. 306–323.

Chadwick, W.W., Jr., Gregg, T.K.P., and Embley, R.W., 1999, Submarine lineated sheet flows; a unique lava morphology formed on subsiding lava ponds: Bulletin of Volcanology, v. 61, no. 3, p. 194–206.

Chadwick, W.W., Jr., Scheirer, D.S., Embley, R.W., and Johnson, H.P., 2001, High-resolution bathymetric surveys using scanning sonars; lava flow morphology, hydrothermal vents, and geologic structure at recent eruption sites on the Juan de Fuca Ridge: Journal of Geophysical Research, v. 106, no. B8, p. 16075–16099.

Chadwick, W.W., Jr., Smith, J.R., Jr., Moore, J.G., Clague, D.A., Garcia, M.O., and Fox, C.G., 1993, Bathymetry of south flank of Kilauea Volcano, Hawaii: U.S. Geological Survey Miscellaneous Field Studies Map MF–2231, scale 1:150,000.

Chase, T.E., Miller, C.P., Seekins, B.A., Normark, W.R., Gutmacher, C.E., Wilde, Pat, and Young, J.D., 1981, Topography of the southern Hawaiian Islands: U.S. Geological Survey Open-File Map 81–120, 3 sheets, scale 1:250,000.

Chitwood, L.A., 1993, Inflated basaltic lava—processes and landforms: Speleograph, v. 29, no. 5, p. 55–64.

Chitwood, L.A., 1994, Inflated basaltic lava—examples of processes and landforms from central and southeast Oregon: Oregon Geology, v. 56, no. 1, p. 11–21.

Clague, D.A., Hagstrum, J.T., Champion, D.E., and Beeson, M.H., 1999, Kīlauea summit overflows; their ages and distribution in the Puna District, Hawaiʻi: Bulletin of Volcanology, v. 61, no. 6, p. 363–381.

Coffin, M.F., Frey, F.A., Wallace, P.J., Antretter, M.J., Arndt, N.T., Barling, Jane, Boehm, Florian, Borre, M.K., Coxall, H.K., Damuth, J.E., Delius, Heike, Duncan, R.A., Inokuchi, Hiroo, Keszthelyi, L.P., Mahoney, J.J., Moore, C.L., Mueller, R.D., Neal, C.R., Nicolaysen, K.E., Pringle, M.S., Reusch, D.N., Saccocia, P.J., Teagle, D.A.H., Waehnert, Veronika, Weis, D.A.M., Wise, S.W., and Zhao, Xixi, 2000, Proceedings of the Ocean Drilling Program, part A. Initial reports; Kerguelen Plateau-Broken Ridge, a large igneous province; covering Leg 183 of the cruises of the drilling vessel JOIDES Resolution, Fremantle, Australia, to Fremantle, Australia, sites 1135–1142, 7 December 1998–11 February 1999 (Ocean Drilling Program, v. 183): College Station, Tex., Texas A&M University, var. pag.

Cooper, K.M., and Kauahikaua, J.P., 1992, Morphology of extinct lava tubes and the implications for tube evolution, Chain of Craters Road, Hawaii Volcanoes National Park, Hawaii: U.S. Geological Survey Open-File Report 92–352, 14 p.

Crisp, J.A., and Baloga, S.M., 1990, A model for lava flows with two thermal components: Journal of Geophysical Research, v. 95, no. B2, p. 1255–1270.

Crisp, J.A., and Baloga, S.M., 1994, Influence of crystallization and entrainment of cooler material on the emplacement of basaltic aa lava flows: Journal of Geophysical Research, v. 99, no. B6, p. 11819–11831.

Crisp, J.A., Cashman, K.V., Bonini, J.A., Hougen, S.B., and Pieri, D.C., 1994, Crystallization history of the 1984 Mauna Loa lava flow: Journal of Geophysical Research, v. 99, no. B4, p. 7177–7198.

Dann, J.C., 2001, Vesicular komatiites, 3.5-Ga Komati Formation, Barberton Greenstone Belt, South Africa; inflation of submarine lavas and origin of spinifex zones: Bulletin of Volcanology, v. 63, no. 7, p. 462–481.

DeGraff, J.M., and Aydin, Atilla, 1993, Effect of thermal regime on growth increment and spacing of contraction joints in basaltic lava: Journal of Geophysical Research, v. 98, no. B4, p. 6411–6430.

Duncan, R.A., Larsen, H.-C., Allan, J.F., Aita, Yoshiaki, Arndt, N.T., Buecker, C.J., Cambray, Herve, Cashman, K.V., Cerney, B.P., Clift, P.D., Fitton, J.G., Le Gall, Bernard, Hooper, P.R., Hurst, S.D., Krissek, L.A., Kudless, K.E., Larsen, L.M., Lesher, C.E., Nakasa, Yukari, Niu, Yaoling, Philipp, Harald, Planke, Sverre, Rehacek, Jakub, Saunders, A.D., Teagle, D.A.H., and Tegner, Christian, 1996, Proceedings of the Ocean Drilling Program, part A. Initial reports; Southeast Greenland

margin; covering Leg 163 of the cruises of the drilling vessel JOIDES Resolution, Reykjavik, Iceland, to Halifax, Nova Scotia, sites 988–990, 3 September–7 October 1995 (Ocean Drilling Program, v. 163): College Station, Tex., Texas A&M University, 623 p.

Duraiswami, R.A., Bondre, N.R., Dole, Gauri, Phadnis, V.M., and Kale, V.S., 2001, Tumuli and associated features from the western Deccan Volcanic Province, India: Bulletin of Volcanology, v. 63, no. 7, p. 435–442.

Eldholm, Olav, Thiede, Jorn, Taylor, Elliott, Barton, Colleen, Bjorklund, K.R., Bleil, Ulrich, Ciesielski, P.F., Desprairies, Alain, Donnally, D.M., Froget, Claude, Goll, R.M., Henrich, Rudigen, Jansen, Eystein, Krissek, L.A., Kvenvolden, K.A., LeHuray, A.P., Love, D.A., Lysne, Peter, McDonald, T.J., Mudie, P.J., Osterman, L.E., Parson, L.M., Phillips, J.D., Pittenger, Alan, Qvale, Gunnbjorg, Schoenharting, Guenther, and Viereck, L.G., 1989, Proceedings of the Ocean Drilling Program, scientific results; Norwegian Sea; covering Leg 104 of the cruises of the drilling vessel JOIDES Resolution, Bremerhaven, Germany, to St. John's, Newfoundland, sites 642–644, 19 June 1985–23 August 1985 (Ocean Drilling Program, v. 104): College Station, Tex., Texas A&M University, 1141 p.

Finch, R.H., and Emerson, O.H., 1925, Sulphate deposits in lava tubes: American Journal of Science, ser. 5, v. 10, p. 39–40.

Finch, R.H., and Macdonald, G.A., 1953, Hawaiian volcanoes during 1950: U.S. Geological Survey Bulletin 996-B, p. 27–89.

Fink, J.H., and Zimbelman, J.R., 1986, Rheology of the 1983 Royal Gardens basalt flows, Kilauea Volcano, Hawaii: Bulletin Volcanologique, v. 48, no. 2–3, p. 87–96.

Fink, J.H., and Zimbelman, J.R., 1990, Longitudinal variations in rheological properties of lavas; Puu Oo basalt flows, Kilauea Volcano, Hawaii, *in* Fink, J.H., ed., Lava flows and domes; emplacement mechanisms and hazard implications (IAVCEI Proceedings in Volcanology, no. 2): Berlin, Springer-Verlag, p. 157–173.

Flynn, L.P., and Mouginis-Mark, P.J., 1992, Cooling rate of an active Hawaiian lava flow from nighttime spectroradiometer measurements: Geophysical Research Letters, v. 19, no. 17, p. 1783–1786.

Flynn, L.P., and Mouginis-Mark, P.J., 1994, Temperature of an active lava channel from spectral measurements, Kilauea Volcano, Hawaii: Bulletin of Volcanology, v. 56, no. 4, p. 297–301.

Flynn, L.P., Mouginis-Mark, P.J., Gradie, J.C., and Lucey, P.G., 1993, Radiative temperature measurements at Kupaianaha lava lake, Kilauea Volcano, Hawaii: Journal of Geophysical Research, v. 98, no. B4, p. 6461–6476.

Friedman, R.C., Taylor, G.J., Keszthelyi, L.P., and Thornber, C.R., 1996, Petrographic textures as indicators of Kilauea lava flow emplacement history [abs.]: Eos (American Geophysical Union Transactions), v. 77, no. 46, supp., p. F807.

Greeley, Ronald, 1971, Observations of actively forming lava tubes and associated structures, Hawaii: Modern Geology, v. 2, no. 3, p. 207–233.

Greeley, Ronald, 1972, Additional observations of actively forming lava tubes and associated structures, Hawaii: Modern Geology, v. 3, no. 3, p. 157–160.

Greeley, Ronald, 1987, The role of lava tubes in Hawaiian volcanoes, chap. 59 *of* Decker, R.W., Wright, T.L., and Stauffer, P.H., eds., Volcanism in Hawaii: U.S. Geological Survey Professional Paper 1350, v. 2, p. 1589–1602.

Greeley, Ronald, Fagents, S.A., Harris, R.S., Kadel, S.D., and Williams, D.A., 1998, Erosion by flowing lava; field evidence: Journal of Geophysical Research, v. 103, no. B11, p. 27325–27345.

Greeley, Ronald, and Hyde, J.H., 1972, Lava tubes of the Cave Basalt, Mount St. Helens, Washington: Geological Society of America Bulletin, v. 83, no. 8, p. 2397–2418.

Gregg, T.K.P., and Chadwick, W.W., Jr., 1996, Submarine lava-flow inflation; a model for the formation of lava pillars: Geology, v. 24, no. 11, p. 981-984.

Guest, J.E., and Murray, J.B., 1979, An analysis of hazard from Mount Etna volcano: Society of London Journal, v. 136, no. 3, p. 347-354.

Guest, J.E., Wood, C.A., and Greeley, Ronald, 1984, Lava tubes, terraces and megatumuli on the 1614–24 pahoehoe lava flow field, Mount Etna, Sicily: Bulletin Volcanologique, v. 47, no. 3, p. 635–648.

Hanley, D.J., and Zimbelman, J.R., 1998, Topographic control of lava flow morphology; putting a number to it [abs.]: Lunar and Planetary Science Conference Abstracts of Papers, v. 29, abstract 1749, n.p.

Hardee, H.C., 1983, Heat transfer measurements in the 1983 Kilauea lava flow: Science, v. 222, no. 4619, p. 47–48.

Harris, A.J.L., Flynn, L.P., Dean, K.G., Pilger, Eric, Wooster, M.J., Okubo, C.H., Mouginis-Mark, P.J., Garbeil, Harold, Thornber, C.R., de la Cruz-Reyna, Servando, Rothery, D.A., and Wright, Robert, 2000, Real-time satellite monitoring of volcanic hot spots, *in* Mouginis-Mark, P.J., Crisp, J.A., and Fink, J.H., eds., Remote sensing of active volcanism: American Geophysical Union Geophysical Monograph 116, p. 139–159.

Harris, A.J.L., Flynn, L.P., Keszthelyi, L.P., Mouginis-Mark, P.J., Rowland, S.K., and Resing, J.A., 1998, Calculation of lava effusion rates from Landsat TM data: Bulletin of Volcanology, v. 60, no. 1, p. 52–71.

Harris, A.J.L., Flynn, L.P., Rothery, D.A., Oppenheimer, Clive, and Sherman, S.B., 1999, Mass flux measurements at active lava lakes; implications for magma recycling: Journal of Geophysical Research, v. 104, no. B4, p. 7117–7136.

Harris, A.J.L., Keszthelyi, L.P., Flynn, L.P., Mouginis-Mark, P.J., Thornber, C.R., Kauahikaua, J.P., Sherrod, D.R., and Trusdell, F.A., 1997a, Chronology of the episode 54 eruption at Kilauea Volcano, Hawaii, from GOES-9 satellite data: Geophysical Research Letters, v. 24, no. 24, p. 3281–3284.

Harris, A.J.L., Keszthelyi, L.P., Flynn, L.P., Mouginis-Mark, P.J., Thornber, C.R., Kauahikaua, J.P., Sherrod, D.R., and Trusdell, F.A., 1997b, Near-real-time monitoring of effusive volcanic eruptions from geostationary satellites [abs.]: Geological Society of America Abstracts with Programs, v. 29, no. 6, p. A–165.

Harris, A.J.L., and Rowland, S.K., 2001, FLOWGO; a kinematic thermo-rheological model for lava flowing in a channel: Bulletin of Volcanology, v. 63, no. 1, p. 20–44.

Harris, A.J.L., and Thornber, C.R., 1999, Complex effusive events at Kīlauea as documented by the GOES satellite and remote video cameras: Bulletin of Volcanology, v. 61, no. 6, p. 382–395.

Heliker, C.C., and Decker, R.W., in press, The Hawai‘i Island eruptions of Kilauea, 1983 to 2001, and Mauna Loa, 1984; living with lava, *in* Guffanti, M.C., Miller, C.D., and Ewert, J.W., eds., Responding to volcanic eruptions and unrest—1980–2000; two decades of scientific experience in applied volcanology: U.S. Geological Survey Circular 1250.

Heliker, C.C., Ulrich, G.E., Margriter, S.C., and Hoffmann, J.P., 2001, Maps showing the development of the Pu‘u ‘Ō‘ō-Kūpaianaha flow field, June 1984–February 1987, Kīlauea Volcano, Hawaii: U.S. Geological Survey Miscellaneous Investigations Series Map I–2685, 4 sheets, scale 1:50,000.

Helz, R.T., Banks, N.G., Heliker, C.C., Neal, C.A., and Wolfe, E.W., 1995, Comparative geothermometry of recent Hawaiian eruptions: Journal of Geophysical Research, v. 100, no. B9, p. 17637–17657.

Helz, R.T., Hon, K.A., and Heliker, C.C., 1993, Thermal efficiency of lava tubes at Kilauea Volcano, Hawaii [abs.], *in* Duggan, M.B., and Knutson, Jan, compilers, Ancient volcanism & modern analogues: IAVCEI General Assembly, Canberra, Australia, 1993, Abstracts, v. 1, no. 1, p. 47.

Helz, R.T., and Thornber, C.R., 1987, Geothermometry of Kilauea Iki lava lake, Hawaii: Bulletin of Volcanology, v. 49, no. 5, p. 651–668.

Hill, R.E.T., and Perring, C.S., 1996, The evolution of Archaean komatiite flow fields— are they inflationary sheet flows? [abs.], *in* Whitehead, P.W., eds., Long lava flows: Chapman Conference on Long Lava Flows, Townsville, Australia, 1996, Abstracts, p. 18–21.

Holcomb, R.T., 1987, Eruptive history and long-term behavior of Kilauea Volcano, chap. 12 *of* Decker, R.W., Wright, T.L., and Stauffer, P.H., eds., Volcanism in Hawaii: U.S. Geological Survey Professional Paper 1350, v. 1, p. 261–350.

Hollamby, Jennifer, 1996, The volcanology of the Tramways area, Kambalda, Western Australia [abs.], *in* Whitehead, P.W., eds., Long lava flows: Chapman Conference on Long Lava Flows, Townsville, Australia, 1996, Abstracts, p. 24–25.

Hon, K.A., Heliker, C.C., and Kjargaard, J.I., 1988, Limu o Pele; a new kind of hydroclastic tephra from Kilauea Volcano, Hawaii [abs.]: Geological Society of America Abstracts with Programs, v. 20, no. 7, p. A112–A113.

Hon, K.A., Kauahikaua, J.P., Denlinger, R.P., and Mackay, Kevin, 1994, Emplacement and inflation of pahoehoe sheet flows; observations and measurements of active lava flows on Kilauea Volcano, Hawaii: Geological Society of America Bulletin, v. 106, no. 3, p. 351–370.

Hon, K.A., Kauahikaua, J.P., and Mackay, Kevin, 1993a, Inflation and cooling data from pahoehoe sheet flows on Kilauea Volcano: U.S. Geological Survey Open-File Report 93–342–A, 27 p.

Hon, K.A., Mattox, T.N., Kauahikaua, J.P., and Kjargaard, J.I., 1993b, The construction of pahoehoe lava deltas on Kilauea volcano, Hawaii [abs.]: Eos (American Geophysical Union Transactions), v. 74, no. 43, supp., p. 616.

Hoover, S.R., Cashman, K.V., and Manga, Michael, 2001, The yield strength of subliquidus basalts—experimental results: Journal of Volcanology and Geothermal Research, v. 107, no. 1–3, p. 1–18.

Hulme, Geoffrey, 1974, The interpretation of lava flow morphology: Royal Astronomical Society Geophysical Journal, v. 39, no. 2, p. 361–383.

Ishihara, Kazuhiro, Iguchi, Masato, and Kamo, Kosuke, 1989, Numerical simulation of some volcanoes in Japan, *in* Fink, J.H, ed., Lava flows and domes; emplacement mechanisms and hazard implications (IAVCEI Proceedings in Volcanology, no. 2): Berlin, Springer-Verlag, p. 174–207.

Jones, A.E., 1937, The formation of basaltic lava flows: Journal of Geology, v. 45, no. 8, p. 872–880.

Jones, A.E., 1943, Classification of lava-surfaces: American Geophysical Union Transactions, v. 24, no. 1, p. 265–268.

Ka ‘Io Productions, 2000, Winter 2000 eruption update; a firsthand account of the current eruption of Kilauea Volcano: Volcano, Hawaii, VHS videotape, 63 min.

Kauahikaua, J.P., Cashman, K.V., Mattox, T.N., Heliker, C.C., Hon, K.A., Mangan, M.T., and Thornber, C.R., 1998a, Observations on basaltic lava streams in tubes from Kilauea Volcano, island of Hawai‘i: Journal of Geophysical Research, v. 103, no. B11, p. 27303–27323.

Kauahikaua, J.P., Denlinger, R.P., Foster, James, and Keszthelyi, L.P., 1993, Lava delta instability; is it mass-wasting or is it triggered by lava flowing through tubes? [abs.]: Eos (American Geophysical Union Transactions), v. 74, no. 43, supp., p. 616.

Kauahikaua, J.P., Mangan, M.T., Heliker, C.C., and Mattox, T.N., 1996, A quantitative look at the demise of a basaltic vent; the death of Kupaianaha, Kilauea Volcano, Hawai‘i: Bulletin of Volcanology, v. 57, no. 8, p. 641–648.

Kauahikaua, J.P., Margriter, S.C., Lockwood, J.P., and Trusdell, F.A., 1995a, Applications of GIS to the estimation of lava flow hazards on Mauna Loa Volcano, Hawai‘i, *in* Rhodes, J.M., and Lockwood, J.P., eds., Mauna Loa revealed; structure, composition, history, and hazards: American Geophysical Union Geophysical Monograph 92, p. 315–325.

Kauahikaua, J.P., Margriter, S.C., and Moore, R.B., 1995b, GIS-aided volcanic activity hazard analysis for the Hawaii Geothermal Project environmental impact statement, *in* Carrara, Alberto, and Guzzetti, Fausto, eds., Geographical Information Systems in assessing natural hazards: Dordrecht, Kluwer Academic Publishers, p. 235–257.

Kauahikaua, J.P., Trusdell, F.A., and Heliker, C.C., 1998b, The probability of lava inundation at the proposed and existing Kulani Prison sites: U.S. Geological Survey Open-File Report 98–794, 21 p.

Kelly, K.M., Hon, K.A., and Tribble, G.W., 1989, Bathymetric and submarine studies of an active lava delta near Kupapau Point, Kilauea Volcano, Hawaii [abs.]: Eos (American Geophysical Union Transactions), v. 70, no. 43, supp., p. 1202.

Kempe, Stephan, 1997, Lavafalls; a major factor for the enlargements of lava tubes on the Kilauea and Hualalai, Hawaii: International Congress of Speleology Proceedings, v. 12, no. 1, p. 445–448.

Kerr, R.C., 2001, Thermal erosion by laminar flows: Journal of Geophysical Research, v. 106, no. B11, p. 26453–26465.

Keszthelyi, L.P., 1993, Portable infrared video system for the reconnaissance of lava flows [abs.]: Eos (American Geophysical Union Transactions), v. 74, no. 43, supp., p. 640.

Keszthelyi, L.P., 1995, Measurements of the cooling at the base of pahoehoe flows: Geophysical Research Letters, v. 22, no. 16, p. 2195–2198.

Keszthelyi, L.P., and Denlinger, R.P., 1996, The initial cooling of pahoehoe flow lobes: Bulletin of Volcanology, v. 58, no. 1, p. 5–18.

Kilburn, C.R.J., 1981, Pahoehoe and aa lavas; a discussion and continuation of the model of Peterson and Tilling: Journal of Volcanology and Geothermal Research, v. 11, no. 2–4, p. 373–382.

Kilburn, C.R.J., 1996, Patterns and predictability in the emplacement of subaerial lava flows and flow fields, *in* Scarpa, Roberto, and Tilling, R.I., eds., Monitoring and mitigation of volcano hazards: Berlin, Springer, p. 491–537.

Kilburn, C.R.J., 2000, Lava flows and flow fields, *in* Sigurdsson, Haraldur, Houghton, B.F., McNutt, S.R., Rymer, Hazel, and Stix, John, eds., Encyclopedia of volcanoes: San Diego, Calif., Academic Press, p. 291–305.

Kilburn, C.R.J., Pinkerton, Harry, and Wilson, Lionel, 1995, Forecasting the behaviour of lava flows, *in* McGuire, W.J., Kilburn, C.R.J., and Murray, J.B., eds., Monitoring active volcanoes; strategies, procedures, and techniques: London, UCL Press, p. 346–368.

Larsen, H.C., Saunders, A.D., Clift, P.D., Ali, J.R., Beget, J.E., Cambray, Herve, Demant, Alain, Fitton, J.G., Fram, M.S., Fukuma, Koji, Gieskes, J.M., Holmes, M.A., Hunt, J.M., Lacasse, Christian, Larsen, L.M., Lykke-Andersen, Holger, Meltser, Alexandr, Morrison, M.L., Nemoto, Naoki, Okay, Nilgun, Saito, Saneatsu, Sinton, Christopher, Spezzaferri, Silvia, Stax, Rainer, Vallier, T.L., Vandamme, Didier, Wei, Wuchang, and Werner, Reinhard, 1994, Proceedings of the Ocean Drilling Program, part A. Initial reports; East Greenland margin; covering Leg 152 of the cruises of the drilling vessel JOIDES Resolution, Reykjavik, Iceland, to St. John's, Newfoundland, sites 914–919, 24 September–22 November 1993 (Ocean Drilling Program, v. 152): College Station, Tex., Texas A&M University, 977 p.

Lipman, P.W., and Banks, N.G., 1987, Aa flow dynamics, Mauna Loa 1984, chap. 57 *of* Decker, R.W., Wright, T.L., and Stauffer, P.H., eds., Volcanism in Hawaii: U.S. Geological Survey Professional Paper 1350, v. 2, p. 1527–1567.

Lipman, P.W., Banks, N.G., and Rhodes, J.M., 1985, Degassing-induced crystallization of basaltic magma and effects on lava rheology: Nature, v. 317, no. 6038, p. 604–607.

Lockwood, J.P., Banks, N.G., English, T.T., Greenland, L.P., Jackson, D.B., Johnson, D.J., Koyanagi, R.Y., McGee, K.A., Okamura, A.T., and Rhodes, J.M., 1985, The 1984 eruption of Mauna Loa Volcano, Hawaii: Eos (American Geophysical Union Transactions), v. 66, no. 16, p. 169–171.

Macdonald, G.A., 1953, Pahoehoe, aa, and block lava: American Journal of Science, v. 251, no. 3, p. 169–191.

Macdonald, G.A., 1967, Forms and structures of extrusive basaltic rocks, *in* Hess, H.H., and Poldervaart, Arie, eds., Basalts; the Poldervaart treatise on rocks of basaltic composition: New York, Interscience, v. 1, p. 1–61.

Mattox, T.N., Heliker, C.C., Kauahikaua, J.P., and Hon, K.A., 1993, Development of the 1990 Kalapana flow field, Kilauea Volcano, Hawaii: Bulletin of Volcanology, v. 55, no. 6, p. 407–413.

Mattox, T.N., and Mangan, M.T., 1997, Littoral hydrovolcanic explosions; a case study of lava-seawater interaction at Kilauea Volcano: Journal of Volcanology and Geothermal Research, v. 75, no. 1–2, p. 1–17.

Miyamoto, Hideaki, and Sasaki, Sho, 1997, Simulating lava flows by an improved cellular automata method: Computers & Geosciences, v. 23, no. 3, p. 283–292.

Miyamoto, Hideaki, and Sasaki, Sho, 1998, Numerical simulations of flood basalt lava flows; roles of parameters on lava flow morphologies: Journal of Geophysical Research, v. 103, no. B11, p. 27489–27502.

Moore, H.J., 1987, Preliminary estimates of the rheological properties of 1984 Mauna Loa lava, chap. 58 *of* Decker, R.W., Wright, T.L., and Stauffer, P.H., eds., Volcanism in Hawaii: U.S. Geological Survey Professional Paper 1350, v. 2, p. 1569–1588.

Moore, J.G., Phillips, R.L., Grigg, R.W., Peterson, D.W., and Swanson, D.A., 1973, Flow of lava into the sea, 1969–1971, Kilauea Volcano, Hawaii: Geological Society of America Bulletin, v. 84, no. 2, p. 537–546.

Moore, R.B., Helz, R.T., Dzurisin, Daniel, Eaton, G.P., Koyanagi, R.Y., Lipman, P.W., Lockwood, J.P., and Puniwai, G.S., 1980, The 1977 eruption of Kilauea volcano, Hawaii, *in* McBirney, A.R., ed., Gordon A. Macdonald memorial volume: Journal of Volcanology and Geothermal Research, v. 7, no. 3–4, p. 189–210.

Newhall, C.G., and Hoblitt, R.P., 2002, Constructing event trees for volcanic crises: Bulletin of Volcanology, v. 64, no. 1, p. 3–20.

Oze, C.J.-P., 1997, A petrological analysis of blue glassy pahoehoe, Kilauea, Hawai'i: Walla Walla, Wash., Whitman College, B.S. thesis, 35 p.

Peitersen, M.N., and Crown, D.A., 1999, Downflow width behavior of Martian and terrestrial lava flows: Journal of Geophysical Research, v. 104, no. E4, p. 8473–8488.

Peitersen, M.N., and Crown, D.A., 2000, Correlations between topography and intraflow width behavior in Martian and terrestrial lava flows: Journal of Geophysical Research, v. 105, no. E2, p. 4123–4134.

Peterson, D.W., 1976, Processes of volcanic island growth, Kilauea Volcano, Hawaii, 1969–1973, *in* Gonzalez-Ferran, Oscar, ed., Symposium on Andean and Antarctic Volcanology Problems, Santiago, Chile, 1974, Proceedings (International Association of Volcanology and Chemistry of the Earth's Interior, special series): Napoli, F. Giannini, p. 172–189.

Peterson, D.W., Holcomb, R.T., Tilling, R.I., and Christiansen, R.L., 1994, Development of lava tubes in the light of observations at Mauna Ulu, Kilauea Volcano, Hawaii: Bulletin of Volcanology, v. 56, no. 5, p. 343–360.

Peterson, D.W., and Swanson, D.A., 1974, Observed formation of lava tubes during 1970–71 at Kilauea Volcano, Hawaii: Studies in Speleology, v. 2, no. 6, p. 209–223.

Peterson, D.W., and Tilling, R.I., 1980, Transition of basaltic lava from pahoehoe to aa, Kilauea volcano Hawaii; field observations and key factors, *in* McBirney, A.R., ed., Gordon A.

Macdonald memorial volume: Journal of Volcanology and Geothermal Research, v. 7, no. 3–4, p. 271–293.

Pieri, D.C., 1986, Eruption rate, area, and length relationships for some Hawaiian lava flows: Journal of Volcanology and Geothermal Research, v. 30, no. 1–2, p. 29–45.

Pinkerton, Harry, James, Mike, and Jones, Alun, 2002, Surface temperature measurements of active lava flows on Kilauea volcano, Hawai′i: Journal of Volcanology and Geothermal Research, v. 113, no. 1–2, p. 159–176.

Pinkerton, Harry, and Wilson, Lionel, 1994, Factors controlling the lengths of channel-fed lava flows: Bulletin of Volcanology, v. 56, no. 2, p. 108–120.

Polacci, Margherita, Cashman, K.V., and Kauahikaua, J.P., 1999, Textural characterization of the pāhoehoe-ʻaʻā transition in Hawaiian basalt: Bulletin of Volcanology, v. 60, no. 8, p. 595–609.

Porter, Andy, 2000, The initial exploration of Lower Laeʻapuki Cave System, Hawaiʻi Volcanoes National Park: NSS News, v. 58, no. 1, p. 10–17.

Realmuto, V.J., Hon, K.A., Kahle, A.B., Abbott, E.A., and Pieri, D.C., 1992, Multispectral thermal infrared mapping of the 1 October 1988 Kupaianaha flow field, Kilauea volcano, Hawaii: Bulletin of Volcanology, v. 55, no. 1, p. 33–44.

Resing, J.A., and Sansone, F.J., 2002, The chemistry of lava-sea-water interactions II; the elemental signature: Geochimica et Cosmochimica Acta, v. 66, no. 11, p. 1925–1941.

Robson, G.R., 1967, Thickness of Etnean lavas: Nature, v. 216, no. 5112, p. 251–252.

Rowland, S.K., MacKay, M.E., Garbeil, Harold, and Mouginis-Mark, P.J., 1997, Using TOPSAR interferometric radar topography to calculate erupted volumes of the ongoing Puu Oo/Kupaianaha/Kamoamoa eruption, Kilauea Volcano, Hawaii [abs.]: Eos (American Geophysical Union Transactions), v. 78, no. 46, supp., p. F776.

Rowland, S.K., and Walker, G.P.L., 1990, Pahoehoe and aa in Hawaii; volumetric flow rate controls the lava structure: Bulletin of Volcanology, v. 52, no. 8, p. 615–628.

Saar, M.O., Manga, Michael, Cashman, K.V., and Fremouw, Sean, 2001, Numerical models of the onset of yield strength in crystal-melt suspensions: Earth and Planetary Science Letters, v. 187, no. 3–4, p. 367–379.

Sage, L.L., and Mattox, T.N., 2000, A study of dense, glassy flows; dense pahoehoe lava flows from Kilauea Volcano, Hawaii: Grand Valley State University McNair Scholars Journal, v. 4, p. 33–41.

Sakimoto, S.E.H., and Gregg, T.K.P., 2001, Channeled flow; analytic solutions, laboratory experiments, and application to lava flows: Journal of Geophysical Research, v. 106, no. B5, p. 8629–8644.

Sansone, F.J., and Resing, J.A., 1995, Hydrography and geochemistry of sea surface hydrothermal plumes resulting from Hawaiian coastal volcanism: Journal of Geophysical Research, v. 100, no. C7, p. 13555–13569.

Sansone, F.J., Resing, J.A., Tribble, G.W., Sedwick, P.N., Kelly, K.M., and Hon, K.A., 1991, Lava-seawater interactions at shallow-water submarine lava flows: Geophysical Research Letters, v. 18, no. 9, p. 1731–1734.

Self, Stephen, Keszthelyi, L.P., and Thordarson, Thorvaldur, 1998, The importance of pāhoehoe: Annual Review of Earth and Planetary Sciences, v. 26, p. 81–110.

Self, Stephen, Keszthelyi, L.P., and Thordarson, Thorvaldur, 2000, Discussion of "Pulsed inflation of pahoehoe lava flows; implications for flood basalt emplacement", by S.W. Anderson, E.R. Stofan, E.R. Smrekar, J.E. Guest, and B. Wood [Earth Planet. Sci. Lett. 168 (1999) 7–18]: Earth and Planetary Science Letters, v. 179, no. 2, p. 421–423.

Self, Stephen, Thordarson, Thorvaldur, and Keszthelyi, L.P., 1997, Emplacement of continental flood basalt lava flows, *in* Mahoney, J.J., and Coffin, M.F., eds., Large igneous provinces; continental, oceanic, and planetary flood volcanism: American Geophysical Union Geophysical Monograph 100, p. 381–410.

Self, Stephen, Thordarson, Thorvaldur, Keszthelyi, L.P., Walker, G.P.L., Hon, K.A., Murphy, M.T., Long, P.E., and Finnemore, S.L., 1996, A new model for the emplacement of Columbia River Basalts as large, inflated pahoehoe lava flow fields: Geophysical Research Letters, v. 23, no. 19, p. 2689–2692.

Smith, D.K., Kong, L.S.L., Johnson, K.T.M., and Reynolds, J.R., 2002, Volcanic morphology of the submarine Puna Ridge, Kilauea Volcano, *in* Takahashi, Eiichi, Lipman, P.W., Garcia, M.O., Naka, Jiro, and Aramaki, Shigeo, eds., Hawaiian volcanoes; deep underwater perspectives: American Geophysical Union Geophysical Monograph 128, p. 125–142.

Stephenson, P.J., Burch-Johnston, A.T., Stanton, D.J., and Whitehead, P.W., 1998, Three long lava flows in north Queensland: Journal of Geophysical Research, v. 103, no. B11, p. 27359–27370.

Summerour, J.H., 1989, The geology of five unusual craters, Aden Basalts, Dona Ana County, New Mexico: El Paso, University of Texas, M.S. thesis, 129 p.

Sutton, A.J., Elias, Tamar, Gerlach, T.M., and Stokes, J.B., 2001, Implications for eruptive processes as indicated by sulfur dioxide emissions from Kīlauea volcano Hawaiʻi, 1979–1997: Journal of Volcanology and Geothermal Research, v. 108, no. 1–4, p. 283–302.

Swanson, D.A., 1973, Pahoehoe flows from the 1969–1971 Mauna Ulu eruption, Kilauea Volcano, Hawaii: Geological Society of America Bulletin, v. 84, no. 2, p. 615–626.

Swanson, D.A., Duffield, W.A., Jackson, D.B., and Peterson, D.W., 1979, Chronological narrative of the 1969–71 Mauna Ulu eruption of Kilauea Volcano, Hawaii: U.S. Geological Survey Professional Paper 1056, 55 p.

Swanson, D.A., and Fabbi, B.P., 1973, Loss of volatiles during fountaining and flowage of basaltic lava at Kilauea Volcano, Hawaii: U.S. Geological Survey Journal of Research, v. 1, no. 6, p. 649–658.

Tallarico, Andrea, and Dragoni, Michele, 2000, A three-dimensional Bingham model for channeled lava flows: Journal of Geophysical Research, v. 105, no. 11, p. 25969–25980.

Thornber, C.R., 1997, HVO/RVTS-1; a prototype remote video telemetry system for monitoring the Kilauea east rift zone eruption, 1997: U.S. Geological Survey Open-File Report 97–537, 19 p.

Thornber, C.R., 2001, Olivine-liquid relations of lava erupted by Kīlauea Volcano from 1994 to 1998; implications for

shallow magmatic processes associated with the ongoing east-rift-zone eruption: Canadian Mineralogist, v. 39, no. 2, p. 239–266.

Thornber, C.R., Meeker, G.P., Hon, K.A., Sutley, Stephen, Camara, Bobby, Kauahikaua, J.P., Lewis, G.B., and Ricketts, Charlie, 1999, Fresh Kilauea lava tubes; the inside story [abs.]: Big Island Science Conference, 15th, Hilo, Hawaii, 1999, Proceedings, v. 15, p. 30.

Tilling, R.I., Christiansen, R.L., Duffield, W.A., Endo, E.T., Holcomb, R.T., Koyanagi, R.Y., Peterson, D.W., and Unger, J.D., 1987, The 1972–1974 Mauna Ulu eruption, Kilauea Volcano; an example of quasi-steady-state magma transfer, chap. 16 *of* Decker, R.W., Wright, T.L., and Stauffer, P.H., eds., Volcanism in Hawaii: U.S. Geological Survey Professional Paper 1350, v. 1, p. 405–469.

Tribble, G.W., 1991, Underwater observations of active lava flows from Kilauea Volcano, Hawaii: Geology, v. 19, no. 6, p. 633–636.

Umino, Susumu, Lipman, P.W., and Obata, Sumie, 2000, Subaqueous lava flow lobes, observed on ROV *KAIKO* dives off Hawaii: Geology, v. 28, no. 6, p. 503–506.

Wadge, Geoffrey, Young, P.A.V., and McKendrick, I.J., 1994, Mapping lava flow hazards using computer simulation: Journal of Geophysical Research, v. 99, no. B1, p. 489–504.

Walker, G.P.L., 1967, Thickness and viscosity of Etnean lavas: Nature, v. 213, no. 5075, p. 484–485.

Walker, G.P.L., 1973, Lengths of lava flows, *in* Guest, J.E., and Skelhorn, R.R., eds., Mount Etna and the 1971 eruption: Royal Society of London Philosophical Transactions, ser. A, v. 274, no. 1238, p. 107–118.

Walker, G.P.L., 1991, Structure, and orgin by injection of lava under surface crust, of tumuli, “lava rises”, “lava-rise pits”, and “lava-inflation clefts” in Hawaii: Bulletin of Volcanology, v. 53, no. 7, p. 546–558.

Wentworth, C.K., and Macdonald, G.A., 1953, Structures and forms of basaltic rocks in Hawaii: U.S. Geological Survey Bulletin 994, 98 p.

Whitehead, P.W., and Stephenson, P.J., 1998, Lava rise ridges of the Toomba basalt flow, north Queensland, Australia: Journal of Geophysical Research, v. 103, no. B11, p. 27370–27382.

Wilmoth, R.A., and Walker, G.P., 1993, P-type and S-type pahoehoe; a study of vesicle distribution patterns in Hawaiian lava flows: Journal of Volcanology and Geothermal Research, v. 55, no. 1–2, p. 129–142.

Wolfe, E.W., Neal, C.A., Banks, N.G., and Duggan, T.J., 1988, Geologic observations and chronology of eruptive events, chap. 1 *of* Wolfe, E.W., ed., The Puu Oo eruption of Kilauea Volcano, Hawaii; episodes 1 through 20, January 3, 1983, through June 8, 1984: U.S. Geological Survey Professional Paper 1463, p. 1–97.

Wood, Chris, 2001, Initial feedback report [of the Laki Underground 2001 Expedition, July 9–Aug. 10, 2001]: Poole, U.K., Bournemouth University/Shepton Mallet Caving Club and Icelandic Speleological Society report, n.p.

Wright, Robert, Blake, Stephen, Harris, A.J.L., and Rothery, D.A., 2001, A simple explanation for the space-based calculation of lava eruption rates: Earth and Planetary Science Letters, v. 192, no. 2, p. 223–233.

Wright, T.L., and Okamura, R.T., 1977, Cooling and crystallization of tholeiitic basalt, 1965 Makaopuhi lava lake, Hawaii: U.S. Geological Survey Professional Paper 1004, p. 78 p.

Young, Philippa, and Wadge, Geoff, 1990, FLOWFRONT; simulation of a lava flow: Computers & Geosciences, v. 16, no. 8, p. 1171–1191.

Zablocki, C.J., 1978, Applications of the VLF induction method for studying some volcanic processes of Kilauea volcano, Hawaii: Journal of Volcanology and Geothermal Research, v. 3, no. 1–2, p. 155–195.

The Transition from ʻAʻā to Pāhoehoe Crust on Flows Emplaced During the Puʻu ʻŌʻō-Kūpaianaha Eruption

By Ken Hon, Cheryl Gansecki *and* Jim Kauahikaua

Abstract

The transition from pāhoehoe to ʻaʻā along a single lava flow is widely accepted as irreversible in volcanology. However, channelized ʻaʻā flows have been repeatedly observed changing into pāhoehoe flows during the low-effusion-rate "pāhoehoe" stage of the Puʻu ʻŌʻō-Kūpaianaha eruption. This change most commonly occurs when flows move from steep slopes to level ground. The transition is marked by the change from ʻaʻā to pāhoehoe crust on the solidified levees. It is here suggested that the definitions of pāhoehoe and ʻaʻā be restricted to solidified crustal products, as those terms were originally defined. Active lava flows can be designated as either pāhoehoe flows or ʻaʻā flows, depending on the type of crust that is being produced at the advancing front. Many difficulties arise from applying the terms pāhoehoe and ʻaʻā to molten lava that has not taken a solid form. Hawaiian tholeiitic lava undergoes an irreversible transition from near-Newtonian to Bingham or other non-Newtonian behavior as it cools, crystallizes, and degases during transport away from the vent. Most Hawaiian pāhoehoe flows are fed by near-Newtonian lava, and most Hawaiian ʻaʻā flows are fed by lava with Bingham or more complex rheologies. Within a restricted rheological range, however, Hawaiian lava can form either a pāhoehoe or an ʻaʻā crust, depending on strain rate. This limited rheologic condition allows an ʻaʻā flow to change into a pāhoehoe flow in response to a reduction in strain rate.

Introduction

Virtually every geologist recognizes the Hawaiian words pāhoehoe and ʻaʻā, used to describe the two principal types of subaerial basaltic lava flows found throughout the world. Pāhoehoe has a continuous smooth, billowy, or ropy crust, and ʻaʻā has a brecciated rough, spiny, or clinkery surface (Macdonald, 1953). Originally used to refer to the solidified lava-flow surfaces, the definitions were expanded to designate entire flows by Macdonald (1953, p. 170), who added ". . . the terms refer to the partly or completely solidified flows, though commonly the surfaces of the molten feeding rivers also are sufficiently distinct in appearance to make possible their recognition as one type or the other." We suggest that the terms ʻaʻā and pāhoehoe be restricted to solidified crusts and thatthe terms ʻaʻā flow and pāhoehoe flow be used when discussing either active or inactive flows. We further recommend that none of these terms be applied to molten lava in channels, because that lava may go on to produce either pāhoehoe or ʻaʻā.

Many Hawaiian lava flows erupt as pāhoehoe and undergo a change to ʻaʻā as they flow away from the vent (fig. 1). This change is particularly common in short-lived flows with high effusion rates, and it is widely believed that this transition is irreversible (Macdonald, 1953; Peterson and Tilling, 1980; Kilburn, 2000). Macdonald (1953) clearly defined the transition as the place where the "solidified" part of the flow changed from predominantly pāhoehoe surfaces to ʻaʻā surfaces. Thus, the pāhoehoe-ʻaʻā transition can be thought of as a facies change from pāhoehoe crust to ʻaʻā crust along a single flow. Whereas Macdonald (1953) acknowledged that the material flowing in the channel generally corresponded to the material on the solidified flow levees, he noted that this did not necessarily have to be the case. Cashman and others (1999) proposed that the transition takes place in the channel, where the lava changes from a well-mixed fluid to a thermally stratified fluid with a cooler surface and edges and a hotter isothermal core. They suggested that the change related directly to an increase in yield strength resulting from an observed increase in the degree of plagioclase crystallinity (to more than 10 or 20 percent microlites).

A typical transitional crustal sequence along a single Mauna Loa flow goes from pāhoehoe to slabby pāhoehoe to scoriaceous-spinose ʻaʻā and, finally, to clinker-dominated ʻaʻā at the distal parts of the flows (Lipman and Banks, 1987). Wolfe and others (1988) reported similar transitions for the large ʻaʻā flows from the early stages of Kīlauea's Puʻu ʻŌʻō eruption. In the large flows they described from Mauna Loa and Kīlauea, the surface textures of the active channels were roughly the same as those of the solidified levees, and the position of the pāhoehoe to ʻaʻā transition remained in a relatively fixed position during the life of the flow (Lipman and Banks, 1987, p. 1529; Wolfe and others, 1988, p. 30). Across the pāhoehoe-to-ʻaʻā transition, vesicularity decreases, deformation of vesicles is greater, and plagioclase microlite crystallinity increases in the solidified lava (Polacci and others, 1999: Cashman and others, 1999).

During the past decade of the Pu‘u ‘Ō‘ō-Kūpaianaha eruption, we have observed numerous examples of the transition of active ‘a‘ā flows into active pāhoehoe flows. This transition is marked by a “reverse” facies change from clinkery ‘a‘ā to spiny ‘a‘ā to slabby pāhoehoe, to pāhoehoe. It is concluded that this process is relatively common, particularly during long-lived eruptions of low and/or variable effusion rates.

The Nature of the Pāhoehoe-‘A‘ā Transition

The original definition of the pāhoehoe-‘a‘ā transition was explicit in specifying it as being a change in flow types away from the vent. “A flow of pāhoehoe may change downslope to ‘a‘ā, but the change of ‘a‘ā to pāhoehoe has never been observed” (Macdonald, 1953, p. 183). The reasons given for this transition (Macdonald, 1953) are an increase in viscosity due to cooling and gas loss during transport away from the vent and the promotion of crystallization by mechanical stirring of the lava. Cashman and others (1999) provided an excellent review of the historical development of ideas regarding the pāhoehoe-‘a‘ā transition.

Peterson and Tilling (1980) elegantly demonstrated that the transition from pāhoehoe to ‘a‘ā is related not only to apparent viscosity, but also to applied shear stress and the rate of shear strain. The factors listed by Macdonald (1953), such as composition, temperature, crystallinity, melt polymerization, volatile content, and vesicularity, affect the apparent viscosity but are not the sole controls on the pāhoehoe-‘a‘ā transition in Hawai‘i. Peterson and Tilling (1980) showed that other variables, such as effusion rate, channel configuration, flow velocity and duration, and ground slope, are directly related to the applied shear stress and affect the shear-strain rate.

Peterson and Tilling (1980) analyzed the pāhoehoe-‘a‘ā transition by examining the change in shear-strain rate and apparent viscosity to which an individual “element” (infinitesimal part) of molten lava is subjected during the transition from pāhoehoe to ‘a‘ā. Because completely molten lava has the properties of neither pāhoehoe nor ‘a‘ā, determining the type of crust that will form upon cooling can be difficult. Furthermore, once a pāhoehoe crust forms, that “element” of lava is no longer capable of changing to ‘a‘ā. Instead, the change in an “element” of lava is really from a nearly Newtonian rheology to either a Bingham or other non-Newtonian rheology. This rheological change is irreversible, as alluded to by Kilburn (1981), but does not necessarily coincide with the pāhoehoe-to-‘a‘ā transition, which is a change in crustal state (Kilburn, 1990). The transition from a pāhoehoe flow to an ‘a‘ā flow, or the reverse, generally takes place at the front of the advancing flow, where most of the crust is being produced. However, the change in rheological behavior of an individual “element” of molten lava as it moves to the flow front may occur anywhere in the transport system, depending upon cooling, gas loss, and other factors. We retain here the original definitions of pāhoehoe and ‘a‘ā as crusts or flows and of the transition from pāhoehoe to ‘a‘ā as a change in flow type (Macdonald, 1953), which is similar to a facies change.

Figure 1. Pāhoehoe-to-‘a‘ā transition occurring in many small flows as they cascade down a steep slope at the base of Pūlama pali on the west side of the Pu‘u ‘Ō‘ō flow field in May 2002.

The pāhoehoe-to-ʻaʻā transition has been widely accepted as irreversible (Macdonald, 1953; Peterson and Tilling, 1980; Kilburn, 1981). Specific examples of misinterpreted reversals of this transition (apparent changes from ʻaʻā to pāhoehoe) were given by Macdonald and others (1983, p. 21) and by Kilburn (2000, p. 299). Kilburn (2000) also summarized the main objection by pointing out that broken ʻaʻā surfaces cannot change into unbroken pāhoehoe surfaces.

During the course of the Puʻu ʻŌʻō-Kūpaianaha eruption, however, we have repeatedly observed ʻaʻā flows changing downslope into pāhoehoe flows. We refer to this change as the ʻaʻā-to-pāhoehoe flow transition and suggest that the pāhoehoe-to-ʻaʻā transition is in fact reversible. Lava that produces most pāhoehoe flows more closely approximates Newtonian rheology, whereas lava that produces ʻaʻā flows has either a Bingham rheology, with a significant yield strength, or demonstrates other non-Newtonian rheological behavior (Shaw, 1969; Pinkerton and Sparks, 1978; Moore, 1987; Pinkerton and Norton, 1995).

We suggest that there is a limited rheological interval in which lava with a yield strength may produce either pāhoehoe or ʻaʻā crust, depending on strain rate. ʻAʻā surfaces do not form by simple rupturing of pāhoehoe surfaces but, rather, by the tearing of clinker from the stiff, viscoelastic molten core of an ʻaʻā flow. An individual piece of ʻaʻā crust can certainly not change to a pāhoehoe crust, but neither can a piece of smooth pāhoehoe crust change to ʻaʻā clinker. Kilburn (1990) suggested that the transition threshold between pāhoehoe and ʻaʻā is a failure envelope, where the crust begins to fragment, instead of being a simple rheological boundary. Cashman and others (1999) proposed a more complex model using crustal stability and rheology to define the transition. These models of the transition are based upon changes in the type of crust and are compatible with the original definition of the pāhoehoe-to-ʻaʻā transition.

Examples of ʻAʻā-to-Pāhoehoe Flow Transitions

Since the onset of nearly continuous effusion from Kīlauea Volcano in July 1986, a number of types of transitions from ʻaʻā to pāhoehoe flows have been observed. Lava from the Puʻu ʻŌʻō and Kūpaianaha vents flowed over gently sloping ground (1–5°), then down a much steeper slope (5–20°), and, finally, onto the flat (<2°) coastal plain (Kauahikaua and others, this volume). Most of the transitions from ʻaʻā flows to pāhoehoe flows occur at the change from steeper to flatter slopes. The transition is, in general, reflected in the types of solidified lava exposed in these two areas. A mixture of ʻaʻā and pāhoehoe flows exists on the steeper slope, whereas on the flat coastal plain virtually no ʻaʻā can be seen.

Owing to a combination of circumstances, the transition from ʻaʻā to pāhoehoe crust along a single flow has gone largely unreported. Macdonald (1953) made many of his observations on active eruptions of Mauna Loa, whose high effusion rates and short durations strongly favor ʻaʻā formation. Peterson and Tilling (1980), who made their observations during the prolonged Mauna Ulu eruption, had easy access to the vent area but had difficulty observing the transition from steep to flat slopes near the coast owing to the lack of roads. In contrast, access to the vent areas has been difficult during the ongoing Puʻu ʻŌʻō eruption, whereas access to lava flows on the flat coastal plain has been relatively easy. In addition, transitions from pāhoehoe to ʻaʻā along single Mauna Loa flows tend to be well preserved, but transitions fromʻaʻā to pāhoehoe flows are rapidly overplated by subsequent pāhoehoe flows during long-lived eruptions.

Channelized ʻAʻā Flows Changing to Pāhoehoe Flows

The most convincing examples of the ʻaʻā-to-pāhoehoe flow transition occur when a channelized ʻaʻā flow advances from the steeper slope onto the coastal flat without stagnating. The distribution of solidified levee morphologies is roughly the reverse of that reported by Lipman and Banks (1987). ʻAʻā grades downflow into slabby pāhoehoe, and then into pāhoehoe (fig. 2). On the morning of August 17, 1998, we arrived at the front of an ʻaʻā flow just as it was changing to a slabby pāhoehoe flow on the coastal flats. The progress and speed of this flow was captured on video (Hon and Gansecki, 2002). By midafternoon (about 6 hours later), the flow front had slowed significantly and consisted of smooth pāhoehoe lobes and toes. The ʻaʻā, slabby pāhoehoe, and pāhoehoe portions of this flow were all fed by an open channel that extended from the flow front approximately 200 m upslope to where it was crusted over (fig. 2).

Another excellent example was observed on September 8–9, 2000, in which a similar transition from ʻaʻā flow to pāhoehoe flow occurred over a 24-hour period. When seen in the late afternoon, the flow front was undergoing a transition from stiff, clinkery ʻaʻā to less viscous, spiny ʻaʻā. By midafternoon of the next day, the flow was in transition from ʻaʻā to slabby pāhoehoe as it began to spread out on the coastal flats. By early evening, the front of the flow had completely changed to a channel-fed pāhoehoe flow.

In both of these cases, the lava channels feeding the flow fronts were crusting over several hundred meters behind the active flow front (fig. 2). The formation of tubes insulates the lava delivered to the flow front and keeps the temperature from decreasing very much as flows lengthen (Helz and others, 1993; Helz and others, this volume). The relative position of the interface between crusted channel and open channel remained at a fairly constant distance behind the flow front as the flow underwent the transition from ʻaʻā to pāhoehoe (that is, lava-tube formation was keeping pace with the advance of the flow front). Once the transition to a pāhoehoe flow is completed, the channel commonly crusts over completely within a few hours to a day, and the lava then advances as a tube-fed sheet flow.

A slightly different variation of the ʻaʻā-to-pāhoehoe flow transition occurs when an ʻaʻā flow reaches a flat area and the front stops advancing. The rubbly snout of the ʻaʻā flow confines additional lava coming into the flow and causes the front to inflate (see, for example, Calvari and Pinkerton, 1998). The front then ruptures, and the fluid interior pours out and forms a pāhoehoe flow (fig. 3*A*). The ʻaʻā flow seen in figure 3*B* was still moving slowly when a lava stream broke out of the flow front and a pāhoehoe lobe spread rapidly in front of the ʻaʻā flow. This pāhoehoe lobe then inflated and formed a sheet flow.

Surges and Overflows from ʻAʻā Channels and Levees

More localized examples of the ʻaʻā-to-pāhoehoe flow transition have been observed along the margins of channels in ʻaʻā flows. Either channel blockages or surges in lava supply can cause lateral overflows from ʻaʻā levees (Lipman and Banks, 1987). In both cases, the overflows at a lower velocity form pāhoehoe crusts rather than ʻaʻā crusts. Overflows generally represent a small volume of the material in the channel and tend to spread laterally rather than downhill,

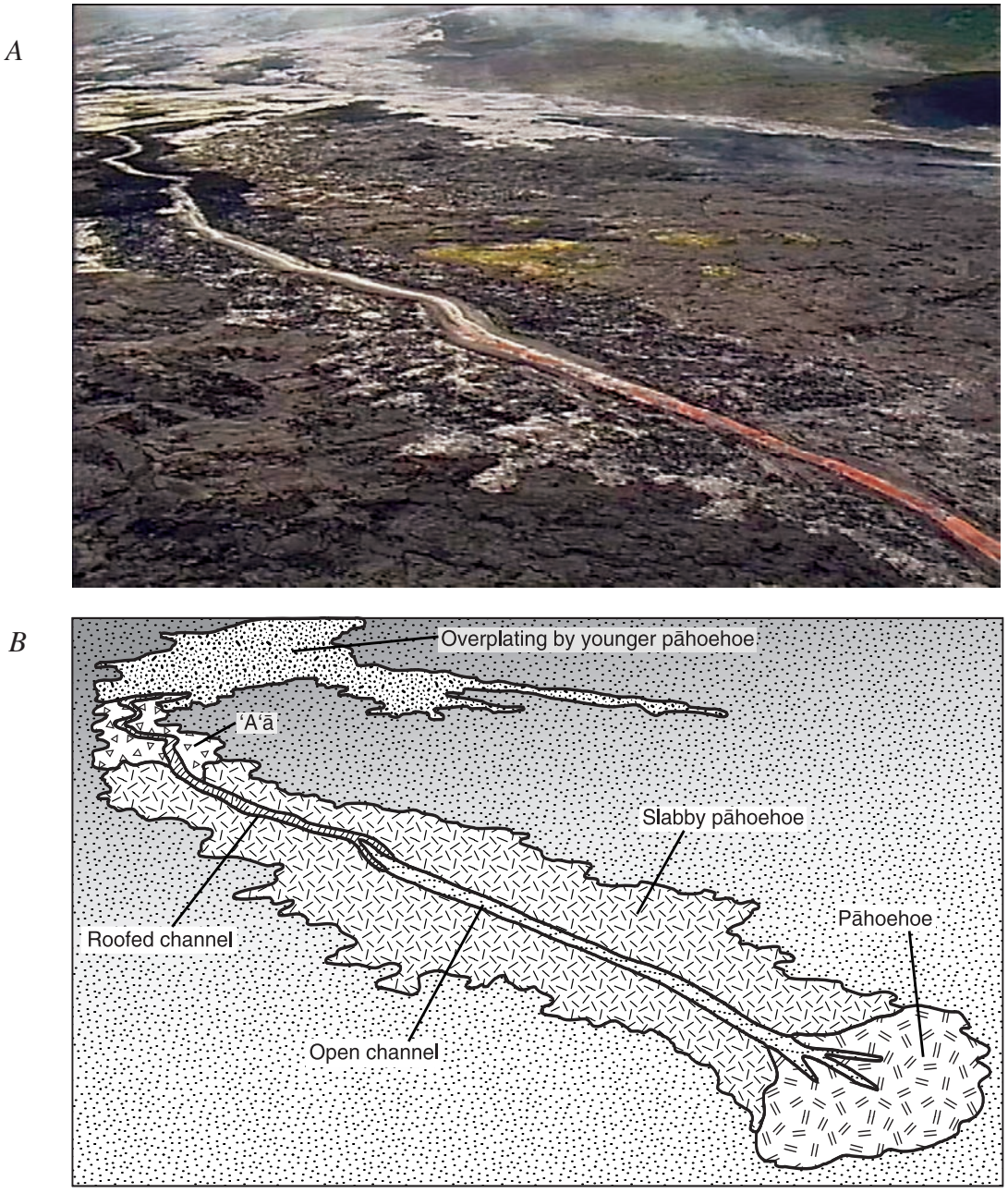

Figure 2. Transition from ʻaʻā to pāhoehoe along a single flow. *A*, Video image of the August 17, 1998, flow (Hon and Gansecki, 2002), showing the ʻaʻā-to-slabby-pāhoehoe part of the transition. The flow is about 75 m wide. *B*, Drawing of the entire ʻaʻā-to-pāhoehoe flow transition on August 17, 1998, showing the pāhoehoe snout of the flow.

reducing both velocity and shear strain on the flow and thereby allowing pāhoehoe to form.

Lipman and Banks (1987) reported pāhoehoe overflows from the channel about 3 km beyond the ʻaʻā transition during the early stages of the 1984 Mauna Loa eruption. Cashman and others (1999) sampled a transitional slabby pāhoehoe flow that broke out about 300 m downstream of the pāhoehoe-to-ʻaʻā transition during the current eruption of Kīlauea. Another excellent example can be seen at Muliwai a Pele in the Mauna Ulu flow field along the Chain of Craters Road. Here, overflows of smooth pāhoehoe deposited pāhoehoe-crusted lava balls on ʻaʻā levees.

Pāhoehoe Leaks from ʻAʻā Flows

Small oozes or leaks of pāhoehoe from dying ʻaʻā fronts have been observed repeatedly during Kīlauea's current eruption and are well documented in other studies (Camp and others, 1987; Wolfe and others, 1988; Jurado-Chichay and Rowland, 1995; Calvari and Pinkerton, 1998). Reduced lava supply to the flow front provides insufficient force to move the front. The small amount of incoming lava pools behind the snout of the ʻaʻā flow and can produce lateral injections (Lipman and Banks, 1987) that "leak" from the levees or the snout. On September 8, 2000, small pāhoehoe flows were observed oozing from the side of an ʻaʻā flow (fig. 4) that had stagnated on flat ground. The lava channel was open for several kilometers upslope, and lava tubes were not present. Wolfe and others (1988) reported similar small pāhoehoe toes oozing from the stagnated fronts of large ʻaʻā flows during the early high fountaining stages of Puʻu ʻŌʻō. Macdonald also noticed pāhoehoe toes leaking from ʻaʻā flows but ascribed them to younger pāhoehoe flows burrowing beneath older ʻaʻā flows, thereby "giving the false appearance of flow changing from ʻaʻā to pāhoehoe" (Macdonald and others, 1983, p. 21).

Jurado-Chichay and Rowland (1995) described a complex example in a 1,300-year-old Mauna Loa flow, where an overflow from an ʻaʻā channel emerged as pāhoehoe and changed to ʻaʻā as it moved away. The ʻaʻā flow appeared to have stopped advancing, inflated, and finally leaked pāhoehoe before stagnating. They interpreted the formation of pāhoehoe at this locality as the result of the crusting-over of earlier flows.

Breakouts from Inflated Pāhoehoe Flows

Large breakouts from the fronts of inflated pāhoehoe flows can show an interesting variation on the ʻaʻā-to-pāhoehoe flow transition. As the flow front breaks open, lava is pushed through a relatively small opening (1–5 m wide) and begins to spread rapidly. Initially, the flow moves very fast, owing to a combination of narrow width and high supply from stored lava (Hon and others, 1994), commonly forming slabby pāhoehoe flows. As the flow spreads out and the lava supply decreases, the velocity of the flow also decreases, and normal pāhoehoe forms at the edge of the flow. We have seen this happen repeatedly on Kīlauea; transitions between slabby pāhoehoe and normal pāhoehoe can also be seen on the inflated McCartys pāhoehoe flow in the Zuni Bandera field of New Mexico (K.A. Hon, unpublished data, 1995).

Changes from ʻAʻā to Pāhoehoe That Are Not Transitions

During some Hawaiian eruptions, a widespread change occurs from ʻaʻā flows to pāhoehoe flows that is related to a drop in effusion rate (Macdonald, 1953; Rowland and Walker, 1990, Kilburn, 2000). The effusion rate may wane during an eruption because of a change in flux or in vent geometry and storage. Rowland and Walker (1990) clearly document these changes for the paired eruptions of Mauna Loa (1859 and 1880–81) and for the Puʻu ʻŌʻō-Kūpaianaha eruption, as well as for a number of other Hawaiian eruptions. High effusion rates are accompanied by relatively high strain rates; cooling rates are also high because tube formation is inhibited in large channels. This change from ʻaʻā to pāhoehoe during the course of an eruption does not represent an example of the ʻaʻā-to-pāhoehoe flow transition. The change generally does not occur along a single flow but, rather, represents a change in style of flow-field development.

Another type of change from ʻaʻā to pāhoehoe may take place when lava tubes form by the crusting-over of channels in ʻaʻā flows (Peterson and Swanson, 1974; Peterson and Tilling, 1980; Calvari and Pinkerton, 1999). As the crust of the tube thickens, it reduces the cross-sectional area of the nascent lava tube. This causes a constriction, which frequently results in breakouts of slow-moving pāhoehoe from the new tube well upslope of the flow front. These pāhoehoe flows, along with other pāhoehoe flows that commonly overplate the earlier ʻaʻā flows, give the appearance of an ʻaʻā-to-pāhoehoe flow transition. The pāhoehoe facies, however, is upslope of the ʻaʻā facies during formation.

Rheological and Crustal Transitions in Hawaiian Lavas

Peterson and Tilling (1980) and Kilburn (1981) altered the discussion about the pāhoehoe-to-ʻaʻā transition from the change in crust morphology along a flow to the change that a discrete "element" of molten lava undergoes as it is transported to the flow front. The pāhoehoe-to-ʻaʻā transition was sketched as the transition threshold zone (TTZ) on a dimensionless graph of apparent viscosity versus shear strain (fig. 9 of Peterson and Tilling, 1980). Within the TTZ, slabby pāhoehoe forms at high strain rates, and viscous spiny pāhoehoe forms at lower strain rates. Peterson and Tilling (1980) gave examples to demonstrate how changes in

A

B

Figure 3. *A*, Pāhoehoe flow breaking out from the front of a stagnated ʻaʻā flow at the base of Pūlama pali on September 10, 2000. *B*, Pāhoehoe flow breaking out from the front of an ʻaʻā flow as it reaches the flat just outside Kalapana (photograph taken April 3, 1990). Notice the incandescent material in the ʻaʻā flow, which was still active as the pāhoehoe flow emerged.

Figure 4. Pāhoehoe lobes oozing from an ʻaʻā levee as the ʻaʻā flow stagnates (photograph by A.M. Burt, September 8, 2000). The active ʻaʻā levee is seen in the picture above the pāhoehoe lobe, which is flowing on older ʻaʻā crust.

shear strain and apparent viscosity could force lava from the pāhoehoe field into the ʻaʻā field.

Kilburn (1981) made some simplifying assumptions, based upon the rheological measurements of Shaw (1969) and Pinkerton and Sparks (1978), to show that the range of apparent Newtonian viscosities (η_a) at a given Bingham viscosity (η_b) and yield strength (σ_y) defines a distinctive curve (fig. 5). Bingham fluids differ from Newtonian fluids in having a yield strength (Shaw and others, 1968; Peterson and Tilling, 1980; Kilburn, 1981). The values of η_a for Bingham lavas asymptotically approach η_b (fig. 5) at high shear-strain rates. As the shear-strain rate decreases, η_a increases dramatically. If there is no change in η_b (for example, no change in temperature, volatile, or crystal content), the fluid follows a η_a curve (white arrows in figure 5) as the shear-strain rate is reduced (for example, the flow slows). If the fluid cools, crystallizes, or otherwise increases in apparent viscosity, the path will shift to the right (black arrows) in figure 5. A black vertical dashed line shows the Newtonian viscosity (η_N) for Hawaiian lava with a temperature of 1,150°C (Shaw, 1969), a temperature common for lavas within a few kilometers of the Puʻu ʻŌʻō vent (Helz and others, this volume; Cashman and others, 1999).

Kilburn (1981) proposed that the TTZ is represented by a family of η_a curves for lava with Bingham rheology. According to this model, lava that passes into the TTZ cannot return to a previous state; the transition is irreversible. Kilburn (1990) later modified this argument to suggest that the TTZ represents a crustal-failure envelope rather than a simple rheological boundary. We have followed this model in constructing a semiquantitative graph of the transition for Hawaiian lava (fig. 6*A*).

Refining the Graphical Transition for Hawaiian Lavas

Apparent Newtonian viscosity η_a curves L, 1, 4, and 8 (table 1, fig. 6*A, B*) have been constructed from data for Kīlauea and Mauna Loa lava with Bingham viscosities (Shaw and others, 1968; Shaw, 1969; Moore, 1987), using equation 3 of Kilburn (1981).

$$\eta_a = \eta_b + (\sigma_y/\dot{\varepsilon}),$$

where σ_y is the yield strength of the lava and $\dot{\varepsilon}$ is the shear-strain rate.

Kilburn (1981) had previously plotted the data of Shaw and others (1968) from Hawaiʻi and the single curve from an Etna ʻaʻā flow (Pinkerton and Sparks, 1978) on a similar plot. The η_a curves from the two volcanoes differ significantly in shape, owing to the very different temperatures and compositions of the lava (Kilburn, 1981). Plotting the viscosity

Table 1. Viscosity data for Hawaiian tholeiite lava with Bingham rheology used to construct figures 5 and 6.

Curve number	Bingham viscosity η_b (Pa·s)	Yield strength σ_y (Pa)	Temperature (°C)	Crystal content (percent)	Principal reference
Curve L	700	95	1130–1135	25	Shaw and others (1968)[1]
Curve 8	1100	150	1128; 1139	22; ---	Moore (1987)[2]
Curve 4	3700	930	1126; 1133	40; 24	Moore (1987)[3]
Curve 1	81000	2225	1125	>40?	Moore (1987)[4]

[1] Average of the two measurements taken from Makaopuhi lava lake.

[2] Viscosity data from station 8 at 2,500-m elevation on Mauna Loa (Moore, 1987, p. 1581). Location given on figure 57.1 and referred to as 1852 vent in table 57.1 of Lipman and Banks (1987). Temperatures taken from table 57.1 for two samples from 2,500-m elevat ion (NER-12/57 and unmarked sample). Crystallinity estimated from table 3 of Crisp and others (1994) for sample NER-12/57 taken at 2,250-m elevation.

[3] Viscosity data from station 4 at 1,900-m elevation on Mauna Loa (Moore, 1987, p. 1582). Yield strength is average of two estimates given. Temperatures are from table 57.1 of Lipman and Banks (1987) for samples NER-12/48, taken at 1,940-m elevation, and NER-12/28, taken at 1,730-m elevation near station 4. Crystallinity (40 percent for NER-12/48 and 24 percent for NER-12/28) is taken from table 3 of Crisp and others (1994) for same samples. Note that Crisp and others (1994) may have mislabeled sample NER-12/28 as NER-12/27 throughout their paper. The sample they label as NER-12/28 is a near-vent sample.

[4] Viscosity data from station 1 at 1,600-m elevation on Mauna Loa (Moore, 1987, p. 1582). Yield strength is lower of two estimates given and was used by Moore (1987). Temperature is from table 57.1 of Lipman and Banks (1987) for a measurement taken in 1984 on 3/31. There are no data on crystallinity for this site, which is even farther from the vent than sample NER-12/28 and is probably at least as crystal rich. This lava did not fit a Bingham rheological model and was thought to exhibit pseudoplastic or other complex behavior by Moore (1987).

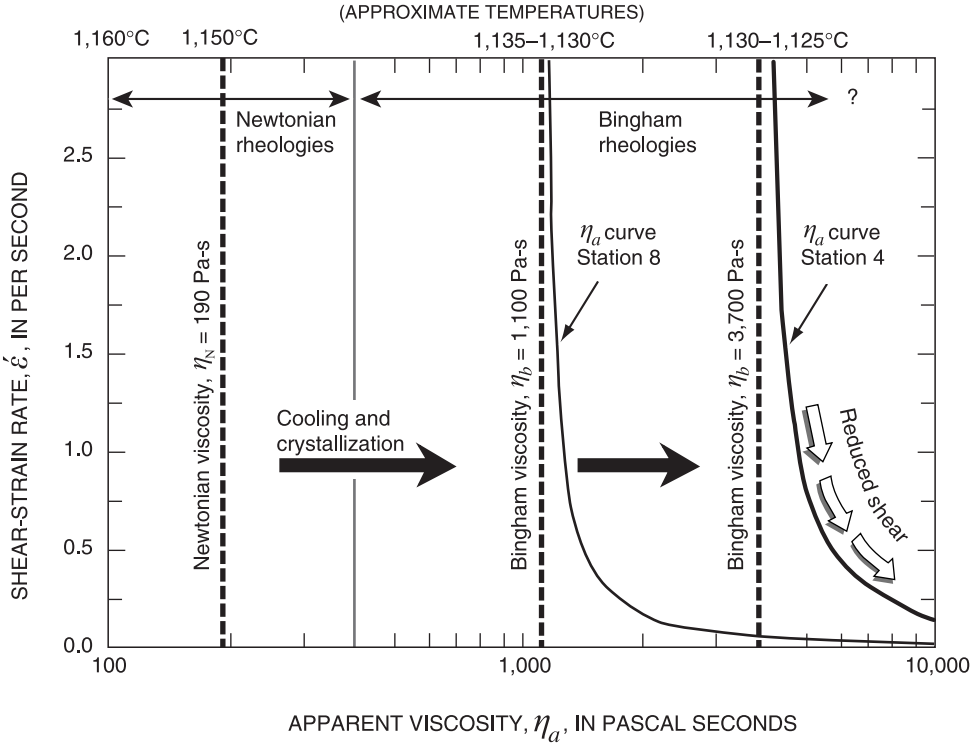

Figure 5. Diagram of shear-strain rate versus apparent Newtonian viscosity of lava, showing difference between a Hawaiian lava with near-Newtonian viscosity (data from Shaw, 1969) and Hawaiian lavas with Bingham viscosities and yield strengths (data in table 1, from Moore, 1987). The development of yield strength may be caused by crystallization of plagioclase microlites (Cashman and others, 1999). The apparent viscosity of the Bingham lava changes with the rate of shear strain (Kilburn, 1981). Both cooling and crystallization increase the Newtonian or Bingham viscosity of the fluid in the direction of the thick black arrows from one vertical Bingham viscosity (η_b) line to another. Decreasing the shear-strain rate causes the apparent Newtonian viscosity (η_a) of Bingham lavas to increase dramatically (white arrows).

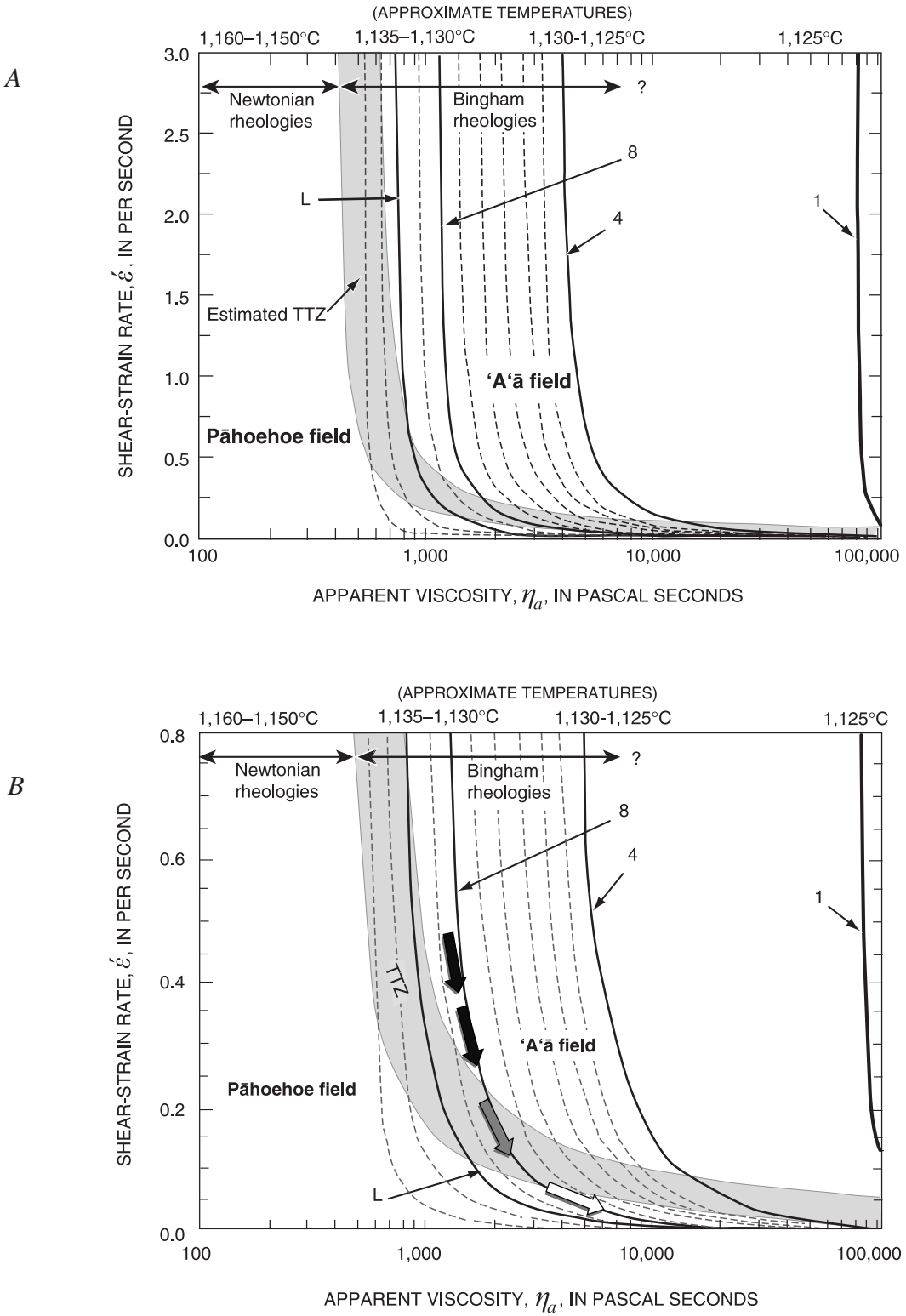

Figure 6. Diagrams of shear-strain rate versus apparent Newtonian viscosity, showing relation of pāhoehoe and 'a'ā lavas. *A*, Approximate stability fields for Hawaiian pāhoehoe and 'a'ā and approximate transition threshold zone (TTZ) within Bingham rheology field. Shaded area represents estimated TTZ. Solid curved lines are apparent Newtonian viscosities (η_a) for specific Bingham viscosities as calculated for Kīlauea (curve L) and for Mauna Loa (curves 8, 4, and 1) (see text and table 1 for explanation). Dashed lines are estimated and represent family of apparent viscosity curves for Hawaiian lavas with Bingham rheology. *B*, Region of figure 6*A* at lower range of shear-strain values (<0.8) showing lower section of TTZ in detail. Possible flow-front conditions during 'a'ā-to-pāhoehoe flow transition are shown by the arrows. The lava begins in the 'a'ā field (black arrows) and approximately follows an apparent viscosity (η_a) curve as shear strain is reduced. Then the lava enters the TTZ (gray arrow) and finally the pāhoehoe field (white arrow).

directly measured (curve L) by Shaw and others (1968) with the empirically estimated viscosities (curves 1, 4, 8) of Moore (1987) allows generation of a set of curves with similar shapes (fig. 6). The Bingham viscosity data (table 1) are estimates of the apparent viscosity of the lava (a mixture of melt, crystals, and bubbles). These two data sets were determined by different methods, but the closeness in shape and position of curves L and 8 for lava with similar temperature and crystallinity (fig. 6*A*) shows that the Bingham viscosity estimates are in reasonable agreement (Moore, 1987, p. 1585).

Viscosity has been plotted on a log scale because it increases roughly exponentially with decreasing temperature (Shaw, 1969). Linear viscosity plots produce a pāhoehoe field that is extremely narrow and de-emphasizes the broad temperature range over which pāhoehoe occurs in Hawai‘i. Approximate temperatures have been placed at the top of figures 6*A* and 6*B* to provide a reference for several specific η_a curves. The dashed lines are interpolated to show the general shape of the η_a curves and possible paths resulting from reduction of shear strain; the spacing of these curves has no temperature significance.

The approximate ranges of Newtonian and Bingham rheologies are shown by arrows at the top of figure 6*A* and 6*B* (also shown on fig. 5). An apparent viscosity of 400 Pa·s was estimated as the boundary between the Newtonian and Bingham viscosity fields. Moore (1987, p. 1,584) estimated that Hawaiian lavas at 1,140°C have viscosities of 300–400 Pa·s. Lava with temperatures between 1,145 and 1,135°C may have crystallinities of 10–20 percent (Crisp and others, 1994; Cashman and others, 1999; Helz and others, this volume). Cashman and others (1999) suggested that lava with crystallinities of 25–30 percent, particularly when consisting of plagioclase microlites, begins to develop significant yield strength.

Cashman and others (1999) concluded that yield strength is necessary to develop ‘a‘ā or transitional crustal morphologies. This idea is supported by the data of Shaw and others (1968) and Moore (1987), who calculated significant yield strengths for fluids with temperatures below 1,135°C. Our field observations of pāhoehoe flows also show that pasty or spiny crusts begin to form at temperatures less than 1,140°C, suggesting the development of yield strength in these lavas. The estimated boundary provides a left-hand limit in figure 6 to the upper extent of the TTZ. The actual boundary may be lower or higher but is probably not less than 300 Pa·s or greater than 600 Pa·s. Changing the estimated position of the Newtonian-Bingham rheology boundary shifts the TTZ slightly but has no significant effect on our argument.

Curve L (Shaw and others, 1968) represents lava subjected to very low shear-strain rates in a lava lake with a pāhoehoe crust. Similar temperatures of 1,130–1,135°C were common for large ‘a‘ā flows during the early Pu‘u ‘Ō‘ō eruption (Neal and others, 1988). Thus, at higher shear-strain rates, Kīlauea lava with the rheology of curve L could produce ‘a‘ā crust. We suggest that curve L must cross the transition threshold zone (TTZ) somewhere in the region shown on figure 6*A*.

Curve 8 is for channelized Mauna Loa lava with ‘a‘ā crust subject to shear-strain rates of 1-3 s^{-1} (station 8 on fig. 58.17 in Moore, 1987). The TTZ must lie to the left of this curve at high shear-strain rates. Lipman and Banks (1987, p. 1,529) observed small pāhoehoe overflows from the channel near station 8 (2,500-m elevation on the 1852 vent) and stated that lava flowing slowly was capable of generating pāhoehoe down to the 2,400-m elevation. These data and observations suggest that curve 8 for Mauna Loa lava must also cross the TTZ. We arbitrarily chose a small value for the shear-strain rate crossover (about 0.1 to 0.2 s^{-1}) to minimize the pāhoehoe field and conditions favorable for the ‘a‘ā-to-pāhoehoe flow transition (fig. 6*B*).

Curve 4 describes Mauna Loa lava subjected to a strain rate of about 1 s^{-1} and producing ‘a‘ā (station 4 on fig. 58.17 in Moore, 1987). Most of the channel overflows in this region were ‘a‘ā, though a slabby pāhoehoe overflow was also reported (Lipman and Banks, 1987). This suggests that curve 4 might enter the TTZ at low strain rates but may not pass through it.

‘A‘ā flows at station 1 (curve 1 in fig. 6*A*; table 1), about 5 km farther from the vent than station 4, have order-of-magnitude higher apparent viscosities but similar temperatures (Moore, 1987; Lipman and Banks, 1987). These flows were not easily modeled as Bingham rheologies (Moore, 1987) and appear to behave pseudoplastically or thixotropically (Shaw, 1969; Moore, 1987; Pinkerton and Norton, 1995). Hawaiian lava with this rheology probably cannot form normal smooth-surfaced pāhoehoe, though more viscous transitional morphologies, such as spiny pāhoehoe (Peterson and Tilling, 1980) and toothpaste lava (Rowland and Walker, 1987), may form at low shear-strain rates.

The semiquantitative graphs (fig. 6*A, B*) of shear-strain rate versus apparent viscosity for Hawaiian lava differ significantly from the earlier dimensionless graphs (Peterson and Tilling, 1980; Kilburn, 1981) by having values on the axes. However, the graphs should not be used to determine absolute numbers, owing to the uncertainties associated with the original viscosity determinations. Nonetheless, estimating these values as a starting point for further work and discussion is a valuable exercise.

The TTZ (fig. 6*A, B*) asymptotically approaches the apparent viscosity axis at low shear-strain rates, rather than being truncated by this axis, as shown by Peterson and Tilling (1980). This allows a larger range of rheologies to produce transitional crustal morphologies (for example, much of the pāhoehoe derived from differentiated Etna lavas would be considered transitional in Hawai‘i). Peterson and Tilling (1980) did not show apparent viscosity curves in relation to their TTZ, and Kilburn (1981) suggested that the TTZ was represented by a family of apparent viscosity curves. Kilburn (1990) modified the TTZ to cut across and truncate apparent viscosity curves on a dimensionless graph. We show the apparent viscosity curves cutting across the TTZ.

Apparent viscosity η_a is plotted on a log scale (fig. 6*A, B*) to expand the vertical part of the TTZ and the relatively narrow viscosity field for Newtonian rheologies. The Newtonian rheologies represent a broad temperature range of 20–30°C that is highly compressed without the log scale. This

small viscosity interval, however, represents a relatively large amount of cooling time compared to that represented by the much larger interval of apparent viscosity between curves 1 and 4 (fig. 6*A*), because cooling and crystallization rates for lava in open channels are roughly uniform for Hawaiian lava (Cashman and others, 1999). As lava cools below 1,140°C, the increasing crystallinity causes a nearly exponential increase in viscosity (Shaw and others, 1968) over a relatively short time period. The temperature data in the region below 1,140°C also become somewhat erratic (table 1; fig. 6), because the heat of crystallization offsets cooling as increasing amounts of plagioclase microlites form (Crisp and others, 1994; Helz and others, this volume).

The position of the transition threshold zone (TTZ) of Peterson and Tilling (1980) has been approximated in this study, largely on the basis of empirical observations discussed earlier. The exact position and shape of the TTZ are tentative. We here purposely minimized the conditions under which lava that produces ʻaʻā crusts at higher shear rates might produce pāhoehoe at lower shear rates. It is here suggested that the TTZ cuts across the family of apparent viscosity curves for Hawaiian lava in the approximate interval of 1,125–1,140°C (fig. 6*A*), which is typical for pāhoehoe on the coastal flat 10–12 km from the vent (Hon and others, 1994; Keszthelyi, 1995; Keszthelyi and Denlinger, 1996). If this is correct, lava can pass back from the ʻaʻā field into the pāhoehoe field under this restricted set of rheological conditions.

Tracking Changes in Shear-Strain Rate and Viscosity

Figure 6*B* shows a possible path for a Bingham lava to change from producing ʻaʻā crust to producing pāhoehoe crust by simply reducing the shear-strain rate. The black arrows represent lava producing ʻaʻā crust at higher strain rates, the gray arrow represents lava within the transition zone producing slabby pāhoehoe crust, and the white arrow represents lava producing pāhoehoe crust. Again, the actual shear-strain rates are speculative. The path assumes that the Bingham viscosity of the fluid producing the ʻaʻā and the pāhoehoe is nearly constant. This case is relatively easy to demonstrate for pāhoehoe-toe breakouts from stagnated ʻaʻā fronts. Since the lava that produced the ʻaʻā and the pāhoehoe must have traveled down the same channel system to arrive at the front, the molten lava that arrives last to produce the pāhoehoe will have cooled more, as a result of waning supply rates and increased storage time in the flow front. This clearly demonstrates that lava feeding these flows was capable of producing either pāhoehoe or ʻaʻā, depending on the strain rate.

The relationship is more complex for the partially tubed ʻaʻā and pāhoehoe flows. For these flows, the length of open channel from the tube mouth to the flow front remains nearly the same as the flow advances. Cooling during open-channel flow is faster (0.0005°C/s) and has a much greater effect on crystallization and lava viscosity than slower cooling (0.0001–0.0002°C/s) during flow in a lava tube (Cashman and others, 1999; Helz and others, this volume). Assuming that the time of transport in the open channel remains nearly constant, the only increase in cooling rate would be caused by lengthening of the lava tube as the flow moves downslope. This condition requires that the flow front advances at about the same rate that the lava tube crusts over, in agreement with our observations. Cooling is time-dependent, so the length of open channel can actually be shorter on flat ground where the velocity of the lava drops and the lava cools more per unit distance traveled. Thus, the viscosity of the flows will increase fairly slowly, as shown on figure 6*B*. In contrast, the shear-strain rate will be controlled mainly by the ground slope, which changes rather rapidly from >5° on the slope to <2° on the coastal flat. The shear-strain rate may also be affected by surges in flux rate, caused by constriction of channels or tubes and fluctuations in vent output.

A hidden difficulty exists in attempting to track paths of discrete elements of molten lava described by Peterson and Tilling (1980, p. 286) on graphs such as that in figure 6*B*. Implicit in any discussion of lava travel paths is transport time, which affects cooling rate and crystallization. Since time is not on one of the axes, plotting any type of path on this graph poses a challenge. Changes in temperature along a flow could be transformed into length of time, using the approximate cooling rates given by Cashman and others (1999), and further transformed into distances if transport velocities along the flow are known. The release of heat during crystallization also adds to the complexity of estimating rates of cooling, and some flows actually appear nearly isothermal while increasing greatly in apparent viscosity (Crisp and others, 1994). As can be seen on figure 6*A* and 6*B*, any attempt to transfer cooling rates into time will produce a highly nonlinear scale.

Another problem with the idea of a path is that the conditions to which lava is subjected when flowing in a channel are not analogous to conditions the same lava will undergo upon reaching the flow front, where most crust forms. Two different, but related, processes are represented on the graphs (fig. 6): one is the change in rheology of the fluid, and the second is the formation of crust. Crust clearly plays an integral part in the emplacement of any lava flow and has a significant effect on the bulk viscosity of the flow (Kilburn, 1993, 2000; Hon and others, 1994; Keszthelyi and Denlinger, 1996; Cashman and others, 1999). Most crust on lava flows begins forming at the flow front, not during transport in a channel or tube system, because lava at the front spreads over a wide area and is exposed to higher shear-strain rates and faster cooling. In contrast, most lava moving from the vent to the flow front generally does not undergo conditions conducive to crust production; otherwise lava in the channel would solidify.

Instead, graphs like those in figure 6*A* and 6*B* are, perhaps, better used to visualize shear-strain rate and viscosity conditions to which lava is exposed at a certain point in time. We suggest that tracking the conditions at the flow front as it moves downslope is as important as tracking the rheological

changes in the lava as it is transported to the flow front. The changes in lava rheology would be tracked on the same graph, but without the TTZ. Once lava reaches the area where crust is being produced, the TTZ is useful in predicting which type of crust will form.

Migration of the Pāhoehoe-to-ʻAʻā Transition

Both Lipman and Banks (1987) and Wolfe and others (1988) found that the position of the pāhoehoe-to-ʻaʻā flow transition on large, open-channel flows remained very close to the initial transition (marked by the change from pāhoehoe to ʻaʻā crust on the levees) throughout the life of the flow. In contrast, the position of the pāhoehoe-to-ʻaʻā flow transition on smaller, partially tubed flows can migrate downstream with respect to where the change occurred on the solidified levees. The migrating transition may be marked along the channel by coatings of smooth pāhoehoe crust on the surrounding ʻaʻā levees.

The migration of the transition along the channel is commonly due to the formation of lava tubes (Peterson and Tilling, 1980, p. 276), which can form in a few hours or days on small channels (1–5 m) but can take weeks or months to form on larger channels. In Hawaiʻi, large eruptions with high effusion rates last only a few days or weeks and generally end before lava tubes can form on their wide channels (10–20 m). An exception is the Kaʻūpūlehu flow on Hualālai Volcano, where the channels were eroded by a bedload of dunite xenoliths. Those channels have a narrow and deep cross section that permitted rapid tube formation (Kauahikaua and others, 2002) and allowed the pāhoehoe-to-ʻaʻā transition to migrate downslope, as indicated by pāhoehoe coatings lining the channel walls. The old, high-effusion-rate flows on Mauna Loa studied by Jurado-Chichay and Rowland (1995) also partially tubed over and allowed the transition zone to migrate to the coastal region.

If the boundary between the crusted channel and the open channel begins to migrate faster downslope than the flow front, the entire channel will eventually be tubed over to the flow front and the flow will then become pāhoehoe. This is the ultimate fate of all the relatively small channelized ʻaʻā and pāhoehoe lava flows that reach the coastal flats. The critical observation is whether the channel crusts over before or after a channelized ʻaʻā flow changes to pāhoehoe. Some flows reach the flat with channel systems that stay open until after the flow has undergone a change from ʻaʻā to pāhoehoe. Other ʻaʻā flows may actually become completely tubed over as they slow down and stop on the flatter ground. This insulates lava delivered to the flow front and produces outbreaks of pāhoehoe from the ʻaʻā front. The rheology of the lava would appear to shift to the left if conditions at the flow front were tracked on a graph like that of fig. 6*A*. Clearly no individual parcel of molten lava can get hotter upon arrival at the flow front.

Do Pāhoehoe and ʻAʻā Liquids Exist?

The terms pāhoehoe and ʻaʻā were expanded by Peterson and Tilling (1980) to include both fluid and crust, in a way similar to the use of the term lava for both molten and solid rock. We suggest, however, that the use of pāhoehoe and ʻaʻā be restricted to the solidified lava surfaces or lava flows dominantly covered by crust, as Macdonald (1953) suggested. Solidified pāhoehoe crust does not change to ʻaʻā crust, nor vice versa. The nature of the molten lava can only be determined by the crust it becomes and not reliably by any morphology of the molten lava itself. Furthermore, the nature of the molten lava beneath the crust cannot always be inferred from the morphology of the crust, particularly in channels.

A number of studies (Kilburn and Guest, 1993; Jurado-Chichay and Rowland, 1995; Cashman and others, 1999) demonstrated that the fluid cores of ʻaʻā flow channels and lobes have a complex thermal stratification. In contrast, the interiors of pāhoehoe flow channels and flow lobes appear to be relatively well mixed (Hon and others, 1994; Cashman and others, 1999). A flow that is undergoing the pāhoehoe-to-ʻaʻā transition defined by Macdonald (1953) would have a fluid core whose outer surfaces are cooling and producing solidified products that change progressively from pāhoehoe to ʻaʻā crusts along the length of the flow. The molten interior of a lava channel can easily be masked by a cooler outer layer that is producing crust (Cashman and others, 1999). Therefore, estimating the rheological properties of lava within a given channel or lobe is not as simple as it appears. If our analysis of the TTZ is correct, some molten lava may also have the ability to form either pāhoehoe or ʻaʻā crusts, depending solely on the strain rate.

The argument in this paper differs little from the original premise of Peterson and Tilling (1980), who demonstrated that it is the shear-strain rate acting on molten lava with a given rheology that determines the type of crust produced. Kilburn (1990) amplified this concept by suggesting that the TTZ is a failure envelope controlled by shear-strain rates that cuts across rheological boundaries. The clarification being made here is that the transition is defined by the type of crust formed and not by the rheology of the molten lava producing the crust.

Discussion

Are the examples given above truly examples of an ʻaʻā-to-pāhoehoe flow transition? Using the original definition given by Macdonald (1953), we believe the answer is "yes" for our first type, in which ʻaʻā flows change sequentially into pāhoehoe flows. This change occurs at the flow front, where the flow displays a morphological sequence of ʻaʻā to slabby pāhoehoe to pāhoehoe on the levees as the flow advances, the exact reverse of the widely accepted pāhoehoe-to-ʻaʻā transition.

The ʻaʻā-to-pāhoehoe flow transition is most commonly associated with a drop in shear stress while the molten lava delivered to the flow front remains at a relatively constant temperature. These conditions can occur for channelized flows advancing from steep to flat ground and for overflows from ʻaʻā flow channels. In such cases, the conditions of apparent viscosity and shear-strain rate stay fairly close to the region between curves L and 8 (fig. 6*A*), if our approximation of the transition is correct.

Kilburn (2000) discounted pāhoehoe outbreaks from ʻaʻā fronts because they incorporate "hotter" lava from the core of the flow. However, the molten lava core that produces the pāhoehoe in this low-shear-strain environment has traveled past the point of pāhoehoe-ʻaʻā transition, as marked by solidified ʻaʻā on the levees of the stagnated flow. Clearly lava that produced an ʻaʻā fan and levees on the steeper slope also produced pāhoehoe upon reaching the flatter ground. The lava that produces pāhoehoe-crusted flows cannot be the same element of lava that earlier produced ʻaʻā crust. Both elements of lava arrived at the front through the same transport system and should be rheologically identical. The only difference is that the later lava experienced lower shear-strain rates on the flatter ground.

Cashman and others (1999) suggested that the molten lava producing transitional pāhoehoe breakouts comes from the hotter inner component (about 1,135°C and 15–20 percent crystals) of the ʻaʻā channel, whereas the cool outer component (~1,100°C and 40 percent crystals) appears to have undergone an irreversible transition and is capable of producing only ʻaʻā crust. They demonstrated that the increasing number of plagioclase microlites below 1,140°C raises the yield strength and is largely responsible for the change in rheology of Hawaiian lava.

Similar data from the 1984 Mauna Loa eruption suggest that molten lava capable of producing either ʻaʻā flow fronts or pāhoehoe overflows has crystallinities of 20–30 percent at temperatures of 1,125–1,140°C (Lipman and Banks, 1987; Crisp and others, 1994). Temperatures of large ʻaʻā flow fronts during the early Puʻu ʻŌʻō stages were commonly about 1,100°C, but large surges from the flow interior had temperatures of about 1,135–1,138°C (Neal and others, 1988). The surges were fluid, spiny ʻaʻā, but small leaks of pāhoehoe from stagnant flows indicate that the same fluid core could produce pāhoehoe at low strain rates (Wolfe and others, 1988).

All of these data suggest that Hawaiian lava in the approximate temperature range of 1,125–1,140°C can produce either ʻaʻā or pāhoehoe crust, depending on the rate of shear strain (fig. 6*A*). Along the course of a channel, the fluid can become pāhoehoe crust in one place, continue over a steep slope and become ʻaʻā clinker, then proceed out onto a flat plain and again form pāhoehoe crust.

When flowing in channels, Hawaiian lava with temperatures between 1,125 and 1,140°C can also have a smooth surface appearance; thus, determining in the field whether pāhoehoe or ʻaʻā crust will form may be difficult. Retaining the original use of the terms pāhoehoe and ʻaʻā for the solidified crust and not for the molten lava is suggested. Where sufficient patches of crust have formed on the channel surface, the lava should be called "lava with pāhoehoe crust" or "lava with ʻaʻā crust," rather than pāhoehoe lava or ʻaʻā lava. Difficulties can arise for lava flows that contain both fragments of pāhoehoe crust and ʻaʻā clinker. In some of these flows, pāhoehoe crust may have formed in the channel and rafted some distance to the front. In transitional slabby pāhoehoe flows, both spiny ʻaʻā crust and pāhoehoe slabs may form simultaneously in response to variable rates of shear strain in the moving front.

Graphs, such as those in figure 6, can be used to track changes in the rheology of lava transported to the flow front. The transition threshold zone (TTZ) can be used separately to evaluate crustal formation at the flow front on the same graph. The type of crust being formed at the flow front can be identified unambiguously in the field, as cooled crustal fragments of either pāhoehoe or ʻaʻā will generally be present. The graph can be used to predict the type of lava flow that might form when a flow front reaches a specific position, given estimations of lava rheology and slope.

Conclusions

Using available data, we constructed a semiquantitative graph (fig. 6) of shear strain versus apparent viscosity for Hawaiian lava. The approximate shape and position of the transition threshold zone (TTZ), estimated from field data and observations, differs from those of previously published estimates (Peterson and Tilling, 1980, Kilburn, 1981). This new interpretation allows an ʻaʻā-to-pāhoehoe flow transition to exist in a limited rheological interval (about 1,125-1,140°C) for Hawaiian tholeiitic lava.

Lava streams in ʻaʻā and transitional flows probably consist of two components (Cashman and others; 1999; Kilburn and Guest, 1993). This stratification allows molten lava still capable of solidifying to pāhoehoe crust to travel in the core of a lava stream, while the surface and outer edges (the cooler and higher shear-strain regions) are producing ʻaʻā clinker. The rapid formation of lava tubes also plays a crucial role in the ʻaʻā-to-pāhoehoe flow transition by keeping the Bingham viscosity and yield strength nearly constant as the shear strain is reduced. This allows the transition zone to migrate downslope, rather than remain in a relatively fixed position as it does in open-channel flows (Lipman and Banks, 1987; Wolfe and others, 1988).

Most authors have stressed the role that high effusion rate plays in creating ʻaʻā fields, while low effusion rates promote the growth of pāhoehoe fields (Macdonald, 1953; Rowland and Walker, 1990; Cashman and others, 1999). ʻAʻā can, however, be a significant component of low-effusion-rate pāhoehoe flow fields. Unlike the simple pāhoehoe-to-ʻaʻā transitions observed on flows with high effusion rates, the nature of the transition on flows with low effusion rates is nearly impossible to decipher after the eruption has ceased, owing to the progressive overplating by pāhoehoe.

The reversible transition between pāhoehoe and ʻaʻā flow types is strongly controlled by slope and local lava supply, rather than by effusion rate.

Additional studies are needed to understand the flow behavior described here. A simple cataloging of temperatures and crystallinities of pāhoehoe found on the coastal region far from the vent, to compare with ʻaʻā crystallinities and temperatures, would be a significant start. A determined attempt to study and sample these ephemeral lava flows in the process of changing from ʻaʻā to pāhoehoe, much like the studies done on the pāhoehoe-to-ʻaʻā transition (Cashman and others, 1999; Polacci and others, 1999), is also needed. Perhaps this current eruption will provide another 20 years of opportunity to answer these questions.

Acknowledgments

The authors are indebted to Don Peterson, Robert Tilling, Chris Kilburn, and Kathy Cashman, whose seminal papers on the pahoehoe-to-ʻaʻā transition have influenced us greatly. We thank Don Swanson, Christina Heliker, Dave Sherrod, and Jenda Johnson of the USGS Hawaiian Volcano Observatory and Dave Clague of the Monterey Bay Aquarium Research Institute for interesting and thought-provoking discussions of the ideas and the manuscript. Scott Rowland, Lazlo Keszthelyi, Chris Kilburn, and Kathy Cashman all provided excellent and insightful review comments that significantly improved the manuscript.

References Cited

Calvari, Sonia, and Pinkerton, Harry, 1998, Formation of lava tubes and extensive flow field during the 1991–1993 eruption of Mount Etna: Journal of Geophysical Research, v. 103, no. B11, p. 27291–27301.

Calvari, Sonia, and Pinkerton, Harry, 1999, Lava tube morphology on Etna and evidence for lava flow emplacement mechanisms: Journal of Volcanology and Geothermal Research, v. 90, no. 3–4, p. 263–280.

Camp, V.E., Hooper, P.R., Roobol, M.J., and White, D.L., 1987, The Madinah eruption, Saudi Arabia; magma mixing and simultaneous extrusion of three basaltic chemical types: Bulletin of Volcanology, v. 49, no. 2, p. 489–508.

Cashman, K.V., Thornber, C.R., and Kauahikaua, J.P., 1999, Cooling and crystallization of lava in open channels, and the transition of pāhoehoe lava to ʻaʻā: Bulletin of Volcanology, v. 61, no. 5, p. 306–323.

Crisp, Joy, Cashman, K.V., Bonini, J.A., Hougen, S.B., and Pieri, D.C., 1994, Crystallization history of the 1984 Mauna Loa lava flow: Journal of Geophysical Research, v. 99, no. B4, p. 7177–7198.

Helz, R.T., Hon, K.A., and Heliker, C.C., 1993, Thermal efficiency of lava tubes at Kilauea Volcano, Hawaii [abs.], *in* Duggan, M.B., and Knutson, Jan, compilers, Ancient volcanism and modern analogues: IAVCEI General Assembly, Canberra, Australia, 1993, Abstracts, v. 1, no. 1, p. 47.

Hon, K.A., and Gansecki, C.A., 2002, Lava flows and lava tubes; what they are, how they form: Volcano, Hawaii, Volcano Video Productions, VHS videotape, 45 min.

Hon, K.A., Kauahikaua, J.P., Denlinger, R.P., and McKay, Kevin, 1994, Emplacement and inflation of pahoehoe sheet flows; observations and measurements of active lava flows on Kilauea Volcano, Hawaii: Geological Society of America Bulletin, v. 106, no. 3, p. 351–370.

Jurado-Chichay, Zinzuni, and Rowland, S.K., 1995, Channel overflows of the Pōhue Bay flow, Mauna Loa, Hawai′i; examples of the contrast between surface and interior lava: Bulletin of Volcanology, v. 57, no. 2, p. 117–126.

Kauahikaua, J.P., Cashman, K.V., Clague, D.A., Champion, Duane, and Hagstrum, J.T., 2002, Emplacement of the most recent lava flows on Hualālai Volcano, Hawai‘i: Bulletin of Volcanology, v. 64, no. 3–4, p. 229–253.

Keszthelyi, L.P., 1995, Measurements of the cooling at the base of pahoehoe flows: Geophysical Research Letters, v. 22, no. 16, p. 2195–2198.

Keszthelyi, L.P., and Denlinger, R.P., 1996, The initial cooling of pahoehoe flow lobes: Bulletin of Volcanology, v. 58, no. 1, p. 5–18.

Kilburn, C.R.J., 1981, Pahoehoe and aa lavas; a discussion and continuation of the model of Peterson and Tilling: Journal of Volcanology and Geothermal Research, v. 11, no. 2–4, p. 373–382.

Kilburn, C.R.J., 1990, Surfaces of aa flow-fields on Mount Etna, Sicily; morphology, rheology, crystallization and scaling phenomena, *in* Fink, J.H., ed., Lava flows and domes; emplacement mechanisms and hazard implications: Berlin, Springer-Verlag, p. 129–156.

Kilburn, C.R.J., 1993, Lava crusts, aa flow lengthening, and the pahoehoe-aa transition, *in* Kilburn, C.R.J., and Luongo, Giuseppe, eds., Active lavas; monitoring and modeling: London, UCL Press, p. 263–280.

Kilburn, C.R.J., 2000, Lava flows and flow fields, *in* Sigurdsson, Haraldar, Houghton, B.F., McNutt, S.R., Rymer, Hazel, and Stix, John, eds., Encyclopedia of volcanoes: San Diego, Calif., Academic Press, p. 291–305.

Kilburn, C.R.J., and Guest, J.E., 1993, Aa lavas of Mount Etna, Sicily, *in* Kilburn, C.R.J., and Luongo, Giuseppe, eds., Active lavas; monitoring and modelling: London, UCL Press, p. 73–106.

Lipman, P.W., and Banks, N.G., 1987, Aa flow dynamics, Mauna Loa, 1984, chap. 57 *of* Decker, R.W., Wright, T.L., and Stauffer, P.H., eds., Volcanism in Hawaii: U.S. Geological Survey Professional Paper 1350, v. 2, p. 1527–1567.

Macdonald, G.A., 1953, Pahoehoe, aa, and block lava: American Journal of Science, v. 251, no. 3, p. 169–191.

Macdonald, G.A., Abbot, A.T., and Peterson, F.L., 1983, Volcanoes in the sea (2d ed.): Honolulu, University of Hawaii Press, 517 p.

Moore, H.J., 1987, Preliminary estimates of the rheological properties of 1984 Mauna Loa lava, chap. 58 *of* Decker, R.W., Wright, T.L., and Stauffer, P.H., eds., Volcanism in Hawaii:

U.S. Geological Survey Professional Paper 1350, v. 2, p. 1569–1588.

Neal, C.A., Duggan, T.J., Wolfe, E.W., and Brandt, E.L., 1988, Lava samples, temperatures, and compositions, chap. 2 *of* Wolfe, E.W., ed., The Puu Oo eruption of Kilauea Volcano, Hawaii; episodes 1 through 20, January 3, 1983, through June 8, 1984: U.S. Geological Survey Professional Paper 1463, p. 99–126.

Peterson, D.W., and Swanson, D.A., 1974, Observed formation of lava tubes during 1970–71 at Kilauea Volcano, Hawaii: Studies in Speleology, v. 2, no. 6, p. 209–223.

Peterson, D.W., and Tilling, R.T., 1980, Transition of basaltic lava from pahoehoe to aa, Kilauea volcano, Hawaii; field observations and key factors, *in* McBirney, A.R., ed., Gordon A. Macdonald memorial volume: Journal of Volcanology and Geothermal Research, v. 7, no. 3–4, p. 271–293.

Pinkerton, Harry, and Norton, Gill, 1995, Rheological properties of basaltic lavas at sub-liquidus temperatures; laboratory and field measurements on lavas from Mount Etna: Journal of Volcanology and Geothermal Research, v. 68, no. 4, p. 307–323.

Pinkerton, Harry, and Sparks, R.S.J., 1978, Field measurements of the rheology of flowing lava: Nature, v. 276, no. 5686, p 383–385.

Polacci, Margherita, Cashman, K.V., and Kauahikaua, J.P., 1999, Textural characterization of the pāhoehoe-ʻaʻā transition in Hawaiian basalt: Bulletin of Volcanology, v. 60, no. 8, p. 595–609.

Rowland, S.K., and Walker, G.P.L., 1987, Toothpaste lava; characteristics and origin of a lava structural type transitional between pahoehoe and aa: Bulletin of Volcanology, v. 49, no. 4, p. 631–641.

Rowland, S.K., and Walker, G.P.L., 1990, Pahoehoe and aa in Hawaii; volumetric flow rate controls the lava structure: Bulletin of Volcanology, v. 52, no. 8, p. 615–628.

Shaw, H.R., 1969, Rheology of basalt in the melting range: Journal of Petrology, v. 10, no. 3, p. 510–535.

Shaw, H.R., Wright, T.L., Peck, D.L., and Okamura, R.T., 1968, The viscosity of basaltic magma; an analysis of field measurements in Makaopuhi lava lake, Hawaii: American Journal of Science, v. 266, no. 4, p. 225–264.

Wolfe, E.W., Neal, C.A., Banks, N.G., and Duggan, T.J., 1988, Geologic observations and chronology of eruptive events, chap. 1 *of* Wolfe, E.W., ed., The Puu Oo eruption of Kilauea Volcano, Hawaii; episodes 1 through 20, January 3, 1983, through June 8, 1984: U.S. Geological Survey Professional Paper 1463, p. 1–97.

Thermal Efficiency of Lava Tubes in the Pu‘u ‘Ō‘ō-Kūpaianaha Eruption

By Rosalind Tuthill Helz, Christina Heliker, Ken Hon, *and* Margaret Mangan

Abstract

We have applied glass geothermometry to a suite of 37 pairs of glassy lava samples collected on Kīlauea's east rift zone, from the upper and lower ends of the episode 48 lava-tube system, when the Kūpaianaha pond was active (1986–90). We also present data on a small suite of skylight samples collected from 1986 through the end of episode 48 (in 1991), plus some data on skylight-coast sample pairs from episodes 51 and 53. The results for the pond-coast pairs are as follows:

(1) From November 1986 through January 1988 (15 months), the average change in inferred quenching temperature from pond to coast (for 12 sample pairs) is 12.4°C, and the average increase in crystal content (inferred from the observed enrichment of TiO_2 and K_2O in glasses in coastal samples) is 11 to 12 weight percent.
(2) From February 1988 through November 1989 (23 months), the average change in inferred quenching temperature from pond to coast (for 25 sample pairs) is 8.4°C, and the average increase in crystal content is 4 to 5 weight percent. Within this part of the data set, pond and coastal temperatures rise and fall together much of the time, even though these temporal fluctuations are at or below the limit of resolution of glass geothermometry $\Delta T \leq 3$°C).
(3) The minimum temperature difference for any pond-coast pair is 7°C. Of 37 sample pairs, 24 have ΔT=7–9°C, over the entire 3-year period.

In about half of the skylight samples, the enclosed glasses have MgO contents consistent with the location at which the samples were collected along the lava-tube system. Glasses in the rest of the skylight samples are displaced to lower MgO contents; such samples may not be consistently as well quenched as the pond and littoral spatter samples. The data from episodes 51 and 53 are from a new tube system that was somewhat shorter than the episode 48 (Kūpaianaha) lava tubes. The best-documented temperature difference observed for this 10-km long lava tube (6°C) gives exactly the same rate of temperature decrease with distance (0.6°/km) as the limiting ΔT value of 7°C observed for the 12-km-long Kūpaianaha lava-tube systems. This cooling rate may represent the limiting thermal efficiency of tubes of the current eruption.

Introduction

Observations of the ongoing long-term eruption of Kīlauea Volcano on the Island of Hawai‘i have enhanced our understanding of many eruptive processes at Kīlauea, in particular, how lava tubes form and function. Lava tubes are common in pāhoehoe flows at both Kīlauea and Mauna Loa (Greeley, 1987), where their formation is favored by low to moderate effusion rates (Rowland and Walker, 1990). In the current eruption, lava tubes have been the dominant means of lava transport from July 1986 to the present.

Glass geothermometry (Helz and Thornber, 1987), which derives quenching temperatures of samples from the MgO content of their glasses, has permitted tracking the thermal history of this long-term eruption in detail. Glass analyses and estimated quenching temperatures are well documented for the period 1983–94 (Helz and others, 1991; Helz and Hearn, 1998); the same technique has also been applied to episodes 49 (Mangan and others, 1995), 50 to 53 (Heliker and others, 1998) and 53 to 55 (Thornber, 2001). In this chapter, we focus on a subset of the data that documents the thermal efficiency of lava tubes from 1986 to 1990, the period when the active lava pond at Kūpaianaha was accessible for sampling.

Background

The early stages of the current Kīlauea eruption were characterized by episodic high lava fountains at the Pu‘u ‘Ō‘ō vent, which fed rapidly moving ‘a‘ā flows. After July 1986, this eruptive style gave way to more continuous effusive activity at a new vent 3 km downrift from Pu‘u ‘Ō‘ō. From July 1986 to mid-1990, lava surfaced at this site, where it formed a large open pond of circulating lava, named the Kūpaianaha vent. The active lava pond gradually crusted over, roofing over completely in late 1990. Eruptive activity continued, however, with lava moving through the site of the former Kūpaianaha pond to the coast by way of well-established lava-tube systems (Heliker and Wright, 1991; see Heliker and Mattox, this volume). The resulting lava aprons of tube-fed pāhoehoe and the mechanism of their emplacement were described in some detail by Mattox and others (1993) and Hon and others (1994).

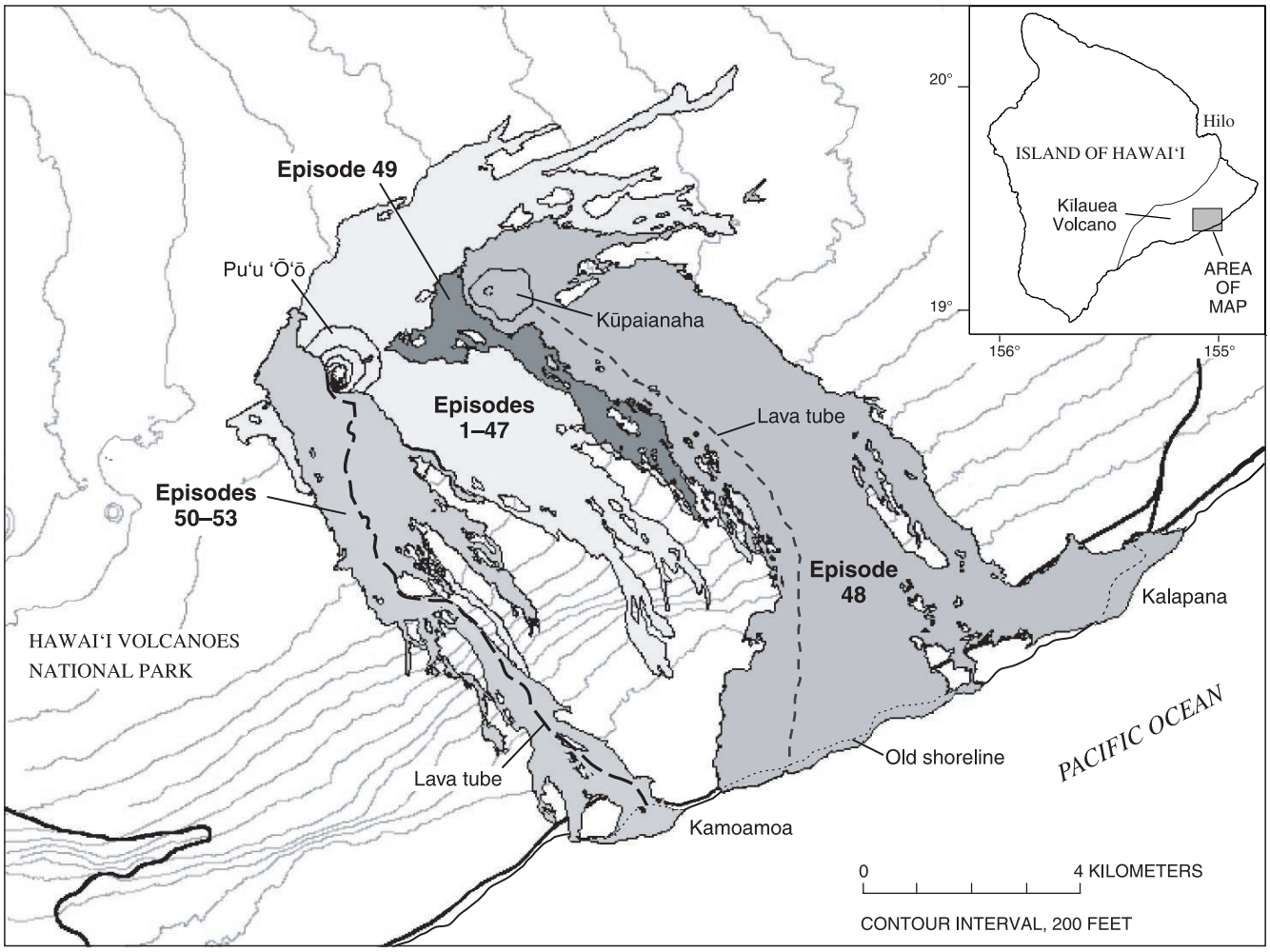

Figure 1. Kīlauea Volcano, Island of Hawai‘i, showing east rift zone through early stages of episode 53 (April 1993). Light dashed line, one of several lava-tube paths of Kūpaianaha period; heavy dashed line, episode 53 lava-tube system.

The Kūpaianaha vent, the extent of the episode 48 lava fields, and the episode 49–53 lava flows are shown in figure 1. Sample lava-tube paths are shown for episodes 48 and 53; these paths are not unique but indicate typical paths of the tube systems studied by Cashman and others (1994) and those discussed here. Scientists at the U.S. Geological Survey's Hawaiian Volcano Observatory (HVO) have measured these lava-tube systems to be 10 to 12 km long (Mattox and others, 1993; Cashman and others, 1994; Kauahikaua and others, 1998; also HVO, unpub. data).

Sample Characteristics

When the Kūpaianaha lava pond was open, and active tube systems delivered lava to the coast, HVO scientists made a special effort to collect paired samples of spatter from both the pond (at the upper end of the lava-tube system) and the coast, preferably of ocean-quenched littoral spatter. We report data on the existing set of 37 such sample pairs. The pairs were usually collected within a day of each other, although some pairs were collected 2 to 5 days apart (see table 1). We also report data for a few samples from the episode 48 suite that were collected through skylights in active lava tubes during the period when the Kūpaianaha lava pond was open (table 2) or after the pond closed up (table 3).

Pond Samples

The pond samples include spatter samples, one sample of pond overflow (KER48-668F) and samples of pond dip. The spatter and overflow samples date from November 1986 through March 1988, when the level of lava in Kūpaianaha was high, and circulation of the lava caused frequent episodes of spattering along the rim. When collected in real time, or when the spatter fell on a relatively cool surface, these samples underwent a rapid quench, making them suitable for geothermometry. All of the pond samples collected from April 1988 through May 1990 (after which the lava pond crusted over completely) are so-called dip samples; that is, they consist of glass that adhered to a rod or hammer thrown into the molten lava, or lowered from a helicopter into the lava. This

sampling method provides a very good quench, so long as the probe is retrieved from the molten lava quickly.

Coast (Littoral) Samples

The early (Nov. 1986–Jan. 1988) coastal samples include those collected where lava flows entered the ocean, plus some material from lava-tube breakouts near the coast. The quality of the quench for individual breakout samples depends on how quickly the sample was collected and whether the collector used water to quench it, or relied on air cooling. After January 1988, all coastal samples in the suite are of spatter from littoral cones or from lava tubes at the shoreline and were well quenched by interaction with seawater. Because the quenching history of the samples depends on where and how they were collected, such details are given in table 1 for all littoral samples.

Skylight Samples

Skylight samples were rarely taken when the Kūpaianaha lava pond was open; the two samples we have (KER48-852F and KER48-875F) were both collected on the same day as their associated pond samples (table 2). In addition, six skylight samples were collected in 1990 during the waning stages of the pond's life (table 2). Finally, we have analyzed several sets of skylight-littoral samples collected after the pond had completely crusted over (table 3). All the skylight samples were collected on a hammer lowered into the lava stream. The surfaces of the walls and roofs within lava tubes are known to be at basalt solidus temperatures (~985–1,000°C; Helz and Thornber, 1987) or higher. Kauahikaua and others (1998) reported a temperature of 1,080°C for the walls of a lava tube. Even the air temperatures over skylights are typically 800°C or higher (Peterson and others, 1994), so these samples may have undergone a different pattern of quenching from most other samples, with rapid cooling not occurring until after the hammer had cleared the skylight.

Petrography of Samples Used in This Study

All of our lava samples consist largely of clear brown glass, with minor amounts of crystals and vesicles. The photomicrographs in figure 2 show two pond-coast pairs that are representative of the whole population. In the first pair, pond sample 961P contains minor amounts of olivine (+ chromite, generally included in olivine), plus tiny crystals of augite. The coastal sample is somewhat more crystalline and contains trace amounts of plagioclase, as well as olivine + augite. In the second pair, both pond and coastal samples contain olivine + augite + plagioclase; again, the coastal sample is more crystalline than the pond sample. Sample 1076S (table 1) is

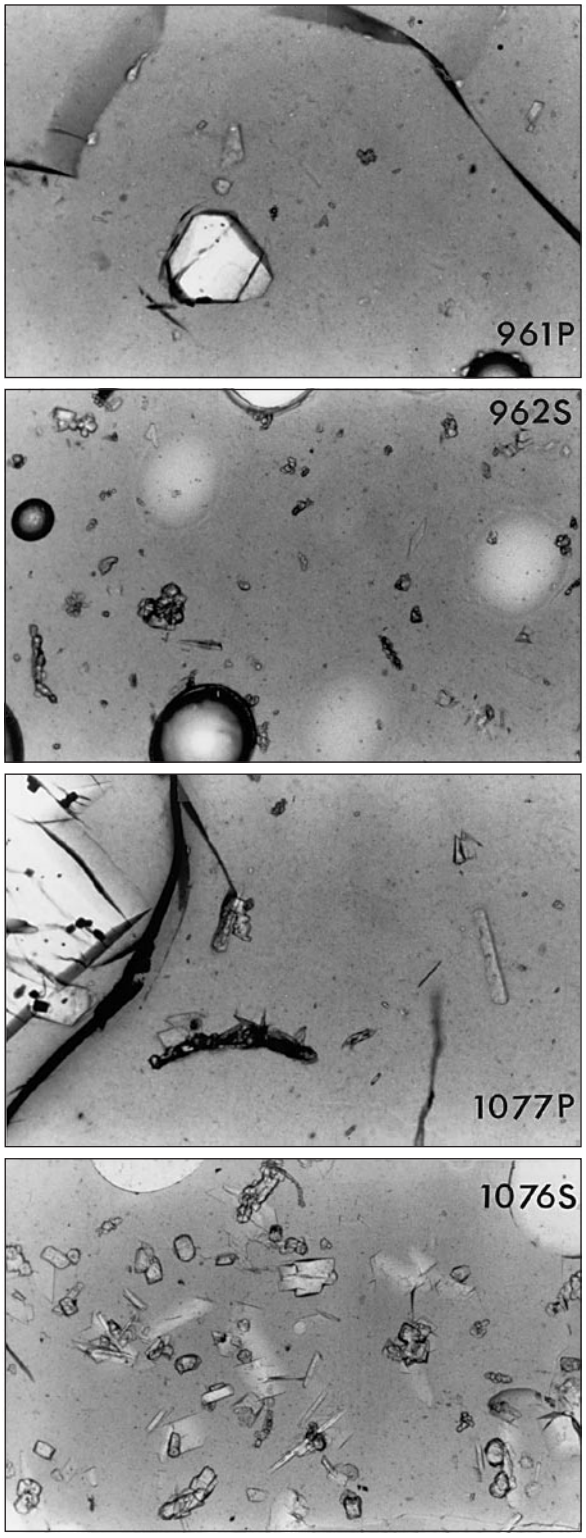

Figure 2. Photomicrographs (plane polarized light) of two pond-coast sample pairs of spatter from Kūpaianaha. Sample pair *A* and *B*; (samples 961P and 962S, table 1) were erupted in September 1988, and *C* and *D* (samples 1077P and 1076S, table 1) in May 1989. Field of view is 1.7 mm across for all images. Crystals present include olivine (+ chromite as inclusions), augite, and plagioclase; rest of area is glass and vesicles. Crystal content of coastal samples is higher and more variable than that of pond samples.

Table 1. Details on paired samples of spatter collected from the Kūpaianaha lava pond and the coast.

Pond sample	Date collected	T_{MgO} °C	Littoral sample	Date collected	T_{MgO} °C	Time difference	ΔT_{MgO} °C	Location of littoral sample	Bulk analysis for samples?
663S	11/25/86	1,148	666F	11/29/86	1,139	4 days	9	Beach	yes for both
668F	12/05/86	1,156	674F	12/04/86	1,143	1 day	14	Under water	"
730S	04/17/87	1,156	739F	04/15/87	1,143	2 days,	13	Tidepool	"
747S	05/12/87	1,156	746F	05/12/87	1,147	same day	9	2-m elevation	"
749S	05/19/87	1,157	748F	05/19/87	1,148	same day	9	350 m from ocean	"
764S	06/17/87	1,155	759F	06/14/87	1,144	3 days	11	3-m elevation	not for 759F
774P	07/07/87	1,157	776F	07/02/87	1,143	5 days	14	9-m elevation	yes for both
790S	09/09/87	1,153	791F	09/10/87	1,140	1 day	13	150 m from ocean	"
822S	11/03/87	1,154	817F	11/04/87	1,139	1 day	15	50 m from ocean	"
853P	12/17/87	1,152	860F	12/17/87	1,135	same day	17	6-m elevation	"
868P	01/14/88	1,153	867F	01/13/88	1,137	1 day	16	20–30 m from ocean	"
874S	01/26/88	1,153	873F	01/25/88	1,146	1 day	7	9-m elevation	"
889S	02/08/88	1,151	891S	02/11/88	1,142	3 days	11	Littoral cone	"
894S	02/15/88	1,152	891S	02/11/88	1,142	5 days	10	Same sample	"
898S	02/25/88	1,157	897S	02/24/88	1,149	1 day	8	0-m elevation	"
902S	03/10/88	1,154	901S	03/11/88	1,147	1 day	7	0-m elevation	"
903S	03/15/88	1,154	904S	03/18/88	1,148	3 days	7	0-m elevation	"
905S	03/24/88	1,156	906S	03/26/88	1,147	2 days	8	0-m elevation	"
911P	04/21/88	1,157	912S	04/22/88	1,147	1 day	9	0-m elevation	"
937P	06/23/88	1,156	935S	06/22/88	1,147	1 day	9	0-m elevation	"
939P	07/07/88	1,156	940S	07/08/88	1,147	1 day	9	0-m elevation	not for 940S
948P	07/22/88	1,156	943S	07/18/88	1,148	4 days	8	0-m elevation	yes for both
956P	08/24/88	1,156	957S	08/28/88	1,149	4 days	7	0-m elevation	"
961P	09/20/88	1,157	962S	09/23/88	1,149	3 days	8	0-m elevation	"
983P	10/06/88	1,157	982S	10/03/88	1,149	3 days	8	0-m elevation	"
990P	11/17/88	1,155	991S	11/19/88	1,146	2 days	9	0-m elevation	"
1000P	01/04/89	1,156	1001S	01/05/89	1,149	1 day	7	0-m elevation	"
1003P	01/19/89	1,157	1004S	01/20/89	1,149	1 day	8	0-m elevation	not for 1004S
1016P	02/17/89	1,157	1014S	02/17/89	1,146	same day	9	0-m elevation	yes for both
1027P	03/09/89	1,158	1026S	03/07/89	1,148	2 days	10	0-m elevation	not for 1026S
1033P	04/06/89	1,156	1034S	04/07/89	1,149	1 day	7	0-m elevation	not for 1034S
1072P	05/05/89	1,157	1073S	05/06/89	1,149	1 day	8	0-m elevation	yes for both
1074P	05/11/89	1,156	1075S	05/11/89	1,148	same day	8	0-m elevation	for neither
1077P	05/19/89	1,155	1076S	05/19/89	1,144	same day	11	0-m elevation	not for 1076S
1078P	05/24/89	1,156	1079F	05/25/89	1,148	1 day	8	Floating pillow	not for 1079S
1087P	08/10/89	1,155	1090S	08/12/89	1,148	2 days	7	0-m elevation	not for 1090S
1107P	11/14/89	1,157	1106S	11/12/89	1,150	2 days	7	0-m elevation	yes for both

one of the coolest late littoral samples in this suite and so is more crystalline than most. The crystal contents of all samples are too low to be readily determined by point-counting the area of one thin section, and so we made no attempt to obtain modes by this method. The principal variations in the entire suite are as follows: (1) some pond samples have been quenched from above plagioclase-in, whereas all the coastal and skylight samples contain three silicate phases (documented in Helz and Hearn, 1998), and (2) all the coastal and skylight samples contain more crystals than their corresponding pond samples.

Glass Analyses and Geothermometry

All the glass analytical data discussed here were obtained at the U.S. Geological Survey laboratory in Reston, Va., using the ARL-SEMQ and JEOL electron microprobes. The actual analyses, further details on analytical techniques, and estimates of glass quenching temperatures were reported by Helz and Hearn (1998). Critical information on pond-coast sample pairs and skylight samples, extracted

from their report and from HVO archives, is summarized in tables 1 through 3.

Glass geothermometry, as developed by Helz and Thornber (1987), depends on the observation that the MgO content of glass varies linearly with temperature for Kīlauea melts in equilibrium with olivine. Thus, the absence of any sign of reaction between olivine and glass in these samples (fig. 2) is important. The reproducibility of the MgO contents of naturally quenched glasses is also critical, because the precision of the MgO analysis determines the limit of resolution of temperature of glass (T_{MgO}) geothermometry. Helz and others (1995, fig. 3) show that the difference between initial and replicate MgO analyses in a large suite of glasses from Kīlauea never exceeds 0.15 weight percent absolute, which corresponds to a 3°C difference in apparent quenching temperature. Thus, within this data set, any temperature difference (ΔT) larger than 3°C is outside the range of analytical noise and may be interpretable.

Results for Pond-Coast Sample Pairs

The MgO contents and quenching temperatures of glasses from all pond-coast sample pairs are plotted against time in figure 3. The most conspicuous feature of this plot is that, without exception, the glasses in the coastal samples have lower MgO contents and, hence, were quenched from lower temperatures than the glasses in the pond samples. This signal is so consistent that it is reasonable to interpret the temperature decrease as due to cooling during transport in the 10 to 12-km-long lava-tube system.

Except for the single earliest pond sample (663S, table 1, containing glass with 6.76 weight percent MgO), all of the pond samples discussed here contain glasses having MgO contents between 6.86–7.19 weight percent. The range in MgO content for all pond glasses (when we include those

Table 2. Data on samples from the episode 48 suite that were collected through skylights in active lava tubes during the period when the Kūpaianaha lava pond was open.

Pond sample	Date collected	T_{MgO} °C	Skylight sample	Date collected	T_{MgO} °C	Elevation (ft)	Littoral sample	Date collected	T_{MgO} °C	Time difference	ΔT_{MgO} (°C)
822S	11/03/87	1,154	--	--	--	--	817F	01/14/87	1,139	1 day	15
845S	11/19/87	1,154	852F	11/19/87	1,147	1,900	--	--	--	same day	7
853P	12/17/87	1,152	--	--	--	--	860F	12/17/87	1,135	same day	17
868S	01/14/88	1,153	--	--	--	--	867F	01/13/88	1,137	1 day	16
874S	01/26/88	1,153	875F	01/26/88	1,145	1,980	--	--	--	same day	8
"	01/26/88	1,153	--	--	--	--	873F	01/25/88	1,146	1 day	7
--	--	--	875F	01/26/88	1,145	1,980	"	01/25/88	1,146	1 day	-1
1129P	02/07/90	1,155	1137F	02/10/90	1,152	1,830	--	--	--	3 days	3
1234P	02/15/90	1,158	1150F	02/15/90	1,147	1,420	--	--	--	same day	12
--	--	--	1202F	03/19/90	1,147	1,650	1220S	03/19/90	1,145	same day	2
--	--	--	1237F	04/08/90	1,154	1,650	--	--	--	--	--
1252P	05/10/90	1,158	--	--	--	--	--	--	--	--	--
1258P	05/31/90	1,156	1257F	05/31/90	1,150	1,850	--	--	--	same day	6
--	--	--	1260F	06/30/90	1,152	1,850	--	--	--	--	--
--	--	--	--	--	--	--	1261S	07/28/90	1,146	--	--

Table 3. Data on samples from the episode 48 suite that were collected through skylights in active lava tubes after the Kūpaianaha lava pond closed up.

Episode	Skylight sample	Date collected	T_{MgO} °C	Elevation (ft)	Littoral sample	Date collected	T_{MgO} °C	Time difference	ΔT_{MgO} °C
48	1305F	02/27/91	1,154	1,845	--	--	--	2 days (1311S)	2
48	1306F	02/27/91	1,155	1,840	--	--	--	2 days (1311S)	3
48	1308F	03/01/91	1,156	2,080	1311S	03/01/92	1,151–1,152	same day	4-5
51	1407F	11/12/92	1,153	2,350	1408S	11/19/92	1,149	5 days	4
53	1430F	04/16/93	1,151	2,010	--	--	--	13 days (1436F)	0
53	1431F	04/16/93	1,156–1,157	2,360	--	--	--	13 days (1436F)	5-6
53	1432F	04/16/93	1155	2,350	--	--	--	13 days (1436F)	4
53	1433F	04/16/93	1151	250	1436F	04/29/93	1,151	13 days	0

without corresponding coastal pairs) is larger (6.76–7.36 weight percent MgO; Helz and Hearn, 1998). The narrow range in MgO content for pond glasses in the suite of paired samples considered here is important because it means that the variable time gaps between collection of samples considered to be pairs, whether a few hours or several days (see table 1), do not contribute significantly to the variation in ΔT values. Figure 3 shows clearly that the bulk of the variation in ΔT results from the variation in MgO content of the glass in the coastal samples. This variation in turn may be due either to (1) variations in the quality of quench undergone by the coastal samples or (2) variation in the efficiency of the lava-tube systems over time.

Can we distinguish between these two possible causes of variation in MgO content of the coastal glasses? A fairly obvious shift in the size of ΔT occurs over time. The ΔT values for the 12 sample pairs collected from November 1986 through January 1988 average 12.3°C, whereas the ΔT values for all subsequent sample pairs average 8.4°C. In many of the first 12 pairs, the littoral sample was collected not at the beach but slightly inland and so may not have been as well quenched as the later samples, all of which were collected at the shore. However, the three earliest littoral samples, which were water-quenched, still have ΔT=9, 13 and 14°C. Many of the other samples were dipped into a can of water after collection on the point of a hammer, and so the larger ΔT in these early sample pairs cannot be dismissed solely as the result of inadequately rapid quenching. Finally, if we consider relative collection times, we see that some of the largest ΔT values are for sample pairs collected on the same day or adjacent days (table 1), and so these samples are not simply mismatched.

We cannot discard any of the early pairs as having unequivocal quenching problems, nor can we define a "best" subset of sample pairs with only small ΔT values. Therefore we regard the variation in ΔT values over time as meaningful, with the data showing that the lava-tube system became more consistent in its behavior and more thermally efficient after January 1988. This conclusion is consistent with field observations that the lava apron fed from Kūpaianaha was thin when it first reached the ocean, but thickened steadily thereafter (see Hon and others, 1994).

Variations in the Later Sample Pairs

The 25 sample pairs collected from February 1988 through November 1989 vary much less in ΔT than the earlier sample pairs. During this period, all littoral samples were retrieved from the surf zone and so were uniformly well quenched. Furthermore, although the pond surface became increasingly hard to reach, cable samples recovered from the rim continued to provide well-quenched material from the upper end of what was a mature tube system in a large lava field.

Within this remarkably uniform part of the data set, two features stand out: the first striking feature is that MgO contents of glass (and quenching temperatures) of the sample

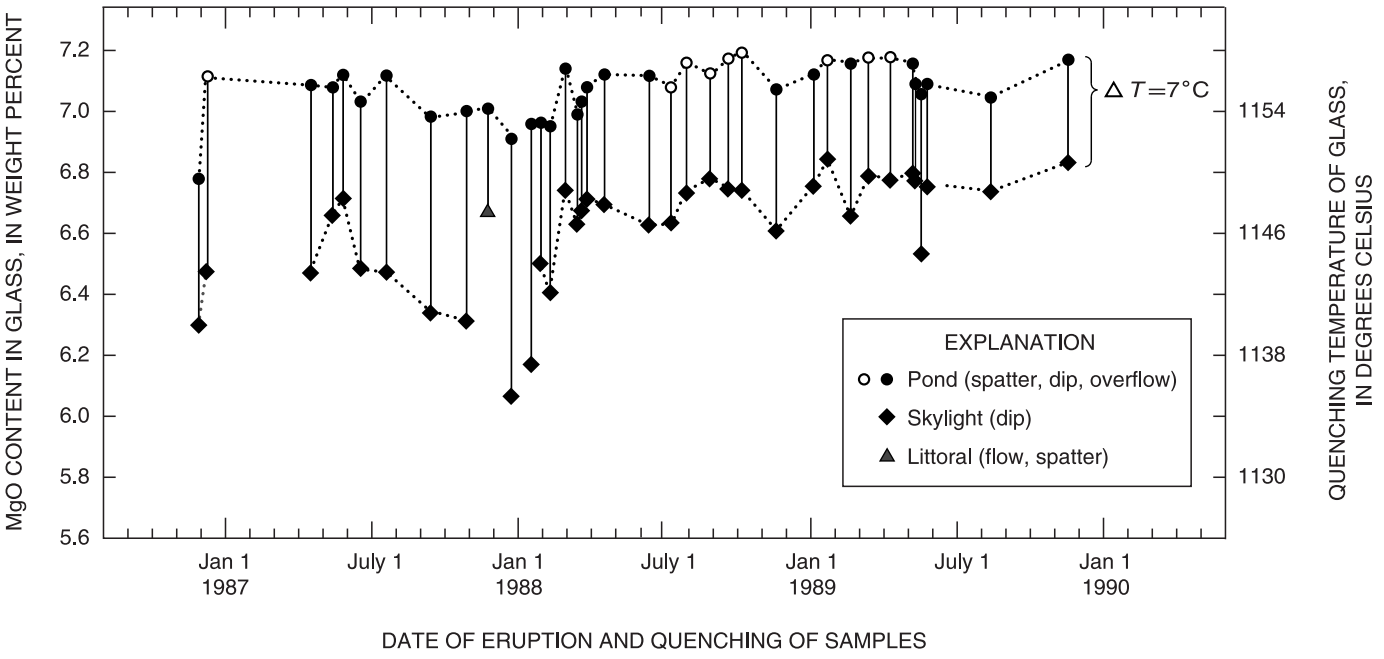

Figure 3. MgO content of glass and inferred quenching temperature versus time for pond-coast sample pairs from Pu‘u ‘Ō‘ō-Kūpaianaha eruption. Small divisions on time scale designate months. Open circles, samples with crystalline assemblage olivine + augite. All filled symbols, samples with three-phase assemblage olivine + augite + plagioclase.

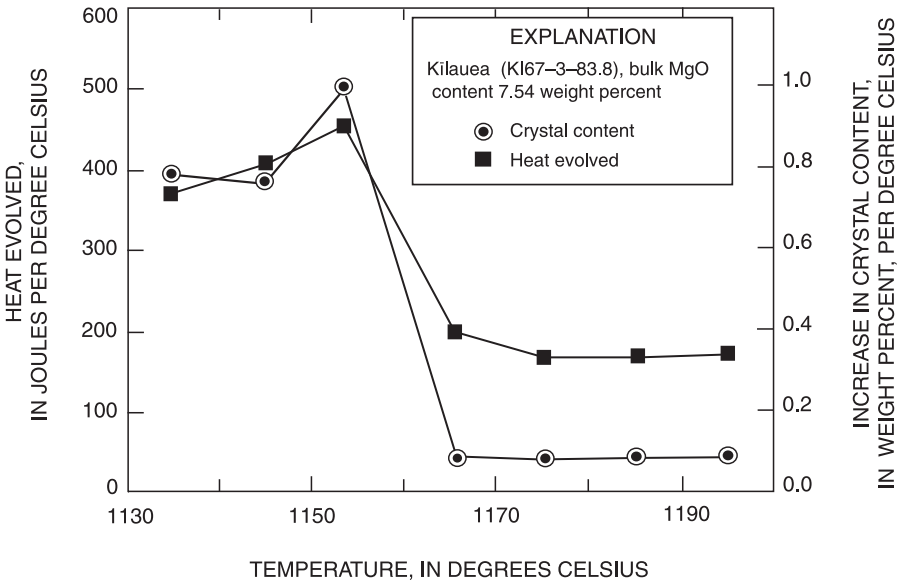

Figure 4. Heat evolved (= decrease in enthalpy) and increase in crystal content that occurs during equilibrium crystallization of a Kīlauea basalt as temperature decreases from 1,195 to 1,125°C, calculated using thermodynamic modeling procedure of Ghiorso (1985).

pairs seem to rise and fall together, with a near-constant ΔT= 7–9°C. This tight coupling of pond and coastal temperatures implies that the time needed for lava to flow from the pond to the coast is short, relative to (1) the gap in collection time between the samples in each pair and (2) the time needed to recharge the lava pond and tube system, either during continuous activity or after a pause in effusive activity, with lava of a slightly different temperature.

The net length of the lava-tube systems fed from Kūpaianaha was 12 km (not considering smaller-scale sinuosities), according to many observers (see Mattox and others, 1993), and the flow rate of lava in the tubes was determined (Kauahikaua and others, 1998) to be 1 to 3 m/s, where lava was visible through skylights. Thus, a particular parcel of lava could have taken as little as a few hours, mostly less than a day, to traverse the lava-tube system and emerge at the shore during periods of steady-state flow.

In contrast, the time scale for obvious fluctuations in magma supply ranged from many hours to a week, as did the collection time between samples (see table 1). Specifically, the April 1988 pause, the only pause within the time frame of figure 3, took place over a week (Heliker and Wright, 1991; see Heliker and Mattox, this volume). The tight correlation in MgO content between glasses in pond and coastal samples is consistent with rapid lava transport, in which the lava-tube system was flushed quickly and was always occupied by only one "batch" of lava, however defined.

The second striking feature of the 1988–89 data set is the well-defined minimum ΔT value of 7°C, observed in 7 (of 25) sample pairs, and corresponding to a temperature decrease of 0.6°C/km over the 12-km tube system. No sample pairs have a smaller ΔT value. We suggest that this limiting ΔT value represents the maximum thermal efficiency for lava transport from pond to coast, given the constancy of all other boundary conditions (slope, magma-supply rate, and physical properties of the lava).

Crystallization Behavior of Kīlauea Basalts

Model Crystallization Behavior

To evaluate more fully the significance of these temperature decreases, in terms of the processes that occur during lava transport in tubes, we need to consider how basaltic lavas crystallize. Specifically, we need to know what phases crystallize, at what temperature, and how much heat must be released as temperature decreases. The amount of heat evolved (the decrease in enthalpy) and the increase in crystal content that will occur, during equilibrium cooling and crystallization of a sample of Kīlauea basalt, are plotted in figure 4. The calculation procedure used is the thermodynamic model of Ghiorso (1985). The conditions of this calculation were equilibrium crystallization, at fo_2 equal to the quartz-fayalite-magnetite (QFM) buffer. The temperature decrement used was 10°, from 1,200 to 1,080°C. This temperature interval was chosen to facilitate comparison with the results of melting experiments, where the interval between runs is typically 10°C. The model calculates olivine and plagioclase compositions fairly closely but does not allow for any components in pyroxene other than the four end members (Di, En, Hd, Fs); thus, the calculated augite contains no Al_2O_3, Cr_2O_3, TiO_2 or Na_2O. Therefore, the calculated results only approximate the observed behavior of natural samples.

The results presented here are for a sample from Kīlauea Iki lava lake, with a bulk MgO content of 7.54 weight percent; calculations using various Kīlauea and Mauna Loa basalts show patterns very similar to those shown in figure 4. The phase relations of this basalt composition were determined experimentally (Helz and Thornber, 1987) and are typical of those of many other Kīlauea basalts that have

been studied experimentally (see Thompson and Tilley, 1969). Olivine ± chromite crystallizes first, at 1,169°C in this bulk composition, followed by augite at 1,165±5°C, and plagioclase at 1,155±5°C (roughly 10°C lower than augite). The calculations, which show olivine crystallizing first, with augite and plagioclase coming in between 1,170° and 1,160°C, do not resolve the difference between augite-in (the temperature at which augite first crystallizes) and plagioclase-in, but otherwise adequately reproduce the actual phase relations. This crystallization sequence is virtually identical to that observed in lava samples from the Pu‘u ‘Ō‘ō-Kūpaianaha eruption (Helz and others, 1991; Helz and Hearn, 1998), where augite-in is at 7.34 weight percent MgO (T=1,162°C) and plagioclase-in is at 7.00 to 7.12 weight percent MgO (T=1,155–1,157°C). Therefore, the data in figure 4 should be applicable to the sample suite considered here.

Figure 4 shows that, in Kīlauea lava compositions, the increase in crystal content and amount of heat released (the decrease in enthalpy, or -ΔH) have two distinct stages. There is a higher-temperature stage where olivine alone is crystallizing; here the enthalpy change is -176 J/°C per 100 g of basalt, and 0.1 weight percent of the melt crystallizes per degree. In the second stage, olivine + augite + plagioclase crystallize together. Along this three-phase cotectic, the change in enthalpy is -418 J/°C per 100 g of basalt, and 0.8 weight percent of the melt crystallizes per degree, or eight times as much as in the first stage.

The narrow (5–10°C) temperature interval within which the crystallizing assemblage is olivine + augite is not captured in the model calculations. In our discussion below, we assume that stage 2 is reached only when plagioclase begins to crystallize. Our lumping of olivine + augite with stage 1 is based on the observation that the amount of augite present in Pu‘u ‘Ō‘ō-Kūpaianaha samples at plagioclase-in is very low (see fig. 2*A*), and hence that the amount of heat released by its crystallization is small.

Virtually all samples in our suite have the assemblage olivine + augite + plagioclase and hence must crystallize and evolve heat at the rates specified for stage two above. Thus, for the range of temperature decreases commonly observed, the model predicts the following changes in enthalpy and crystal content:

for ΔT = -7°C	ΔH= -2930 J	5.6% more crystals in coastal samples
for ΔT = -9°C	ΔH= -3760 J	7.2% more crystals in coastal samples
for ΔT = -11°C	ΔH= -4600 J	8.8% more crystals in coastal samples

Translating these values to changes per kilometer, for 100 grams of basalt in a 12-km tube system, we obtain the following:

for ΔT = -7°C	0.6°/km cooling	ΔH= -240 J/km	0.47% crystals/km
for ΔT = -9°C	0.75°/km cooling	ΔH= -310 J/km	0.60% crystals/km
for ΔT = -11°C	0.9°/km cooling	ΔH= -380 J/km	0.73% crystals/km

These values show the range of increases in crystal content and decrease in enthalpy of the basalt that the thermodynamic equilibrium-crystallization model would predict for most pairs in this sample suite.

Observations on Crystallization and Differentiation of Samples

We cannot directly observe the heat lost during transport of lava in the 1986–89 tube systems, years after the fact. We can, however, evaluate whether the crystal content of the samples varies as expected. Two processes are potentially involved: (1) within-tube crystallization of the glass and (2) bulk differentiation of the lava. In the first process, some of the melt will have crystallized to produce additional olivine + augite + plagioclase. The new crystals will be tiny, having grown during the few hours of transport time in the lava tube, so they are unlikely to separate during flow. The second process would occur if some of the larger crystals present in the pond samples were lost during flow, or picked up by erosion of the walls and floor of the lava tube. The crystals most likely to be affected are the olivine phenocrysts and microphenocrysts (fig. 2).

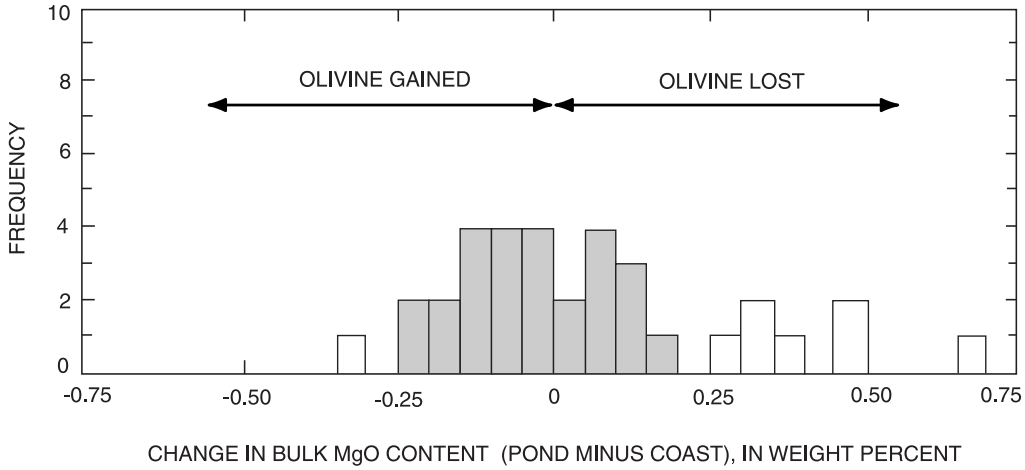

Figure 5. Histogram showing change in bulk MgO content for 35 pond-coast sample pairs, for which whole-rock analyses are available. Most sample pairs (shaded) show less than 0.25 weight per cent change in MgO content during transport in lava tube between pond and coast.

Table 4. Changes in crystal content for pond-coast pairs from the Kūpaianaha tube system, estimated from thermodynamic calculations and from changes in glass composition.

	Early pairs	Later pairs
Number of pairs	12	25
Average ΔT value and range, in degrees Celsius	12.25 (7–17)	8.4 (7–11)
Theoretical increase in crystal content and range, in weight percent	9.8 (5.6–13.6)	6.7 (5.6–8.8)
Average ΔTiO_2 and range, in weight percent	11.3 (5–20)	4.8 (1–9)
Average ΔK_2O and range, in weight percent	12.3 (4–27)	4.1 (0–11)
Average ΔP_2O_5 and range, in weight percent	13.5 (4–23)	8.2 (0–24)

Let us first consider whether bulk composition has been affected by either gain or loss of crystals between the flowing lava and the floor or walls of the lava tube. The difference in bulk MgO content between pond and coastal samples is shown in figure 5, for all pairs for which bulk analyses exist (as noted in table 1). We chose to plot MgO because it has the largest range in Kīlauea lavas (Wright, 1971) and because it will most strongly show the effects of any olivine fractionation in these samples.

In figure 5, the shift in bulk MgO for most of the 34 analysis pairs falls within $\pm$0.25 weight percent MgO (corresponding to $\pm$0.6 weight percent olivine), and the distribution of these samples is random around zero. We suggest that this part of the variation is dominated by sampling noise, presumably reflecting heterogeneity in bulk lava composition, perhaps with slight mismatches caused by varying time gaps in sampling. Seven analysis pairs have larger ΔMgO shifts, consistent with loss of 0.7–1.3 weight percent olivine, but this process is not pervasive. Changes in other aspects of bulk composition are small, so we conclude that lava bulk composition does not change significantly because of flow through the tubes.

The most straightforward way to estimate how much glass crystallizes during transport in the lava-tube system is to calculate the increase in the less-compatible oxides in glasses from coastal samples relative to glasses from pond samples. The most suitable oxides, based on looking at the microprobe analyses (Helz and Hearn, 1998), are TiO_2, K_2O and P_2O_5. Because the absolute values of some of these oxides are low, and the differences between analyses in the sample pairs are small, the differentials (such as ΔK_2O) from one pair of analyses to the next can be quite variable. Therefore, in table 4, we have shown averages for the differences in oxide concentration for the 12 early pairs and for the 25 later pairs, with the ranges of values for individual pairs indicated in parentheses. The increases in crystal content predicted by thermodynamic modeling, for the average ΔT of the early and later sample pairs, are included in table 4 for comparison. These results show that TiO_2, K_2O and P_2O_5 contents of glasses in coastal samples are consistently higher than those of the pond samples; therefore, the coastal samples have crystallized during transport by approximately the percentages shown. Glasses in the early coastal samples (with larger average ΔT) have crystallized more extensively than glasses in the later coastal samples. Finally, for both data sets, the estimated increases based on ΔTiO_2 and ΔK_2O are broadly consistent with theoretical predictions. The observed increase in P_2O_5 is larger than the theoretical prediction, but this difference (especially for the later pairs) is probably insignificant because the absolute P_2O_5 contents of these glasses are low (0.21 to 0.29 weight percent), and ΔP_2O_5 is very small and may be dominated by analytical noise.

Petrographic examination of the samples (fig. 2) suggests that the estimated 5 to 12 percent increases in microlite contents are reasonable. These results, together with earlier observations that bulk lava composition does not vary significantly during transport, lead us to conclude that (1) the melt in these lava tubes follows the equilibrium crystallization path quite closely and (2) the theoretical model (SILMIN) adequately models the actual (near-equilibrium) crystallization processes in the episode 48 lava tubes.

Heat Versus Temperature

The crystallization model of Ghiorso (1985) gives an approximate rate at which heat must be evolved during equilibrium crystallization of these basaltic liquids. Various studies of the actual cooling behavior of basalts (Keszthelyi, 1994, 1995a, b) have shown that heat loss is not uniquely related to temperature changes. For example, Keszthelyi (1995a) was able to detect increases in temperature following sudden bursts of nucleation of crystals. Such complications, though they do not occur under near-equilibrium conditions, nevertheless show directly that evaluating the thermal efficiency of lava tubes may involve more than simply monitoring changes in glass composition and inferred temperature.

We can illustrate one complication with some simple calculations. We assume a 12-km-long lava tube, with a total heat loss of 2,930 J (equivalent to ΔT= -7°C along the three-phase cotectic). However, for this calculation we assume that the input at the upper ("pond") end of the tube has a melt like the most magnesian glasses of the current Kīlauea east rift zone eruption, namely glasses from episode 30 at Pu‘u ‘Ō‘ō, with MgO contents of 7.90 to 7.99 weight percent and quenching temperatures of 1,174–1,175°C. We use the actual phase relations of the lava (plagioclase-in at 1,155°C for Pu‘u ‘Ō‘ō; Helz and others, 1991) to determine when the lava shifts from stage 1 (olivine-only) parameters to stage 2 (multiphase crystallization) parameters, as given above.

Because this hypothetical lava starts in stage 1, we begin our calculation with the change in heat content (ΔH) of -176 J/°C (versus -418 J/°C for stage 2). To lose 2,930 J of heat per 100 g of lava, the temperature must decrease by 16.6°C. Thus, the temperature at the coast for our hypothetical lava would be 1,158°C, still 3° above plagioclase-in. The lava will have been in stage 1 for the entire 12-km trip and will have undergone a total temperature decrease 2.4 times as great as a three-phase lava would, *at the identical thermal efficiency of the lava-tube system*.

If we assume a total heat loss of 3,760 J (corresponding to ΔT= -9°C under stage 2 conditions), we find that the entire range of 20°C at stage 1 does not quite consume all of the heat that must be dissipated. The remaining 242 J requires a further stage 2 temperature decrease of 0.6°C, for a total temperature decrease in the lava tube of 21°C. The change from one-phase to three-phase crystallization occurs 11.2 km down the lava tube, so the hypothetical lava will have been crystallizing only olivine for almost the entire distance, and the temperature change is more than twice what we observe in the actual samples. In evaluating the significance of rates of temperature decrease in tubes (here or as in Thornber, 2001), clearly the nature of the crystallizing assemblage is an important variable that must always be verified by inspection of the samples.

Results for Skylight Samples

Results comparing skylight samples to corresponding pond and/or coastal samples are summarized in figures 6 and 7, which plot the elevation at which the samples were collected against MgO content of glass. Figure 6 shows the early skylight samples (from Nov. 1987 to Jan. 1988), plus a larger set of skylight samples taken at the very end of the Kūpaianaha lava pond activity (see table 2). The shaded area in each set of data shows the range of slopes (ΔMgO, which is effectively ΔT) versus elevation generated by the range of MgO contents of glass in the pond and coastal samples. Other lines connect individual samples collected closest to each other in time. The most obvious feature in figure 6 is that some of the skylight samples do not fall on straight lines between the population of pond and coastal samples. The MgO contents of half the skylight glasses are low by 0.20 to 0.45 weight percent absolute, at the elevation of collection. The total range in replicate MgO analyses of glasses is 0.15 weight percent absolute, so these larger deviations in MgO content should be analytically significant, as are the deviations in temperature from straight-line decreases.

MgO contents of glasses from skylight and littoral samples from an episode 48 tube of February 1991, a single sample pair from episode 51 (November 1992) and a last

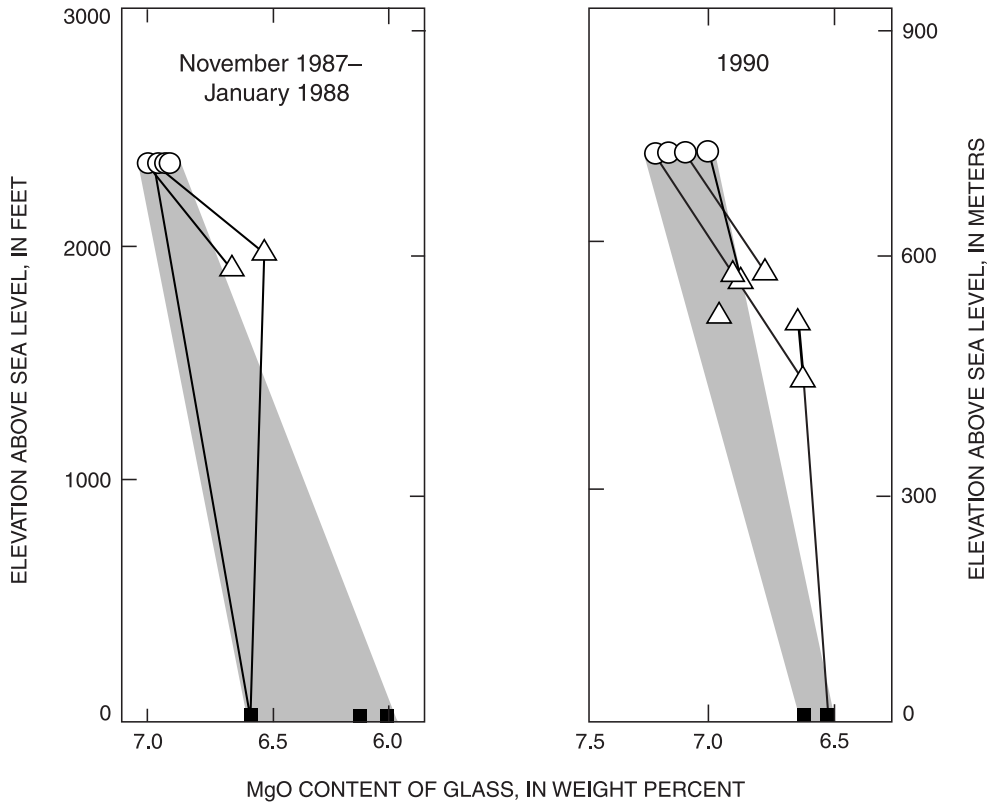

Figure 6. MgO content of glass from pond samples (circles), skylight samples (triangles), and coastal samples (squares) versus elevation at which samples were collected, from two different time periods. Heavy lines connect samples closely associated in time. Shaded areas indicate range of slopes shown by pond-coast data alone.

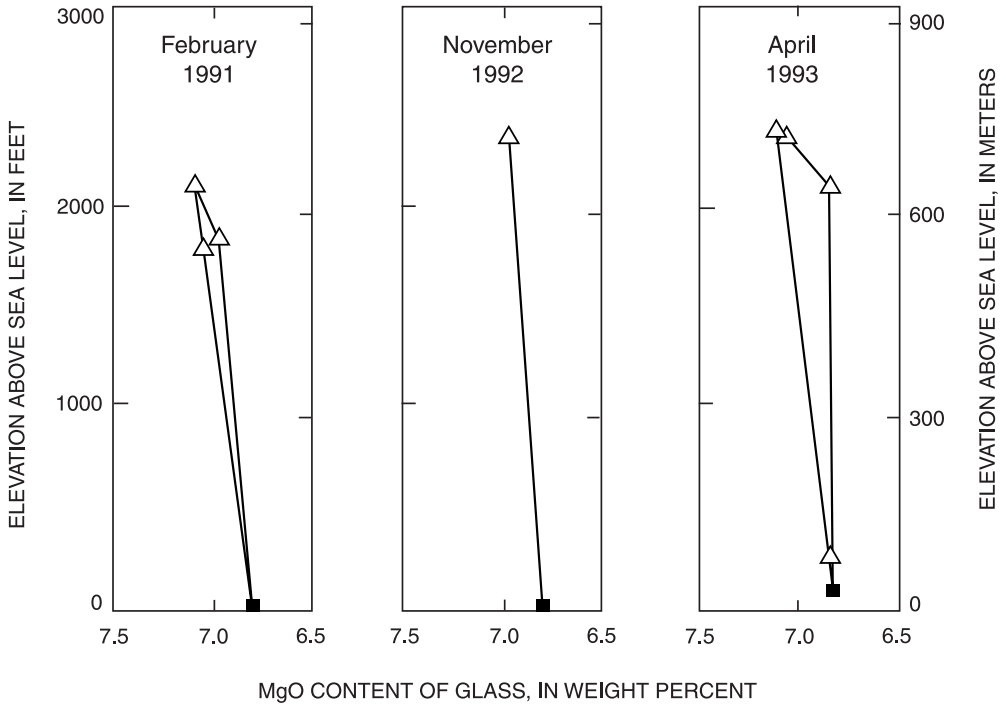

Figure 7. MgO content of glass from skylight samples (triangles) and coastal samples (squares) versus the elevation at which the samples were collected, during three different time periods. MgO content of glass in coastal samples is virtually constant throughout the entire period.

sample set from episode 53 (April 1993) are shown in figure 7. The latter two episodes were fed from Pu‘u ‘Ō‘ō itself, not from Kūpaianaha (fig. 1). The 1991 and 1992 data sets were previously described by Cashman and others (1994); the analyses used here are those of Helz and Hearn (1998). The various analyses, regardless of source, are very similar; in particular MgO contents differ by no more than 0.1 weight percent absolute in all instances. The skylight and coastal data in figure 7 resemble those in figure 6: the lines are steep to vertical, with a spread in MgO content in the upper skylight samples.

What is causing the nonlinearity evident in figure 6 (and, to a lesser extent, in fig. 7), such that so many skylight-littoral analysis pairs have calculated ΔT values in the range -1 to 4°C (see tables 2 and 3)? Clearly the behavior of the lava-tube system is unchanged: MgO in the skylight glasses has deviated on the low side from early in the lifespan of Kūpaianaha. Two possible explanations are (1) the upper part of the tube system loses heat much faster than the lower part, in which case the kinks seen in figures 6 and 7 are real, or (2) the skylight samples, which are difficult to retrieve, are less well quenched than the pond samples.

What could make the upper 2- to 4-km section of the lava-tube system thermally less efficient than the lower 6 to 8 km? One possibility would be enhanced loss of volatiles (mostly H_2O) because of the loss of the heat of vaporization that would accompany H_2O loss. However, the lava in the pond already had the opportunity to degas as it flowed under Pu‘u ‘Ō‘ō on its way to Kūpaianaha; also, the Kūpaianaha pond itself was effectively an immense skylight and must have allowed for extensive H_2O loss before lava entered the upper part of the tube system. In fact, Helz and others (1991) and Mangan and others (1995) noted the extreme dryness of the pond samples, as evidenced by their elevated plagioclase-in temperature (7.12 weight percent MgO, T=1,157°C) relative to that of Pu‘u ‘Ō‘ō samples and to samples taken after the pond crusted over (7.00 weight percent MgO, T=1,155°C). Finally, it is difficult to see why spontaneous degassing should become more efficient after the lava reenters a confined passageway. We believe that variable degassing rates are not responsible for the nonlinearity in glass MgO content.

A related possibility, suggested by Keszthelyi (1994), is that higher rainfall at higher elevations may cause more cooling in the uppermost part of the lava tube. However, if the rain falling on Pu‘u ‘Ō‘ō, on the 3 km of ground between Pu‘u ‘Ō‘ō and Kūpaianaha, and on Kūpaianaha itself was not enough to affect the condition of the pond samples, why should rainfall on the next 2 to 4 km of the tube system have so much effect on the skylight samples? In a more detailed analysis, Keszthelyi (1995b) divided the tube path into five segments and calculated their thermal budgets separately. His results, which consider many possible parameters, show that the rate of heat loss should be similar along most of the length of the tube, except for a small segment in the middle.

The alternative explanation (occasional quenching problems) is suggested by the fact that temperatures within the lava tube and even in air above skylights are very high (800–1,080°C; Peterson and others, 1994; Kauahikaua and

others, 1998). The process of withdrawing a sample from the lava stream, up through the airspace within the tube and out the skylight, is not instantaneous but takes minutes. The pond samples may not all be perfectly quenched, but they probably were more rapidly and more consistently quenched than the skylight samples.

This latter interpretation makes sense for the whole array of data in figures 3, 6, and 7, especially because half of the skylight data points in figure 6 are colinear with those of the pond-coast pairs. The idea that temperature decline in these lava tubes is approximately linear with distance is supported by the results of Thornber (2001), who presented detailed data for tube samples from the later part of episode 53. In his study, five sets of samples crystallizing at or below plagioclase-in (with up to six samples collected along the tube on a single day) show linear decreases in temperature from the Pu‘u ‘Ō‘ō vent out to almost 10 km.

Thus, we assume that the decrease in temperature (and heat loss, for a given crystallizing assemblage) is nearly linear with distance, so that skylight samples colinear with the pond-coast pairs (or having parallel slopes) represent successful sampling through skylights. To compare the total temperature changes for skylight-coast sample sets from episodes 51 and 53 with those from episode 48, we need to recall that the later tube systems were shorter than those fed from Kūpaianaha (10 km versus 12 km). Thus, ΔT=6°C for the 10-km-long lava tube system of episode 53 corresponds almost exactly to ΔT=7°C for the 12-km long Kūpaianaha system: both show a temperature decrease of 0.6°C/km. Thornber's (2001) minimum observed temperature decrease is 0.55°C/km. The close agreement in minimum cooling rate from these three studies strongly suggests that there is a limiting thermal efficiency for the lava tubes of the current Kīlauea east-rift-zone eruption.

Discussion

Repeated attempts have been made to quantify the change in temperature during flow of lava in tubes or along flows at Hawaiian volcanoes. In particular, the lava tube systems of the Mauna Ulu eruption were studied by Swanson (1973), who used an optical pyrometer to measure temperatures through skylights. He reported that "the highest optical-pyrometer temperatures of lava visible in each window of the tube system were 1,150° to 1,155°C, with no recognizable tendency for cooling downslope." Similarly, in their study of the 1984 Mauna Loa channelized ‘a‘ā flow, Lipman and Banks (1987) presented infrared-pyrometry and thermocouple data that showed unsystematic temperature variations along the flow, apparently all within 10–15°C of each other. The question posed by these and other early studies was, is the transport of lava really isothermal, or is the temperature variation too small to be defined by such measurements?

The consistent results of the present study and others (Cashman and others, 1994; Thornber, 2001) using glass geothermometry make it clear that the problem was the limited precision of field temperature determinations and that temperature decreases in lava tubes are readily quantifiable, given sets of well-quenched samples and an appropriate calibration. The calibration of Montierth and others (1995) will allow similar studies to be made on Mauna Loa lava, in the event of renewed eruptive activity and the formation of active tube systems on that volcano.

We have already noted that the minimum temperature loss per kilometer is the same in all three glass-geothermometry-based studies of the present Kīlauea eruption. We further note that the observed range of this parameter is fairly narrow (0.6–0.9°C/km for practically all sample pairs in this study from January 1988 through November 1989), and that this range of values has also been replicated by Thornber (2001), even though the sampling strategies used in the two studies were very different. We conclude that (1) there is a consistent and reproducible range of operating efficiency for Kīlauea lava tubes, at the magma-production rate of the ongoing east-rift-zone eruption, which can be documented over at least 10 years and (2) the sporadic lower ΔT values observed for skylight-coast pairs (tables 2, 3) are very unlikely to be significant.

Three additional features of these results deserve comment. First, the higher temperature decreases observed for pond-coast pairs collected before January 1988 result from variable but low quenching temperatures of the early littoral samples, at more or less constant temperatures for pond samples. We believe that these are caused by (unseen) variations in the thickness of the floor under the lava tubes in the new, relatively thin lava apron. The flows were thick enough for stable roofs to develop all the way to the coast; however, observers had no way of knowing whether the floor of a particular tube was entirely underlain by new lava, or by cold, older flows. We attribute the lower temperature decreases and more consistent littoral quenching temperatures observed after January 1988 to the development of a consistent floor across the area of the flow field.

Second, we should consider whether the differences in quenching temperatures shown in figure 3 are maximum or minimum values. That is, do the pond samples represent the average temperature in Kūpaianaha or just its surface temperature? We cannot be completely sure of the extent to which the temperature in the Kūpaianaha lava pond may have varied with depth. We suggest that any temperature gradients were small because the pond was constantly circulating and overturning, and because the range of MgO content in the pond glasses is quite limited (fig. 3). Moreover, Pu‘u ‘Ō‘ō spatter samples collected during episode 48 (from July 1991 on) are no hotter than the hottest of the Kūpaianaha samples (Helz and Hearn, 1998). The pond samples are surface samples, however, so to the extent that any bias exists, the ΔT values given in table 1 and figure 3 are minimums.

The coastal samples must be strongly biased toward sampling the hottest, fastest-moving part of the lava stream in the tube. The observed variation in stream velocity in the lava tube (Kauahikaua and others, 1998) may reflect variations in temperature across the lava stream; thus, the temperature decreases observed are (again) minimums for the system.

Table 5. Data on ʻAilāʻau selvage glasses, with estimated source temperatures.

[Parenthetical values indicate that the initial temperature estimate was higher than 1,155°C (plagioclase-in). For these samples, temperatures above 1,155°C are assumed to correspond to single-phase (olivine-only) crystallization, and the initial estimates were corrected accordingly. The resulting temperatures imply original (vent) MgO contents of 6.87–7.97 per cent by weight. Data from Clague and others (1999)]

Sample batch	No. of specimens	Distance from inferred vent	T_{MgO}°C for average selvage glass	Estimated source T_{MgO}°C (minimum)
1	5	0–5 km	1,153	1,153–(1,165)
2	2	5–10 km	1,145	1,148–1,151
3	10	10–15 km	1,143	1,149–1,152
4	4	15–20 km	1,150	(1,165)–(1,171)
5	6	20–25 km	1,142	1,154–(1,160)
6	2	25–30 km	1,143	(1,162)–(1,169)
7	9	30–35 km	1,142	(1,167)–(1,174)
8	15	35–40 km	1,139	(1,167)–(1,174)

Third, it is important to remember that the observed temperature decreases are all for lava undergoing multiphase crystallization (olivine + augite + plagioclase). The rate of temperature decrease for lavas crystallizing only olivine will be 2.4 times greater: the corresponding ΔT values would be 1.44–2.16°C/km, at exactly the same rate of heat loss along a lava tube. The controlling variable is heat loss, not temperature decrease, so petrographic examination of samples is required.

Other Studies of Lava Temperatures at Kīlauea

Studies of variations in lava temperature at Kīlauea have not focused exclusively on evaluating lava-tube systems. Cashman and others (1999) reported data on samples collected along an open lava channel, to elucidate factors controlling the transition from pāhoehoe to ʻaʻā observed in the channel. Application of glass geothermometry to these samples showed temperature decreases of 4.4–6.8°C/km, almost an order of magnitude higher than those observed in lava tubes, as would be expected from field observations. Modal analysis of these samples showed that the crystal content along the flow channel increased by 0.83 percent crystals per degree, as temperature decreased. This rate is similar to crystallization rates inferred in the present study (table 4), and also compares well with results of theoretical calculations (fig. 4), which showed an increase in crystal content of 0.8 weight percent per degree. Deviations from equilibrium are apparently not large in the hottest part of active lava flows, even in open channels. This observation is important, because the MgO glass geothermometer is valid only at equilibrium (Helz and others, 1995).

Glass geothermometry can be applied to older lava flow or tube systems, but the results must be interpreted carefully. For example, Clague and others (1999), in their excellent study of the ʻAilāʻau lava flow field (dated at A.D. 1445±30), reported average glass analyses of selvages from various parts of the flow field and translated the MgO contents of those glasses to temperature. Their results (summarized in table 5 by sample group, inferred distance from vent, and apparent quenching temperature of the glasses) show a relatively coherent decrease in the MgO content of glass with distance from the inferred vent (near the present Kīlauea Iki Crater), with a corresponding inferred temperature decrease of 0.35°C/km. The authors correctly note that this is much less than the observed cooling rate in tubes, being half the minimum rate of temperature decrease observed in the lava tubes of the current eruption.

The probable explanation for the limited compositional range of the ʻAilāʻau glasses is that they are not well-quenched samples; they are merely naturally occurring flow selvages, subject to a period of undercooling and disequilibrium crystallization prior to becoming rigid. Undercooling in pāhoehoe toes and flow margins has been observed in sampling of active flows (Helz and others 1995); under these conditions, MgO glass geothermometry (controlled by olivine crystallization) failed to keep up with actual measured temperature decreases. This process is probably responsible for the convergence in selvage glass compositions in the ʻAilāʻau lava flows. The sample base of Clague and others (1999) may include samples equivalent to the distal (littoral) samples presented here. For an eruption that occurred in A.D. 1445, however, we cannot obtain samples equivalent to pond spatter, tears from Puʻu ʻŌʻō, or dip samples from skylights or other active flow channels. Such samples require diligent real-time collection, an artificial quench, or both.

What have we learned about the ʻAilāʻau eruption from these glass data? First, the general decrease in MgO content of glasses with distance from the vent should be real and would reflect the decline in maximum MgO in the melt in

the original tubes/channels. Second, the existence of sample group 4 (table 5), with distinctly more magnesian glasses for their distance from the summit, suggests that the temperature of ʻAilāʻau lavas erupted at the vent varied over the course of the eruption or, conceivably, that some of the lava was erupted from a different vent.

What were source temperatures likely to have been? If we assume the maximum observed thermal efficiency for well-developed lava tubes of the present eruption (0.6°C/km for multiphase crystallization, or 1.4°C/km for olivine-only crystallization), we can use the distances from the inferred vent to arrive at minimum source temperatures for the lavas. These temperature estimates, given in the last column of table 5, range from 1,153 to 1,174°C. Most of the more distant samples (groups 4–8) have probable temperatures above plagioclase-in, at the low end of olivine-only crystallization. This temperature range is plausible for lavas originating at Kīlauea's summit (Wright, 1971).

We have a modern analogue that supports this interpretation. Melts in the same temperature range inferred for the ʻAilāʻau lavas were actually erupted during the high-fountaining episodes at Puʻu ʻŌʻō; however, such magnesian melts were not recovered from flow margins, even close to the vents. Instead all flow (selvage) samples contained the three-phase assemblage olivine + augite + plagioclase (Helz and others, 1991; Helz and Hearn, 1998). If these hotter melts are not recoverable from flow margins, even for samples collected and quenched by human intervention, they almost certainly would not be preserved in flow margins collected centuries after the eruption.

Other Aspects of Lava Transport in Tubes

Most studies of lava tube systems focus on the question, what is the maximum distance that tube systems can deliver lava? Keszthelyi (1995b) provides a good summary on this subject, reviewing many factors that go into quantifying the thermal budget of tube systems. A more specific question that we consider here is, what more can we learn from the active tube systems at Kīlauea?

We have consistent determinations of the maximum thermal efficiency for transport of lava in the present tube system. However, lava at the coast has not reached a limiting crystal content (figs. 2*B*, 2*D*), so no direct estimation of maximum possible length can be made. Even longer Hawaiian lava-tube systems, such as the 1859 Mauna Loa system (see Greeley, 1987), are stopped by the ocean, not by high viscosity produced by high crystal contents (Helz and others, 1993, and R.T. Helz, unpub. data, 1995). Also, our ability to evaluate the effect of variation in slope is limited by the small range of slopes found on tholeiitic shield volcanoes, in addition to the relatively short distances involved. In fact, extremely long lava flows, such as those of the Columbia River Basalt Group (Tolan and others, 1989) and those of North Queensland (Stephenson and Griffin, 1976) have traveled many times farther on lower slopes than the longest Hawaiian lava flows or tubes. This observation suggests that regional slope is not particularly critical in limiting lava tube lengths.

Other parameters of interest that have been investigated include actual structure, flow velocity of lava tubes, and the cross-sectional area of the lava stream. Thermal imaging obtained by Realmuto and others (1992) shows an intricate and fairly regular pattern of sinuosity and bifurcation of the Kūpaianaha lava-tube system of October 1988. Analysis of the observed structure by Keszthelyi (1994, 1995b) suggests that bifurcations have little effect on overall heat loss. The regularity in pattern implies a fairly predictable difference between net length and actual length of the lava tubes. Although length is not a major source of uncertainty in thermal efficiency, knowing true length would enable us to refine the estimates of temperature decrease and rate of heat loss. Kauahikaua and others (1998) and Kauahikaua and others (this volume) present unique data on velocity variations and on cross-sectional areas of the lava stream that are essential to increasing our understanding of the dynamics of the whole lava-tube system.

Another dynamic parameter, which remains relatively unknown, is lava flux rate along the length of the tube. Specifically, we do not know what fraction of the lava that enters the top of the lava-tube system emerges at the bottom. Evidence for downcutting of the tube floor (Kauahikaua and others, 1998) documents the erosion of material and its incorporation into the lava stream. Yet it is thermodynamically impossible for more lava to come out the bottom of the tube than flowed in at the top, so any erosion must be more than compensated by loss of material from the lava stream to the walls or floor elsewhere along the tube.

We presume this "lost" material is lodged in the inflating, thickening flow field (Hon and others, 1994), where it must represent a large part of the thermal budget of these lava-tube systems. Initial modeling by Keszthelyi (1994) led him to conclude that the temperature decrease during transport must be much greater than the 1°C/km that he used in his model, an estimate based loosely on the present results (as reported by Helz and others, 1991, 1993). However, if even a fairly small fraction of the lava that enters the tube never emerges, the ΔT values observed for the lava stream are not sufficient to define the thermal budget (integrated heat loss) for the whole tube system. Keszthelyi (1995b) subsequently recognized that lava effusion rate is a critical parameter, but his treatment of this parameter was necessarily theoretical.

We may be able to obtain data on lava flux in Kīlauea's lava tubes if the present activity continues, but can we recover any information applicable to the past 20 years' activity? One possible approach would be to look more closely for changes in bulk composition of the lava stream. We have looked briefly at changes in bulk MgO content of the pond-coast sample pairs and concluded that systematic changes in bulk composition, as a result of either cooling or flow differentiation in the lava tubes, appear to be small. Nonetheless, it might be fruitful to look more closely for changes in bulk composition at the trace element level, especially for anomalous increases in incompatible elements.

Summary and Conclusions

This chapter presents the results of applying the glass geothermometer of Helz and Thornber (1987) to a suite of 37 sample pairs of very glassy lava collected from the upper and lower ends of the episode 48 tube system, while the Kūpaianaha lava pond was open and accessible. We also include data on a smaller suite of skylight samples collected from early in the lifetime of Kūpaianaha through the end of episode 48 (in 1991), plus some data on skylight-coast sample pairs collected during episodes 51 and 53. The results are as follows:

(1) From November 1986 through January 1988 (15 months), the average change in inferred quenching temperature (for 12 sample pairs) is 12.4°C, and the average increase in crystal content (inferred from observed enrichment of TiO_2 and K_2O in the coastal glasses) is about 11 to 12 weight percent.

(2) From February 1988 through November 1989 (23 months), the average change in inferred quenching temperature (for 25 sample pairs) is 8.4°C, and the average increase in crystal content is 4 to 5 weight percent. Within this part of the data set, pond and coastal temperatures seem to rise and fall together much of the time, even though these temporal fluctuations are at or below the limit of resolution of glass geothermometry ($\Delta T \leq 3$°C).

(3) The minimum difference in temperature (ΔT) for any pond-coast pair is 7°C. Of 37 sample pairs, 24 have ΔT=7–9°C, over the entire 3-year period. These data, which form a coherent set, give us a well-defined range of temperature decreases in the episode 48 tube system, over its lifetime.

(4) The skylight samples are somewhat equivocal in their significance. About half the glasses in the skylight samples have MgO contents consistent with their position along the lava-tube system, and the other half have lower MgO contents. Apparently some of the skylight samples are not as well quenched as the pond and littoral spatter samples.

Other studies using glass geothermometry to evaluate temperature decreases in lava tubes of the ongoing Kīlauea eruption have produced similar results. The well-documented ΔT value of 6°C for some episode 53 samples (Cashman and others, 1994), collected from the 10-km long tube fed from Pu‘u ‘Ō‘ō, gives exactly the same temperature decrease with distance (0.6°C/km) as the limiting ΔT of 7°C observed for the 12-km tubes fed from Kūpaianaha. The range of efficiencies observed in the present study has been replicated by the results of Thornber (2001) for samples collected in 1996–98 during episode 53.

Better information on the actual length of the path traversed by lava in these tube systems would help establish the limits of overall thermal efficiency of Kīlauea lava tubes. However, the biggest gap in our understanding of these lava tube systems is lack of information on the efficiency of mass flux through the tubes. Without estimates of how much lava is retained in the lava-field system, the best-quantified changes in lava temperature give us only part of the story.

Acknowledgments

We wish to acknowledge the dedication of the HVO staff from 1986 through 1993. This chapter depends heavily on their continuous efforts to make rigorous field observations and to collect well-quenched and well-documented samples. In addition, we acknowledge B. Carter Hearn's meticulous electron microprobe analyses, which form part of the data base discussed here. The manuscript was greatly improved by reviews from Kathy Cashman and Jim Kauahikaua.

References Cited

Cashman, K.V., Mangan, M.T., and Newman, Sally, 1994, Surface degassing and modifications to vesicle size distributions in active basalt flows: Journal of Volcanology and Geothermal Research, v. 61, no. 1–4, p. 45–68.

Cashman, K.V., Thornber, C.R., and Kauahikaua, J.P., 1999, Cooling and crystallization of lava in open channels, and the transition of pāhoehoe lava to ‘a‘ā: Bulletin of Volcanology, v. 61, no. 5, p. 306–323.

Clague, D.A., Hagstrum, J.T., Champion, D.E., and Beeson, M.H., 1999, Kīlauea summit overflows; their ages and distribution in the Puna District, Hawai‘i: Bulletin of Volcanology, v. 61, no. 6, p. 363–381.

Ghiorso, M.S., 1985, Chemical mass transfer in magmatic processes, I. Thermodynamic relations and numerical algorithms: Contributions to Mineralogy and Petrology, v. 90, no. 2–3, p. 107–120.

Greeley, Ronald, 1987, The role of lava tubes in Hawaiian volcanoes, chap. 59 *of* Decker, R.W., Wright, T.L., and Stauffer, P.H., eds., Volcanism in Hawaii: U.S. Geological Survey Professional Paper 1350, v. 2, p. 1589–1602.

Heliker, C.C., Mangan, M.T., Mattox, T.N., Kauahikaua, J.P., and Helz, R.T., 1998, The character of long-term eruptions; inferences from episodes 50–53 of the Pu‘u ‘Ō‘ō-Kūpaianaha eruption of Kīlauea Volcano: Bulletin of Volcanology, v. 59, no. 6, p. 381–393.

Heliker, C.C., and Wright, T.L., 1991, The Puu Oo-Kupaianaha eruption of Kilauea: Eos (American Geophysical Union Transactions), v. 72, no. 47, p. 521, 526, 530.

Helz, R.T., Banks, N.G., Heliker, C.C., Neal, C.A., and Wolfe, E.W., 1995, Comparative geothermometry of recent Hawaiian eruptions: Journal of Geophysical Research, v. 100, no. B9, p. 17637–17657.

Helz, R.T., and Hearn, B.C., Jr., 1998, Compositions of glasses from the Pu`u O`o-Kūpaianaha eruption of Kilauea Volcano, Hawaii, January 1983 through December 1994: U.S. Geological Survey Open-File Report 98–511, 75 p.

Helz, R.T., Heliker, C.C., Mangan, M.T., Hon, K.A., Neal, C.A., and Simmons, L.K., 1991, Thermal history of the current

Kilauean east rift eruption: Eos (American Geophysical Union Transactions), v. 72, no. 44, supp., p. 557–558.

Helz, R.T., Hon, K.A., and Heliker, C.C., 1993, Thermal efficiency of lava tubes at Kilauea Volcano, Hawaii [abs.], *in* Duggan, M.B., and Knutson, Jan, compilers, Ancient volcanism & modern analogues: IAVCEI General Assembly, Canberra, Australia, 1993, Abstracts, v. 1, no. 1, p. 47.

Helz, R.T., and Thornber, C.R., 1987, Geothermometry of Kilauea Iki lava lake, Hawaii: Bulletin of Volcanology, v. 49, no. 5, p. 651–668.

Hon, K.A., Kauahikaua, J.P., Denlinger, R.P., and Mackay, Kevin, 1994, Emplacement and inflation of pahoehoe sheet flows; observations and measurements of active lava flows on Kilauea Volcano, Hawaii: Geological Society of America Bulletin, v. 106, no. 3, p. 351–370.

Kauahikaua, J.P., Cashman, K.V., Mattox, T.N., Heliker, C.C., Hon, K.A., Mangan, M.T., and Thornber, C.R., 1998, Observations on basaltic lava streams in tubes from Kilauea Volcano, island of Hawai‘i: Journal of Geophysical Research, v. 103, no. B11, p. 27303–27323.

Keszthelyi, L.P., 1994, On the thermal budget of pahoehoe lava flows: Pasadena, California Institute of Technology, Ph.D. dissertation, 269 p.

Keszthelyi, L.P., 1995a, Measurements of the cooling at the base of pahoehoe flows: Geophysical Research Letters, v. 22, no. 16, p. 2195–2198.

Keszthelyi, L.P., 1995b, A preliminary thermal budget for lava tubes on the Earth and planets: Journal of Geophysical Research, v. 100, no. B10, p. 20411–20420.

Lipman, P.W., and Banks, N.G., 1987, Aa flow dynamics, Mauna Loa 1984, chap. 57 *of* Decker, R.W., Wright, T.L., and Stauffer, P.H., eds., Volcanism in Hawaii: U.S. Geological Survey Professional Paper 1350, v. 2, p. 1527–1567.

Mangan, M.T., Heliker, C.C., Mattox, T.N., Kauahikaua, J.P., and Helz, R.T., 1995, Episode 49 of the Pu‘u ‘O‘o-Kupaianaha eruption of Kilauea Volcano—breakdown of a steady-state eruptive era: Bulletin of Volcanology, v. 57, no. 2, p. 127–135.

Mattox, T.N., Heliker, C.C., Kauahikaua, J.P., and Hon, K.A., 1993, Development of the 1990 Kalapana flow field, Kilauea volcano, Hawaii: Bulletin of Volcanology, v. 55, no. 6, p. 407–413.

Montierth, Charlene, Johnston, A.D., and Cashman, K.V., 1995, An empirical glass-composition-based geothermometer for Mauna Loa lavas, *in* Rhodes, J.M., and Lockwood, J.P., eds., Mauna Loa revealed; structure, composition, history, and hazards: American Geophysical Union Geophysical Monograph 92, p. 207–217.

Peterson, D.W., Holcomb, R.T., Tilling, R.I., and Christiansen, R.L., 1994, Development of lava tubes in the light of observations at Mauna Ulu, Kilauea Volcano, Hawaii: Bulletin of Volcanology, v. 56, no. 5, p. 343–360.

Realmuto, V.J., Hon, K.A., Kahle, A.B., Abbott, E.A., and Pieri, D.C., 1992, Multispectral thermal infrared mapping of the 1 October 1988 Kupaianaha flow field, Kilauea volcano, Hawaii: Bulletin of Volcanology, v. 55, no. 1, p. 33–44.

Rowland, S.K., and Walker, G.P.L., 1990, Pahoehoe and aa in Hawaii; volumetric flow rate controls the lava structure: Bulletin of Volcanology, v. 52, no. 8, p. 615–628.

Stephenson, P.J., and Griffin, T.J., 1976, Some long basaltic lava flows in North Queensland, *in* Johnson, R.W., ed., Volcanism in Australasia: New York, Elsevier, p. 41–51.

Swanson, D.A., 1973, Pahoehoe flows from the 1969–1971 Mauna Ulu eruption, Kilauea Volcano, Hawaii: Geological Society of America Bulletin, v. 84, no. 2, p. 612–626.

Thompson, R.N., and Tilley, C.E., 1969, Melting and crystallisation relations of Kilauean basalts of Hawaii; the lavas of the 1959–60 Kilauea eruption: Earth and Planetary Science Letters, v. 5, no. 7, p. 469–477.

Thornber, C.R., 2001, Olivine-liquid relations of lava erupted by Kīlauea Volcano from 1994 to 1998; implications for shallow magmatic processes associated with the ongoing east-rift-zone eruption: Canadian Mineralogist, v. 39, no. 2, p. 239–266.

Tolan, T.L., Reidel, S.P., Beeson, M.H., Anderson, J.L., Fecht, K.R., and Swanson, D.A., 1989, Revisions to the estimates of the areal extent and volume of the Columbia River Basalt Group, *in* Reidel, S.P., and Hooper, P.R., eds., Volcanism and tectonism in the Columbia River flood-basalt province: Geological Society of America Special Paper 239, p. 1–20.

Wright, T.L., 1971, Chemistry of Kilauea and Mauna Loa lava in space and time: U.S. Geological Survey Professional Paper 735, 40 p.

Magma-Reservoir Processes Revealed by Geochemistry of the Pu‘u ‘Ō‘ō-Kūpaianaha Eruption

By Carl R. Thornber

Abstract

Geochemical data were examined for a suite of approximately 1,000 near-vent lava samples, collected from January 1983 to October 2001, from the Pu‘u ‘Ō‘ō-Kūpaianaha eruption of Kīlauea Volcano, Hawai‘i. Bulk lava and glass compositions reveal short- and long-term changes in preeruptive magma conditions that can be correlated with changes in edifice deformation, shallow magma transfer, and eruptive behavior. Nearly two decades of eruption on Kīlauea's east rift zone have yielded about 2.3 km^3 of lava, 97 percent of which is sparsely olivine-phyric with an MgO range of 6.8 to 9.6 weight percent. During separate brief intervals of low-volume fissure eruption (episodes 1 to 3 and 54), isolated rift-zone magma pods with lower-MgO compositions and with phenocrysts of olivine, clinopyroxene, and plagioclase were mixed with more mafic magma immediately before eruption. During prolonged, near-continuous eruption (episodes 48 through 53 and most of 55), steady-state effusion was marked by cyclic variations in olivine-saturated magma composition. Bulk-lava MgO content and eruption temperatures vary in cycles of monthly to biennial frequency, while olivine-incompatible elements vary inversely to these cycles. MgO-normalized values and ratios of highly to moderately incompatible elements, which are not affected by olivine fractionation, however, reveal cycles in magma composition that occur before olivine crystallization over the magmatic temperature range tapped by this eruption (1,205–1,155ºC). These short-term cycles are superimposed on a long-term decrease of incompatible element ratios, which has been proposed to reflect a progressive 20-year change in mantle-source conditions. Such variation in primitive recharge magma cannot be ruled out, but the short-term fluctuations of this signature may require unreasonably complex mantle variations. Alternatively, the correspondence of geochemical cycles with edifice deformation and eruptive behavior suggests that the long-term evolving magmatic condition is a result of a prolonged succession of short-term shallow magmatic events. The long-term trends can be explained by episodic mixing of chemically uniform recharge melt with diminishing proportions of pre-1983 summit magma (maintained at near-cotectic conditions). The occurrence of long-term summit deflation since the 1982 eruption suggests that progressive summit-reservoir depletion may be responsible for observed geochemical and isotopic trends in post-1982 steady-state eruption products. New magma derived from a uniform mantle source has apparently flushed out older resident magma and may now completely occupy the shallow magmatic plumbing system.

Introduction—Magmatic Setting

During the past two decades, geophysical and geochemical monitoring have helped define how and where magma is transported, stored, erupted, and recharged within the edifice of Kīlauea Volcano. Recent geophysical interpretations of the magmatic plumbing system are consistent with earlier models summarized and refined by Tilling and Dvorak (1993). Magma generated at depths greater than 60 km within the Hawaiian hotspot is transported to storage beneath Kīlauea's summit. Subsequently, behind an unbuttressed and seaward-moving flank, the magma is transported via episodic dike injection to the two rift zones that radiate from the summit.

Interpretations of variations in seismic velocity beneath the summit caldera (Dawson and others, 1999; Ohminato and others, 1998) reveal that a body of magma is presently located 1 to 4 km below an area southeast of Halemaumau, and a magma conduit connects this summit reservoir to the uppermost east rift zone (see fig. 1). Carbon dioxide (CO_2) concentrations in summit and rift-zone gas fumaroles, measured since 1983, suggest that magma recharge is restricted to the summit, beneath the vicinity of Halemaumau (Gerlach and others, 2002). Gerlach and others provide reasonable evidence that turbulent magma mixing occurs at the base of the summit reservoir as primitive (CO_2-rich) melts are introduced. A shallow summit magma reservoir has probably been maintained by such open-system recharge for more than two centuries of episodic summit eruptions (Pietruszka and Garcia, 1999a).

Before the Pu‘u ‘Ō‘ō-Kūpaianaha eruption began, an estimated 55 percent of magma supplied to the shallow edifice from 1952 to 1983 intruded along the rift zones (Dzurisin and others, 1984). Despite the intrusion and eruption that occurred at the summit during the same time period, Dzurisin and others indicate that little or no net change occurred in the volume of magma stored in the summit reservoir. Since 1983, however, amidst near-continual rift eruption and influx

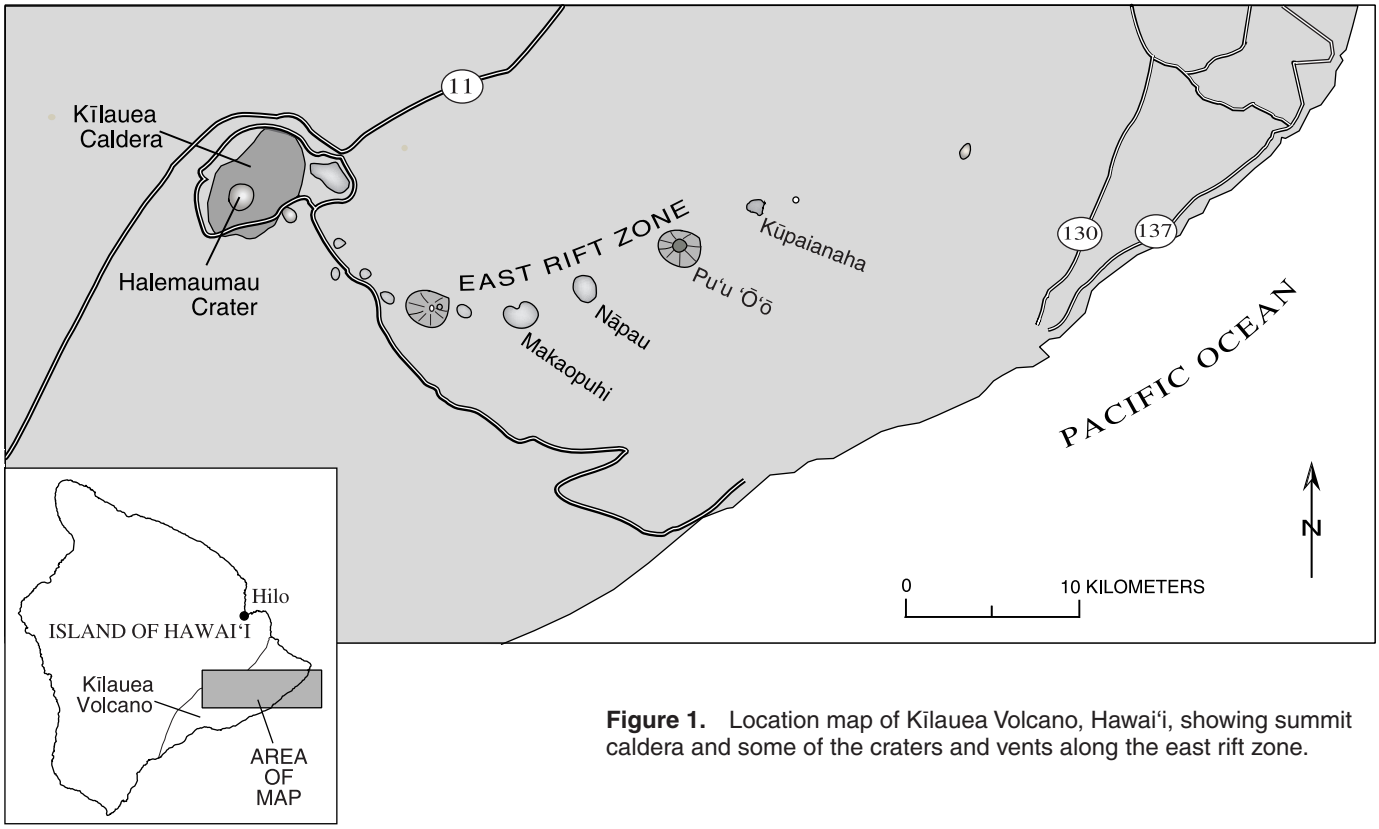

Figure 1. Location map of Kīlauea Volcano, Hawai'i, showing summit caldera and some of the craters and vents along the east rift zone.

of new magma into the summit reservoir, the shallow reservoir has steadily deflated. This deflation indicates that the summit magma chamber has gradually lost stored magma.

In concert with this 20-year-long deflationary trend at the summit, progressive outward movement of the south flank has accommodated development of an increasingly efficient magma conduit through the shallow upper and middle east rift zone. Evidence that pockets of magma also exist along the east rift conduit is shown in geophysical and petrologic studies (Thornber and others, in press; Garcia and others, 1989, 1992; Hoffman and others, 1990; Okamura and others, 1988). Such pockets of rift-resident magma may be physically isolated from magma flowing continuously through the shallow rift zone or may persist as open-system reservoirs, maintained in connection with fresh magma supplied from the summit region.

Changes in vent location and eruptive vigor throughout the Pu'u 'Ō'ō-Kūpaianaha eruption (Heliker and Mattox, this volume) are a consequence of the ebb and flow of magma within this dynamically evolving system. Over the short term (year-to-year, month-to-month, and day-to-day), seemingly erratic cycles of summit inflation and deflation result from magma intrusion into, or withdrawal from, the summit reservoir, combined with magma transport into and along the east rift zone (Wolfe and others, 1987; Okamura and others, 1988; Denlinger, 1997; Garcia and others, 1996; Owen and others, 2000; Thornber, 2001; Cervelli and others, 2002; Thornber and others, in press; Cervelli and Miklius, this volume). Surges and lulls in downrift vent activity, which correlate with these cycles, demonstrate that a fluid-pressure balance is maintained between the summit and the east rift zone.

Geochemical Data

The geochemical data in this paper are culled from the Hawaiian Volcano Observatory (HVO) database of lava samples from the Pu'u 'Ō'ō-Kūpaianaha eruption. As an integral part of the ongoing eruption-monitoring effort, such data have been continuously obtained, using U.S. Geological Survey analytical laboratories. Sampling information and complete analyses for about 1,000 near-vent samples collected from episodes 1 through 55 (up to October 2001) are available from the author.

The selected suite of HVO's lava samples from the eruption is limited mostly to rapidly quenched eruptive products of spatter; tephra (reticulite and Pele's hairs and tears) collected near the vent; lava collected from skylights of lava tubes; and lava from pond or surface flows collected at the vent. Collection techniques used were similar to those described by Thornber (2001). Glass and whole-rock chemistry tends to change during emplacement of distal surface flows (Cashman and others, 1999; Sharma and others, 1999) and in sluggish lava-tube flows associated with eruptive pauses; such samples are not included in this database. Eruption temperatures were

determined, using the Kīlauea MgO-glass thermometry of Helz and Thornber (1987), with an average distance correction factor of 0.9ºC/km applied to lava-tube flow samples collected at variable distances from the vent (Thornber, 2001).

Geochemical data compiled for near-vent samples includes 793 bulk lava major-element analyses obtained by wavelength dispersive x-ray fluorescence (WDXRF) techniques; 652 major-element glass compositions, each an average of 10 electron microprobe analyses (EMPA) per sample; and 85 instrumental neutron activation analyses (INAA) of trace elements from representative bulk lava samples. Glasses in a subsuite of 37 samples of Pele's tears erupted from 1995 to 1996 were analyzed for trace elements, using laser-ablation inductive-coupled plasma mass spectrometry (LAICPMS). The database also includes Nd, Sr, and Pb isotopic data obtained for 10 of the samples analyzed by INAA that erupted between 1983 and 1994. For this report, two vent-spatter samples from the last summit eruptions in April and September 1982 were also collected and analyzed for major elements.

Overview of Eruption Geochemistry, January 1983 to October 2001

Nearly continuous magma infusion beneath the summit for 19 years has yielded about 2 km^3 of lava on the rift zone (fig. 1). Approximately 97 percent of this lava is weakly olivine-phyric, with minor chromian spinel, and has MgO contents of 6.8 to 9.6 weight percent. Small volumes of cooler and relatively MgO-poor magma, erupted during episodes 1 through 3 (January to April 1983) and during episode 54 (January 30–31, 1997), are saturated in clinopyroxene and plagioclase. MgO variation diagrams for major and trace elements that are incompatible with crystallization of olivine and spinel define different geochemical trends of erupted lava (fig. 2). At or below about 7 weight percent MgO, moderately incompatible elements that are incorporated by plagioclase and clinopyroxene (such as Ca and Sc) are depleted, whereas highly incompatible elements (such as large-ion lithophile elements, rare earth elements and Ti, Zr, and Hf) are variably enriched, relative to olivine-controlled compositions. Above about 7 weight percent MgO, the incompatible element variation is consistent with olivine-only fractionation from a limited range of magmatic temperatures and delineates an olivine-control trend of slightly increasing incompatible elements with decreasing MgO. As indicated in figure 2, this olivine-saturated liquid line of descent (LLD) shifts progressively, from episode 48 to 55, toward lower concentrations of K_2O and other incompatible elements.

Throughout most of the eruption, matrix glass compositions varied with bulk lava compositions. Increases and decreases of MgO content in bulk lava correlated positively with changes in eruption temperature, as determined by MgO content of the glass (fig. 3*A, B*). In addition to having relatively low MgO content and temperature, the bulk signature of lava erupted during episodes 1–3 and 54 is clearly distinguished from the common olivine-controlled composition in temporal variation plots of olivine-incompatible elements, such as Ca and Ti (figs. 3*C, D*).

Concentrations of incompatible elements in olivine-phyric lava vary inversely with bulk lava MgO and eruption temperature over periods of 6 months to 2 years (fig. 3). On this time scale, cycles of variation in temperature and in MgO and incompatible-element concentrations are broadly consistent with repeated cycles of olivine fractionation from melts of about 10 to 7 weight percent MgO. When normalized to constant MgO (7 and 10 percent), variation owing to olivine fractionation is nullified, revealing short-term incompatible-element cycles between end members of 7 and 10 weight percent MgO, superimposed on a long-term decrease of concentrations, independent of olivine fractionation (fig. 3*C, E*).

The trend of long-term decrease, more pronounced for more highly incompatible elements, results in well-defined temporal decreases in ratios of incompatible elements, such as Ca/Al and K/Ti (fig. 4*A, B*). These ratios track a gradual and persistent change in the composition of olivine-saturated magma that feeds the eruption. Such progressive changes of an olivine-controlled LLD are apparent in a temporal decrease in ratios of highly to moderately incompatible trace elements (for example, La/Yb, fig. 4*C*) and in the change of averaged olivine-normalized trace element patterns for successive intervals of steady-state eruption (fig. 5). The long-term trends of elements incompatible with olivine in lava erupted during episodes of prolonged effusion extend back in time to the last magma erupted from the summit in September 1982, four months before the onset of the current eruption (figs. 3, 4, and 5). As discussed later, these post-1983 trends are coincident with that of long-term summit deflation (fig. 4*D*).

Within estimated analytical errors for matrix glasses (Thornber and others, 2002), incompatible elements show the same overall temporal trends observed for whole-rock data, but with more scatter. The greater variability of glass data is due to minor cooling and crystallization associated with drainback at the vents and transport of lava in tubes. Some of the variation can be attributed to microlite development in poorly quenched vent samples. The variability of glass data is minimized for ratios of olivine-incompatible elements, which reveal the same overall long-term trends as bulk-lava ratios (fig. 4*A, B*). Incompatible trace element concentrations for Pele's tears (glass) collected from mid-1995 to mid-1996 are consistent with the temporal variations observed for major and minor elements (fig. 5).

Isotopic determinations of Sr, Nd, and Pb for 10 representative olivine-phyric samples erupted from 1983 to 1993 complement similar determinations for 14 samples collected between 1983 and January 1998, reported by Garcia and others (1996, 2000), and for 1982 summit magma (Pietruszka and Garcia, 1999a). For all three datasets, $^{143}Nd/^{144}Nd$ and $^{87}Sr/^{86}Sr$ remain fairly constant (within analytical error), but, in a fashion similar to olivine-incompatible element ratios, $^{206}Pb/^{204}Pb$ decreases steadily from the values of 1982 summit lava until 1988, then increases slightly again (fig. 6).

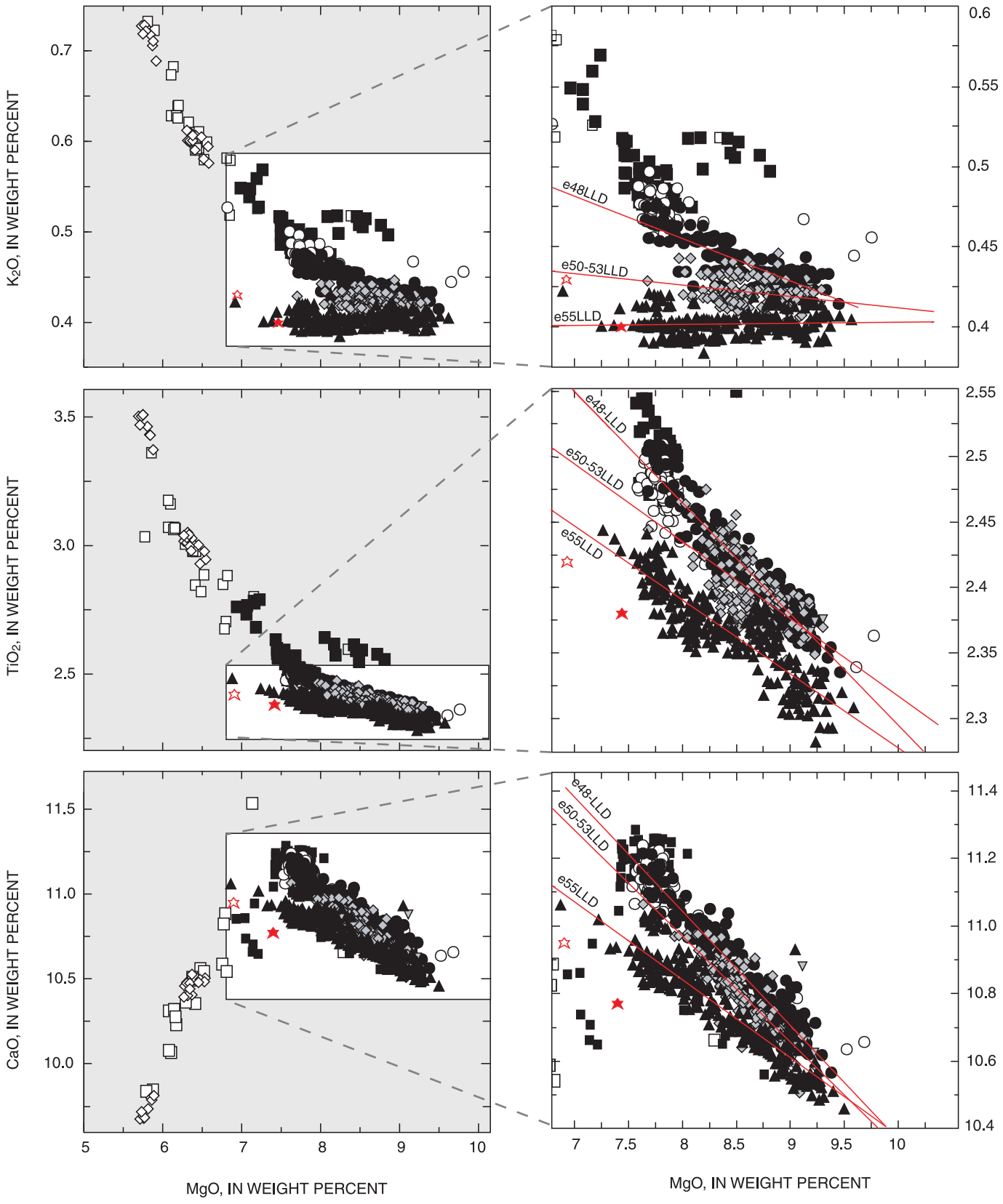

Figure 2. MgO variation diagrams for selected incompatible elements. Symbols (facing page) pertain to groups of eruptive episodes, as indicated in figure. All values are for bulk lava analyses except the averaged compositions of glasses in Pele's tears collected during episodes 53 (open red star) and 55 (filled red star) (from Thornber, 2001). Scales are expanded in duplicate figures for K_2O, TiO_2, and CaO to show progressive shift in an olivine-saturated liquid line of descent (LLD) toward lower concentrations of incompatible elements, shown by red lines fit to data for episodes 48 (e48LLD), 50–53 (e50–53LLD) and 55 (55LLD).

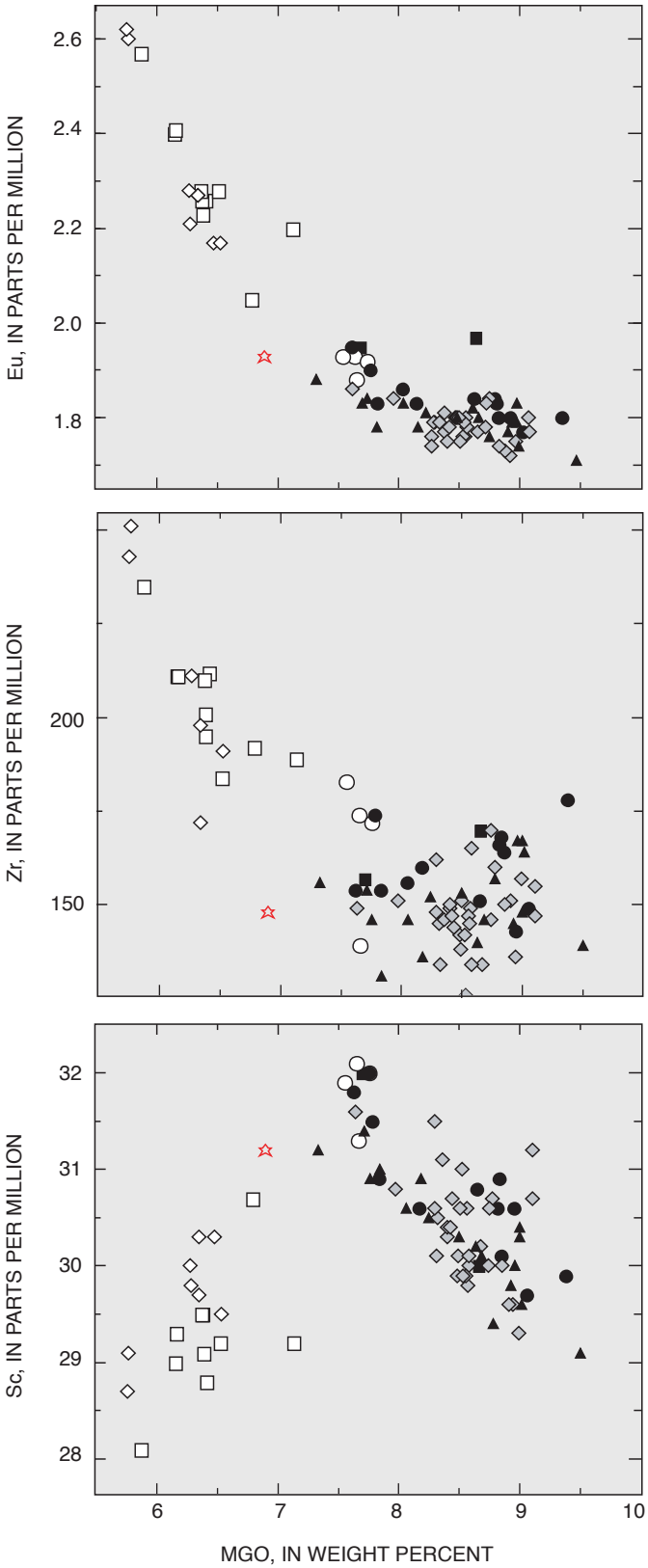

Figure 2. Continued.

Chronological Evolution of Volcanic and Magmatic Conditions

The eruption began with lava of a historically preponderant Kīlauea composition extruded from a small fissure that is still exposed on the west side of Nāpau Crater (Wolfe and others, 1988). At 6.8 weight percent MgO, its composition is at the low end of an olivine-control trend. Garcia and others (1989) found no petrographic evidence for preeruptive magma mixing in this initial 1983 lava, which is similar in character and composition to that which last erupted at the summit in September 1982. Those authors provide evidence that subsequent early fissure eruptions during episodes 1 to 3, extending 7.5 km from the west edge of Nāpau, were fed by mixing of this near-cotectic magma with cooler magma stored beneath the rift.

During the vigorous Pu‘u ‘Ō‘ō eruptive intervals (episodes 4 to 47) that followed the mixing events of episodes 1 to 3, cycles of low to high MgO are repeated within and between episodes (fig. 3*B*). Tephra deposited by waxing and waning fountains contains heterogeneous glass fragments that yield eruption temperatures from 1,161 to 1,173ºC (fig. 3*A*). High-temperature glass data are correlated with high-MgO in bulk lava for some samples collected during episodes 5 to 10 and 30 to 31, but high-temperature glasses in low-MgO bulk lava are more common in these episodes and may reflect olivine loss after drainback and recirculation associated with eruptive pulses.

During episodes 4 to 29, erupted lava became gradually hotter, richer in MgO, and more depleted in incompatible elements (figs. 2–4). In the light of additional petrologic and geophysical evidence, Garcia and others (1988, 1992) interpreted this trend to be a result of progressive flushing of rift magma reservoirs intersected by the developing conduit between the summit and the Pu‘u ‘Ō‘ō vent. The final flushing of hybrid magma at Pu‘u ‘Ō‘ō had occurred by episodes 30 and 31, when the hottest and most MgO-rich magma was erupted (1,173ºC matrix glass temperature and 9.6 weight percent bulk lava MgO).

From episodes 32 to 47 of the eruption, bulk lava and glass compositions portray cyclic fractionation over a limited range of olivine-saturated magma conditions (1,161º–1,165ºC). Through this interval, olivine phenocrysts formed at near-equilibrium conditions in host liquids, possibly within the conduit beneath Pu‘u ‘Ō‘ō during lengthy repose periods between these episodes (Garcia and others, 1992).

A failure of the conduit beneath Pu‘u ‘Ō‘ō resulted in downrift propagation of fissure vents and the establishment of long-term continuous eruption from the Kūpaianaha vent (episode 48). From July 1986 to February 1987, during the building of the Kūpaianaha shield, bulk-lava MgO steadily climbed (to about 8.6 weight percent from the lower values of about 7.6 weight percent for magma erupted during episodes 32 through 47) as hot, summit-derived magma moved through the newly developed extension of the shallow rift conduit. Determination of MgO glass temperatures remained erratic, owing to difficulties in obtaining well-quenched near-vent samples.

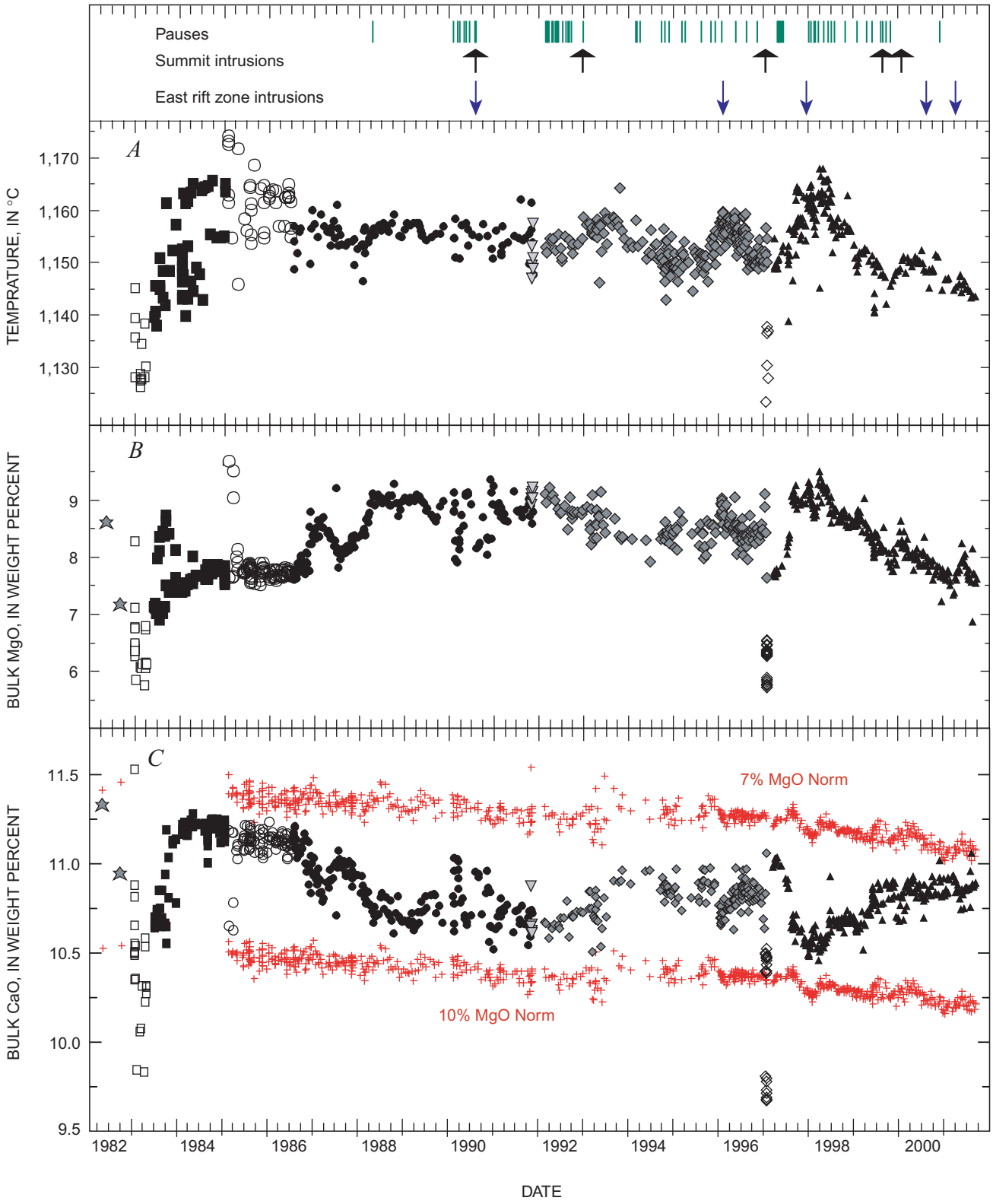

Figure 3. Time-series plots of eruption temperature and lava composition from January 1983 to October 2001, plus 1982 summit compositions. Summit lava of 1982 is indicated with gray stars. The crosses plotted above and below data in *C* and *E* are CaO and TiO_2 values for olivine-phyric samples normalized to 7 weight percent and 10 weight percent MgO, by removal or addition of equilibrium olivine, respectively. Shown above *A* is a timeline of summit intrusions (upward arrows), rift zone intrusions (downward arrows), and eruptive pauses (hash marks). *A,* Eruption temperature, as determined by MgO glass thermometry and corrected for distance to vent for distal tube samples (see text). *B,* Bulk lava MgO variation. *C,* Bulk lava CaO variation. *D,* Bulk lava TiO_2 variation. *E,* Expanded scale for bulk lava TiO_2 variation in olivine-saturated lava, episodes 30–53 and 55.

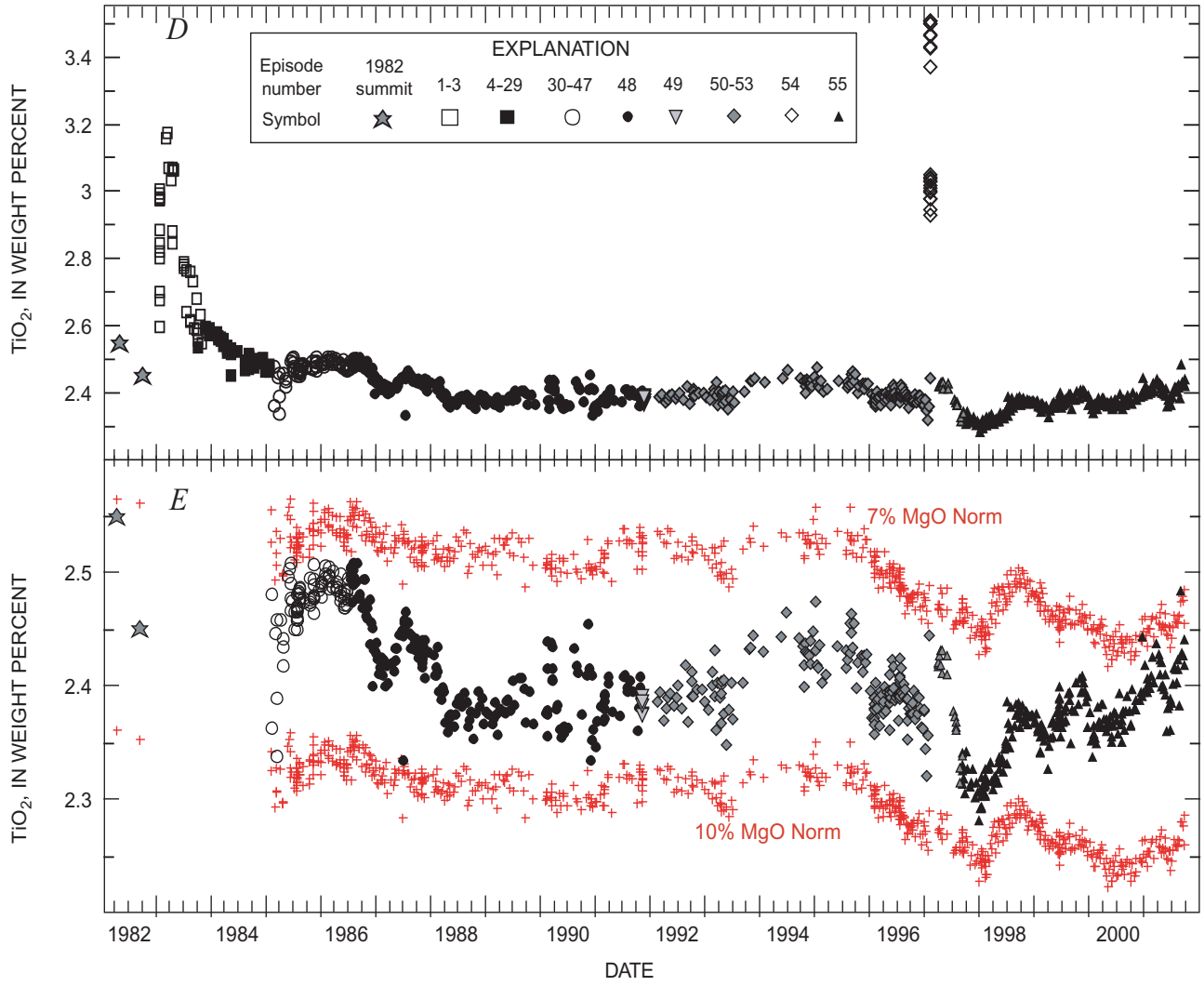

Figure 3. Continued.

After peaking in February 1987, bulk lava MgO and eruption temperature declined simultaneously until July 1987 in the first of numerous magmatic cycles that typify prolonged eruptive intervals. In this relatively steady-state situation, the conduit delivered hotter and cooler olivine-saturated magma as pulses and lulls in the eruption occurred in response to summit deformation and in accordance with a delicate pressure balance within the shallow magmatic plumbing system (Garcia and others, 1996; Thornber, 2001).

Cyclic variation of MgO and temperature persisted for 11½ years (episodes 48 though 53), undisrupted by the interlude of uprift vent migration back to Pu‘u ‘Ō‘ō from November 1991 to February 1992 (late episode 48, episodes 49 and 50; Mangan and others, 1995; Heliker and others, 1998). The uprift shift to Pu‘u ‘Ō‘ō coincided with three intrusions along the rift zone, after a period of 9 eruptive pauses during 1990 and 1991 (Heliker and Mattox, this volume) when the Kūpaianaha pond crusted over as magma flux waned (Kauahikaua and others, 1996) and bulk lava MgO and eruption temperature showed an overall decline amidst sporadic highs and lows (fig. 3).

In January 1997, the near-steady-state flow of olivine-saturated magma through a well-developed conduit from summit to rift zone was disrupted by shallow rift-zone extension and a brief eruption at Nāpau Crater (episode 54; Owen and others, 2000; Thornber and others, in press). Geophysical and petrologic evidence indicates preeruptive mixing of hotter, olivine-saturated melts with older and colder fractionated pockets of magma within the shallow rift during this event (Thornber and others, in press). Mixing resulted from passive intrusion associated with rift extension during episode 54, in contrast to the forceful dike intrusion of summit magma into rift magma during episodes 1 through 3. The first five months of episode 55 until July 1997 were characterized by a steady increase in temperature and bulk-lava MgO in samples erupted from several sporadically active Pu‘u ‘Ō‘ō flank vents. A gradual return to steady-state eruptive conditions occurred as the summit steadily reinflated, indicating that the shallow magmatic plumbing system was being repressurized. Major- and trace-element variation during early episode 55 is consistent with the gradual flushing of cooler, near-cotectic magma residing within the conduit (Thornber and others, in

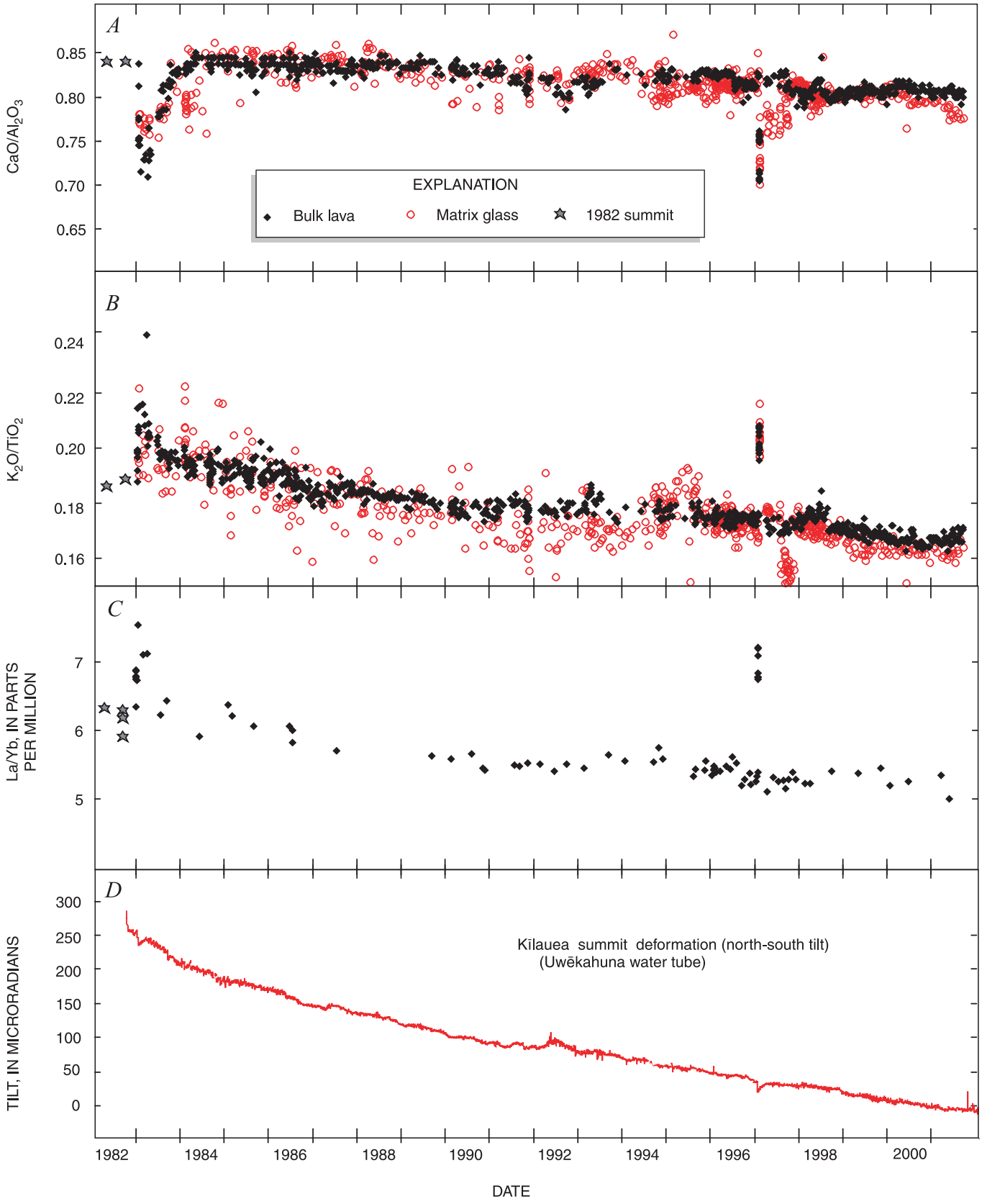

Figure 4. Time-series plots of bulk lava composition (data in weight percent) from January 1983 to October 2001 showing selected incompatible-element ratios for major elements in bulk lava and matrix glasses, and Kīlauea summit deflation during this period. Gray stars denote April and September 1982 summit lava; *A,* CaO/Al_2O_3; *B,* K_2O/TiO_2; *C,* La/Yb (data are from Pietruzska and Garcia, 1999a); *D,* Long-term Kīlauea summit deflation, as represented by Uwēkahuna north-south water-tube tilt data.

press). Since mid-1997, episode 55 lava compositions have varied cyclically, like those of episodes 48 through 53, and are superimposed on an overall decline of bulk-lava MgO and eruption temperature (Thornber, 2001; fig. 3).

Relation Between Geochemical Cycles and Open-System Shallow Magmatism

Throughout periods of nearly continuous eruption (episodes 48 to 53 and most of 55), olivine-liquid relations predicate near-equilibrium olivine crystallization from melts equivalent to the lava's bulk composition, without significant loss or accumulation of olivine during transit along the length of the rift conduit (Garcia and others 1996; Thornber, 2001). The cyclic variation of olivine-controlled compositions indicates repetition of a limited range of olivine-saturated magmatic conditions that may be typical of nearly continuous magma recharge.

As documented for the pre-Kūpaianaha/post-mixing stages of the eruption (episodes 30 to 47), the hottest and most MgO-rich magmas erupted during subsequent episodes of prolonged effusion are also correlated to temporary increases in eruption rate and vigor that occur in association with intrusion or displacement of summit magma. Such events include the dramatic surges in eruption flux on February 1, 1996 (episode 53), and on January 14, 1998 (episode 55) (see fig. 3). The highest eruption temperatures since episode 30, observed in April 1998, were associated with summit inflation and high eruptive flux. In this event, magma with about 9.5 weight percent MgO that was tran sported to the vent originated at about 1,205ºC, in equilibrium with $Fo_{84.5}$ olivine. Cyclic variation accompanying overall decreasing trends in temperature and MgO content occurred during waning stages of episode 48, throughout the pause-riddled episodes 50 to 53 until late 1995, after the summit intrusion of February 1, 1996, and from April 1998 until October 2001. The low-temperature end of these olivine-controlled cycles occurred at the end of the latter sampling interval, when magma with about 7.5 weight percent MgO, saturated with $Fo_{81.5}$ olivine at about 1,165ºC, was tapped by the eruption.

The MgO variability during prolonged steady-state eruption is within the range shown by olivine-controlled magma erupted before episode 48 (6.8 weight percent MgO at the onset of eruption and 9.8 weight percent MgO during episode 30). This overall range is consistent with the combined range of MgO in glass of summit tephra and of Kīlauea Iki lava (Mastin and others, 2001; Murata and Richter, 1966) and with bulk lava MgO for historic summit eruptions other than the 1959 Kīlauea Iki eruption (Wright, 1971). Such characteristic and recurring compositions suggest that these represent end-member magmatic conditions within the shallow magmatic plumbing system. The low end of MgO variation approaches a stable end-member condition maintained at the low-pressure multiphase cotectic for Kīlauea basalt (about 7 weight percent MgO at about 1,155ºC; Thompson and Tilley, 1969; Helz and Thornber, 1987; Yang and others, 1996). As pointed out in numerous studies of olivine-basalt systematics (O'Hara, 1977; O'Hara and Matthews, 1981; Defant and Nielson, 1990; Rhodes and Hart, 1995), the lack of differentiation below the multiphase cotectic is attributed to "buffering" effects of open-system replenishment of a persistent magma reservoir. This dynamic magma-buffering process accounts for the preponderance of Kīlauea and Mauna Loa lava compositions at the low end of an olivine-controlled liquid line of descent (see Rhodes, 1995). The high-temperature end member of about 10 weight percent MgO is regulated by the amount of olivine that fractionates from the recharge magma when it is turbulently mixed with a portion of near-cotectic resident magma. The consistent limit of magmatic temperatures reflected by eruptive products richest in MgO is likely to be controlled by a constant composition of primitive melt entering the system, estimated at about 15 weight percent MgO (Clague

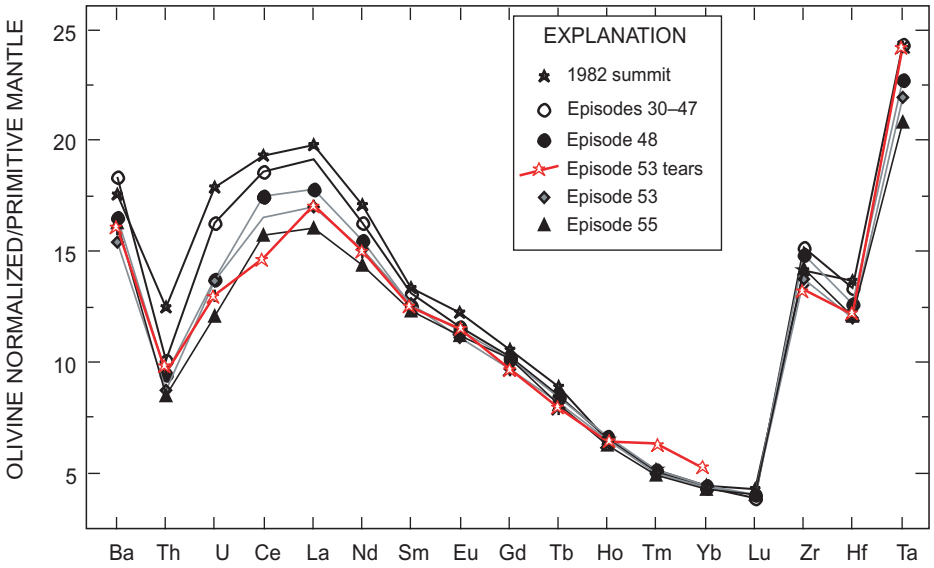

Figure 5. Trace-element spidergram comparing range of highly to moderately incompatible elements in bulk lava averaged for successive episode groups (symbols are same as in figures 1 and 2). Values (ppm) were all normalized to 7 weight percent MgO by olivine subtraction and plotted relative to primitive mantle values of Sun and McDonough (1989). Summit data for 1982 are from Pietruzka and Garcia (1999a; sample number 1982–s14). Red line portrays average trace-element composition of Pele's tears collected from mid-1995 to mid-1996 (analyzed by LAICPMS).

and others, 1995). Fractionation of more forsteritic olivine (~Fo_{85} to ~Fo_{90}), below the zone of replenishment and turbulent mixing tapped by the current Kīlauea eruption, feeds a layer of olivine cumulate within the edifice at depths greater than 4 to 5 km beneath the summit and south flank (Clague and Denlinger, 1994; Delaney and others, 1998; Denlinger and Okubo, 1995).

Concentrations of incompatible elements in steady-state eruption products inversely mimic the cyclical repetition of eruption temperature and bulk-lava MgO content between compositions normalized to 7 and 10 weight percent MgO end members (fig. 3*C, E*). These variations are consistent with olivine fractionation during cooling after intermittent recharge. However, the temporal variation of major and minor incompatible-element ratios (and olivine-normalized compositions) indicates that subtle but analytically significant short-term fluctuations in the relative concentrations of these components must occur before olivine crystallization over the magmatic temperature range of about 1,200 to about 1,160ºC that is tapped by this eruption.

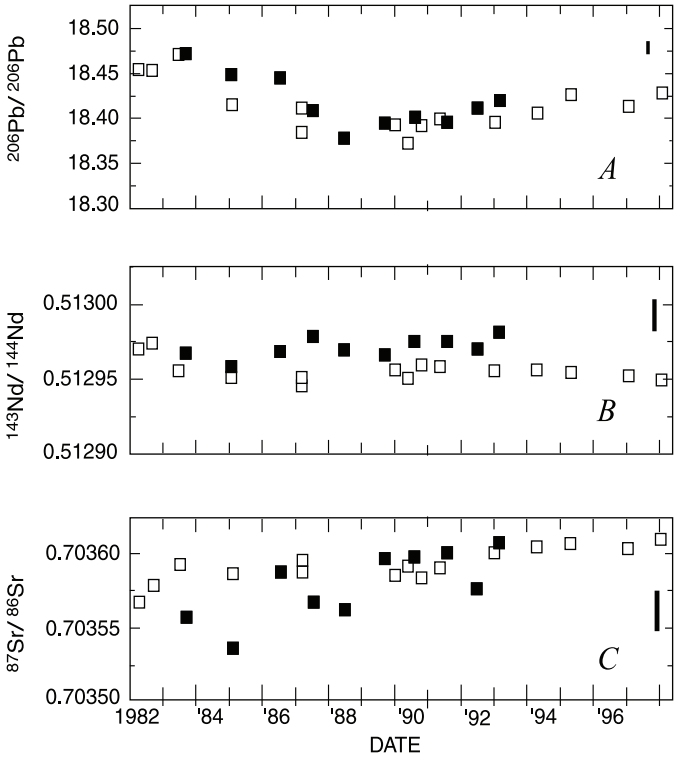

Figure 6. Time-series plots of Pb, Nd, and Sr isotope variation in Kīlauea lava samples erupted from 1982 to 1998. Filled squares are previously unpublished values determined by D. Unruh, U.S. Geological Survey (Denver) on samples submitted by the author (see Thornber and others, in press, for details on techniques and precision). Open squares are data compiled from Peitruszka and Garcia (1999a) and Garcia and others (1996, 2000). No interlaboratory corrections were made to the data. The error bars (thick vertical lines) shown at the right of each figure represent 2-sigma errors for U.S. Geological Survey data, as established by the analyst.

Cyclic variations of olivine-incompatible element ratios (such as Ti/Ca and K/Ti) have monthly and annual-to-biennial durations and generally increase and decrease in delayed response to cycles of increasing and decreasing magmatic temperatures (fig. 7), as reflected by bulk-lava MgO changes. Comparison with continuous GPS measurements of summit deformation (since mid-1996) shows trends of increasing and decreasing incompatible-element ratios associated with intervals of summit inflation and deflation (fig. 8).

Precise temporal correlations between this subtle petrogenetic signature and documented intrusive events and eruptive surges are clouded by the physical complexities of the dynamic open-system magmatic setting. The general tendency of these ratios to increase coincident with summit inflation, however, suggests that variably fractionated melts are incorporated during mixing between mantle-derived magma and pre-1983 near-cotectic magma residing within the edifice.
The feasibility of this shallow mixing hypothesis is supported by linear trends in plots of incompatible-element ratios versus incompatible elements for successive sampling intervals from February 1996 to October 2001. These trends can be extended back to 1982 summit magma compositions and are consistent with periods of summit inflation and deflation (fig. 9).

The short-term cycles of increasing and decreasing olivine-incompatible element ratios are superimposed on the long-term decrease in olivine-saturated magma delivered to the vent. It is unlikely that such frequent and erratic changes can be attributed to the mantle source of Kīlauea basalt. An interpretation involving a prolonged succession of short-term shallow mixing events may account for the long-term evolving magmatic condition. This interpretation does not require a gradual change in mantle-melting conditions over the 20-year duration of this eruption.

Is Evolution of Eruption Geochemistry Effected from the Bottom Up or from the Top Down?

Trace-element geochemical trends in lava erupted over the past two decades have been interpreted to reflect a gradual change in source melting components or processes in the mantle (Garcia and others, 1992, 1996, and 2000). Garcia and others presented justified and feasible geochemical models for the source evolution of Pu‘u ‘Ō‘ō-Kūpaianaha basalt. The models range from progressive depletion amid greater degrees of adiabatic melting of a constant mantle source to mixing of primitive melts derived from multiple and heterogeneous sources within the zone of mantle melting. Such changes of source conditions cannot be ruled out as factors affecting the systematic long-term decrease in olivine-incompatible element ratios. This trend, however, is consistent with an equally plausible process involving the evolution of an almost continuously recharged shallow magmatic plumbing system.

Subtle geochemical differences in terms of dynamic processes that persist in continuously fed, shallow magma chambers must be understood before ascribing dynamic source characteristics to monogenetic basalt eruption (O'Hara, 1977). The correlations of inflation-deflation cycles with incompatible-element geochemistry lend credibility to the idea that such changes in geochemistry reflect an evolution of shallow magmatic conditions during prolonged rift-zone eruption. If the temporal decrease of incompatible-element ratios were to be effected from the top down rather than from the bottom up, then the geochemical signature of this eruption would approach that of steady-state flux from a consistent and uniform mantle source.

Pietruzska and Garcia (1999b) provide minimal estimates of a 30- to 40-year residence time for late 20th century summit magma. By their reasoning, the 1982 summit eruption is representative of magma that may still reside in a summit reservoir, persisting at cotectic conditions (about 7 weight percent MgO). Geochemically, isotopically, and geophysically, the long-term trends of the Pu‘u ‘Ō‘ō-Kūpaianaha eruption can be explained by efficient turbulent mixing of chemically uniform recharge melt with diminishing proportions of 1982 summit magma maintained at near-cotectic conditions. The 20-year decline in ratios of highly to moderately incompatible elements may signify either that a progressively greater proportion of recharge magma is being diverted directly to Pu‘u ‘Ō‘ō, with minimal summit interaction, or that the mass ratio of those mixing end members has changed, owing to a shrinking summit chamber, or both. The coincidence of steady, long-term summit deflation since 1982 and the continuous trend of decreasing incompatible-element ratios and Pb isotopes in steady-state eruption products from those of 1982 summit magma (figs. 3, 4, 5 and 6)

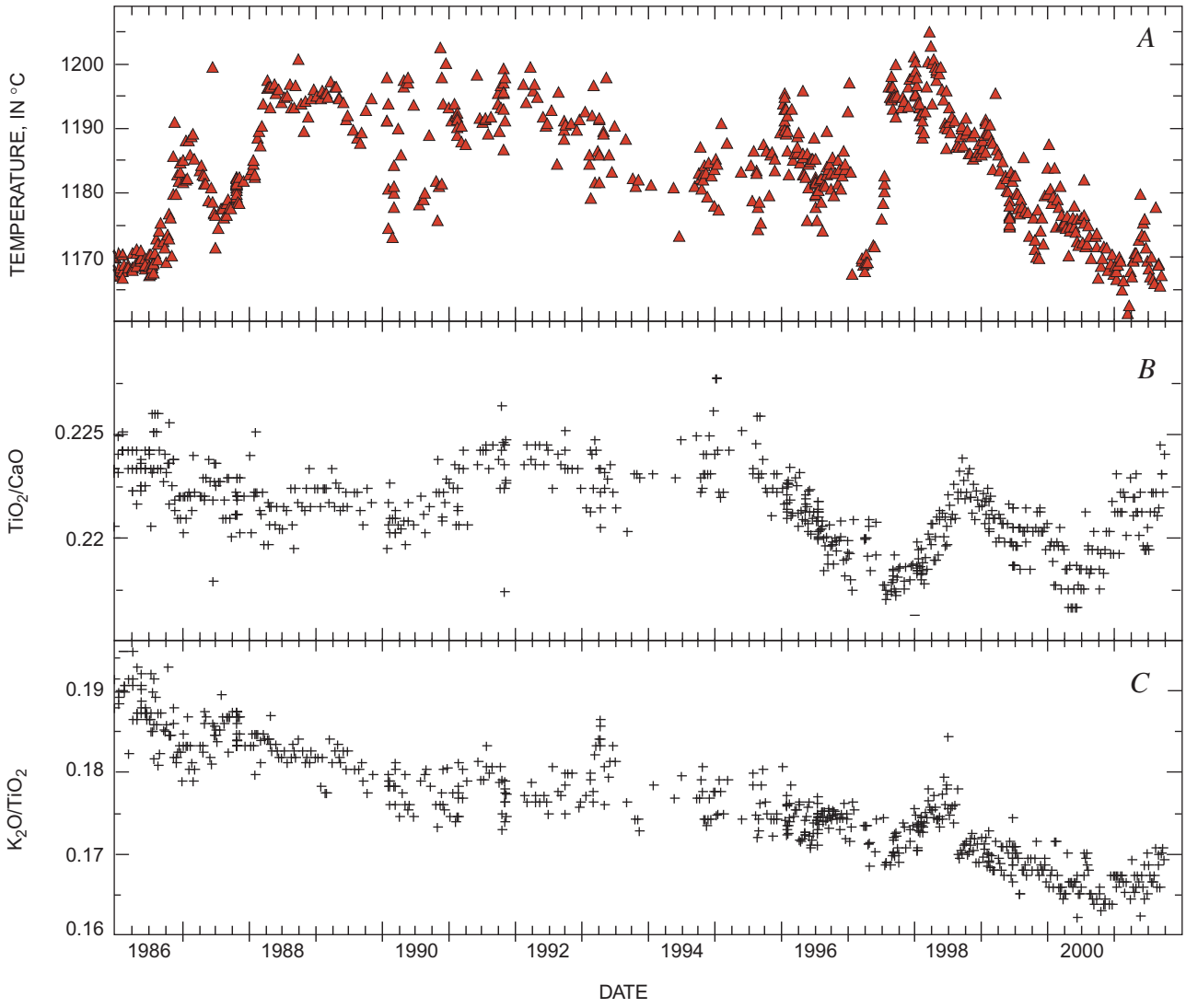

Figure 7. Time-series plots comparing inferred magmatic temperature and incompatible-element ratios of steady-state eruption products from January 1986 to October 2001. Original chemical data in weight percent. *A,* Magmatic temperature derived using bulk-lava MgO in MgO thermometry calculation of Helz and Thornber (1987), assuming melts have compositions equivalent to bulk lava (see Thornber, 2001). *B,* TiO_2/CaO (1-sigma error is 0.0004, based on reproducibility of this ratio in standard analyses over time). *C,* K_2O/TiO_2 (1-sigma error of 0.001).

suggest the possibility of a long-term evolution of erupted magma composition inherently linked to summit reservoir shrinkage.

To test this relation, parameters for a single spherical chamber of about 2–3 km^3 volume extending to 4 km depth (Pietruska and Garcia, 1999b) were used for geodetic modeling of recent cross-summit continuous GPS data (UWEV-AHUP line), combined with older leveling and electronic distance measurement (EDM) data across the summit, to yield a Mogi-modeled volume reduction of 2 percent per year since 1982 (M. Lisowski, written commun., June 2002). A similar volume reduction of about 2 percent per year is independently ascertained from the gradual change in La/Yb from September 1982 to October 2001. This result is achieved, using the

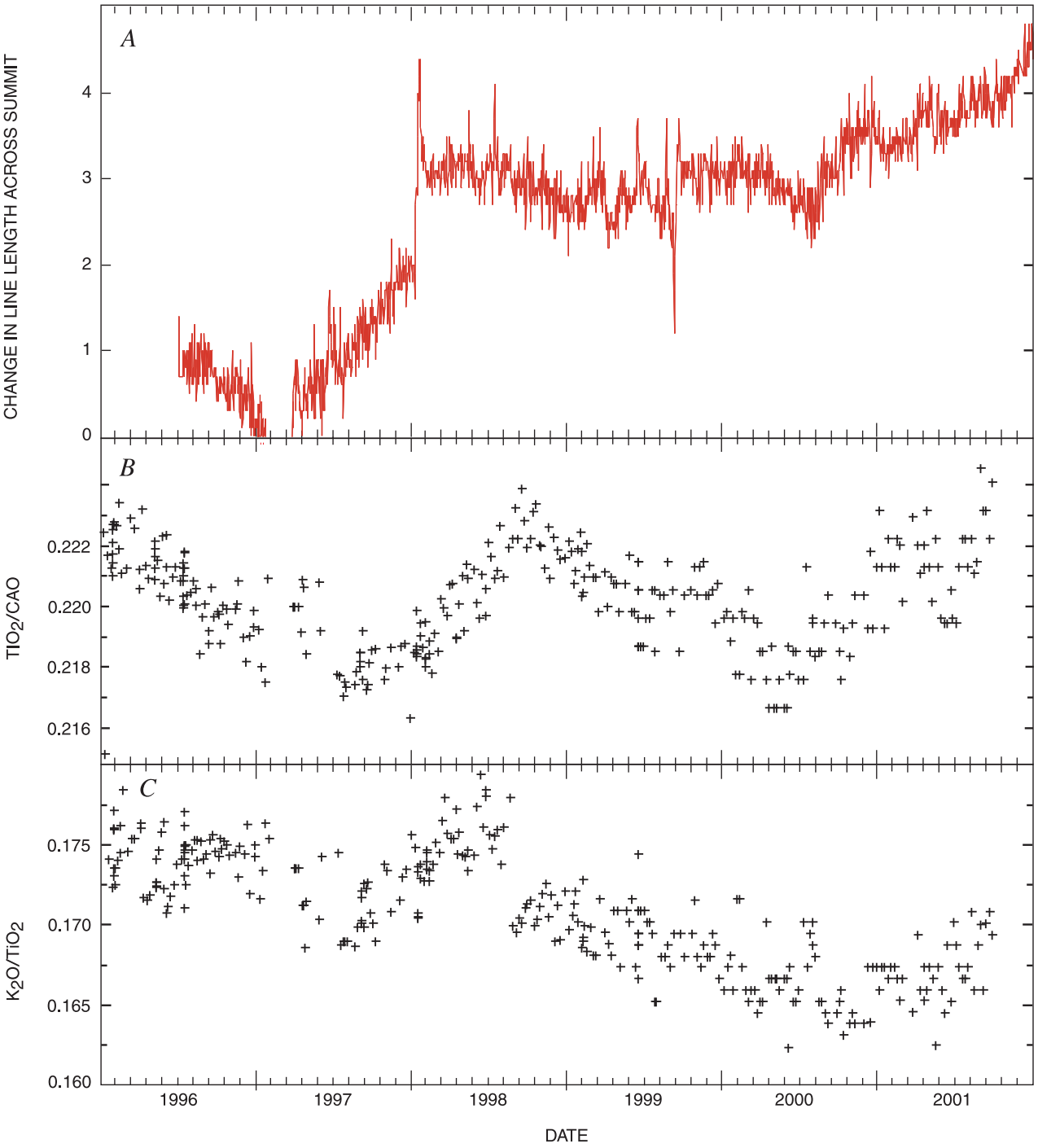

Figure 8. Time-series plots comparing summit deformation and incompatible-element ratios in lava produced during steady-state eruption from January 1996 to October 2001 (excluding episode 54). Original chemical data in weight percent. *A,* Continuous GPS measurement of line-length changes across summit. *B,* TiO_2/CaO (1-sigma error of 0.0004). *C,* K_2O/TiO_2 (1-sigma error of 0.001).

mixing equations presented in Pietruzska and Garcia (1999b), assuming that the 2001 end product is representative of chemically uniform and constant mantle flux of 0.1 km^3 per year. The mixing of 1982 and episode 55 end members is also reflected in the progressive change in incompatible trace-element patterns with time (fig. 5). Both deformation and petrologic models suggest that the eruption is an outlet for repeated flushing of magma that was resident within the edifice at the onset of near-continuous activity.

Further geochemical evidence for progressive batch mixing between 1982 summit magma and October 2001, episode 55 magma is suggested by linear relations between incompatible-element ratios and incompatible elements (fig. 10*A*). The array of K_2O/TiO_2 versus K_2O for steady-state eruptive products from late episode 48 through 53 and episode 55 straddles a mixing line between these end members, using binary mixing equations of Langmuir and others (1978). Likewise, a comparison of La/Yb versus Ce data from September 1982 summit magmas (Pietruszka and Garcia, 1999a) and the compositional range of steady-state eruption products defines a similar binary mixing relation between these temporally distinguished end members (fig. 10*B*). These relations verify the plausibility of a shallow mixing scenario, though they do not preclude a progressive change in source characteristics.

In this model of shallow, open-system magmatism, a zone of magmatic buffering between resident and recharge magma approaches a condition in which all of the resident magma is derived from a uniform long-term source. Intrusive recharge events enhance the efficiency of mixing and removal of a limited supply of pre-1983 cotectic magma, producing short-term cyclic increases of incompatible elements that are contrary to their overall long-term decrease. The net effect of prolonged magma supply and eruption is increasing efficiency of the plumbing system that transports mantle-derived melt into the shallow summit region and out through the east rift zone.

Summary

Correlations of geochemical and geophysical data indicate that three magma sources have contributed to the Pu‘u ‘Ō‘ō-Kūpaianaha eruption: (1) magma from a uniform mantle source, (2) pre-1983 summit magma, and (3) pre-1983 fractionated rift magma. Two processes are responsible for the array of non-olivine-controlled geochemical traits observed: turbulent mixing of old and new source magmas at the base of

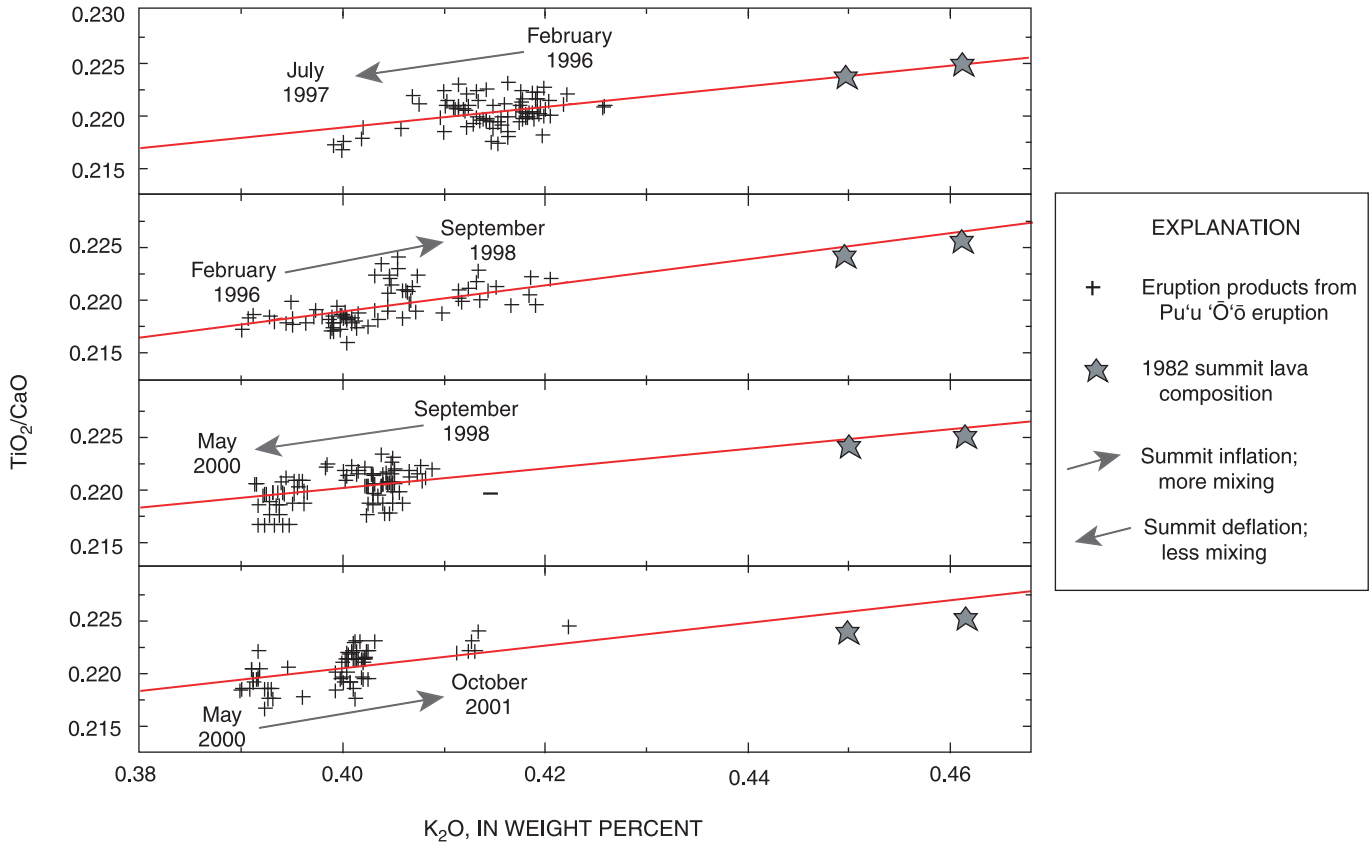

Figure 9. Plots comparing incompatible-element ratio (TiO_2/CaO) and incompatible-element (K_2O) content of steady-state eruption products from 1996 to 2001. Original chemical data in weight percent. Intervals shown correspond to cycles depicted in figure 8*B*. Red lines in each plot correspond to linear fit to eruption data, which project through or near 1982 summit composition and are consistent with binary mixing lines between averaged 1982 summit magma and episode 55 magma.

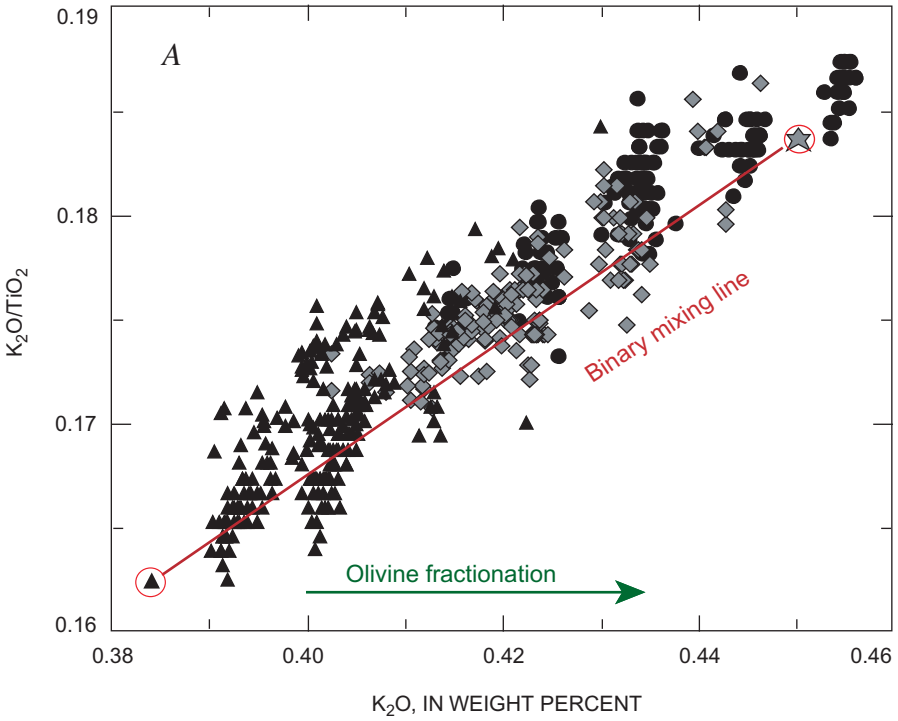

Figure 10. Variations of incompatible-element ratios, independent of olivine crystallization, in lava of episodes 48, 50–53, and 55 for *(A)* K_2O/TiO_2 versus K_2O and *(B)* La/Yb versus Ce. Symbols are same as in figures 1 and 2 and indicate progressive in compatible element ratio depletion in successive steady-state eruptive intervals. Red lines in each figure are calculated binary mixing lines between averaged 1982 summit magma and October 2001, episode 55 magma (see text). Trace-element data for 1982 summit magma are the averaged values of three September 1982 ICPMS analyses from Pietruszka and Garcia (1999a).

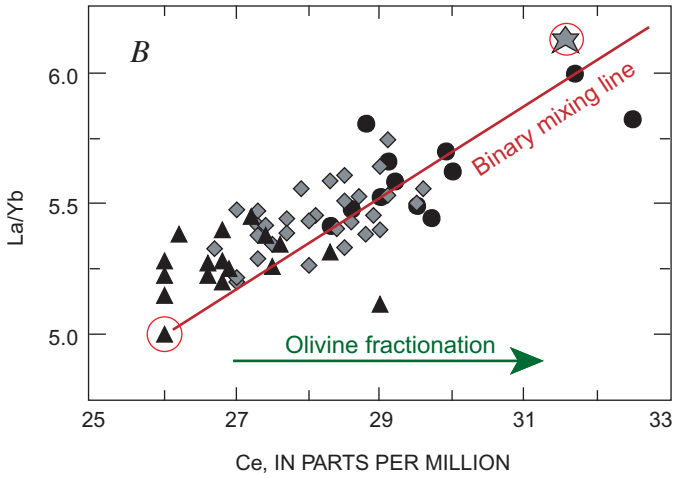

the summit reservoir, and mixing of summit-derived olivine-controlled magma with rift-fractionated magma.

Primitive magma, entering through the base of the summit region, is mixed with a reservoir of near-cotectic magma at 1- to 4-km depth. Such mixtures produce an intermediate range of olivine-saturated magma compositions that reflect the buffering capacity of the mixture before it is routed through the east rift zone to the vent. Near-equilibrium crystallization from the newly mixed olivine-saturated melt ensues with cooling during transport down the rift. The hottest magma tends to initiate compositional cycles of irregular duration, as vigorous eruption pulses occur in response to intrusive events at the summit. Subsequent cyclic change toward lower, near-cotectic magmatic temperatures is associated with periods of overall summit deflation, relatively low-level effusion, and frequent eruptive pauses. These short- and intermediate-term geochemical and eruptive cycles record the ebb and flow within a complex, delicately balanced, shallow plumbing system that is open to nearly continuous magmatic recharge.

Significant proportions of rift-stored magma were incorporated by more mafic magma immediately prior to geochemically aberrant and volumetrically insignificant eruptive intervals (episodes 1 to 3 and 54). As long as isolated pods of cooling magma exist near the active rift conduit, they may be flushed from the edifice by a near-continuous flux of magma derived from the summit region.

Geochemical variations observed throughout periods of prolonged rift-zone effusion constrain dynamic processes of recharge, assimilation, displacement, and eruption associated with a complex and continuously evolving shallow magmatic plumbing system. The consistent limits to repeated compositional and temperature variation of steady-state rift-eruption products are within the slightly larger range of historical summit lava. These limits of cyclic MgO variation define a persistent temperature range of olivine-saturated, end-member magmatic conditions regulated by recharge of the shallow magmatic plumbing system that feeds the prolonged eruption.

Cyclic variations in the concentrations of olivine-incompatible elements consistent with olivine-fractionation trends are superimposed upon cycles in which the relative concentrations of these elements increase and decrease, independent of subsequent crystallization of olivine. Variations in this compositional signature of erupted lava are interpreted to result from episodic assimilation of pre-1983 magma, maintained within the shallow edifice at near-cotectic conditions by long-term magmatic recharge. Repeated short-term assimilation cycles have resulted in the gradual flushing of a limited supply of older resident magma, as is reflected in the steady, long-term decrease in incompatible-element ratios and Pb isotopic ratios from values of magma last erupted at the summit in 1982.

This model of shallow magmatic processes accounts for the long-term evolution of erupted magma compositions and is consistent with 20-year trends in deformation of the shallow edifice. Amid nearly continuous magma influx, overall summit deflation requires a gradually diminishing volume of summit reservoir magma. Long-term summit deflation is accompanied by continual outward flank movement, which has accommodated an increasingly efficient magma conduit from the summit to the east rift zone. These overall trends in volcanic and magmatic behavior support an interpretation of prolonged effusive eruption approaching a steady-state tectonomagmatic condition in which magma derived from a uniform mantle source, having purged older resident magma, may now completely occupy the shallow magmatic plumbing system.

Acknowledgments

This work owes much to the vision of Ken Hon, who, in 1992, originated the HVO eruption database as an ongoing depository of geochemical analyses. In addition to myself and Ken Hon, other HVO staff geologists who collected lava samples used in this study include Christina Heliker, Ed Wolfe, George Ulrich, Maggie Mangan, Jim Kauahikaua, Dave Sherrod, Tari Mattox, Frank Trusdell, and Rick Hoblitt. I also acknowledge the collaborative contribution and precise analytical work of James Budahn (INAA), Ian Ridley (LAICPMS), and Dan Unruh (isotopic data). Thomas Wright and Wendell Duffield provided insightful and helpful reviews. Editorial revisions by Christina Heliker, Jane Takahashi, Jenda Johnson, and Don Swanson are greatly appreciated.

References Cited

Cashman, K.V., Thornber, C.R., and Kauahikaua, J.P., 1999, Cooling and crystallization of lava in open channels, and the transition of pāhoehoe to ʻaʻā lava: Bulletin of Volcanology, v. 61, no. 5, p. 306–323.

Cervelli, P.F., Segall, Paul, Amelung, Falk, Garbeil, Harold, Meertens, C.M., Owen, S.E., Miklius, Asta, and Lisowski, Michael, 2002, The 12 September 1999 Upper East Rift Zone dike intrusion at Kilauea Volcano, Hawaii: Journal of Geophysical Research, v. 107, no. B7, p. ECV 3–1 – ECV 3–13.

Clague, D.A., and Denlinger, R.P., 1994, Role of olivine cumulates in destabilizing the flanks of Hawaiian volcanoes: Bulletin of Volcanology, v. 56, no. 6–7, p. 425–434.

Clague, D.A., Moore, J.G., Dixon, J.E., and Friesen, W.B., 1995, Petrology of submarine lavas from Kilauea's Puna Ridge, Hawaii: Journal of Petrology, v. 36, no. 2, p. 299–349.

Dawson, P.B., Chouet, B.A., Okubo, P.B., Villeseñor, Antonio, and Benz, H.M., 1999, Three-dimensional velocity structure of the Kilauea caldera, Hawaii: Geophysical Research Letters, v. 26, no. 18, p. 2805–2808.

Defant, M.J., and Nielsen, R.L., 1990, Interpretation of open system petrogenetic processes; phase equilibria constraints on magma evolution: Geochimica et Cosmochimica Acta, v. 54, no. 1, p. 87–102.

Delaney, P.T., Denlinger, R.P., Lisowski, Michael, Miklius, Asta, Okubo, P.G., Okamura, A.T., and Sako, M.K., 1998, Volcanic spreading at Kilauea, 1976–1996: Journal of Geophysical Research, v. 103, no. B8, p. 18003–18023.

Denlinger, R.P., 1997, A dynamic balance between magma supply and eruption rate at Kilauea volcano, Hawaii: Journal of Geophysical Research, v. 102, no. B8, p. 18091–18100.

Denlinger, R.P., and Okubo P.G., 1995, Structure of the mobile south flank of Kilauea Volcano, Hawaii: Journal of Geophysical Research, v. 100, no. B12, p. 24499–24507.

Dzurizin, Daniel, Koyanagi, R.Y., and English, T.T., 1984, Magma supply and storage at Kilauea Volcano, Hawaii, 1956–1983: Journal of Volcanology and Geothermal Research, v. 21, no. 3–4, p. 177–206.

Garcia, M.O., Ho, R.A., Rhodes, J.M., and Wolfe, E.W., 1989, Petrologic constraints on rift-zone processes: Bulletin of Volcanology, v. 52, no. 2, p. 81–96.

Garcia, M.O., Pietruszka, A.J., Rhodes J.M., and Swanson, K.A., 2000, Magmatic processes during prolonged Pu′u ′O′o eruption of Kilauea Volcano, Hawaii: Journal of Petrology, v. 41, no. 7, p. 967–990.

Garcia, M.O., Rhodes, J.M., Trusdell, F.A., and Pietruszka, A.J., 1996, Petrology of lavas from the Puu Oo eruption of Kilauea Volcano; III. The Kupaianaha episode (1986–1992): Bulletin of Volcanology, v. 58, no. 5, p. 359–379.

Garcia, M.O., Rhodes, J.M., Wolfe, E.W., Ulrich, G.E., and Ho, R.A., 1992, Petrology of lavas from episodes 2–47 of the Puu Oo eruption of Kilauea Volcano, Hawaii; evaluation of magmatic processes: Bulletin of Volcanology, v. 55, no. 1–2, p. 1–16.

Garcia, M.O., and Wolfe, E.W., 1988, Petrology of the erupted lava, chap. 3 *of* Wolfe, E.W., ed., The Puu Oo eruption of Kilauea Volcano, Hawaii; episodes 1 through 20, January 3, 1983, through June 8, 1984: U.S. Geological Survey Professional Paper 1463, p. 127–143.

Gerlach, T.M., McGee, K.A., Elias, Tamar, Sutton, A.J., and Doukas, M.P., 2002, The carbon dioxide emission rate of Kīlauea Volcano; implications for primary magma CO_2 content and summit reservoir dynamics: Journal of Geophysical Research, v. 107, no. B9, 2189, doi:10.1029/2001JB000407.

Heliker, C.C., Mangan, M.T., Mattox, T.N., Kauahikaua, J.P., and Helz, R.T., 1998, The character of long-term eruptions; inferences from episodes 50–53 of the Puʻu ʻŌʻō-Kūpaianaha eruption of Kīlauea Volcano: Bulletin of Volcanology, v. 59, no. 6, p. 381–393.

Helz, R.T., and Thornber, C.R., 1987, Geothermometry of Kilauea Iki lava lake, Hawaii: Bulletin of Volcanology, v. 49, no. 5, p. 651–668.

Hoffmann, J.P., Ulrich, G.E., and Garcia, M.O., 1990, Horizontal ground deformation patterns and magma storage during the Puu Oo eruption of Kilauea volcano, Hawaii; episodes 22–42: Bulletin of Volcanology, v. 52, no. 6, p. 522–531.

Kauahikaua, J.P., Mangan, M.T., Heliker, C.C., and Mattox, T.N., 1996, A quantitative look at the demise of a basaltic vent; the death of Kupaianaha, Kilauea Volcano, Hawai‘i: Bulletin of Volcanology, v. 57, no. 8, p. 641–648.

Langmuir, C.H., Vocke, R.D., Jr., Hanson, G.N., and Hart, S.R., 1978, A general mixing equation with applications to Icelandic basalts: Earth and Planetary Science Letters, v. 37, no. 3, p. 380–392.

Mangan, M.T., Heliker, C.C., Mattox, T.N., Kauahikaua, J.P., and Helz, R.T., 1995, Episode 49 of the Pu‘u ‘O‘o-Kupaianaha eruption of Kilauea volcano—breakdown of a steady-state eruptive era: Bulletin of Volcanology, v. 57, no. 2, p. 127–135.

Mastin, L.G., Christiansen, R. L., Thornber, C.R., Lowenstern, J.B., and Beeson, Melvin, 2001, Evidence for incomplete magma degassing during hydromagmatic explosions that produced the Keanakako′i Ash, Kilauea Volcano, Hawaii [abs.]: Eos (American Geophysical Union Transactions), v. 82, no. 47, p. F1347–1348.

Murata, K.J., and Richter, D.H., 1966, Chemistry of the lavas of the 1959–60 eruption of Kilauea Volcano, Hawaii: U.S. Geological Survey Professional Paper 537–A, 26 p.

O’Hara, M.J., 1977, Geochemical evolution during fractional crystallization of a periodically refilled magma chamber: Nature, v. 266, no. 5602, p. 503–507.

O’Hara, M.J., and Mathews, R.E., 1981, Geochemical evolution in an advancing, periodically replenished, periodically tapped and continuously fractionating magma chamber: Journal of the Geological Society of London, v. 138, no. 3, p. 237–277.

Ohminato, Takao, Chouet, B.A., Dawson, Phillip, and Kedar, Sharon, 1998, Waveform inversion of very long period impulsive signals assoiciated with magmatic injection beneath Kilauea Volcano, Hawaii: Journal of Geophysical Research, v. 103, no. B10, p. 23839–23862.

Okamura, A.T., Dvorak, J.J., Koyanagi, R.Y., and Tanigawa, W.R., 1988, Surface deformation during dike propagation, chap. 6 *of* Wolfe, E.W., ed., The Puu Oo eruption of Kilauea Volcano, Hawaii; episodes 1 through 20, January 3, 1983, through June 8, 1984: U. S. Geological Survey Professional Paper 1463, p. 165–182.

Owen, S.E., Segall, Paul, Lisowski, Michael, Miklius, Asta, Murrray, Michael, Bevis, M.G., and Foster, James, 2000, January 30, 1997 eruptive event on Kilauea Volcano, Hawaii, as monitored by continuous GPS: Geophysical Research Letters, v. 27, no. 17, p. 2757–2760.

Pietruszka, A.J., and Garcia, M.O., 1999a, A rapid fluctuation in the mantle source and melting history of Kilauea Volcano inferred from the geochemistry of its historical summit lavas (1790–1982): Journal of Petrology, v. 40, no. 8, p. 1321–1342.

Pietruszka, A.J., and Garcia, 1999b, The size and shape of Kilauea Volcano’s summit magma storage reservoir; a geochemical probe: Earth and Planetary Science Letters, v. 167, no. 3–4, p. 311–320.

Rhodes, J.M., 1995, The 1852 and 1868 Mauna Loa picrite eruptions; clues to parental magma compositions and the magmatic plumbing system, *in* Rhodes, J.M., and Lockwood, J.P., eds., Mauna Loa revealed; structure, composition, history, and hazards: American Geophysical Union Geophysical Monograph 92, p. 241–262.

Rhodes, J.M., and Hart, S.R., 1995, Episodic trace element and isotopic variations in historical Mauna Loa lavas; implications for magma plume dynamics, *in* Rhodes, J.M., and Lockwood, J.P., eds., Mauna Loa revealed; structure, composition, history, and hazards: American Geophysical Union Geophysical Monograph 92, p. 263–288.

Sharma, Kirti, Self, Stephen, Thornber, C.R., and Keszthelyi, L.P., 1999, Textural variations through inflated pahoehoe flow lobes from Kilauea, Hawaii [abs.]: Eos (American Geophysical Union Transactions), v. 80, no. 46, supp., p. F1090.

Sun, S.-S., and McDonough, W.F., 1989, Chemical and isotopic systematics of oceanic basalts; implications for mantle composition and processes, *in* Saunders, A.D., and Norry, M.J., eds., Magmatism in the ocean basins: Geological Society Special Publications, v. 42, p. 313–345.

Thompson, R.N., and Tilley, C.E., 1969, Melting and crystallisation relations of Kilauean basalts of Hawaii; the lavas of the 1959–60 Kilauea eruption: Earth and Planetary Science Letters, v. 5, no. 7, p. 469–477.

Thornber, C.R., 2001, Olivine-liquid relations of lava erupted by Kīlauea Volcano from 1994–1998; implications for shallow magmatic processes associated with the ongoing east-rift-zone eruption: Canadian Mineralogist, v. 39, no. 2, p. 239–266.

Thornber, C.R., Heliker, C.C., Sherrod, D.R., Kauahikaua, J.P., Miklius, Asta, Okubo, P.G., Trusdell, F.A., Budahn, J.R., Ridley, W.I., and Meeker, G.P., in press, Kilauea east rift zone magmatism; an episode 54 perspective: Journal of Petrology.

Thornber, C.R., Sherrod, D.R., Siems, D.F., Heliker, C.C., Meeker, G.P., Oscarson, R.L., and Kauahikaua, J.P., 2002, Whole-rock and glass major-element geochemistry of Kilauea Volcano, Hawaii, near-vent eruptive products; September 1994 through September 2001: U.S. Geological Survey Open-File Report 02–17, 41 p.

Tilling, R.I., and Dvorak, J.J., 1993, Anatomy of a basaltic volcano: Nature, v. 363, no. 6425, p. 125–132.

Wolfe, E.W., Garcia, M.O., Jackson, D.B., Koyanagi, R.Y., Neal, C.A., and Okamura, A.T., 1987, The Puu Oo eruption of Kilauea Volcano, episodes 1–20, January 3, 1983 to June 8, 1984, chap. 17 *of* Decker, R.W., Wright, T.L., and Stauffer, P.H., eds., Volcanism in Hawaii: U.S. Geological Survey Professional Paper 1350, v. 1, p. 471–508.

Wolfe, E.W., Neal, C.A., Banks, N.G., and Duggan, T.J., 1988, Geologic observations and chronology of eruptive events, chap. 1 *of* Wolfe, E.W., ed., The Puu Oo eruption of Kilauea Volcano, Hawaii; episodes 1 through 20, January 3, 1983, through June 8, 1984: U. S. Geological Survey Professional Paper 1463, p. 1–97.

Wright, T.L., 1971, Chemistry of Kilauea and Mauna Loa lava in space and time: U.S. Geological Survey Professional Paper 735, 40 p.

Yang, H.-J., Kinzler, R.J., and Grove, T.L., 1996, Experiments and models of anhydrous, basaltic olivine-plagioclase-augite saturated melts from 0.001–10kbar: Contributions to Mineralogy and Petrology, v. 124, no. 1, p. 1–18.

Lava-Effusion Rates for the Pu‘u ‘Ō‘ō-Kūpaianaha Eruption Derived from SO_2 Emissions and Very Low Frequency (VLF) Measurements

By A. Jeff Sutton, Tamar Elias, *and* Jim Kauahikaua

Abstract

Lava-effusion rates have been estimated on a regular basis throughout the Pu‘u ‘Ō‘ō-Kūpaianaha eruption by several techniques, including mapping of lava-flow surface area and thickness, very low frequency (VLF) electromagnetic-profiling measurements over active lava tubes, and measurements of SO_2 discharge. Together, these three techniques indicate that Kīlauea erupted roughly 0.13 km^3/yr or about 2.4 to 2.6 km^3 of dense-rock-equivalent (DRE) lava between January 1983 and May 2002. VLF and SO_2 measurements produce total-volume estimates for the eruption within 10 percent of each other. SO_2- and VLF-derived lava-effusion rates are statistically correlated at the 99-percent-confidence level for the extent of both datasets but show the best agreement for the period 1997–2002, when sampling density for both datasets was highest and activity varied; they produced instantaneous lava-effusion rates episodically exceeding 1 million m^3d^{-1} per day. The data, which are consistent with magma at a CO_2-equilibration depth of 1.0 to 1.5 km, may indicate the minimum depth of the duct feeding magma in the east rift zone. The reliability of east rift SO_2 data, in combination with a rapidly evolving technology for inexpensively and remotely measuring plume SO_2, points toward the practical application of this technique to continuously monitor lava-effusion rates during this and similar eruptions.

Introduction

Knowledge of lava-effusion rates is a key to understanding magma supply and transport and for improving real-time lava-flow-hazard assessments. From January 1983 to July 1986, lava-effusion rates for the Pu‘u ‘Ō‘ō-Kūpaianaha eruption were derived by using the duration of discrete eruptive intervals and the lava volume calculated from the mapped area and thickness of the flows produced (Ulrich and others, 1984, 1985, 1987; Wolfe, 1988; Ulrich and others, written commun., 2002; see Heliker and others, this volume). This approach was effective during the period of episodic fountaining that characterized the first 3.5 years of the eruption, because the lava flows during each episode could be completely mapped and because the episodes had specific start and end times. This technique could no longer be easily applied, however, when the style of the eruption changed to continuous, lower-rate effusion that built the shield around the Kūpaianaha vent. A substantial amount of the volume increase of the shield was endogenous and difficult to measure, particularly during 1987. During the same year, lava carried by newly developed tubes reached the sea and so could not be quantified by surface mapping. New techniques to estimate lava-effusion rates were needed.

In this chapter, we describe the methods used to derive lava-effusion rates from eruptive-gas emissions and measurements of the volume rate of flow through lava tubes. We also present a comprehensive record of annual lava-effusion rates obtained by these techniques throughout the current east-rift-zone eruption and compare them with the rates obtained by traditional mapping methods.

Background and Methods

Jackson and others (1988) showed that very low frequency (VLF) electromagnetic profiling could be used at Kīlauea to quantify the instantaneous volume rate of flow through a lava tube. Kauahikaua and others (1996) improved the technique and, by intensive monitoring throughout 1991, used it to accurately predict the February 1992 demise of the Kūpaianaha vent. Since that time, VLF profiling has been used routinely to estimate lava-effusion rates for the eruption and to map active tubes as deep as 20 m beneath the ground surface (Kauahikaua and others, 1998).

The volume rate of lava flow through a tube can be estimated by using the VLF electromagnetic technique (Zablocki, 1978). The measurements consist of sets of data obtained on a profile over the tube. These data are reduced by using an empirical relation (Kauahikaua and others, 1996) to a single estimate of cross-sectional area of fluid of an assumed

electrical conductivity in the tube. A flow velocity can be measured either by timing the transit of objects or by using a Doppler radar gun, if there is a skylight nearby where the lava stream is actually visible. The product of the average flow velocity and cross-sectional area results in an estimate of the volume rate of lava flow through the tube at that site, typically reported as the dense-rock-equivalent (DRE) lava-effusion rate (Kauahikaua and others, 1996; Heliker and others, 1998, and this volume).

VLF data not previously published are included here from monthly summaries and, in some cases, more frequent field measurements (J.P. Kauahikaua, unpub. data, 1997, 2001–2).

Lava-effusion rates may also be estimated by using geochemical data related to measured eruptive-gas release (Greenland and others, 1988; Andres and others, 1989; Sutton and others, 2001). Mass-balance calculations give a CO_2 content of 0.0195 weight percent for early production of lava from the eruption, corresponding to the shallowest equilibration depth of 1.0 to 1.5 km reached within the summit reservoir or during transport down the rift zone (Gerlach and Graeber, 1985; Gerlach, 1986). Bottinga and Javoy (1991) estimated the CO_2 content at 0.021 weight percent, and Greenland at 0.02 weight percent (Greenland and others, 1985, 1988). Essentially all of this CO_2 is lost on eruption after migration down the rift zone. This observation, in combination with the CO_2/SO_2 molar ratio measured in eruptive-gas samples along the rift zone and the east-rift-zone SO_2-emission rate, can be used to estimate the lava-effusion rate, using the equation

$$W_{CO_2}/W_{SO_2} = [CO_2/SO_2]\,(f_{CO_2}/f_{SO_2}), \quad (1)$$

where W_{CO_2}/W_{SO_2} is the eruptive CO_2/SO_2 weight-fraction ratio, $[CO_2/SO_2]$ is the average molar eruptive-gas ratio, and f_{CO_2}/f_{SO_2} is the ratio of their formula weights. Solving equation 1 for W_{SO_2} yields

$$W_{SO_2} = ([SO_2/CO_2]\,(f_{SO_2}/f_{CO_2}))\,W_{CO_2} \quad (2)$$
$$= 1.49 \text{ kg } SO_2 \text{ released per tonne of lava erupted.}$$

We calculated W_{SO_2} by using $[CO_2]/[SO_2]=0.19\pm0.01$, the average of 204 analyses of eruptive gas collected from the east-rift-zone eruption site. These analyses, which were carried out by several investigators from 1983 to 1997, were summarized by Gerlach and others (1998).

Knowing the value of W_{SO_2}, the volume of DRE lava discharged and degassed on eruption, V_m, is related to the mass of SO_2 emitted, E_{SO_2}, by the equation

$$E_{SO_2} = V_m\, W_{SO_2}\, \rho_m \quad (3)$$

Kīlauea's SO_2 emissions during the Pu'u 'Ō'ō-Kūpaianaha eruption have been measured on a nearly weekly basis by using correlation spectrometry (COSPEC) (Casadevall and others, 1987; Elias and others, 1998; Sutton and others, 2001; Elias and Sutton, 2002). The void-free lava density, ρ_m, is taken as 2.8 ± 0.1 t/m^3, on the basis of the DRE densities of the glassy rinds of 24 lavas from Kīlauea's submarine east rift zone (Clague and others, 1995). Rearranging equation 3 to solve for V_m, we obtain

$$V_m = E_{SO_2}/(W_{SO_2}\,\rho_m), \quad (4)$$

where $(W_{SO_2}\,\rho_m)^{-1}$ is a degassing constant, for the current eruption equal to 233 ± 80 m^3 of lava per tonne of SO_2. If we call this value K_d, then from COSPEC-based measurements of E_{SO_2} and the equation

$$V_m = E_{SO_2}\,K_d, \quad (5)$$

we can estimate east-rift-zone lava-effusion rates for this eruption. In an earlier report, Sutton and others (2001) calculated SO_2-derived lava-effusion rates by using a preliminary K_d value of 207.

Estimates of the lava-effusion rate based on intermittent SO_2 emission-rate measurements using equations 1 through 5 are necessarily inexact. In equation 5, we estimate the uncertainty in E_{SO_2} as typical for COSPEC measurements, at about 20 percent, and that of K_d at about 35 percent, largely owing to the uncertainty in W_{CO_2} and ρ_m. The absolute value of the constant W_{CO_2}, in particular, strongly affects K_d. Thus, we estimate the absolute uncertainty in V_m at about ±40 percent. Because both W_{CO_2} and ρ_m are constants, we expect the precision of our reported lava-effusion rates to be substantially better, likely closer to ±30 percent.

The earliest lava-effusion rates calculated by using equation 5 use COSPEC data collected in September 1986 for this study. From 1986 to 1991, we used emission data recorded at the Pu'u 'Ō'ō cone, even though the main eruptive vent was Kūpaianaha, 3 km downrift, because the cone continued to act as a degassing chimney for magma that passed beneath it on the way to the Kūpaianaha vent. The lava-effusion rates through 2001 are derived from SO_2-emission measurements included in previously published reports (Elias and others, 1998; Elias and Sutton, 2002), and those for 2002 are based on USGS-HVO data.

An instrumental data set spanning more than 15 years inevitably incorporates changes, generally from improvements in method and processing techniques. Changes also occur as investigators respond to variations in the system under study, and conclusions based on long-time-series data sets must take these changes into account. For example, we have learned that east-rift-zone lava-emission rates calculated from near-vent, tripod-based COSPEC data are generally lower than those based on vehicle measurements along Chain of Craters Road (Andres and others, 1989; Elias and others, 1998; Sutton and others, 2001; Elias and Sutton, 2002). Because routine Chain of Craters Road measurements did not begin until 1992, emission-rate data from early in the eruption are all near-vent and tripod-based. In their raw form, these data likely represent a minimum estimate of east-rift zone SO_2 emissions.

We therefore applied a correction factor to SO_2-emission data from 1986 to 1991 based on comparisons showing that the Chain of Craters Road vehicle-based emission rates were

2.1 times higher than the tripod-based emission rates on contemporaneous days (r=0.95). This relation, which was established by using the small available number of paired data points (n=7), brackets the 1986–91 range of data values. We believe that the corrected tripod data, though not as reliable as data obtained along Chain of Craters Road, more reasonably represent the total east-rift-zone SO_2 emissions than do the raw, east-rift-zone tripod-based rates themselves.

Results and Discussion

The Big Picture: Annual Pu‘u ‘Ō‘ō-Kūpaianaha Lava-Effusion Rates, 1983–2002

Table 1, which summarizes void-free lava (DRE) lava-effusion rates based on COSPEC, mapping, and VLF measurements for January 1983 through mid-May 2002, is organized in two sections: SO_2 plus mapping-derived effusion rates and VLF plus mapping-derived effusion rates. It includes descriptive statistics for SO_2- and VLF-derived lava-rates on a cubic-meters-per-day basis.

We estimated the integrated annual discharges listed in table 1 by applying the nonparametric digital filter (NPDF) contained in the Peakfit software (version 4, Jandel Scientific, San Rafael, California) to generate a refined data set with an evenly spaced (daily) time base from the intermittent measurements. Using the NPDF, generating one data point per day simplified exact annual integrations for the years when data were not obtained precisely on the first and last days of the year. Integration of each year of daily values yielded the annual estimates. Annual integrations for the data filtered with the NPDF agreed with nonfiltered data within 1 percent. Lava-effusion rates for the first 19.5 years of the eruption peaked in 1998, at about 0.19 km^3/yr, and were lowest during the first three years, at about 0.11 km^3/yr.

The data listed in table 1 show that Kīlauea has discharged a total of about 2.4 to 2.6 km^3 of lava in the 19.5 years of the current eruption. Our estimates, based on mapping plus VLF profiling and mapping plus SO_2 profiling, yield integrated lava-effusion rates for the eruption that agree within 10 percent.

The data plotted in figure 1 and listed in table 1 show how the respective estimates of lava-effusion rates and sampling frequencies compare for each year. No VLF or surface-mapping measurements were available for the period 1989–90, when much of the lava produced by the eruption

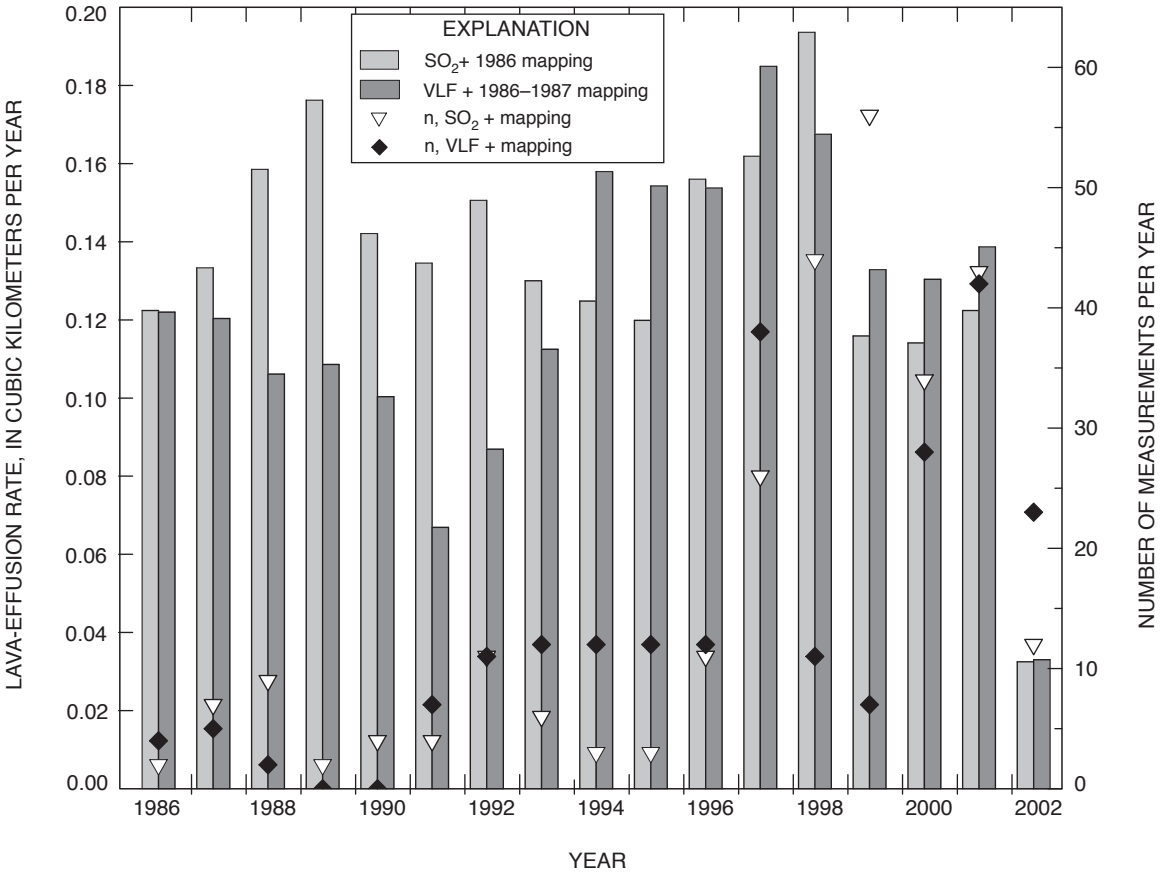

Figure 1. Integrated annual lava-effusion rates derived from SO_2-emission rates plus 1986 mapping data, and very low frequency (VLF) electromagnetic profiling plus 1986–87 mapping data, and number of samples (n) for each year.

Table 1. Annual effusion rates for the Pu‘u ‘Ō‘ō-Kūpaianaha eruption, 1983 through mid-2002.

[From 1983 to mid-1986, effusion rates were calculated solely on mapped flow area and thickness. SO_2-emission measurements began in September 1986. Very low frequency (VLF) electromagnetic profiling began in 1991, except for two data points in 1988, and continued through mid-May 2002. All lava-effusion rates listed in dense-rock equivalent (DRE). Shaded area of table (1983 through mid-1986 and 1987 includes flow-mapping data adapted from Ulrich and others (1985, 1987, 2002), Wolfe and others (1987, 1988, written commun., 2002), and Heliker and Mattox (this volume). Minimum, maximum, mean, and SD (standard deviation) values derived from N field data points processed with a non-parametric digital filter to obtain a daily rate.]

	SO_2-emission-rate and mapping-derived lava-effusion rates						VLF electromagnetic profiling-derived lava-effusion rates					
	Total volume	Daily lava effusion rate (10^5)					Total volume	Daily lava effusion rate (10^5)				
Year	(km^3)	Minimum	Maximum	Mean	SD	n	(km^3)	Minimum	Maximum	Mean	SD	n
1983	0.11	--	--	--	--	--	0.11	--	--	--	--	--
1984	.10	--	--	--	--	--	.10	--	--	--	--	--
1985	.11	--	--	--	--	--	.11	--	--	--	--	--
1986	.12	--	--	--	--	--	.12	--	--	--	--	--
1987	.13	2.80	4.63	3.67	.56	7	.12	--	--	--	--	--
1988	.16	3.36	5.76	4.34	.33	9	.10	2.53	2.77	2.63	.56	2
1989	.18	4.41	5.12	4.84	.18	2	.10	2.69	2.73	2.71	.12	0
1990	.14	3.27	4.70	3.90	.44	4	.10	2.73	2.77	2.76	.11	0
1991	.13	3.44	4.06	3.69	.36	4	.07	0.70	2.76	1.84	.76	7
1992	.15	2.14	6.42	4.12	.95	11	.09	1.33	2.75	2.38	.48	11
1993	.13	1.24	4.63	3.57	.85	6	.11	2.65	3.89	3.09	.30	12
1994	.12	3.16	3.60	3.43	1.12	3	.16	3.00	5.00	4.33	.74	12
1995	.12	2.83	4.35	3.30	.37	3	.15	3.02	5.58	2.56	.55	12
1996	.16	1.98	5.48	4.27	.68	11	.15	4.06	4.64	4.22	.16	12
1997	.16	0.33	15.86	4.45	3.37	26	.18	0.95	7.48	5.08	1.83	38
1998	.19	3.44	9.00	5.32	1.16	44	.17	3.03	8.08	4.60	1.28	11
1999	.12	1.72	5.39	3.18	1.10	56	.13	2.99	4.23	3.65	.41	7
2000	.11	2.26	4.07	3.13	.48	34	13	1.12	5.06	3.57	.48	28
2001	.12	1.98	9.10	3.36	.92	43	.14	2.88	4.73	3.81	.51	42
2002	.03	0.42	3.34	2.41	0.37	12	.03	1.37	3.74	2.43	.64	23
Totals	2.62						2.38					

flowed directly into the sea. Thus, SO_2-derived lava-effusion rates were the only measure of lava effusion during these 2 years; the VLF-mapping values in figure 1 and table 1 are interpolated. The sampling frequency for both techniques has increased since 1996, as has overall agreement between the SO_2- and VLF-derived data sets.

The average SO_2- and VLF-derived annual lava-effusion rates for the 19.5-year duration of this study, of 0.13 and 0.12 km^3/yr, are similar to the rate of 0.12 km^3/yr reported by Swanson (1972) for the Halemaumau eruption of 1967–68 and the first 7 months of the Mauna Ulu eruption of 1969. They also compare well with the overall lava-effusion rate of 0.11 km^3/yr reported by Swanson for sustained eruptions during the 19-year period beginning in 1952. Dvorak and Dzurisin (1993), who studied both eruption rate and magma-supply rate at Kīlauea over the past 160 years, reported that an average and fairly constant magma-supply rate of 0.09 km^3/yr has been characteristic for sustained eruptive periods at Kīlauea since 1950. More recently, Cayol and others (2000) calculated an average magma-supply rate to Kīlauea between 1961 and 1991 of 0.18 km^3/yr. This value, 50 percent more than the previous estimate (Swanson, 1972), would—given our measured lava-effusion rate—require that much of the magma supplied to Kīlauea has been stored in the rift zones. Gerlach and others (2002) showed that a magma supply rate of 0.18 km^3/yr is supported by an attendantly high CO_2-emission rate from Kīlauea's summit.

Shorter-Term Variation: Daily Lava-Effusion Rates, 1986–2002

Raw, intermittent-time series of daily estimates for SO_2- and VLF-derived lava-effusion rates show a short-term variation (fig. 2*A*). Both figure 2*A* and the FFT-smoothed traces in figure 2*B* show the good overall agreement of the two data sets, with visibly improved tracking during years when sampling density is higher. A notable discrepancy between the VLF- and SO_2-derived lava-effusion rates occurs from 1988 through 1991, when SO_2-derived lava-effusion rates exceed those based on VLF and mapping. Just previously, substantial endogenous shield building occurred at Kūpaianaha, culminating in lava extrusion from the base of the shield (Heliker and Wright, 1991). The volume of endogenous shield growth was difficult to quantify. During this period, SO_2 emissions at Kīlauea's summit, 23 km uprift, were the highest recorded since the eruption began, possibly indicating increasing magma throughput in the summit reservoir (Sutton and others, 2001). Unfortunately, few mapping-derived lava-volume estimates, no VLF lava-effusion data, and only a few measurements of SO_2-emission rate were available for this period.

Notably, a decrease in the SO_2-derived lava-effusion rate did not accompany the decline in lava extrusion at Kūpaianaha in 1991 as tracked by VLF profiling (Kauahikaua and others, 1996). Kūpaianaha may have been shutting down as new magma was aseismically intruding and degassing in and near the Pu'u 'Ō'ō edifice, priming the middle east rift zone for episode 49 in November 1991 (Mangan and others, 1995).

The period of more frequent measurements, including 1996 through 2002, is shown in figure 3. Both techniques captured the eruptive pause and slow restart after episode 54 in early 1997 (Thornber and others, 1997). In late 1997, SO_2 and VLF data recorded some of the highest extrusion rates since the continuously effusive stage of the eruption began in 1986. These high lava-effusion rates, more than 1 million m^3/d, were mirrored by the eruptive activity as Pu'u 'Ō'ō's crater filled and overflowed for the first time since 1986 (Heliker and others, 1997). Flank vent activity and shield building on the cone also increased.

Correlation of SO_2-and VLF-Derived Lava-Effusion Rates: Statistical Considerations

We examined the SO_2 and VLF time series statistically for two periods: (1) 1991–2002, the entire duration of simultaneous VLF and SO_2 data collection; and (2) 1996–2002, a subset of more frequent data collection and the period of greatest variation for both the VLF and SO_2 time series. SO_2 data were seldom collected on the same day as VLF data, and so we interpolated each data set by using Peakfit's NPDF to produce two identically spaced time series, at the smaller data-point sample size of the VLF data set.

Linear regression shows that both data subsets correlate significantly at both the 95- and 99-percent-confidence levels. The subset of more frequently obtained data in 1996–2002 produced the most significant linear correlation, with r=0.53, between SO_2-and VLF-derived lava-effusion rates at the 99-percent-confidence level. The regression and residual plots and statistics for these two periods are plotted in figure 4 and listed in table 2. The slope of the regression plot, 0.75, is not

Table 2. Parameters for linear regression $y=a+bx$, where y is the SO_2-emission-rate-derived lava-effusion rate, x is the very low frequency (VLF) electromagnetic-profiling-derived lava-effusion rate, and b is the slope $d(SO_2)/d(VLF)$.

[The two time periods were chosen based on sampling frequency and eruptive activity.]

	Time Period	
Parameter	3/1991–5/2002	1/1996–5/2002
Intercept, a	238,211	78,334
Slope, b	0.36	0.75
Correlation coefficient, r	.34	.53
Coefficient of determination, r_2	.12	.28
Degrees of freedom	213	121
Critical r at 99 percent confidence	.181	.228
Critical r at 95 percent confidence	.138	.174

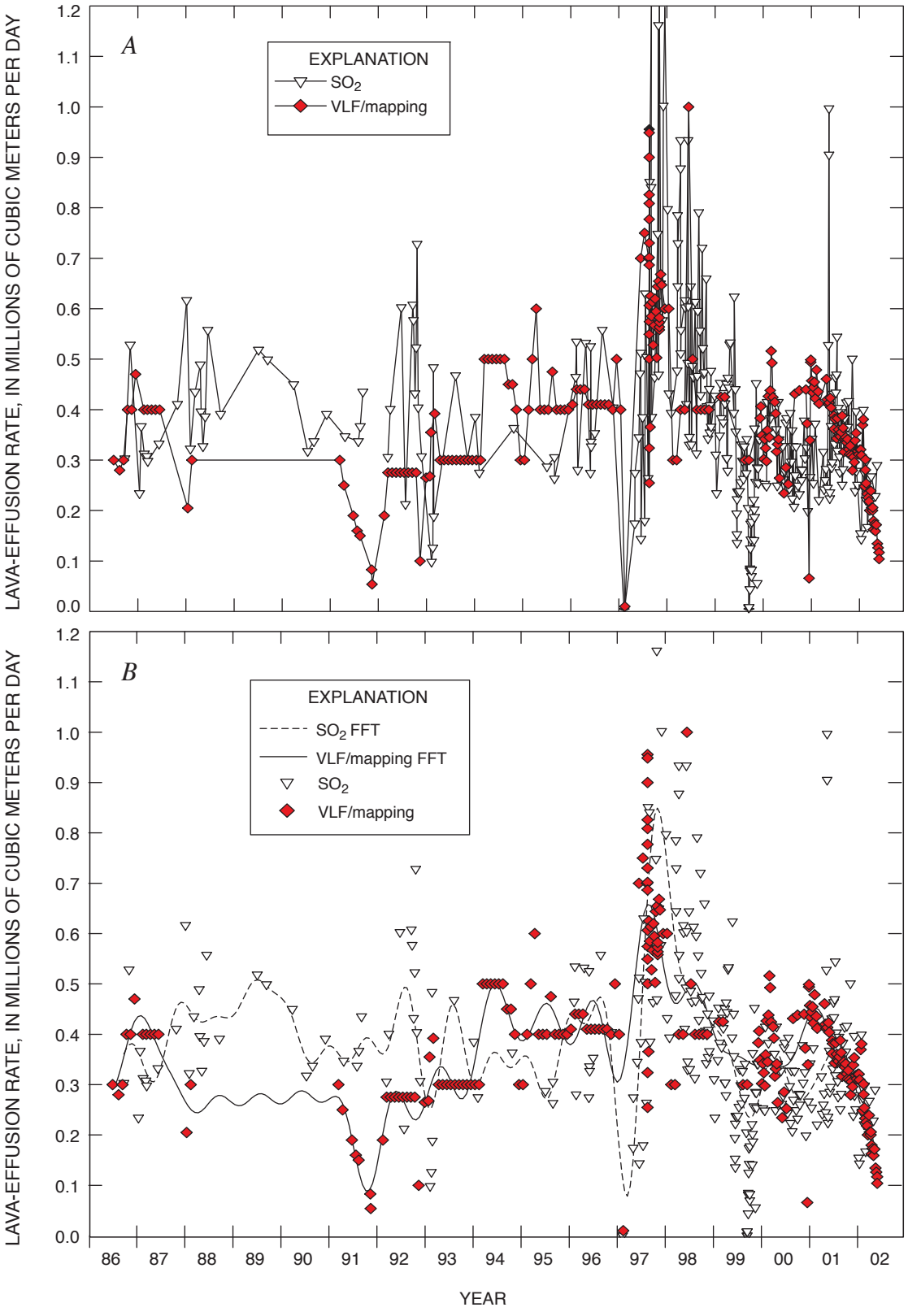

Figure 2. Long-term change in lava-effusion rate over time. *A*, SO_2-emission-rate-based and very low frequency (VLF) electromagnetic-profiling-based estimates of lava-effusion rate. Except for two measurements in 1988, VLF profiling plus mapping measurements reported before 1991 are based on mapping data only. Monthly lava-flux estimates from these data are used through 1996 and individual measurements for 1997–2002. SO_2-emission rates use east-rift-zone vehicle-based data (1992–2002) and corrected, tripod-mounted correlation-spectrometric (COSPEC) data (1986–91). *B*, Raw data (triangles and diamonds) were fast Fourier transform (FFT)- smoothed to produce dashed and solid lines that show data trends.

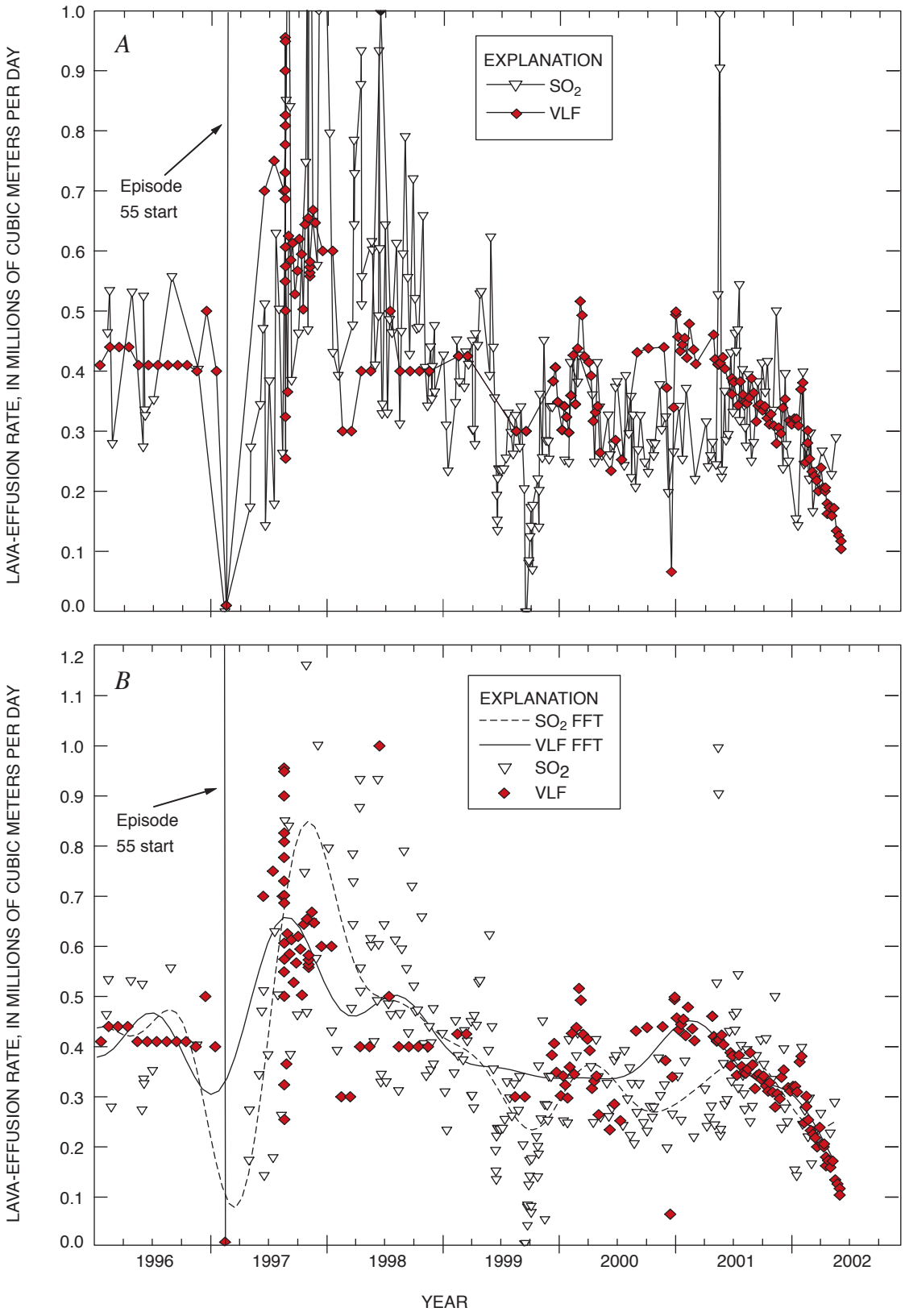

Figure 3. Short-term change in effusion rate over time. *A*, Comparison of SO_2-emission-rate-derived and very low frequency (VLF) electromagnetic-profiling-derived lava-effusion rates shows that effusion rates climbed markedly through third quarter of 1997. During this period, Pu‘u ‘Ō‘ō’s crater and flank-vent activity increased, and lava eventually overflowed crater. Tracking for these two data sets improved markedly as sampling frequency increased. *B,* Raw data (triangles and diamonds) were fast Fourier transform (FFT)-smoothed to produce dashed and solid lines that more clearly show data trends.

unity as for a perfect correlation, but the intercept of 0.07 million m^3/d is fairly close to 0 for data sets ranging as high as 0.9 million m^3/d for the interpolated data.

The regression residuals for both periods show a maximum deviation at high lava-effusion rates. These results are expected because high variation in both the SO_2 and VLF data accompanied the large (up to 1.0 million m^3/d) lava-effusion rates observed. The absence of precisely coincident VLF and SO_2 data degrades the overall correlation and magnifies the problem of deviating residuals. The large variation during a high-effusion-rate event recorded in August 1997, using the VLF technique, is plotted in figure 5. This large variation, 0.7 million m^3/d, constitutes 75 percent of the total signal. No accompanying SO_2 data are available for this period.

The variation in lava-effusion rates derived from SO_2 emissions also increases in the higher ranges. The variation in SO_2-emission rates is reported as the standard deviation of measurements during an observation day (Elias and others, 1998). Higher SO_2-derived lava-effusion rates have higher standard deviations (fig. 6).

Although the foregoing discussion demonstrates the overall agreement between SO_2- and VLF-derived lava-effusion

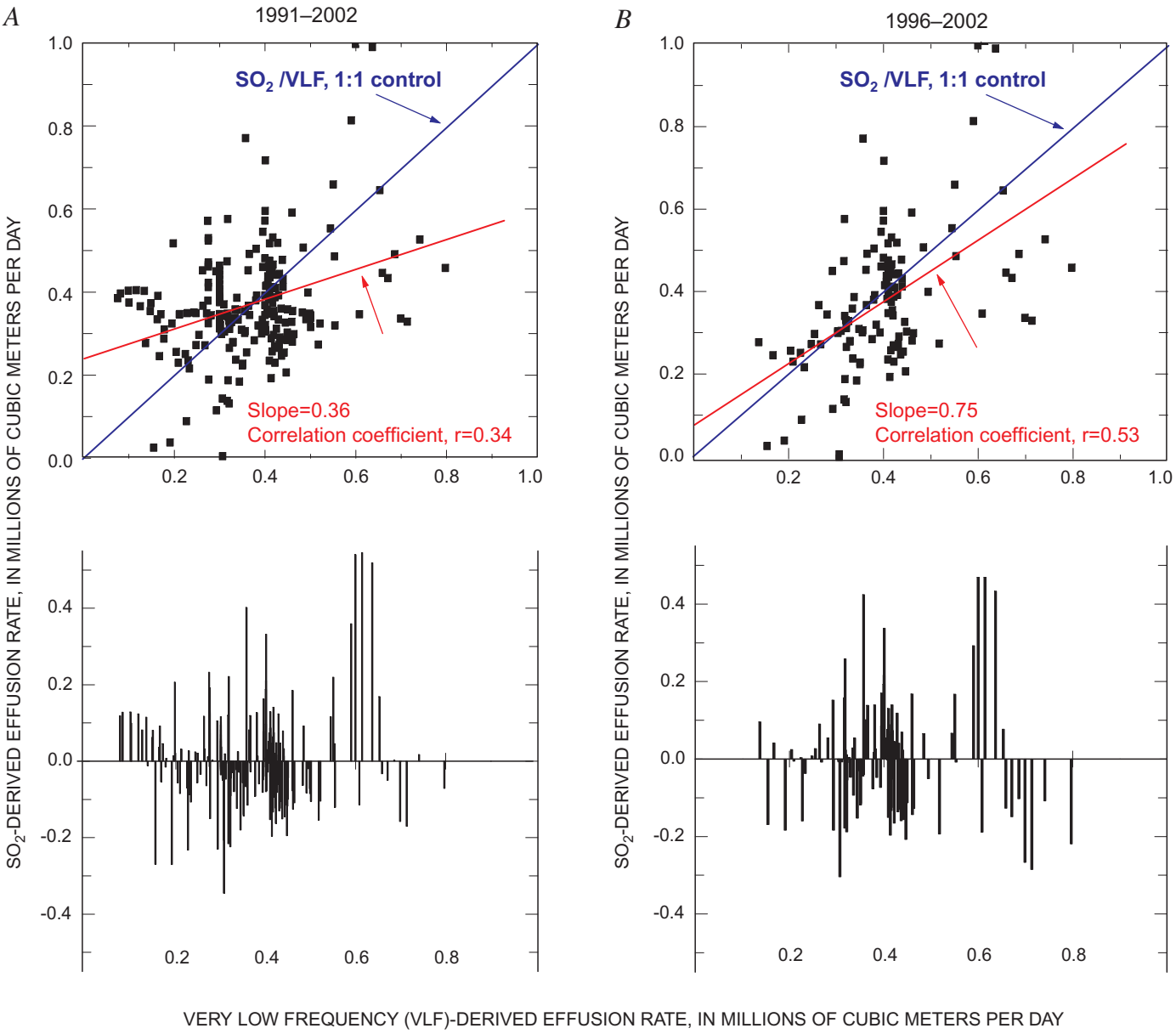

Figure 4. Lava-effusion rates derived from very low frequency (VLF) electromagnetic profiles and SO_2-emission rates statistically correlated at 95- and 99-percent-confidence levels for periods 1991–2002 (*A*), and 1996–2002 (*B*). Correlation during 1996–2002, when sampling frequency was higher, is stronger (see table 2). Residuals (lower plots) show notable deviation toward region of higher lava-effusion rate, when effusion rate shows large temporal variation.

rates, a precisely contemporaneous data set including SO_2 and VLF data is needed to rigorously test the agreement between the two techniques.

Other Remote Techniques for Measuring Lava-Effusion Rates

Several space-based techniques have been used to infer lava-effusion rates on Kīlauea. Topographic synthetic-aperture radar (TOPSAR) was used to estimate lava-effusion rates for episodes 50 through 53 of the eruption. These estimates agree with direct VLF measurements within 6 to 30 percent (Rowland and others, 1999). Harris and others (1998) showed that lava-effusion rates could be derived by leveraging the high spatial resolution of Landsat Thematic Mapper (TM) data with coarser but more frequent data obtained by an advanced very high resolution radiometer (AVHRR). These two data streams were used to sequentially image the flow field and detect changes in heat from one satellite pass to another, deriving lava-effusion rates from these data (Wright and others, 2001). Although remote space-based techniques show promise, they are significantly challenged by cloud cover and the absence of remotely visible surface flows.

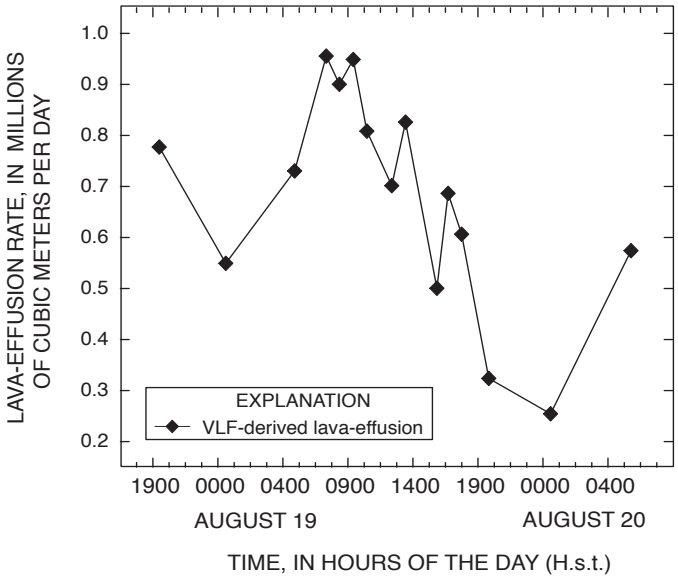

Figure 5. Very low frequency (VLF) electromagnetic-profiling-derived lava-effusion rates near Pu‘u ‘Ō‘ō record the large variation in volume rate of flow through primary tube that carries lava away from vent during period of increasing eruptive activity. SO_2 emissions, though not quantified precisely during this interval, show similar variation during other periods of increased activity.

Conclusions

VLF data and SO_2 profiling, in combination with surface-thickness measurements and area mapping, show that the Pu‘u ‘Ō‘ō-Kūpaianaha eruption produced from 2.4 to 2.6 km^3 of DRE lava between January 1983 and May 2002. The total volumes of magma calculated by SO_2 and VLF techniques for the 19.5 years of the current eruption agree within 10 percent. Heliker and others (this volume) report 2.3 km^3 of lava erupted through the end of 2001, based onVLF and mapping data. With the notable deviation during the period from about 1996 through 1998, the overall eruption rate has been fairly steady at about 0.13 km^3/yr.

We believe that the CO_2/SO_2-ratio approach used in this study accurately approximates the east-rift-zone lava-effusion rate. The simplicity of equations 2 and 5 applies a system-specific empirical measure, $[CO_2]/[SO_2]$, the value of which has been exhaustively refined at the vent and within the plume (Gerlach and others, 1998), where COSPEC SO_2-emission rates are measured. Furthermore, lava-effusion rates calculated in this way are supported by those calculated independently from VLF measurements. The agreement of lava-effusion rates calculated by using two fundamentally different techniques, VLF and COSPEC, demonstrates that monitoring SO_2 emissions, at least at Kīlauea, can serve as a useful proxy for tracking lava-effusion rates.

The results from the CO_2/SO_2-ratio approach imply that the magma supplying the current eruption is equilibrated at 1.0- to 1.5-km depth before being erupted on the east rift zone. This equilibration could be occurring within a shallow part of the summit reservoir or, alternatively, on the way to the east rift zone. Dawson and others (1999) found a high-V_p/V_s zone 1 to 2 km beneath the summit, consistent with possible summit-reservoir equilibration. This equilibration point might, in turn, indicate the depth of the duct leading outward to the east rift zone.

The excellent agreement between the VLF- and SO_2-derived lava-effusion rates for the Pu‘u ‘Ō‘ō-Kūpaianaha eruption since 1991 and especially since 1992, when regular east-rift-zone SO_2 measurements began, has resulted in these two techniques becoming the mainstay of eruption-rate monitoring at Kīlauea. Under certain conditions, however, it is difficult or impossible to make measurements with one technique or the other. East-rift-zone COSPEC measurements along Chain of Craters Road require brisk winds within a fairly narrow range of wind direction (Sutton and others, 2001). Thus, seasonal interruption of northeasterly trade winds disturbs measurement frequency and overall data quality. Similarly, VLF measurements on the eruptive flow field requires the existence of lava tubes and a skylight high on the tube with an unobscured view to the lava stream to measure flow velocity. Both types of measurements are compromised and can be hazardous in poor weather conditions.

The degree of VLF-COSPEC temporal correlation is encouraging, considering that both techniques function as effusion-rate monitors by scaling up measurements, gathered over a few hours or less, to report a daily rate. Both COSPEC measurements of east-rift-zone SO_2 and VLF

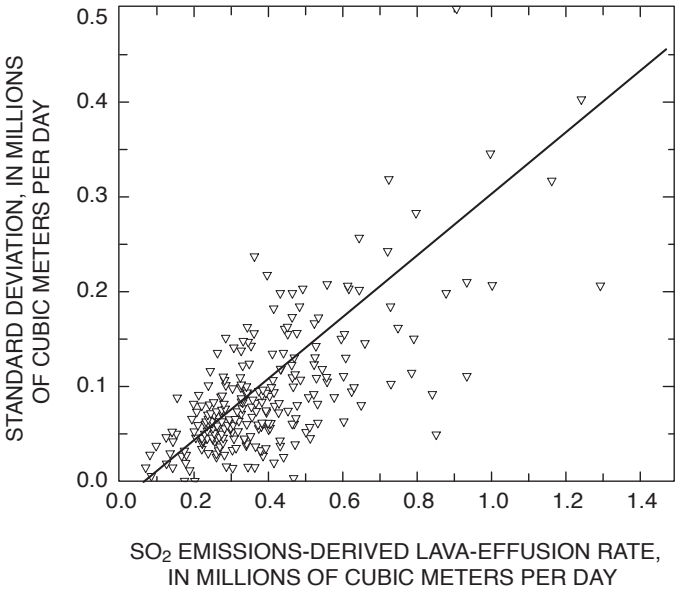

Figure 6. Standard deviation of lava-effusion rates based on daily average SO_2-emission-rate measurements, shows a positive linear trend with increasing effusion, corroborating large variation in lava-effusion-rate data shown by very low frequency (VLF) electromagnetic-profiling data in figure 5 and supporting finding of deviating residuals at high lava-effusion rates.

measurements are typically conducted only once each week at Kīlauea. A more thorough evaluation of the agreement between the two methods for effusion-rate monitoring is warranted but requires contemporaneous measurements.

Weekly VLF- and SO_2-emission-rate measurements have significantly improved our ability to track changes in the status of the Pu‘u ‘Ō‘ō eruption over periods of weeks to months. Short periods of more frequent data collection with these techniques have illuminated eruptive processes, such as gas pistoning and hornito formation, at and near the vent.

Recent availability of miniaturized, high-resolution ultraviolet spectrometers, coupled with practical, real-time data processing, has led researchers to pursue development of lower-cost alternatives to the electromechanical COSPEC developed in the 1960s (Horton and others, 2002; Galle and others, 2002). The potential of automating such low-power devices shows promise toward deployment of a continuous SO_2-emission and effusion-rate monitor at Kīlauea.

Acknowledgments

We gratefully acknowledge the many hours of hard work contributed by participants in the USGS Volunteers for Science program. The manuscript benefited from helpful reviews by Dave Clague, Peter Cervelli, and Terry Gerlach.

References Cited

Andres, R.J., Kyle, P.R., Stokes, J.B., and Rose, W.I., 1989, SO_2 from episode 48A eruption, Hawaii; sulfur dioxide emissions from the episode 48A east rift zone eruption of Kilauea volcano, Hawaii: Bulletin of Volcanology, v. 52, no. 2, p. 113–117.

Bottinga, Yan, and Javoy, Marc, 1991, The degassing of Hawaiian tholeiite: Bulletin of Volcanology, v. 53, no. 2, p. 73–85.

Casadevall, T.J., Stokes, J.B., Greenland, L.P., Malinconico, L.L., Casadevall, J.R., and Furukawa, B.T., 1987, SO_2 and CO_2 emission rates at Kilauea Volcano, 1979–1984, chap. 29 *of* Decker, R.W., Wright, T.L., and Stauffer, P.H., eds., Volcanism in Hawaii: U.S. Geological Survey Professional Paper 1350, p. 771–780.

Cayol, Valérie, Dieterich, J.H., Okamura, A.T., and Miklius, Asta, 2000, High magma storage rates before the 1983 eruption of Kilauea, Hawaii: Science, v. 288, no. 5475, p. 2343–2346.

Clague, D.A., Moore, J.G., Dixon, J.E., and Friesen, W.B., 1995, Petrology of submarine lavas from Kilauea's Puna Ridge, Hawaii: Journal of Petrology, v. 36, no. 2, p. 299–349.

Dixon, J.E., Clague, D.A., and Stolper, E.M., 1991, Degassing history of water, sulfur, and carbon in submarine lavas from Kilauea Volcano, Hawaii: Journal of Geology, v. 99, no. 2, p. 371–394.

Dvorak, J.J., and Dzurisin, Daniel, 1993, Variations in magma supply rate at Kilauea Volcano, Hawaii: Journal of Geophysical Research, v. 98, no. B12, p. 22255–22268.

Elias, Tamar, Sutton, A.J., Stokes, J.B., and Casadevall, T.J., 1998, Sulfur dioxide emission rates of Kilauea Volcano, Hawaii, 1979–1997: U.S. Geological Survey Open-File Report 98–462, 40 p.

Elias, Tamar, and Sutton, A.J., 2002, Sulfur dioxide emission rates from Kilauea Volcano, Hawaii, an update; 1998–2001: U.S. Geological Survey Open-File Report 02–460, 10 p., figs. 23 p.

Galle, Bo, Oppenheimer, Clive, Geyer, Andreas, McGonigle, A.J.S., Edmonds, Marie, and Horrocks, Lisa, 2002, A miniaturized ultraviolet spectrometer for remote sensing of SO_2 fluxes; a new tool for volcano surveillance: Journal of Volcanology and Geothermal Research, v. 119, no. 1–4, p. 241–254.

Gerlach, T.M., 1986, Exsolution of H_2O, CO_2, and S during eruptive episodes at Kilauea volcano, Hawaii: Journal of Geophysical Research, v. 91, no. B12, p. 12177–12185.

Gerlach, T.M., 1993, Thermodynamic evaluation and restoration of volcanic gas analyses; an example based on modern collection and analytical methods: Geochemical Journal, v. 27, no. 4–5, p. 305–322.

Gerlach, T.M., and Graeber, E.J., 1985, Volatile budget of Kilauea volcano: Nature, v. 313, no. 6000, p. 273–277.

Gerlach, T.M., Hinkley, T.K., Briggs, P.H., and Stokes, J.B., 1991, Fumarole gases of Halemaumau pit crater and summit magma chamber degassing models for Kilauea Volcano [abs.]: Eos (American Geophysical Union Transactions), v. 72, no. 44, supp., p. 562.

Gerlach, T.M., McGee, K.A., Sutton, A.J., and Elias, Tamar, 1998, Rates of volcanic CO_2 degassing from airborne determinations

of SO_2 emission rates and plume CO_2/SO_2; test study at Pu′u ′O′o cone, Kilauea volcano, Hawaii: Geophysical Research Letters, v. 25, no. 14, p. 2675–2678.

Gerlach, T.M., McGee, K.A., Elias, Tamar, Sutton, A.J., and Doukas, M.P., 2002, The carbon dioxide emission rate of Kīlauea Volcano; implications for primary magma CO_2 content and summit reservoir dynamics: Journal of Geophysical Research, v. 107, no. B9, 2189, doi:10.1029/2001JB000407.

Greenland, L.P., 1986, Gas analyses from the Pu′u O′o eruption in 1985, Kilauea volcano, Hawaii: Bulletin of Volcanology, v. 48, no. 6, p. 341–348.

Greenland, L.P., 1987, Hawaiian eruptive gases, chap. 28 *of* Decker, R.W., Wright, T.L., and Stauffer, P.H., eds., Volcanism in Hawaii: U.S. Geological Survey Professional Paper 1350, p. 759–770.

Greenland, L.P., 1988, Gases from the 1983–84 east-rift eruption, chap. 4 *of* Wolfe, E.W., ed., The Puu Oo eruption of Kilauea Volcano, Hawaii; episodes 1 through 20, January 3, 1983, through June 8, 1984: U.S. Geological Survey Professional Paper 1463, p. 145–153.

Greenland, L.P., Okamura, A.T., and Stokes, J.B., 1988, Constraints on the mechanics of the eruption, chap. 5 *of* Wolfe, E.W., ed., The Puu Oo eruption of Kilauea Volcano, Hawaii; episodes 1 through 20, January 3, 1983, through June 8, 1984: U.S. Geological Survey Professional Paper 1463, p. 155–164.

Greenland, L.P., Rose, W.I., and Stokes, J.B., 1985, An estimate of gas emissions and magmatic gas content from Kilauea volcano: Geochimica et Cosmochimica Acta, v. 49, no. 1, p. 125–129.

Harris, A.J.L., Flynn, L.P., Keszthelyi, L.P., Mouginis-Mark, P.J., Rowland, S.K., and Resing, J.A., 1998, Calculation of lava effusion rates from Landsat TM data: Bulletin of Volcanology, v. 60, no. 1, p. 52–71.

Heliker, C.C., Sherrod, D.R., Thornber, C.R., and Kauahikaua, J.P., 1997, Kilauea Volcano east rift zone eruption update; 1997 brings era of instability [abs.]: Eos (American Geophysical Union Transactions), v. 78, no. 46, supp., p. F648.

Heliker, C.C., and Wright, T.L., 1991, The Pu′u ′O′o-Kupaianaha eruption of Kilauea: Eos (American Geophysical Union Transactions), v. 72, no. 47, p. 521, 526, 530.

Horton, K.A., Mouginis-Mark, P.J., Garbeil, Harold, Porter, J.N., Sutton, A.J., Elias, Tamar, and Oppenheimer, C.M.M., 2002, FLYSPEC; Expanding options for low-cost instruments to remotely monitor volcanic gas emissions [abs.]: Chapman Conference on Volcanism and the Earth's Atmosphere, Thera, Greece, 2000, Abstracts, p. 31.

Jackson, D.B., Kauahikaua, J.P., Hon, K.A., and Heliker, C.C., 1988, Rate and variation of magma supply to the active lava lake on the middle east rift zone of Kilauea Volcano, Hawaii [abs.]: Geological Society of America Abstracts with Programs, v. 20, no. 7, p. A397.

Kauahikaua, J.P., 1993, Geophysical characteristics of the hydrothermal systems of Kilauea volcano, Hawai′i: Geothermics, v. 22, no. 4, p. 271–299.

Kauahikaua, J.P., Cashman, K.V., Mattox, T.N., Heliker, C.C., Hon, K.A., Mangan, M.T., and Thornber, C.R., 1998, Observations on basaltic lava streams in tubes from Kilauea Volcano, island of Hawai′i: Journal of Geophysical Research, v. 103, no. B11, p. 27303–27323.

Kauahikaua, J.P., Mangan, M.T., Heliker, C.C., and Mattox, T.N., 1996, A quantitative look at the demise of a basaltic vent; the death of Kupaianaha, Kilauea Volcano, Hawai′i: Bulletin of Volcanology, v. 57, no. 8, p. 641–648.

Mangan, M.T., Heliker, C.C., Mattox, T.N., Kauahikaua, J.P., and Helz, R.T., 1995, Episode 49 of the Pu′u ′O′ o-Kupaianaha eruption of Kilauea volcano—breakdown of a steady-state eruptive era: Bulletin of Volcanology, v. 57, no. 2, p. 127–135.

Moore, J.G., and Fabbi, B.P., 1971, An estimate of the juvenile sulfur content of basalt: Contributions to Mineralogy and Petrology, v. 33, no. 2, p. 118–127.

Rowland, S.K., MacKay, M.E., and Garbeil, Harold, 1999, Topographic analyses of Kīlauea Volcano, Hawai′i, from interferometric airborne radar: Bulletin of Volcanology, v. 61, no. 1, p. 1–14.

Strange, W.E., Woollard, G.P., and Rose, J.C., 1965, An analysis of the gravity field over the Hawaiian Islands in terms of crustal structure: Pacific Science, v. 19, no. 3, p. 381–389.

Sutton, A.J., Elias, Tamar, Gerlach, T.M., and Stokes, J.B., 2001, Implications for eruptive processes as indicated by sulfur dioxide emissions from Kīlauea Volcano, Hawai′i, 1979–1997: Journal of Volcanology and Geothermal Research, v. 108, no. 1–4, p. 283–302.

Swanson, D.A., 1972, Magma supply rate at Kilauea Volcano, 1952–1971: Science, v. 175, no. 4018, p. 169–170.

Swanson, D.A., and Fabbi, B.P., 1973, Loss of volatiles during fountaining and flowage of basaltic lava at Kilauea Volcano, Hawaii: U.S. Geological Survey Journal of Research, v. 1, no. 6, p. 649–658.

Symonds, R.B., Gerlach, T.M., and Reed, M.H., 2001, Magmatic gas scrubbing; implications for volcano monitoring: Journal of Volcanology and Geothermal Research, v. 108, no. 1–4, p. 303–341.

Thornber, C.R., Sherrod, D.R., Heliker, C.C., Kauahikaua, J.P., Trusdell, F.A., Lisowski, Michael, and Okubo, P.G., 1997, Kilauea's ongoing eruption; Napau Crater revisted after 14 years [abs.]: Eos (American Geophysical Union Transactions), v. 78, no. 17, supp., p. S329.

Thornber, C.R., Sherrod, D.R., Siems, D.F., Heliker, C.C., Meeker, G.P., Oscarson, R.L., and Kauahikaua, J.P., 2002, Whole-rock and glass major-element geochemistry of Kilauea Volcano, Hawaii, near-vent eruptive products; September 1994 through September 2001: U.S. Geological Survey Open-File Report 02–17, 41 p.

Ulrich, G.E., Heliker, C.C., and Hoffmann, J.P., 1985, Kilauea Volcano, Hawaii, continued eruption [abs.]: Eos (American Geophysical Union Transactions), v. 66, no. 46, p. 1132.

Ulrich, G.E., Wolfe, E.W., Heliker, C.C., and Neal, C.A., 1987, Pu'u 'O'o IV; evolution of a plumbing system [abs.], *in* Decker, R.W., Halbig, J.B., Hazlett, R.W., Okamura, R.T., and Wright, T.L., eds., Hawaii Symposium on How Volcanoes Work, Hilo, Hawaii, 1987, Abstract volume: Honolulu, University of Hawaii, Hawaii Institute of Geophysics, p. 259.

Ulrich, G.E., Wolfe, E.W., Hoffmann, J.P., and Neal, C.A., 1984, Continuing eruption of east rift zone, Kilauea Volcano, Hawaii [abs.]: Eos (American Geophysical Union Transactions), v. 65, no. 45, p. 1130.

Wolfe, E.W., ed., 1988, The Puu Oo eruption of Kilauea Volcano, Hawaii; episodes 1 through 20, January 3, 1983, through June 8, 1984: U.S. Geological Survey Professional Paper 1463, 251 p.

Wolfe, E.W., Garcia, M.O., Jackson, D.B., Koyanagi, R.Y., Neal, C.A., and Okamura, A.T., 1987, The Puu Oo eruption of Kilauea Volcano, episodes 1–20, January 3, 1983, to June 8, 1984, chap. 17 *of* Decker, R.W., Wright, T.L., and Stauffer, P.H., eds., Volcanism in Hawaii: U.S. Geological Survey Professional Paper 1350, v. 1, p. 471–508.

Wolfe, E.W., Neal, C.A., Banks, N.G., and Duggan, T.J., 1988, Geologic observations and chronology of eruptive events, chap. 1 *of* Wolfe, E.W., ed., The Puu Oo eruption of Kilauea Volcano, Hawaii; episodes 1 through 20, January 3, 1983, through June 8, 1984: U.S. Geological Survey Professional Paper 1463, p. 1–97.

Wright, Robert, Blake, Stephen, Harris, A.J.L., and Rothery, D.A., 2001, A simple explanation for the space-based calculation of lava eruption rates: Earth and Planetary Science Letters, v. 192, no. 2, p. 223–233.

Zablocki, C.J., 1978, Applications of the VLF induction method for studying some volcanic processes of Kilauea volcano, Hawaii: Journal of Volcanology and Geothermal Research, v. 3, no. 1–2, p. 155–195.

The Shallow Magmatic System of Kīlauea Volcano

By Peter F. Cervelli *and* Asta Miklius

Abstract

The shallow magmatic system of Kīlauea Volcano currently consists of two distinct summit magma reservoirs, a vent at Pu‘u ‘Ō‘ō, and a conduit connecting that vent to the shallower of the two summit reservoirs. Global Positioning System (GPS) measurements and leveling surveys record long-term subsidence over a magma reservoir near the southeast border of the summit caldera, centered no deeper than about 3.5 km below ground level (2.5 km below sea level). The yearly volume loss from this source is, at most, 2.5 million m^3, approximately 2 percent of the annual eruption output from Pu‘u ‘Ō‘ō. Electronic borehole tiltmeters image another, much shallower magma reservoir about 0.5 km east of Halemaumau at a depth of 500 to 700 m above sea level (500 to 700 m below ground level). The deformation from this shallow reservoir is episodic and short-lived, each event persisting for only a few days. Four of these deformation events, which occurred from 2000 to 2002, are highly self-similar and appear to reflect a brief interruption of magma supply. We conclude, from the style of deformation and from the timing of seismicity during these events, that the conduit from the summit to Pu‘u ‘Ō‘ō leaves from the shallower reservoir. From there it runs horizontally along the rift zone until it intersects the surface topography at Pu‘u ‘Ō‘ō. We estimate the radius of this cylindrical conduit at about 2.75 m.

Introduction

In this chapter, we infer the structure of the shallow magmatic system beneath Kīlauea summit, as well as the location and dimensions of the feeder conduit to Pu‘u ‘Ō‘ō. Toward this end, we use various data sets, including continuous Global Positioning System (GPS) and borehole tilt, leveling campaigns, seismic measurements, and estimates of lava flux and gas effusion. All of these data lead to a fundamental observation about the magma system—there exists a quasisteady long-term mode of deformation interrupted by occasional short-lived episodes of deformation both at Kīlauea's summit and at Pu‘u ‘Ō‘ō. Many of these episodes share striking similarities that suggest a corresponding similarity of process, which, if understood, could provide clues about the structure of Kīlauea's shallow magmatic system.

Over the course of the current Pu‘u ‘Ō‘ō eruption, the deformation observed at Kīlauea has been characterized by high rates of south-flank motion (max 8 cm/yr) and summit subsidence (max 11 cm/yr), punctuated by episodes of faster motion associated with earthquakes and intrusions (Delaney and others, 1993). Delaney and others (1993, 1998) and Owen and others (2000), who summarized the data up to 1996, modeled the sources of deformation as consisting of slip along low-angle south-flank faults, deep rift-zone opening, and deflation in the summit caldera. We interpret deformation measurements between 1996 and the present but do not attempt to model all the sources contributing to the deformation patterns observed on Kīlauea. Instead, we concentrate on the summit area because it gives the most information about the structure of the shallow magmatic system.

Long-term summit deformation during the current eruption is primarily vertical, consisting of persistent subsidence in the southern part of Kīlauea's caldera. Numerous workers have attributed similar patterns of subsidence in the past to a deflating magma reservoir at about 3- to 5-km depth (Mogi, 1958; Fiske and Kinoshita, 1969; Tilling and Dvorak, 1993). Delaney and others (1993) and Owen and others (2000) determined that most of the current subsidence is attributable to this deflating reservoir but that rifting of the summit area is required by the horizontal data. Rifting, in fact, may cause about 35 percent of the subsidence. Recent data, primarily leveling and GPS, collected since 1996 clearly image the deflating magma reservoir in the southern caldera, although we do not model the contribution from rifting.

Superimposed on the long-term subsidence are self-similar deformation events, which image a shallow magma reservoir slightly east of Halemaumau (fig. 1). These episodes, and what they imply about the shallow magmatic system beneath Kīlauea, are the primary focus of this chapter.

Data

Continuous GPS

The U.S. Geological Survey's Hawaiian Volcano Observatory (HVO), Stanford University, and the University of Hawai‘i operate a network of continuously recording dual-frequency GPS receivers on Kīlauea (fig. 1). Data from these receivers are processed in daily batches with the Gipsy/Oasis II software package (Lichten and Border, 1987). Time series

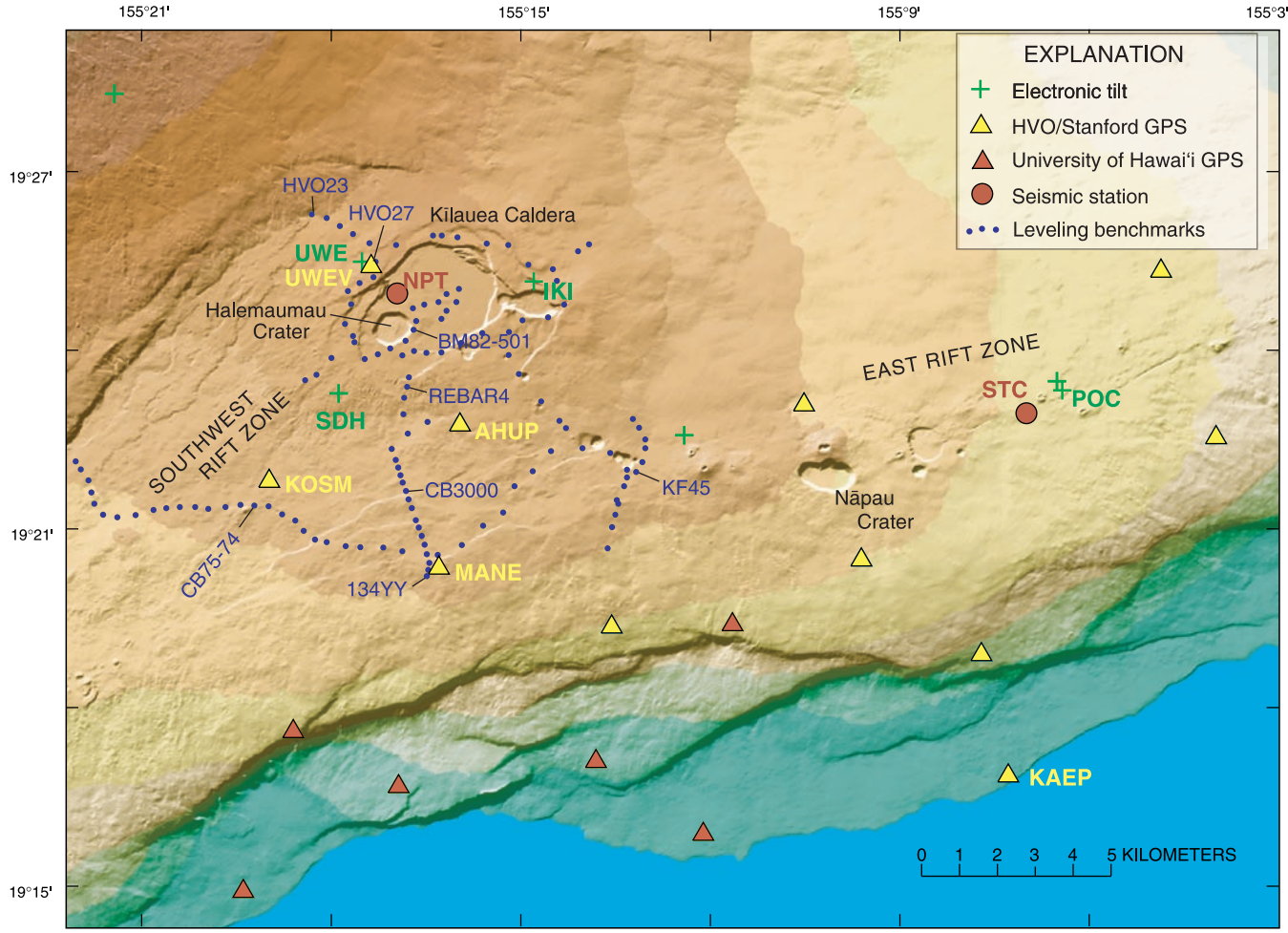

Figure 1. Kīlauea Volcano, Island of Hawai'i, showing locations of stations in electronic-tilt, leveling, and continuous Global Positioning System (GPS) networks and seismic stations mentioned in text. Digital elevation model used to construct figure is not recent enough to include Pu'u 'Ō'ō and effects of its eruption. Tiltmeter at station POC is located on northwest flank of Pu'u 'Ō'ō. Contour interval, 500 ft.

from two selected summit stations (UWEV, AHUP) are shown in figure 2. We filtered all the time series to minimize the effect of reference-frame errors and to calculate long-term station velocities (Cervelli and others, 2002a). This procedure allows geologic offsets, such as earthquakes and intrusions, to exist in the time series without biasing estimates of the long-term deformation rates. The horizontal velocities of the Kīlauea continuous GPS stations, after subtracting the velocity of a continuous station on Mauna Kea (approx 50 km north of Kīlauea's caldera), are mapped in figure 3. No evidence exists for active deformation at Mauna Kea; and so its station velocity serves as a proxy for the velocity of the Pacific Plate.

The predominant horizontal signal in the GPS data is a persistent southeastward migration of Kīlauea's south flank (fig. 3). Maximum rates of about 8 cm/yr are observed at station KAEP on the south coast (fig. 1). Station UWEV, north of the topographic caldera but within the structural caldera, and station AHUP, south of the caldera, both show southeastward motion of about 2.5 cm/yr. Station AHUP is moving slightly faster than station UWEV, leading to a small (0.5 cm/yr) extension across the caldera. The rate at station KOSM, in the southwest rift zone, is nearly 5 cm/yr and is directed much more easterly than at the other summit stations.

Since 1996, many geologic events, including two east-rift-zone intrusions and several earthquakes, have affected the GPS time series. The long-term deformation pattern, however, seems unperturbed by these events. Indeed, even the largest event, the January 1997 Nāpau Crater eruption, introduced only a transient signal into the time series.

Apart from horizontal motion, the continuous GPS network is also sensitive to long-term vertical signals. The GPS data show uplift along the coast of about 3 cm/yr and subsidence in the south caldera of more than 4 cm/yr. The sign change between subsidence and uplift runs between the Koa'e and Hilina fault systems (fig. 3).

In the modeling and discussion that follows, we consider only the four GPS stations located around Kīlauea's summit: AHUP, KOSM, MANE, and UWEV (fig. 1). This subset of stations is sufficient to address the question of magma-system structure that is the primary focus of this chapter.

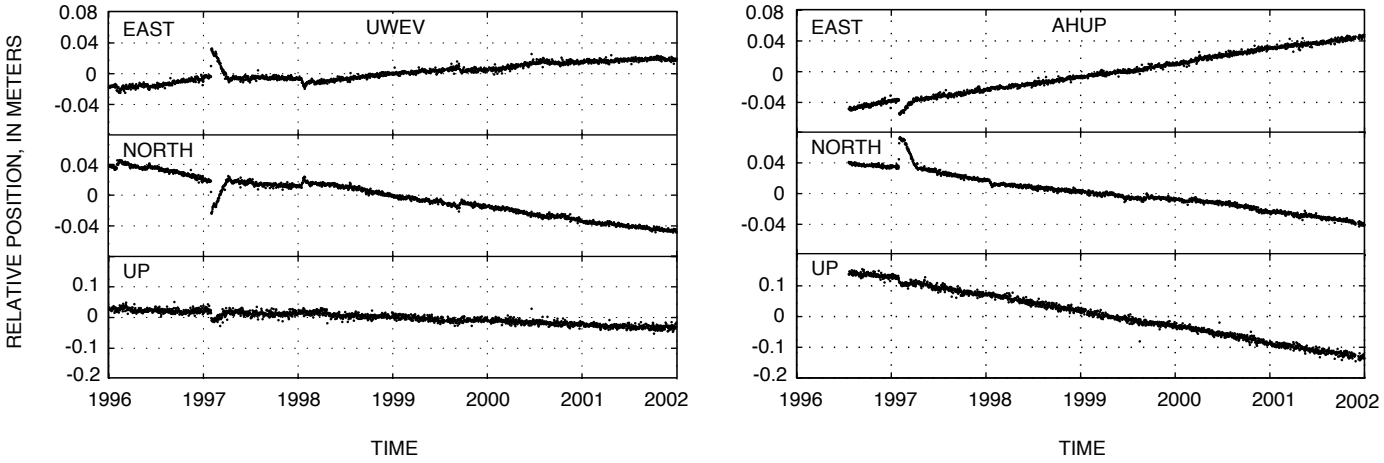

Figure 2. Time series from two summit Global Positioning System (GPS) stations with respect to a fixed Pacific Plate. Station AHUP is south of Kīlauea's summit caldera; station UWEV is just northwest of topographic caldera (fig. 1). Striking departure from long-term trend in early 1997 is effect of Nāpau Crater eruption (eruptive episode 54). Note long-term subsidence at station AHUP that exceeds 5 cm/yr. Effect of episodic events discussed in text is too short-lived to appear on these time series.

Leveling

A leveling traverse crossing Kīlauea's summit and upper rift zones (fig. 1) is measured nearly annually. Leveling surveys are conducted to first-order, second-class standards (Federal Geodetic Control Committee, 1984) and have an expected error propagation of 2 mm/km$^{1/2}$. Loop closures in the network permit us to empirically calibrate the expected error; on Kīlauea's summit, we achieve about 2.2 mm/km$^{1/2}$.

Selected time series of elevations relative to a reference station, HV023, northwest of Kīlauea's caldera (fig. 1) show a steady rate of subsidence from 1996 through 2002 (fig. 4), with a transient perturbation resulting from the January 1997 Nāpau Crater eruption. Contours of average rates of elevation change across the summit (fig. 5) show broad, asymmetric subsidence, with the locus of maximum subsidence in the southern caldera. The maximum subsidence rate is about 6 cm/yr, slightly lower than the 8 cm/yr measured during the early part of the Pu'u 'Ō'ō eruption from 1983 to 1990 (Delaney and others, 1998). The rate of vertical motion at station HVO23 over this time period is unknown. The vertical GPS data seem to systematically exceed the rates implied by the leveling data at the GPS stations by about 5 mm/yr. This small discrepancy likely reflects slow subsidence at leveling reference station, HVO23.

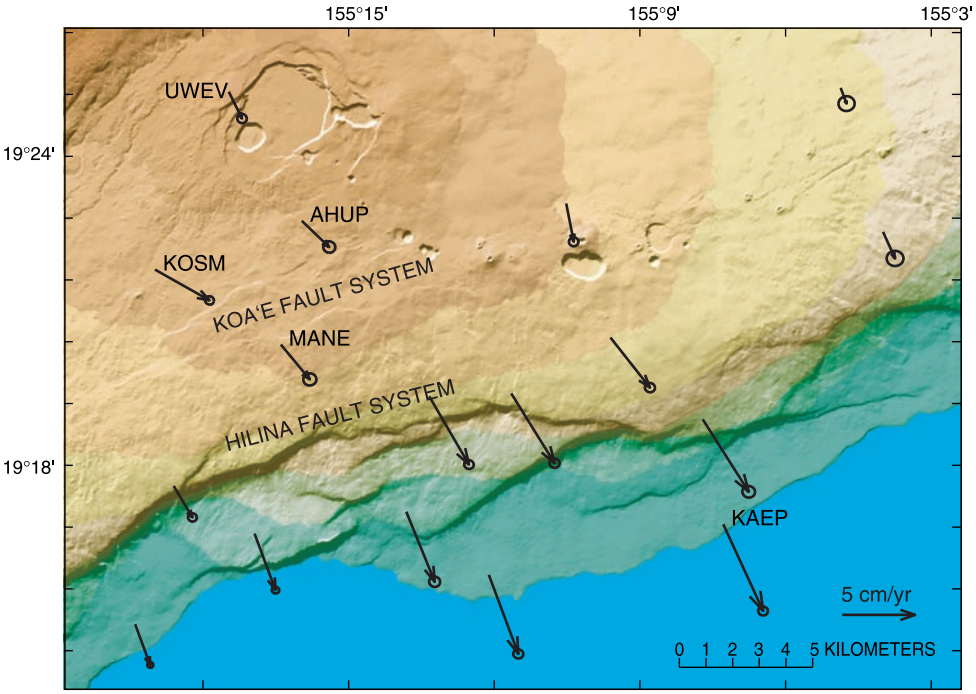

Figure 3. Kīlauea Volcano showing vectors of horizontal Global Positioning System (GPS) velocity from 1996 to 2002 with respect to a fixed Pacific Plate. Error ellipses at 95-percent-confidence level are scaled by repeatability about constant-velocity model. Major signal depicted is southeastward displacement of south flank, which reaches a maximum at coast and decays northward.

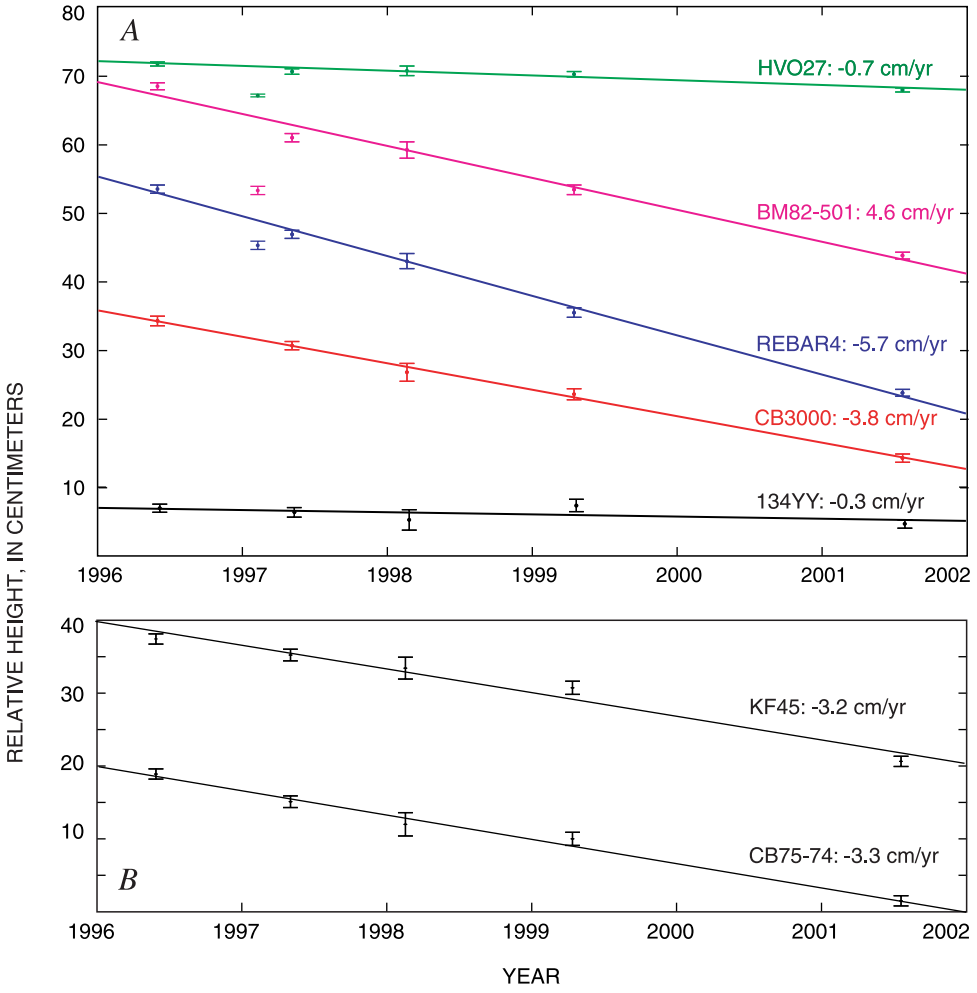

Figure 4. Time series of elevations at leveling stations with respect to reference station HVO23 (fig. 1). *A*, Stations along line crossing summit caldera. *B*, Stations on rift zones. Station KF45 is on upper east rift zone; station CB75-74 is on southwest rift zone. Data from partial survey of leveling network just after early 1997 Nāpau Crater eruption mark only departure from steady rate of subsidence in summit area over this interval. These early 1997 data were not used in calculating average vertical velocities.

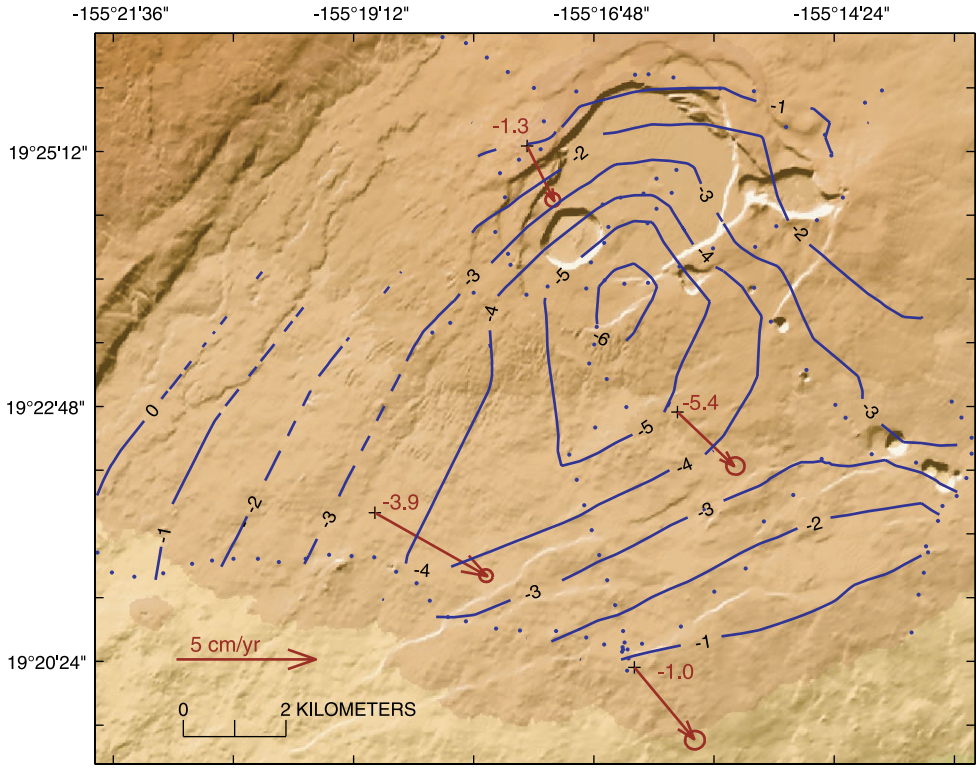

Figure 5. Summit of Kīlauea Volcano, showing contours of vertical-deformation rates and horizontal Global Positioning System (GPS) velocities from 1996 to 2002. Contours, in 0.01-m/yr intervals, are with respect to reference station HVO23. Vertical velocities at GPS stations (red) in meters per year. Vertical GPS velocities systematically exceed those from leveling data by about 5 mm/yr, probably because of subsidence at reference station HVO23.

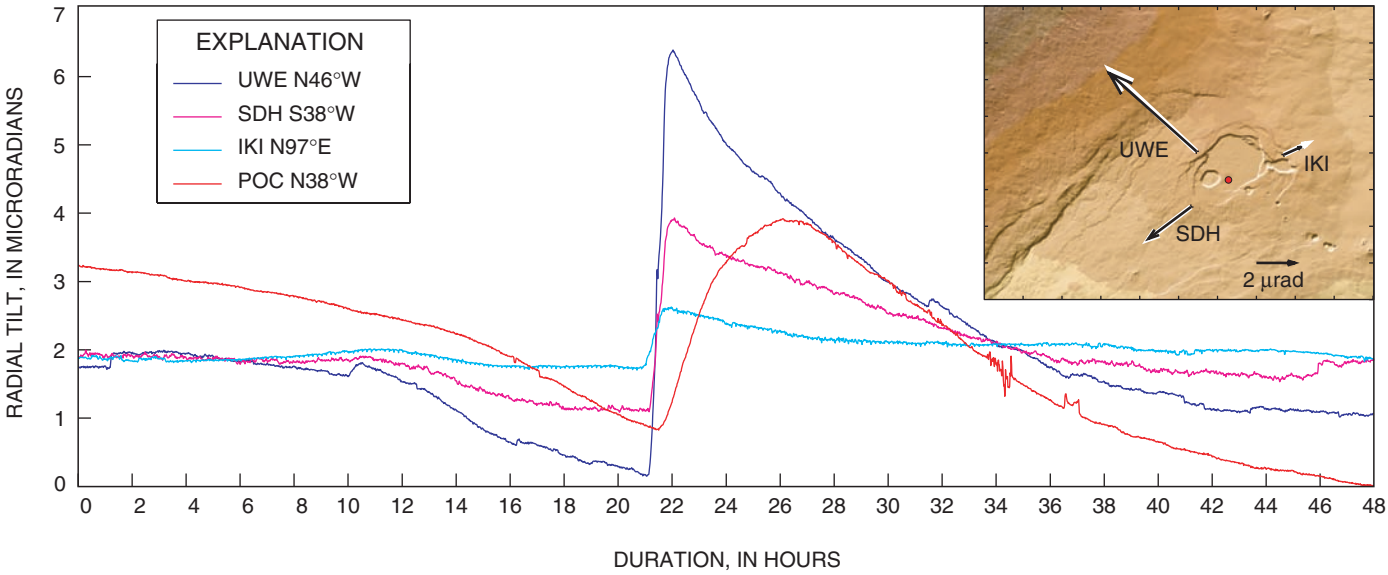

Figure 6*A*. Time series of tilt from borehole tiltmeter stations at summit and Pu‘u ‘Ō‘ō (POC) (fig. 1) for September 24–26, 2000. We plot component of tilt radial to source, that is, tilt in the direction that, on average, maximizes magnitude of signal. Inset map shows tilt vectors (in black) at summit for hour-long inflation. In white are tilts predicted by model for inflating point source at location shown by red circle. At Pu‘u ‘Ō‘ō, maximum tilt points away from cone's summit crater area.

Electronic Tilt

HVO operates a network of 12 electronic tiltmeters, each set into a borehole ranging in depth from 5 to 40 m. The locations of the six tiltmeters that monitor Kīlauea's summit and Pu‘u ‘Ō‘ō are shown in figure 1. Data from the tiltmeters are logged on site at a 1-minute sampling rate and telemetered back to the observatory every 10 minutes. The first electronic borehole tiltmeter (sta. UWE, fig. 1) was installed in 1998.

The tiltmeter located on Pu‘u ‘Ō‘ō (sta. POC, fig. 1), just northwest of its rim, was installed in early 2000. Since then, it has recorded about 10 tilt events that started at Kīlauea's summit and propagated toward the vent, indicating a change in pressure over the entire shallow magmatic system. Four of these events are highly self-similar. At both the summit and at Pu‘u ‘Ō‘ō, these 2- to 3-day-long events are characterized by a period of slow deflation, then rapid inflation, followed by another period of slow deflation, bringing the final tilt close to the pre-event level. Three of these events were associated with a surge in the effusion rate at Pu‘u ‘Ō‘ō, the one exception being the December 2001 event.

The three stages of the surge-type tilt events start at the summit and propagate to Pu‘u ‘Ō‘ō (figs. 6*A*–*6C*). The initial deflation of 1 to 3 microradians at stations UWE and POC (fig. 1) takes 8 to 20 hours. The time between the onset of the tilt change at station UWE and the onset at station POC ranges from 1.5 to 2.5 hours. The inflationary stage is very rapid, with station UWE gaining 6 to 10 µrad in 1 hour. Station POC starts inflating 20 to 30 minutes later and takes from 5 to 14 hours to gain 4 to 6 µrad. The final deflation, its rate decaying exponentially, takes from 8 to more than 20 hours.

At the summit, an intense burst of seismic energy precedes the rapid inflation by a few minutes. Seismicity ceases just before the inflation begins, and resumes again as the inflation reaches its peak (figs. 6*B*–6*D*). At the vent, seismic energy seems to decrease with the initial inflation and then increases as the inflation continues. Low-frequency seismicity remains relatively high as the tilt slowly decays to the pre-event level.

At Pu‘u ‘Ō‘ō, the April 2002 deformation event (fig. 6*D*) differed from previous events in several ways. The initial deflation there was much greater than at station UWE (fig. 1), and the final deflation included numerous small tilt oscillations. During the deflationary periods of the oscillations, markedly increased seismic activity was observed. This oscillatory behavior may be related to increased pressure in Pu‘u ‘Ō‘ō's shallow magmatic system during this time and does not necessarily imply a different process from the other events.

Tilt vectors at the summit clearly point to a source of deflation and inflation slightly east of Halemaumau (fig. 6). At Pu‘u ‘Ō‘ō, tilt directions vary slightly more but generally point toward and away from the crater. Of the four deformation events described above, three were associated with eruptive surges, but the December 2001 event had no discernible effect on the eruption. The first signs of increased lava flux at the eruption site were generally observed shortly after Pu‘u ‘Ō‘ō started inflating.

Model

Clearly, the deformation field from the long-term source at the summit is qualitatively different from the deformation field associated with the episodic events, both in terms of their time scales and their spatial patterns. For this reason, we model the two modes of deformation separately. The long-

term deformation consists mostly of persistent subsidence in the caldera and upper rift zones, combined with the effects of south-flank motion, whereas the episodic deformation consists of a short-lived (~2 days) signal throughout Kīlauea's shallow magmatic system.

General Methods

To model the observed deformation fields, we use basic elasticity theory to predict tilts and displacements from point sources (Anderson, 1936; Mogi, 1958). Though mathematically simple, point sources are known to approximate the effects of a finite spherical magma reservoir quite well (McTigue, 1987). For the episodic source, the strength of the data, consisting of three tilt vectors, is insufficient to resolve fine detail in the reservoir structure. Thus, models more complex than a point source are probably not warranted. For the long-term source, we are interested in identifying the deformation arising from magma withdrawal beneath the southern caldera, as opposed to, for example, rifting. For this reason, the point source is again appropriate because more complex magma-reservoir models have a greater potential for absorbing deformation signals arising from other sources.

We represent the Earth as a homogenous, linear, isotropic, elastic half-space. Although this representation of the Earth ignores surface topography, the effect of topography on a shield volcano like Kīlauea is small (McTigue and Segall, 1988). Nonetheless, for episodic deformation events, which appear to be quite shallow, we include a topographic correction for two reasons. First, use of a topographic correction permits the establishment of a vertical datum, which is essential when the source depth is not much greater than the scale of the topography. Second, approximation of a topographic correction for the vertical displacements (and tilts) from a point source is straightforward (Williams and Wadge, 2001). The effect of elastic heterogeneity is also small, although failure to include realistic elastic properties may bias source depths as too shallow by about 10 percent (Johnson and others, 2001).

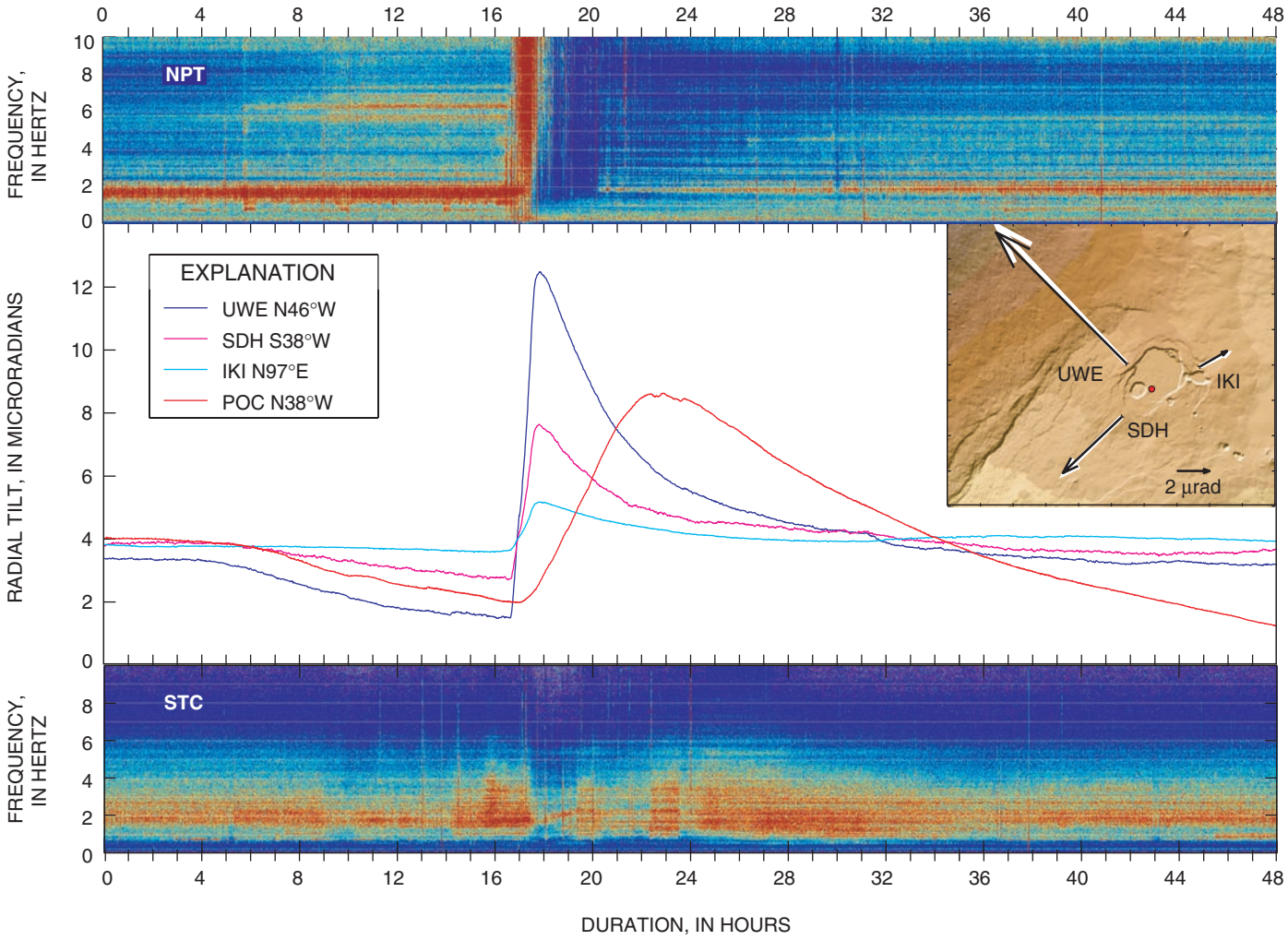

Figure 6*B*. Time series of radial component of tilt and seismic energy spectra for May 20–22, 2001. Spectrograms are from stations NPT, near Halemaumau, and STC, near Pu'u 'Ō'ō (fig. 1). Inset map shows tilt vectors (in black) at summit for hour-long inflation. In white are tilts predicted by model of inflating point source at location shown by red circle.

To invert the deformation fields for source location and strength, we cast the inversion problem as a nonlinear optimization (Cervelli and others, 2001). Specifically, we seek a source model that minimizes the difference between model predictions and observations. For the optimization, the quantity to be minimized is the mean square error, defined as

$$\mathrm{MSE} = r^T \Sigma^{-1} r / \nu,$$

where r is the residual vector (difference between observation and prediction), Σ is the data-covariance matrix, and ν is the number of degrees of freedom (the number of data points minus the number of model parameters). A χ^2 test can be applied to the MSE to check whether the data have been fitted within errors at some confidence level. To be meaningful, however, the χ^2 test requires that the data covariance be well known. For the tilt data, the covariance is poorly known, because we have not accounted for uncertainties in tiltmeter azimuth, the scale factor from millivolts to microradians, and other factors. In the case of the leveling and GPS data, the data covariance is better known but still may be off by a scale factor. Moreover, the χ^2 test strictly applies only when a linear relation exists between model parameters and data. For a point source, only the volume change is linear. Therefore, even though we use the MSE as a quantitative representation of the misfit, we do so only as a matter of convenience and not because of the statistical properties of the MSE under the circumstances described above.

Long-Term Deformation

The long-term pattern of deformation evident at Kīlauea's summit, well characterized by the continuous GPS and leveling data, is quite complex. This observation is not surprising because at least three separate geologic processes lead to significant deformation signals in this region: (1) motion of Kīlauea's south flank, (2) deflation in the summit magmatic system, and (3) rifting in the rift zones. Although south-flank motion and rifting introduce potentially large deformation signals in the summit region, we can partially separate them from magmatic deflation, the primary concern of this chapter. This separation is possible because the patterns of deformation from the two other sources differ considerably from the radial symmetry of a deflating magma reservoir. We are mindful,

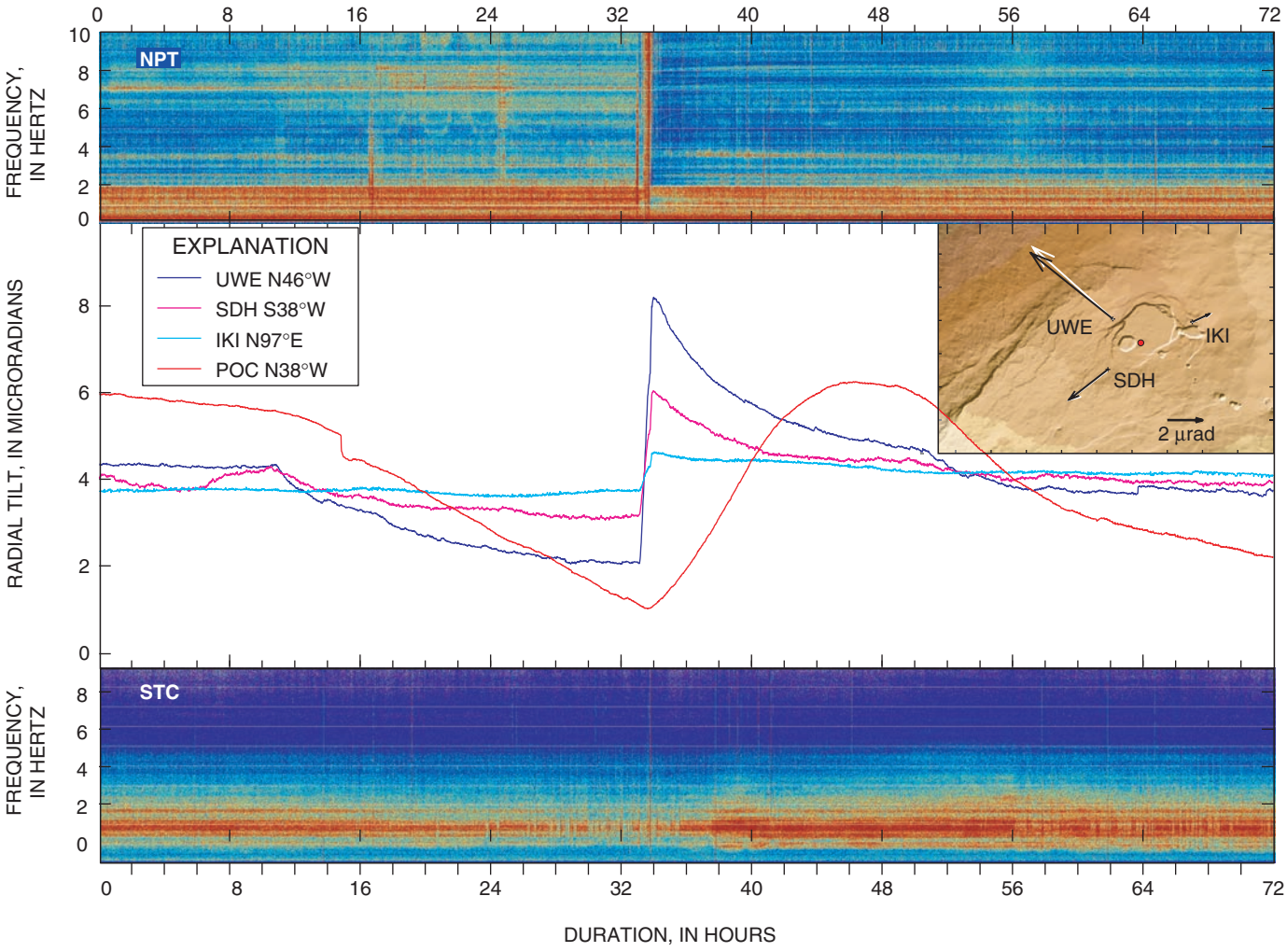

Figure 6*C*. Time series of radial component of tilt and seismic energy spectra for December 8–11, 2001. Inset map shows tilt vectors (in black) at summit for hour-long inflation. In white are tilts predicted by model of inflating point source at location shown by red circle.

however, as discussed in detail below, that a point source may absorb signals from other deformation sources.

We use the full covariance of the leveling data (Árnadóttir and others, 1992), which accounts for the correlations among these data introduced by summing the section-height differences. The covariances from both the GPS and leveling data are scaled by their repeatability about a constant velocity. Inverting these two data sets for a single point source results in a model located in the southern caldera (figs. 7*A*–7*B*) at 2.5 km below sea level and deflating at about 2.5 million km^3/yr. Henceforward, we refer to this deformation source as the "south-caldera magma reservoir."

The residual (fig. 7*C*) between model predictions (fig. 7*B*) and observations (fig. 7*A*) shows that, although most of the subsidence is attributable to a point source, significant deformation remains unexplained by the simple point-source model. This result is consistent with our expectation. The horizontal component of the GPS data shows a clear southeastward displacement, almost certainly related to south-flank deformation, that cannot be explained by a symmetrical deflation. The long-wavelength signal in the vertical residual suggests an extensional process coincident with the rift zones. The closed contours of the residual near the center of the caldera may result from minor deflation at the more shallow episodic source discussed in detail below.

We expect that modeling all of the summit deformation with only a point source of deflation will somewhat bias our estimate of the point source's strength and location. Specifically, we expect that our depth and volume-change estimates will be biased on the high side, because deepening and strengthening the source will widen the wavelength of the predicted data, enabling the single point source to soak up some of the signal from the other deformation sources. To estimate how large this bias might be, we conducted an experiment, using the deformation model of Owen and others (2000). This model is complete in the sense that it contains deformation sources corresponding to each of the structures thought to contribute to summit deformation—a slipping décollement, opening rift zones, and a deflating magma chamber.

We began our experiment by calculating the deformation predicted by the model at each of the leveling benchmarks and GPS stations. Then we inverted this synthetic data set as

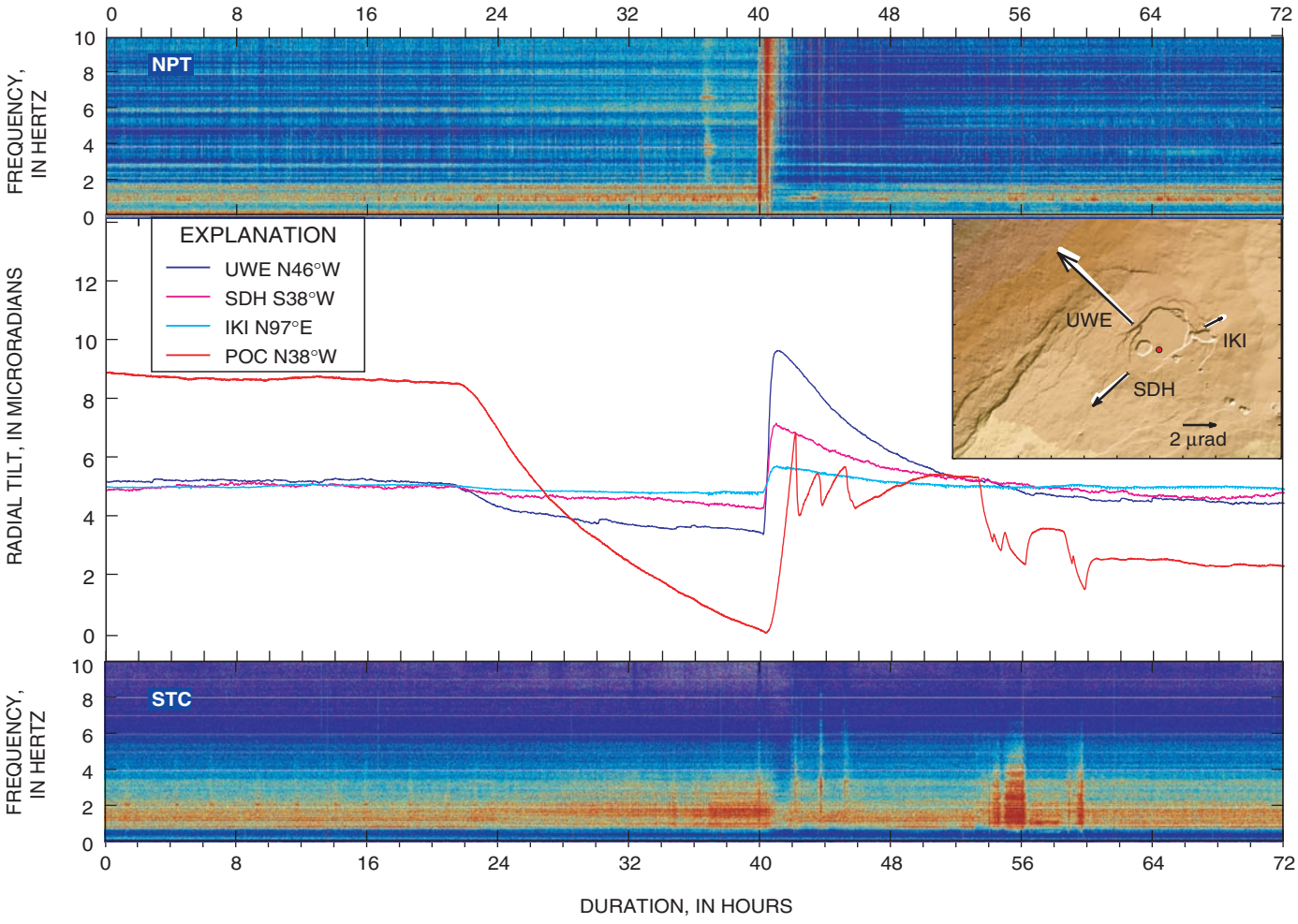

Figure 6*D*. Time series of radial component of tilt and seismic energy spectra for April 4–7, 2002. Inset map shows tilt vectors (in black) at summit for hour-long inflation. In white are tilts predicted by model of inflating point source at location shown by red circle.

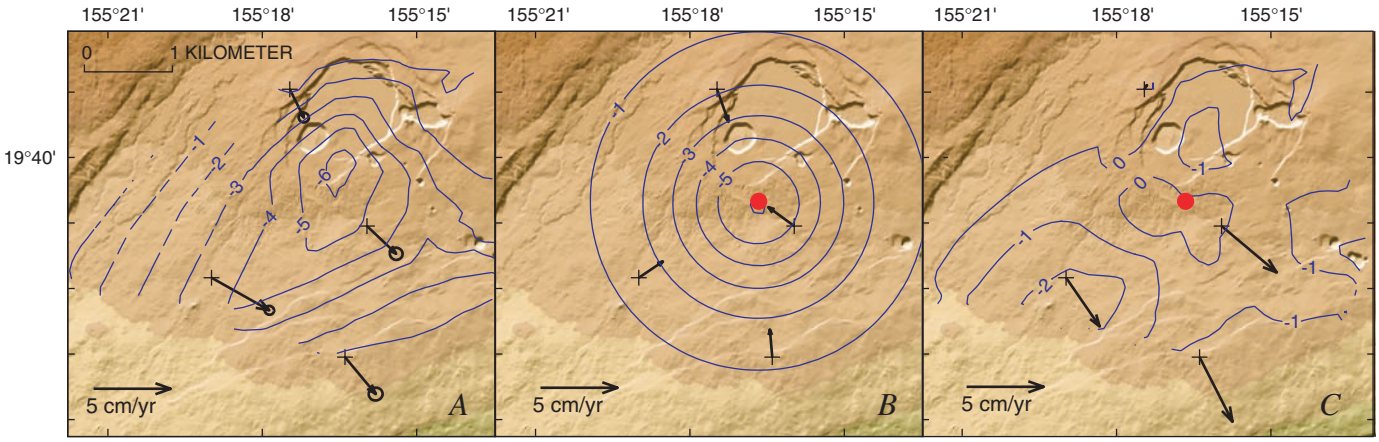

Figure 7. Comparison of observed deformation at Kīlauea's summit (fig. 1) from 1996 to 2002 and deformation predicted by model of spherical source located beneath southern caldera (red dot), about 2.5 km below sea level. *A*, 1-cm/yr contours of subsidence from leveling data relative to reference station HVO23, and horizontal motions of Global Positioning System (GPS) stations. *B*, Predicted displacements. *C*, Residual between model prediction and observation, that is, deformation not accounted for by point-source model.

above for a single point source. The synthetic data contain signals from all the deformation sources; we attempt to model the synthetic data, using only a point source. As expected, the inversion led to a source deeper and stronger than the original source given by Owen and others (2000), because the single point source absorbed some of the signal from the other deformation sources. The horizontal position was not significantly biased. Owen and others' point source was at 1.7-km depth (below the top of an elastic half-space, a datum different from the one used elsewhere in this chapter), whereas the depth resulting from our experiment was 2.2 km. More significantly, our estimated volume-change rate was almost twice that of Owen and others.

Our initial estimates of volume-change rate and depth are clearly too high. Conservatively stated, the reservoir depth is no deeper than 2.5 km and is probably closer to 2 km below sea level; the volume-change rate is about 10^6 m^3/yr and is certainly no greater than 2.5 million m^3/yr. We remain confident of our estimated horizontal position, which is well constrained by the circular symmetry of the deformation field. The question of exactly how much of the vertical-deformation signal at the summit is explained by deflation of the south-caldera magma reservoir remains murky; however, we can say that a significant fraction of the vertical deformation (approx 25 percent) is attributable to other sources.

Episodic Deformation

We estimate the location and volume change of the magma reservoir that deforms during episodic events by using the total magnitude and orientation of the tilt signals at stations UWE, IKI, and SDH (fig. 1) for rapid-inflation intervals. The tilt vectors for these intervals are especially well resolved because they are large and last only about an hour. The short duration limits contamination of the signal by various noise sources with predominantly diurnal frequencies. We account for uncertainties in the tilt vectors by considering the scatter about the mean for short periods of time before and after rapid-inflation intervals, resulting in a (diagonal) covariance matrix that we can use to appropriately weight the data in the subsequent inversion.

Model predictions and observations for each of the four deformation events and the horizontal locations of the source models are plotted in figure 6. The depths of the four sources vary considerably over a range of 130 to 450 m below ground level, or 975 to 650 m above sea level (fig. 8). This depth variation could represent a deepening of the source region over time or, alternatively, may simply reflect a large uncertainty in the depth estimate. Indeed, forward models reveal that the current summit tilt network does not provide good resolution of the depth of sources within about 1 km of the surface.

Convinced that the four deformation events share a common horizontal coordinate, we performed an inversion, using all the data simultaneously to invert for a single three-dimensional coordinate plus four volume changes corresponding to the four different events. To the extent that the errors contaminating the data are not correlated from event to event, this procedure should strengthen the inversion considerably. Three two-component tiltmeters observing the four events give 24 data points to estimate the seven model parameters, in contrast to the event-by-event analysis, which gives only 6 data points to estimate four model parameters per event. The inversion is probably not strengthened as much as it seems, because many of the errors contaminating the data are systematic over time; for example, any azimuth misalignment of the tiltmeter does not change from event to event. Nonetheless, we expect some improvement by using this "stacked" source-inversion method, given that at least some of the errors are not temporally correlated.

The green circle in figure 8 is the stacked estimate for the horizontal coordinate of the deformation source. We refer to this source as the "Halemaumau magma reservoir" because of its proximity to the prominent crater. The green line in figure 8

shows the stacked estimate of the depth—about 850 m above sea level (350 m below ground level). Our estimated location of the Halemaumau magma reservoir agrees closely with that inferred from broadband seismic data (Ohminato and others, 1998). However, our estimate of the reservoir depth is somewhat shallower; Ohminato and others imaged a finite spherical source centered about 200 m above sea level (950 m below ground level), with a radius of about 0.5 km. As discussed below, we do not believe that this discrepancy is statistically significant at the 95-percent-confidence level.

Another advantage of stacking the data over time is that we then have enough data points to estimate uncertainties in the model parameters by using the bootstrap method (Efron and Tibshirani, 1993). Briefly, this method involves randomly resampling the data vector (with replacement) numerous times and then estimating a new optimal source model for each resample. The empirical probability distribution of the model parameters is given by the parameter distribution resulting from the bootstrap. Histograms for the three model coordinates show that the horizontal coordinates are well constrained, but the depth shows a more asymmetric, long-tailed range of possibilities (fig. 9). Also shown in figure 9 is a scatter plot of depth versus volume change for the largest deformation event (May 2001). The clear correlation between these two model parameters implies that the parameters are not separable, given the current spatial distribution of data. Qualitatively, this result means that increased volume change can compensate for deeper sources, but only up to a point; the data do constrain the depth to be shallower than about sea level at a high confidence level.

In the following discussion, we use the volume changes from four episodic deformation events to estimate magma-supply rates. The geometry of the current tilt network results in poor source-depth resolution and a high correlation between depth and volume change. To obtain unbiased estimates of volume change, we decided to fix the source depth to 700 m above sea level (450 m below ground surface). This depth is not completely arbitrary because it lies well within the 95-percent-confidence level estimated by the bootstrap method, although it is not the most probable depth. Inversions in a homogeneous source tend to bias source depths as too shallow, but this bias is probably only about 50 m. Our primary reason for choosing the 700-m depth is that this depth agrees well with the depth estimates from other geophysical methods (Ohminato and others, 1998) and, moreover, does not contradict the tilt data. As of this writing, we are installing a new tiltmeter north of Halemaumau that should help resolve the source-depth question.

Discussion

We interpret these tilt events as resulting from an interruption or blockage in magma supply that affects both the Halemaumau magma reservoir and the conduit to Pu‘u ‘Ō‘ō. At the onset of the interruption, deflation begins at the summit (and slightly later at Pu‘u ‘Ō‘ō) as lava continues to exit the system through flank vents on Pu‘u ‘Ō‘ō. This deflation is the result of continued withdrawal at a time of interrupted supply. When the interruption ends, rapid inflation ensues as the accumulated and overpressurized magma below the locus of interruption rushes up into the shallow magma system. We do not speculate here about the cause of the interruption, except to note that there are several possible explanations.

If this “blocked pipe” model is correct, then the magnitude of the inflation should scale with the duration of the deflation times the magma-supply rate times an efficiency factor that measures what percentage of the magma supply is blocked. Assuming complete blockage, the magma-supply rate

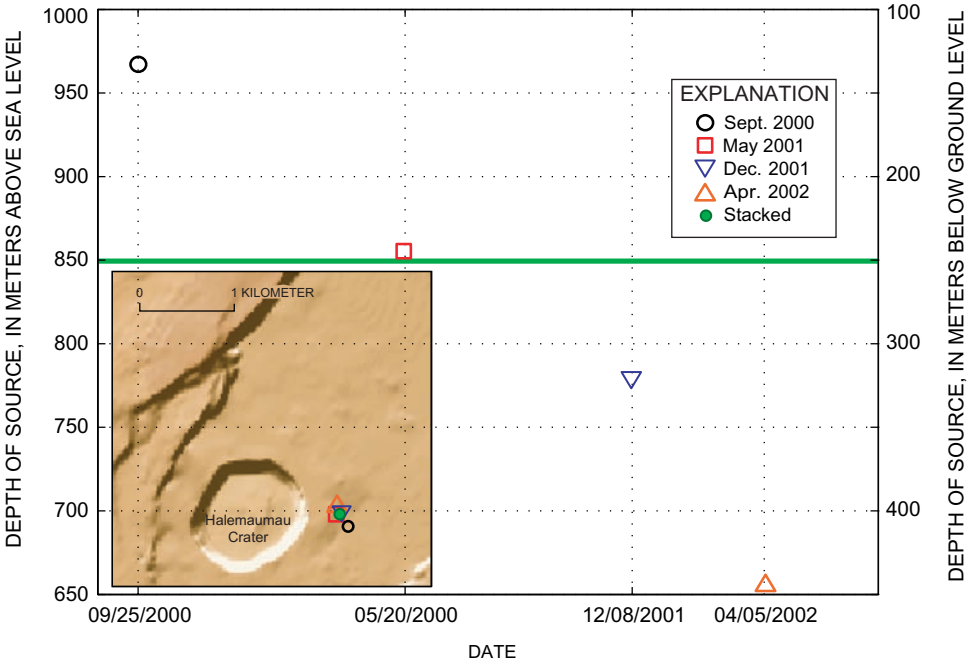

Figure 8. Depth of modeled Halemaumau magma reservoir versus time for four short-lived tilt events. Horizontal line indicates depth estimated with “stacked” model, which combines data from all four events into a single inversion. Inset map shows narrow range of horizontal locations of each modeled source.

can be estimated directly. The duration of deflation, magnitude of inflation, and estimated magma-supply rates for the four events are listed in table 1.

Table 1. Characteristics of four self-similar tilt events.

[Parameters are duration of deflationary stage, estimated volume change during inflation, and corresponding magma-supply rate, assuming a blocked-pipe model.]

Date	Duration (hours)	Volume change (10^5 m^3)	Magma supply rate (10^6 m^3/day)
09/24/2000	19.9	4.8	0.58
05/20/2001	12.8	8.4	1.58
12/09/2001	22.0	4.9	.54
04/05/2002	18.8	4.8	.61

Other estimates of magma-supply rates come from very low frequency (VLF) measurements across lava tubes leading from Pu‘u ‘Ō‘ō (Kauahikaua and others, 1996) and from SO_2 emission measurements from the eruption site (Sutton and others, 2001). The VLF data estimate just the rate of lava leaving Pu‘u ‘Ō‘ō; they are insensitive to the volume of magma being stored or emplaced elsewhere. Thus, the VLF measurements represent a minimum magma-supply rate into Kīlauea's magmatic system. Eruption-site SO_2 emissions also represent a minimum estimate for similar reasons. As expected, the magma-supply rates implied by the blocked-pipe model are systematically larger than those estimated by these two methods (fig. 10). The relative magnitudes of observed magma-supply rates seem to agree well with those predicted from the blocked-pipe model. Moreover, the exceptionally high rate we estimated during the May 2001 event corresponds to a large spike in SO_2 emissions, although curiously this spike is absent in the VLF data. However, because VLF measurements give only the cross-sectional area of the flowing lava, the conversion to lava flux rate requires a velocity estimate. Therefore, if a direct measurement of flow velocity is unavailable, VLF measurements can miss a flux spike, provided the cross-sectional area of the flowing lava (the tube) does not increase.

The tilt records give unambiguous estimates of the time lag between the onset of inflation at Kīlauea's summit and at Pu‘u ‘Ō‘ō. Using a nominal distance of 20 km from the summit to Pu‘u ‘Ō‘ō, we can estimate a propagation velocity. The tilt records also provide a direct estimate of the instantaneous flux rate into the shallow magmatic system during the inflationary stage. The propagation velocity is probably a reasonable proxy for the flow velocity through the conduit from the summit to Pu‘u ‘Ō‘ō, because, owing to the blockage, the conduit

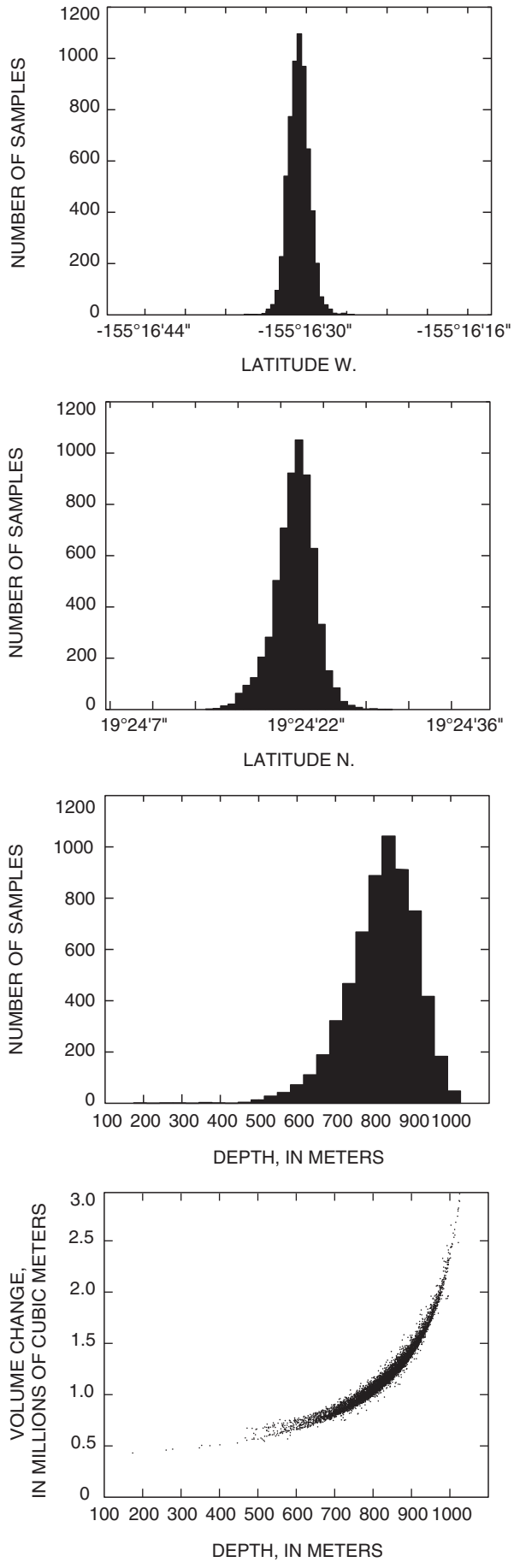

Figure 9. Probability distribution of model parameters (latitude, longitude, depth), estimated with bootstrap method. Plot of depth versus volume change (for May 2000 event) shows close correlation between these parameters. All depths below sea level; ground surface is about 1,100 m above sea level.

was in a state of low pressure before the onset of inflation. Moreover, if the propagation were really a pressure pulse, we would expect the velocity of the pulse to approximate the *P*-wave velocity of the magma, more than 1,000 m/s (Murase and McBirney, 1973).

If we assume that the flux rate through the conduit were the same as that measured at the summit, then we can estimate the radius of the conduit. Of course, this estimate assumes a cylindrical conduit, but this geometry seems likely for thermal and mechanical reasons. After the initial dike intrusion, we suggest that magma flow quickly centralized into a cylindrical conduit, much as a fissure eruption rapidly evolves into a single circular vent.

Poiseuille flow, frequently used to model the flow of viscous fluid through a pipe, gives the following relation:

$$r = (2\,Q / \pi\,u)^{1/2},$$

where r is the conduit radius, Q is the flux rate, and u is the flow velocity. Because the radius is a function of the square root of the ratio of flux to velocity, it is fairly well constrained, even given large uncertainties in Q and u. We estimate a mean conduit radius of 2.75±0.5 m (table 2). A radius of this size, in combination with the maximum flow velocities and a typical viscosity for basaltic magma (100 Pa·s), leads to Reynolds numbers averaging about 1,750. This result implies laminar flow, possibly explaining why the conduit can survive the high flow velocities associated with these deformation events. Laminar, rather than turbulent, flow may also explain the observed absence of volcanic tremor along the inferred (see below) path of the conduit.

Table 2. Estimates of conduit radius based on inferred magma-supply rate and velocity for four self-similar tilt events discussed in text.

Date	Velocity (m/s)	Rate (m^3/s)	Radius (m)
09/24/2000	16.5	150	2.4
05/20/2001	14.1	204	3.0
12/09/2001	11.7	155	2.9
04/05/2002	13.8	162	2.7

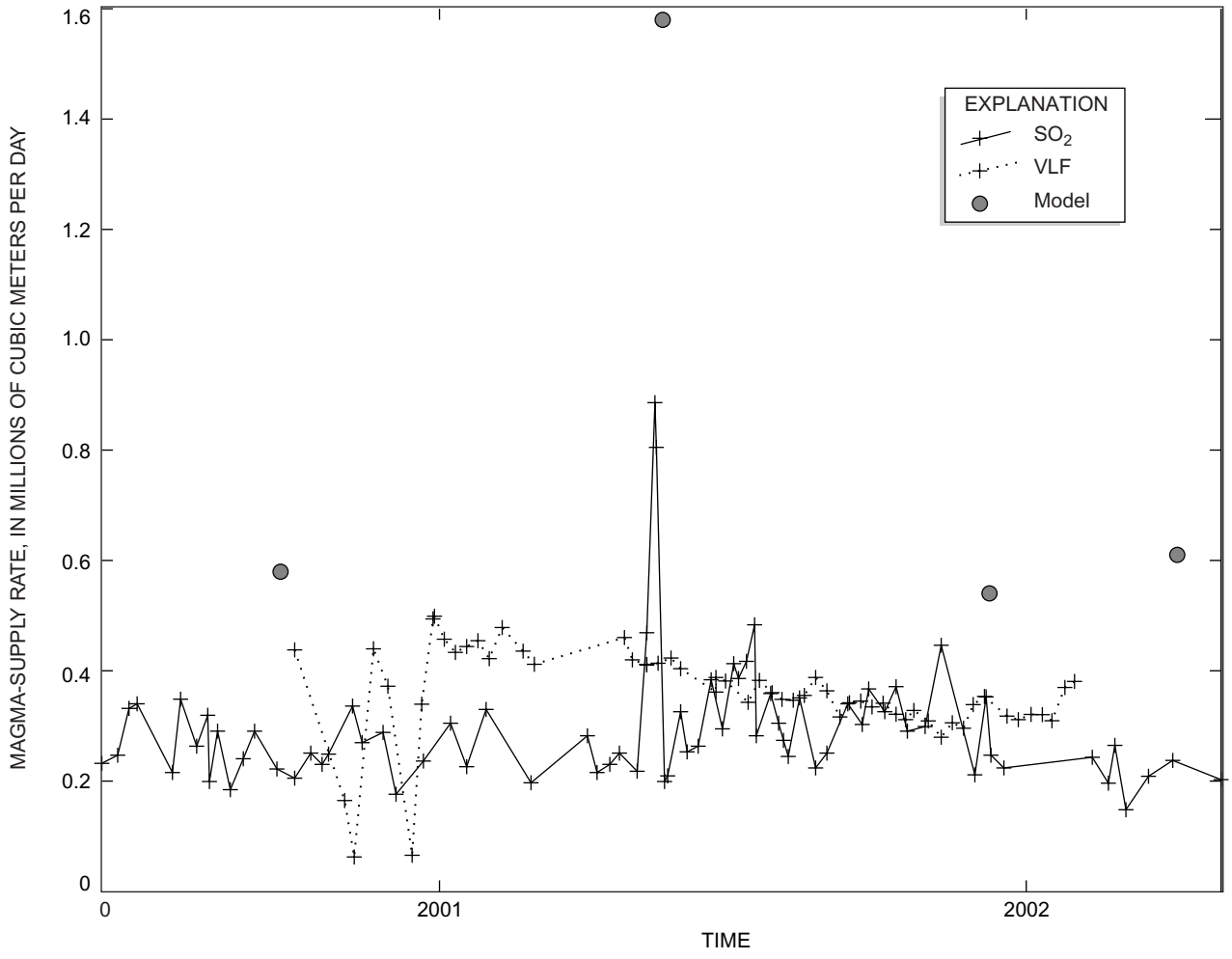

Figure 10. Comparison of magma-supply rates estimated from blocked-pipe model with (1) estimates of lava-effusion rates derived from SO_2 emissions from the eruption site, and (2) estimates of lava flux from Pu‘u ‘Ō‘ō based on very low frequency (VLF) measurements across lava tubes.

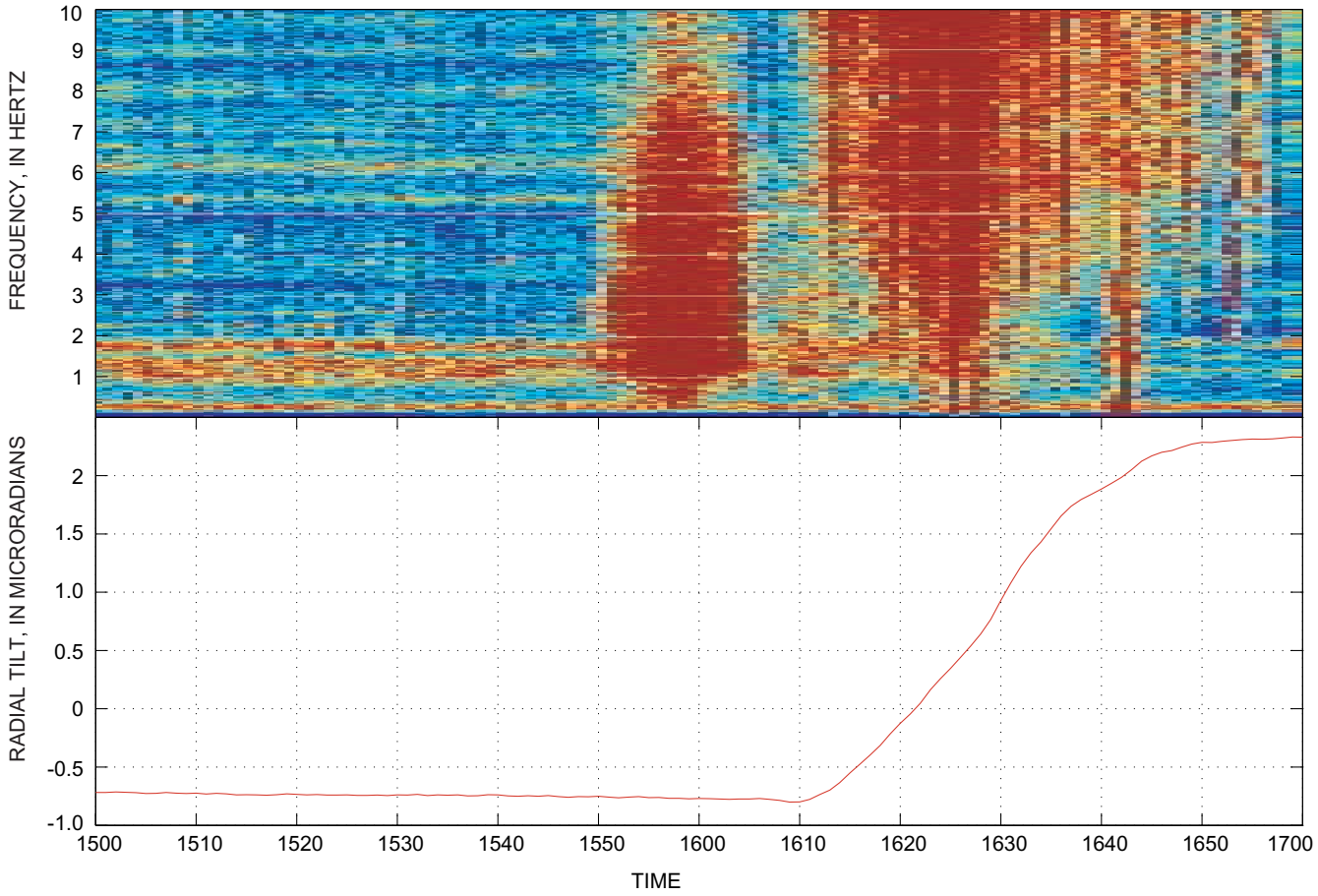

Figure 11. Detail of station NPT (fig. 1) spectrogram and station UWE radial tilt from April 5, 2002, tilt event. Note burst of seismic energy preceding inflation, followed by marked pause in seismicity until well after inflationary stage is underway.

Neither the episodic events nor the long-term deformation gives any direct indication of the depth of the conduit from Kīlauea's summit to Pu‘u ‘Ō‘ō. We consider two possible scenarios. First, the conduit could leave the Halemaumau magma reservoir and run subhorizontally until it intersects the surface topography at Pu‘u ‘Ō‘ō. Second, the conduit could leave from the deeper south-caldera reservoir and run obliquely upward to the vent. Both the summit and Pu‘u ‘Ō‘ō deflated more or less concurrently during the first phase of each deformation event, and so the interruption must have occurred below both the conduit and the Halemaumau magma reservoir. Although this information is insufficient to decide between these two possible scenarios, the fact that the interruption affected the whole shallow magmatic system leads to several interesting observations.

A closeup of the spectrogram from a seismometer located at station NPT, just north of Halemaumau (fig. 1), during the April 2002 deformation event is shown in the upper part of figure 11, and the radial tilt at station UWE in the lower part. Note that an intense burst of seismic energy begins about 19 minutes before inflation is first recorded by the tiltmeter, and then ends abruptly about 15 minutes after it began and 4 minutes before inflation. We interpret this burst of seismic energy as volcanic tremor resulting from magma flow at or near the point of interruption as the blockage is breached. Another burst of seismic energy appears on the spectrogram about 4 minutes into the inflation at the summit and lasts for another 45 minutes, ending approximately simultaneously with the inflation. This second burst of seismic energy could have resulted from tremor associated with flow out of the Halemaumau magma reservoir into the conduit toward Pu‘u ‘Ō‘ō. Other equally plausible hypotheses remain because the nature of tremor is not well understood and the locus of tremor is extremely difficult to determine. For example, the second burst of seismic energy could be a combination of numerous small summit earthquakes, triggered by the sudden inflation, and tremor from flow into a conduit toward Pu‘u ‘Ō‘ō situated well below the Halemaumau magma reservoir. Indeed, since the location of the blockage is unknown, the conduit to Pu‘u ‘Ō‘ō could originate from the south-caldera reservoir and still not contradict the data.

The connection between the south caldera reservoir, the Halemaumau magma reservoir, and Pu‘u ‘Ō‘ō can be represented by two simple models: (1) a Y-shaped model with two branches from the south-caldera reservoir, one to the Halemaumau magma reservoir, the other to Pu‘u ‘Ō‘ō; and (2) a Γ-shaped model characterized by a single "vertical" conduit from the south-caldera reservoir to the Halemaumau magma

reservoir and a single "horizontal" conduit from the Halemaumau magma reservoir to Pu‘u ‘Ō‘ō. We favor the Γ-shaped model, for the following reasons.

First, a shallow conduit is more likely than a deep conduit to remain open during the frequent pauses that have characterized many intervals of this eruption (see Heliker and Mattox, this volume), because a deep conduit would undergo significantly higher lithostatic pressures. During a pause, magma pressure within the conduit is presumed to drop; without high magma pressure, it is difficult to see how a deep conduit could remain open. Yet, after every pause to date, the eruption at Pu‘u ‘Ō‘ō has resumed.

Second, because the Halemaumau magma reservoir shows marked inflation during episodic deformation events and then deflates back to pre-event levels, the question arises of where the excess magma goes during deflation. A Y-shaped system implies that the magma drains back down, because there is no place else for it to go. In contrast, in a Γ-shaped system, the excess magma simply makes its way to Pu‘u ‘Ō‘ō and erupts onto the surface. It is difficult to understand why the Halemaumau magma reservoir would remain a persistently active part of the magmatic system under the Y-shaped scenario.

Finally, shallow intrusions into the upper east rift zone are known to affect both the Halemaumau magma reservoir and Pu‘u ‘Ō‘ō (Cervelli and others, 2002b). These dikes are probably too shallow to intersect a deep conduit to Pu‘u ‘Ō‘ō, suggesting that a Γ-shaped system is more plausible.

Conclusions

The shallow magma system of Kīlauea consists of two distinct magma reservoirs: the Halemaumau reservoir at a depth of about 700 m above sea level, and the south-caldera reservoir at a depth of about 2,500 m below sea level. The south-caldera reservoir is slowly deflating at a rate of no more than about 2.5×10^6 m^3 per year, which is about 2 percent of the total volume of lava erupted from Pu‘u ‘Ō‘ō each year.

The Halemaumau magma reservoir undergoes characteristic, episodic deflation-inflation events that we interpret as resulting from an interruption in magma supply from depth. These events occur with no obvious periodicity. The duration of the deflation and the magnitude of the inflation permit estimates of the total flux through the shallow magma system. Our flux estimates show a good qualitative agreement with other flux estimates inferred from VLF and SO_2-emission measurements.

The location of the conduit from Kīlauea's summit to Pu‘u ‘Ō‘ō is not well resolved by the available geodetic data. We argue, however, that the conduit probably emanates from the Halemaumau magma reservoir at a depth of about 700 m below the surface, with an inferred radius of about 2.75 m.

Acknowledgments

We thank Rick Hoblitt for detailed early discussions about the blocked-pipe interpretation of the episodic tilt events. The manuscript could not even have been started without the efforts of Mike Lisowski, who built the current electronic borehole tiltmeter network on Kīlauea and was also instrumental in building the continuous GPS network. Mike had help; Maurice Sako and Fran Coloma contributed especially long hours of labor and planning. Maurice also led the small army of people needed to conduct the annual leveling surveys, and we thank all of them. Paul Okubo and Jean Battaglia provided us with spectrograms and helped us understand how to interpret them. Jim Kauahikaua and Jeff Sutton gave us the measurements we needed to compare our predicted flux estimates with some realistic benchmark. Thanks to Paul Segall and Susan Owen for their contributions to the Stanford/-HVO GPS network. Michael Bevis and James Foster kindly provided data from the University of Hawai‘i's Kīlauea GPS network. Sigurjon Jonsson and Jim Kauahikaua gave quick and thorough reviews; their comments greatly improved the manuscript. Finally, we thank the editors, Christina Heliker, Don Swanson, and Jane Takahashi, for taking on the task of organizing this volume and bringing it to completion.

References Cited

Anderson, E.M., 1936, Dynamics of the formation of cone-sheets, ring-dykes, and cauldron-subsidences: Royal Society of Edinburgh Proceedings, v. 56, p. 128–157.

Árnadóttir, Thóra, Segall, Paul, and Matthews, M.V., 1992, Resolving the discrepancy between geodetic and seismic fault models for the 1989 Loma Prieta, California, earthquake: Seismological Society of America Bulletin, v. 82, no. 5, p. 2248–2255.

Cervelli, P.F., Murray, Michael, Segall, Paul, Aoki, Yosuke, and Kato, Teruyuki, 2001, Estimating source parameters from deformation data, with an application to the March 1997 earthquake swarm off the Izu Peninsula, Japan: Journal of Geophysical Research, v. 106, no. B6, p. 11217–11238.

Cervelli, P.F., Segall, Paul, Amelung, Falk, Garbeil, Harold, Meertens, C.M., Owen, S.E., Miklius, Asta, and Lisowski, Michael, 2002, The 12 September 1999 Upper East Rift Zone dike intrusion at Kilauea Volcano, Hawaii: Journal of Geophysical Research, v. 107, no. B7, p. ECV 3–1 – ECV 3–13.

Cervelli, P.F., Segall, Paul, Johnson, K.M., Lisowski, Michael, and Miklius, Asta, 2002, Sudden aseismic fault slip on the south flank of Kilauea volcano: Nature, v. 415, no. 6875, p. 1014–1018.

Delaney, P.T., Miklius, Asta, Árnadóttir, Thóra, Okamura, A.T., and Sako, M.K., 1993, Motion of Kilauea Volcano during sustained eruption from the Puu Oo and Kupaianaha vents, 1983–1991: Journal of Geophysical Research, v. 98, no. B10, p. 17801–17820.

Efron, Bradley, and Tibshirani, R.J., 1993, An introduction to the bootstrap (Monographs on Statistics and Applied Probability, no. 57): New York, Chapman & Hall/CRC, 436 p.

Fiske, R.S., and Kinoshita, W.T., 1969, Inflation of Kilauea Volcano prior to its 1967–1968 eruption: Science, v. 165, no. 3891, p. 341–349.

Johnson, K.M., Segall, Paul, and Cervelli, P.F., 2001, Analytical methods for including vertical and lateral heterogeneity of elastic properties in dislocation models and applications to two coseismic GPS data sets [abs.]: Eos (American Geophysical Union Transactions), v. 82, no. 47, supp., p. F296–F297.

Kauahikaua, J.P., Mangan, M.T., Heliker, C.C., and Mattox, T.N., 1996, A quantitative look at the demise of a basaltic vent; the death of Kupaianaha, Kilauea Volcano, Hawai‘i: Bulletin of Volcanology, v. 57, no. 8, p. 641–648.

Lichten, S.M., 1990, Estimation and filtering for high-precision GPS positioning applications: Manuscripta Geodetica, v. 15, p. 159–176.

Lichten, S.M., and Border, J.S., 1987, Strategies for high-precision global positioning system orbit determination: Journal of Geophysical Research, v. 92, no. B12, p. 12751–12762.

McTigue, D.F., 1987, Elastic stress and deformation near a finite spherical magma body; resolution of the point source paradox: Journal of Geophysical Research, v. 92, no. B12, p. 12931–12940.

McTigue, D.F., and Segall, Paul, 1988, Displacements and tilts from dip-slip faults and magma chamber beneath irregular surface topography: Geophysical Research Letters, v. 15, no. 6, p. 601–604.

Mogi, Kiyoo, 1958, Relations between the eruptions of various volcanoes and the deformation of the ground surfaces above them: University of Tokyo, Earthquake Research Institute Bulletin, v. 36, no. 2, p. 99–134.

Murase, Tsutomu, and McBirney, A.R., 1973, Properties of some common igneous rocks and their melts at high temperatures: Geological Society of America, v. 84, no. 11, p. 3563–3592.

Ohminato, Takao, Chouet, B.A., Dawson, P.B., and Kedar, Sharon, 1998, Waveform inversion of very long period impulsive signals associated with magmatic injection beneath Kilauea Volcano, Hawaii: Journal of Geophysical Research, v. 103, no. B10, p. 23839–23862.

Okada, Yoshimitsu, 1985, Surface deformation due to shear and tensile faults in a half-space: Seismological Society of America Bulletin, v. 75, no. 4, p. 1135–1154.

Owen, S.E., Segall, Paul, Lisowski, Michael, Miklius, Asta, Denlinger, R.P., and Sako, M.K., 2000, Rapid deformation of Kilauea Volcano; global positioning system measurements between 1990 and 1996: Journal of Geophysical Research, v. 105, no. B8, p. 18983–18998.

Segall, Paul, Cervelli, P.F., Owen, S.E., Lisowski, Michael, and Miklius, Asta, 2001, Constraints on dike propagation from continuous GPS measurements: Journal of Geophysical Research, v. 106, no. B9, p. 19301–19317.

Sutton, A.J., Elias, Tamar, Gerlach, T.M., and Stokes, J.B., 2001, Implications for eruptive processes as indicated by sulfur dioxide emissions from Kīlauea Volcano, Hawai‘i, 1979–1997: Journal of Volcanology and Geothermal Research, v. 108, no. 1–4, p. 283–302.

Tilling, R.I., and Dvorak, J.J., 1993, Anatomy of a basaltic volcano: Nature, v. 363, no. 6425, p. 125–133.

Williams, C.A., and Wadge, Geoffrey, 2000, An accurate and efficient method for including the effects of topography in three-dimensional elastic models of ground deformation with applications to radar interferometry: Journal of Geophysical Research, v. 105, no. B4, p. 8103–8120.

Long-Term Trends in Microgravity at Kīlauea's Summit During the Pu‘u ‘Ō‘ō-Kūpaianaha Eruption

By Jim Kauahikaua *and* Asta Miklius

Abstract

Microgravity measurements at the summit of Kīlauea Volcano over the course of the Pu‘u ‘Ō‘ō-Kūpaianaha eruption show distinctly different trends during different periods of the eruption. Rates of mass accumulation and withdrawal during these periods, computed from excess gravity changes after correction for measured elevation changes, reveal that the rates of mass change beneath the summit were only a few percent of the total volume of magma going through the volcano plumbing system and erupting at Pu‘u ‘Ō‘ō. Furthermore, the rate of net mass change in the summit reservoir was not constant; indeed, the data suggest that magma was accumulating beneath the summit from 1983 to mid-1985 and from 1991 to mid-1993. The changes in excess gravity correspond to both changes in the stress regime at the summit and changes in eruptive style. Geodetic data show that the summit was extending during periods of magma accumulation and contracting during most of the period of magma withdrawal. The periods of net loss from the summit reservoir were characterized by efficient magma transport to the eruption site. The current precise gravity monitoring of a few benchmarks can provide information about subsurface accumulation or withdrawal of mass, but monitoring can be improved by either continuous measurement at a few benchmarks or frequent measurement over a network of benchmarks.

Introduction

Precise gravity monitoring of volcanoes has come of age in the last decade or so, judging by its inclusion in recent books on volcano monitoring (Murray and others, 2000). With a spatially dense network, gravity and elevation measurements can be used to determine the amount of subsurface mass that has been added or withdrawn beneath or within a volcano. Even with a sparse network, gravity and elevation data can provide information about the density of the material added or withdrawn, if the signal is large enough and if the elevation changes are associated only with the same source as the mass change. The density can indicate the state of compression of the source material (Johnson and others, 2000).

Two early applications of the method were on Kīlauea (Dzurisin and others, 1980; Jachens and Eaton, 1980), where three distinctly different gravity-elevation relationships were observed in 1975–77, during a time of a major earthquake, rift zone intrusions, and a rift zone eruption. When the current eruption started, gravity monitoring was an obvious technique to pursue. Johnson (1992) found that mass changes in the magma reservoir could be elucidated with gravity measurements during the several-days-long inflation-deflation events associated with fountaining episodes at the beginning of the Pu‘u ‘Ō‘ō eruption. During these episodes, the large volumes of magma that were moving from the summit to the east rift in a short amount of time resulted in relatively large gravity and deformation signals. From 1984 through 1985, however, Johnson (1987) found that the ratio of gravity change to elevation change at the summit was near the free-air value; apparently no mass change was associated with the subsidence over that time. He suggested, rather, that the subsidence was due to long-term extension across the summit.

On the basis of geodetic data, Delaney and others (1998) modeled deformation rates during the current eruption using a combination of sources that fit the subsidence and extension across the summit. They found that approximately 60 percent of the subsidence from 1983 to 1991 could be attributed to deflation of a point source beneath the summit. Cervelli and Miklius (this volume) reached a similar conclusion for the 1996–2002 time period. These conclusions are based on average deformation rates over long time periods during the eruption. Changes in the deformation rates at Kīlauea's summit over the past 20 years—subtle in contrast to the large fluctuations in deformation rates in historical time (see, for example, Delaney and others, 1998)—can be correlated in time with changes in both the eruption and gravity rates. Before the advent of continuously recording geodetic networks, temporal resolution was insufficient to fully model small changes in the rate of magma withdrawal or accumulation in the summit reservoir. The gravity rate changes are subtle, as well, with average gravity-change/elevation-change ratios over the course of the eruption near the free-air gradient. The small signal-to-noise ratio, together with multiple sources of elevation change, complicate the interpretation of the gravity data.

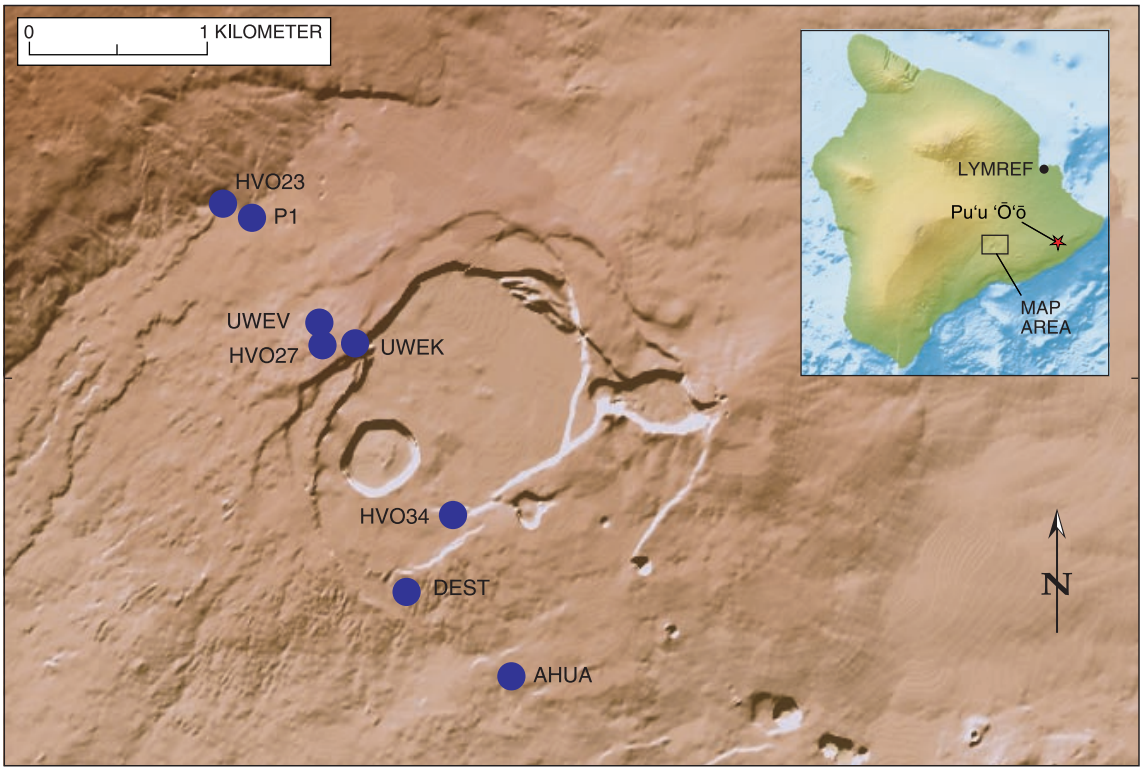

Figure 1. Shaded relief map of Kīlauea summit region showing location of gravity and elevation monitoring sites (blue dots). Inset shows location of station LYMREF and box indicating area of larger map. The Hawaiian Volcano Observatory (HVO) is located between UWEK and HVO27.

In this chapter, we use rates of gravity and elevation change, combined with the good resolution of the magma-source location provided by the long-term geodetic data, to elucidate the subtle differences in mass withdrawal and accumulation in the summit reservoir during the past 20 years of the current eruption.

Data Reduction Methods

Each precise gravity measurement consists of multiple readings with two LaCoste & Romberg gravity meters, G615 and G721, employed simultaneously. Measurements were usually continued until the standard errors were reduced below 10 µGals. The data were corrected for the effects of meter drift and tides.

Over the course of the current eruption, frequent microgravity measurements were made at two benchmarks in the summit area of Kīlauea (fig. 1). Those locations are benchmarks HVO27, on the caldera rim near the Hawaiian Volcano Observatory (HVO), and HVO34, less than 1 km from the persistent center of vertical deformation in the southern part of the Kīlauea caldera (Delaney and others, 1998; Cervelli and Miklius, this volume). The gravity measurements at these benchmarks were made relative to benchmarks LYMREF, 41 km distant in Hilo and, more frequently, P1, 2 km northwest of HVO27 (fig. 1).

Elevation changes were measured by precise leveling, usually yearly, although more frequent measurements were made early in the eruption. Expected random error of leveling surveys prior to 1988 propagates as 7 mm/km$^{1/2}$, and after 1988, as 2 mm/km$^{1/2}$ (Delaney and others, 1994). Vertical displacements in the Kīlauea summit network are measured relative to a local datum, HVO23 (fig. 1). The gravity reference site P1, only 200 m from HVO23, is also part of the leveling network, as are HVO27 and HVO34. Thus, the vertical motion of the summit gravity sites, relative to P1, is well constrained. However, only three leveling surveys originating in Hilo, far from active deformation, have been conducted since the start of the Pu‘u ‘Ō‘ō eruption; these were in 1986, 1988, and 1989.

Additional vertical information is available from GPS measurements, but reasonable resolution of the vertical signal has only been possible since about 1993. All GPS data were collected on dual-frequency receivers and processed with Gipsy/Oasis II software (Lichten and Border, 1987). The data are filtered to minimize the effects of reference frame errors (Cervelli and others, 2002).

Long-Term Data Trends

Precise gravity monitoring of a volcanically active region generally requires interpretation of gravity and elevation changes measured over the same time period at several sites.

Table 1. Computed rates of gravity and elevation change at benchmark HVO34 relative to P1.

[g is the observed gravity rate of change; Δh is the observed elevation rate of change; Δg* is the gravity rate of change corrected for the observed elevation rate of change; and s.e. is the standard error. Dashes indicate insufficient data for estimate.]

Period	Δg, mGals/yr	s.e.	Δh, m/yr	s.e.	Δg*, mGals/yr	s.e.
1983–1991	0.036	0.0004	-0.0976	0.00134	+0.0042	0.0039
1983–Apr 1985	.053	.00082	-.0976	.00134	+.021	.0040
Apr 1985–1991	.030	.00085	-.0976	.00134	-.0022	.0040
1991–1993	.0097	--	-.0142	--	+.0050	.0011
1993–2002	.019	.00067	-.060	.00054	-.0008	.0027

Table 2. Computed rates of gravity and elevation change at benchmark HVO27 relative to P1.

Period	Δg, mGals/yr	s.e.	Δh, m/yr	s.e.	Δg*, mGals/yr	s.e.
1983–1991	+0.00884	0.00075	-0.0187	0.00072	+0.0027	0.0034
1983–Apr 1985	+.0175	.00242	-.0187	.00072	+.0011	.0040
Apr 1985–1991	+.0159	.00314	-.0187	.00072	+.0097	.0045
1991–1993	.0	--	+.0163	--	+.0054	--
1993–2002	-.00383	.00186	-.0074	.00036	-.0063	.0032

Table 3. Computed rates of gravity and elevation change at benchmark HVO34 relative to LYMREF.

Period	Δg, mGals/yr	s.e.	Δh, m/yr	s.e.	Δg*, mGals/yr	s.e.
1988–1991	+0.0547	--	--		--	0.0034
1991–1993	-.00385	--	--		--	--
1993–2002	+.0229	--	[1]-0.0718		-0.00085	--

[1]Data from GPS station DEST.

Table 4. Computed rates of gravity and elevation change at benchmark HVO27 relative to LYMREF.

Period	Δg, mGals/yr	s.e.	Δh, m/yr	s.e.	Δg*, mGals/yr	s.e.
1988–1991	+0.0473	--	--	--	--	--
1991–1993	[1] -.0309	0.00184	--	--	--	--
1993–2002	+.00154	--	[2] -0.0144	--	-0.0032	--

[1] Data from BSMT instead of HVO27
[2] Data from continuous GPS station UWEV

The approach in this paper is a little different, using long-term trends in both the gravity and elevation data at two sites to determine simultaneous rates of gravity and elevation change for several different periods during the current eruption.

The rates of gravity and elevation change during specific periods were computed to minimize χ^2 in fitting the data to a line. The measured rate of elevation change was then multiplied by the measured free-air gradient and subtracted from the measured gravity change to get the residual gravity change. Formulating the rate as a χ^2 problem allowed the calculation of a standard error for each rate. These errors allowed the calculation of the standard error (s.e.) of the residual gravity rate by error propagation. The results are shown in tables 1–4.

The ratio of gravity to elevation change at the Earth's surface, called the free-air gradient, is –0.33025 (±0.0055) mGals/m at Kīlauea's summit. This value is the result of 5 measurements over the last 10 years on the 4 floors (total elevation range of 9.0 m) within the Hawaiian Volcano Observatory building on the rim of Kīlauea's caldera and agrees well with the value of –0.3273 that Johnson (1992) measured for elevation changes of about 1 m within the caldera. The free-air gradient measured at Kīlauea is nearly 10 percent more negative than the theoretical value of –0.3086 mGals/m.

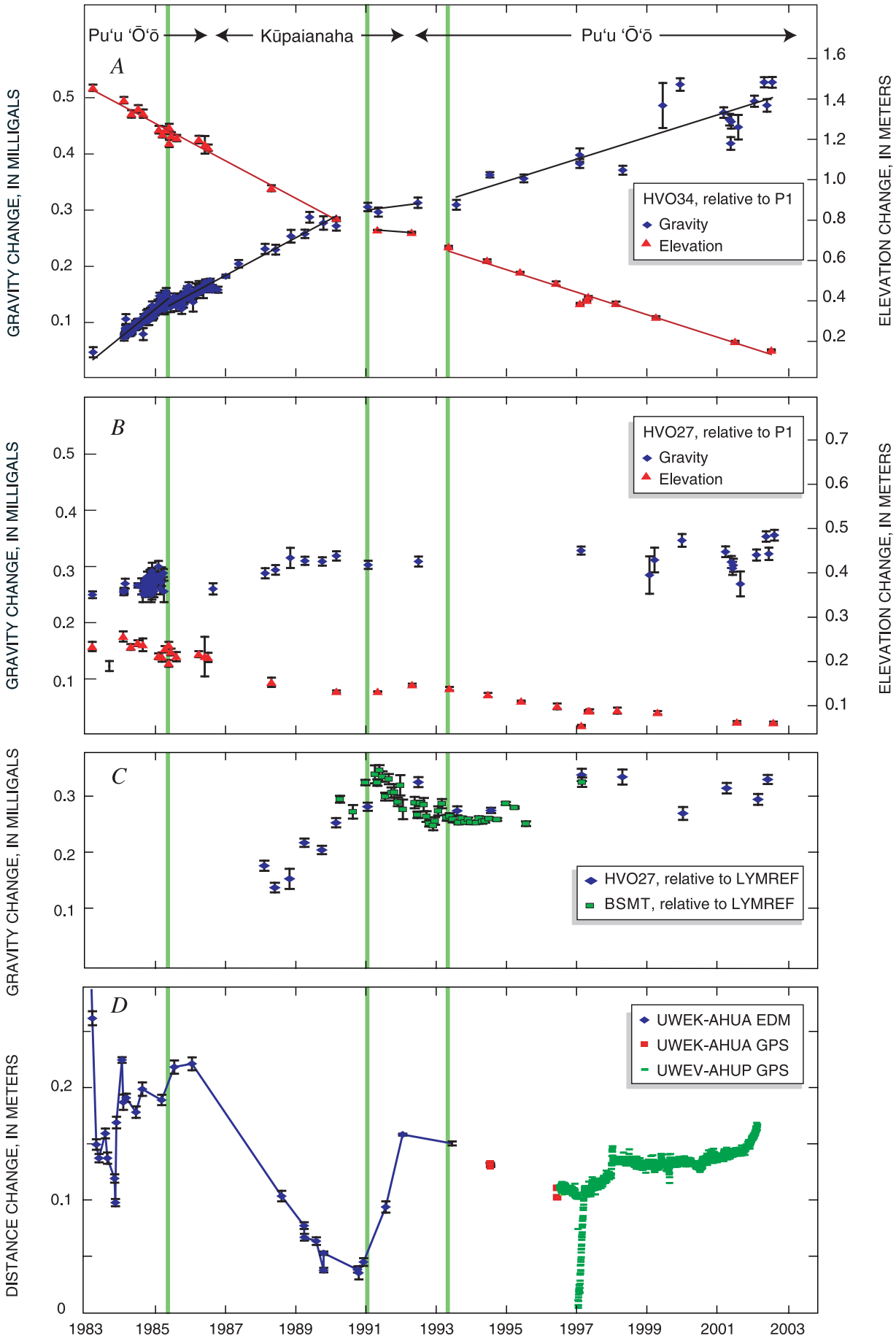
Pu‘u ‘Ō‘ō
Kūpaianaha
Pu‘u ‘Ō‘ō
A
HVO34, relative to P1
Gravity
Elevation
GRAVITY CHANGE, IN MILLIGALS
ELEVATION CHANGE, IN METERS
B
HVO27, relative to P1
Gravity
Elevation
C
HVO27, relative to LYMREF
BSMT, relative to LYMREF
D
UWEK-AHUA EDM
UWEK-AHUA GPS
UWEV-AHUP GPS
DISTANCE CHANGE, IN METERS
1983
1985
1987
1989
1991
1993
1995
1997
1999
2001
2003

The general trends for the entire 20-year span examined here are characterized by elevation decreases and corresponding gravity increases (fig. 2). The average ratio of gravity change to elevation change is very close to the free-air gradient and indicates very small mass changes beneath the summit. Several changes in rate of gravity increase correspond with changes in rate of elevation decrease and with the rate of extension/contraction across Kīlauea's summit area. Furthermore, these changes can be correlated with distinct periods of the Pu'u 'Ō'ō eruption. The time series of gravity at HVO34 relative to P1 (fig. 2*A*) best illustrates most of these changes, as this pair of stations has the densest temporal sampling of both gravity and relative elevation measurements. In addition, HVO34 is the station closest to the magma reservoir and thus records the largest rates of change, increasing the signal-to-noise ratio.

The microgravity data can be separated into four periods for which there are distinct differences in linear trend: 1983–April 1985, April 1985–January 1991, January 1991–April 1993, and April 1993–September 2002 (time of this writing).

From 1983 to mid-1985, gravity at HVO34, relative to P1, was increasing 0.05 mGals/yr, and the elevation was decreasing about 10 cm/yr (fig. 2*A*). Following an initial contraction in response to the start of the eruption, the northwest-southeast summit-crossing baseline (UWEK-AHUA, fig.1) extended about 4 cm/yr (fig. 2*D*).

As the Pu'u 'Ō'ō fountaining episodes became more regular in mid-1985, progressing to continuous effusion in mid-1986 at Kūpaianaha, the HVO34-P1 gravity trend slowed to 0.03 mGals/yr, while the elevation of HVO34 relative to P1 continued to decrease about 10 cm/yr. The summit-crossing baseline changed from extension to contraction around this time, and it contracted at a rate of about 4.5 cm/yr until 1991.

In early 1991, the lava output from Kūpaianaha began to decline (Kauahikaua and others, 1996), and gravity and elevation measurements started to record a period of very little change relative to P1. An additional gravity time series for BSMT (HVO basement), relative to the distant station LYMREF, pinpoints the inflection very clearly (fig. 2*C*). This dense, but brief, gravity time series was obtained between 1990 and 1994 in support of a cryogenic gravimetry experiment. Gravity differences between BSMT and LYMREF were measured several times a year during this experiment and are shown in figure 2*C*, along with data from nearby HVO27. These data clearly show a gravity decrease that started in early 1991 and flattened out during 1993. The rate of elevation change at the summit relative to P1 was greatly reduced during this period, although few measurements exist (fig. 2*B*). No elevation data relative to Hilo are available for this period. Stress across the summit changed from contraction to extension in early 1991 (fig. 2*D*).

Gravity measurements were sparse from 1993 to 2002. On average, gravity increased 0.02 mGals/yr and the elevation of HVO34 relative to P1 decreased at a rate of 6.0 cm/yr.

Interpretation

Quantitative interpretation of microgravity data requires precise elevation measurements at the same locations because of the dominant effect that elevation change has on gravity. Without subsurface mass changes, gravity at the Earth's surface will vary with elevation changes brought about by earth movements in a predictable fashion, defined by the free-air gradient (*FAG*). Subsurface mass changes will be evident by non-zero residual gravity changes, Δg^*,

$$g\Delta^* = \Delta g - FAG \times \Delta h ,$$

where Δg is the observed gravity change and Δh is the observed elevation change. If the subsurface mass change, ΔM_{magma}, can be approximated as a point source at horizontal distance X and depth Z from the measurement location, the resulting residual gravity can be computed

$$g\Delta^* = \Delta M_{magma}\, G \frac{Z}{(Z^2 + X^2)^{3/2}}$$

(Dzurisin and others, 1980), where G is the gravitational constant. One can solve for the mass change (or volume change assuming the density) responsible for the residual gravity response, knowing the source location. The source location cannot be determined uniquely from this sparse set of gravity data alone.

Magma accumulation and withdrawal rates for the summit chamber of Kīlauea have been estimated using these equations and the source location determined by Cervelli and Miklius (this volume). Using the average source-volume change during the eruption determined from geodetic modeling (about 0.002 km^3/yr; Delaney and others, 1993; Cervelli and Miklius, this volume) yields unrealistic magma densities. Therefore, rates of mass change were converted to rates of volume change of uncompressed magma, assuming a density of 2,600 kg/m^3 (Fujii and Kushiro, 1977) and tabulated in table 5. The horizontal parameters of this source location, determined by others (for example, Delaney and others, 1993; Owen and others, 2000), are almost identical to those used here, but depth estimates vary by about 0.5 km. An increase in source depth of 0.5 km corresponds to a 20 percent increase in estimated mass at HVO34, within the error of the estimates, and no significant increase at HVO27.

This simple model, applied to the P1-referenced data, suggests that magma accumulation occurred in the first and

Figure 2. Time series of gravity and deformation data. Green vertical lines denote time periods discussed in text. Error bars, 1 sigma. *A*, Gravity and elevation data for HVO34 relative to P1, *B,* Gravity and elevation data for HVO27 relative to P1, *C,* Gravity data for HVO27 and BSMT relative to LYMREF, and *D*, Line-length changes across summit between UWEK and AHUA. Blue symbols are EDM measurements; red, campaign GPS measurements; and green, continuous GPS measurements between UWEV and AHUP (immediately adjacent to AHUA). Rapid fluctuations in line length,1983–86 caused by episodic fountaining at Pu'u 'Ō'ō and by M6.6 Ka'ōiki earthquake, November 1983. Large contraction/extension in January 1997 corresponds to Nāpau intrusion.

Table 5. Estimated magma accumulation or withdrawal rates at Kīlauea summit, in km³/yr as computed from data for four pairs of benchmarks (see tables 1–4).

[Assumed density is 2,600 kg/m³ (Fujii and Kushiro, 1977). Mogi source is 1.11 km south of HVO34 and at 3.0 km depth (Cervelli and Miklius, this volume). Dashes indicate insufficient data for estimate.]

Period	HVO34 (P1)	HVO27 (P1)	HVO34 (LYMREF)	HVO27 (LYMREF)
1983–April 85	+0.020±.004	+0.038±.01	--	--
April 85–June 91	-.0021±.004	+.033±.01	--	--
June 91–1993	+.0047±.001	+.018	--	--
1993–2002	-.00075±.003	-.021±.01	-0.0010	-0.011

third periods and magma withdrawal during the current period. There is agreement in sign between estimates made using data from different benchmarks for the same period, although the values differ by a factor of as much as 2 or 3. The results from HVO34 and HVO27 appear to conflict for the second period; the estimate with the lowest error suggests no appreciable change in mass (HVO34), and the other available estimate suggests mass accumulation (HVO27). The results from HVO34 and HVO27 are somewhat equivocal for the current period; the estimate from HVO34 is not significantly different from zero, but the estimate from HVO27 indicates magma withdrawal. The estimated accumulation rates for the Hilo-based (LYMREF-referenced) data can be calculated only for the last period and are within two-sigma agreement with the P1-based data, indicating a small amount of magma withdrawal. In all cases, the absolute value of the estimated rates is much smaller than the estimated rate of eruption of material during the current eruption, typically around 0.13 km³/yr (Sutton and others, this volume). In other words, the magma accumulating in, or draining from, the summit reservoir is only a small fraction of the amount of lava erupted from the east rift zone.

Insights Offered into Eruption Mechanism

The estimated amounts of mass accumulation or withdrawal are only a few percent of the total magma throughput of around 0.13 km³/yr in the Kīlauea summit-Pu‘u ‘Ō‘ō system. Even though the accumulation or withdrawal rates are very small, they reflect important behavioral changes in the ongoing eruption.

The gravity data from both HVO27 and HVO34 indicate that residual amounts of magma accumulated beneath the summit area in two periods. During the first period (1983–April 1985), Pu‘u ‘Ō‘ō fountain heights were increasing, reaching their maximum by late 1984 through early 1985. The average discharge continued to increase until late 1985, when average discharge, repose-period lengths, and total summit deflation stabilized (George Ulrich, unpub. data, 1986). These trends suggest that the magma-transport system between the summit reservoir and Pu‘u ‘Ō‘ō became more streamlined as the eruption progressed.

During the second period of magma accumulation (early 1991 to 1993), lava output from Kūpaianaha declined almost linearly to zero by early 1992, when lava returned to Pu‘u ‘Ō‘ō (Kauahikaua and others, 1996). Estimated lava output rates did not return to average until early 1993. Magma-accumulation rates at the summit are estimated at 4 and 15 percent of the average rate at which lava was erupted during this period.

The final, post-1993, period is a time of sparse gravity measurements. Since lava returned to Pu‘u ‘Ō‘ō in early 1992, it has continued to issue from flank vents on the cone as of November 2002. Many short-term events have occurred since 1992, but the gravity data are too sparse to provide more information. Within errors, the data in this period suggest long-term magma withdrawal from the summit amounting to a few percent of the eruptive flux, in agreement with Cervelli and Miklius (this volume). In other words, slightly more lava is being erupted than is supplied to the summit magma reservoir.

Sutton and others (this volume) and Heliker and Mattox (this volume) show that the average eruption rate during the first 19.5 years of this eruption has been about 0.13 km³/yr. By comparison, our gravity and elevation results show that magma has been either accumulating or withdrawing from the summit magma chamber during that time at rates amounting to only a few percent of the erupted rate. The temporal correspondence between residual accumulation or withdrawal at the summit magma reservoir and the dynamics of the Pu‘u ‘Ō‘ō-Kūpaianaha eruption supports the well-accepted idea that erupting lava is supplied through the summit magma chamber (Dvorak and others, 1992). The mass changes at Kīlauea’s summit are much smaller than the erupted mass, and the erupted magma is clearly not supplied mainly from storage in the summit magma reservoir. Rather, the summit magma chamber is only a waypoint for magma en route to eruption.

Lessons for the Future of Precise Gravity Monitoring

In principle, the combination of precise gravity and elevation measurements can be useful in monitoring magma accumulation and withdrawal in the Kīlauea summit region. This paper demonstrates what can be done with limited microgravity data at two benchmarks during an eruption. Coincident elevation data allow calculation of residual gravity changes with time. However, gravity and elevation, infrequently measured at a few benchmarks, are not sufficient to determine source location or density when more than one deformation source exists. Interpretation of such data requires an estimate of source location derived from other geodetic data. The source volumes estimated by Delaney and others (1993) and Cervelli and Miklius (this volume) are

broadly consistent with those calculated from gravity and elevation data in this paper. Therefore, the current sparse gravity-monitoring data can corroborate and, perhaps, refine some aspects of an eruption model determined with the modern geodetic network. The effectiveness of gravity-monitoring measurements can be increased by making continuous measurements at a few key sites in order to better constrain the rates (Zerbini and others, 2001) or by making frequent measurements at a network of sites. Inclusion of gravity data within the geodetic data sets remains the only way to measure the accumulation or withdrawal of subsurface mass and is, therefore, worthy of this increased effort.

Acknowledgments

Our thanks to Gary Puniwai, who acquired most of the gravity data between 1988 and 1995, and to the various student volunteers who filled in the gravity time series data after 1997. Dan Johnson and Tom Wright made the gravity measurements before 1988. No HVO staff member, nor summer volunteer, escaped conscription onto leveling crews at some point. Thanks to all who contributed, and especially to Maurice Sako, who headed the majority of the crews. Constructive reviews and comments were graciously given by Peter Cervelli, Rick Hoblitt, Christina Heliker, Jane Takahashi, Don Swanson, and Dan Johnson.

References

Cervelli, P.F., Segall, Paul, Johnson, K. M., Lisowski, Michael, and Miklius, Asta, 2002, Sudden aseismic fault slip on the south flank of Kilauea volcano: Nature, v. 415, no. 6875, p. 1014–1018.

Delaney, P.T., Denlinger, R.P., Lisowski, Michael, Miklius, Asta, Okubo, P.G., Okamura, A.T., and Sako, M.K. , 1998, Volcanic spreading at Kilauea, 1976–1996: Journal of Geophysical Research, v. 103, no. B8, p. 18003–18023.

Delaney, P.T., Miklius, Asta, Árnadóttir, Thóra, Okamura, A.T., and Sako, M.K., 1993, Motion of Kilauea Volcano during sustained eruption from the Puu Oo and Kupaianaha vents, 1983–1991: Journal of Geophysical Research, v. 98, no. B10, p. 17801–17820.

Delaney, P.T., Miklius, Asta, Árnadóttir, Thóra, Okamura, A.T., and Sako, M.K., 1994, Motion of Kilauea Volcano during sustained eruption from the Puu Oo and Kupaianaha vents, 1983–1991; supplemental information: U.S. Geological Survey Open-File Report 94–567, 23 p.

Dvorak, J.J., Johnson, C.E., and Tilling, R.I., 1992, Dynamics of Kilauea Volcano: Scientific American, v. 267, no. 2, p. 46–53.

Dzurisin, Daniel, Anderson, L.A., Eaton, G.P., Koyanagi, R.Y., Lipman, P.W., Lockwood, J.P., Okamura, R.T., Puniwai, G.S., Sako, M.K., and Yamashita, K.M., 1980, Geophysical observations of Kilauea volcano, Hawaii; 2. Constraints on the magma supply during November 1975–September 1977, *in* McBirney, A.R., ed., Gordon A. Macdonald memorial volume: Journal of Volcanology and Geothermal Research, v. 7, no. 3–4, p. 241–269.

Fujii, Toshitsugu, and Kushiro, Ikuo, 1977, Density, viscosity, and compressibility of basaltic liquid at high pressures: Carnegie Institution of Washington Year Book 76, no. 1730, p. 419–424.

Jachens, R.C., and Eaton, G.P., 1980, Geophysical observations of Kilauea volcano, Hawaii; l. Temporal gravity variations related to the 29 November, 1975, *M*=7.2 earthquake and associated summit collapse, *in* McBirney, A.R., ed., Gordon A. Macdonald memorial volume: Journal of Volcanology and Geothermal Research, v. 7, no. 3–4, p. 225–240.

Johnson, D.J., 1987, Elastic and inelastic magma storage at Kilauea Volcano, chap. 47 *of* Decker, R.W., Wright, T.L., and Stauffer, P.H., eds., Volcanism in Hawaii: U.S. Geological Survey Professional Paper 1350, v. 2, p. 1297–1306.

Johnson, D.J., 1992, Dynamics of magma storage in the summit reservoir of Kilauea Volcano, Hawaii: Journal of Geophysical Research, v. 97, no. B2, p. 1807–1820.

Johnson, D.J., Sigmundsson, Freysteinn, and Delaney, P.T., 2000, Comment on "Volume of magma accumulation or withdrawal estimated from surface uplift or subsidence, with application to the 1960 collapse of Kīlauea volcano" by P.T. Delaney and D.F. McTigue: Bulletin of Volcanology, v. 61, no. 7, p. 491–493.

Kauahikaua, J.P., Mangan, M.T., Heliker, C.C., and Mattox, T.N., 1996, A quantitative look at the demise of a basaltic vent; the death of Kupaianaha, Kilauea Volcano, Hawai'i: Bulletin of Volcanology, v. 57, no. 8, p. 641–648.

Lichten, S.M., and Border, J.S., 1987, Strategies for high-precision global positioning system orbit determination: Journal of Geophysical Research, v. 92, no. 12, p. 12751–12762.

Murray, J.B., Rymer, Hazel, and Locke, C.A., 2000, Ground deformation, gravity, and magnetics, *in* Sigurdsson, Haraldur, Houghton, B.F., McNutt, S.R., Rymer, Hazel, and Stix, John, eds., Encyclopedia of volcanoes: San Diego, Calif., Academic Press, p. 1121–1140.

Owen, S.E., Segall, Paul, Lisowski, Michael, Miklius, Asta, Denlinger, R.P., and Sako, M.K., 2000, Rapid deformation of Kilauea Volcano; global positioning system measurements between 1990 and 1996: Journal of Geophysical Research, v. 105, no. B8, p. 18983–18998.

Zerbini, Susanna, Richter, Bernd, Negusini, Monia, Romagnoli, Claudia, Simon, Dietrich, Domenichini, Francesco, and Schwahn, Wolfgang, 2001, Height and gravity variations by continuous GPS, gravity and environmental parameter observations in the southern Po Plain, near Bologna, Italy: Earth and Planetary Science Letters, v. 192, no. 3, p. 267–279.

Tectonic Pulses During Kīlauea's Current Long-Term Eruption

By Paul Okubo *and* Jennifer S. Nakata

Abstract

The 20-year-old eruption of Kīlauea Volcano at Pu'u 'Ō'ō and Kūpaianaha in the east rift zone has afforded unprecedented opportunities to observe and monitor sustained, long-term eruptive behaviors. In Hawai'i, surface deformation rates are such that, over the course of this eruption, tectonic processes might significantly influence or couple with volcanic processes. When the eruption shifted its center of activity uprift to Pu'u 'Ō'ō, the principal vent, from downrift Kūpaianaha, we observed magmatic pulses, in the form of intrusions, into Kilauea's summit caldera or east rift zone. These pulses were apparently coupled with occasional earthquake swarms or sequences of faulting along the Ka'ōiki system of normal faults bordering Kīlauea's summit caldera. These normal faults have experienced a renewed rate of seismogenic activity since the 1983 M6.6 Ka'ōiki earthquake beneath Mauna Loa's southeast flank. We present our observations suggesting that the Ka'ōiki faulting does indeed couple with the series of dike intrusions that marked a transitional eruptive stage.

Introduction

As of 2003, Pu'u 'Ō'ō-Kūpaianaha eruption has continued for 20 years. It has featured numerous distinct episodes (Wolfe and others, 1987; Mangan and others, 1995; Heliker and others, 1998). The different eruptive styles and shifting vent locations in these episodes are suggestive of different eruptive stages. The detailed observations associated with present eruption monitoring will no doubt lead to improved insights on the evolution of, and transition between, these different eruptive stages. Perhaps as important, given the high average rates of measured surface displacements (Owen and others, 1995), tectonic plate motions, and recurrence of large earthquakes (Klein and others, 2001) in Hawai'i, the 20-year duration of the Pu'u 'Ō'ō-Kūpaianaha eruption can be productively studied in terms of the relationship and possible interactions between magmatic and tectonic processes.

In late 1990, an earthquake swarm signaled a magmatic intrusion into Kīlauea's summit caldera following more than 4 years of steady, effusive eruption from Kūpaianaha—a vent 3 km downrift of Pu'u 'Ō'ō. Such earthquake swarms had been absent from Kīlauea since the earliest stages of the eruption. Between 1990 and 1993, four more magma intrusions—announced by their respective earthquake swarms—occurred between Kīlauea's summit and Pu'u 'Ō'ō. This paper describes these intrusions and points out their association with a family of tectonic earthquakes reactivated by a M6.6 earthquake in 1983 beneath the flank of Mauna Loa (P. Okubo and J. Nakata, unpub. data, 2002). The work uses data from catalogs of hypocentral parameters and other seismic observations, derived according to standard HVO seismic data processing practice (for example, Nakata, 2002).

Overview of Eruption-Related Seismicity

Seismicity patterns preceding the January 3, 1983, beginning of the current eruption have been described in Klein and others (1987) and Koyanagi and others (1988). We agree with those authors in interpreting some of the patterns in microseismicity, especially increased seismicity in the summit and rift zones, to indicate magma transport through Kīlauea's magma storage and transport complex. Figure 1 is a map of the summit and rift zones of Kīlauea, showing various geologic features and locations of seismographic stations.

The early stages of the eruption were marked by repeating episodes of high lava fountains from Pu'u 'Ō'ō. Koyanagi and others (1988) describe their characteristic seismic pattern: (1) an increase in the level of short-period summit earthquake activity (SPC), coincident with inflation of the caldera region as monitored via an electronic tiltmeter on the northwest side of the caldera; (2) shallow long-period (LPC-A) earthquakes beneath the summit caldera, following the rapid deflation of the summit region accompanying the onset of a fountaining episode; and (3) the emergence of deeper long-period (LPC-C) earthquakes within the summit caldera, with lower dominant frequency of oscillation than the LPC-A earthquakes. Hypocentral coordinates, calculated from seismic-wave first-arrival times for larger LP events

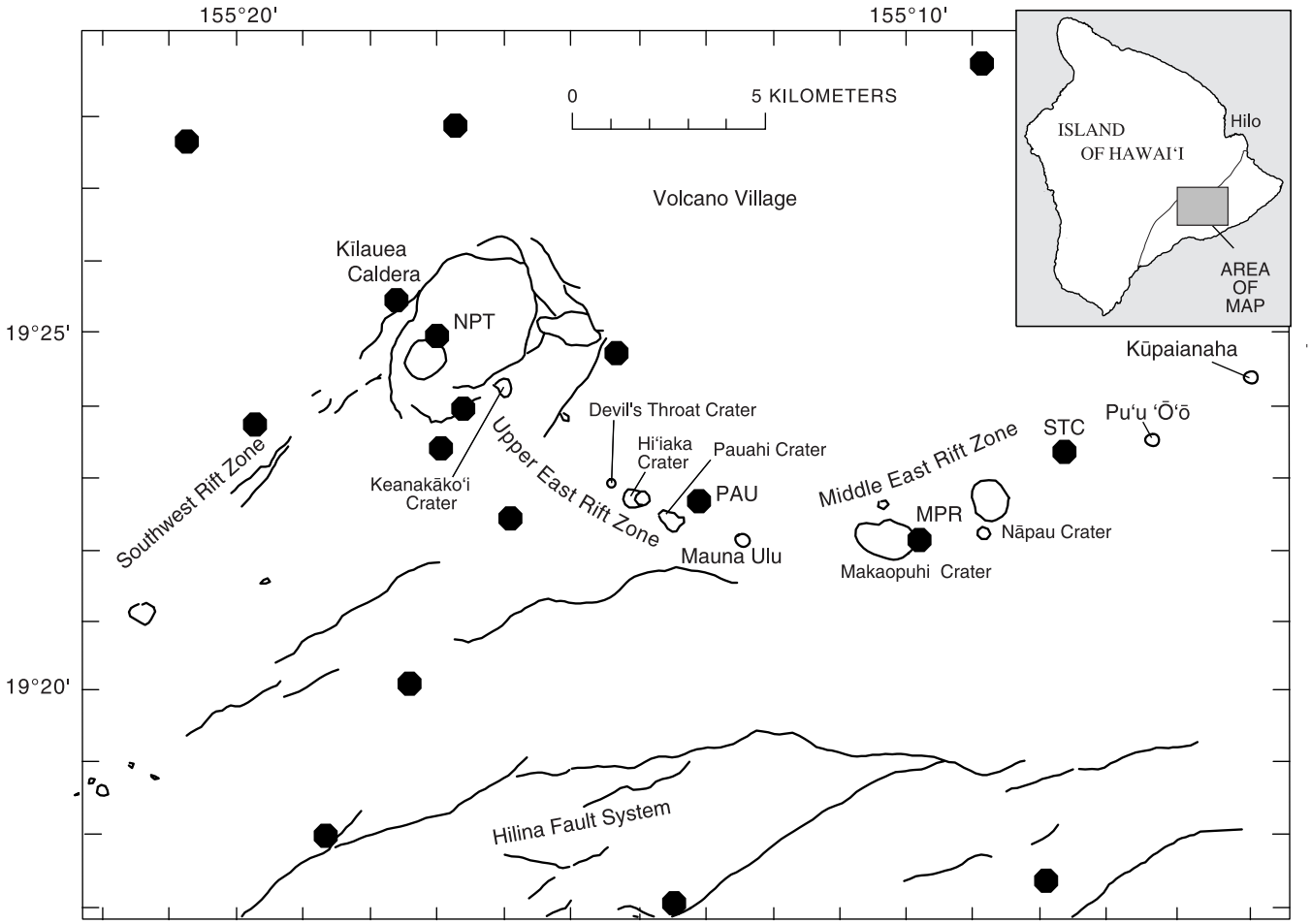

Figure 1. Map showing Kīlauea summit and east rift zone, including seismographic stations (black octagons), faults (lines), craters, and other features.

and events whose first-arrivals were adequately identified, show that LPC-A earthquakes have focal depths of 0–5 km and LPC-C earthquakes, 5–13 km (Koyanagi and others, 1988).

This pattern of seismicity is illustrated in figure 2, which shows 1985 earthquake-count data derived from the daily scanning of a continuous recording of seismic data traces on a Develocorder microfilm recorder. Event counts were compiled by recognizing combinations of waveform characteristics and dominant frequencies of oscillation, principally at station NPT in Kīlauea's caldera; distributions of waveform arrivals and amplitudes about the broader network were used to distinguish between SPC and LPC-A or LPC-C. These scanning procedures and classification criteria result in a qualitative compilation of Kīlauea seismicity. The overall trends in earthquake number, and the ability to calculate hypocentral coordinates for subsets of these earthquakes, afford some confidence toward incorporating these observations into a broader volcanic context. Also included in figure 2 are daily counts of earthquakes from the upper to middle east rift (UER/MER) zone of Kīlauea.

In July 1986, activity shifted from Pu'u 'Ō'ō to Kūpaianaha, a vent that developed a standing lava pond 3 km downrift of Pu'u 'Ō'ō. Flows from this lava pond built a shield and eventually extended downslope via a system of lava tubes (Mangan and others, 1995; Heliker and others, 1998). During the period from July 1986 through November 1990, earthquake swarm activity typically associated with magmatic dike intrusion was absent, consistent with the steady rates of lava production from the eruptive vents.

Figure 3 shows daily earthquake counts for the years 1986 through 1993. This period spans most of Kūpaianaha's eruptive duration of July 1986 to February 1992. The first half of 1986 shows the repeating pattern of earthquake variation beneath Kīlauea's summit caldera associated with the last of the 44 Pu'u 'Ō'ō fountaining episodes. Through much of Kūpaianaha's span, seismicity in the east rift zone, as recorded by counted UER/MER microseismicity, averaged approximately 100 events per day.

Clear departures from the steady UER/MER counts of earthquakes in Kīlauea's east rift zone are seen beginning in June 1987, in September 1988, in June 1989, and at several times during 1990 (see fig. 3). In June 1987, the eruptive vent at Pu'u 'Ō'ō enlarged significantly, and the elevated levels of counted UER/MER microearthquakes are largely due to numerous earthquakes and rockfalls associated with the collapse of the walls of the newly formed crater. On September

17, 1988, a swarm of earthquakes occurred in Kīlauea's upper east rift zone, extending between Kīlauea's caldera and Mauna Ulu. No other observations indicative of magmatic intrusion were associated with these earthquakes. On June 25, 1989, at 1727 H.s.t., the steady seismicity levels in the east rift zone were punctuated by the mainshock/aftershock sequence of a M6.1 Kīlauea south flank earthquake near Kalapana. Despite the size of that earthquake, no direct influence on the eruption was observed. The fluctuations in east-rift seismicity through 1990 are associated with a series of pauses in the eruption, when the extrusion of lava through the Kūpaianaha tube system stopped for different lengths of time and subsequently restarted (Okubo, 1994; Heliker and others, 1998; Heliker and Mattox, this volume).

Kīlauea's summit microseismicity, classified in the manner described above, shows greater variability during the time period from 1986 through 1990. Overall SPC counts appear to decrease from 1987 through 1990. In April 1988, a week-long pause in lava-flow activity was observed at Kūpaianaha. The large numbers of SPC earthquakes in late April, continuing into May 1988 (fig. 3), are associated with this pause. The sporadic spikes in SPC counts registered through 1990 are related to the series of eruption pauses at Kūpaianaha (Heliker and others, 1998). Long-period caldera earthquakes (both LPC-A and LPC-C) occurred in swarms not clearly related to changes in the eruption. Beginning in February 1989, elevated levels of LPC-C counts became apparent. These higher levels continued into early 1990, ending with the onset of the series of eruptive pauses mentioned above. Like other aspects of the eruption, summit microseismicity appeared relatively unaffected by the M6.1 earthquake in June 1989.

Intrusive Swarms

The Kūpaianaha eruptive pauses during 1990 have been described as precursory to the eventual demise of the down-rift vent (Mangan and others, 1995). From mid-1990 through 1991, activity gradually shifted from Kūpaianaha back to Pu‘u ‘Ō‘ō, and the last Kūpaianaha pause was observed in November 1990. Shortly after that pause a series of magma intrusions began while both Kūpaianaha and the lava pond at Pu‘u ‘Ō‘ō remained active. The period of Kūpaianaha pauses and rift-zone intrusions has been described as a transitional stage as the eruption returned to Pu‘u ‘Ō‘ō (Mangan and others, 1995).

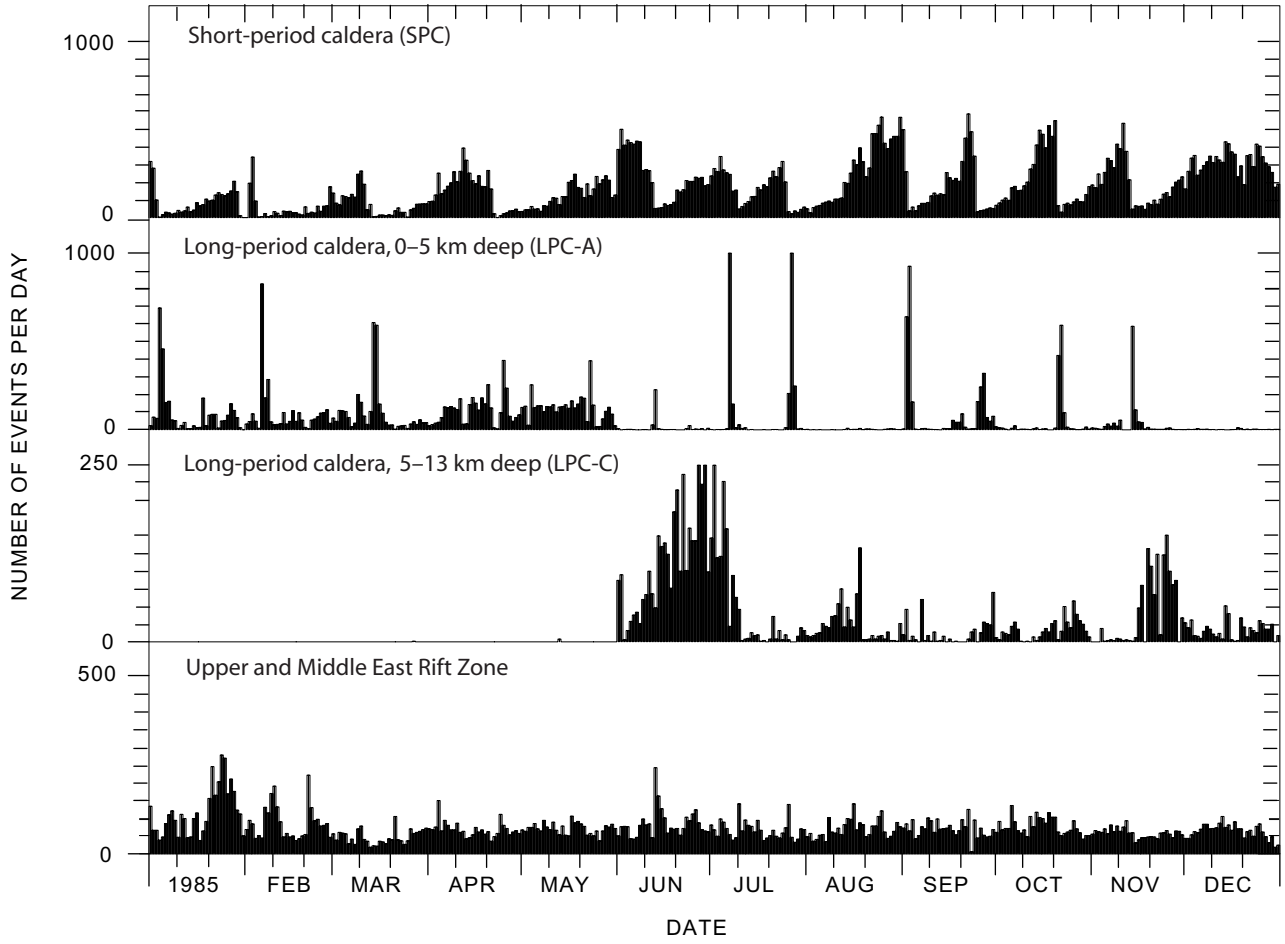

Figure 2. Daily earthquake classification for Kīlauea during 1985, assembled from daily scanning of HVO Develocorder microfilm record.

On December 4, 1990, an intrusion occurred beneath the eastern portion of Kīlauea summit and extended into the uppermost east rift zone. At approximately 1630 H.s.t., a microearthquake swarm started near Keanakāko‘i Crater. This activity was immediately preceded by a small M2 earthquake near Makaopuhi Crater. Approximately 15 minutes after the onset of the swarm near Keanakāko‘i, rapid summit inflation started, and both the amplitude of continuous tremor and summit earthquake activity increased. Maximum tremor amplitude occurred between 1735 and 1810 H.s.t. on December 4. Following this peak, the microearthquake activity continued beneath the summit and extended southeastward toward Mauna Ulu (fig. 4*A*). Elevated seismicity beneath the summit and upper east rift zone continued into the next morning, and the peak in microearthquake activity was followed by another burst of intermediate-depth long-period earthquakes (fig. 3).

This intrusion appears to have involved principally the upward transport of magma to shallower depths beneath the summit and into the adjacent east rift zone of the volcano. Following the intrusion on December 4, Kīlauea's summit gradually reinflated through the month without marked variations in seismicity.

Shallow LP activity continued through the first 3 months of 1991 (fig. 3). This pattern changed with the second intrusion into the east rift zone in March 1991. At approximately 0532 H.s.t. on March 26, a shallow earthquake swarm (depths less than 5 km) started in the upper east rift zone, between Pauahi Crater and Mauna Ulu, 6 km southeast of the caldera rim and 15 km uprift of the active Kūpaianaha vent (fig. 4*B*). Five minutes later, a very sharp deflation of the summit began, and, in two stages, 7–8 microradians of deflation was registered at the summit by late March 27. Intense seismic activity occurred between 0530 and 0830 H.s.t. on March 26 before tapering off. Many of these earthquakes were felt, both in Volcano village and by field workers near Pauahi Crater. Seismicity along the upper east rift zone continued through the end of March at a higher level than the average rate for the early part of the month. On March 28, three earthquakes in the magnitude-4 range occurred beneath Kilauea's south flank, along the Hilina fault system. These

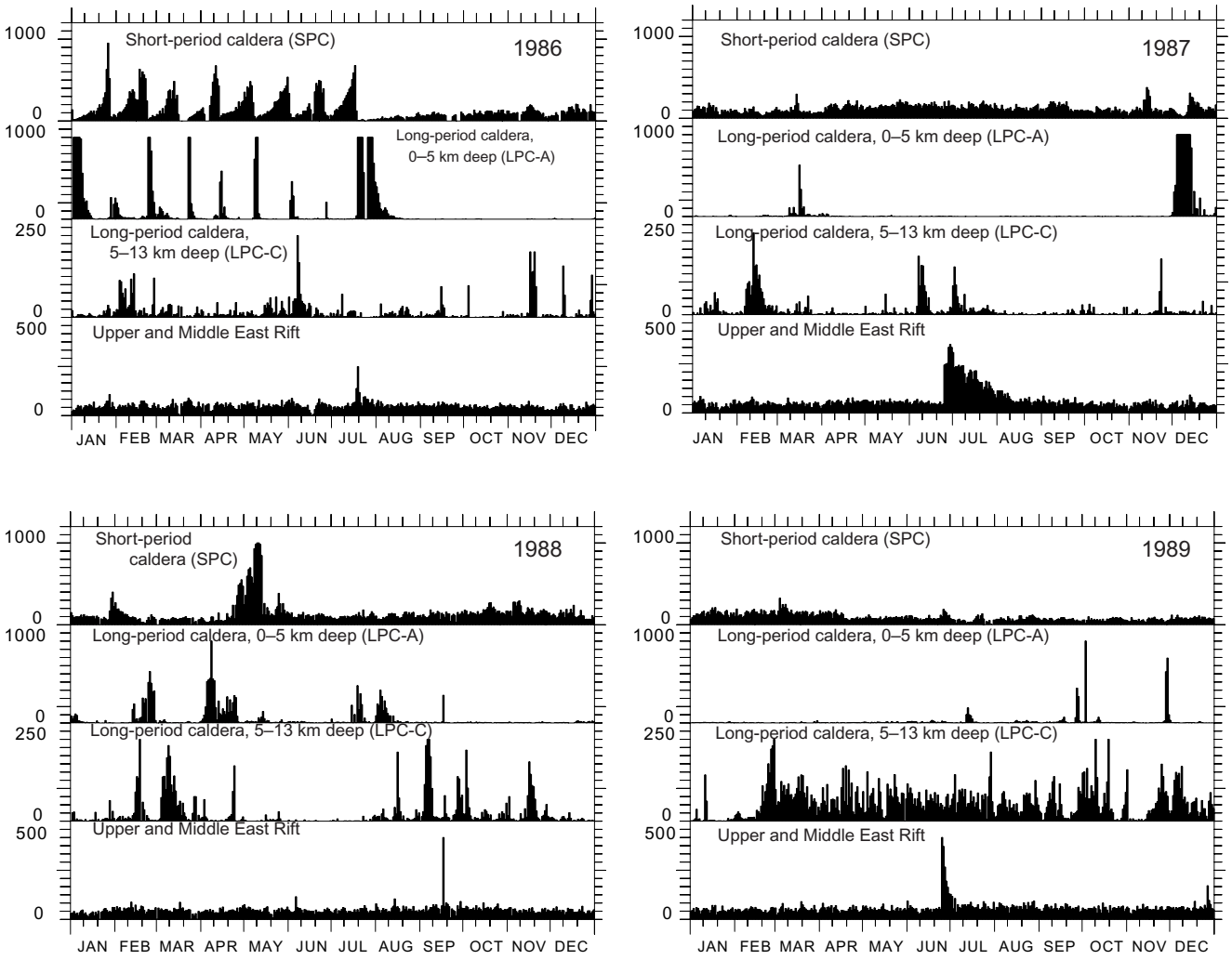

Figure 3. Daily earthquake classification for Kīlauea, 1986 to 1991, assembled from daily scanning of Develocorder microfilm record.

earthquakes were possibly triggered by the intrusion into the upper section of the east rift zone.

The third intrusion accompanied by a swarm of shallow rift-zone microearthquakes occurred on August 21, 1991. Between 1100 and 1200 H.s.t., more than 200 shallow summit microearthquakes were registered. The earthquake count quickly dropped off in the next hour, but elevated levels of seismicity continued in the upper east rift zone through the next day. The largest concentration of events was just southeast of Kīlauea's caldera, and very few events were located beyond Hi'iaka Crater (fig. 4*C*). Most of the events beneath the summit and uppermost section of the east rift zone were related to the intrusive swarm.

The next intrusion, in March 1992, was accompanied by an intense swarm of shallow earthquakes along the rift zone between Devil's Throat and Pauahi Crater (fig. 4*D*). The swarm began at approximately 0045 H.s.t. on March 3, with more than 2,000 events listed in the hourly counts obtained from the HVO Develocorder between 0000 and 0500 that day. During these hours, 139 events were recorded well enough to allow precise computer estimation of hypocentral parameters. The intrusion and the earthquake swarm were coincident with summit deflation and apparent downrift inflation. Seismicity did not migrate either uprift or downrift. These events are also linked to the termination of eruptive episode 50 (Mangan and others, 1995). Renewed eruptive activity, designated as eruptive episode 51 (Heliker and others, 1998), began on March 7 following a period of elevated volcanic tremor at Pu'u 'Ō'ō that registered at the STC seismographic station. With the onset of episode 51, seismicity along the Devil's Throat-to-Pauahi Crater segment returned to levels observed before episode 50.

The fifth intrusive swarm occurred in February 1993 (fig. 4*E*). A dramatic increase of activity occurred at 2325 H.s.t. on February 7. Strong responses were observed both at Kīlauea's summit and in the rift zone. High-amplitude volcanic tremor began at 2325 H.s.t. and essentially saturated the record at station MPR for two hours. During this period, the amplitude of volcanic tremor at NPT and throughout Kīlauea's summit area gradually increased as the summit rapidly deflated. At

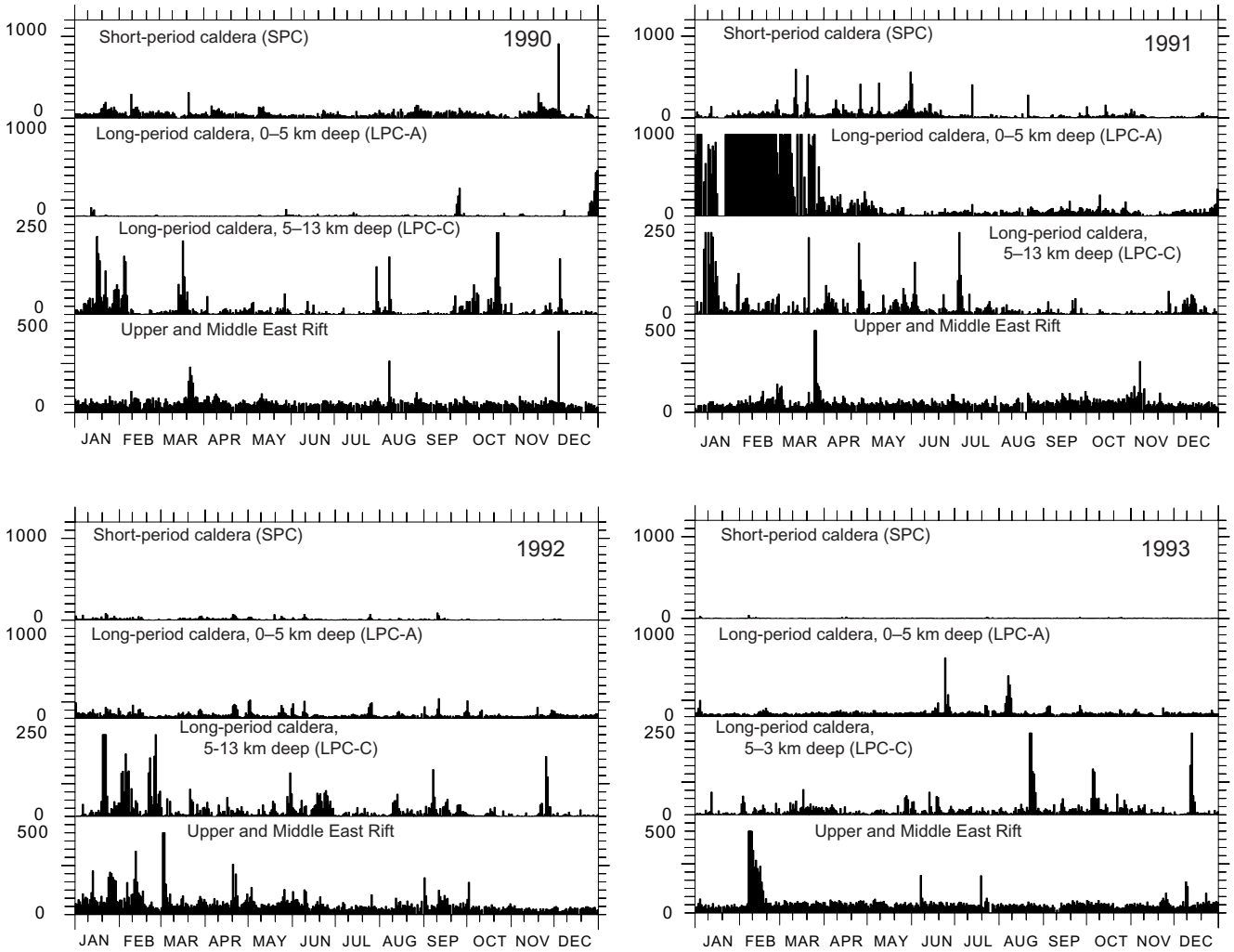

Figure 3. Continued.

0100 H.s.t. on February 8, decreasing amplitude of continuous tremor made it possible to distinguish discrete events on the upper east rift seismic records as the summit continued to register strong tremor and deflation. By 0400 H.s.t. on February 8, eruption tremor had dropped to quiet background levels in the east rift zone.

From the morning of February 8, earthquake activity continued to taper to lower, steady levels. Through the first 48 hours of the swarm, more than 5,000 events were counted. Many of the located events clustered near Makaopuhi Crater (fig. 4*E*). The strong shallow tremor beneath Kīlauea caldera, registered at station NPT, continued for approximately 18 hours before gradually returning to background levels. As the intensity of activity near Makaopuhi Crater decreased, increased numbers of deeper (6 km and greater) earthquakes were recorded beneath the south flank.

Ka‘ōiki Earthquakes

On November 16, 1983, a M6.6 earthquake occurred in the Ka‘ōiki fault system, which lies between the summits of Kīlauea and Mauna Loa volcanoes (fig. 5). In addition to the immediate effects of this earthquake, Lockwood and others (1987) suggested that it was a precursor to the 1984 eruption of Mauna Loa. The earthquake was followed by numerous aftershocks, including seismicity extending eastward toward Kīlauea's summit caldera.

Earthquakes located between the Ka‘ōiki fault system and Kīlauea's caldera are referred to as Nāmakani earthquakes because of their proximity to the Nāmakani Paio Campground. Figure 6 shows the cumulative numbers of Nāmakani earthquakes between January 1974 and December 2001. One effect of the 1983 M6.6 mainshock is to introduce a jump in the number of Nāmakani earthquakes. After 1983 the rate of Nāmakani earthquakes remains elevated compared to the pre-1983 rate. The typical aftershock decay evident after 1983 is interrupted by a swarm of microearthquakes in mid-November 1990, 2 weeks before the December 1990 summit intrusion.

Each of the five intrusive swarms of earthquakes from December 1990 to February 1993 was preceded by a recognizable cluster of Nāmakani earthquakes. Windows for each swarm are defined to begin 1 month before and to end 1 month after the swarm. For example, for the February 7, 1993 swarm, earthquakes that occurred between January 7, and March 7, 1993, are plotted. The located seismicity for the 5 intrusive swarms is combined in figure 7. The timing of the intrusive swarms and the Nāmakani earthquakes is seen in figure 8, where epicenters are projected onto plane A–A′ shown in figure 7, and plotted as a function of time. In the case of each intrusive swarm, a cluster of Nāmakani earthquakes occurs precursory to the dike intrusion by 2 to 3 weeks.

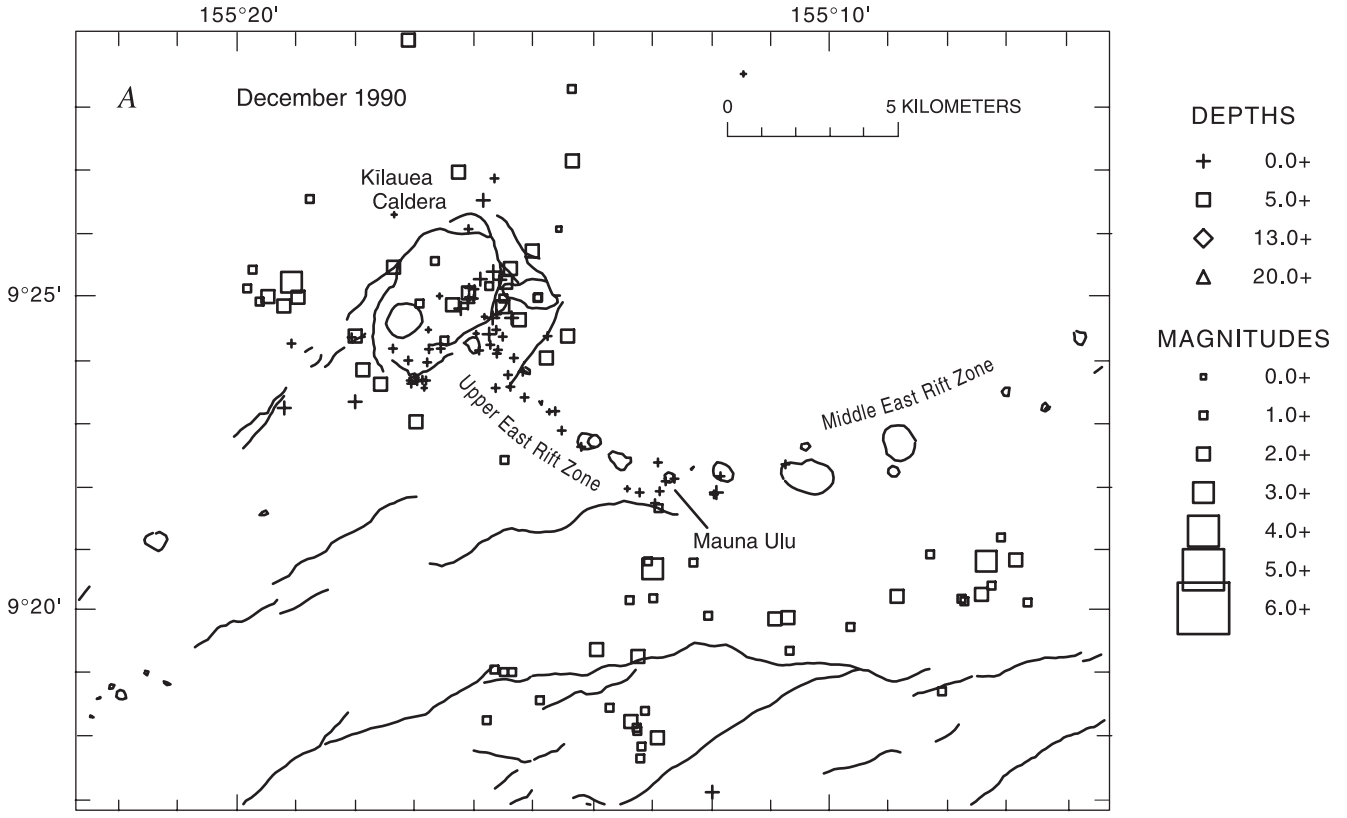

Figure 4. Seismicity, presented as earthquake epicenters coded according to earthquake focal depth and sized according to magnitude, for intrusive swarms, 1990 to 1993. *A*, December 1990. *B*, March 1991. *C*, August 1991. *D*, March 1992. *E*, February 1993.

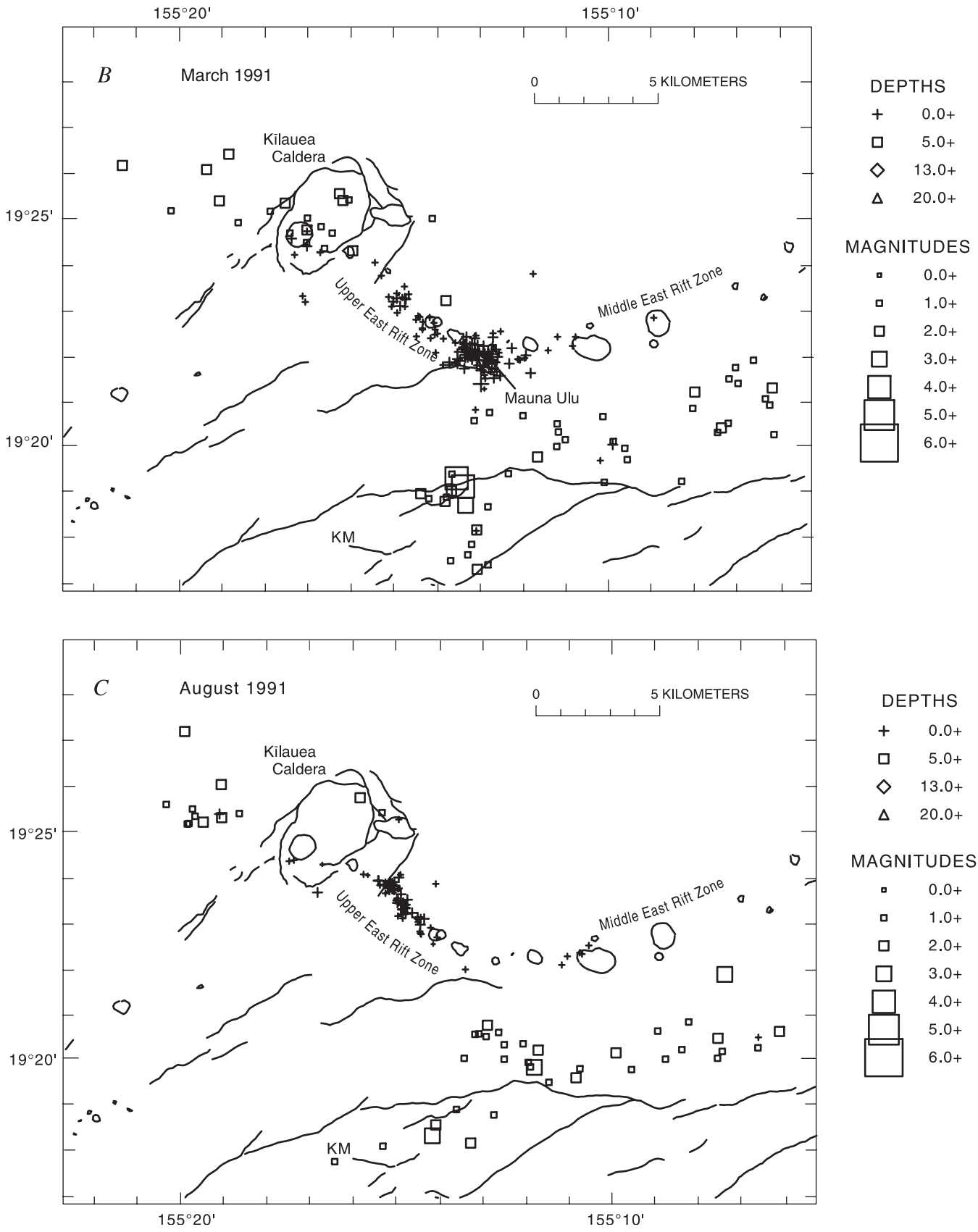

Figure 4. Continued.

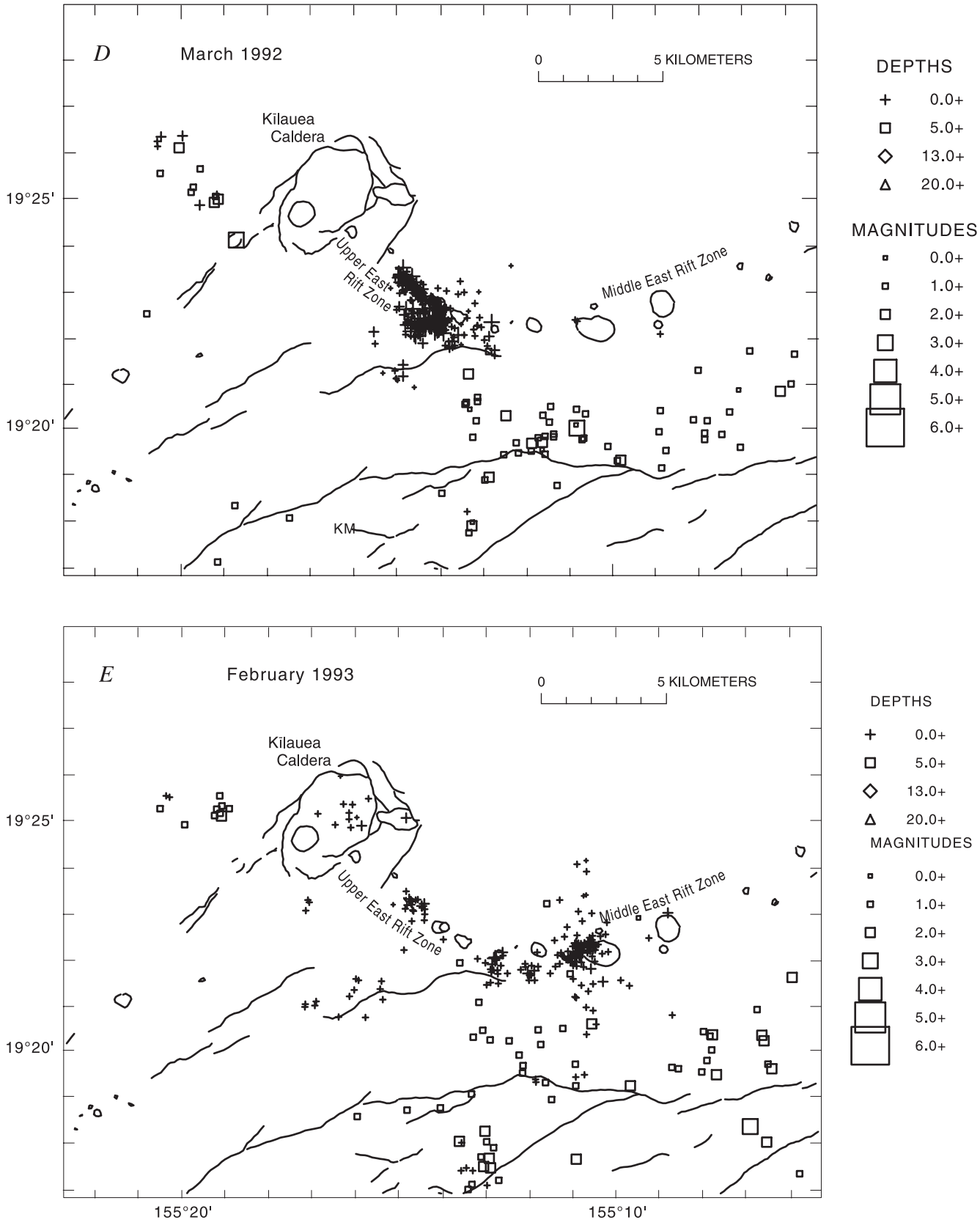

Figure 4. Continued.

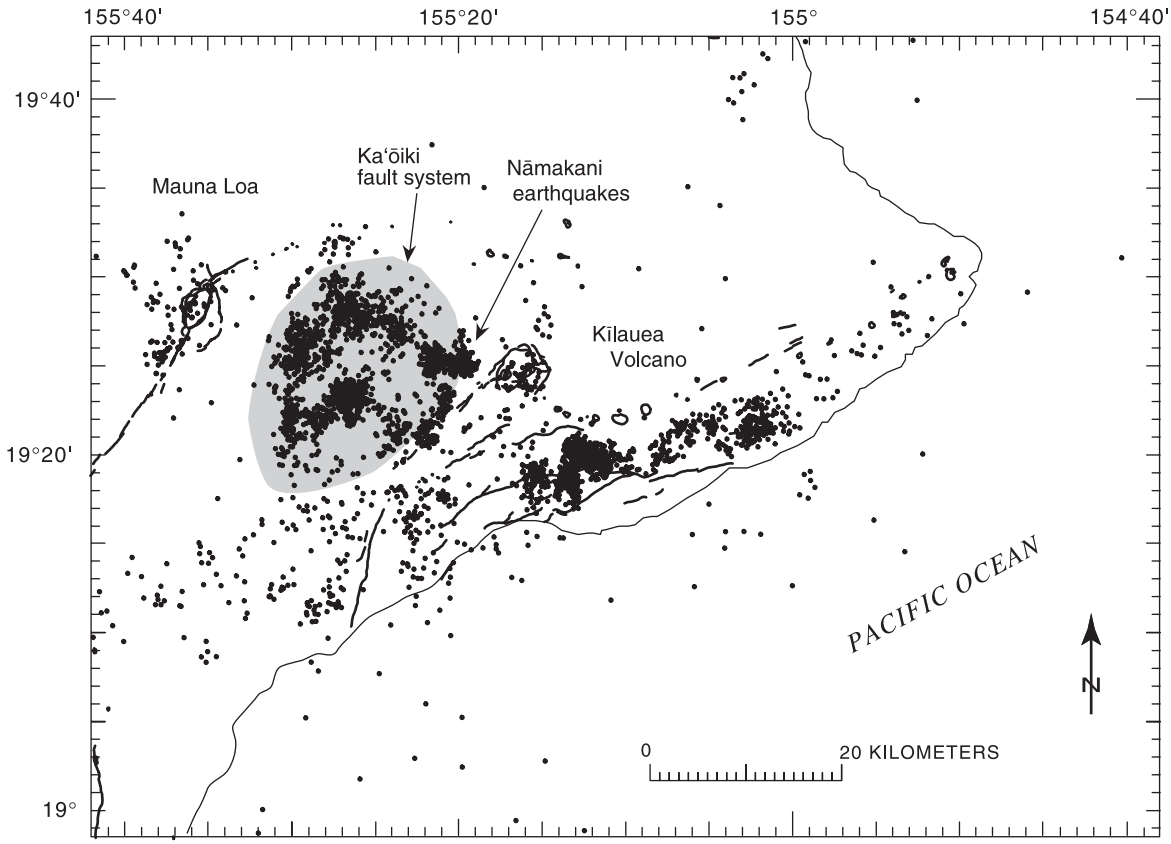

Figure 5. Southeast Hawai‘i earthquakes (black dots), November 16, 1983–November 16, 1984, including aftershocks of the M6.6 November 16, 1983, Ka‘ōiki earthquake. Gray area encloses Ka‘ōiki fault system.

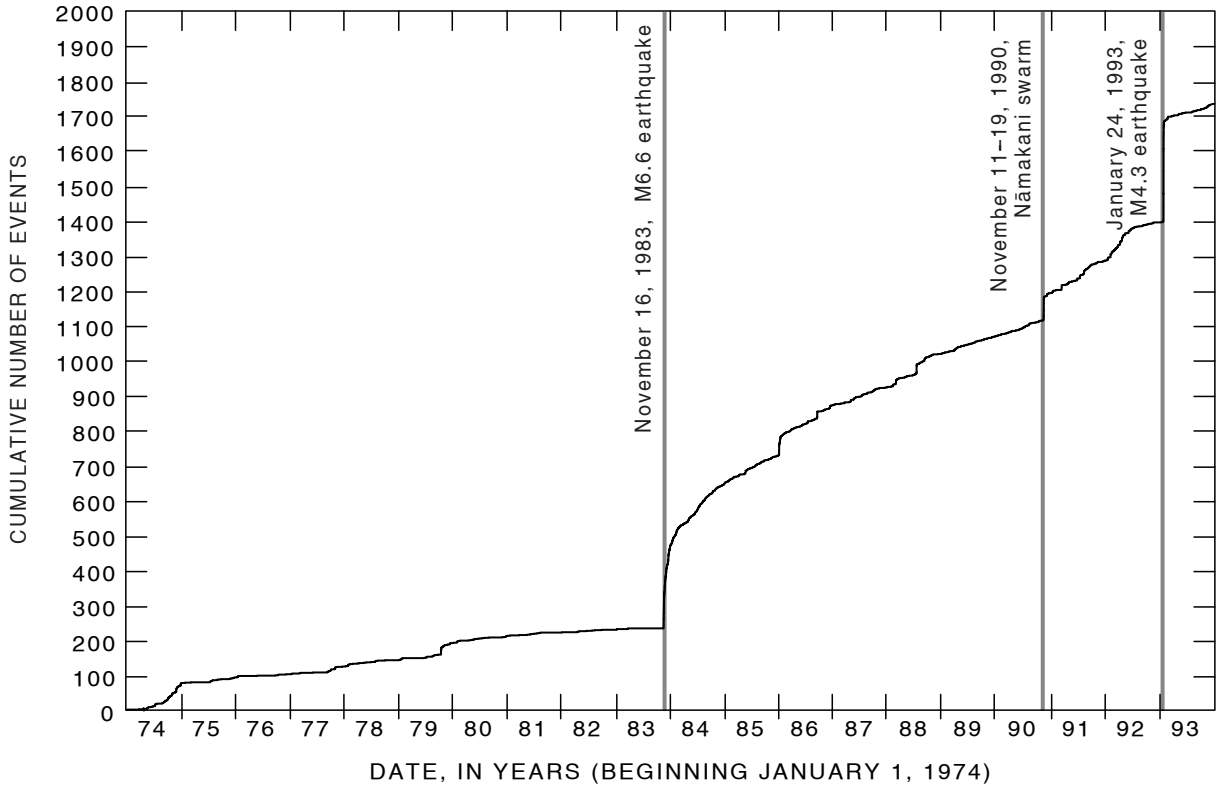

Figure 6. Cumulative number of Nāmakani earthquakes, 1974–1993.

Discussion

The composite seismicity of figure 7 is shown in cross section in figure 9. The levels of seismicity beneath the summit caldera of Kīlauea during these periods are lower than those in the neighboring regions. The caldera earthquakes shallower than 5 km are of the SPC type, and those extending to 13 km are LPC-C. The relatively aseismic region between the two sparse groups of hypocenters beneath Kīlauea's summit caldera has traditionally been interpreted as Kīlauea's principal magma-storage complex.

Seismicity clusters in different parts of the east rift zone activated during the different intrusions. Between the summit caldera and Mauna Ulu are three larger clusters of shallow earthquakes. The weakly seismic zone that separates the upper and the lower clusters of shallow earthquakes may represent an active conduit or a storage reservoir. The southeasternmost shallow cluster of earthquakes at 3-km depth is beneath the west side of Makaopuhi Crater. Swanson and others (1975) suggested that a secondary magma-storage chamber underlies Makaopuhi, so the swarm seismicity there might indicate occasional activation of this feature.

Gillard and others (1996) have examined the 1991 seismic swarms in detail using waveform-correlation techniques. This analysis allows precise relative relocation of earthquakes whose waveforms strongly correlate with waveforms of other earthquakes. In the March and August 1991 swarms, the relocated seismicity defines streaks within the rift zone at approximately 3 km below the surface, and the focal mechanisms are consistent with right-lateral strike-slip faulting between Kīlauea's caldera and Mauna Ulu. Gillard and others (1996) interpret the seismicity to define a transition between the stably active, deeper rift zone (e.g., Delaney and others, 1990) and an overlying elastic-brittle crust, not the propagating tip of a dike. The presumed increased presence of magma during the intrusions facilitated this faulting.

We see the Nāmakani seismicity in figure 9 as a cluster of epicenters west-northwest of Kīlauea's summit caldera. In cross-section, the hypocenters align along a moderately

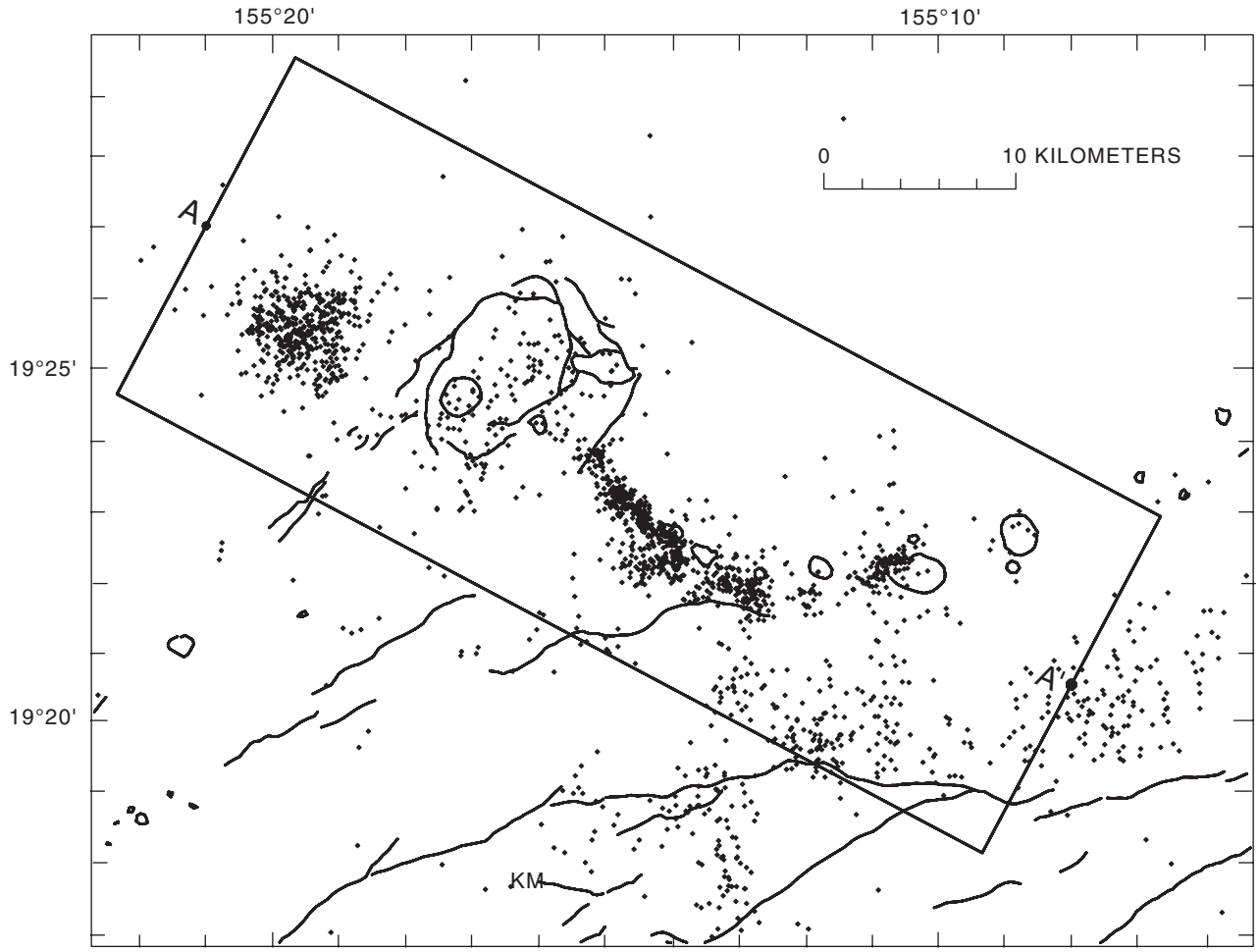

Figure 7. Composite seismicity map of Kīlauea showing epicenters of earthquakes associated with five intrusive swarm periods, 1990 to 1993 (see also figure 8). Earthquakes within box labeled A–A′ used for plots in figures 8 and 9.

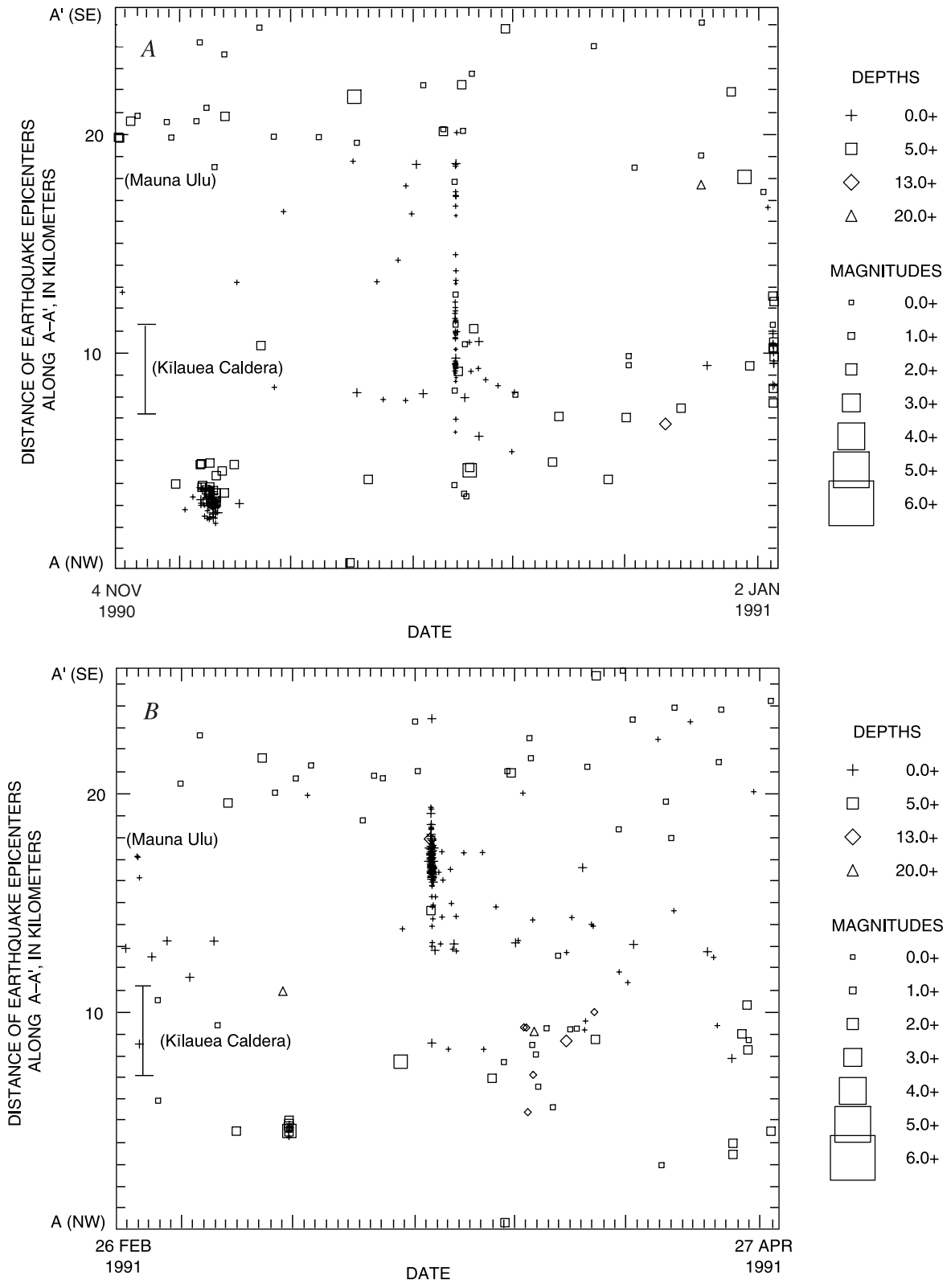

Figure 8. Distance-versus-time plots of earthquake epicenters. Symbols for geologic features as in figure 1. Earthquakes within box labelled A–A′ (fig. 7) for 2-month windows centered about five east-rift-zone intrusions. Epicenters are projected onto a plane parallel to A–A′ shown in figure 7. Epicentral symbols coded as in figure 4. Nāmakani earthquakes appear as cluster at lower left of figures, and east rift intrusions appear as nearly vertical streaks of shallow earthquake symbols. *A*, December 1990. *B*, March 1991. *C*, August 1991. *D*, March 1992. *E*, February 1993.

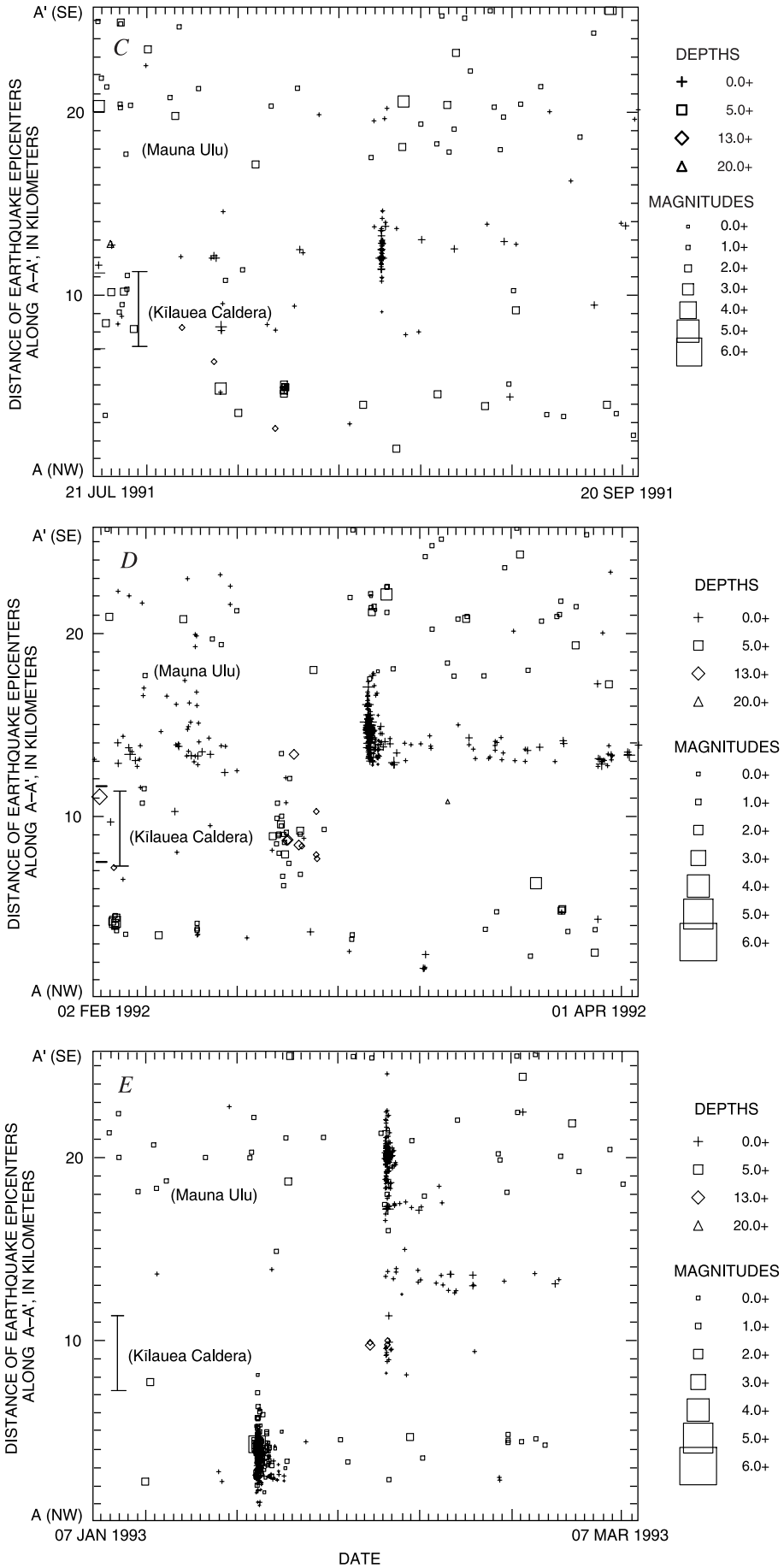

Figure 8. Continued.

southeast-dipping structure that, if projected updip toward the surface, would coincide with part of the Ka‘ōiki fault system. P-wave first motions of the largest of the Nāmakani earthquakes show a nodal plane that is consistent with normal faulting along a fault dipping to the southeast at approximately 60°.

The hypocentral cross-section (fig. 9) suggests an explanation for the association between the Nāmakani earthquakes and the east-rift-zone intrusions. The predominant structure defined by the Nāmakani earthquakes is a southeast-dipping normal fault, extending to 8-km depth toward Kīlauea's caldera. The focal mechanisms of the Nāmakani earthquakes are not restrictively dip-slip, but those of the largest Nāmakani earthquakes are consistent with normal faulting. We suggest that a swarm of Nāmakani earthquakes indicates normal faulting along the southeast-dipping fault. Thus, either a relatively large Nāmakani earthquake or a Nāmakani swarm has the effect of changing stresses near Kīlauea's summit caldera. We infer that, for these stress changes to then lead to dike intrusions along the east rift zone, stress conditions in Kīlauea's summit magma-storage complex, and possibly through the east-rift-zone magma conduit, must be finely balanced.

Since 1993, additional Nāmakani earthquake sequences and east-rift-zone intrusions have occurred. In February 1996, a summit intrusion closely resembling the December 1990 intrusion took place. In January 1997, lava erupted in and near Nāpau Crater, uprift of Pu‘u ‘Ō‘ō (Thornber, 2001). On January 27, 1998, an energetic Nāmakani sequence, with 2 M4.1 earthquakes followed by numerous aftershocks, was observed. Another M4.3 Nāmakani earthquake occurred on May 26, 1999. The pattern of Nāmakani earthquakes preceding east-rift-zone intrusions is not as clearly apparent as it was before 1994 (Okubo and others, 1996).

Conclusions

Swarms of tectonic Nāmakani microearthquakes preceded magma intrusions on Kīlauea's east rift zone from 1990 to 1993. This association, admittedly qualitative, suggests the potential to integrate aspects of Kīlauea's eruptive behavior into a broader regional context. Somewhat paradoxically, swarms or sequences of microearthquakes were directly linked

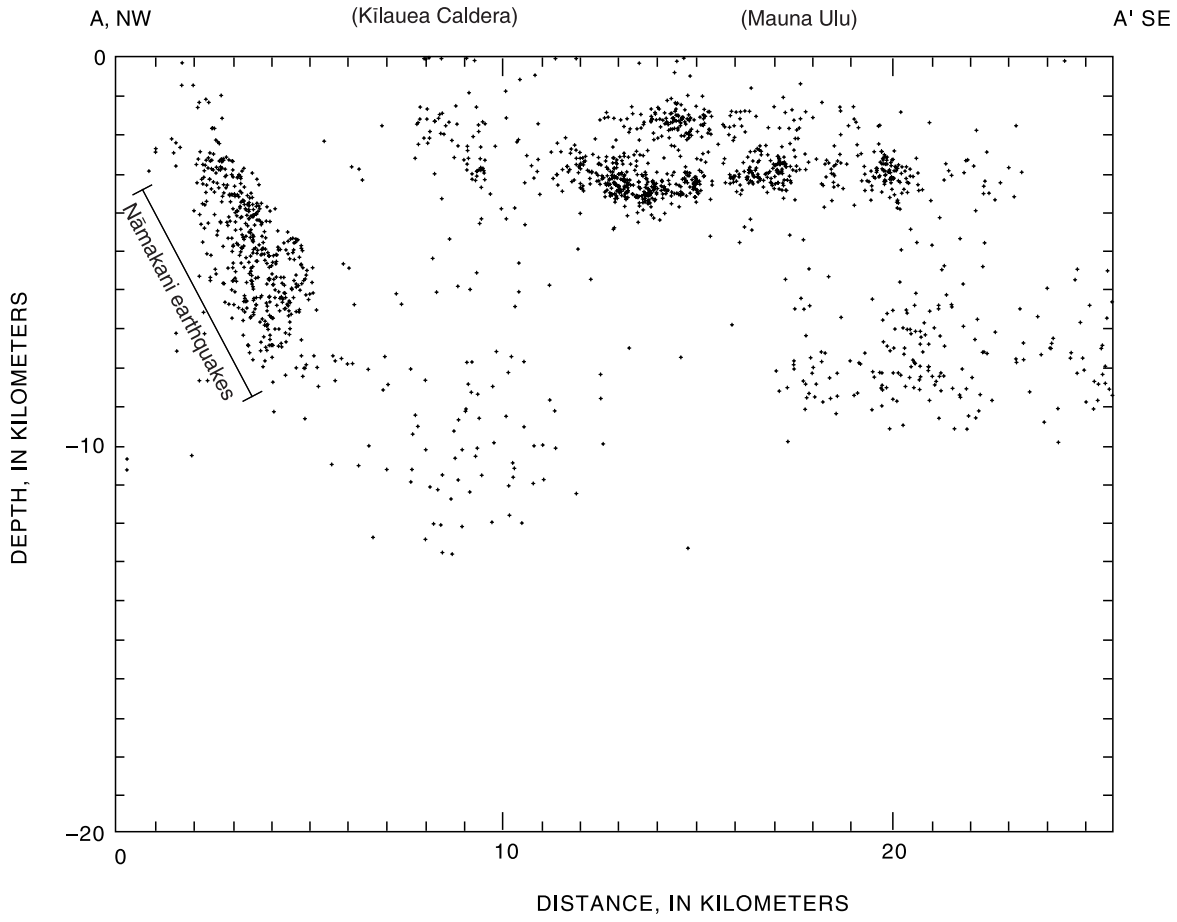

Figure 9. Hypocenters of earthquakes shown in box labeled A–A′ in figure 7, projected onto a vertical plane parallel to A–A′. The cross-section extends from the Ka‘ōiki fault system (NW) to Kīlauea's east rift zone (SE).

to visible eruptive changes, but moderate earthquakes in 1983 and 1989 had no apparent effects on the eruption.

The rate of Nāmakani earthquakes increased dramatically as part of the 1983 M6.6 Kaʻōiki aftershock sequence. Ongoing high rates of seaward displacement of Kīlauea's south flank, and extension and subsidence of its summit caldera persist (Owen and others, 1995; Cervelli and Miklius, this volume), suggesting that continuing Nāmakani seismicity reflects extension reaching inland to Mauna Loa's flank. If the Puʻu ʻŌʻō-Kūpaianaha eruption helps fuel Kīlauea's flank deformations, it can be expected that the Nāmakani seismicity will continue as the eruption continues. With the eruption again in a stable mode at Puʻu ʻŌʻō, we have apparently lost the direct link between Nāmakani seismicity pulses and east-rift-zone intrusions.

Quantitative descriptions of the effects of the Nāmakani earthquakes remain problematic. The source depths, focal mechanisms, and low magnitudes of even the largest of these earthquakes (M4.3) are not likely to produce large surface deformations. No comprehensive and continuous geodetic monitors of Mauna Loa and the Kaʻōiki fault system were in place in the early 1990s, when Kīlauea's east-rift-zone eruption was adjusting back from Kūpaianaha to Puʻu ʻŌʻō. Ongoing improvements in such monitors afford the possibility of more detailed modeling of future Nāmakani earthquakes and of similar interactions of tectonic and magmatic processes.

Acknowledgments

The ability to study and discuss long-term seismicity patterns and behaviors is only afforded by ongoing field maintenance and data processing and archiving performed by the electronics and seismic data analysis teams at the Hawaiian Volcano Observatory. The efforts of Robert Koyanagi, George Kojima, Kenneth Honma, Renee Ellorda, Gary Honzaki, Steven Fuke, Wilfred Tanigawa, and Alvin Tomori are appreciated and gratefully acknowledged.

References Cited

Delaney, P.T., Fiske, R.S., Miklius, Asta, Okamura, A.T., and Sako, M.K., 1990, Deep magma body beneath the summit and rift zones of Kilauea Volcano, Hawaii: Science, v. 247, no. 4948, p. 1311–1316.

Gillard, Dominique, Rubin, A.M., and Okubo, P.G., 1996, Highly concentrated seismicity caused by deformation of Kilauea's deep magma system: Nature, v. 384, no. 6607, p. 343–346.

Heliker, C.C., Mangan, M.T., Mattox, T.N., Kauahikaua, J.P., and Helz, R.T., 1998, The character of long-term eruptions; inferences from episodes 50–53 of the Puʻu ʻŌʻō-Kūpaianaha eruption of Kīlauea Volcano: Bulletin of Volcanology, v. 59, no. 6, p. 381–393.

Klein, F.W., Frankel, A.D., Mueller, C.S., Wesson, R.L., and Okubo, P.G., 2001, Seismic hazard in Hawaii; high rate of large earthquakes and probabilistic ground-motion maps: Seismological Society of America Bulletin, v. 91, no. 3, p. 479–498.

Klein, F.W., Koyanagi, R.Y., Nakata, J.S., and Tanigawa, W.R., 1987, The seismicity of Kilauea's magma system, chap. 43 *of* Decker, R.W., Wright, T.L., and Stauffer, P.H., eds., Volcanism in Hawaii: U.S. Geological Survey Professional Paper 1350, v. *2*, p. 1019–1185.

Koyanagi, R.Y., Tanigawa, W.R., and Nakata, J.S., 1988, Seismicity associated with the eruption, chap. 7 *of* Wolfe, E.W., ed., The Puu Oo eruption of Kilauea Volcano, Hawaii; episodes 1 through 20, January 3, 1983, through June 8, 1984: U.S. Geological Survey Professional Paper 1463, p. 183–235.

Lockwood, J.P., Dvorak, J.J., English, T.T., Koyanagi, R.Y., Okamura, A.T., Summers, M.L., and Tanigawa, W.R., 1987, Mauna Loa 1974–1984; a decade of intrusive and extrusive activity, chap. 19 *of* Decker, R.W., Wright, T.L., and Stauffer, P.H., eds., Volcanism in Hawaii: U.S. Geological Survey Professional Paper 1350, v. 1, p. 537–570.

Mangan, M.T., Heliker, C.C., Mattox, T.N., Kauahikaua, J.P., and Helz, R.T., 1995, Episode 49 of the Puʻu ʻOʻo-Kupaianaha eruption of Kilauea volcano—breakdown of a steady-state eruptive era: Bulletin of Volcanology, v. 57, no. 2, p. 127–135.

Nakata, J.S., 2000, Hawaiian Volcano Observatory summary 99; part I, seismic data, January to December 1999 (Chronological summary by C.C. Heliker and D.R. Sherrod): U.S. Geological Survey Open-File Report 00–433, 61 p.

Nakata, J.S., 2002, Hawaiian Volcano Observatory summary 101; part I, seismic data, January to December 2001 (Chronological summary by C.C. Heliker): U.S. Geological Survey Open-File Report 02–157, 70 p.

Okubo, P.G., 1994, Seismicity associated with the continuing eruption at Kilauea Volcano, Hawaii [abs.]: Seismological Research Letters, v. 65, no. 1, p. 55.

Okubo, P.G., Nakata, J.S., Chouet, B.A., and Dawson, P.B., 1996, The February 1, 1996, Kilauea summit earthquake swarm [abs.]: Eos (American Geophysical Union Transactions), v. 77, no. 46, supp., p. F798.

Owen, S.E., Segall, Paul, Freymueller, J.T., Miklius, Asta, Denlinger, R.P., Árnadóttir, Thóra, Sako, M.K., and Bürgmann, R.B., 1995, Rapid deformation of the south flank of Kilauea volcano, Hawaii: Science, v. 267, no. 5202, p. 1328–1332.

Owen, S.E., Segall, Paul, Lisowski, Michael, Miklius, Asta, Denlinger, R.P., and Sako, M.K., 2000, Rapid deformation of Kilauea Volcano; global positioning system measurements between 1990 and 1996: Journal of Geophysical Research, v. 105, no. B8, p. 18983–18998.

Swanson, D.A., Jackson, D.B, Koyanagi, R.Y., and Wright, T.L., 1975, The February 1969 east rift eruption of Kilauea Volcano, Hawaii: U.S. Geological Survey Professional Paper 891, 30 p.

Thornber, C.R., 2001, Olivine-liquid relations of lava erupted by Kīlauea Volcano from 1994 to 1998; implications for shallow magmatic processes associated with the ongoing east-rift-zone eruption: Canadian Mineralogist, v. 39, no. 2, p. 239–266.

Wolfe, E.W., Garcia, M.O., Jackson, D.B., Koyanagi, R.Y., Neal, C.A., and Okamura, A.T., 1987, The Puu Oo eruption of Kilauea Volcano, episodes 1–20, Januray 3, 1983, to June 8, 1984, chap. 17 *of* Decker, R.W., Wright, T.L., and Stauffer, P.H., eds., Volcanism in Hawaii: U.S. Geological Survey Professional Paper 1350, v. 1, p. 471–508.

Stress Changes Before and During the Pu‘u ‘Ō‘ō-Kūpaianaha Eruption

By James H. Dieterich, Valérie Cayol, *and* Paul Okubo

Abstract

Surface deformation and earthquake data for Kīlauea Volcano have been analyzed as they pertain to stress interactions before and during the Pu‘u ‘Ō‘ō-Kūpaianaha eruption. A newly developed method was used to solve for Coulomb stress changes from earthquake rate changes that facilitates quantitative comparisons between earthquake and deformation data sets. Between the 1975 M7.2 Kalapana earthquake and the start of the Pu‘u ‘Ō‘ō-Kūpaianaha eruption in 1983, deformation rates of Kīlauea Volcano were the most rapid ever recorded. During this period, deformation was characterized by expansion of a dike-like magma system within Kīlauea's rift zones, coupled with aseismic creep over a narrow zone of a low-angle fault located beneath the volcano's south flank. For the 1976–83 period, the rate of rift opening is estimated to have averaged 40 cm per year on the basis of ground deformation. At the onset of the Pu‘u ‘Ō‘ō-Kūpaianaha eruption in January 1983, the dike propagated to the surface to form the eruptive fissures. Deformation data and seismicity stress solutions indicate that a fivefold slowing of stressing rates in Kīlauea's south flank occurred either in late 1979 or at the start of the of Pu‘u ‘Ō‘ō-Kūpaianaha eruption in January 1983, depending on location. The stressing rates before and after the onset of the eruption are consistent with changes in volume of magma stored before and after the onset of the Pu‘u ‘Ō‘ō-Kūpaianaha eruption.

Introduction

Seismic activity often signals the occurrence of magmatic processes within volcanoes, such as the intrusion of new magma bodies and the inflation, or deflation, of existing bodies. Indeed, major volcanic events are often associated with large earthquakes or, in extreme cases, edifice collapse. The intimate association of seismicity with volcanic activity indicates that interactions between faulting and magma bodies are a fundamental aspect of volcanic processes. Stress changes induced by magmatic processes can drive faulting and earthquake activity. Conversely, faulting, by relieving stresses from previous intrusive processes, can establish stress states favorable to new or continued intrusion. That is, faulting can create "room" to accommodate the added volume of intruded magma.

At Kīlauea, these interactions are very evident. Changes of seismic activity characterize the onset of eruptions and are primary indicators of subsurface movements of magma (Klein and others, 1987). Additionally, interactions between rift-zone magmatic expansion and detachment faulting at the base of the volcano appear to underlie both the formation and the persistence of Kīlauea's rift zones (Dieterich, 1988).

This paper presents a combined analysis of deformation and earthquake rates data related to the Pu‘u ‘Ō‘ō-Kūpaianaha eruption. Its focus is the south flank of Kīlauea and the adjacent east rift zone in the region of the Pu‘u ‘Ō‘ō-Kūpaianaha eruptive fissures (fig. 1). The work attempts to identify and delineate stress interactions within the south flank of Kīlauea and to develop a consistent model of magmatic and earthquake processes within Kīlauea particularly as they relate to the Pu‘u ‘Ō‘ō-Kūpaianaha eruption.

The analysis includes the period following the M7.2 Kalapana earthquake in 1975 and continues through the onset of the Pu‘u ‘Ō‘ō-Kūpaianaha eruption in 1983. The 1975 Kalapana earthquake marks a point of major change in the behavior of Kīlauea. In the 15 years before that earthquake, eruptive activity was prevalent, but from the 1975 Kalapana earthquake to the 1983 eruption, magmatic activity was predominately intrusive (Dzurisin and others, 1984). The interval between the 1975 earthquake and the onset of the Pu‘u ‘Ō‘ō-Kūpaianaha eruption was also a period of exceptionally rapid deformation (fig. 2) and intense seismic activity (fig. 1), with extension rates across Kīlauea caldera averaging about 25 cm/yr. Following the onset of the 1983 Pu‘u ‘Ō‘ō-Kūpaianaha eruption, activity changed from intrusion to nearly continuous rift eruption, and deformation rates decreased to about 4 cm/yr (Delaney and others, 1998).

Model of Kīlauea's Rift Zone and South Flank

Previous investigations have identified the principal structural elements of Kīlauea Volcano. Geodetic and seismologic observations (for example, Fiske and Kinoshita, 1969; Klein and others, 1987) indicate that magma rises from the mantle

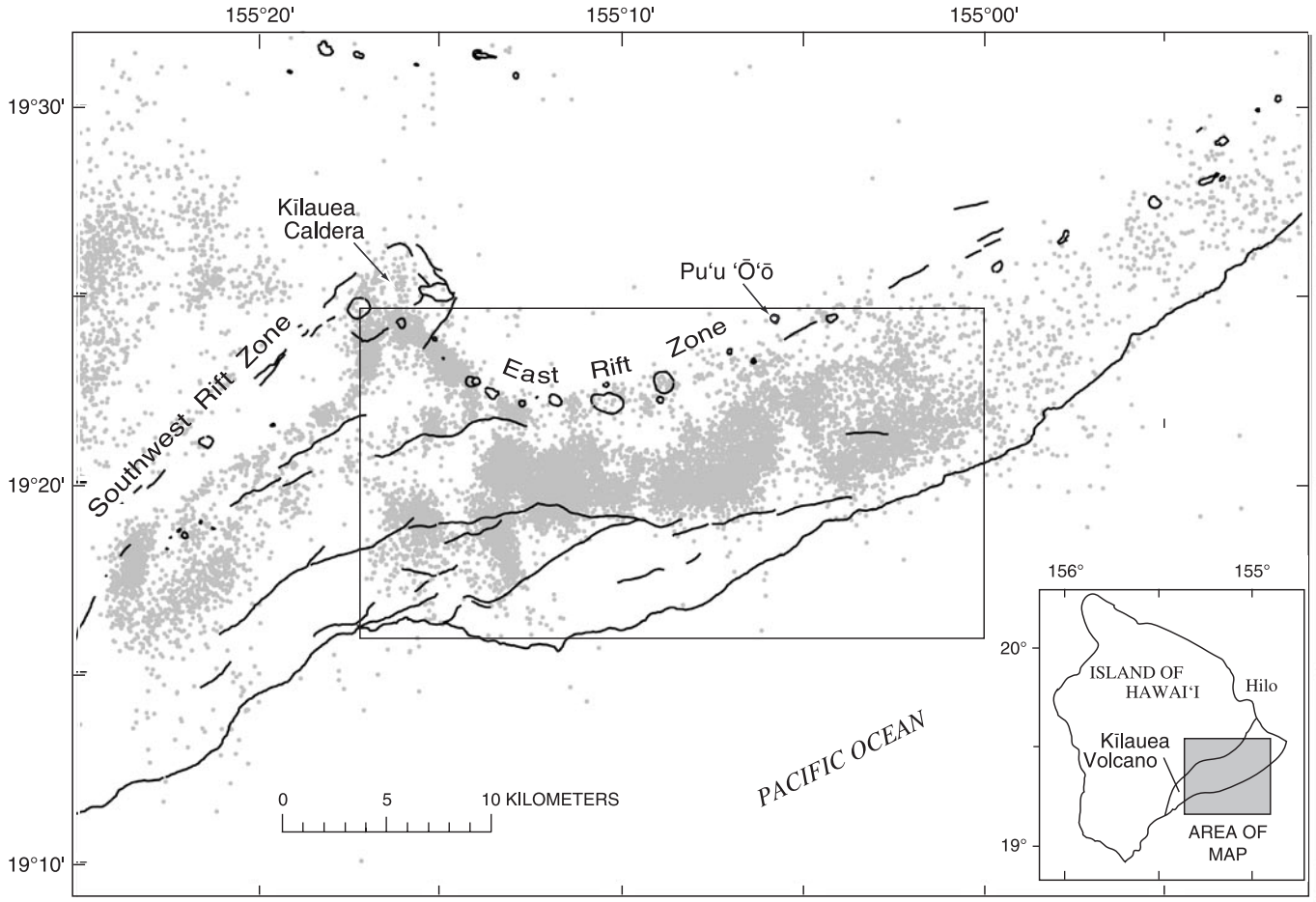

Figure 1. Map showing principal features of Kīlauea Volcano. Study area for analysis of the seismicity data (inner rectangle) consists of the east rift zone (including the Pu'u 'Ō'ō-Kūpaianaha eruption site) and the seismically active south flank of Kīlauea. Black lines are faults; open circles are volcanic craters. Earthquake locations, M≥2, recorded from 1976 to 1982, are shown by gray dots.

through a conduit located below Kīlauea's summit. From the summit region, magma is then laterally supplied to Kīlauea's two rift zones—the east and the southwest rift zones (fig. 1). Magma is stored within these rift zones, as evidenced from petrologic data (Wright and Fiske, 1971) and geophysical studies (Hill and Zucca, 1987; Okubo and others, 1997). Precise relative relocations of shallow rift earthquakes (Gillard and others, 1996; Rubin and others, 1998) define narrow ribbons that are interpreted to mark the highly stressed zone at the top of a vertical tabular magma reservoir. This observation, together with the long wavelength of deformations across the rift system (Delaney and others, 1990), suggest the dilation of a dike-like reservoir that extends from a depth of about 3 km downward to the pre-volcano sea floor, which is depressed to a depth of 9 to 10 km beneath sea level in the vicinity of the rift zones (fig. 3). The continuous deformation at sites widespread on the volcano indicates that the injection of magma into the deep rift zones is a steady process (Delaney and others, 1990). In addition, supply of magma to the rift zones is sometimes accompanied by swarms of shallow (1–4 km) earthquakes corresponding to the rapid intrusion of shallow dikes, which may lead to the formation of eruptive fissures (Klein and others, 1987).

Geodetic monitoring provides a number of data sets that record the surface deformations of Kīlauea's rift zones and flank. In the present study, we model trilateration, leveling, and sea-level data using a three-dimensional mixed boundary element method that takes topography into account (Cayol and Cornet, 1998). This method employs stress boundary conditions and permits simultaneous representation of stress interactions among the faults and magma bodies that make up the structural elements of Kīlauea. The medium is assumed to be elastic.

The southwest and east rift zones are represented as a single steeply dipping dike that extends to the base of the volcano (fig. 3). The horizontal location of the dike is defined by shallow seismicity along the rift zones and by the locus of maximum subsidence, determined by leveling. Where available at the time of the study, relocated earthquakes (Gillard and others, 1996; Rubin and others, 1998) were used. In the boundary element model, rift zone expansion occurs by intrusion of magma into the rift zones (Swanson and others, 1976) and is coupled to, and accommodated by, fault slip at the interface between the volcano and the pre-existing sea floor (Nakamura, 1982, Dieterich, 1988). Evidence for a decollement at the base

of the volcano is provided by the 1975 M7.2 and the 1989 M6.1 earthquakes, which were caused by seaward motion on a low-angle fault (Ando, 1979; Bryan, 1992), probably located at the interface between the volcanic edifice and the depressed former sea floor. Additionally, high rates of seismicity at depths ranging from 6 to 12 km characterize the south flank of Kīlauea. Relative relocations (Got and others, 1994) showed that some of the earthquakes reveal a low-angle, northward dipping fault corresponding to the base of the edifice.

The starting model assumes that this low-angle fault is located at 9-km depth at the rift zones. Results presented below indicate that the scarcity of earthquakes close to the rift zones is probably related to aseismic fault creep of the fault. This could be caused by elevated temperatures in the rift system, which favor fault creep (Tse and Rice, 1986), and possibly by the creep of hot, olivine-rich magma and olivine cumulates, which may be present at the base of the rifts (Clague and Denlinger, 1994). Consequently, the fault in the starting model is allowed to slip over a narrow area corresponding to the aseismic region south of the rift zones (fig. 3). The dip of this fault is assumed to be 5° to the northwest, a compromise between various independent estimates (Got and others, 1994; Crosson and Endo, 1982; Thurber and Gripp, 1988). The boundary conditions are stresses. All parts of the rift system are assumed to be hydraulically connected, resulting in a single overpressure for the dike. The fault is assumed to move passively in response to the reservoir dilation and, consequently, has a null stress perturbation. Young's modulus is taken at 50 GPa, a value deduced from the P-wave velocity in the south flank (Okubo and others, 1997) and corrected by a factor of 0.7 to account for the difference between the static and dynamic modulus at a confining pressure of 100 MPa (Cheng and Johnston, 1981). Poisson's ratio is assumed to be 0.25.

Model variables are the depth, height, width, dip, and opening of the rift-zone dike, the dip and depth of the low-angle fault, and the width of the creeping portion of the fault adjacent to the rifts. The two principal outputs of the model are (1) predicted surface deformations, and (2) stress changes within Kīlauea. To compare among the deformation solutions, the error χ^2 was computed on relative displacements along the trilateration baselines (Cayol and others, 2000). The indeterminate components of the velocity field are adjusted using the model coordinate method of network adjustment (Segall and Matthews, 1988). The stress solutions are compared with the results of the seismicity analysis.

Analysis of Earthquake Rate Data

For analysis of seismicity data, a recently developed method (Dieterich and others, 2000) was employed that uses seismicity rate changes to determine changes of stress. That study presented preliminary results from Kīlauea and made

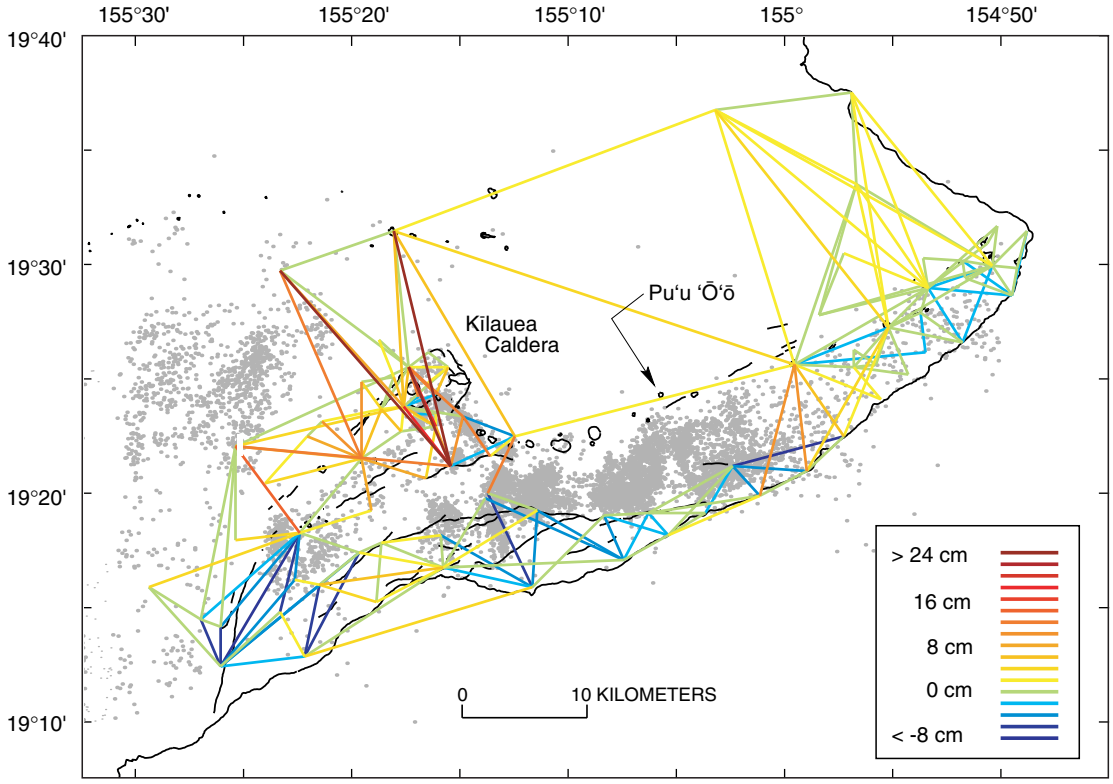

Figure 2. Map of Kīlauea showing rates of relative displacements (in centimeters per year) recorded by trilateration between 1976 and 1982. Positive values are extension; negative values are shortening. Trilateration measurements are estimated to have a fixed error of 1 cm and a scale error of 1 ppm (Delaney and others, 1994, table C-1).

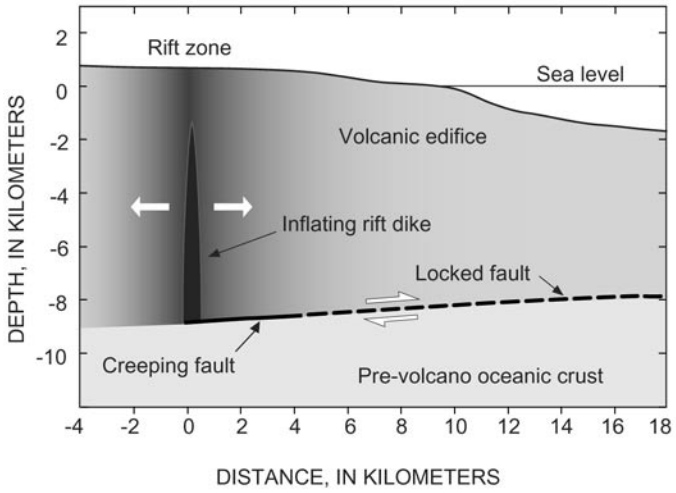

Figure 3. Schematic cross section across the east rift zone of Kīlauea showing principal structural elements used in modeling deformation data. Overpressure in dike drives flank deformation. Dashed line indicates locked portion of the basal fault.

quantitative comparisons between the stresses obtained from modeling the deformation data with stresses obtained from seismicity. The method is summarized here.

This method builds on the widespread demonstration that changes of stress correlate with changes of earthquake-activity rates (Simpson and Reasenberg, 1994; King and others, 1994; Jaumé and Sykes, 1996; Harris and others, 1995; Stein, 1999). Specifically, earthquake rates tend to increase (or decrease) in regions where the Coulomb failure stress function increases (or decreases). Coulomb stress S is defined as

$$S = \tau - \mu\sigma, \qquad (1)$$

where τ is the shear stress acting across fault planes that generate earthquakes (positive in the slip direction), σ is the normal stress (less pore fluid pressure), and μ is the coefficient of fault friction. However, stress changes and earthquake rate changes are not linearly correlated, and earthquake rate changes are strongly time-dependent. Consequently, estimating stress changes from changes of earthquake activity is not straightforward. These nonlinear effects are quite apparent at Kīlauea, where magmatically induced stress changes of a few MPa give rise to swarms of earthquake activity in which earthquake rates may temporarily jump by a factor of 100 or more and then decay with time in the manner of an aftershock sequence, with rates falling by t^{-1} (where t is time following the stress change).

To account for these nonlinear effects, changes of Coulomb stress are determined from changes of earthquake rates using a formulation (Dieterich, 1994) derived from laboratory observations of rate- and state-dependence of fault friction. This formulation includes the non-linear dependence of earthquake rates on stress and provides a physical model for aftershocks including the time-dependence of the Omori aftershock decay law. Earthquake rate R (in a specified magnitude range) is

$$R = \frac{r}{\gamma \dot{S}_r}, \text{ where } d\gamma = \frac{1}{A\sigma}[dt - \gamma dS] \qquad (2)$$

and where γ is a state variable, t is time, and S is a Coulomb stress function in which the friction term in equation (1) is defined as $\mu=\tau/\sigma-a$. The constant r is defined as the steady-state earthquake rate within the selected volume, at the reference stressing rate $\dot{S}_r$. A is a dimensionless fault constitutive parameter with values, measured in laboratory experiments, usually in the range 0.005 to 0.015 (Dieterich, 1994; Dieterich and Kilgore, 1996; Scholz, 1998). We assume μ=0.35 in computing Coulomb stresses from the deformation model to compare with the seismicity stress solutions. This value is based on an assumed sliding friction (τ/σ) of 0.6, which is reduced by the parameter a, estimated as 0.25 from laboratory studies (Linker and Dieterich, 1992; Dieterich, 1994).

To determine stress changes in some volume, the observed seismicity rate as a function of time $R(t)$ is used to directly calculate γ as a function of time (that is, from equation 2, $\gamma(t)=r/R(t)\dot{S}_r$). Using a time-marching procedure, the differential equation 2 is then solved for the Coulomb stress as a function of time. Dieterich and others (2000) provide additional information. The earthquake rates are smoothed before solving for S to reduce noise in the solution, which arises from the random component of earthquake occurrence. This procedure gives the change of Coulomb stress that is driving the earthquake process. On average, we assume earthquakes occur on faults that are optimally oriented in the stress field. The stress field may not have a constant orientation across the region and may change orientation with time. The procedure, as currently implemented, does not provide information on stress orientation.

The calculation for γ requires estimates of r and $\dot{S}_r$; r is taken to be the average earthquake rate in the volume over the entire time interval from January 1976 to January 2000. The calculations are performed in terms of the normalized Coulomb stress ($S/A\sigma$), which permits the parameter $\dot{S}_r$ to be replaced by the observable quantity t_a, the aftershock duration. From Dieterich (1994),

$$t_a = A\sigma/\dot{S}_r \qquad (3)$$

and is defined as the characteristic time for seismicity rates to return to the background rate r. Finally, the scaling of results to stress in MPa requires the additional estimation of the term $A\sigma$. Comparisons between the normalized Coulomb stresses and results of deformation modeling indicate $A\sigma$ has values in the range 0.25 to 0.45 MPa. For this study all results have been scaled using $A\sigma$=0.30MPa.

Maps of Coulomb stress change over specified time intervals were derived by repeating these calculations at nodes in a grid superimposed over Kīlauea. The grid has a regular node spacing of 1 km in both the x and y directions. Seismicity rates were obtained within cylindrical volumes, between hypocentral depths of 6 and 13 km, centered on each node. Within each volume, with a starting radius of $\sqrt{0.5}$ km, we required a minimum average seismicity rate of eight events per year, M≥1.5. If the seismicity within the initial volume did not meet this criterion, the search radius about that node was increased in increments of $\sqrt{0.5}$ km until the minimum average rate of eight events per year was obtained or the maximum search radius of $4\sqrt{0.5}$ km=2.83 km was exceeded. At 2.83 km, if

the corresponding volume did not produce at least eight earthquakes per year, Coulomb stress change was not computed. Using these procedures, we mapped Coulomb stress changes for most of Kīlauea's south flank. A similar procedure was used to obtain stress solutions for selected cross sections.

Figure 4 shows examples of calculations at representative nodes in the study area. The eight-per-year criterion used for these solutions, together with randomness in earthquake times, results in somewhat noisy solutions. However, the noise due to earthquake randomness is not spatially coherent, while changes due to underlying stress changes have spatial coherence. The eight-per-year criterion provides a reasonable balance between optimizing for spatial resolution and enhancing signal to noise at each node.

Results

Deformation and Stress Changes, 1976 to 1983

This time interval consists of the period following the 1975 Kalapana earthquake and before the onset of the Pu'u 'Ō'ō-Kūpaianaha eruption. The spatial and temporal resolution of the deformation data for this interval precludes detailed modeling of local events and small-scale structures. Consequently, the deformation models seek principally to represent the overall deformation of the volcano, and they assume that both the sporadic shallow dike intrusions and the steady magma reservoir can be modeled as the cumulative deformation of a single dike.

During the period from 1976 to 1983, trilateration baselines (fig. 2) show rapid horizontal extension across the caldera and rift zones. This extension is particularly fast in the upper parts of the rift zones, and the maximum extension of as much as 26 cm/yr occurs across the summit caldera. Most of the baselines that span the south flank, particularly those perpendicular to the rift zones, experienced compression of as much as 9 cm/yr. The flank compression during this period differs from measurements after 1983, which show flank extension (Delaney and others, 1998; Owen and others, 1995). Negligible deformation rates are recorded in the easternmost part of the rift system, as well as on the north flank of the volcano. Subsidence along the rift-system axis (up to 7 cm/yr) and uplift of the south flank (up to 2.5 cm/yr) accompany the large horizontal displacements (fig. 5). This uplift is confirmed by data from tide gauges and water-well level data (table 1).

On the basis of deformation modeling, the depth of the top of the rift-zone dike, its dip, and the area of fault creep are reasonably well constrained by the trilateration observations. For a fault depth of 9 km, our preferred model (fig. 6) gives the best fit to the trilateration data (smallest χ^2 error on relative displacements) with a vertical dike 8.5 km high, dilating at an average rate of 40 cm/yr, and coupled slip on a fault dipping 5° to the northwest. The low-angle fault creeps passively (constant stress) over the narrow aseismic area south

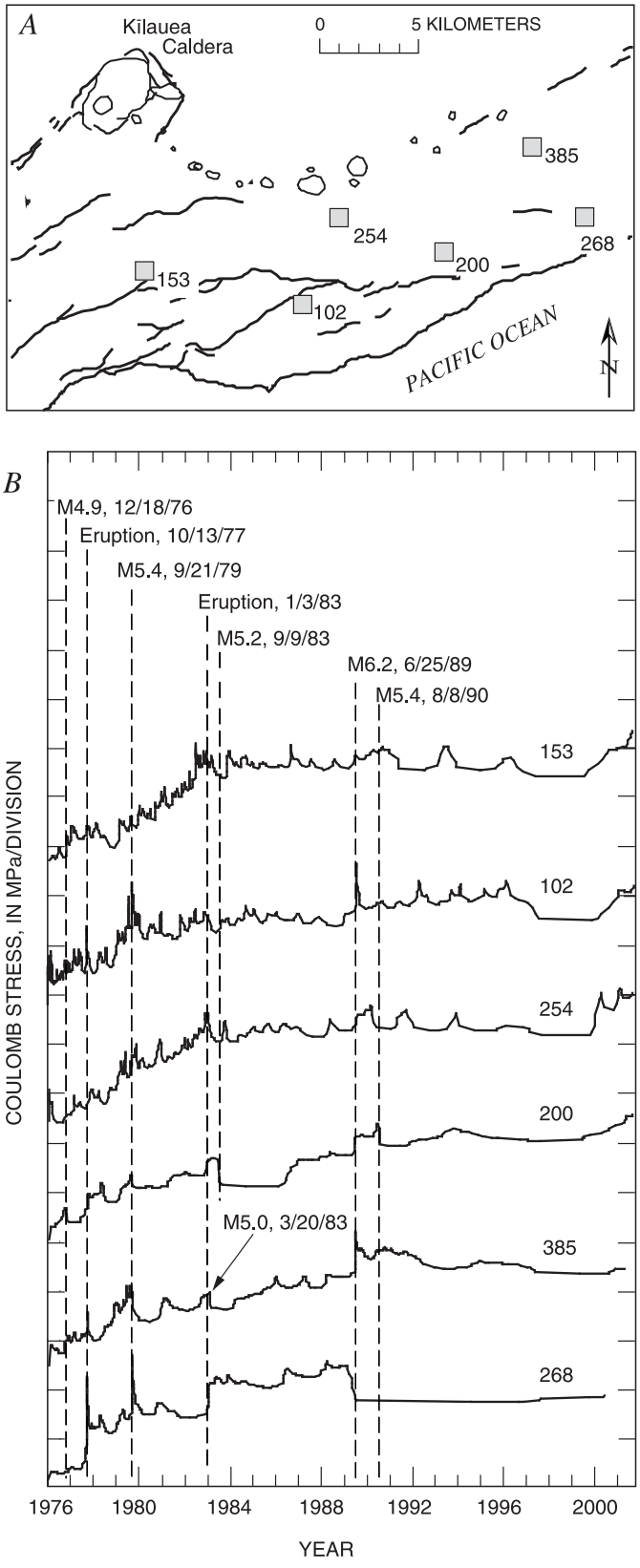

Figure 4. *A*, Index map of study region for solution of Coulomb stress changes from seismicity rate changes. Numbered symbols indicate locations of selected records of stress vs. time given in *B*. *B*, Representative solutions for Coulomb stress vs. time solutions. Vertical dashed lines indicate times of earthquakes and east-rift-zone eruption onsets.

of the rift zone. At the ground surface, this model results in an average rift-zone opening of 20 cm/yr. This model also gives the best fit of the leveling data (fig. 5). However, the sharp subsidence along line b–b′ (fig. 5) associated with the August 1981 southwest rift intrusion cannot be resolved by the elastic modeling (Pollard and others, 1983). Modeled height changes are also comparable to those obtained from sea-level measurements (table 1).

Table 1. Comparison between measured and predicted elevation changes at water wells and tide gauge for 1976–82.

[Water well and Āpua tide gauge data (Āpua tide) are derived from the interpolations given by Delaney and others (1998).]

Location	Latitude and Longitude	Elevation (cm/year)	
		Measured	Modeled
Kapoho	19°30', 154°50'	-1.4±0.7	0.2
Mālama Ki	19°27', 154°53'	-1.7±0.6	0.7
Pūlama	19°21', 155°20'	5.0±1.2	7.0
ʻĀpua tide	19°16', 155°12'	5.7±1.3	6.0

Models with dike dilation but no fault slip fit the trilateration data, but they lead to an underestimation (as much as 50 percent) of rift-zone subsidence (line a–a′). Compared to the best-fit solution, in which the fault is allowed to slip over a larger uniform width of 10 km, the error (χ^2) on distance variation increases by 10 percent, south flank compression is not accounted for, and the rift zone subsidence is overestimated by as much as 40 percent. The overestimation of the south flank uplift remains the same when the fault is horizontal. Trilateration data give little constraint on the fault depths and dike height nor on the precise western and eastern extent of the dike. Indeed, trilateration data are equally well explained by a fault located in the depth range 6 to 11 km and for a rift system 4 km shorter or longer to the west or to the east.

The total calculated Coulomb stress change in the preferred model along a cross section that includes the location of the January 1983 eruptive fissures is shown in figure 7*A*. For calculation of Coulomb stress in the deformation model, we assume μ=0.35 and resolve stress changes on fault planes parallel to the decollement with a sense of slip such that the upper block moves away from the rift zone. Projected onto this cross section are earthquakes from the start of 1980 to the start of 1983, as well as the M7.2 earthquake of 1975 and the M6.2 earthquake of 1989. Note the good correspondence between earthquake activity and the region of high Coulomb stress.

Coulomb stress changes have been determined from earthquake rate changes along the cross section of figure 7*A*. At this location, the seismicity stress solution over the 1976 to 1983 interval (fig. 7*B*) may not be equivalent to the regional deformation model, because significant local stressing events altered the local stress conditions in this area but are not resolvable in the deformation data. These local events are discussed below and include the dike intrusion and eruption of September 1977 and several earthquakes in the magnitude range 4.6 to 5.4. Consequently, we believe the stress change calculated for the interval from 1980 to 1983 (fig. 7*C*), which lacks eruptive events or significant earthquakes, is probably a more appropriate comparison with the deformation model. The seismicity stress solution for 1980 to 1983 agrees with the deformation model in the overall pattern of stress changes, including the region of maximum stress increase adjacent to the end of the zone of inferred fault creep. However, the average maximum stress change is about 0.6 MPa/yr (1976–83) in the

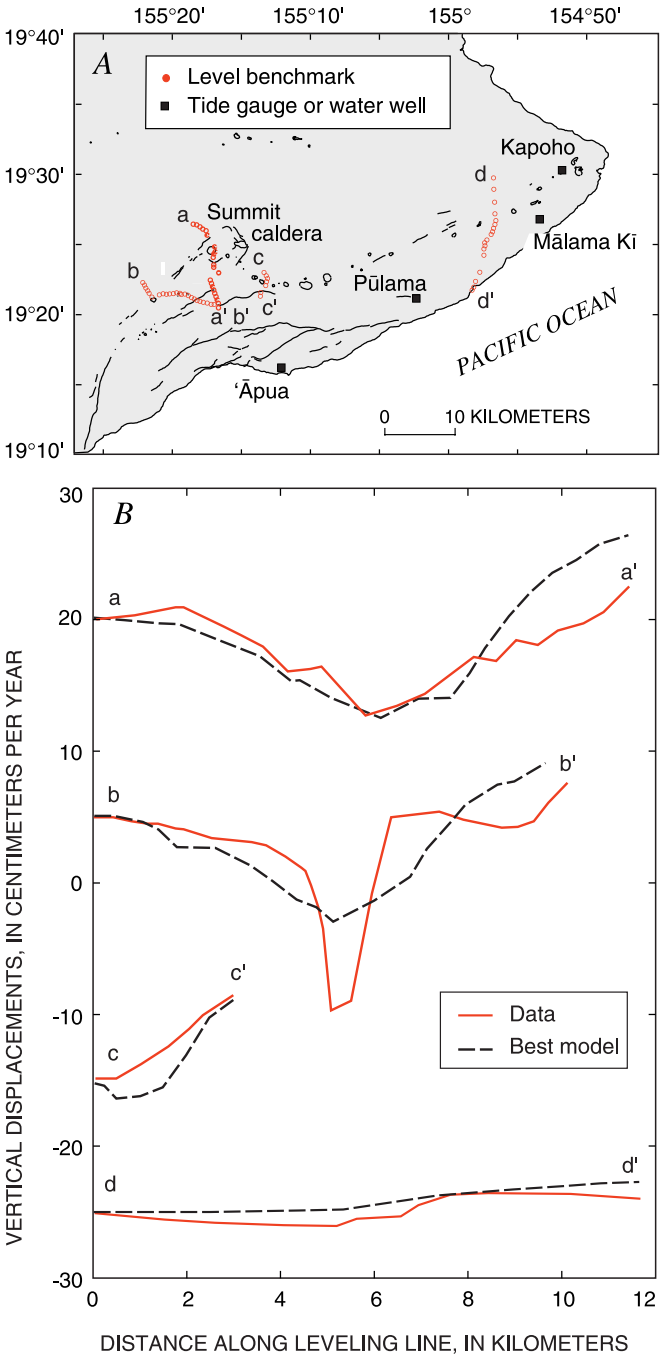

Figure 5. *A*, Location of leveling lines, tide gauge, and water wells used in deformation modeling of Kīlauea Volcano for the period from 1976 to 1983. *B*, Comparison of relative vertical velocities measured (red lines) and predicted by best-fitting model (black lines) along four lines shown in *A*.

deformation model compared to about 0.2 MPa/yr (1980–83) for the seismicity solution. Below we show that this difference is consistent with a regional slowing of stressing rates that occurred in this area around the start of 1980.

The pattern of stress change from the seismicity solution (fig. 7*C*) provides added support for the preferred deformation model. This model, with a narrow zone of fault slip, differs substantially from those obtained for 1983–91 by Delaney and others (1993) and for 1990–93 by Owen and others (1995). Coulomb stresses in models with much wider zones of fault creep, as employed by Delaney and others (1993) to model the 1983–91 period and by Owen and others (1995) to model the 1990–93 period, appear to be inconsistent with the earthquake data. Indeed, models lacking a zone of fault creep, or with a wider zone of fault creep than used here, place the greatest stress change in regions devoid of earthquakes and have low stress in the area of earthquake activity.

The Eruptions of 1983 and 1977

The Pu‘u ‘Ō‘ō-Kūpaianaha eruption was initiated by a shallow intrusion that opened the rift zone by about 2 m (Dvorak and others, 1986; Okamura and others, 1988; Hall Wallace and Delaney, 1995) and, on January 3, 1983, reached the surface to form a line of eruptive fissures (fig. 8 *A*, *B*, *C*). The boundary element models for Coulomb stress change for the onset of the 1983 eruption are based on horizontal displacements from trilateration measurements and on dry tilt data. We have computed deformation and stress changes for a model in which the inferred deep, pre-existing, inflating rift dike propagates from a depth of 3 km to the free surface, and for a model of an isolated intrusion of a shallow dike (Okamura and others, 1988; Hall Wallace and Delaney, 1995) in which the deeper dike and fault are not involved. Both models fit the deformation data equally well and have a dike opening at the surface of 2.1 m.

Several factors lead us to strongly favor the deep-dike model (fig. 8*B*) over the shallow-dike model (fig. 8*A*). First, it is a mechanically consistent extension of the preferred model for the 1976–83 period. Second, the pressure required to open the shallow dike in the preferred model is internally consistent with that model—the dike opens in response to a stress increase equivalent to the increased pressure required to lift magma the 3 km to the surface. The pressure in the shallow-dike model was adjusted to give the best fit to the data and is nearly twice that in the deep-dike model. The large pressure increase required for the shallow-dike model appears difficult to justify on physical grounds. Third, the preferred model agrees with both earthquake locations and seismicity stress solutions (fig. 8*C*), while the shallow-dike model agrees with neither. At the time of the intrusion, seismicity rates in this region of the south flank immediately increased by as much as a factor of 100. Relative to the pre-intrusion period, activity shifted away from the rift zone, and more shallow events occurred in regions of increased stress (compare figure 7*A* with figure 8*B*). Stress changes obtained from the seismicity (fig. 8*C*) are in good agreement with the stress-change calculations in the preferred model of a deep pre-existing dike (fig. 8*B*). In particular, in the depth range of 6 to 10 km (fig. 8 maps), the preferred deformation model and the seismicity solution (fig. 8*C*) show a region adjacent to the rift zone that undergoes a modest stress decrease. This pattern arises in the preferred deformation model specifically because the basal fault adjacent to the rift zone is allowed to slip in response to the intrusion and to increased pressure in the pre-existing rift dike. Farther away from the rift is a region of large stress increase that originates from the combined effect of the shallow rift expansion and the

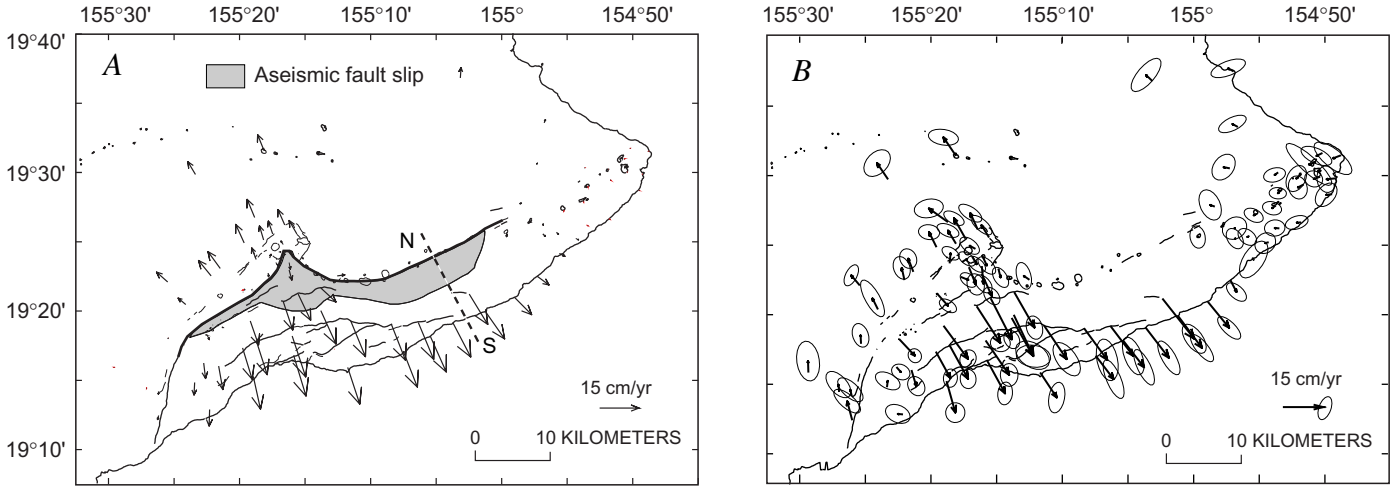

Figure 6. *A*, Horizontal velocities at ground surface of Kīlauea Volcano predicted by best-fit model for the period from 1976 to 1983. Location of model dike is indicated by bold line. Creeping portion of low-angle fault at base of the volcano is indicated by gray. The remainder of the fault is locked. Dashed line indicates location of cross sections in figure 7. *B*, Measured velocities determined from model coordinate network adjustment (Segall and Matthews, 1988) performed with reference to velocity model given in *A*. Ellipses are 95-percent confidence interval.

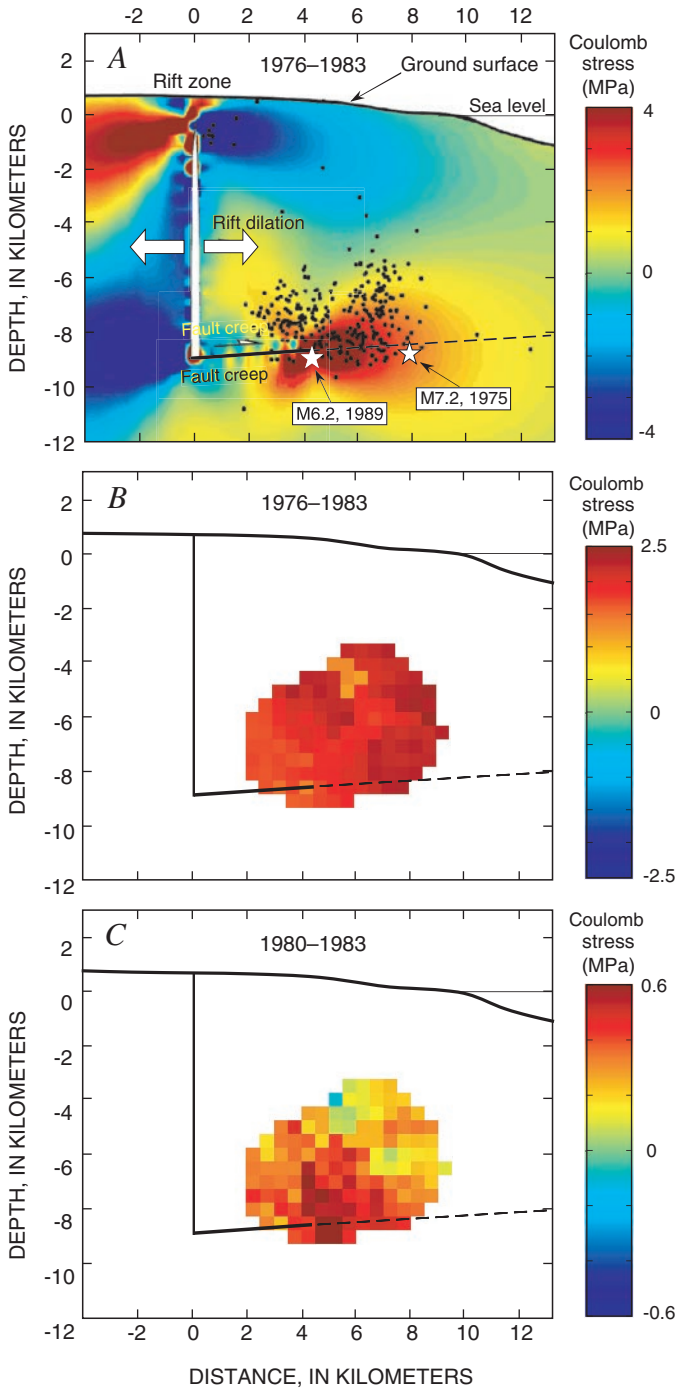

Figure 7. Coulomb stress changes prior to onset of Pu‘u ‘Ō‘ō-Kūpaianaha eruption of January 3, 1983, shown on cross sections of south flank and east rift zone through zone of Pu‘u ‘Ō‘ō-Kūpaianaha eruptive fissures. See figure 8 for location of cross section. *A*, Coulomb stress changes from preferred deformation model for the period from 1976 to 1983 and earthquakes (M≥1.5) (shown as dots and stars) for the period from 1980 to 1983. Coulomb stress computation assumes failure planes parallel to basal fault such that positive Coulomb stress promotes seaward (SSE) motion of upper block. *B*, Seismicity stress solution for the period from 1976.0 to 1982.9 (using decimal notation for parts of years). *C*, Seismicity stress solution for the period from 1980.0 to 1983.0.

deep fault slip. In contrast, the stress changes derived from the shallow-dike model (fig. 8*A*) bear little resemblance to stresses from the seismicity solution. Also, the region of high stress increase north of the rift zone, in the depth range of 6 to 10 km (fig. 8*A*), is devoid of earthquake activity.

Previously, Cayol and others (2000) presented a quantitative comparison of results for the cross-sectional stresses resulting from the 1983 intrusion (but using a somewhat different approach to solving equation 2 with stresses from this boundary element model). Regression of the Coulomb stresses from the boundary element model of the intrusion against stresses from the seismicity calculation yielded a slope of 1.1 and a correlation coefficient of 0.80.

The preferred deformation model of the 1983 intrusion also appears to be a reasonable representation of the stress changes for the September 1977 intrusion and eruption. Each intrusion occurred in the same region, and the limited deformation data for the 1977 event are consistent with the more extensive 1983 data set. Significantly, each resulted in similar changes in seismicity patterns and rates. Consequently, the resulting seismicity stress solution for the 1977 intrusion (fig. 8*D*) is very similar to the 1983 solutions. The principal difference appears to be a somewhat larger magnitude of stress increases in 1977. This is consistent with measurements made of geodimeter lines (Pūlama-Kupapa‘u and Queen’s Bath-Ford), which suggest much larger flank compression at the time of the 1977 intrusion compared to the 1983 intrusion (Arnold Okamura, oral commun., 2002).

Flank Earthquakes

In addition to the magmatic deformation sources in the east rift zone, the adjacent region of the south flank is also subjected to internal stressing from earthquakes. Since 1976, significant earthquakes in this area include the 1989 M6.1 Kalapana earthquake and several moderate earthquakes in the range M4.7 to M5.4 (fig. 9). The somewhat limited deformation data related to the 1989 Kalapana earthquake have been analyzed by Arnadottír and others (1991), who determined that the best-fitting dislocation source was a gently dipping thrust fault extending east of the hypocenter, into a region of low seismicity. The M4.9–M5.4 earthquakes, which are typically at depths of 7 to 10 km, are generally too small and too deep to result in diagnostic surface deformations adequate for modeling purposes. However, such events are expected to significantly alter stress conditions on length scales on the order of one or two source dimensions (that is, 5 to 10 km) by amounts comparable to those of larger earthquakes, because earthquake stress drops are independent of magnitude. This is apparent in the seismicity stress solutions for these moderate flank earthquakes (fig. 9).

Detailed comparisons of these solutions with models based on deformation observations are not possible, but it is instructive to compare them to a generalized boundary element model of a moderate earthquake (fig. 10*A*). The model represents an earthquake of about M5.0 and consists of a

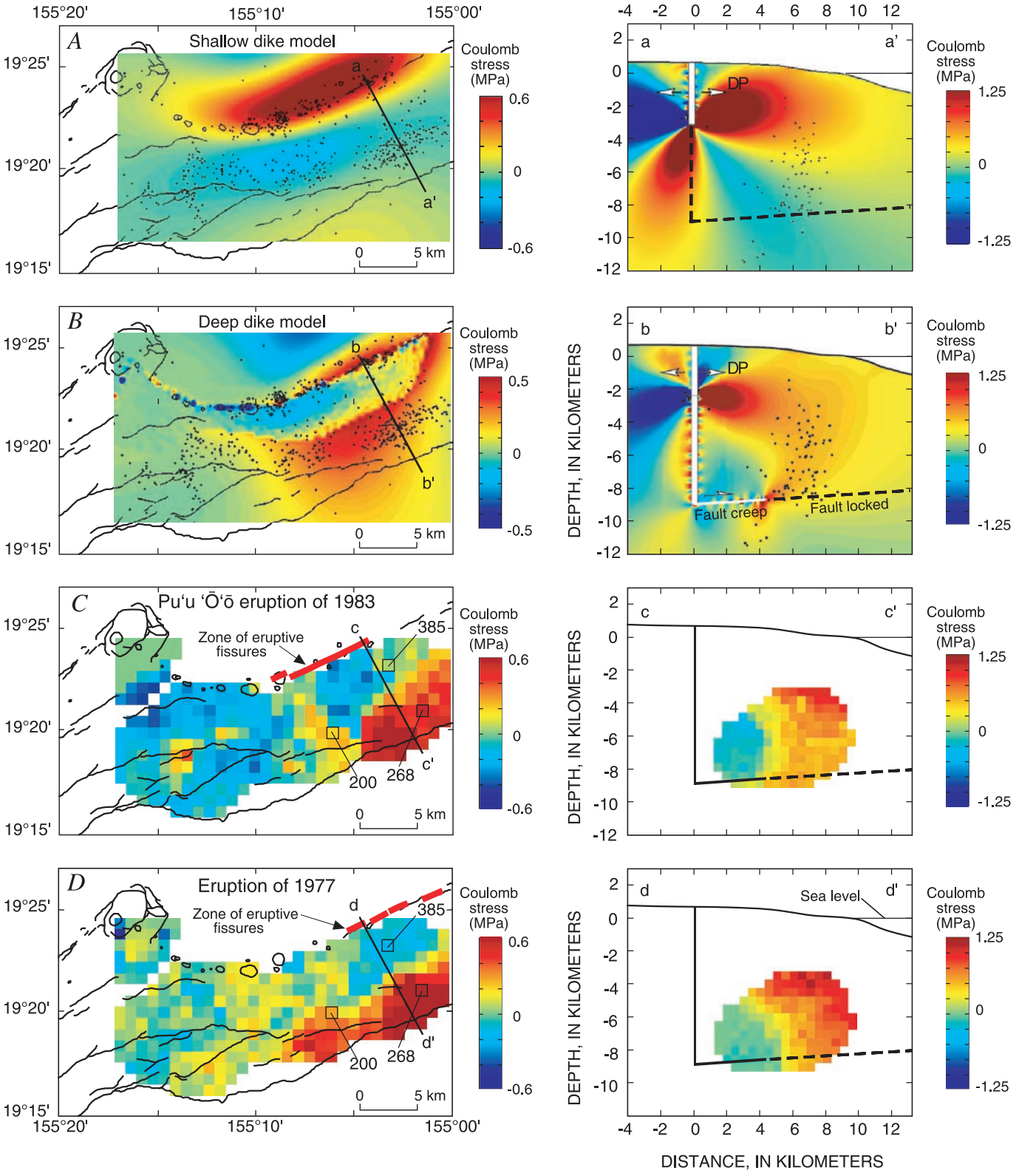

Figure 8. Coulomb stress changes at time of September 13, 1977, and January 3, 1983, east rift eruptions. *A*, Map and cross section of Coulomb stress changes computed from deformation model of onset of 1983 Pu‘u ‘Ō‘ō-Kūpaianaha eruption using shallow-dike model. Earthquakes shown (as dots) are M≥1.5 for 90 days following the onset of Pu‘u ‘Ō‘ō-Kūpaianaha eruption. *B*, Map and cross section of Coulomb stress changes computed from deformation model of onset of 1983 Pu‘u ‘Ō‘ō-Kūpaianaha eruption using preferred deep-dike model. Earthquakes shown as in *A*. *C*, Coulomb stress changes from seismicity rate changes at onset of the Pu‘u ‘Ō‘ō-Kūpaianaha eruption. See figure 4 for records of stress vs. time for the indicated nodes. *D*, Coulomb stress changes from seismicity rate changes at the onset of the September 1977 eruption.

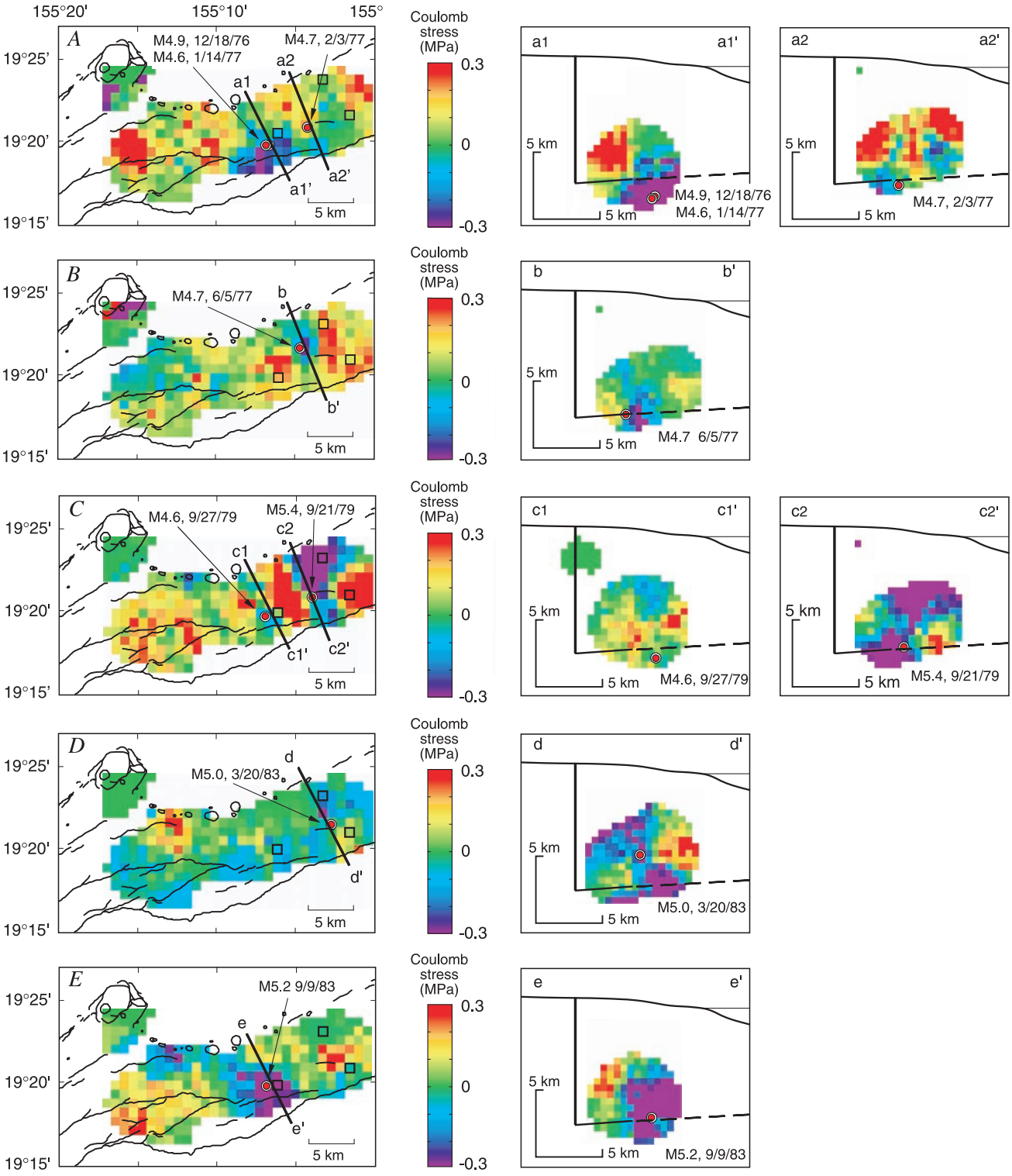

Figure 9. Coulomb stress changes computed from seismicity rate changes for earthquakes M≥4.7 in vicinity of Pu‘u ‘Ō‘ō-Kūpaianaha eruption. Small squares on map view indicate locations of records of stress vs. time in figure 4.

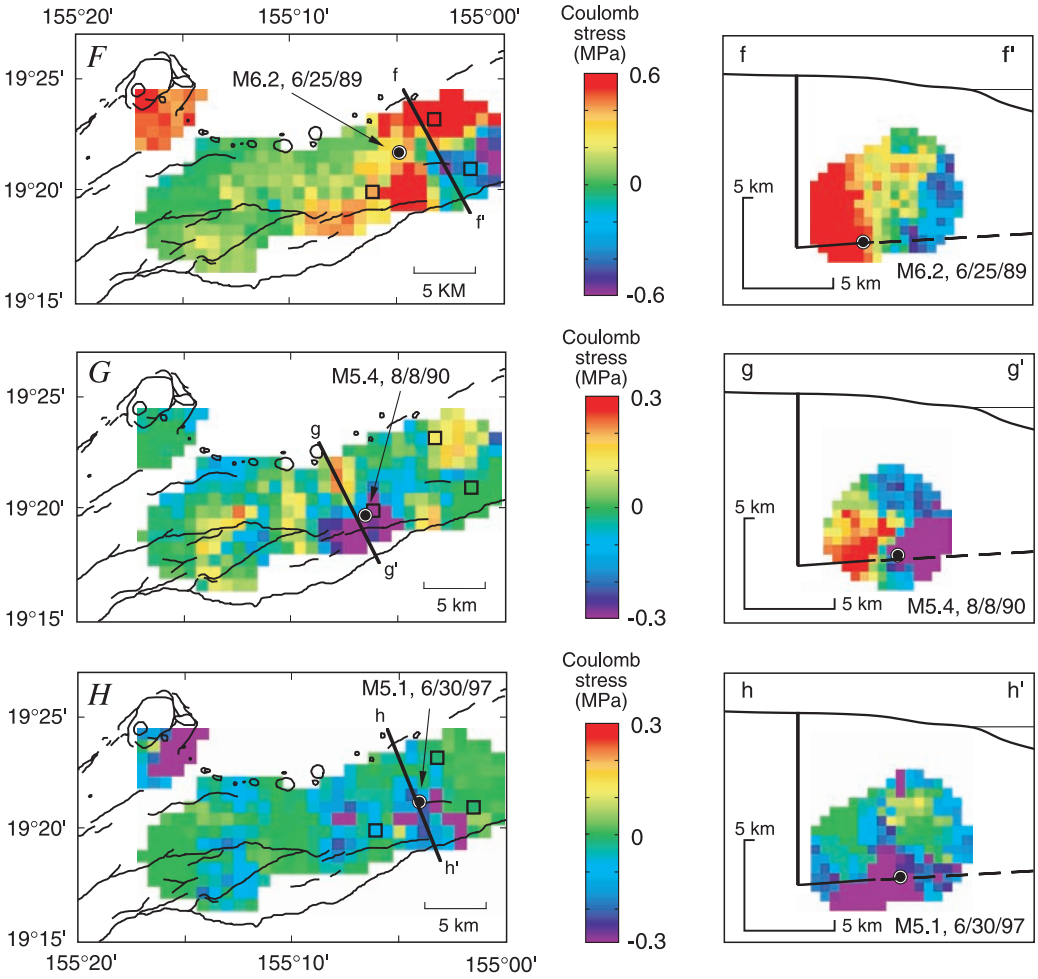

Figure 9. Continued.

horizontal circular rupture source 5 km in diameter and a uniform stress drop of 1 MPa. To facilitate comparisons with the seismicity solutions, which use earthquakes principally in the depth range of 6 to 10 km, the Coulomb stresses have been averaged over a depth interval of ±2 km centered on the fault plane. Figure 10*B* shows a simulated seismicity stress solution based on the boundary element model. In this simulation, earthquake rates as a function of time and position were first calculated from the stress changes of the boundary element model using equation 2. Next, using the predicted rates, earthquake event times were randomly drawn to produce a synthetic earthquake catalog. The unperturbed earthquake rates of the synthetic catalog (r in equation 2) were chosen to be representative of the south flank rates. Finally, the synthetic catalog was used to solve for the stress changes using the procedures employed for the real data (fig. 10*B*). The simulation indicates that sources 5 km in diameter, or somewhat smaller, should be resolvable using the seismicity solution method.

In map view, the solutions for stress changes at the time of earthquakes of M≥4.7 give regions of stress decrease near the earthquake hypocenter and stress increase in adjacent regions. These patterns are in general agreement with the model earthquake. Most prominent in these solutions are the regions of stress decrease, or "stress shadows," where seismic activity slowed following the earthquake. The dimensions of the regions of stress decrease are typically 4 to 8 km, consistent with fault slip lengths expected for earthquakes of these magnitudes.

In cross section, the Coulomb stress solutions of four earthquakes (M4.7, 6/5/77; M4.6, 9/27/79; M5.4 9/21/79; M5.0, 3/20/83) in figure 9*B*, *C*, and *D* show the characteristic pattern of stress decrease and increase expected for slip on a fault patch. That pattern has a region of stress drop between two zones of stress increase, presumably marking the region of fault slip and regions of stress concentration at the ends of the slip zone, respectively. Four other events (M4.9, 12/18/76; M5.2, 9/9/83; M6.2, 6/25/89; M5.4, 8/8/90) in figure 9*A*, *E*, *F*, and *G* appear to have incomplete patterns of stress change consisting of a single region of stress increase adjacent to the region of stress decrease. The earthquakes with these patterns are, on average, larger than those events showing the more complete pattern, and all lie at the edge of the region where seismicity stress solutions are possible according to our

criteria. Consequently, we interpret these cross sections to represent sources that lie partly outside the solution region. Two earthquakes (M4.7, 2/3/77; M5.1, 6/30/97) in figure 9*A* and *H* have complicated patterns that may represent complex, multi-segment events or sources that are misoriented with respect to the cross sections.

South flank earthquakes, especially the larger events, relieve rift expansion stresses and thereby permit continued expansion of the rifts and the accompanying intrusion of magma into the rifts (Dieterich, 1988). The intrusion and eruption of September 13, 1977, were preceded by the M4.7 earthquake of June 5, 1977, and followed by the M5.4 earthquake of September 2, 1979 (figs. 9*B* and 9*C*, respectively). The 1979 event, in particular, relieved the 1977 intrusion stresses and may have permitted movement of magma into the portion of the rift zone that resulted in the eruption of Pu‘u ‘Ō‘ō-Kūpaianaha on January 3, 1983.

Following the onset of the Pu‘u ‘Ō‘ō-Kūpaianaha eruption, most larger earthquakes initiated within the region of stress increase that developed at the time of the 1983 intrusion and eruption (fig. 7). The single exception is the M6.2 1989 earthquake, which initiated outside that zone of stress increase. However, the region of maximum stress drop for that earthquake did coincide with this region of maximum stress increase (compare figure 8*B* with figure 9*F*). This is also evident in the stress/time record of node 268 (fig. 4), which clearly shows the stress increases at the times of the 1977 and 1983 eruptions and the stress decrease at the time of the 1989 earthquake.

In the vicinity of node 200, there were repeated moderate earthquakes of M4.9, M4.6, M5.2 and M5.4 on 12/18/76, 9/2/79, 9/9/83, and 8/8/90, respectively (figs. 4 and 9*A*, *C*, *E,* and *G*). These events are evident as stress drops at node 200 (fig. 4). In addition, this location experienced stress increases at the times of the 1977 and 1983 intrusions as well as the 1989 earthquake. This record gives an impression of recurring fault failure at a threshold stress.

Stressing Rate Changes in 1979 and 1983

Comparison of the trilateration line length changes in the 1976–82 period with those after 1983 shows widespread slowing of deformation rates sometime around the time that the Pu‘u ‘Ō‘ō-Kūpaianaha eruption began. Extension rates across Kīlauea caldera averaged about 25 cm/yr in the years leading up to the Pu‘u ‘Ō‘ō-Kūpaianaha eruption and decreased to about 4 cm/yr at the onset of the eruption (Delaney and others, 1998), a slowing by a factor of about five. Across the east rift zone, a similar slowing of rates of extension occurred, and south-flank lines oriented perpendicular to the rift zone changed from compression to extension (Delaney and others, 1998). South of the east rift zone, a slowing of stressing rates is very evident in the seismicity solutions. For much of the region, the stress versus time data (fig. 4) indicate average stressing rates of about 0.25±0.10 MPa/yr in the 1976–80 period and about 0.05±0.02 MPa/yr after 1983, roughly a factor of five decrease that is consistent with the deformation data. This slowing occurred quite abruptly around the end of 1979 in some regions (fig. 4, nodes 102, 385, and 268) and at the start of 1983 in other areas (fig. 4, nodes 153, 254, and possibly 200).

Regions affected by a change of stressing rates near the end of 1979 are shown in figure 11*A*, which plots the average stressing rate in the interval from 1980.0 to 1982.5 (the exact temporal midpoint of the year 1982) minus the average

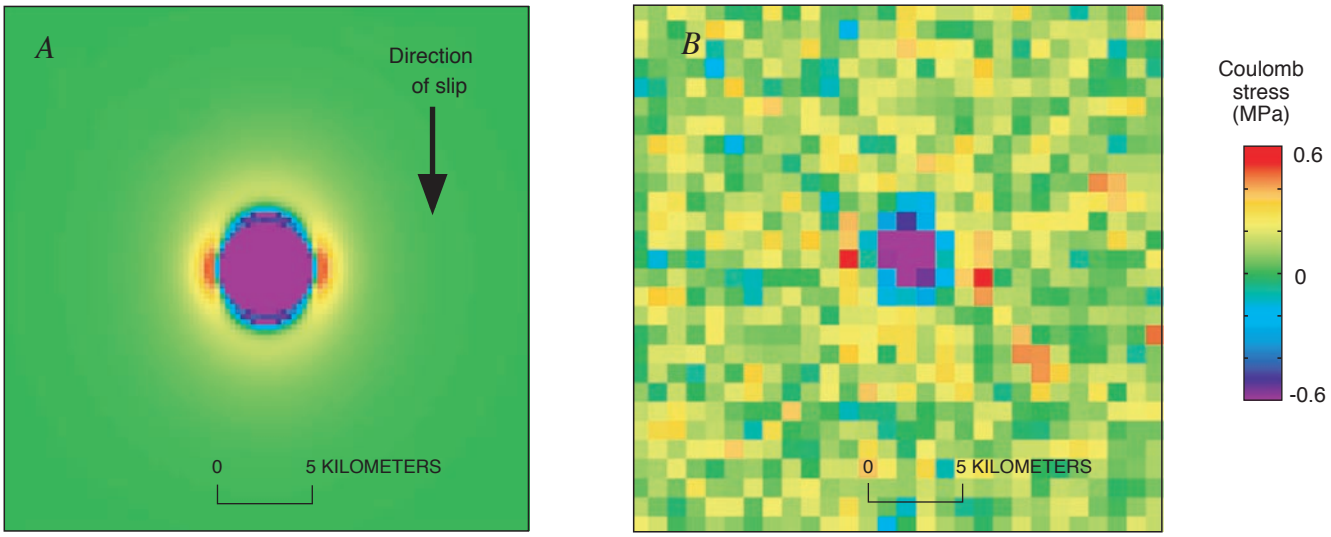

Figure 10. Generalized model of M~5 earthquake. View is perpendicular to fault plane. *A*, Boundary element model of slip in which stresses have been averaged over a width of ±2 km of the fault surface. *B*, Solution for stress changes from simulated earthquake catalog derived from boundary element model of *A*, together with earthquake rate formulation given by equation 2.

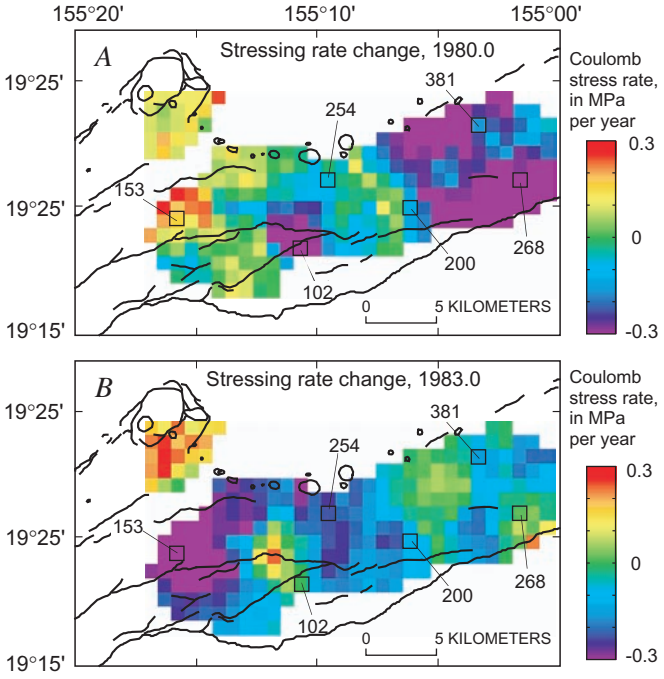

Figure 11. Change of Coulomb stressing rates. Plots give change of stressing rate $\Delta\dot{S}_r=\dot{S}_2-\dot{S}_1$, where $\dot{S}_1$ and $\dot{S}_2$ are average Coulomb stressing rates in successive time intervals 1 and 2, respectively. Numbered squares indicate the locations of the records of time vs. stress in figure 4. *A*, Change of stressing rate near the start of 1980 using average stressing rates in time intervals 1976.0–1980.0 and 1980.0–1982.5 (using decimal notation for parts of years). *B*, Change of stressing rate at start of 1983, using average stressing rates in time intervals 1980.0–1983.0 and 1983.0–1988.5.

stressing rate in the interval from 1976.0 to 1980.0 from the seismicity stress solutions. The region most affected by this slowing coincides quite closely with the area affected by the M5.4 earthquake of 9/21/79 (fig. 9). In addition, the stressing rate of an isolated region to the west (in the area of node 102) also slowed dramatically. Figure 11*B* shows regions affected by slowing at the start of 1983.

The slowing of flank stressing at the start of 1983 indicates that the volume of lava for the Pu‘u ‘Ō‘ō-Kūpaianaha eruption represents a major fraction of the magma supplied to Kīlauea. On the basis of rift-zone volume change in the preferred deformation model for the 1976–83 period, the rate of supply of magma to the rift zones has been modeled to be 0.18 km^3/yr (Cayol and others, 2000). Wolfe and others (1987) estimated an average eruption rate of 0.12 km^3/yr from February 1983 to June 1984, and Heliker and Mattox (this volume) obtained a rate of 0.12 km^3/yr over the first 19 years of the eruption. Assuming a constant supply rate of 0.18 km^3/yr and eruptive rates of 0.12 km^3/yr, the volume of magma available to drive rift expansion decreased from 0.18 km^3/year to 0.06 km^3/yr after the onset of the eruption. Within the uncertainties of these estimates, this inferred three-fold reduction of magma to drive rift expansion at the start of the Pu‘u ‘Ō‘ō-Kūpaianaha eruption is reasonably consistent with the five-fold reduction of deformation and stressing rates noted previously.

The cause for the slowing of deformation rates in the eastern portion of the study area around the time of the 1979 earthquake is somewhat problematic. If, as we have argued, deformation of the south flank is driven by movement of magma into the rift system, then the earthquake, which appears to have created a stress condition amenable to continuing intrusion in this area, should have not have resulted in slowing of the deformation. We speculate that the supply of magma to the east rift zone in the area of the Pu‘u ‘Ō‘ō-Kūpaianaha eruptive fissures became temporarily blocked at the time of the earthquake. If this interpretation is correct, then stressing rates in the uprift direction from the blockage (to the west) should have increased around the time of the 1979 earthquake, because the same volume of magma was then driving the deformation over a smaller region. Evidence for this is seen in the weak increase of stressing rates that is evident over much of the western portion of the study area, with a strong increase in stressing rates in the vicinity of node 153, where they increased from about 0.3 MPa/yr to about 0.6 MPa/yr (see the stress vs. time solution for node 153 of figure 4). Additionally, the pattern of slowing at the start of the 1983 eruption (fig. 10*B*) is restricted to the western half of the study area, indicating that magma that was driving the deformation in that region was diverted to feed the 1983 eruption.

Conclusions

An analysis of surface deformation and earthquake data has been carried out for Kīlauea Volcano as it pertains to stress interactions before and during the Pu‘u ‘Ō‘ō-Kūpaianaha eruption. The seismicity analysis employs a newly developed method to solve for Coulomb stress changes from earthquake rate changes. The period following the M7.2 Kalapana earthquake in 1975 and before the start of the Pu‘u ‘Ō‘ō-Kūpaianaha eruption in 1983 was characterized by the rapid expansion of a dike-like magma body within the rift zones of Kīlauea. Both the deformation models and the seismicity stress solutions indicate rift expansion was coupled to aseismic fault slip over a narrow region of a low-angle fault beneath the south flank. The rate of rift opening averaged 40 cm/yr, which is much higher than estimates for any previously analyzed period of Kīlauea deformation. At the onset of the Pu‘u ‘Ō‘ō-Kūpaianaha eruption in January 1983, the inflating rift-zone dike propagated to the surface to form the eruptive fissures. The exceptionally high seismic activity in the south flank adjacent to the east rift zone, and the locations of earthquakes within this zone, are consistent with rapid stressing by an expanding rift zone. In late 1979 and at the start of the Pu‘u ‘Ō‘ō-Kūpaianaha eruption in January 1983, deformation data and seismicity stress solutions indicate a dramatic slowing of deformation and stressing rates in Kīlauea’s south flank. The magnitude of the slowing is roughly consistent with our estimates of magma supply to Kīlauea, based on the deformation modeling of the 1976–83 period.

Acknowledgments

We thank the staff of the Hawaiian Volcano Observatory, particularly Arnold Okamura and Asta Miklius for providing us with the deformation data. Thanks also to Peter Cervelli, Christina Heliker, Ross Stein, and Don Swanson for their thoughtful reviews.

References Cited

Ando, Masataka, 1979, The Hawaii earthquake of November 29, 1975; low dip angle faulting due to forceful injection of magma: Journal of Geophysical Research, v. 84, no. B13, p. 7616–7626.

Árnadóttir, Thóra, Segall, Paul, and Delaney, P.T., 1991, A fault model for the 1989 Kilauea south flank earthquake from levelling and seismic data: Geophysical Research Letters, v. 18, no. 12, p. 2217–2220.

Bryan, C.J., 1992, A possible triggering mechanism for large Hawaiian earthquakes derived from analysis of the 26 June 1989 Kilauea south flank sequence: Seismological Society of America Bulletin, v. 82, no. 6, p. 2368–2390.

Cayol, Valérie, and Cornet, F.H., 1998, Three-dimensional modeling of the 1983–1984 eruption at Piton de la Fournaise Volcano, Réunion Island: Journal of Geophysical Research, v. 103, no. B8, p. 18025–18037.

Cayol, Valérie, Dieterich, J.H., Okamura, A.T., and Miklius, Asta, 2000, High magma storage rates before the 1983 eruption of Kilauea, Hawaii: Science, v. 288, no. 5475, p. 2343–2346.

Cheng, C.H., and Johnston, D.H., 1981, Dynamic and static moduli: Geophysical Research Letters, v. 8, no. 1, p. 39–42.

Clague, D.A., and Denlinger, R.P., 1994, Role of olivine cumulates in destabilizing the flanks of Hawaiian volcanoes: Bulletin of Volcanology, v. 56, no. 6–7, p. 425–434.

Crosson, R.S., and Endo, E.T., 1982, Focal mechanisms and locations of earthquakes in the vicinity of the 1975 Kalapana aftershock zone 1970–1979; implications for tectonics of the south flank of Kilauea Volcano, island of Hawaii: Tectonics, v. 1, no. 6, p. 495–542.

Delaney, P.T., Denlinger, R.P., Lisowski, Michael, Miklius, Asta, Okubo, P.G., Okamura, A.T., and Sako, M.K., 1998, Volcanic spreading at Kilauea, 1976–1996: Journal of Geophysical Research, v. 103, no. B8, p. 18003–18023.

Delaney, P.T., Fiske, R.S., Miklius, Asta, Okamura, A.T., and Sako, M.K., 1990, Deep magma body beneath the summit and rift zones of Kilauea Volcano, Hawaii: Science, v. 247, no. 4948, p. 1311–1316.

Delaney, P.T., Miklius, Asta, Árnadóttir, Thóra, Okamura, A.T., and Sako, M.K., 1993, Motion of Kilauea Volcano during sustained eruption from the Puu Oo and Kupaianaha vents, 1983–1991: Journal of Geophysical Research, v. 98, no. B10, p. 17801–17820.

Delaney, P.T., Miklius, Asta, Árnadóttir, Thóra, Okamura, A.T., and Sako, M.K, 1994, Motion of Kilauea Volcano during sustained eruption from the Puu Oo and Kupaianaha vents, 1983–1991; supplemental information: U.S. Geological Survey Open-File Report 94–567, 23 p.

Dieterich, J.H., 1988, Growth and persistence of Hawaiian volcanic rift zones: Journal of Geophysical Research, v. 93, no. B5, p. 4258–4270.

Dieterich, J.H., 1994, A constitutive law for rate of earthquake production and its applications to earthquake clustering: Journal of Geophysical Research, v. 99, no. B2, p. 2601–2618.

Dieterich, J.H., Cayol, Valérie, and Okubo, P.G., 2000, The use of earthquake rate changes as a stress meter at Kilauea volcano: Nature, v. 408, no. 6811, p. 457–460.

Dieterich, J.H., and Kilgore, B.D., 1996, Implications of fault constitutive properties for earthquake prediction: National Academy of Sciences Proceedings, v. 93, p. 3787–3794.

Dvorak, J.J., Okamura, A.T., English, T.T., Koyanagi, R.Y., Nakata, J.S., Sako, M.K., Tanigawa, W.R., and Yamashita, K.M., 1986, Mechanical response of the south flank of Kilauea volcano, Hawaii, to intrusive events along the rift systems: Tectonophysics, v. 124, no. 3–4, p. 193–209.

Dzurisin, Daniel, Koyanagi, R.Y., and English, T.T., 1984, Magma supply and storage at Kilauea Volcano, Hawaii, 1956–1983: Journal of Volcanology and Geothermal Research, v. 21, no. 3–4, p. 177–206.

Fiske, R.S., and Kinoshita, W.T., 1969, Inflation of Kilauea Volcano prior to its 1967–1968 eruption: Science, v. 165, no. 3891, p. 341–349.

Gillard, Dominique, Rubin, A.M., and Okubo, P.G., 1996, Highly concentrated seismicity caused by deformation of Kilauea's deep magma system: Nature, v. 384, no. 6607, p. 343–346.

Got, J.-L., Fréchet, Julien, and Klein, F.W., 1994, Deep fault plane geometry inferred from multiplet relative relocation beneath the south flank of Kilauea: Journal of Geophysical Research, v. 99, no. B8, p. 15375–15386.

Hall Wallace, M.K., and Delaney, P.T., 1995, Deformation of Kilauea volcano during 1982 and 1983; a transition period: Journal of Geophysical Research, v. 100, no. B5, p. 8201–8219.

Harris, R.A., Simpson, R.W., and Reasenberg, P.A., 1995, Influence of static stress changes on earthquake locations in southern California: Nature, v. 375, no. 6528, p. 221–224.

Hill, D.P., and Zucca, J.J., 1987, Geophysical constraints on the structure of Kilauea and Mauna Loa Volcanoes and some implications for seismomagmatic processes, chap. 37 *of* Decker, R.W., Wright, T.L., and Stauffer, P.H., eds., Volcanism in Hawaii: U.S. Geological Survey Professional Paper 1350, v. 2, p. 903–917.

Jaumé, S.C., and Sykes, L.R., 1996, Evolution of moderate seismicity in the San Francisco Bay region, 1850 to 1993; seismicity changes related to the occurrence of large and great earthquakes: Journal of Geophysical Research, v. 101, no. B1, p. 765–789.

King, G.C.P., Stein, R.S., and Lin, Jian, 1994, Static stress changes and the triggering of earthquakes: Seismological Society of America Bulletin, v. 84, no. 3, p. 935–953.

Klein, F.W., Koyanagi, R.Y., Nakata, J.S., and Tanigawa, W.R., 1987, The seismicity of Kilauea's magma system, chap.

43 *of* Decker, R.W., Wright, T.L., and Stauffer, P.H., eds., Volcanism in Hawaii: U.S. Geological Survey Professional Paper 1350, v. 2, p. 1019–1185.

Linker, M.F., and Dieterich, J.H., 1992, Effects of variable normal stress on rock friction; observations and constitutive equations: Journal of Geophysical Research, v. 97, no. B4, p. 4923–4940.

Nakamura, Kazuaki, 1982, Why do long rift zones develop in Hawaiian volcanoes—a possible role of thick oceanic sediments, *in* Schmincke, H.-U., Baker, P.E., and Forjaz, V.H., eds., Activity of ocean volcanoes, International Symposium on the Activity of Oceanic Volcanoes, July 1982, Proceedings: Ponta Delgada, Universidade dos Azores, Serie Ciencias da Naturezam, no. 3, p. 59–73.

Okamura, A.T., Dvorak, J.J., Koyanagi, R.Y., and Tanigawa, W.R., 1988, Surface deformation during dike propagation, chap. 6 *of* Wolfe, E.W., ed., The Puu Oo eruption of Kilauea Volcano, Hawaii; episodes 1 through 20, January 3, 1983, through June 8, 1984: U.S. Geological Survey Professional Paper 1463, p. 165–182.

Okubo, P.G., Benz, H.M., and Chouet, B.A., 1997, Imaging the crustal magma sources beneath Mauna Loa and Kilauea volcanoes, Hawaii: Geology, v. 25, no. 10, p. 867–870.

Owen, S.E., Segall, Paul, Freymueller, J.T., Miklius, Asta, Denlinger, R.P., Árnadóttir, Thóra, Sako, M.K., and Bürgmann, R.B., 1995, Rapid deformation of the south flank of Kilauea volcano, Hawaii: Science, v. 267, no. 5202, p. 1328–1332.

Pollard, D.D., Delaney, P.T., Duffield, W.A., Endo, E.T., and Okamura, A.T., 1983, Surface deformation in volcanic rift zones: Tectonophysics, v. 94, no. 1–4, p. 541–584.

Rubin, A.M., Gillard, Dominique, and Got, J.-L., 1998, A reinterpretation of seismicity associated with the January 1983 dike intrusion at Kilauea Volcano, Hawaii: Journal of Geophysical Research, v. 103, no. B5, p. 10003–10015.

Scholz, C.H., 1998, Earthquakes and friction laws: Nature, v. 391, no. 6662, p. 37–42.

Segall, Paul, and Matthews, M.V., 1988, Displacement calculations from geodetic data and the testing of geophysical deformation models: Journal of Geophysical Research, v. 93, no. B12, p. 14954–14966.

Simpson, R.W., and Reasenberg, P.A., 1994, Earthquake-induced static-stress changes on central California faults, *in* Simpson, R.W., ed., The Loma Prieta, California earthquake of October 17, 1989; tectonic processes and models: U.S. Geological Survey Professional Paper 1550–F, p. 55–89.

Stein, R.S., 1999, The role of stress transfer in earthquake occurrence: Nature, v. 402, no. 6762, p. 605–609.

Swanson, D.A, Duffield, W.A., and Fiske, R.S., 1976, Displacement of the south flank of Kilauea Volcano; the result of forceful intrusion of magma into the rift zones: U.S. Geological Survey Professional Paper 963, 39 p.

Thurber, C.H., and Gripp, A.E., 1988, Flexure and seismicity beneath the south flank of Kilauea volcano and tectonic implications: Journal of Geophysical Research, v. 93, no. B5, p. 4271–4278.

Tse, S.T., and Rice, J.R., 1986, Crustal earthquake instability in relation to the depth variation of frictional properties: Journal of Geophysical Research, v. 91, no. B9, p. 9452–9472.

Wolfe, E.W., Garcia, M.O., Jackson, D.B., Koyanagi, R.Y., Neal, C.A., and Okamura, A.T., 1987, The Puu Oo eruption of Kilauea Volcano, episodes 1–20, January 3, 1983, to June 8, 1984, chap. 17 Decker, R.W., Wright, T.L., and Stauffer, P.H., eds., Volcanism in Hawaii: U.S. Geological Survey Professional Paper 1350, v. 1, p. 471–508.

Wright, T.L., and Fiske, R.S., 1971, Origin of differentiated and hybrid lavas of Kilauea Volcano, Hawaii: Journal of Petrology, v. 12, no. 1, p. 1–65.

Volunteers at the Hawaiian Volcano Observatory, 1983–2002

By Steven R. Brantley

During the 20 years of the Pu‘u ‘Ō‘ō-Kūpaianaha eruption, the Hawaiian Volcano Observatory (HVO) has relied heavily on the help of more than 300 volunteers from Hawai‘i, the mainland United States, and many other countries around the world. Most volunteers have been of college age, undergraduates or graduates in the earth sciences. But they have also included professors on sabbatical leave, retirees, the children and spouses of HVO staff who were pressed into service, and itinerant volcano-watchers of various persuasions.

In each year of the past decade, volunteers contributed more than 10,000 hours to help monitor the active volcanoes of Hawai‘i and conduct research on Hawaiian volcanism. They, in turn, gained experience working on active volcanoes and participating in scientific research—collecting and analyzing data, building and installing instruments, preparing maps and writing reports, or helping with administrative, library, or archival tasks. Many have gone on to become our colleagues: earth scientists working in Hawaii and many other parts of the world.

Listed below are the names of the volunteers, most of whom worked at the observatory for at least three months under the auspices of the USGS Volunteer Program. I have tried to include the names of all those who volunteered for at least a month during the 20-year span of the eruption, but records from the early years are scanty, and I apologize for any omissions or errors. The observatory staff thanks all who contributed their time, energy, and ideas to our work and takes pride in watching the volunteers grow personally and professionally from their experience at HVO.

Albrecht, William	1981–2001	Andres, Bob	1986
Milholland, Cheney	1983	Amit, Tom	1986
Pedit, Bern	1983–85	Weisel, Dorian	1986–90
Peterson, Lisa	1983–87	Carter, Norma	1986–92
Chadwick, Bill	1984	Hort, Matthias	1987
Atwill, Teresa	1984	Cagle, Deane	1987
Johnson, Daniel	1984–86	Gaspari, Mary	1987
Servos, Kurt	1985	Huey, Christie	1987
Kaiser, Claudia	1985	Harmon, Kim	1987
Rowland, Scott	1985–87	Browning, Kerry	1987
White, Ed	1985	Jackson, Tracy	1987
Miller, Katie	1985	Koyanagi, Stuart	1987
Swoboda, Peter	1985	Richardson, Adele	1987
Bower, Jane Elizabeth	1985	Kern, Gunter	1987
Dixon, Eleanor	1985	MacKay, Kevin	1997
Park, Conny	1985	Rapp, Juergen	1987
Jackson, Michael	1985	Boyer, Steve	1987–88
Chartier, Torrie	1985	Durkoop, Anke	1988
Stone, Mike	1986	Druckenbrod, Peter	1988
Nadermann, Frank	1986	Springer, Martine	1988
Davis, Clara	1986	Schmidt, Christof	1988
Ouchida, Joyce	1986	Thomson, Toni	1988–2002
Steinle, Uwe	1986	Stewart, Tom	1989

Reiff, Holger	1989
Powell, Debbie	1989
Lege, Thomas	1989
Birkle, Peter	1989
Lim, Peggy	1989–90
Schickman, Kaye	1989
Lockwood, Martha	1989–93
Bryan, Carol J.	1989, 1992–93
Mattox, Tari	1989, 2000
MacKenzie, Kris	1990
Westphal, Hildegard	1990
Staesche, Astrid	1990
Wright, John L.	1990
DeGroot, Trish	1990
Jones, Alun C.	1990
Davaille, Anne	1990
Kech, Michael	1990
Andreas, Klein	1990–91
Wienbruch, Christian	1990–91
Babb, Janet	1990–91
Mattox, Steve	1990–93
Hultgrien, Lynn	1990, 1998
Paulick, Holger	1991
Stover, Robert	1991
McClurg, Joseph	1991–92
Stroncik, Nicole	1991–92
Yamaguchi, Shoji	1991–95
Tirelli, Andrea Csillag	1991, 1994
Keszthelyi, Laszlo	1991–92, 1994–99
Simmons, Philip W.	1992
Burkley, Erin	1992
Schaaf, Michael	1992
Dorn, Susanne	1992
Gregg, Christopher Eric	1992
Foster, James	1992–93
Camara, Bobby	1992–94
Timmermans, Mary–Louise	1993
Kanjorski, Nancy	1993
Wilson, David G.	1993
King, Lance	1993
Lamson, Geoffrey M.	1993
Hack, Paul J.	1993
Galcher, William M.	1993
Wilson, William C.	1993–94
Roberts, George B.	1993–94
Horsman, Jennifer L.	1993–94
Pallon, Jennifer E.	1993–94
Riesenberg, Kathryn M.	1993–94
Kekaulike-Maby, Pua	1993–94
Kater, Lorien	1993–94
Pitka, Steven	1993–94
Thorne, Zoe	1993–2002
Kauahikaua, Lilinoe	1994
Jacobi, Emmett	1994
Orr, Tim R.	1994
Gowing, Yukiko Sato	1994
Kuhns, Birgit	1994
Zumbro, David S.	1994
Moss, Jane	1994
Olmsted, Valerie	1994
Sachnoff, Lisa	1994
Kimberly, Paul	1994
Yoon, Elim	1994
Brodsky, Emily E.	1994
Benumof, Benjamin	1994
Lohr, Walter	1994
Halsor, Sid P.	1994
Miller, Amy	1994
Tozer, Craig	1994
MacDonald Lara K.	1994
Kretschmar, Laura	1994
Corley-Ogilvie, Chris	1994–95
Tuin, Martin	1994–95
Meijer, Peter	1994–95
White, Scott	1994–95
Wilburn, Christopher G.	1994–95
Wills, Mack	1994–99
Gertisser, Ralf	1995
Oram, Suzy	1995
Sanchez, Irene	1995
Surmonte, Christopher	1995
Harnetiaux, Jonathan	1995
Ballentine, Greg	1995
Rusk, Brian	1995
Hunt, Emily	1995
Hoover, Sarah E.	1995
Maceri, Stella E.	1995
Cortez, Renee	1995
Ton-That, Thao	1995
Davies, Ansley B.	1995
Evison, Deborah L.	1995
Widham, Jennifer L.	1995
Novak, Elizabeth A.	1995–96
Zwaan, Jonathan	1995–96
Haspels, Jeffrey	1995–96
Eisenger, Chris	1995–96, 1998–99
O'Meara, Stephen	1995–2000
Sharma, Kirti	1995–96, 1999–2001

Bonsey, Ed	1995–2002
Warshauer, Kent	1995–2002
Forman, Laura	1996
Breuninger, Anna B.	1996
Zenk, Andrew Michael	1996
Friedman, Rachel	1996
Csaky, Marcus	1996
Ficker, Edward	1996
McGee, Jennifer	1996
Solywoda, Kathy	1996
Settle, Jennifer Lee	1996
Musante, Susan	1996
Licameli, Anna Maria	1996
Calis, Nadine	1996
Webb, Patrick R.	1996
Page, Delia	1996
Honma, Andrew	1996
Sweeney, Edward	1996
Miura, Elizabeth H.	1996
Feineman, Maureen	1996
Poole, Anne P.	1996
Ulstad, Kristin	1996
Coon, Leslie	1996
Ching, Cleo L.	1996
Ahearn, Dylan	1996–97
Pauk, Benjamin August	1996, 1998
Goehring, Douglas	1996–98
Johnson, Jenda	1996–2002
van Koolwyk, Marye	1997
Workman, Rhea	1997
Weiss, Daniel	1997
Webb, Patrick R.	1997
Gardner, Chris	1997
Wekker, Rodney	1997
Owens, John J.	1997
Klee, Robert	1997
Miller, Noel	1997
Diener, Ben	1997
Bacon, Steven	1997
Cazeneuve, Michael	1997
Kellogg, Melissa	1997
Holm, Richard	1997
Krahenbuhl, Richard	1997–98
Duarte, Kaeo	1997–98
Graves, Peter	1997–98, 2000–01
Santos, Sharon	1998
MacFadyen, Amy	1998
Rossi, Matti J.	1998
Kenedi, Kate Lewis	1998
Kenedi, Chris	1998
Turner, Miralani	1998
Sigurdson, David	1998
Oshiro, Peter	1998
Sander, Kathleen	1998
Watson, Deborah	1998
Smith, W. Ryan	1998
Lindner, Thomas	1998
Llewellin, Edward	1998
Doust, Roeland Pieter	1998
Su, Chun-Yen	1998
Owen, Richard	1998
Gaffney, Amy	1998
Hanley, Diane	1998
Petersen, Tanya	1998
Benson, Kristian	1998–99
Seaman, Caroline	1998–99
Doughty, Georgina	1998–99
McGiffert, Heather	1998–99
Nakata, Ian	1998–99
Gripp, Alice	1999
Miller, Vicky	1999
Merrill, Mary	1999
Merrill, Joseph	1999
Pusic, Daria	1999
Bend, Jochen	1999
Lewis, Ancret	1999
Wightman, Joe	1999
Petrycki, Jennifer	1999
Dance, Michelle	1999
Simon, Karen	1999
Turnbull, Joy	1999
Cochrane, Anna	1999
White, Scott	1999
Fra, Urbano Paleo	1999
Jeffcoate, Alistair Bryan	1999
Lundberg, Matthew	1999
Colclough, Sarah	1999
Krug, Ralf	1999–2000
Helbling, Angela Herta	1999–2000
Royer, Geraldine	1999–2000
Ong, Phillip	1999–2000
Hager, Stacey	1999–2000
Barker, Stephen	1999–2000
Van Dalfsen, Elske	1999–2000
Haslinger, Florian	1999–2000
Stolar, Drew	1999–2000
Stolar, Stephanie	1999–2000
Tincher, Kit	1999, 2001–02

Steiner, Michael	2000
Woods, Lindsay Anne	2000
Head, Elisabet	2000
French, Kirsty	2000
Soule, Samuel Adam	2000
Pirie, Dawn	2000
Cantu, Guadalupe	2000
Schipper, C. Ian	2000
James, Brian	2000
Kaye, Grant	2000
Hungerford, Jefferson	2000
Squire, Robert	2000
Thaw, Jonathan	2000
Adleman, Jennifer	2000
McQuade, Yume	2000–01
Haig, Sawyer	2000–01
Flude, Stephanie	2000–01
Garofalo, Kristin	2000–01
Pfeiffer, Tom	2000–01
Stine, Larry L.	2000–01
Stine, Mary Kay	2000–01
Shaner, Kelsey	2001
Henderson, John	2001
Beran, Laurens	2001
Barr, Mary	2001
Sawyer, Georgina	2001
Neuman, Gregory S.	2001
Swannell, Philippa	2001
Wanless, Dorsey	2001
Nesvadba, Nicole	2001
Godard, Vincent	2001
Meyer, Jason	2001
LaChance, Frederick	2001
Pressling, Nicola	2001
Ano, Marion	2001
Donegan, Stephen James	2001
Dobson, Katherine	2001–02
Edmunds, Paul	2001–02
Duncan, Alec S.	2001–02
Vierra, Sherry	2001–02
Cole, Matthew	2001–02
Avis, Christopher	2001–02
Sheppard, Deborah E.	2002
Meier, Vanessa Lynn	2002
Matiella, Maria	2002
James, Sarah	2002
Chattey, Leanne	2002
Dalton, Marika	2002
Synowsky, Eva	2002
Durant, Adam J.	2002
Douglas, Anne	2002
Shu, Wen-Yi	2002
Fairweather, Ian	2002
Castenada, Rosalinda	2002
Wagner, Christine	2002
Goodrich, Whitney	2002
Rutherford, Eric	2002
Williams, Rebecca	2002
Jenkins, Kelley	2002
Modinou, Ivvet	2002
Weldon, Christopher	2002
Stewart, Lisa	2002